Determination of abundance, composition, and sources of carbonaceous components within particulate matter from urban environments within the UK

Melissa Nikkhah-Eshghi

Submitted in fulfilment of the requirements for the degree of

Doctor of Philosophy

Scottish Universities Environmental Research Centre

College of Science and Engineering

University of Glasgow

July 2023

Abstract

Airborne ambient particulate matter (PM) has detrimental effects on human health and the environment and its concentrations are usually higher in urban areas. The carbonaceous component is a major constituent of particulate matter with an aerodynamic diameter of ≤2.5 μM ($PM_{2.5}$). It comprises of black carbon (BC) and many individual species of organic compounds such as polycyclic aromatic hydrocarbons (PAHs) and n-alkanes. Despite this importance, BC remains a poorly quantified and poorly characterised component of PM, relative to other PM fractions. The aims of this work were therefore to:

1) Determine the abundance and spatiotemporal trends of airborne BC in Glasgow, Scotland's largest city.
2) Obtain samples of airborne PM from Glasgow and elsewhere in the UK, quantify the concentrations of PM-bound PAHs and estimate the associated health risks of exposure to these PM-bound PAHs.
3) Develop hydropyrolysis (hypy) methodology to isolate BC_{hypy} from airborne ambient PM, obtaining BC/Total Carbon % (BC/TC%) measurements.
4) Undertake source apportionment of the carbonaceous components (PAHs, n-alkanes, TC and BC) of PM from Glasgow and elsewhere. Radiocarbon (^{14}C) analysis and delta carbon-13 ($\delta^{13}C$) were to be used for source apportionment of TC and BC. Principal component analysis (PCA) were to be used to determine sources of PAHs and n-alkanes.

To determine the abundance and spatiotemporal trends in Glasgow, two portable microaethalometer instruments were used. These were calibrated through co-location against the UK BC network aethalometer at the Glasgow Townhead urban background site. In four Glasgow wards, one microaethalometer was placed at a fixed location whilst the other was used in mobile measurements to determine the relative and absolute spatiotemporal variations in BC. BC increment concentrations calculated through subtracting the background BC concentrations from Glasgow Townhead site and absolute concentrations exhibited spatial variation across the wards. The 'mobile' measurements showed the city centre to be a hotspot whilst Baillieston, a residential ward on the outskirts of the city, had the lowest BC increments. Population, population densities and socio-economic data could be used as valuable BC indicators to determine other BC hotspots in Glasgow and beyond. Temporally, median BC increments were significantly higher in mid-morning (10:30 – 11:30)

than earlier morning (08:00 – 09:00). However, absolute BC concentrations had the opposite trend showing that background BC contributes highly to morning BC concentrations. This suggests that use of BC increments rather than BC concentrations can help improve understanding of local pollution events by removing background influences. BC increments were correlated strongly with NOx concentrations and bus/heavy goods vehicles average daily traffic counts at the sampling sites. This showed that Glasgow City Council could focus local air quality measures towards reducing emissions from buses and HGVs.

Samples of $PM_{2.5}$ were collected from two sites in Glasgow using a low volume air sampler: GLA-HH (University Avenue, Hillhead), GLA-CC (George Street, City). Samples of $PM_{2.5,}$ and of particulate matter with an aerodynamic diameter of ≤10 μM (PM_{10}), from GLA-KS (Hope Street, City) were provided by Ricardo, an environmental consulting services company. Samples were also collected from a comparison site, an urban background site located in Manchester Fallowfield Campus (MAN-FF). The GLA-KS and MAN-FF samples were collected by high volume air samplers. For n-alkane and PAH analysis, samples were extracted by accelerated solvent extraction (ASE) using hexane and acetone, and then compound groups were separated using column chromatography.

GLA-KS benzo(a)pyrene (BaP) concentrations exceeded the UK National Air Quality Objective (NAQO) of 0.25 ng m^{-3} and were close to the EU Fourth Air Quality Daughter Directive (FAQDD) limit value of 1 ng m^{-3}. This implied that inhalation of $PM_{2.5}$ from GLA-KS could be associated with potential health effects such as lung cancer. BaP concentrations in the MAN-FF samples did not exceed the NAQO or FAQDD values, suggesting that suburban areas had lower associated health risks than inner-city areas. The increased lung cancer risk through inhalation ($ILCR_{inh}$) was calculated for PM-bound PAHs. The $ILCR_{inh}$ using the World Health Organization IUR_{Bap} value resulted in $ILCR_{inh}$ of 2.09×10^{-4} for GLA-KS($PM_{2.5}$) and 4.60×10^{-5} for GLA-KS(PM_{10}). This equated to 209 excess lung cancer cases per 1,000,000 people for $PM_{2.5}$ and 46 excess lung cancer cases per 1,000,000 people for PM_{10}. When applied to the Anderston, City and Yorkhill ward population this translated to 6 excess annual cases of lung cancer, assuming continuous and homogenous exposure of inhabitants. This shows that health risks posed to those living in Anderston, City and Yorkhill ward is not negligible and should be improved through $PM_{2.5}$ reductions.

The hypy methodology was tested on various different materials. Purchased aerosol and dust standards (NIST 1649b Urban Dust, NIST 1648a Urban PM, BCR-723 Road dust and ERMCZ100 Fine Dust PM_{10}-like) were used in the study. Two of these materials represented

urban aerosols (NIST 1649b and 1648a), and the other two materials (BCR-723 road dust and ERMCZ100 Fine Dust) represented aerosols with dominant vehicular emission sources as they were collected from traffic tunnels. An in-house road dust sample from Glasgow Hillhead was collected for analysis. Materials that represented end-members of BC were also used. NIST 2975 diesel PM was used to represent high BC concentrations, whilst in-house charred biomass materials were used to represent lower BC concentrations. A purchased lignite material was used to represent a material with low BC content.

Hypy successfully determined BC/TC% in materials that contain low, moderate and high BC contents. As expected the BC/TC% of NIST 2975 Diesel PM was around 100 %BC/TC, for the lignite material (BZ) it was around 2 %BC/TC. The biomass materials showed variability with BT/TC% of 16 % (DB) and 63 % (EB). The urban aerosols had similar BC/TC% (25 – 28 %). The road dusts had different BC/TC% due to different sampling site characteristics (14 – 41 %). The variability between replicates was extremely low with a maximum standard deviation of 5.3 %BC/TC and standard error of 1.3 %BC/TC across all materials. The BC/TC% for NIST 1649b (28 %BC/TC) was in agreement with other hypy-derived BC/TC% reported in the literature. A method was then developed for the use of hypy on airborne ambient PM for subsequent ^{14}C analysis for source apportionment.

Airborne ambient PM from two sites in Glasgow (Glasgow City Centre GLA-CC, and Glasgow Hillhead GLA-HH) and Fallowfield Manchester (MAN-FF) underwent ^{14}C analysis for both TC and BC components. The results for the percentage modern carbon (%MC) for the TC were compared to other UK sites. The MC% to percentage fossil carbon (%FC), (%MC:%FC), proportions in TC sample for GLA-CC and GLA-HH were 46%:54% showing dominant fossil sources. Whilst for MAN-FF the %MC:%FC proportion was 63%:37%, hence exhibiting dominant modern carbon sources. Due to COVID-19 comparisons with other UK sites did not represent source apportionments for business-as-usual scenarios. The %MC (TC) followed this order:

Auchencorth Moss > London Honor Oak Park > Chilbolton Observatory > Manchester Fallowfield > Glasgow Hillhead > Glasgow City Centre.

Auchencorth Moss, a rural background site, had the highest proportion of modern carbon sources and Glasgow City Centre had the highest proportion of fossil carbon sources.

The PAH and n-alkane and PAH sources were in agreement with those %MC (TC) for GLA-CC and GLA-HH as fossil fuel combustion sources were dominant sources according to source categorisations from PAH diagnostic ratios (PAH DRs) and carbon preference index

(CPI) for n-alkanes. Principal component analysis showed that the variance in PAH and n-alkane concentrations could be explained by two principal components (PC), PC 1 (79.6 % of the variance) and PC 2 (20.1 % of the variance). These components represented diesel and wood combustion emissions (PC 1) and vehicular emissions (direct and indirect) (PC 2). The n-alkane distributions showed the presence of epicuticular wax n-alkanes (C_{29}, C_{31} and C_{33}) suggesting biogenic vegetative detritus sources in GLA-KS samples, with the possibility of regionally transported biomass combustion PM-bound PAHs. The n-alkanes showing odd/even carbon preference in MAN-FF differed from GLA-KS, suggesting different sources of epicuticular waxes.

BC_{hypy} was successfully isolated for urban aerosols and dust materials. The NIST 1649b %MC (BC_{hypy}) of 6 %MC was in agreement with previous studies. BC_{hypy} was then isolated for MAN-FF and GLA-HH samples. The reported %MC (BC_{hypy}) was 24 % for GLA-HH and 20 – 25 % for MAN-FF. The two replicates of MAN-FF showed a good level of precision both yielding 25 %MC (BC_{hypy}). The sources of carbonaceous components from GLA-HH and MAN-FF therefore dominantly fossil carbon. However, the ^{14}C was higher than urban aerosol materials (6 – 12 %MC) and reported values in the literature for a UK site, Birmingham (11 % average %MC). This shows that the modern nature of BC has increased due to decreasing fossil fuel combustion emissions and an increase in biomass combustion sources.

This project provided a valuable overview of the abundance and spatiotemporal trends of BC in Glasgow, health risks of PM-bound PAHs in Glasgow and Manchester and the sources of BC, TC, and organic carbon (OC) components in PM within the UK.

Table of Contents

List of tables

List of figures

Acknowledgements

I would like to sincerely thank my patient supervisors Phillipa Ascough, Mathew Heal and Jaime Toney firstly for giving me an opportunity to work on this project. I am forever grateful for the opportunity and the guidance you've given me. I am especially grateful to Philippa, my first supervisor, for her drive and commitment, which continually pushed me and the project forward. To the staff members from SUERC, Chris, Josanne, Mark, Richard, Rona, Jason and Gillian, thank you for providing help and kindness throughout the project. To Ali Salik, who is integral to the running of the BECS lab, thank you for sharing your expertise and being extremely kind and patient in the process.

I would also like to thank the individuals and organisations who collaborated with me: SEPA, (Collin Gillepsie), Ricardo (Stuart Sneddon and others), The National Physics Laboratory, the University of Manchester (James Allan and Nick Marsden) and University of Glasgow Engineering (Ian Watson and Prashant).

I would also like to thank Iain Beverland, Fiona, Caitlin and the security team for allowing me to collect samples at the University of Strathclyde and accompanying me at Townhead during measurements. Thanks to Charlotte and Anca for helping me with carrying sampling equipment and collect road dust samples.

To the friends I met along the way Annette and Jakub, thank you for the bright weekends we shared together. Thank you to Adam, Calum, Hara, Jamal, Lewis, Nicole and Orestis who provided me with the much-needed emotional support. Thank you to my family, who supported in any way they could.

And lastly, in the spirit of self-love, I thank myself for the patience, perseverance, and strength I have exhibited. This has been a turbulent journey, with many ups and downs, so I am proud of myself for finishing the thesis. I eagerly await the start of a new chapter.

Author's Declaration

I declare, except where explicit reference is made to the contribution of others, that this thesis is the result of my own work and has not been submitted for any other degree at the University of Glasgow or any other institution.

Printed Name: Melissa Nikkhah-Eshghi

Signature:

Glossary of Abbreviations used in Text

General Terms

ASE – Accelerated Solvent Extraction

BC – Black carbon

BC_{hypy} – Reported carbon content in the hypy residue

^{14}C – Radiocarbon isotope

EC – Elemental carbon

FC – Fossil carbon

GC-FID – Gas chromatography flame ionisation detection

GC-MS – Gas chromatography mass spectrometry

FAQDD – Fourth Air Quality Daughter Directive

Hypy – Hydropyrolsyis measurement technique

OC – Organic carbon

MC – Modern carbon

NAQO – National Air Quality Objectives

Non-BC_{hypy} – Semi-labile organics removed from the hypy residue

NOx – Nitrogen oxides

NO_2 – Nitrogen dioxide

PAHs – Polycyclic aromatic hydrocarbons

PAH DRs – Polycyclic aromatic hydrocarbons diagnostic ratios

PCA – Principal component analysis

PM – Particulate matter

$PM_{2.5}$ – Particulate matter with an aerodynamic diameter of ≤ 2.5 µm

PM_{10} – Particulate matter with an aerodynamic diameter of ≤ 10 µm

PAH Abbreviations

NAPH – Napthalene

ACY – Acenapthylene

ACE – Acenapthene

FLU – Fluorene

PHEN – Phenanthrene

ANTH -Anthracene

FLA – Fluoranthene

PYR – Pyrene

CHRY – Chrysene

BaA – Benzo(a)anthracene

BbF – Benzo(b)fluorene

BkF – Benzo(k)fluorene

BaP – Benzo(a)pyrene

DahA – Dibenzo(a,h)anthracene

IcdP – Indeno(1,2,3,c,d)pyrene

Bghi – Benzo(g,h,i)perylene

LMW PAHs – Low molecular weight PAHs (NAPH, ACY, ACE, FLU, PHEN and ANTH)

MMW PAHs – Moderate molecular weight PAHs (FLA, PYR, CHRY, BaA)

HMW PAHs – High molecular weight PAHs (BbF, BkF, BaP, DahA, IcdP, BghiP)

1. Introduction

Air pollution is detrimental to human health as it is strongly associated with occurrence and severity of respiratory and cardiovascular diseases (Alexis et al., 2004; Folinsbee, 1993; Kampa & Castanas, 2008; Kurt et al., 2016). The World Health Organisation estimates that overall, air pollution leads to 7 million premature deaths per year worldwide (World Health Organisation). In the UK, the Committee on the Medical Effects of Air Pollution (COMEAP), estimated that air pollution, in particular, particulate matter, caused 29,000 premature deaths in the year 2008 (COMEAP, 2010).

The economic cost from impacts of air pollution, such as costs associated with hospital admissions, in the UK were estimated to be £157 million in 2017 with findings in a recent report from Public Health England warning that these costs could reach £18.6 billion by 2035 unless action is taken (Public Health England, 2018).

Air pollution can also lead to severe environmental effects, as certain air pollutants, such as black carbon (BC), introduce a net warming effect on the Earth's atmosphere, which can exacerbate climate change effects through temperature rises (Bond et al., 2013; Bytnerowicz et al., 2007; IPCC, 2018; Madronich et al., 2023; Sicard & Dalstein-Richier, 2015). The International Panel on Climate Change (IPCC) stated that climate models project significant differences in regional climate characteristics between present-day and global warming of 1.5 and 1.5 – 2 °C with a high degree of confidence. The differences will likely include increases of mean temperature in land and ocean regions, hot extremes, heavy precipitation and the probability of drought and precipitation deficits; such changes are likely to affect nature conservation (IPCC, 2018). The IPCC deemed BC to be a short-term climate forcer, contributing to such effects (IPCC, 2018).

As a result of the above, it is important to assess ambient concentrations of air pollution. Air pollution is a complex mixture of solid and liquid particles and gaseous species; therefore, to assess air quality, air pollutants are measured and monitored based on their chemical composition or physical states. Monitoring of air pollution provides real-time and temporal trends in concentrations at monitoring locations. The monitoring and reporting of certain air pollutants is required by law in current legislation such as the Air Quality Standards England 2010 and amendment in 2016 which has equivalent regulations existing in Scotland, Wales and Northern Ireland (The Air Quality Standards Regulations, 2010; The Air Quality

Standards Regulations Amendment, 2016). The purpose of the legislation is to reduce public exposure to air pollution and to limit environmental degradation as a result of air pollution.

In the UK, local authorities play a role in ensuring air quality improvements are delivered effectively to areas exceeding air pollutant annual mean concentration targets set by law, under the Air Quality regulation England (2000) with equivalents in Scotland, Wales and Northern Ireland (The Air Quality England Regulations, 2000).

In the UK the five key pollutants that are usually quantified to determine air quality are: nitrogen dioxide (NO_2), ozone (O_3), sulphur dioxide (SO_2), particulate matter (PM) with an aerodynamic diameter of <10 µm (PM_{10}) and of <2.5 µm ($PM_{2.5}$) (UK Air, n.d.-b). When NO_2, PM_{10} /$PM_{2.5}$ and SO_2 concentrations breach The National Air Quality Standards, an air quality management area (AQMA) is declared by the local authority in question who then manage and reduce the concentrations in the area to bring these below the limit value. Glasgow City currently has two AQMAs for NO_2 and PM_{10}/$PM_{2.5}$ (UK Air, n.d.-c).

1.1. Particulate Matter (PM)

National policy, national legislation and local authorities are crucial to air quality improvements as required by UK and international legislation. It is currently clear that PM concentrations in certain areas within the UK do not meet the National Air Quality Standards; there are currently 83 PM_{10} air quality management areas in the UK (UK Air, n.d.-a). Unlike the other key pollutants identified above, PM is not a single chemically-defined entity (e.g., a single molecule) and consists of many different chemical components from different sources. The main components of PM are a variety of carbonaceous components, sulphates, nitrates, ammonia, sodium chloride, mineral dust, and water (AQEG, 2005;2012). PM has a wide range of natural sources (pollen, sea spray and Saharan dust) as well as anthropogenic sources (e.g., fuel combustion).

Particulate matter can also be formed in the atmosphere through chemical reactions of gaseous pollutants from anthropogenic sources such as ammonia from agriculture and biogenic sources such as volatile organic compounds (VOCs) from vegetation – this is known as secondary PM (Air Quality Expert Group, 2005).

Dry and wet atmospheric deposition removes PM from the atmosphere to aquatic and terrestrial ecosystems. Until final deposition PM remains suspended in the atmosphere,

where it can travel long distances. This means that PM sources in a single location can be regional as well as local (Beverland et al., 2000). The distances travelled by PM are affected by the size of the particles and meteorological conditions (Pérez et al., 2020).

The health risks associated with the inhalation of PM depend on the size of the particles. Inhalation of coarse particles ($PM_{2.5-10}$), leads to deposition in the extrathoracic and upper tracheobronchial regions, whilst inhalation of fine particles ($PM_{2.5}$) is more likely to lead to penetration into tracheobronchial and alveolar regions (Brook et al., 2004). Short-term PM_{10} inhalation has been associated to chronic obstructive pulmonary disease and cardiovascular disease (Anderson et al., 2001; Arbex et al., 2009; Ballester et al., 2006; Belch et al., 2021; Zhang et al., 2017). Long-term $PM_{2.5}$ exposure has been associated with a larger increase for cardiovascular mortality than short-term $PM_{2.5}$ exposure (Brook et al., 2010). A study found that long-term $PM_{2.5}$ exposure is an important environment risk factor for global type 2 diabetes burden (Liu et al., 2021). The health risks associated with inhalation of PM also depend on the composition of PM. For example, a strong association was found between exposure to carbonaceous $PM_{2.5}$ and infant mortality, particularly neonatal mortality (Goyal et al., 2019). Furthermore, a study that analysed daily concentrations of $PM_{2.5}$ constituents over five years to investigate daily mortality found mortality relative risks estimated for BC and organic carbon (OC) were larger than those for sulphate and nitrate (Kim et al., 2012). This shows the importance in the speciation of $PM_{2.5}$ mass, in particular the carbonaceous constituents if the links between PM and the variety of different associated health risk are to be properly explored.

1.2. PM Carbonaceous Constituents: Black Carbon (BC)

Black carbon (BC) is a component of $PM_{2.5}$ formed during the incomplete combustion of a variety of carbon-based fuel sources: plants, woods, fossil fuels and industrially-produced substances such as cokes (Paul, 2012). These combustion processes are predominantly related to anthropogenic activities such as transport, energy generation, residential heating and biomass burning, and to non-anthropogenic factors such as wildfires. In the UK, the predominant source of BC aerosol load is via anthropogenic activities. The current biggest contributors of BC in the UK are industrial biomass combustion, small-scale waste burning and domestic combustion of wood (NAEI, 2020).

Research has shown that BC is more strongly associated to adverse health effects than PM ; some studies have suggested BC to be used as an additional indicator for adverse health effects (Janssen et al., 2011). A review of ambient PM toxicological and epidemiological literature found BC to be more causally involved in all-cause lung cancer and cardiovascular mortality, morbidity and adverse birth and nervous system effects (Grahame et al., 2014). Epidemiological evidence was also found linking BC with cardiopulmonary hospital admissions and all-cause cardiopulmonary and cardiovascular mortality (Janssen et al., 2012). Another study found that after controlling for $PM_{2.5}$ mass, associations remained between all-cause mortality and BC and potassium (Achilleos et al., 2017).

Black carbon also has detrimental environmental effects through the absorption and scattering of radiation, alteration of cloud properties and deposition on snow and sea ice (Bond et al., 2013). The International Panel on Climate Change stated reducing concentrations of short-lived climate forcers, such as BC, could contribute to efforts that endeavour to limit climate warming to 1.5 °C (IPCC, 2018). It was also stated that these reductions would have co- benefits such as improved air quality, reduced risk to human health and agricultural yields.

1.2.1. BC Definitions, Composition and Structure

BC is a conventional 'umbrella' term, used interchangeably with 'elemental carbon' (EC) and 'soot' (Andreae & Gelencsér, 2006; Petzold et al., 2013b). This often refers to a form of carbon that has polyaromatic chemistry, is very dark in colour under natural light, and is produced as a direct result of combustion processes. However, there is no agreed clear unambiguous terminology available for the quantification of this type of carbonaceous matter in atmospheric aerosols. The measurement of highly light-absorbing/black carbonaceous matter in atmospheric aerosols spans many different disciplinary fields including atmospheric science, climatology, environmental science, biogeochemistry, and paleoclimatology. As a consequence, this has led to conflicting terminologies despite the requirement for clear concise terminology being more crucial due to the inter-disciplinary nature of the research (Petzold et al., 2013b). Due to the lack of a consensus terminology, numerous publications in the scientific literature refer to the same property with different terms and use the same term for a different property (Petzold et al., 2013b).

For clarity, each of the terms BC, EC and soot is defined in this thesis as follows:

Black Carbon: BC - Refers to the highly light-absorbing refractory carbonaceous matter in aerosols which have low reflectivity throughout the visible spectrum, thus appearing black. An issue with this term is that it does not inherently specify any details about the formation process (Andreae & Gelencsér, 2006), and can cover any material with a dark coloration, but which is not produced by any combustion process. BC has also been defined by Bond et al. (2013) by its properties such as:

1) Strong absorption of visible light

2) Refractory nature with a vaporisation temperature near 4000 K

3) Aggregate morphology of small spheres

4) Insoluble in water and common organic solvents.

Elemental Carbon: EC - Refers to a set of substances consisting entirely of carbon all of which are highly absorbing throughout the visible spectrum. The issue with this term is that it assumes that the particle is 100 % pure carbon, and it could imply one or more allotropes of carbon (diamond, graphite, C_{60}, carbon nanotubes) (Petzold et al., 2013b).

Soot – Refers to a broad set of substances produced by incomplete combustion of carbonaceous fuels, and is hence defined by a formation mechanism, not optical properties, composition, or structure. The definition of soot links this term to its source: combustion. Soot is a useful term because it does not imply 100 % pure carbon, stating the presence of other elements. It has a variable structure that can be amorphous, graphitic or fullerene (Andreae & Gelencsér, 2006; Long et al., 2013). Unlike the term BC and EC, the term soot includes components such as OC from chars, coke-oven emission and organic-based carbon particles.

To align with other literature in the atmospheric science community, the term BC will be used throughout the thesis. Nevertheless, the inherent issue with the term ‘black carbon’ is that it implies the air pollutant in question is a single entity, similar to ‘carbon black’ (CB) which is a manufactured product, consisting of fine black powder of nearly pure elemental carbon. CB is nearly pure elemental carbon with low quantities of extractable organic carbon (OC) and total inorganics (Long et al., 2013; Watson & Valberg, 2001). It has a morphology with ‘grape-like’ aggregates of highly fused spherical primary particles, with aggregates clustered into larger-sized agglomerates. CB is often used as a proxy for BC in studies; for example, laboratory animals were exposed to CB, and this was mistaken as giving evidence

of the potential health effects of airborne ambient BC (Tankersley et al., 2007; Tankersley et al., 2004). This shows that using ambiguous terms like BC, that assume a single entity, can be detrimental to research within the field. A critical point here is that the ambiguity over BC arises in a large part due to difficulties in chemically characterising and isolating this component of the carbonaceous aerosol load. This therefore leads to ambiguity between studies as different fractions of the aerosol loads are being targeted for investigation.

Many research studies have shown that airborne ambient BC particles differ from CB in composition and morphology, as particles are more heterogenous with higher ash and extractable OC contents (Long et al., 2013). One type of airborne ambient BC particle that particularly resembles CB are particles emitted from biomass burning; they have chain-like aggregates and spherical primary particles, with the primary particles having turbostratic microstructures similar to those reported for CB (Chakrabarty et al., 2010; Kocbach et al., 2006; Kocbach Bølling et al., 2009; Long et al., 2013). However, there is a lot more variability in particles emitted from biomass burning due to variability in fuel and combustion conditions. This leads to particles with different structures, such as spherical particles with high organic carbon, sphere-like particles with ash content, chain aggregates with solid irregulars and liquid/spherical shapes from open biomass burning (Kocbach Bølling et al., 2009; Long et al., 2013; Reid et al., 2005). Particles from biomass burning also have a large water-soluble fraction (Andreae & Gelencsér, 2006; Decesari et al., 2006; Hoffer et al., 2006).

Another type of airborne ambient BC particle similar to CB is diesel exhaust particulates (DEP). DEP have solid elemental carbon cores, like CB but with smaller diameters (Burtscher, 2005; Long et al., 2013; Shi et al., 2000). They have more strongly bent graphene, which is due to more defects. The defects are correlated to surface functionalisation, so DEP has more oxygen and hydrogen atoms, than CB (Long et al., 2013; Müller et al., 2007). Another key difference between DEP and CB is that DEP involves a layer of volatile and semi-volatile hydrocarbons and sulphates that lie atop the solid elemental carbon cores unlike CB (Kittelson, 1998; Long et al., 2013; Shi et al., 2000).

This shows that airborne ambient BC particles exist in conjunction with OC, hence their morphologies exhibit variation depending on the source and combustion conditions (Hays & Vander Wal, 2007; Long et al., 2013). The OC fraction tends to exceed the BC content (Fernandes et al., 2003; Long et al., 2013; Reid et al., 2005). Moreover, airborne ambient BC particles are less pure in terms of carbon content, as DEP had a higher degree of surface functionalisation. Another issue is that if BC has surface functionalisation, i.e. heteroatoms

like hydrogen and oxygen, BC becomes a three-dimensional organic polymer capable of transferring electrons rather than a mere amorphous form of EC (Andreae & Gelencsér, 2006; Chang et al., 1982). More efficient combustion regimes result in higher abundance of oxygen and defective structures in BC particles, which in turn increases their chemical reactivity and wettability in the atmosphere (Andreae & Gelencsér, 2006; Chughtai et al., 2002; Su et al., 2004). This is inconsistent with the Bond et al. (2013) definition that BC is refractory.

To summarise, the properties of airborne ambient BC particles described in much of the literature do not always match those described in the definition by Bond et al. (2013) most likely because primary BC particles seldom exist in the atmosphere; they aggregate and, once emitted, externally and internally mix with other atmospheric particles present in ambient air (Weingartner et al., 1997; Zhang et al., 2008). BC is better represented with the combustion continuum model (see Figure 1.1). Figure 1.1 was first assembled by John I. Hedges (Hedges et al., 2000; Masiello, 2004). The BC continuum successfully highlights that BC is not a single entity, rather a continuum of chemically heterogenous substances, where increased heating and chemical reformation yields a spectrum of progressively carbon-rich and refractory organic materials (Hedges et al., 2000). The BC continuum is more logically applicable to airborne ambient aerosols than the belief that BC is a single highly refractory entity, as if that was the case, there would be large pool sizes of BC present, due to slow or non-existent loss processes of BC, and considering little is known about loss processes of BC, this seems unlikely (Masiello, 2004). The BC continuum is supported by evidence, using ^{13}C Nuclear Magnetic Resonance (NMR). When pinewood is charred, it loses signal intensity associated with cellulose and gains signal intensity in the aryl and O-aryl regions due to an increasingly aromatic chemical structure. This shows aromaticity of BC increases with charring (Baldock & Smernik, 2002; Masiello, 2004). The size of particles is important in the BC continuum, as it effects their transportability. Smaller BC particles remain airborne for longer whilst larger particles undergo deposition, so the initial reservoir that the particles enter is dependent on size (Clark & Patterson, 1997; Masiello, 2004; Ogren & Charlson, 1983).

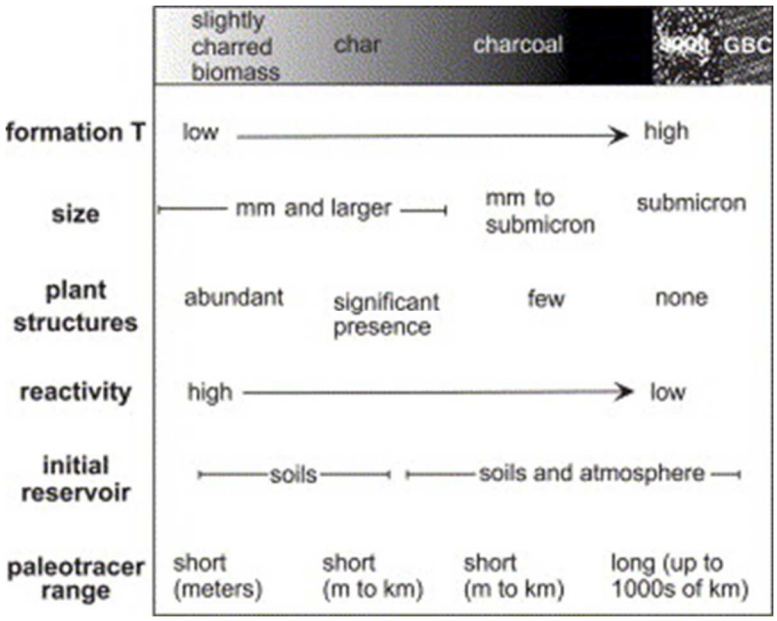

Figure 1.1. The BC continuum reprinted from: *New directions in black carbon organic geochemistry,* volume 92, C.A. Masiello, Marine Chemistry, 201-213, Copyright (2004), with permission from Elsevier.

It is generally thought polycyclic aromatic hydrocarbons (PAHs) play a role in the formation of BC particles, through two carbon radicals joining into PAHs, with PAHs continuing to assemble into larger aromatic rings, eventually condensing into solid spheres (Masiello, 2004). This mode of production suggests that the presence of PAHs is intrinsic to the structure of BC particles (Akhter et al., 1984; Akhter et al., 1985; Masiello, 2004; Sergides et al., 1987). Precise chemical characterisation of numerous organic species in BC particles is very challenging, with Reid et al. (2005) noting an absence of any full quantification of the organic species comprising the carbon-based components of biomass smoke particles (Chakrabarty et al., 2010). This could be due to the difficulty in separating BC from other components in PM. Moreover, Long et al. (2013) reported uncertainties in PAH data across studies and particle types due to differences in collection or extraction methods and lack of uniform analyte specification (Long et al., 2013).

In summary, the BC continuum shows that BC is extremely variable in composition, properties, and morphology. Airborne ambient BC particles rarely exist solely, as they externally and internally mix with other atmospheric particles in the air. This makes isolating and measuring BC from chemically complex matrices such as aerosols extremely difficult and leads to the use of operational definitions of BC. To characterise and measure the refractory component of the BC continuum often used to describe BC, BC must be separated from the other OC components in airborne ambient aerosols. Once separated, BC is best

defined as stable polyaromatic structure. This definition will be used here on to describe BC as there is a consensus that BC is formed from combustion processes, and that its chemistry is polyaromatic in nature. These issues are discussed further in Section 1.2.2.

1.2.2. Characterisation of BC

Chemical characterisation of BC includes obtaining information on abundance of BC, its chemical composition, and its morphology/structure. The characterisation of BC in a range of environmental matrices, generally falls into six broad categories of measurement approach: chemical, microscopic, molecular tracer, optical, spectroscopic, and thermal. Sometimes combinations of these categories are made e.g., thermal-optical techniques or combinations of techniques such as thermal methods and ^{14}C analysis. The advantages and disadvantages of the various BC measurement techniques are presented in Table 1.3.

What makes BC unique are its light absorption, microstructure, morphology, solubility, and thermal stability properties. It is important to note that all these are a function of the underlying chemistry of BC. As seen in Figure 1.2 not all measurement techniques can capture the full range of BC continuum. This then leads to BC being measured on an operational basis rather than based on all 5 of its key properties listed above. This means that individual techniques identify specific segments of the BC continuum as shown in Figure 1.2. Consequently, large variability is observed when quantifying BC with different methods; Currie et al. (2002a) reported that the proportion of BC in an 'urban dust' standard (NIST SRM 1649a) ranged from 6.8 to 52 % using 13 different quantification methods. Descriptions of some of the common methodologies used to characterise BC is provided below.

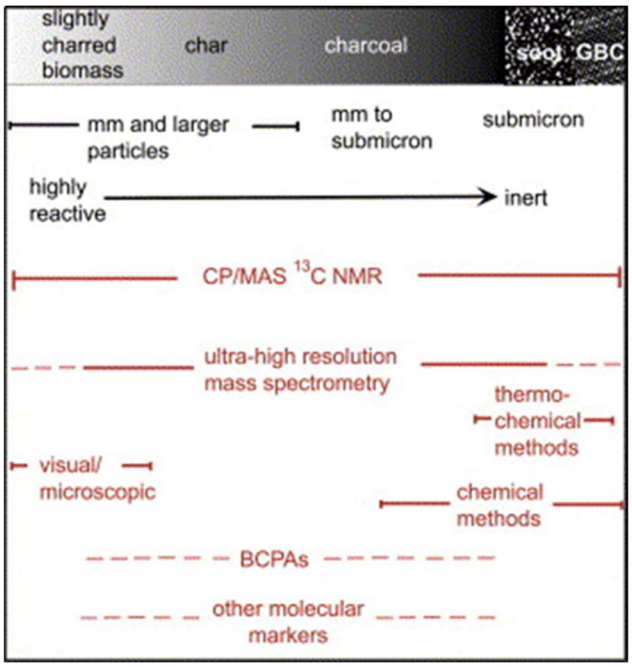

Figure 1.2 The BC methods continuum reprinted from: *New directions in black carbon organic geochemistry,* volume 92, C.A. Masiello, Marine Chemistry, 201-213, Copyright (2004), with permission from Elsevier.

Chemical Techniques

Chemical methods use oxidants to oxidise organic material, to isolate the resistant carbon residue and quantify it. These methods operate on the basis that BC consists of chemically highly recalcitrant carbon, as a function of its polyaromatic structure. Typically, a wet chemical oxidation is used, at a molarity and time interval chosen by the experimenter. Common chemical oxidants include potassium dichromate (Hammes et al., 2007). This involves adding aliquots of acidified dichromate solution to the sample and maintaining the sample at an elevated temperature in an orbital incubator shaker (Meredith et al., 2012). The sample is recovered using a centrifuge, then washed and then suspended in deionised water. The sample then undergoes freeze-drying and is quantified as BC. The aim is that the oxidation processes sufficiently remove non-BC carbon but do not degrade BC itself.

The issues with this method are that there are many stages where the sample loss can occur. This is problem when analysing airborne ambient aerosol, as it is harder to collect larger sample sizes compared to other environmental matrices such as soil. Moreover, results in Hammes et al. (2007) showed dichromate oxidation led to variation in BC results, which was thought to reflect variation in methods used by different laboratories (Meredith et al., 2012). Knicker et al. (2007) determined BC concentrations relied strongly on the applied

time of dichromate oxidation. This shows that BC could be overestimated if oxidation was not complete, hence quantifying non-BC as BC. Contrastingly, BC could be underestimated if the applied time for oxidation is too long hence BC itself becoming oxidised.

Microscopic Techniques

Electron microscopy can give information on the particle morphology and microstructure through transmission (TEM) or scanning (SEM) mode. It is a promising technique for identifying 3D structures of nanoparticles. Quantifiable parameters such as fractal dimension D*f,* can be applied to the image (Lack et al., 2014). However, electron microscopy is labour intensive in terms of sample preparation and data analysis. Computer-controlled image processing approaches are however enabling automatic characterisation of morphology of thousands of particles deposited on a filter (Petzold et al., 2013a).

Optical Techniques

Optical techniques to measure BC include aethalometers and photoacoustic instruments. The volumetric cross-section for light absorption (σ_{ap}) is the principal measure of any optical technique for measuring light-absorbing particles. The cross-section for light absorption, also known as the light absorption coefficient, helps derive a light-absorbing carbon mass concentration (BC) based on the relationship $BC = \sigma_{ap} \times MAC^{-1}$. MAC, which is the mass absorption coefficient, varies significantly in time and space dependent on certain factors such as source emissions and transformation during transport (Healy et al., 2017; Petzold et al., 2013a). Therefore, a single value is not representative of all BC particles.

The MAC value of primary spheres is independent when particles are fractal-like agglomerates, as particle absorption depends on the size of the spherules not the aggregates. For other particles, the MAC may depend on the sizes of individual particle hence the effective MAC of the aerosol will depend on the size distribution of the individual particles. Hence morphologies of particles must be known to ensure the correct MAC value is being used. This is not common practice, as MAC values are often fixed, hence this contributed to uncertainty in reported BC concentrations (Chakraborty et al., 2023; Petzold et al., 2013a). The application of this conversion between optical absorption and mass concentration also assumes BC is the only light-absorbing particulate species present. This is untrue, as mineral dust and non-BC light-absorbing carbonaceous matter such as brown carbon, are also light-

absorbing particulate species (Andreae & Gelencsér, 2006; Petzold et al., 2013a). Such influences must be excluded or corrected. Another issue is that coated particles enhance absorption as well as relative humidity effects (Petzold et al., 2013a).

Molecular Tracers (BPCA)

A common molecular tracer method is the benzene polycarboxylic acid (BPCA) method which used uses BPCA as a proxy of BC to determine BC concentrations (Glaser et al., 1998; Schneider et al., 2011). This method converts BC to benzene rings substituted with varying number of carboxylic acid groups forming benzene polycarboxylic acids (BPCA). This is completed through digestion with nitric acid followed by conversion to BPCA. After filtering and clean-up steps the sample is freeze-dried and can be analysed using GC-MS (after derivatisation) or HPLC. The BPCA is quantified and is used to determine BC concentration via ratio scale-up (Goldberg, 1985; Schneider et al., 2011).

A disadvantage of this method is that there are many stages where sample loss can occur. This is problem when analysing airborne ambient aerosol, as it is harder to collect larger sample sizes compared to other environmental matrices such as soil. Furthermore, prolonged digestion can lead to partial decomposition and reduced yields of BPCA leading to underestimations in reported BC (Glaser et al., 1998).

Thermal Techniques

Thermal and gas-analytical approaches are based on the analysis of gasification products that evolve from a heating filter sample either in an oxidising or inert atmosphere. To isolate and quantify BC (usually referred to as elemental carbon) the sample is heated to temperatures above 340 degrees C, to volatilise OC and convert it into gases, either CO_2 or CH_4, which are then detected using specific detection methods. The rest of the carbon is oxidised and counted as BC. There are a range of protocols such as IMPROVE, NIOSH, EUSAAR-2, each of which displays variation in the selectivity of separating BC from the bulk carbonaceous matter. Corrections for pyrolysis and charring of carbonaceous matter to BC are done through measurement of transmission or reflectance during the thermal-optical analysis step. The correction differs significantly between the transmission measurement (TOR, thermal-optical reflectance) and temperature protocol (Petzold et al., 2013a). Thermal

methods can be used in conjunction with ^{14}C quantification to determine sources of OC and BC (Heal et al., 2011).

Hydropyrolysis is also a thermal technique utilising high hydrogen pressures to reductively remove the semi-labile OC, which is retained on a silica trap, leaving behind the hypy residue, BC_{hypy} (Ascough et al., 2009; Meredith et al., 2012; Wurster et al., 2012; Wurster et al., 2013). The residue will also contain inorganic materials, not volatilised through the hypy process. The carbon content of the residue is determined through elemental carbon analysis and deemed as BC_{hypy}. This method allows for quantification of BC but also further analysis such as ^{14}C dating for source apportionment and GC-MS analysis of the semi-labile OC components referred to as non-BC_{hypy}.

Spectroscopic Techniques

Raman Spectroscopy

Raman spectroscopy measures the inelastic scattering of light when the vibrational mode of a chemical bond shifts the wavelength of some of the incident light. It is sensitive to the structural order of carbon atoms in aerosol particles. A direct link has been shown between graphite-like carbon structures and strong light absorption properties. As long as Raman spectroscopy is combined with calibration methods, this relationship can be used for the measurement of graphite-like carbon in atmospheric particle samples (Petzold et al., 2013a).

Cross Polarisation and Magnetic Angle spinning ^{13}C Nuclear Magnetic Resonance (CP/MAS ^{13}C NMR)

Nuclear Magnetic Resonance (NMR) is a useful technique for identifying and analysing organic compounds (Balci, 2005). ^{13}C NMR is one of the few techniques capable of providing direct measures of relative numbers of aromatic and non-aromatic carbons in coal and related materials (Akhter et al., 1984). Solid-state measurements using ^{13}C NMR with use of cross polarisation (CP) and Magic Angle Spinning (MAS) techniques, has been used with promising results in the study of coal and related materials and appeared applicable on hexane BC (Akhter et al., 1984).

Laser-induced incandescence

Laser-induced incandescence methods utilise laser heating of light-absorbing particles and subsequent analysis of emitted radiation. They look at an ensemble of particles or single particles (single particle soot photometer SP2), detecting carbon-containing particles which

are transformed to heat and the results in the re-emission of thermal radiation. It is a mass-based method, but the instrument response depends on the type of carbonaceous particle and the conversion of thermal radiation to carbon mass has to be established by proper calibration. Calibration of these instruments must be performed using a reference carbon material such as fullerene (Petzold et al., 2013a).

Aerosol Mass Spectrometry

Aerosol mass spectrometry (AMS) methods such as soot particle AMS (SP-AMS) and aerosol time-of-flight MS utilise single particle laser ablation systems based on laser induced plasma or multi-photo ionisation or laser vaporisation methods under incandescent conditions combined with heated filaments and subsequent mass-spectrometry techniques for analysing the chemical composition of individual carbon clusters in the mass spectra. Such methods target elemental chemical composition of the particles (Petzold et al., 2013a).

Table 1.1. Advantages and disadvantages of BC characterisation techniques.

Characterisation Technique	Advantages	Disadvantages
Chemical	• Wet oxidation methods avoid the problem of charring. [1] • Potassium dichromate method is an inexpensive technique. [2] • Potassium dichromate method has good reproducibility for soot, char, bituminous coal samples. [2]	• Rate of decomposition of organic matter may vary between different sources e.g., deep-sea sediments and terrestrial. [4] • Survival of non-BC material such as paraffinic and aliphatic structures. [5] • Chemical oxidation also attacks charcoal BC. [6] • Wet oxidation methods may cause loss of light soot particles during rinsing of sample. [7] • Potassium dichromate method fails to recover parts of BC dissolved in acid fraction. [2] • Potassium dichromate has poor reproducibility for soils and sediments. [2] • Positive artefacts. [3]
Hydropyrolysis *(thermal)*	• Reproducible BC_{hypy} determinations. [18] • Matrix independent. [18] • BC/TC% obtained from hypy were within the range of other results in the International BC Ring Trial of 12 reference materials, highlighting the accuracy of the technique. [2. 18] • Hypy appears to discriminate between relatively labile biochars reporting low BC_{hypy} values, from more refractory, high BC_{hypy} soot in pure samples. [18]	• Carbonate carbon can be allocated to either OC or EC; acid pre-treatment can remove interference. [17] • Cannot distinguish between pyrogenic-derived BC from highly mature sedimentary organic matter. [18]

	• Retains semi-labile organic carbon from sample for further analysis. [18]	
Microscopic	• Reveals the structure of monomers of BC. [8] • Ensemble method has a low uncertainty. [8]	• Different aggregate morphology characterization techniques have different drawbacks: Ensemble Method: Difficulty in obtaining accurate 3D information about aggregate morphologic variables required for calculating the three-dimensional D*f* of aggregates. Nested Squares Method and Perimeter Method: Assumptions made that 2D D*f* equals 3D D*f,* causing systematic differences between the two from a 2D projection of a 3D structure. [8] • Nested squares and perimeter method have large uncertainties. [8]
Molecular Tracer (BPCA)	• Benzene Polycarboxylic Acid (BPCA) tracer method requires nitric acid oxidation after digestion; this removes interfering organic substances that complicate the subsequent procedure. [11]	• BPCAs may originate from biological sources as well as BC, e.g., pigment aspergillin. [12] • Standard substances not containing BC showed high BPCA content. [13]
Optical (Filter Systems)	• Field deployable. • Simple and inexpensive operation. [8] • Different wavelengths to measure BC and organic carbon. [9] • Insensitivity to gas phase absorption. [8] • Non-destructive.	• Certain organic compounds may contribute to light absorption in atmospheric aerosols e.g., brown carbon. [9] • Artefacts caused by filter-aerosol interactions, and fluctuations in humidity, temperature and pressure. [8] • Corrections needed: multiple light scattering within filter, filter loading, particle scattering. [8] • Lack of calibration/corrections for certain artefacts. [8] • Relies on sample layer being thin to avoid multiple scattering effects of radiation between

		particles. These conditions are usually not met. [8] • Uncertainty 12 – 30 %. [8]
Spectroscopic Raman Spectroscopy	• Subtle difference between Raman Spectroscopy (RS) modes can provide detailed information on size and morphology of graphite crystals. [8] • Standards available for RS. [8]	• Other materials can change modes, e.g., co-emitted species. [8] • Interferences at 1500 cm^{-1} affect wavenumber integration used for BC (referred to as EC) quantification. [8] • Organic material can produce high background fluorescence. [8] • Relatively large sample quantity required for high signal to noise. This means a lot of sampling for atmospheric aerosols. [8] • High laser power can damage samples. [8] • Uncertainty ≥13 % or larger if calibration material does not match spectral features of BC (referred to as EC) [8]
CP/MAS ^{13}C NMR	• Identifies non-refractory and refractory organics	
Laser-induced incandescence	• Field and laboratory measurements	• At high laser intensities, BC particles vaporize and can undergo restructuring, which alters their optical properties and LII signals.
Thermal	• Straightforward measurement technique. [8] • Extraction with aqueous or organic solvents can reduce charring. [14]	• Soil, road dust, metals can cause the evolution of light-absorbing compounds to occur prematurely. [15] • Precision dependent on temperature of sample, location of temperature sensor in oven can affect this. [16]

		• Carbonate carbon can be allocated to either OC or BC (referred to as EC) acid pre-treatment can remove interference. [17] • No consensus on reference material to calibrate response of BC content. [17] • Charring bias can lead to overestimations in BC. [11] • Harshest thermal methods measure only soot and graphite [3] • Pollen contamination can lead to an overestimation of BC by 10 – 25 %. [3] • Brown carbon can be accounted as BC or OC. [43] • In thermal optical systems, brown carbon 'invisible' to instruments charring correction processes as brown carbon absorbs the lasers wavelength less strongly that BC. [9] • Uncertainty ±20 – 50 %. [8]

References: [1] Cornelissen et al. (2005), [2] Hammes et al. (2007), [3] Masiello (2004), [4] Masiello et al. (2002), [5] Meredith et al. (2013), [6] Knicker et al. (2007), [7] Dargie (2010), [8] Lack et al. (2014), [9] Andreae and Gelencsér (2006), [10] Kuo et al. (2008), [11] Glaser et al. (1998), [12] Brodowski et al. (2005), [13] Chang et al. (2018), [14] Novakov and Corrigan (1995), [15] Khan et al. (2012). [16] Phuah et al. (2009), [17] Karanasiou et al. (2007), [18] Meredith et al. (2012).

A technique that has not previously been explored in depth for its application for isolation of BC in aerosol studies is hydropyrolysis (hypy). However, this method has been proven as a highly advantageous approach for isolation, quantification, and characterisation of BC in other environmental matrices, such as charcoals, soils, and sediments (e.g. Ascough et al. (2009); Ascough et al. (2010); Meredith et al. (2012); Wurster et al. (2012); Wurster et al. (2013); Zhang et al. (2019a)).

It has been found that hypy leads to conversions of around 100 % of solid organic matter to DCM-soluble oil in kerogens, clays and biomass (Beramendi-Orosco et al., 2004; Love et al., 1997; Murray et al., 1998; Rocha et al., 1999) High conversions > 60 % were also found

for coal (Li et al., 1996; Snape et al., 1994). This provides evidence that hypy removes labile organic matter from refractory carbon, isolating BC.

The BC remaining after hypy (BC_{hypy}) has been shown to have an atomic H/C ratio of less than 0.5 across different sample matrices. This showed that BC_{hypy} comprises of a chemically well-defined polyaromatic structure in terms of the average size of peri-condensed aromatic clusters of >7 rings. This suggests that hypy is a matrix independent method for BC quantification (Meredith et al., 2012). It was also found that PAHs in the organic compounds removed from BC_{hypy} (referred to as non-BC_{hypy}) were no bigger than 7-rings (Meredith et al., 2013). Hypy was also found to yield reproducible BC determinations, with minimal charring and instrument artefacts (Ascough et al., 2009; Meredith et al., 2012). BC determinations using hypy were compared to reported BC values from other measurement techniques reported in Hammes et al. (2007) (Meredith et al., 2012). The results were shown to be higher compared to methods that under-estimate BC and lower than methods that tend to over-estimate BC (Meredith et al., 2012).

Hydropyrolysis therefore could prove to be a useful alternative to thermal methods for the determination of BC in filter samples. Advantages of hypy are that it is matrix-independent, reproducible, has minimal charring and less likely to have instrument artefacts.

1.3. PM Carbonaceous Constituents: Organic Carbon Aerosol

OC aerosol components can be classified as primary organic aerosol (POA) or secondary organic aerosol (SOA) (Boucher, 2015; Pöschl, 2005). POA are emitted directly from their source as liquid or solid particles in the condensed phase, or as semi-volatile vapours, which then may condense into a solid or liquid form depending on atmospheric conditions. Common sources of POA include natural and anthropogenic biomass burning, fossil fuel combustion and wind or traffic induced resuspension of soil and road dust, biological materials (plant and animal debris, pollen, spores, microorganisms etc.), and organic compounds dissolved in surface waters. In contrast, SOA is formed through gas-to-particle chemical reactions of volatile organic compounds (VOCs) in the atmosphere (Boucher, 2015; Pöschl, 2005). There are many different organic compounds within PM.

Table 1.2. Common organic PM components and their sources, adapted from (Pöschl, 2005). The article was published in Atmospheric Aerosols: Composition, Transformation, Climate and Health Effects, 44, Pöschl, U., pp. 7520 – 7540, Copyright Elsevier (2005).

Substance Classes	Sources
Aliphatic hydrocarbons	Biomass, fossil-fuel combustion
Aliphatic alcohols and carbonyls	Biomass, SOA/aging
Aliphatic dicarboxylic acids	SOA/aging
Aromatic poly-carboxylic acids	SOA/aging, soil/dust
Cellulose and other carbohydrates	Biomass
Fatty acids and other alkanoic acids	Biomass, SOA/aging
Levoglucosan	Biomass burning
Multifunctional aliphatic and aromatic compounds	SOA/aging, soil/dust
PAHs including nitro- and oxy- PAHs	Fossil fuel combustion, biomass burning and SOA/aging for nitro- and oxy- PAHs
Secondary organic oligomers/polymers and humic-like substances	SOA/aging, soil/dust

Table 1.2 shows some of the common organic PM components and their sources. Identification and quantification of organic carbonaceous compounds within PM usually includes extraction of aerosol samples collected on filters, to draw these compounds into solution, using appropriate solvents. The extracts are then analysed by techniques that can separate and detect components (Pöschl, 2005).

Polycyclic aromatic hydrocarbons are a component of OC in PM (Pöschl, 2005). They are a group of chemically related compounds, with varying structures, which are persistent within the environment (Dat & Chang, 2017). PAHs have petrogenic origins such as crude and refined petroleum and pyrogenic origins from the combustion of fuels such as fossil fuels and biomass. PAHs can also be emitted from natural sources such as forest fires, diagenesis, volcanic eruptions (Dat & Chang, 2017; Zakaria et al., 2002). In the atmosphere, PAHs exist in both gas and solid/particulate phase. Low molecular weight (LMW) PAHs (2- to 3- ring) have higher vapour pressures and are dominant in gas phase, moderate molecular weight (MMW) PAHs are distributed in both gas and particulate phases, whilst high molecular weight (HMW) PAHs (5- to 6- ring) have low vapour pressures so are dominant in the particulate phase (Dat & Chang, 2017). Most HMW PAHs are considered to be human carcinogens, for example benzo(a)pyrene (BaP) (Dat & Chang, 2017; Ravindra et al., 2008a; USEPA, 1993). PAHs are also considered to have mutagenic potential and are hence a potent

source of human disease due to their ability to induce genetic instability, and therefore accelerate the evolution of human cancers or lead to the development of genetically inherited diseases (Gordon et al., 2009; Gout et al., 2017; Saxowsky et al., 2008; Van Leeuwen, De Kleijn, et al., 1998; Van Leeuwen, Hol, et al., 1998; Vermulst et al., 2015). A study found that the total concentration of carcinogenic PAHs in PM correlated positively with mutagenicity of PM as well as induction of DNA adducts and oxidative DNA damage (de Kok et al., 2005). Furthermore, mutagens also contribute to transcription errors, which arise in dividing and non-dividing cells, affecting every class of transcripts inside cells. Such errors can alter fate of cells, initiate oncogenic programs, deregulate metabolism, cause protein misfolding or shorten cellular lifespan. Additionally, transcription errors were shown to generate the toxic proteins found in nonfamilial cases of Alzheimer's disease (Gordon et al., 2009; Gout et al., 2017; Saxowsky et al., 2008; Van Leeuwen et al., 1998a; Van Leeuwen et al., 1998b; Vermulst et al., 2015). Fritsch et al. (2020) found that DNA repair is required to mitigate against transcriptional mutagenesis after exposure. It was stated that without such repair, DNA damage would continue to induce transcription errors over time. Results suggested that DNA damage can directly contribute to the loss of proteostasis seen in aging cells, a key component of the etiology of numerous age-related diseases, including Alzheimer's disease and Parkinson's disease (Fritsch et al., 2020).

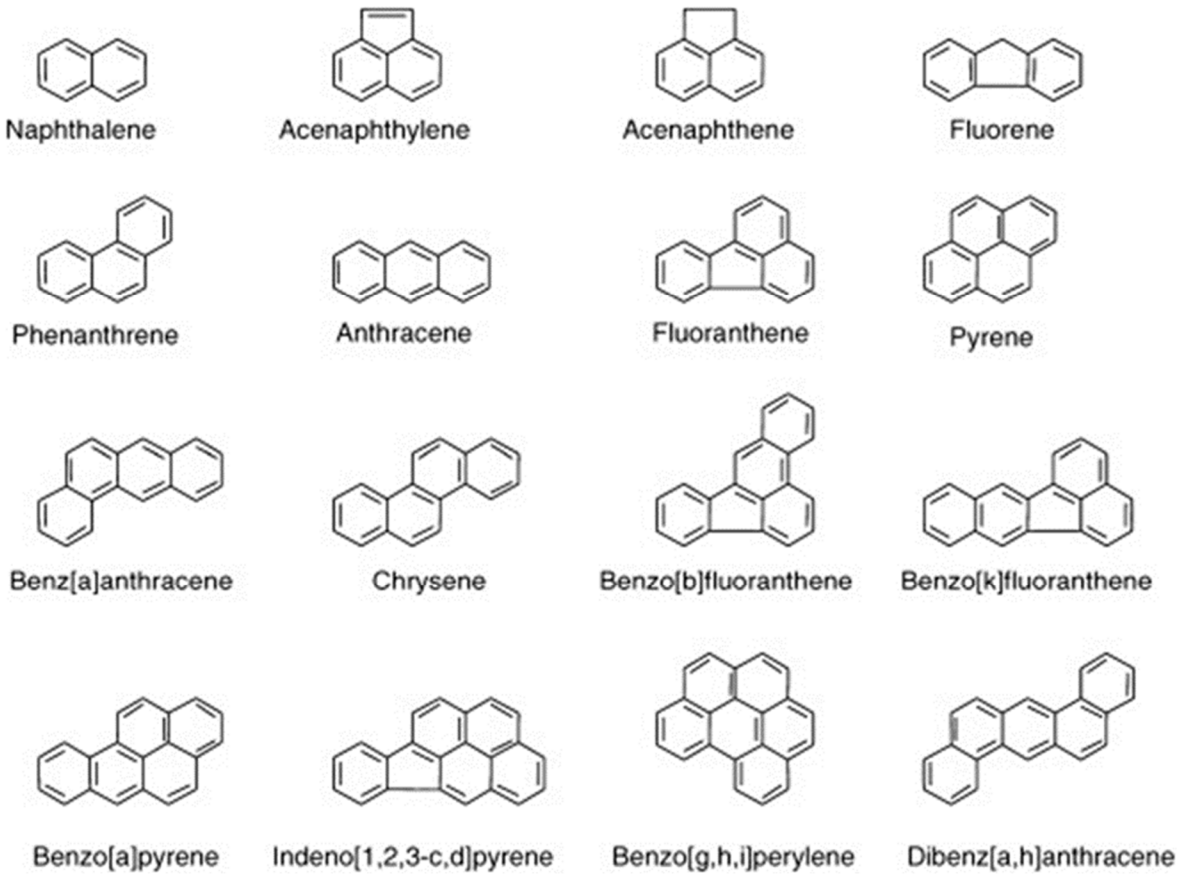

Figure 1.3. The molecular structure of the 16 PAHs considered priority pollutants by the United States Environmental Protection Agency (US EPA) reprinted from Microbial Biodegradation and Bioremediation, edition 1, Sudhir et al., Biofilm-Mediated Bioremediation of Polycyclic Aromatic Hydrocarbons, 203-232, Copyright (2014), with permission from Elsevier.

Given the information above there is considerable interest in identifying the sources of PAH pollutants. Identification of sources is important if policy decisions are to target the correct areas for mitigation and ultimately be effective. PAH emission profiles can give insight to their sources, for example low temperature processes such as wood burning usually emit LMW PAHs whilst high temperature processes such as fuel combustion in vehicle engines emit HMW PAHs (Mostert et al., 2010; Tobiszewski & Namieśnik, 2012). The high temperatures crack other present organic compounds into reactive radicals. These form stable PAHs, that have a lower degree of alkylation and higher degree of aromaticity than petrogenic PAHs (Hwang et al., 2003; Tobiszewski & Namieśnik, 2012). PAH diagnostic ratios have been used frequently in the literature to distinguish between PAH emission

sources, particularly petrogenic versus pyrogenic sources, in airborne ambient PM (Callén et al., 2011; Oliveira et al., 2011; Ravindra et al., 2008b). n-Alkanes are also used as source indicators in airborne ambient PM as they are relatively non-reactive (Caumo et al., 2020; Cincinelli et al., 2003; Flores et al., 2022; Harrison & Yin, 2010). n-Alkanes have anthropogenic sources (combustion of fossil fuels, biomass) as well as natural sources (epicuticular waxes, pollen and micro-organisms) (Yassaa et al., 2001).

Chromatographic techniques play an important role in the analysis of air pollutants. There are different chromatographic techniques used to analyse PAHs in airborne ambient PM such as thin-layer chromatography (TLC), gel-permeation chromatography (GPC), high-performance liquid chromatography and gas chromatography combined with different techniques or detectors such mass spectrometry, flame ionisation detectors or UV. GC-MS is a widely used technique due to its strengths in qualitative and quantitative assessments of PAHs (Li-bin et al., 2007).

GC-MS combines two microanalytical techniques as demonstrated in Figure 1.4. Gas chromatography enables the separation of components in a mixture in time, whilst the mass spectrometer uses ionisation techniques for qualitative and quantitative determinations as it creates a mass spectrum for each analyte component as it elutes from the column (Houck & Siegel, 2010b; Sparkman et al., 2011). The volatility of the analytes works particularly well with the mass spectrometer which requires gas-phase analytes. Selected ion monitoring (SIM) mode can lower the limits of detection, through the use of three-ion ratios for unambiguous identification (Sparkman et al., 2011).

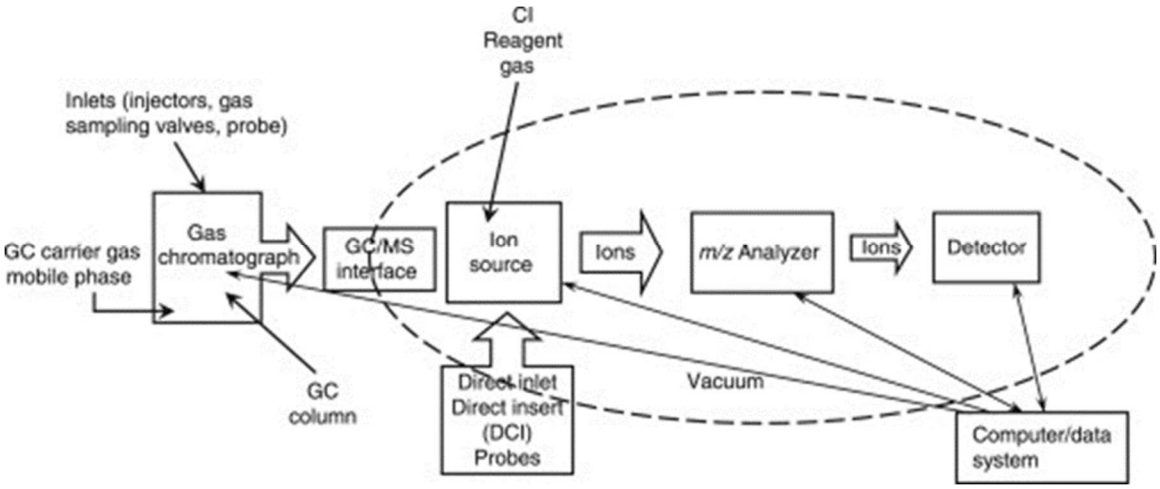

Figure 1.4. Schematic of a GC-MS reprinted from Gas Chromatography and Mass Spectrometry, Edition 2, Sparkman et al., Introduction and History, 2-13, Copyright (2011), with permission from Elsevier.

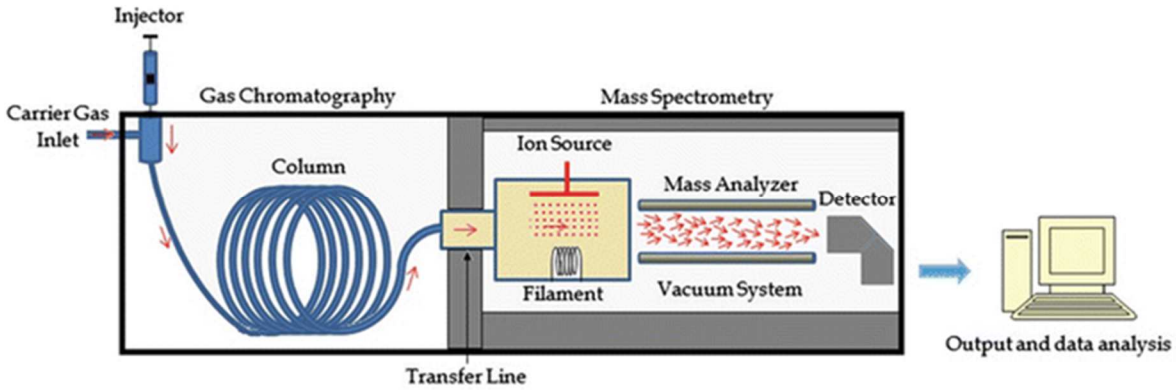

Figure 1.5. Visual representation of a GC-MS reprinted from Methods in Molecular Biology, Emwas et al., Gas Chromatography–Mass Spectrometry of Biofluids and Extracts, Metabonomics, volume 1277, Copyright (2015), reproduced with permission from Springer Nature.

Once the sample mixture is injected (see Figure 1.5) the gas chromatograph uses capillary columns, known as the stationary phase, which can be polar or non-polar, and rely on the interaction of the stationary phase with the substances within the mixture, known as the mobile phase. The weaker the retention, the quicker the elution from the column, and vice

versa. Variables such as column stationary phase, column length, internal diameter and film thickness can affect resolution (Hübschmann, 2009).

The mass spectrometer has an ionisation source which ionises each substance as it elutes, in the ionisation chamber, commonly by bombardment of electrons (see Figure 1.5). The ionised substance, known as the parent ion, can then break down into smaller ions, decomposing or reacting with other energetic species to form new daughter ions. With constant conditions, the fragmentation pattern formed by a substance will be highly reproducible. In the magnetic sector, the ions are accelerated through a curved magnetic field, moving towards the detector with smaller ions being deflected to a greater extent. The current is amplified, and then detected (Houck & Siegel, 2010a).

For n-alkanes, a flame ionisation detector can be used. It works by burning the substances in a sample in a hydrogen flame, causing the substances to lose an electron and become ionised, whilst the mobile phase carrier gas will not be affected. An electric current is made from the electrons during ionisation, and the current is amplified and detected, with the magnitude of the current being proportional to the amount of a substance present (Houck & Siegel, 2010b).

1.4. Source Apportionment of Carbonaceous Components of PM

Source apportionment of air pollutants is crucial for air quality management as it enables the identification of emission sources contributing to air concentrations of one or more pollutants (Briggs & Long, 2016). As BC may be a better indicator for health effects than PM (as discussed in Section 1.2.), source apportionment of BC could help inform policymakers with regards to appropriate mitigation methods to reduce potential health risks associated with inhalation of PM. There are two approaches for source apportionment: bottom-up methods (emission inventories and air dispersion modelling) or top-down methods (receptor models) but bottom-up methods often have uncertainties, as reported by Monks et al. (2009) who found emission inventories had uncertainties up to factors of 3.4 and 80 for primary and secondary carbonaceous particles (Briggs & Long, 2016; Monks et al., 2009).

Table 1.3 shows the advantages and disadvantages of top-down methods when used to determine sources of BC. It should be noted these methods can be used to determine sources of PM as well as solely BC. As highlighted in Table 1.3, there is no gold standard for source apportionment of different carbonaceous components of aerosols, thus combinations of different approaches can be useful (Briggs & Long, 2016). However, the use of ^{14}C measurements for source apportionment of BC can be particularly useful. The long half-life of ^{14}C (5730 years) means that the $^{14}C/^{12}C$ ratios do not change significantly over the time of emission from the source to collection of the sample. ^{14}C is a sensitive method, allowing for small differences in the proportion of fossil versus modern biomass sources to be identified (Belis et al., 2014; Schuur et al., 2016). Sources are divided into broad groups fossil and modern. A disadvantage of this is that it cannot differentiate between natural biogenic sources (biogenic SOA) and biomass combustion (natural and anthropogenic). However, when ^{14}C measurements are applied to BC (a combustion product), source apportionment can give better indications with regards to anthropogenic sources. Ascough et al. (2009) found that ^{14}C analysis of BC_{hypy} removed organic contaminants that caused different ^{14}C ages leading to highly reproducible ^{14}C ages. This showed that ^{14}C measurements on BC_{hypy} can be used to derive the fossil versus biomass combustion proportions.

The basis of the ^{14}C method is the measurement of the radioactive carbon isotope, ^{14}C which is formed by the interaction of cosmic particles with ^{14}N in the Earth's atmosphere. After formation, ^{14}C is rapidly oxidised to $^{14}CO_2$ and is cycled in the Earth and its environmental

systems as ^{14}C in a vast range of compounds, in living material (plants, animals, microbes), in equilibrium with CO_2 in the atmosphere (Heaton et al., 2021; Schuur et al., 2016). Once the living material dies or undergoes its final formation, the material becomes a closed system with regards to ^{14}C, as no new ^{14}C can be incorporated, but existing ^{14}C undergoes radioactive decay leading to a decrease in the $^{14}C/^{12}C$ ratio with time (Schuur et al., 2016; Wood, 2015). The half-life of ^{14}C is 5370 years, and after approximately 9 half-lives (c.50,000 years) the amount of ^{14}C in a material becomes indistinguishable from background ^{14}C levels, with modern techniques (Bronk Ramsey, 2008; Schuur et al., 2016). Materials with levels of ^{14}C that are indistinguishable from laboratory measurement background are referred to as '^{14}C-dead' such as fossil fuels and geological age carbon. However, samples with abundant ^{14}C (i.e. $^{14}C/^{12}C$ ratios of 1.0 and above, relative to the international standard, Oxalic Acid II), are referred to as 'modern carbon', have carbon that has been recently fixed from the atmosphere (Heal et al., 2011; Schuur et al., 2016). The two categories are extremely distinct making the technique appropriate for source apportionment. Several studies have utilised ^{14}C for source apportionment of BC, but BC and OC separation is required before ^{14}C analysis. Thermal methods are commonly used, and they operationally define BC, so are prone to artefacts (see Section 1.2.2) (Andersson et al., 2011; Bernardoni et al., 2013; Heal et al., 2011; Szidat et al., 2004b; Zenker et al., 2017).

Table 1.3. Advantages and disadvantages of source apportionment methods for BC. This table was reprinted and adapted, with permission from Elsevier, from Critical review of black carbon and elemental carbon source apportionment in Europe and the United States, Briggs and Long, Atmospheric Environment, 144, pp. 409-427, Copyright 2016.

Method	Strengths	Weaknesses
Aethalometer method Measures BC and OC through light-absorbing properties, with set wavelengths for each category.	• Attributes all BC source categories. • Does not require supplemental data sources.	• Can only identify two source categories: fossil fuels and biomass burning. • Requires assumptions for parameter values (Angstrom exponents).
Chemical Mass Balance A multivariate model that uses a least squares solution to a set of linear equations, with data comprising of organic molecular tracers in source profiles for example levoglucosan for biomass burning.	• Attributes all BC source categories. • Can distinguish between all source categories.	• May not identify all sources of BC. • Requires emission profiles for all sources considered by model. • Requires multiple data sources beyond BC or EC measurements.
Macro-tracer Method Using a set of linear equations, to describe the relationship between key tracers such as levoglucosan, OC and BC.	• Attributes all BC to source categories. • Requires few data sources (i.e., only a few key species).	• Can only identify two source categories: fossil fuels and biomass burning. • Requires assumptions for parameter values (e.g., average emission factors).
Positive Matrix Factorisation (Multivariate Model)	• Can attribute BC to many source categories. • Can attribute BC to source categories that are not well characterized.	• May not distinguish between BC contributions from two or more sources. • May not attribute all BC to source categories (may have residual BC). • Requires multiple data sources beyond BC or EC measurements.
Principal Component Analysis Converts a set of observations of possibly correlated variables into a value of linearly uncorrelated variables, named principal components. The results are then interpreted by the modeler.	• Can attribute BC to many source categories. • Can attribute BC to source categories that are not well characterized.	• Principal components can reflect a mixture of sources but are often interpreted as independent sources. • May not attribute all BC to source categories (may have residual BC). • Requires multiple data sources beyond BC or EC measurements.

Radiocarbon Method Ratio of $^{14}C/^{12}C$ in a sample compared to $^{14}C/^{12}C$ in reference year of 1950.	• Attributes all BC to source categories. • Does not require supplemental data sources.	• Can only identify two source categories: fossil fuels and biomass burning.
Specialised models A range of models developed specifically for source apportionment such as Community Multi-Scale Air Quality (CMAQ) Model.	• Can attribute BC to many source categories. • Can attribute BC to source categories that are not well characterized.	• May not identify all sources of BC. • May not attribute all BC to source categories (may have residual BC). • Requires multiple data sources beyond BC or EC measurements such as accurate emission inventories.

1.5. Project Aims and Thesis Outline

To summarise BC and PM can have detrimental effects on the environment and human health. Glasgow currently has two AQMAs hence it is important to understand the spatiotemporal variation of BC for air quality management purposes. The health risks of inhalation of PM should also be understood and quantified in determined hotspots. As current BC measurement techniques exhibit positive and negative artefacts, a novel methodology, hypy, will be developed so that it can be used to determine BC in airborne ambient PM. The sources of BC_{hypy} will also be determined.

The aims of this thesis were:

1. To determine the abundance of BC in Glasgow and the spatiotemporal trends exhibited by BC in an urban area, Glasgow. Chapter 2 used portable BC monitors to determine areas of high BC pollution and gain an understanding of the spatiotemporal variation of BC increments and concentrations in Glasgow.
2. To understand the health risks associated with carbonaceous component of PM, through analysis of PAHs, in the identified hotspot in Glasgow.
   Chapter 3 analysed PM_{10} and $PM_{2.5}$ samples in the BC hotspot area determined in Chapter 2, as well as another site within the UK.
3. To gain an understanding of the variation in BC content amongst different sources of airborne ambient aerosols using novel methodology hydropyrolysis. Chapter 4 demonstrates the use of hypy to determine the BC/TC% of different standards that were used to represent different sources of airborne ambient aerosols.
4. Build an understanding of the sources of carbonaceous components within PM and test a novel method for separation of BC + OC, prior to ^{14}C analysis. Chapter 5 uses ^{14}C to analyse proportions of fossil and modern carbon at sites across the UK. The hypy methodology is developed for airborne ambient PM using a range of standards and is then tested on airborne ambient PM samples. Chapter 3 determines the sources of OC components of PM; PAHs and n-alkanes.

2. The Abundance and Spatiotemporal Variability of Black Carbon in Glasgow

2.1. Introduction

Air pollution is a global issue, particularly in densely populated regions, where human health effects of air pollutants are most concentrated. As mentioned in Section 1.2.1, BC is an air pollutant that is major constituent of fine particulate matter ($PM_{2.5}$) (AQEG, 2005, 2012). Black carbon is a substance with a highly polyaromatic chemical composition; it is formed from incomplete combustion of carbonaceous fuels in residential heating and cooking, transportation, power generation and other industrial processes (Petzold et al., 2013). Research strongly suggests that BC is detrimental to health as BC particles are small enough to penetrate deep into the lungs, and to pass into the circulatory system. Black carbon may be a stronger marker for respiratory and cardiovascular morbidity and mortality than $PM_{2.5}$ (Grahame et al., 2014; Janssen et al., 2011; Luben et al., 2017). Furthermore, BC is a short-lived climate forcer whose emissions exacerbate climate warming effects through diminishing snow albedo and changing cloud properties (WMO/UNEP, 2011). Consequently, there are considerable 'win-wins' for mitigation of both air pollution and climate forcing effects in reducing BC emissions (IPCC, 2018; UNEP, 2011).

Despite the negative impacts of BC on health and the environment it is currently not a regulatory requirement anywhere to monitor BC concentrations. Consequently, there are no international or national guideline or limit values for BC, rendering it difficult to determine if BC concentrations are unacceptably 'high' or acceptably 'low' for issues such as public health or environmental quality. However, BC is measured at 13 sites across the UK, in the UK Black Carbon Network (https://uk-air.defra.gov.uk/networks/network-info?view=ukbsn). The UK BC Network sites in Glasgow are Glasgow Townhead and Glasgow High Street. These two sites provide valuable data on long-term trends of BC in the city, however, clearly two static sites cannot provide comprehensive information on the spatial variation in BC abundance within a city, which is needed to improve understanding and estimations of personal exposure to BC, the latter being required for epidemiological and health burden evaluations of BC.

Air pollution monitoring is moving away from the sole use of stationary sites to a combination of fixed and mobile monitoring and modelling, driven by the increased

availability of portable, battery-operated instruments (Kuhlbusch et al., 2014; Snyder et al., 2013; Steinle et al., 2013). These instruments can be used in mobile and peripatetic (short periods of deployments at multiple sites) measurement designs (e.g. (Delgado-Saborit, 2012; Dons et al., 2013; Gillespie et al., 2017; Wu et al., 2015).

The portable monitor mostly commonly used to quantify BC is the microAethalometer (AethLabs, San Francisco, CA, USA). However, despite the increasing number of studies reporting measurements with this instrument, data for spatiotemporal variability of BC in UK cities remains sparse. The aim of this study was to:

1. Examine spatiotemporal BC trends within an urban area, Glasgow, across four different electoral wards to increase spatial representativeness of BC measurements.
2. Assess the effectiveness of different monitoring methods (mobile versus fixed) for capturing an accurate picture of BC. The findings are used to make recommendations on future monitoring within Glasgow.
3. Form and test hypotheses using socioeconomic data, about which electoral wards will be BC hotspots to understand factors that may influence BC pollution levels. These factors can then be used to formulate sampling plans for future BC monitoring campaigns.

2.2. Experimental Methodology

2.2.1. Study Area

The rationale for this research was to investigate the spatiotemporal variations of air pollution (as characterised by BC) within a typical large city, since cities contain a large number of individuals travelling to and from places of residence, work/education and recreation, who are exposed to air quality while so doing. Such activities are defined here as socioeconomic activity.

Glasgow is the most populous city in Scotland. The city itself has a population of ~600,000, but the greater Glasgow urban area has a population at least double this dependent on the extent of contiguous urban areas included. The city is divided into 23 electoral wards (see Figure 2.1). To select suitable sampling sites for the research, geographic information systems (QGIS) were used to identify wards that represent potential areas that could be BC hotspots. Spatial data such as ward populations, schools and shopping centres were added to GIS maps as seen in Figure 2.1 and Figure 2.2. The population data was taken from Glasgow City Council website, which contained 2015 data on populations per ward. The population density of each ward was calculated to distinguish wards with higher population densities as research has shown increases in population density led to increases in air pollutant concentrations (Borck & Schrauth, 2021; Carozzi & Roth, 2023). This could be due to higher traffic densities and a greater degree of urbanisation. The number of educational institutions and shopping centres were used as proxies for socioeconomic activity, i.e., intraurban mobility. The educational institutions count included nursery, primary, secondary, further, and higher educational facilities. The educational institution counts consist predominantly of primary and secondary schools; hence this was used as determinant as children are more vulnerable to air pollution.

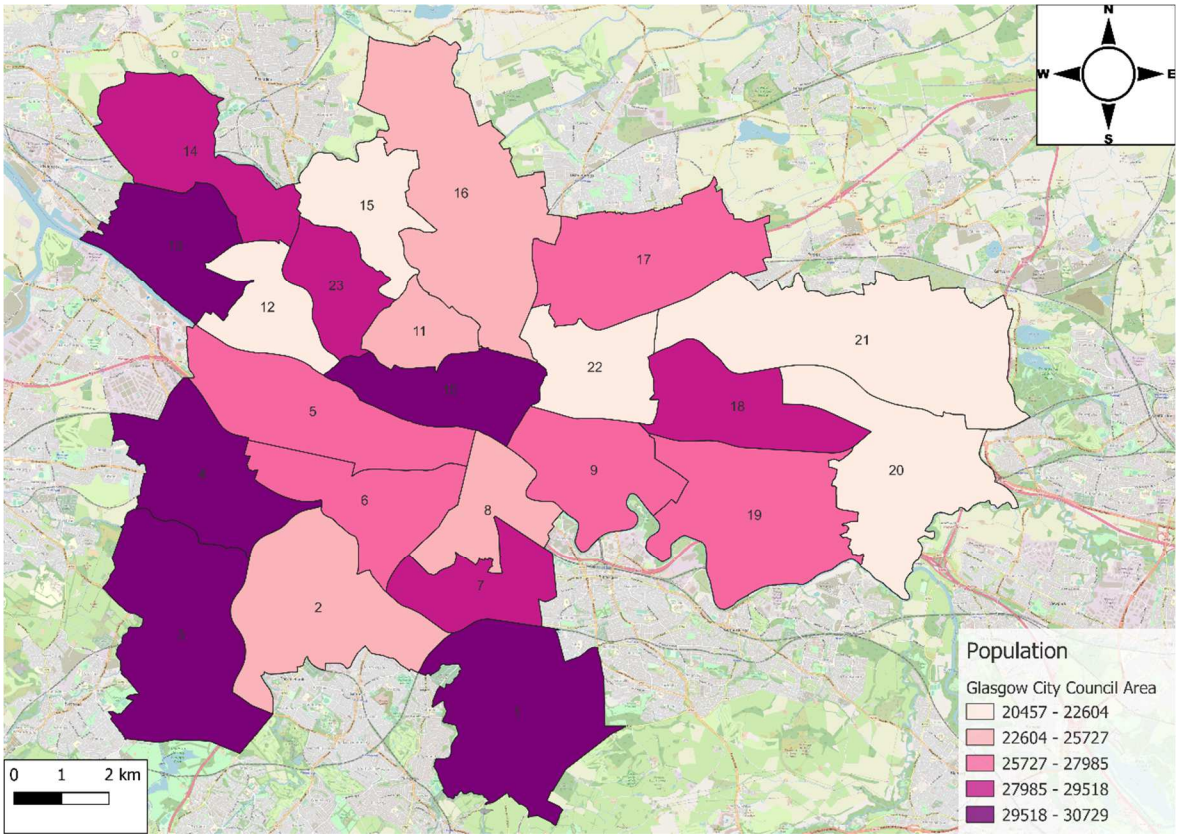

Figure 2.1. Glasgow ward populations (2015 data). Ward names are: 1) Linn, 2) Newlands/Auldburn, 3) Greater Pollok, 4) Cardonald, 5) Govan, 6) Pollokshields, 7) Langside, 8) Southside Central, 9) Calton, 10) Anderston/City/Yorkhill, 11) Hillhead, 12) Victoria Park, 13) Garscadden/Scotstounhill, 14) Drumchapel/Anniesland, 15) Maryhill, 16) Canal, 17) Springburn/Robroyston, 18) East Centre, 19) Shettleston, 20) Baillieston, 21) North East, 22) Dennistoun, 23) Partick East/Kelvindale. The map layer used was Open Street Map.

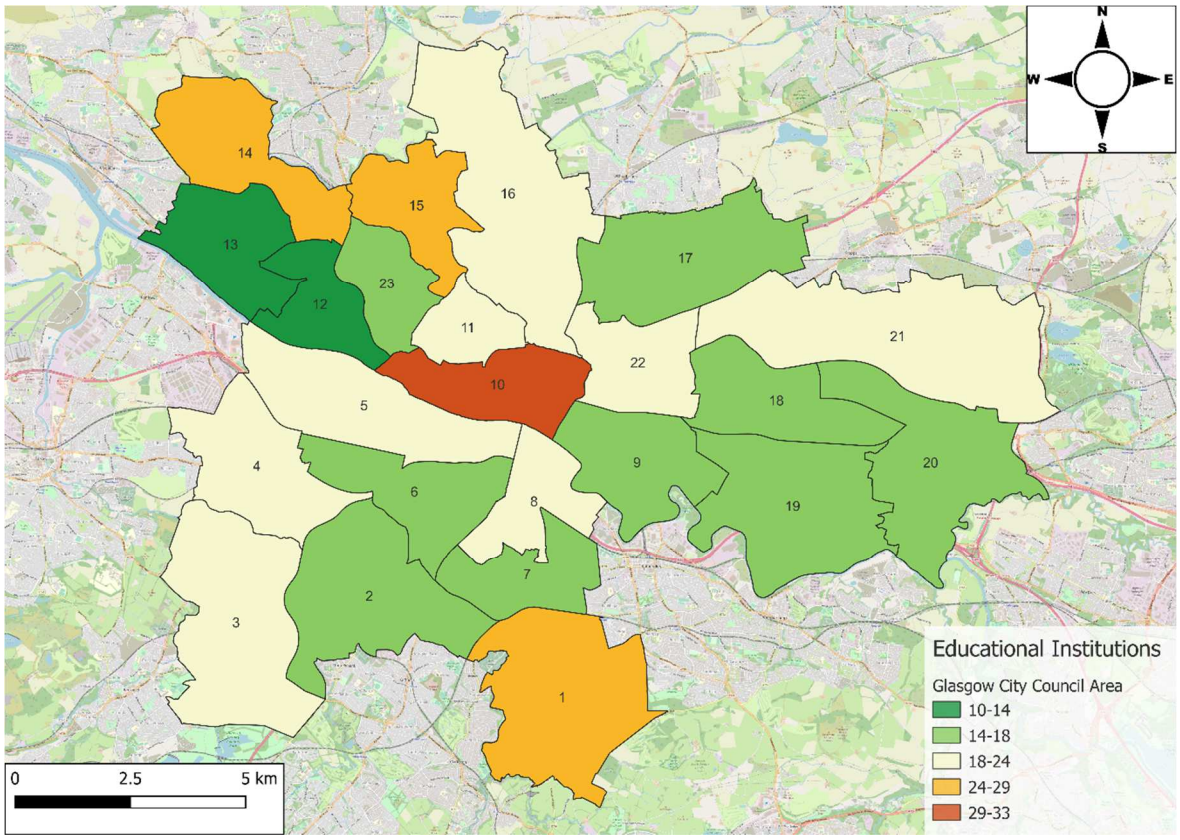

Figure 2.2. Number of educational institutions within the 23 wards of Glasgow. Ward names are: 1) Linn, 2) Newlands/Auldburn, 3) Greater Pollok, 4) Cardonald, 5) Govan, 6) Pollokshields, 7) Langside, 8) Southside Central, 9) Calton, 10) Anderston/City/Yorkhill, 11) Hillhead, 12) Victoria Park, 13) Garscadden/Scotstounhill, 14) Drumchapel/Anniesland, 15) Maryhill, 16) Canal, 17) Springburn/Robroyston, 18) East Centre, 19) Shettleston, 20) Baillieston, 21) North East, 22) Dennistoun, 23) Partick East/Kelvindale. The map layer used was Open Street Map.

Spatial queries were used in QGIS to determine potential areas in Glasgow exhibiting low, medium and high BC concentrations through the use of population data and educational facility counts. The results are summarised in Table 2.1. From this analysis, the following four wards were chosen to represent the anticipated range in BC abundance across Glasgow: Anderston/City/Yorkhill (referred to as city from here on), Hillhead, Partick East/Kelvindale (referred to as Partick ward from here on) and Baillieston. The city ward is the central hub of Glasgow in terms of transport connections and recreational facilities such as restaurants, bars and cinemas. As a result, this ward was likely to have high BC concentrations. Partick and Hillhead were selected as wards with potentially intermediate BC concentrations as both wards have recreational facilities such as restaurants and pubs. Hillhead is also home to the University of Glasgow, thus large numbers of students and staff will be travelling to campus.

However, Partick had a higher population and educational institution counts therefore is likely to have higher BC concentrations than Hillhead. Baillieston ward is a residential area with no shopping centres, and lower number of educational institutions and a lower population, and therefore potentially has lower BC concentrations than the other wards.

Table 2.1. Summary of Glasgow wards satisfying criteria for different combinations of high, intermediate, and low population and socio-economic facilities.

Characteristics	Attribute Query	Result
High socioeconomic activity and population	Population >= 29518 AND Educational institution counts >= 29 AND Population density >= 53.4	City
Intermediate socioeconomic activity and population	Population >= 27985 AND Educational institution counts >= 14 AND Population density >= 53.4	City and Partick
	Population >= 22604 AND Educational institution counts >= 14 AND Population density >= 53.4	City, Partick, Langside, Hillhead
Low socioeconomic activity and population	Population >= 22604 AND Educational institution counts >= 14 AND Population density >= 25.4	Baillieston and North East

2.2.2. Sampling Strategy for BC Measurements

Mobile and fixed measurements of BC were undertaken in the four Glasgow wards intermittently between 09 Jul 2019 and 29 Aug 2019, with one ward being visited on a given day of measurement (see Figure 2.3). To determine when sampling should take place, to capture times when BC concentrations peak, using the openair R package a time variation plot was produced for Glasgow Townhead AURN site (urban background site) and Glasgow High Street (urban traffic site), using 2017 and 2018 data (see Figure 2.4). The plots showed peak BC concentrations at 9:00 at Glasgow Townhead whereas Glasgow High Street showed a peak at 8:00. Based on this data mobile and fixed measurements were undertaken during rush hour 08:00 – 09:00, and during a mid-morning period (10:30 – 11:30) with lower BC concentrations.

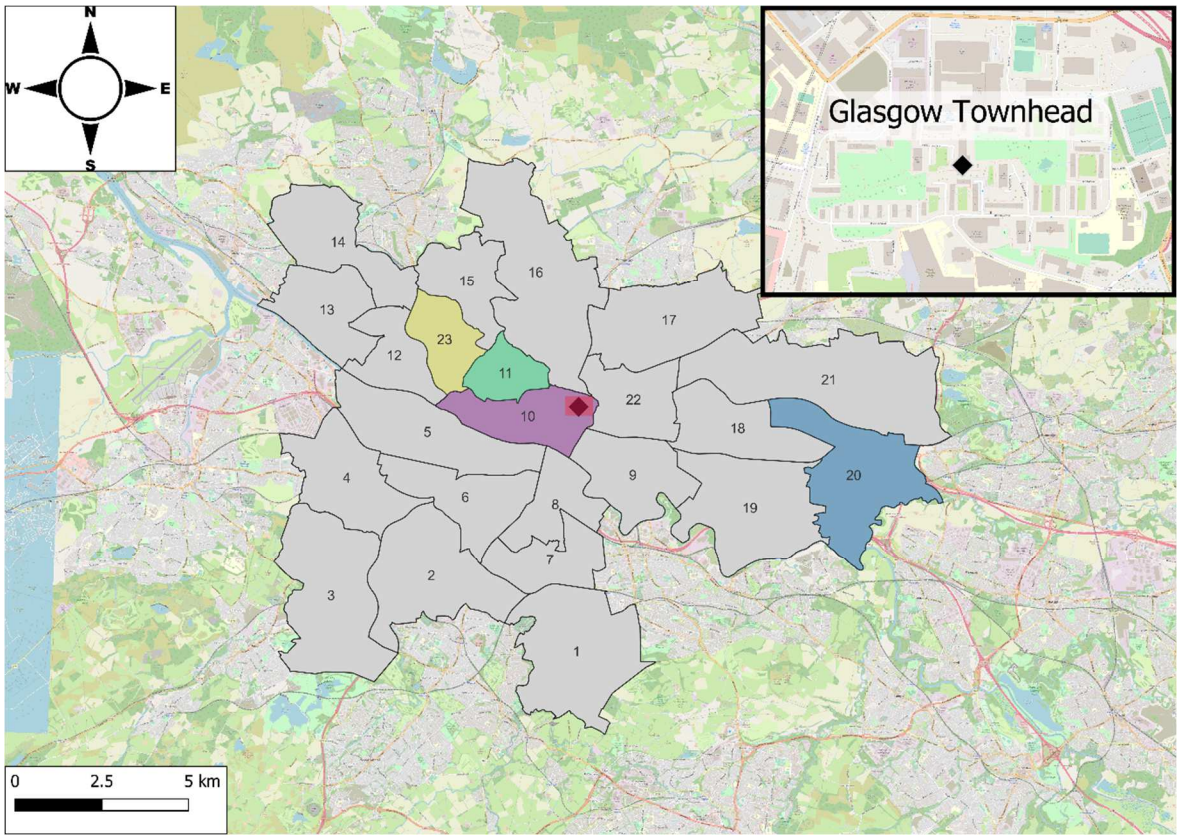

Figure 2.3. BC measurements were taken from the 4 wards in the figure. The purple shows the City ward, the green Hillhead ward, the yellow Partick ward, and the blue Baillieston ward. Glasgow Townhead, urban background site, is shown in the figure. The map layer used was Open Street Map.

Concentrations of BC were measured using two AE51 microAeth aethalometers (Aethlabs, San Francisco, CA). The microAeth designated microAeth 1 was used for the measurements in the four wards. The instrument designated microAeth 2 was permanently deployed at the Glasgow Townhead site shown in Figure 2.3. Measurements from this instrument were used to provide a means of normalisation of the data from microAeth 1 to take account of fluctuations in urban background levels of BC caused by variations in meteorology.

In each ward, there was one fixed site and four 'mobile' sites. The names of the fixed and mobile locations are given in Table 2.2 and maps of the sampling wards and locations in each ward are shown in Figure 2.5, Figure 2.6, Figure 2.7 and Figure 2.8. The 'mobile' sites were locations at which the researcher carrying microAeth 1 transiently paused for 11 minutes during the rush-hour and mid-morning sampling periods. These locations were generally close to bus stops and encompassed two busy roads and two quieter roads within that ward. The first minute of the time spent at each location was to allow for stabilisation

of the microAeth. Only the subsequent 10 minutes were used to collect the BC measurements. Each set of fixed and mobile measurements in each ward was replicated on four days.

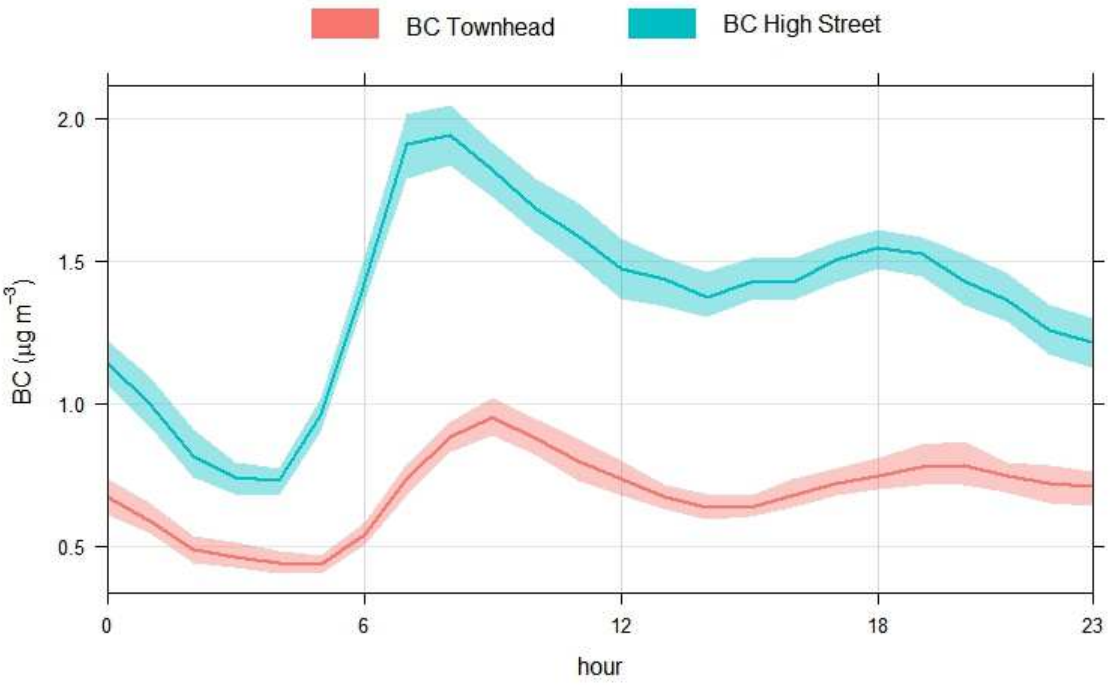

Figure 2.4. Time plot for Glasgow High Street (blue) and Glasgow Townhead (red) BC concentrations from 2017-2018.

For the fixed measurements, microAeth 1 was kept within a locked cage, in a waterproof box through which the sampling inlet passed. Fixed measurements were not possible in Baillieston because of lack of a secure location to house the microAeth. For the mobile measurements, microAeth 1 was carried in a backpack with the manufacturer-supplied 1 m conductive plastic tubing inlet mounted on the shoulder strap, around breathing level height.

MicroAeth 2 was stationed at Glasgow Townhead urban background site (shown in Figure 2.3.) and was housed in a waterproof box locked within a Peli™ case on the roof of the monitoring station. It was connected to mains electricity.

MicroAeths 1 and 2 were set to record data at 10 s and 30 s resolution, respectively. The flow rates were set at 100 mL min^{-1} during the first week of sampling but due to instances of negative BC concentrations were subsequently increased to 150 mL min^{-1}. To avoid overloading the filter strips, the microAeth filter strips were changed regularly to avoid ATN values exceeding 75 (although on four occurrences ATN did exceed 75).

Table 2.2. Details of the sampling strategy listing the mobile and fixed sites within the four wards of Glasgow, where BC measurements were taken.

Wards				
	Baillieston	**City**	**Hillhead**	**Partick**
Fixed Measurements Site	N/A	George Street	University Avenue	Dumbarton Road
Mobile Measurements Sites	1. Glasgow Rd. 2. Weirwood Av. 3. Barachnie Rd. 4. Springhill Av.	1. George St. 2. Cochrane St. 3. Ingram St. 4. Union St.	1.Great Western Rd. 2. Eldon St. 3. Kelvin Way 4. University Av.	1. Dumbarton Rd. 2. Hyndland St. 3. Highburgh Rd. 4. Byres Rd.
Replicates	Mobile – 4 N/A	Mobile – 4 Fixed – 4	Mobile – 4 Fixed – 4	Mobile – 4 Fixed – 4
Sampling times	Morning 08:00 – 09:00 Mid-morning 10:30 – 11:30	Morning 08:00 – 09:00 Mid-morning 10:30 – 11:30	Morning 08:00 – 09:00 Mid-morning 10:30 – 11:30	Morning 08:00 – 09:00 Mid-morning 10:30 – 11:30

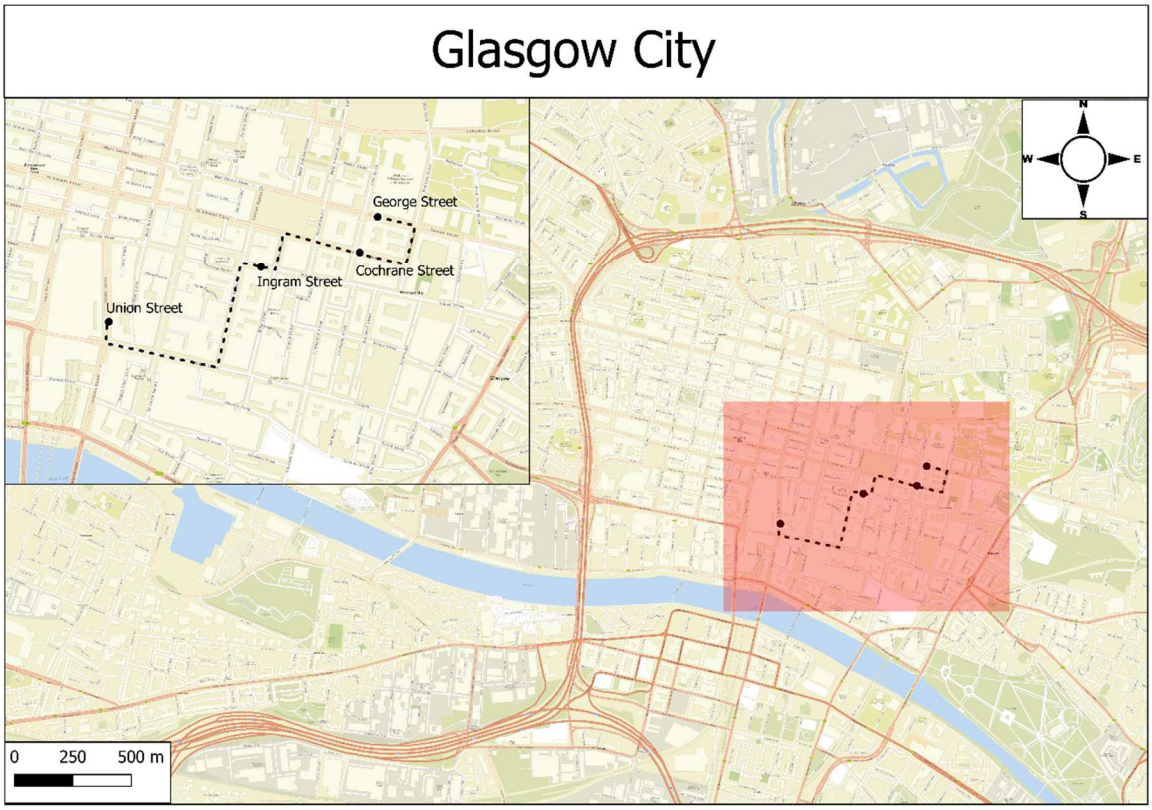

Figure 2.5. City ward sampling stops. George Street was used for fixed monitoring. The map layer used was provided by Esri (Esri standard map).

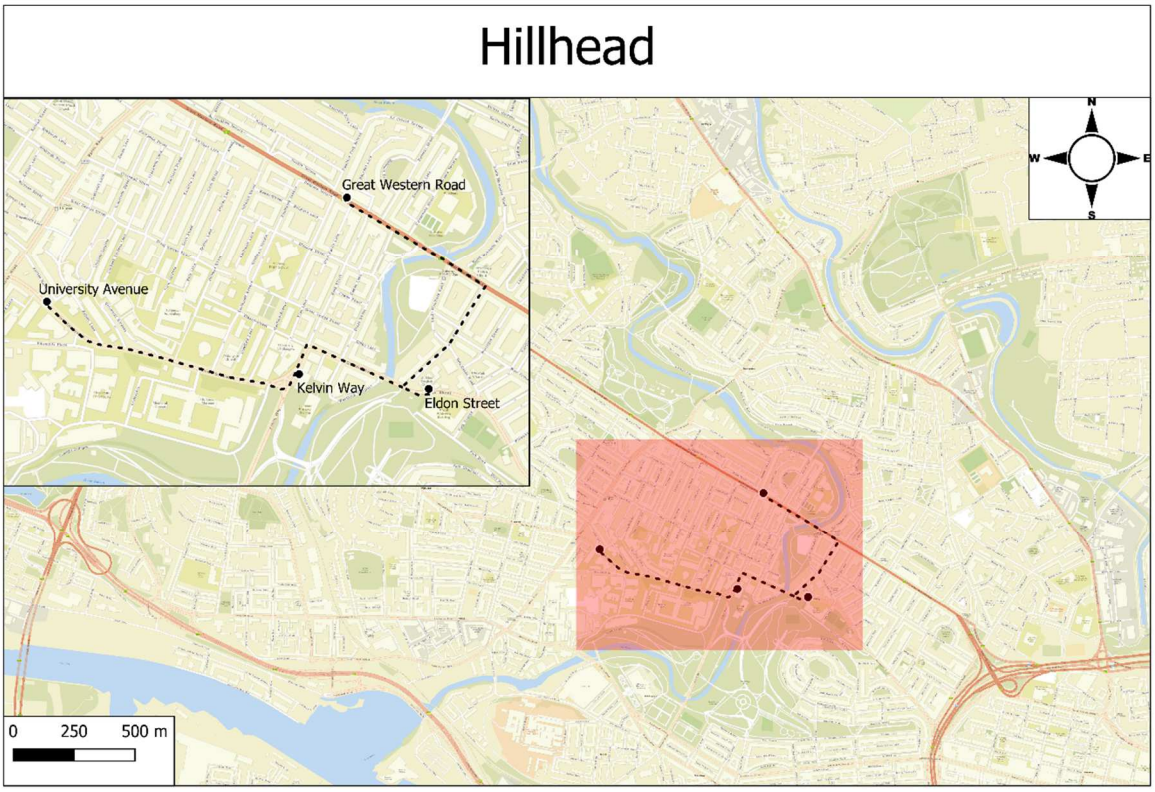

Figure 2.6. Hillhead ward sampling stops. University Avenue stop was used for fixed monitoring. The map layer used was provided by Esri (Esri standard map).

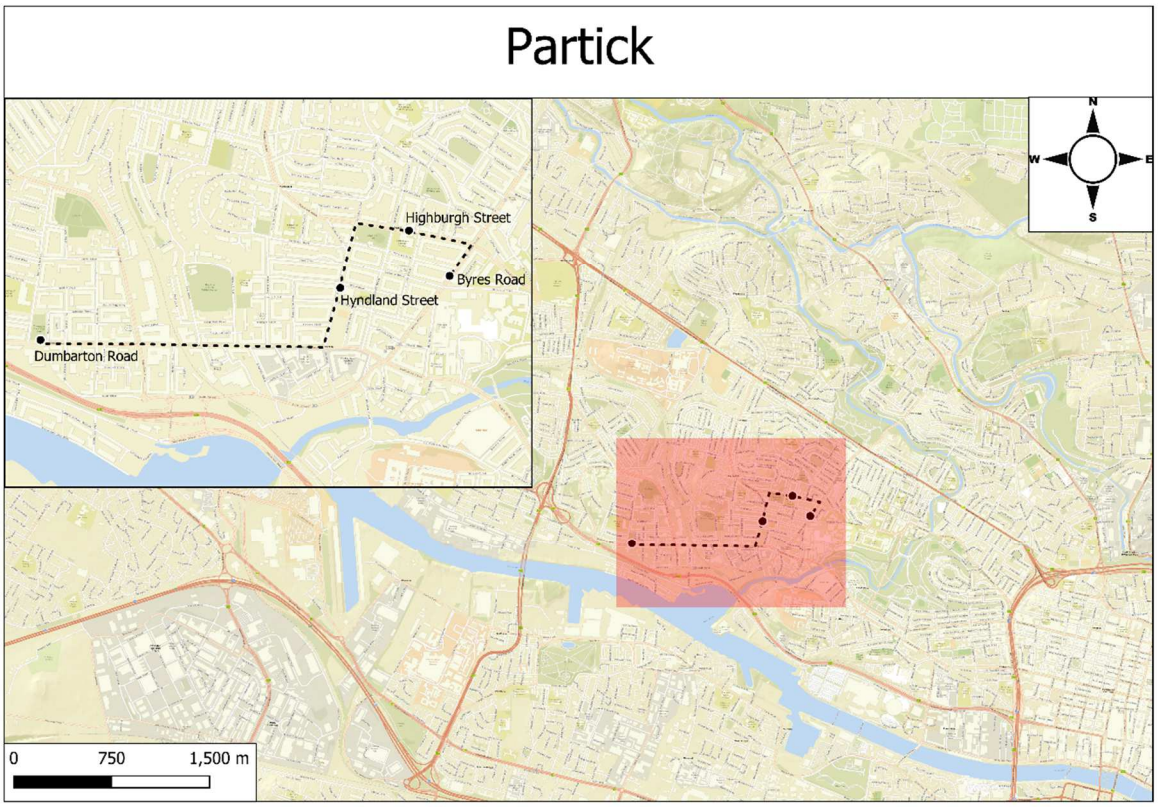

Figure 2.7. Partick ward sampling stops. Dumbarton Road stop was used for fixed monitoring. The map layer used was provided by Esri (Esri standard map).

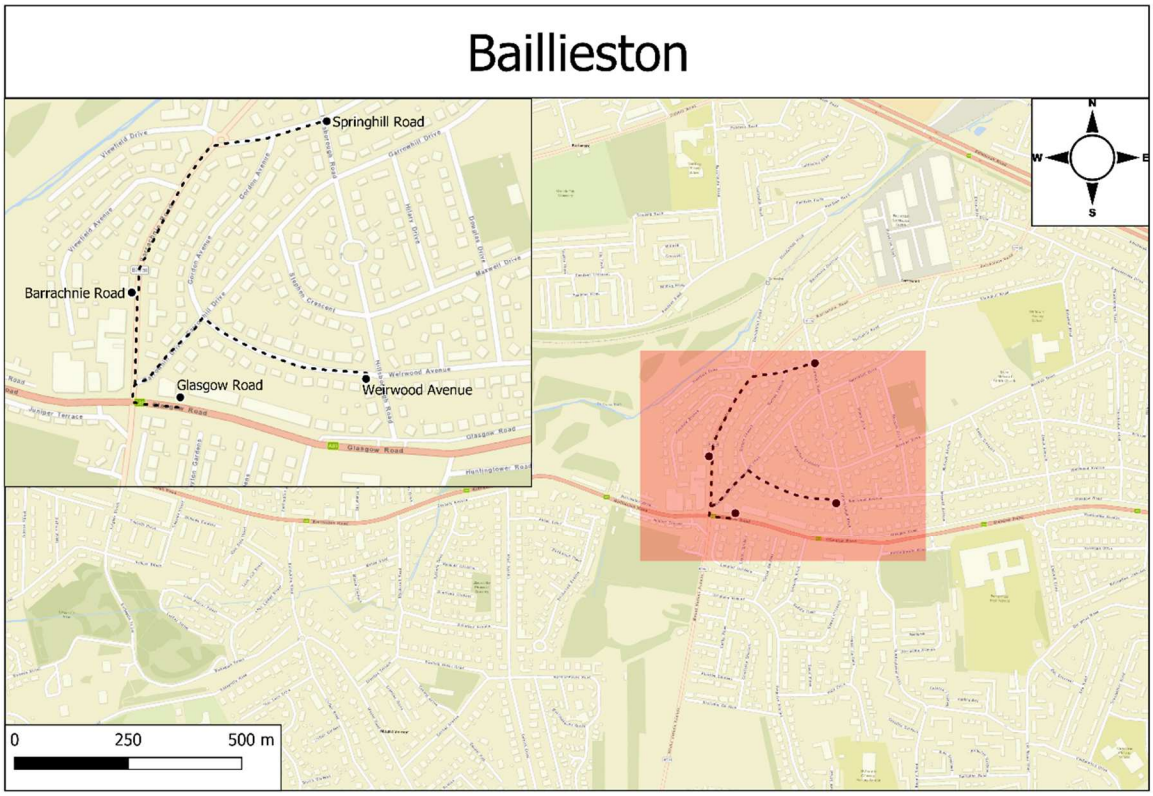

Figure 2.8. Baillieston ward sampling stops. The map layer used was provided by Esri (Esri standard map).

2.2.3. Data Processing of BC Data

Post-processing of microAeth data

The microAeth raw data (at 10 s and 30 s resolution for microAeth units 1 and 2, respectively) was uploaded to the Aethlabs website (https://aethlabs.com/) where an optimised noise-reduction algorithm (ONA) with an attenuation coefficient (ATN) threshold set to ΔATN = 0.01 was used to smooth out instrumental noise in the data.

The smoothed data was then further processed using Equation 1 (Kirchstetter & Novakov, 2007) to account for non-linear response with increasing BC deposition on the filter (Apte et al., 2011).

$$\mathrm{BC}_{corrected} = \mathrm{BC}_o(0.88Tr + 0.12)^{-1} \quad (1)$$

In this equation, BC_o is the instrument-reported concentration and T_r = exp(-ATN/100) is the Aethalometer filter transmission derived from the instrument-reported attenuation coefficient (ATN). Concentration units were also converted from ng m^{-3} to µg m^{-3}.

Calibration of the microAethalometers

The two microAeth instruments were co-located at the Glasgow Townhead urban background site for 3 days. The purpose of this was to compare microAeth measurements against each other and to establish quantitative calibration relationships against the reference AE22 Aethalometer (Magee Scientific, USA) at this site. The reference analyser is part of the UK BC network and is subject to documented quality assurance procedures (uk-air.defra.gov.uk/networks/network-info?view=ukbsn).

Data from the microAeth instruments were averaged to hourly values to construct the calibration curves in Figure 2.9 and Figure 2.10 against the reference analyser BC concentrations. Four data values from the microAeths had extremely low BC concentrations which clearly did not fit the relationships displayed by the rest of the data, so were deemed anomalous and removed. The hourly $BC_{corrected}$ concentrations from microAeth 1 and 2 were highly significantly linearly correlated with each other, with little scatter (R^2 value = 0.99, m = 0.72). The two calibration plots of microAeth vs reference Aethalometer concentrations had insignificant intercepts so linear regressions were performed with the intercept set to zero. The R^2 values were 0.92 (microAeth 1) and 0.90 (microAeth 2). The post-processed $BC_{corrected}$ sample data from each microAeth instrument was adjusted by its respective calibration gradient from Equation 2 on a 1-min average basis to yield $BC_{corrected}$ calibration-adjusted concentrations.

$$\text{microAeth 1: } y = 1.592x \quad \text{microAeth 2: } y = 1.197x \tag{2}$$

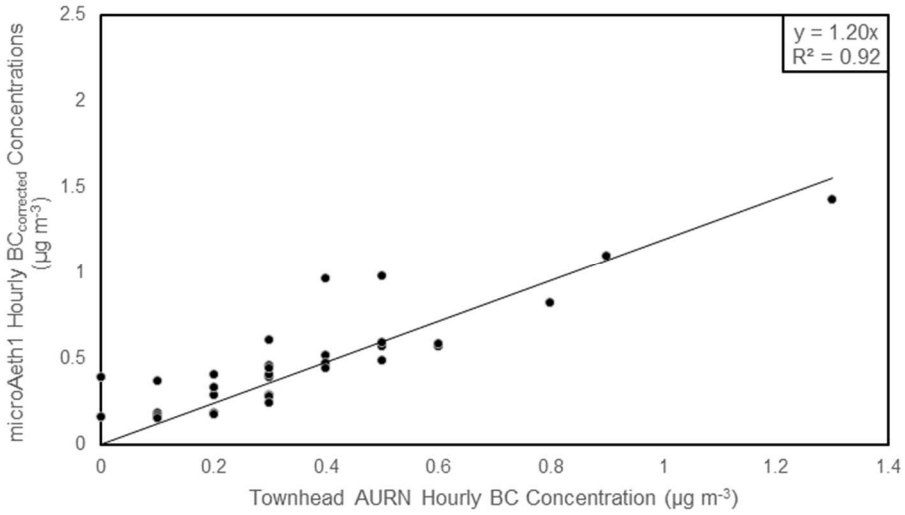

Figure 2.9. Co-location calibration curve for MicroAeth 1 at Glasgow Townhead.

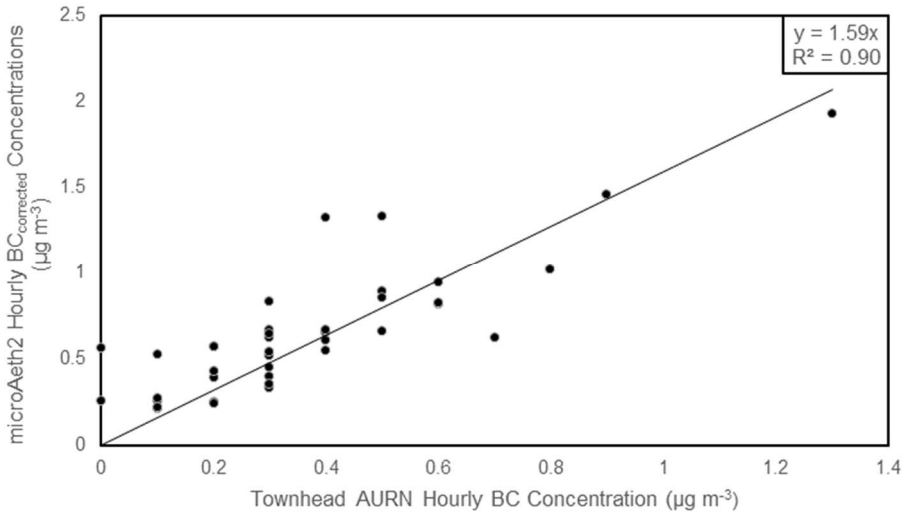

Figure 2.10. Co-location calibration curve for MicroAeth 2 at Glasgow Townhead.

Normalisation against urban background concentrations

To take into account the between-sampling-period variation in levels of BC, the fixed and mobile data collected by microAeth 1 are reported here as increments with respect to the BC concentrations recorded by microAeth 2 at the Glasgow Townhead urban background site. Thus, in the final data-processing step, the 1-min average $BC_{corrected}$ calibration-adjusted concentration from microAeth 2 at Townhead was subtracted from the contemporaneous 1-min average $BC_{corrected}$ calibration-adjusted concentration derived from microAeth 1.

Statistical Analyses

The distribution of the data was non-normal, so non-parametric tests were used to interpret the data. SPSS statistics software was used. Details of the tests, and their purpose, are listed in Table 2.3.

Table 2.3. The array of statistical tests performed on different combinations of the BC measurements.

Statistical Tests			
	Friedman Test	**Wilcoxon Signed Rank Test**	**Kruskal-Wallis test**
Purpose	Evidence for differences between replicate BC concentration increments in each ward.	Evidence for differences in BC concentration increments between morning and mid-morning measurements in each ward	Evidence for differences in BC concentration increments between the four wards
Confidence	95 %	95 %	95 %
Test Groups	Morning and mid-morning measurements were separated for all tests. Tests were undertaken on a) mobile measurements b) fixed measurements	Morning and mid-morning measurements were separated, for all tests. Tests were undertaken on a) mobile measurements b) fixed measurements c) mobile and fixed measurements combined	Morning and mid-morning data were combined for all tests. Tests were undertaken on a) mobile measurements b) fixed measurements c) mobile and fixed measurements combined
Post-Hoc Test	Wilcoxon To gain information on which days were significantly different to others.	N/A	N/A

Negative Values

Around 2 % of all $BC_{corrected}$ concentrations were negative. Table 2.4 shows the sampling wards and dates with negative values. Some of the negative data were associated with microAeth 2 at Glasgow Townhead. To ensure these values did not affect the overall observed trends of BC, statistical tests were performed with datasets containing the negative values and datasets not containing the negative values. There was no difference between the broad conclusions drawn from both data sets, so the negative values were retained; however,

the potential effect of the negative values on more detailed data interpretations is discussed. For example, due to retention of negative values the BC concentrations in Hillhead and Baillieston may have been slightly higher than is reported here.

Table 2.4. Negative measured BC concentrations.

Site	Morning			Mid-morning		
	Date	Duration	Townhead Data?	Date	Duration	Townhead Data?
Hillhead	25.07.19	6 minutes	No	12.07.19	40 minutes	Yes
Baillieston	30.07.19	30 minutes	No	30.07.19	40 minutes	Yes
				15.08.19	40 minutes	Yes

2.2.4. SEPA Traffic Counts and Model

Traffic data was shared by the Scottish Environment Protection Agency to help determine whether BC concentrations could be linked to vehicle compositions for the sampling sites road link. The traffic data was collected in 2017 to build a more detailed picture of traffic flow and composition, and used a mixture of junction turn counts, automatic traffic counters and number plate recognition cameras. The Scottish Environment Protection Agency calculated the Annual Average Daily Traffic flows (AADT) counts from this data to represent typical flows of vehicles along a road section in 24 hours. The Scottish Environment Protection Agency used Defra's emission factor toolkit to calculate vehicle fleet composition. This uses national fleet data for 2017, however the bus composition data was altered to reflect Glasgow's bus fleet's euro classes.

The Scottish Environment Protection Agency also shared modelled annual NO_2 and PM_{10} concentrations. These were determined through running a dispersion model, ADMS-Urban model, and inputting hourly meteorological data from Glasgow Bishopton meteorological station, vehicle emission factors, background emissions from Defra background maps and rural concentrations to account for pollution transported from elsewhere.

2.3. Results and Discussion

A table detailing definitions of shorthand notations used for terms used throughout the results and discussion chapter has been provided.

BC_{f}	1-minute averaged fixed black carbon measurements (μg m^{-3}).
$BC_{f,morn}$	1-minute averaged fixed black carbon morning measurements (μg m^{-3}), all wards combined
$BC_{f,mid}$	1-minute averaged fixed black carbon mid-morning measurements (μg m^{-3}), all wards combined
$BC_{f,combined}$	1-minute averaged fixed black carbon measurements (μg m^{-3}), with morning, mid-morning & all wards combined
BC_{m}	1-minute averaged mobile black carbon measurements (μg m^{-3})
$BC_{,m,morn}$	1-minute averaged mobile black carbon morning measurements (μg m^{-3}), all wards combined
$BC_{m,mid}$	1-minute averaged mobile black carbon mid-morning measurements (μg m^{-3}), all wards combined
$BC_{m,combined}$	1-minute averaged mobile black carbon measurements (μg m^{-3}), with morning, mid-morning & all wards combined
BC_{fm}	1-minute averaged black carbon fixed and mobile measurements (μg m^{-3})
$BC_{fulldataset}$	1-minute averaged fixed and mobile measurements, all wards and time resolutions

2.3.1. Replicates

Each set of fixed and mobile measurements were replicated four times, across four different days. It was important to consider the precision of the 'replicates' per ward. By performing the Friedman statistical test (see Table 2.3 for more details), it could be determined if the BC measurements for each 'replicate' per ward were similar. Significantly different replicates were identified, after which statistical tests were performed on the full dataset and with a dataset excluding divergent replicate data (see Table 2.5 for medians). In most cases, conclusions from statistical tests using both datasets were consistent. However, there were a few cases where conclusions differed. For example, the Friedman statistical test showed a significant difference between morning and mid-morning trends in the dataset excluding divergent replicate data, with mid-morning being higher (P = 0.02) but not for the full dataset. Examination of the medians showed lower medians for the full dataset of $BC_{fulldataset,}$

$BC_{f,morn}$ and $BC_{f,mid}$ (Table 2.5). However, for $BC_{m,morn}$ and $BC_{m,mid}$, the medians were higher. In general, mobile measurement medians increased, and fixed measurement medians decreased. This shift made mobile and fixed BC increment concentration medians more similar.

Table 2.5. The difference in BC increment medians calculated from the original dataset and the dataset which excluded divergent replicate data.

	$BC_{combined}$	**BC_m morning, mid-morning and all wards combined**	**BC_f morning, mid-morning and all wards combined**	**BC_m morning (all wards combined)**	**BC_m mid-morning (all wards combined)**	**BC_f morning (all wards combined)**	**BC_f mid-morning (all wards combined)**
Original dataset	0.5	0.38	0.59	0.29	0.41	0.57	0.61
Dataset excluding divergent replicate data	0.45	0.46	0.43	0.42	0.53	0.43	0.42

To determine if the divergent replicate data could be attributed to variation of general pollution levels on the day of measurement, monitoring station data was observed for nitrogen dioxide (NO_2) and particulate matter with an aerodynamic diameter of ≤ 2.5 µm ($PM_{2.5}$) from 08:00 – 11:00. Glasgow Townhead NO_2 and $PM_{2.5}$ concentrations were subtracted from the monitoring site data to give increment concentrations. The air pollution monitoring stations used to obtain this data were Glasgow High Street (City), Byres Road (Hillhead), Dumbarton Road (Partick) and Cambuslang (Baillieston).

The divergent replicate days per ward for mobile measurements are shown in Table 2.6. In general, there were more significantly different replicates during morning measurements. This could be due to the variability in traffic during morning rush hour. Baillieston and Hillhead exhibited the largest difference between replicates.

Table 2.6. Statistically significant replicate days, from mobile BC increments.

Site	Morning			Mid-morning		
	Replicate Date	**Mean Rank Higher or Lower when removed?**	**Replicates significantly different from**	**Replicate Date**	**Mean Rank Higher or Lower when removed?**	**Replicates significantly different from**
Baillieston	30.07.19	Lower	15.08.19, 23.08.19, 28.08.19	30.07.19	Lower	15.08.19, 23.08.19, 28.08.19
	23.08.19	Lower	15.08.19	15.08.19	Higher	30.07.19, 23.08.19, 28.08.19
City	29.08.19	Lower	09.07.19 and 17.07.19	-	-	-
Hillhead	12.07.19	Lower	25.07.19, 05.08.19, 21.08.19	All replicates	Variable	All replicates
Partick	18.08.19	Lower	20.08.19	-	-	-

$PM_{2.5}$ and NO_2 increments were able to explain the differences between replicates in the city. Data obtained from Glasgow High Street monitoring station showed the NO_2 increment concentrations on 29 Aug 2019, were low from 08:00 – 11:00 compared to other replicate days. $PM_{2.5}$ values were lowest at 9:00 but increased at 10:00 potentially explaining why mid-morning replicates were statistically similar.

For Partick, the $PM_{2.5}$ increment concentrations at 8:00 were highest on the 20 Aug 2019 and lowest on 18 Aug 2019 and a similar trend was observed for the NO_2 increment concentrations. This could explain why measurements made on those days were significantly different. $PM_{2.5}$ values were more similar at 10:00 – 11:00 which explains why replicates were not statistically different during mid-morning.

In Hillhead, NO_2 increments were lowest between 08:00 – 11:00 on the 12 Jul 2019 compared to other replicate days. The $PM_{2.5}$ values, however, were highest from 08:00 – 10:00. The NO_2 increment concentrations help explain why 12 Jul 2019 measurement day was statistically different to other replicate days.

The morning sampling session in Baillieston, that occurred on 30 Jul 2019 was determined to be significantly different to other replicates, as it had a lower BC concentration increment. This was not explained by general pollution, as NO_2 and $PM_{2.5}$ increment concentrations on that day were the highest or second highest compared to other replicates. The NO_2 and $PM_{2.5}$

on 15 Aug 2019 and 23 Aug 2019 were not particularly different, therefore this difference could not be explained by general pollution either. The same was apparent for mid-morning; the general pollution could not explain the differences between the replicates.

For City and Partick wards, the difference between replicates was more fully explained by NO_2 and $PM_{2.5}$ increment concentrations combined, however for Hillhead, it was solely explained by the NO_2 increment concentration.

Table 2.7 shows the statistically different replicate days identified from fixed measurements. In the city, the 29 Jul 2019 exhibited a higher BC increment concentration than all other replicate days. The general air pollution concentration increments were low, therefore high BC increment concentrations on that day, could not be explained by the general pollution.

In Hillhead, the replicate day that was significantly different to others was 01 Aug 2019 (lower than other replicates) and 14 Aug 2019 (higher than other replicates) both in the morning and mid-morning. NO_2 increments on 01 Aug 2019 were generally lower than other replicate days in both NO_2 and $PM_{2.5}$ increments. However, the general pollution on 14 Aug 2019 was not the highest out of all replicate days, therefore this cannot be explained by general pollution.

In Partick, the 28 Aug 2019 was statistically different to all other replicates as the BC increment concentration was higher. $PM_{2.5}$ increment concentrations on this day were highest compared to other replicate days at 9:00, and second highest at 8:00. NO_2 increment concentration were highest at 8:00 and 9:00. General pollution was consistently higher on 24 Jul 2019 than on 22 Aug 2019.

Table 2.7. Statistically significant replicate days, from fixed BC increments.

Site	Morning			Mid-morning		
	Replicate Date	Mean Rank Higher or Lower?	Replicates significantly different from	Replicate Date	Mean Rank Higher or Lower?	Replicates significantly different from
City	29.07.19	Higher	19.07.19 07.08.19 19.08.19	29.07.19	Higher	19.07.19 07.08.19 19.08.19
				07.08.19	Higher	19.08.19
Hillhead	01.08.19	Lower	06.08.19 14.08.19	01.08.19	Lower	06.08.19 14.08.19
	14.08.19	Higher	06.08.19 27.08.19	14.08.19	Higher	06.08.19 27.08.19
Partick	28.08.19	Higher	24.07.19 02.08.19 22.08.19	24.07.19	Higher	22.08.19

To summarise replicate BC increment data showed variations between sampling days despite background BC concentrations being removed. The differences in replicate data could sometimes be explained by general pollution levels on the day of sampling. Where it could not be explained by general pollution levels on the day of sampling, the variation was likely to be from differences in local air pollution on the day of sampling. This could be due to changes in number of vehicles on the road and congestion levels. Therefore, divergent replicate data was retained within the dataset.

2.3.2. Abundance of BC in Glasgow - BC Increments and Absolute Concentrations

Descriptive statistics for absolute and increment BC concentrations are presented in Table 2.8 and Table 2.9 for i) $BC_{f,combined}$ ii) $BC_{m,combined}$ and iii) $BC_{combined}$.

Table 2.8. Descriptive statistics calculated from 1-minute averaged BC absolute concentrations (μg m^{-3}) with all wards combined.

	N	1st percentile	99th percentile	Median	Mean	Standard Deviation
All Mobile & Fixed	2720	-1.68	13.28	1.03	1.81	3.47
All Fixed	1440	0.03	10.40	1.24	1.90	2.18
All Mobile	1280	-1.68	21.97	0.70	1.70	4.50

Fixed and Mobile	N	1st percentile	99th percentile	Median	Mean	Standard Deviation
Morning	1360	-1.03	14.33	1.16	2.06	3.82
Mid-morning	1360	-1.68	11.21	0.86	1.55	3.06

Fixed	N	1st percentile	99th percentile	Median	Mean	Standard Deviation
Morning	720	0.03	10.37	1.45	2.08	2.13
Mid-morning	720	0.03	10.26	1.07	1.71	2.21

Mobile	N	1st percentile	99th percentile	Median	Mean	Standard Deviation
Morning	640	-1.03	24.69	0.86	2.03	5.09
Mid-morning	640	-1.68	13.09	0.61	1.37	3.78

Table 2.9. Descriptive statistics calculated from 1-minute averaged BC increment concentrations (μg m^{-3}) with all wards and sampling intervals combined.

	N	1st percentile	99th percentile	Median	Mean	Standard Deviation
All Mobile & Fixed	2720	-2.65	12.46	0.50	1.16	3.50
All Fixed	1440	-1.24	9.87	0.59	1.16	2.14
All Mobile	1280	-5.27	21.02	0.38	1.16	4.57

Fixed and Mobile	N	1st percentile	99th percentile	Median	Mean	Standard Deviation
Morning	1360	-3.45	13.35	0.45	1.18	3.87
Mid-morning	1360	-1.69	10.91	0.53	1.14	3.09

Fixed	N	1st percentile	99th percentile	Median	Mean	Standard Deviation
Morning	720	-1.40	9.63	0.57	1.16	2.09
Mid-morning	720	-0.97	9.74	0.61	1.16	2.18

Mobile	N	1st percentile	99th percentile	Median	Mean	Standard Deviation
Morning	640	-6.46	23.94	0.29	1.21	5.19
Mid-morning	640	-4.10	12.65	0.41	1.12	3.86

Median $BC_{f,\text{combined}}$ and $BC_{m,combined}$ increment concentrations were similar, though $BC_{m,combined}$ measurements exhibited a slightly lower median (see Figure 2.11). This is because quieter roads were included in the set of mobile measurement sites, so as to provide better spatial representativity overall at a given ward, whilst the fixed measurements were at a single busier road site. On the other hand, 99th percentile $BC_{m,combined}$ concentrations were larger (see Figure 2.12) because these data were collected closer to roadside, i.e., closer to vehicle emission sources. Consequently, the standard deviations in groups of $BC_{m,combined}$ were also larger than equivalent datasets from $BC_{f,\text{combined}}$.

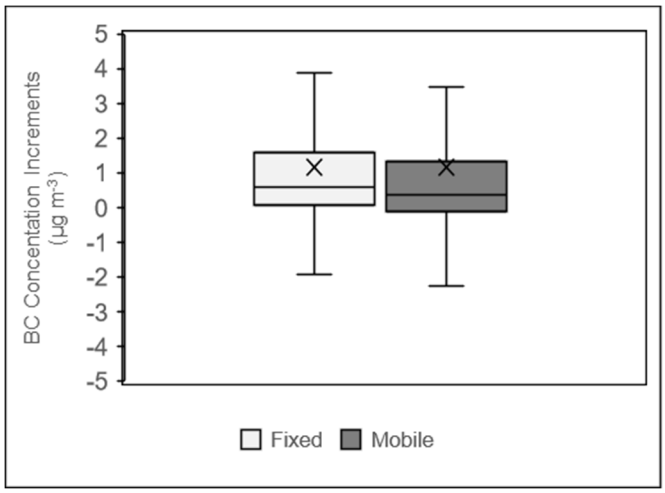

Figure 2.11. Boxplots of $BC_{f,combined}$ and $BC_{m,combined}$ without outlier data points.

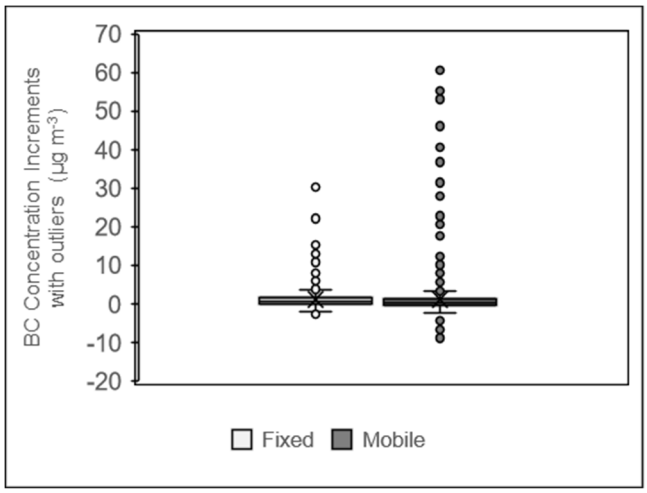

Figure 2.12 Boxplots of $BC_{f,combined}$ and $BC_{m,combined}$ with the outliers of the boxplots.

The absolute median concentration of $BC_{fulldataset}$ was compared to annual median and July-August medians from other sites in the UK BC Network in Figure 2.13 (excluding Birmingham and Chilbolton sites which had no data for 2019) . As the measurements in this study occurred during July-August, the latter medians represent a more representative comparison. The median absolute $BC_{fulldataset}$ concentration of 1.03 µg m^{-3} in this study was higher than the annual and July-August medians at 10 of the 11 network monitoring stations, including the Glasgow High Street and Glasgow Townhead stations. The London Marylebone Road site had the highest annual and July-August medians of 1.70 and 2.20 µg m^{-3} respectively. This is expected as London is by far the most populated city in the UK, with a population more than one order of magnitude greater than Glasgow, and the

Marylebone Road site is adjacent to a heavily trafficked road. The difference between the BC concentrations measured in this study and from the two network Glasgow monitoring stations illustrates the existence in spatial variability in BC concentrations, and hence in BC exposure, across the city. The median absolute $BC_{fulldataset}$ concentration in this study corresponded better with the median at the Glasgow High Street site (0.70 µg m^{-3}) than at the Glasgow Townhead (0.40 µg m^{-3}) since, as noted already, Glasgow Townhead is a background site whilst measurements in this study were made near roads. The median for absolute BC concentrations of $BC_{combined}$ were greater than BC network sites in Northern Ireland (Belfast, Strabane and Ballymena) where some solid-fuel burning for domestic heating still occurs. This indicates traffic must be a dominant source of BC in Glasgow. The median for absolute BC concentrations of $BC_{combined}$ were higher than Glasgow High Street July-August median as measurements were only made during two relatively highly trafficked times of day rather than reflecting a full daily average which includes night-time.

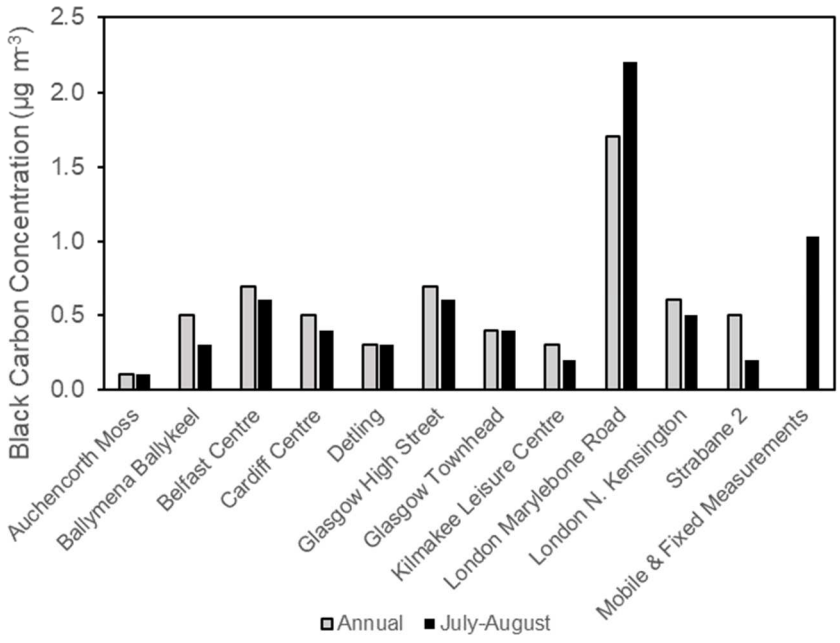

Figure 2.13. Annual medians and the July-August medians from monitoring stations including in the BC Network and the median absolute $BC_{fulldataset}$ concentration from this study.

Figure 2.14 shows plotted $BC_{fulldataset}$ absolute and increment concentrations. The World Health Organisation (WHO) guideline for 24-hour $PM_{2.5}$ concentrations was used to help provide context for BC concentrations, in terms of 'elevated' levels, as there is no BC

guideline value for the UK. The $BC_{fulldataset}$ absolute and increment concentrations exhibited transient exceedances of the 24-hour $PM_{2.5}$ guideline value of 15 µg m^{-3}. There were 19 and 20 transient exceedances for increment BC concentrations and absolute BC concentrations respectively . These exceedances occurred in 3 of 4 wards: City (12 and 13 cases), Baillieston (3 cases) and Partick (4 cases).

Fig. 2.14A **Fig. 2.14B**

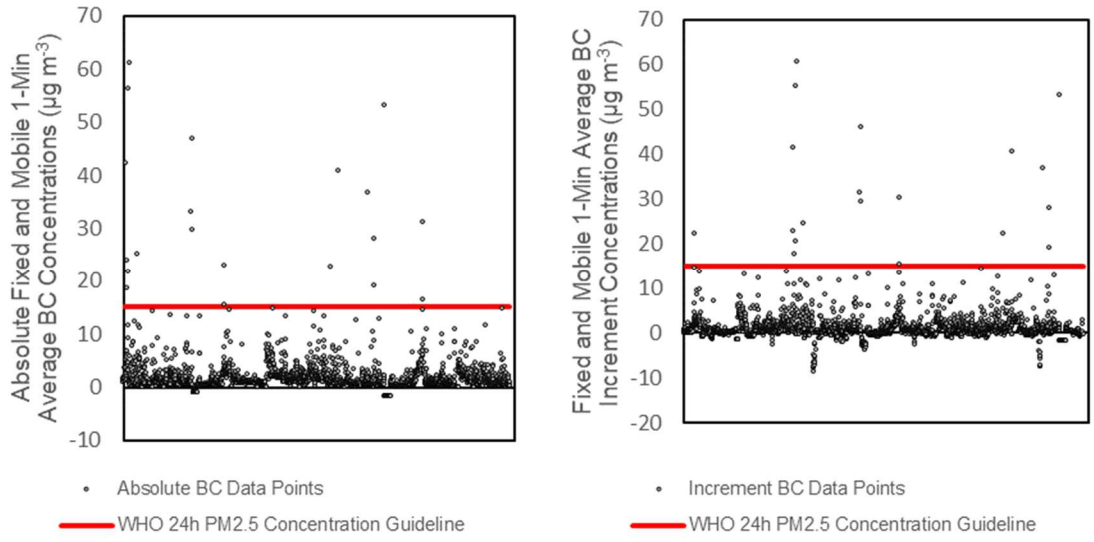

Figure 2.14. Plotted 1-minute averaged data points of $BC_{fulldataset}$ for A) absolute concentrations and B) increments.

The median BC increment for all fixed measurements in Glasgow was 0.59 µg m^{-3}, for mobile measurements ≥8 µg m^{-3} and for fixed and mobile measurements combined 0.50 µg m^{-3}. The median absolute BC concentration for all fixed measurements in Glasgow was 1.24 µg m^{-3}, for mobile measurements 0.70 µg m^{-3} and for fixed and mobile measurements combined 1.03 µg m^{-3}. The BC concentrations were compared to the WHO 24-hour $PM_{2.5}$ concentrations to help identify periods of 'elevated' levels of BC, as there is no limit value for BC in the UK. There were transient exceedances observed in the $BC_{fulldataset}$ before 1-min averages were taken. 19 and 20 transient exceedances were observed in 3 out of 4 wards (City, Baillieston and Partick) for BC increment concentrations and absolute concentrations respectively. From a health perspective, physiological responses such as increased blood pressure, which is a known risk factor for cardiovascular disease, occur with small increases in BC concentration, meaning transient high BC concentrations can lead to negative health effects (De Prins et al., 2014; Mordukhovich et al., 2009; Niranjan & Thakur, 2017; Provost et al., 2016). When comparing the absolute BC concentrations to Glasgow sites in the BC network, Glasgow High Street (0.60 µg m^{-3} July/August median) and Glasgow Townhead

(0.4 µg m^{-3} July/August median) the fixed, mobile, and combined fixed and mobile measurements were all higher than medians of the Glasgow BC Network sites. The BC_m measurements for Glasgow were more comparable to Glasgow High Street, as it was an urban traffic site. It is likely that the measurements had higher concentrations because they were made during two relatively high trafficked times of the day rather than reflecting a full daily average. The latter includes periods of low traffic volumes overnight. However, the mobile and fixed BC measurements taken here, were more spatially representative of Glasgow as a whole than single monitoring station sites as they were taken from 4 different wards. The disparity between medians of Glasgow BC Network sites may also show that Glasgow BC Network sites are not fully representative of Glasgow as a whole, and important additional value is obtained through sampling multiple sites across a wider area of the city.

When comparing the absolute average of $BC_{fulldataset}$ concentrations, 1.81 µg m^{-3}, to previous research, the measurements indicate there has been a decline in BC concentrations in Glasgow compared with the 2009 – 2011 average of 2.94 µg m^{-3} (Singh et al., 2018). This is likely to be mostly from technological advancements such as filters in diesel vehicles which reduce particulate emissions (Ban-Weiss et al., 2008). When compared to a more recent study, conducted in 2015 in Glasgow City by Ezani (2017), the absolute average reported here was slightly below the minimum of the reported absolute BC concentration average range of 2.20 – 4.00 µg m^{-3} in July 2015.

The absolute $BC_{m,morn}$ and $BC_{m,mid}$ average for the City was 3.99 and 2.64 µg m^{-3} respectively. The median for absolute BC concentration in Hillhead (mobile 0.47 – 0.83 µg m^{-3}, fixed 1.21 – 1.37 µg m^{-3}) corresponded well with the reported median, 1.41 µg m^{-3}, which was calculated across 5 weeks of sampling in Hillhead during 2013 (Gillespie et al., 2017). Fixed measurements in Hillhead showed a better agreement to the reported median, despite both studies conducting peripatetic measurements. Difference in mobile measurement medians could represent a general decrease in BC concentrations in Glasgow since 2013.

2.3.3. Temporal Variation – Morning vs. Mid-morning

BC_{fm} increment concentrations from 08:00 – 09:00 and 10:30 – 11:30 were aggregated into a dataset for each time period from all four wards. The mid-morning median calculated from this dataset was higher than the morning median. The same trend was observed with the separated datasets of fixed and mobile BC increments for each time period across all four wards.

For the BC_{fm} aggregated dataset, a Wilcoxon Signed-Ranks test indicated that the morning measurements (mean rank = 698.50) were not significantly different to the mid-morning measurements (mean rank = 664.01), P = 0.128. This implies that the higher BC increment concentrations noted above for mid-morning measurements were not statistically significant. Thus, when discussing the overall trends of mobile and fixed measurements combined, the results do not need to be separated out into morning and mid-morning categories.

However, significance testing of the mobile BC increment concentrations only showed that the higher median BC concentration observed for the mid-morning mobile measurements compared with the morning period was statistically significant (P = 0.01). Consequently, when examining trends in solely mobile or solely fixed measurements, the data needed to be separated out into morning and mid-morning periods. Although the fixed measurement BC concentrations showed no significant difference between morning and mid-morning (P = 0.472), for consistency, fixed measurements are also separated into the two sampling times.

The higher mid-morning mobile measurements could be due to mobile measurements being closer to the roadside as opposed to fixed measurements, hence the mobile measurements may be more sensitive to fluctuations in BC concentration caused by traffic sources. Alternatively, mobile measurements were comprised of measurements from 4 different sampling points, meaning they were more spatially representative of the ward than fixed measurements. The lower BC_f increments could have been caused by fewer sampling points. Previous research by Singh et al. (2018) found BC concentrations averaged from 2009-2016 in Glasgow, had the highest BC concentrations during the morning (3.60 µg m^{-3}) and afternoon peaks were found to be lower (2.70 µg m^{-3}). However, these values include background BC concentration. Absolute measurements obtained in this study were also higher in the morning compared to mid-morning, however, when background concentrations were subtracted, the opposite trend was seen. This suggests high BC concentrations during

08:00 – 09:00 largely constitute of background air pollution. Ezani (2017) found midday measurements (13:00 - 14:30) in Glasgow were 22 % higher than the average morning and afternoon, indicating temporal variability in BC, caused by traffic emissions.

2.3.4. Spatial Variation – BC increments Across Wards

Descriptive statistics were calculated for the absolute (Table 2.10) and increment (Table 2.11) BC concentrations in each of the four wards in which measurements were made, as a first step in investigation of spatiotemporal variation in and between the four wards. Morning and mid-morning measurements were not combined.

Table 2.10. Absolute BC morning and mid-morning concentrations (μg m^{-3}) for each ward.

Ward	Time of Day	N	1st Percentile	99th Percentile	Median	Mean	SD
City Mobile	Morning	160	0.03	48.06	1.76	3.99	7.99
	Mid-morning	160	0.00	17.15	1.60	2.64	4.03
Hillhead Mobile	Morning	160	-0.04	8.29	0.83	1.26	1.77
	Mid-morning	160	0.05	7.19	0.47	0.86	1.49
Partick Mobile	Morning	160	0.01	10.31	1.09	1.73	2.03
	Mid-morning	160	0.07	31.61	0.74	2.11	5.78
Baillieston Mobile	Morning	160	-1.03	31.21	0.30	1.14	5.27
	Mid-morning	160	-1.69	2.16	0.19	-0.12	1.00
City Fixed	Morning	240	0.03	12.88	1.23	1.94	2.42
	Mid-morning	240	0.17	13.11	1.03	1.97	2.91
Hillhead Fixed	Morning	240	0.04	9.25	1.21	2.11	2.09
	Mid-morning	240	0.03	8.50	1.37	1.79	1.88
Partick Fixed	Morning	240	0.14	10.44	1.78	2.19	1.83
	Mid-morning	240	0.07	7.60	0.99	1.34	1.63

Table 2.11. Increment BC morning and mid-morning concentrations (µg m^{-3}) for each ward.

Ward	Time of Day	N	1st Percentile	99th Percentile	Median	Mean	SD
City Mobile	Morning	160	-1.19	47.11	1.06	3.38	7.94
	Mid-morning	160	-0.36	16.48	0.94	2.05	4.02
Hillhead Mobile	Morning	160	-7.73	7.53	0.18	0.15	2.53
	Mid-morning	160	-0.65	7.82	0.51	1.10	1.74
Partick Mobile	Morning	160	-1.80	9.32	0.53	0.92	1.97
	Mid-morning	160	-7.16	31.56	0.54	1.55	6.06
Baillieston Mobile	Morning	160	-3.47	30.29	-0.29	0.38	5.30
	Mid-morning	160	-1.69	2.09	0.07	-0.24	0.95
City Fixed	Morning	240	-1.10	12.12	0.64	1.23	2.38
	Mid-morning	240	-0.95	12.48	0.70	1.47	2.80
Hillhead Fixed	Morning	240	-1.44	7.50	0.16	0.74	1.94
	Mid-morning	240	-0.96	8.18	0.58	1.10	1.92
Partick Fixed	Morning	240	-0.74	9.87	1.08	1.51	1.85
	Mid-morning	240	-0.85	7.05	0.51	0.91	1.63

Kruksal-Wallis tests on the BC increments in the four different wards showed that there were significant differences between the wards irrespective of whether testing the BC_m, BC_f or BC_{fm} (P = 0.0 in each case). This highlighted that there were differences in fixed and mobile measurement concentrations across all wards. The only wards that did not show a significant difference were BC_f increments from City and Partick wards.

The median BC_m increment for morning measurements in the 4 wards were:

City (1.06 µg m^{-3}) > Partick (0.53 µg m^{-3}) > Hillhead (0.18 µg m^{-3}) > Baillieston (-0.29 µg m^{-3})

The median BC_m increment for mid-morning measurements in the 4 wards were:

City (0.94 µg m^{-3}) > Partick (0.54 µg m^{-3}) > Hillhead (0.51 µg m^{-3}) > Baillieston (0.07 µg m^{-3})

The median BC_f increment for morning measurements in the 3 wards were:

Partick (1.08 µg m^{-3}) > City (0.64 µg m^{-3}) > Hillhead (0.16 µg m^{-3})

The median BC_f increment for mid-morning measurements in the 3 wards were:

City (0.70 µg m^{-3}) > Hillhead (0.58 µg m^{-3}) > Partick (0.51 µg m^{-3})

The overall BC_{fm} per ward, with morning and mid-morning combined was:

City (0.80 µg m^{-3}) > Partick (0.63 µg m^{-3}) > Hillhead (0.27 µg m^{-3})

The mobile measurements showed that the City ward had the highest BC increment for morning and mid-morning, then Partick, Hillhead and Baillieston. This was in line with the initial hypothesis, except that, Partick had a higher BC increment than Hillhead. The reason for this could be due to Hillhead having a lower bus and heavy goods vehicles (HGV) AADT as shown in Table 2.12.

The AADT values for buses and HGVs in the 3 wards rank in the order:

City (4137) > Partick (2749) > Hillhead (1874)

A scatterplot of BC_m increment against AADT per sampling site road link, for each vehicle category. The only vehicle category with a positive correlation with an R^2 >0.5 was the bus and HGV category (R^2 = 0.58). This shows that buses and HGVs are more strongly correlated to BC increments suggesting that they are a dominant BC source in Glasgow.

For fixed measurements the AADT values for buses and HGVs rank in the order:

Partick – Dumbarton Road (1438) > Hillhead – University Avenue (480) > City - George Street (293).

This order does not correlate with the measured median BC_f increments, which did not show a consistent trend unlike BC_m increments. Overall traffic counts may have been lower in the Hillhead area during the dates that sampling was completed due to the university being closed for the summer holidays therefore undergraduate teaching was not taking place during July – August. Additionally, during the sampling period, University Avenue in Hillhead was undergoing road works, which may have caused drivers who would have normally used this route, to re-route their journeys. In the City ward, during the July – August, near George

Street, tour buses were observed to be idling, which could have contributed to the higher BC increments for that site.

Table 2.12. Annual average daily traffic flows (AADT) measured by SEPA, split into different categories of vehicle.

Glasgow City Centre - SEPA Measured AADT						
Sampling Site Number	**Car**	**Taxi**	**LGV**	**Bus and HGV**	**Motorcycle**	**Total**
1. George St	2455	874	431	293	65	4118
2. Cochrane St	4881	632	820	308	97	6738
3. Ingram St	1125	480	253	1209	12	3079
4. Union St	4530	1316	891	2327	84	9148
Total	12991	3302	2395	4137	258	23083
Glasgow Hillhead - SEPA Measured AADT						
Sampling Site Number	**Car**	**Taxi**	**LGV**	**Bus and HGV**	**Motorcycle**	**Total**
1. Great Western Rd	16427	884	2234	803	119	20467
2. Eldon St	9671	646	938	482	99	11836
3. Kelvin Way	5966	577	641	109	59	7352
4. University Avenue	7379	650	762	480	74	9345
Total	39443	2757	4575	1874	351	49000
Glasgow Partick - SEPA Measured AADT						
Sampling Site Number	**Car**	**Taxi**	**LGV**	**Bus and HGV**	**Motorcycle**	**Total**
1. Dumbarton Rd	12434	591	1598	1438	47	16108
2. Hyndland St	7261	428	733	86	39	8547
3. Highburgh St	7926	592	779	473	66	9836
4. Byres Rd	7660	541	1189	752	108	10250
Total	35281	2152	4299	2749	260	44741

The results showed that areas of high population and socioeconomic activity had higher BC increments. The city centre had the highest BC_m increments for morning and midday and the highest BC_f for midday. Partick had the second highest BC_m increments followed by Hillhead and Baillieston. This showed that areas with socioeconomic activity was a good indicator of high BC pollution levels. The results were less consistent for BC_f increment measurements. This shows that socioeconomic activity may only be a good indicator of high BC_m measurements as opposed to BC_f. This is because the fixed measurements were taken at one site hence were less spatially representative of the ward. Perhaps with more sites, fixed measurements could still be representative of the ward's pollution levels. The overall BC_{fm} also show BC increments were highest in city, followed by Partick and then Hillhead. Further research could determine which factors (e.g., socioeconomic activity, population density/population and traffic counts) are better indicators of pollution hotspots. This shows the need for more sites within the BC network to represent more wards within Greater Glasgow. These sites could consist of a network of mobile instruments to improve the spatial representativeness of BC measurements for Glasgow. This could help to understand the sources of air pollution specific to the wards and help Glasgow City Council tailor the air quality actions on a ward-by-ward basis. Moreover, a more spatially representative BC network can also help with epidemiological studies linking hospital admissions to local pollution episodes which seemed to be picked up better by mobile measurements.

2.3.5. BC Correlations with Other Pollutants

Scatterplots were produced using 2019 BC data from Glasgow Townhead and Glasgow High Street. As seen in Figure 2.15 and Figure 2.16 BC concentrations from Glasgow Townhead and High Street, had higher R^2 correlations with NOx (R^2 = 0.84) compared with NO_2 (R^2 = 0.63 and 0.61), $PM_{2.5}$ (R^2 = 0.3 and 0.24) and PM_{10} (R^2 = 0.23 and 0.18). This suggests traffic sources were a strong contributor to BC concentrations, as road transport accounted for 27 % of emissions of NOx in the UK in 2021 (Defra, 2023).

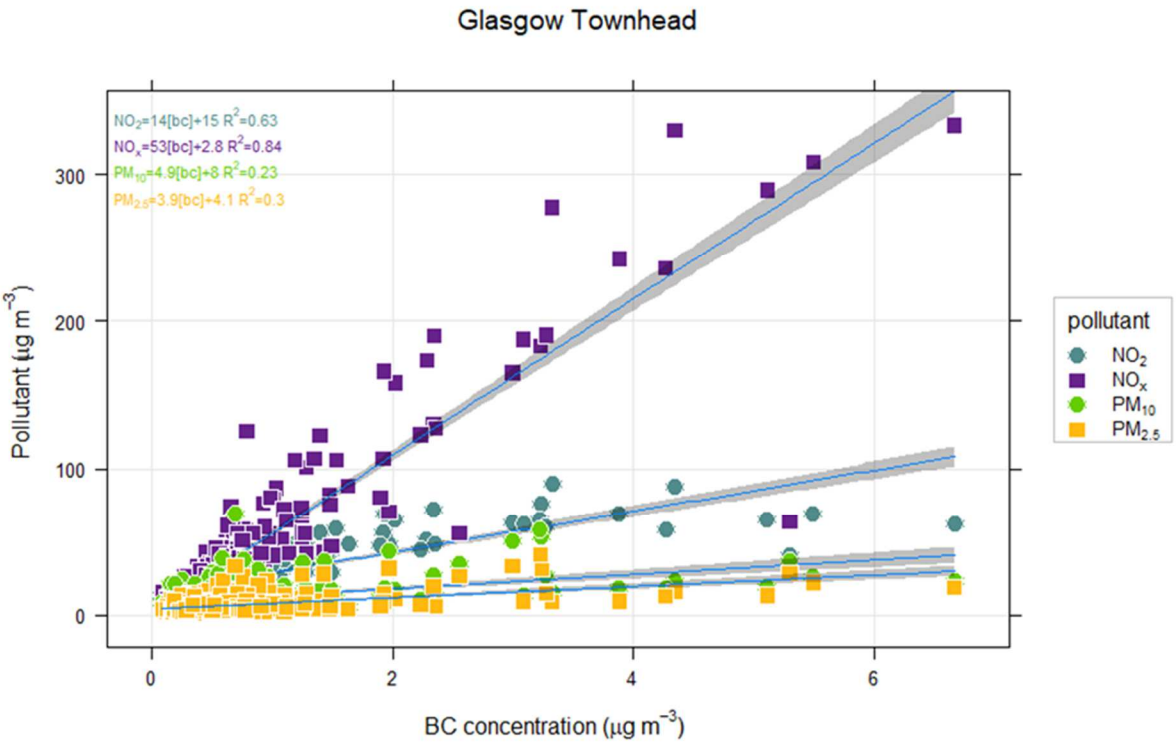

Figure 2.15. Scatterplots of BC (x-axis) and NOx, NO_2, PM_{10} and $PM_{2.5}$ (y-axis) concentrations from Glasgow Townhead.

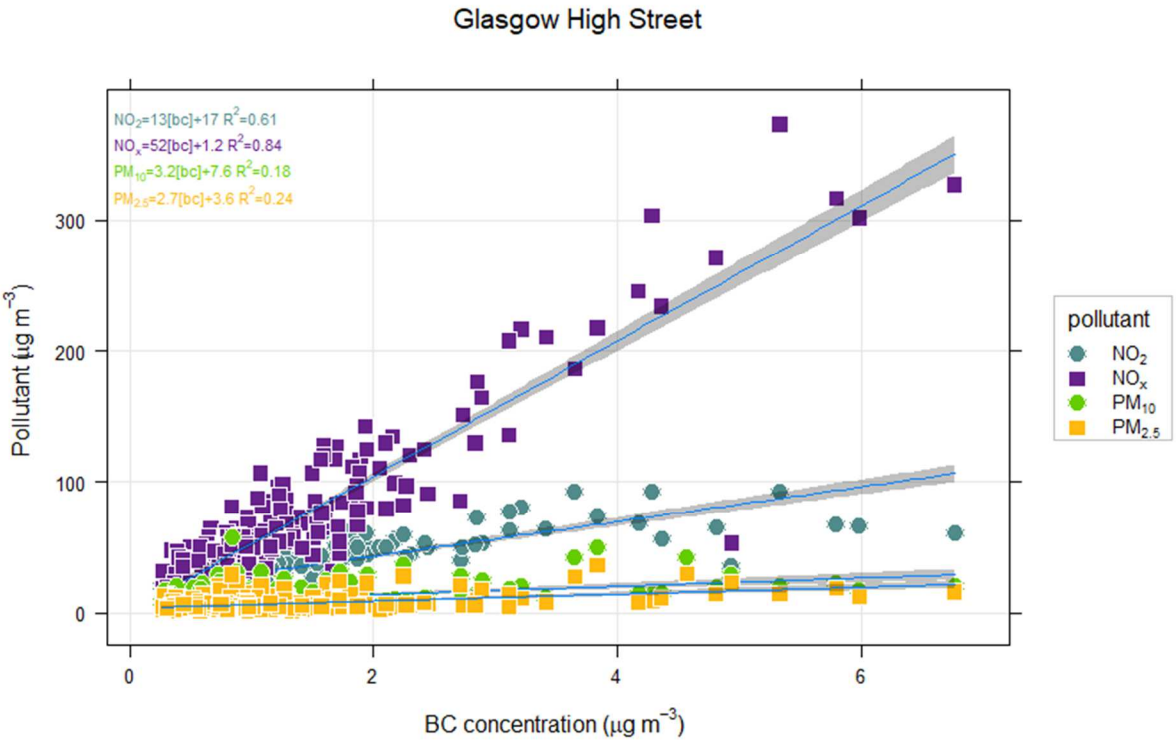

Figure 2.16. Scatterplots of BC (x-axis) and NOx, NO_2, PM_{10} and $PM_{2.5}$ (y-axis) concentrations from Glasgow High Street.

The polar plots in Figure 2.17 and Figure 2.18 show that high BC and NOx concentrations, from Glasgow High Street during summer 2019, were coming from the direction of the city centre outskirts. The roads nearby such as Rottenrow East and Collins Street are side roads with parking bays by the University of Strathclyde. The BC and NOx concentrations from Glasgow Townhead showed that emission sources were likely to be local with small contributions from the M8 motorway and the city centre. In Figure 2.18 the NOx polar plot from Great Western Road also showed high concentrations from Great Western Road and the M8 motorway.

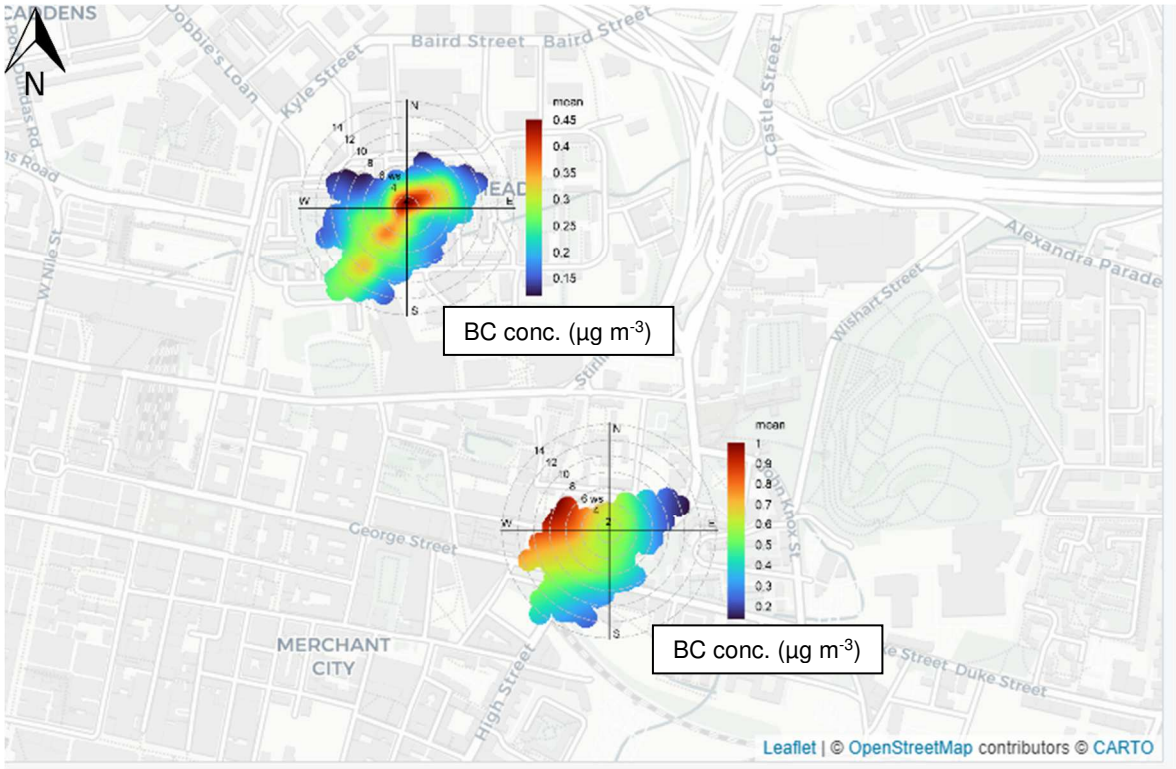

Figure 2.17. Polar plots using BC concentrations from summer 2019 from Glasgow Townhead and Glasgow High Street.

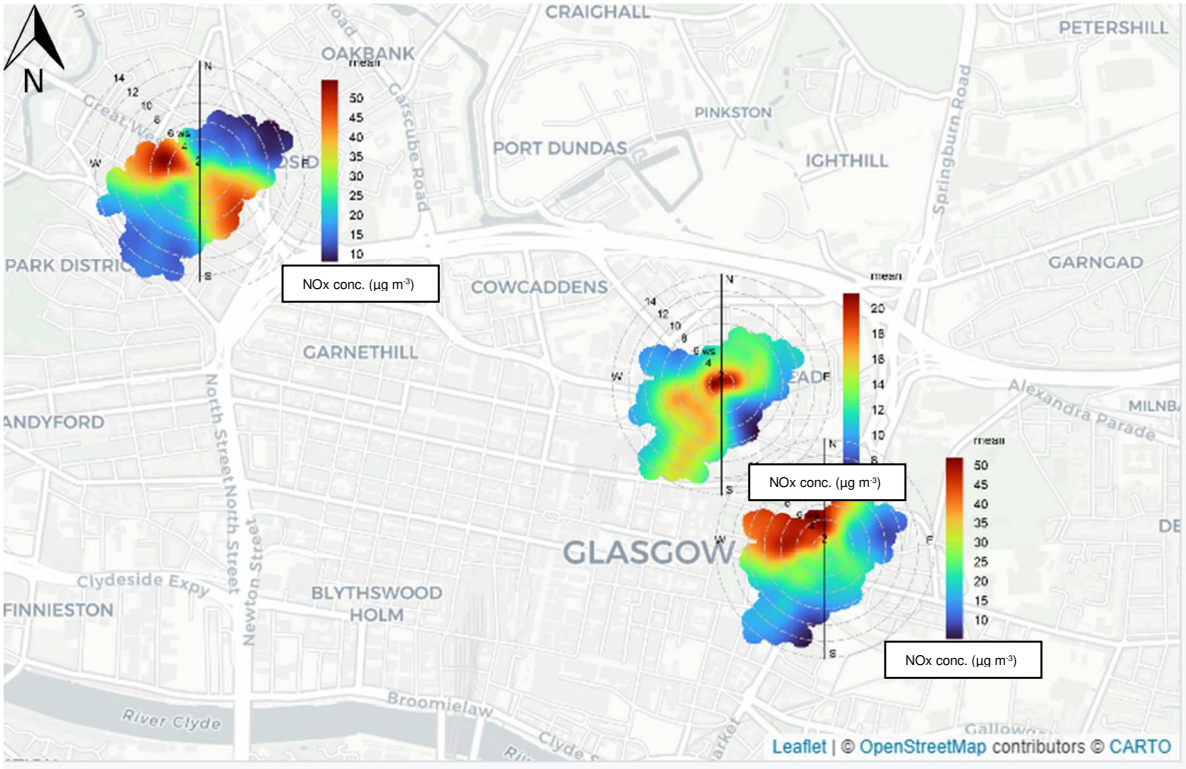

Figure 2.18. Polar plots using NOx concentrations from summer 2019 from Great Western Road, Glasgow Townhead and Glasgow High Street.

2.3.6. Correlations of BC Increments with Modelled NO_2 and PM_{10} Increments

Modelled annual PM_{10} and NO_2 concentrations provided by SEPA were subtracted from modelled PM_{10} and NO_2 concentrations from a road nearby (~0.3 km distance) the Glasgow Townhead AURN station. The median BC concentration increment per site of each ward, was plotted against the modelled NO_2 and PM_{10} increment concentrations. The purpose of this was to examine spatiotemporal relationships between urban pollutants.

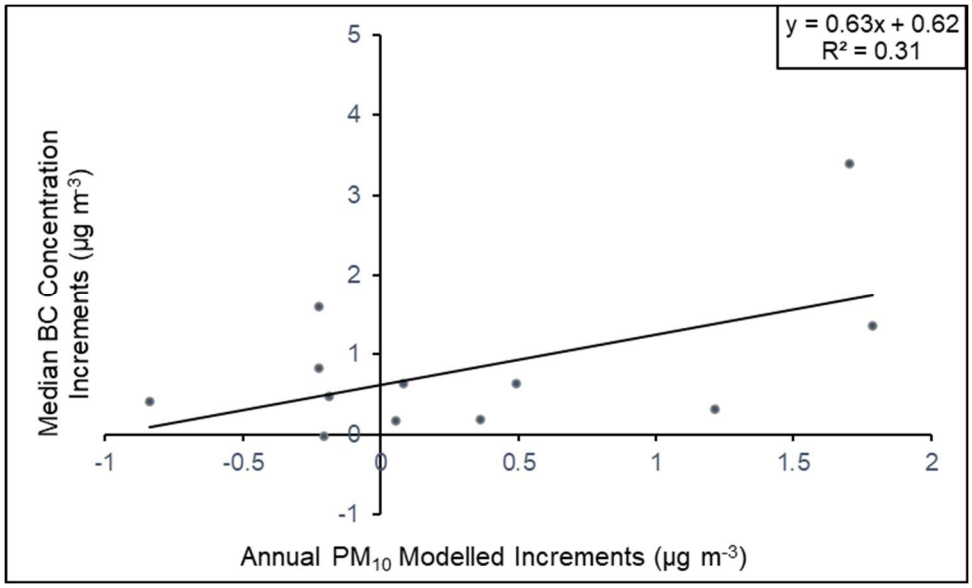

Figure 2.19. Scatterplot between the median BC concentration increments (y-axis) per site across all wards and the modelled PM_{10} concentration increments (x-axis).

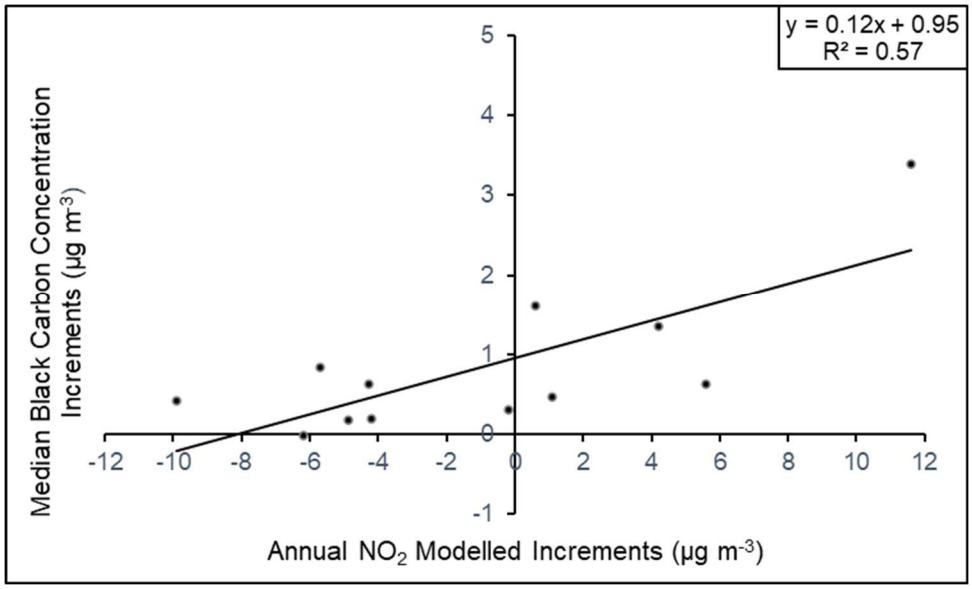

Figure 2.20. Scatterplot between the median BC concentration increments (y-axis) per site across all wards and the modelled NO_2 concentration increments (x-axis).

The R^2 values from scatterplots of measured BC concentration increments against modelled NO_2 and PM_{10} increment concentrations were 0.57 and 0.31 respectively. This is expected as NO_2 and BC are more closely linked to traffic emission sources (Levy et al., 2014).

Whereas PM_{10} may have less spatially specific sources, due to long-range transport which was found to effect PM10 concentrations in three different cities in the UK (Beverland et al., 2000).

The figures also show that whilst Townhead generally has lower BC increments than the BC increments at the four chosen monitoring sites per ward (BC increments are nearly all positive), this is not the case for NO_2 and PM_{10}, where the site nearby Townhead had higher NO_2 and PM_{10} concentrations than quite a lot of the chosen monitoring locations. This could be due to the modelled concentrations being taken from a road nearby the monitoring station (~0.3 km).

These findings were in line with correlations between BC, NO_2 and PM_{10} concentrations measured at Glasgow Townhead and High Street mentioned in Section 2.3.5. Modelled NO_2 increment R^2 value with BC increments (0.57) were close to those between measured BC and NO_2 at Glasgow Townhead (0.63) and Glasgow High Street (0.61). Modelled PM_{10} increment R^2 value with BC increments (0.31) were slightly higher than those between measured BC and NO_2 at Glasgow Townhead (0.23) and Glasgow High Street (0.18).

2.4. Conclusions

Black carbon increments and concentrations were measured in 4 wards within Glasgow during the morning and mid-morning. Mid-morning median increments were higher than morning median increments yet were only deemed to be significantly different for BC_m increments. This suggests that 'mobile' measurements were better at capturing changes in local air pollution, perhaps due to more sampling sites and closer proximity to the roads. Absolute BC concentrations showed the opposite trend, showing that background BC may contribute highly to morning BC concentrations. This shows that BC increments are a better measure for local air pollution. The spatiotemporal trends showed that BC_m increments were highest in the city ward and lowest in Baillieston ward showing population, population density and socioeconomic factors were good indicators of BC pollution levels. The BC_f trends were less consistent which could have been due to a larger distance from the road hence the sources in question or spatial representativeness of the ward. Strong correlations were observed with modelled NO_2 increments and BC increments. Data from AURN and BC Network sites showed stronger correlations between NOx and BC concentrations supporting that NOx and BC may have similar sources in Glasgow. Polar plots from this data showed

that emissions sources could be local to the city centre as well as from side roads with parking bays and the M8 motorway. Strong correlations were observed between BC increments and bus/HGV AADTs, suggesting local air quality actions could focus on bus retrofitting, electrification of bus fleets and freight. To improve the BC network in Glasgow, a more spatially diverse network could help improve knowledge on BC sources and links to health conditions caused by air pollution.

3. Chemical Characterisation of n-Alkanes and PAHs within BC-containing Known-Source Materials and Samples, to Develop an Understanding of the Sources, Structure and Health Risks of OC Associated with BC.

3.1. Introduction

Organic compounds have been used as markers to identify and attribute emission sources in urban areas. n-Alkanes are commonly used as organic molecular markers of the sources of compounds as they react slowly in the atmosphere and are therefore conserved during transport from the source to the receptor sampling site (Lin et al., 2010; Schauer et al., 1996). n-Alkanes can allow differentiation between potential sources, such as fossil fuel and biogenic material, for example wind erosion of epicuticular waxes, direct suspension of pollen, vegetation debris and microbial degradation (Karanasiou et al., 2007; Rogge et al., 1993b;1993c; Rogge et al., 1993a). Sources can be determined through the use of well-established diagnostic parameters such as carbon preference index (CPI), wax n-alkanes percent (WNA%), and the maximum carbon number (C_{max}) (Mazurek & Simoneit, 1984; Simoneit et al., 1991). Another group of organic compounds, PAHs, can also provide information that allows the emission sources to be identified. Polycyclic aromatic hydrocarbon diagnostic ratios (PAH DRs) are widely used in the literature as markers for PAH emission source categories; for example, the ratio of BaP/BghiP can indicate traffic and non-traffic sources (Famiyeh et al., 2021; Tobiszewski & Namieśnik, 2012). Polycyclic aromatic hydrocarbon diagnostic ratios (PAH DRs) are most useful when applied to HMW PAHs as they are strongly resistant to photochemical degradation (Famiyeh et al., 2021; Masri et al., 2018; Tobiszewski & Namieśnik, 2012). Polycyclic aromatic hydrocarbon and n-alkane data can also be used in conjunction with statistical tools like principal component analysis (PCA) to determine source contributions in complex mixtures (Boreddy et al., 2018; Caumo et al., 2020; Caumo et al., 2018; Kang et al., 2020; Lyu et al., 2019).

As a component of PM, PAHs can also present potential carcinogenic and mutagenic health risks associated with inhalation of PM (Claxton et al., 2004; de Kok et al., 2005). Mutagenic compounds are an underlying factor in human disease due to their ability to induce genetic instability and hence to accelerate the evolution of human cancers or the development of

genetically inherited diseases. Furthermore, mutagens also contribute to transcription errors, which arise in dividing and non-dividing cells, affecting every class of transcripts inside cells. Such errors can alter the fate of cells, initiate oncogenic programs, deregulate metabolism, cause protein misfolding or shorten cellular lifespan. Additionally, transcription errors were shown to generate the toxic proteins found in nonfamilial cases of Alzheimer's disease (Gordon et al., 2009; Gout et al., 2017; Saxowsky et al., 2008; Van Leeuwen et al., 1998a; Van Leeuwen et al., 1998b; Vermulst et al., 2015).

Fritsch et al. (2020) found that DNA repair is required to mitigate against transcriptional mutagenesis after exposure. Without such repair, DNA damage would continue to induce transcription errors over extended periods of time; therefore, patients with DNA-repair deficiency syndromes can exhibit prolonged episodes of transcriptional mutagenesis. Because these transcription errors can greatly exceed the number of genetic mutations that arise, they may even elicit the symptoms that characterise these diseases. Results suggest that DNA damage can directly contribute to the loss of proteostasis seen in aging cells, a key component of the etiology of numerous age-related diseases, including Alzheimer's disease and Parkinson's disease (Fritsch et al., 2020). Benzo(a)pyrene is one of the most carcinogenic PAHs and has been classified as carcinogenic to humans by the International Agency for Research on Cancer. The UK National Air Quality Objective (NAQO) for PAHs in ambient air is an annual mean of 0.25 ng m^{-3} for benzo(a)pyrene, BaP, published in the UK Air Quality Strategy 2007. (*The Air Quality Strategy for England, Scotland, Wales and Northern Ireland*, 2007; *Directive 2004/107/EC of the European Parliament and of the Council of 15 December 2004 relating to arsenic, cadmium, mercury, nickel and polycyclic aromatic hydrocarbons in ambient air*, 2005). The EU Fourth Air Quality Daughter Directive 2004 (FAQDD) has an annual mean target value of 1 ng m^{-3} for BaP. Both the UK AQO and the FAQDD use BaP as a marker for the carcinogenic risk of PAHs in ambient air. However, the carcinogenic potential of BaP in PAH mixtures varies, for example Tadsanaprasittipol et al. (2021) found contributions of 40 % total carcinogenicity from BaP at urban background and industrial sites and 60 % at roadside sites. Underestimates of the overall health risks associated to exposure to PAHs in ambient air are likely if only 40 – 60 % of the total carcinogenicity of PAH mixtures are accounted for.

The work presented in this chapter had two aims. The first aim was to determine the origins of n-alkanes and PAHs in PM samples. This is done first by analysing solvent-extracted n-alkanes and PAHs in a variety of known-source materials so as to test the accuracy of

diagnostic tools and PCA approaches (described in Section 1.4) to provide information on PAH distributions from known sources. Secondly, having established the above for the known-source materials, these methods are applied to determine sources of PAHs and n-alkanes in airborne ambient PM. These data are used later in conjunction with ^{14}C source apportionment data to deliver a more holistic approach to source apportionment of airborne ambient aerosols.

The second aim was to investigate the potential health risks from inhalation of PAHs associated with PM_{10} and $PM_{2.5}$ from Glasgow Kerbside sampling site (GLA-KS) in the city ward, which was shown to have the highest BC concentrations out of the four wards investigated in Chapter 2. The potential health risks were also determined for samples from Manchester Fallowfield (MAN-FF) an urban background site. This is done through determination of BaP toxicity equivalent and mutagenic equivalent concentrations in PM samples, as well as through the calculation of the lifetime excess cancer risk.

3.2. Determination of Sources of Solvent-Extractable Polycyclic Aromatic Hydrocarbon And n-Alkanes in Standards and Particulate Matter Samples

To determine the sources of PAHs and n-alkanes in airborne ambient PM, PAHs and n-alkanes were analysed in a range of known-source materials to determine patterns in PAH and n-alkane distributions that could identify sources in airborne ambient PM. Moreover, diagnostic tests that can give information about PAH and n-alkane sources such as PAH DRs, CPI and WNA%, were tested on known-source materials as a verification step. PCA was applied to PAH and n-alkane data from known-source materials and airborne ambient PM separately due to differences in units. The compilation of this data was used to determine sources in airborne ambient PM from GLA-KS and MAN-FF and draw conclusions.

3.2.1. Materials: Known-Source Materials

Aerosol and Dust Materials

The use of materials with the same environmental matrix as airborne ambient PM samples was important for quality control purposes when testing the overall sample preparation and GC-MS method. Additionally, using materials with similar emission sources (vehicular emissions) or site characteristics (urban areas) can help verify the source categorisations using PAHs and n-alkanes.

BCR723 Road dust (trace elements) (BCR-RD)

BCR723 Road dust (BCR-RD) was purchased from Merck. BCR-RD was used to typify road dust with dominant vehicular emission sources, as it was collected from Tanzenberg tunnel in Styria, Austria, in 1998, from a ventilation drain in the tunnel (Zischka et al., 2002). Although the standard was sold as a CRM for metal analysis, it was used here to determine PAHs and n-alkanes originating mainly from vehicular emissions. The reported matrix components were silicate compounds (45-50 %), sulfur (2 -5 %) and total carbon (10%) (Zischka et al., 2002). As the dominant emission sources of the material were known it could act as a standard for PAH diagnostic ratios.

ERMCZ100 Fine Dust (PM_{10}-like) (PAHs) (FD)

ERMCZ100 Fine Dust (FD) was used to typify airborne ambient PM emitted from vehicular traffic as it was collected from a road tunnel called Wisłostrada tunnel, in Warsaw, Poland, from the walls and sidewalks during 2006 (Piascik et al., 2010). This standard was used to determine PAH and n-alkanes originating mainly from vehicular emissions. This standard was used for quality control purposes, as well as the testing of PAH diagnostic ratios.

Road Dust, from University Avenue, Hillhead, Glasgow (HH-RD)

Road dust was collected for this study from University Avenue, Hillhead, Glasgow (55.873456, -4.293445) (HH-RD). Resuspended road dusts are often contributors to PM_{10} and $PM_{2.5}$ samples. HH-RD was collected to represent this potential source of airborne ambient PM from Glasgow.

During sample collection, a new university building was under construction, so temporary traffic lights were being used, inducing a one-way usage of the road, making one direction of traffic wait, whilst the other direction of traffic passed along. Fine bristle brushes were used to collected street kerb and road dust into a dustpan, which had been cleaned with isopropyl alcohol beforehand. To minimise contamination, brushes had not been used prior to sample collection and thick gloves were worn during the sample collection. The collected dust was poured into Ziplock bags. The sample was homogenised through a sieve shaker which had two different meshes (90 µm and 38 µm). The particle fraction with diameters ≤38 µm were collected in a pan and used as the sample. This sample was used as an example of a road dust from an urban area.

NIST 1649b Urban Dust (UD)

NIST Standard Urban Dust, 1649b (UD) was purchased from Merck. UD was used to represent a typical urban ambient airborne aerosol sample as it was collected from atmospheric particulate material in Washington, DC, in 1976 and 1977. This standard was used for quality control purposes, as well as the testing of PAH diagnostic ratios.

NIST 1648a Urban Particulate Matter (UPM)

NIST Standard Urban Particulate Matter, 1648a (UPM) which was purchased from Merck. UPM was used to represent a typical urban aerosol as it was collected in an

urban industrial area of St. Louis, MO, USA in 1976 and 1977. This standard was used for quality control purposes, as well as the testing of PAH diagnostic ratios.

Fossil Fuel Materials

Petrogenic and pyrogenic fossil fuel standards were used to verify source categorisations determined through PAH DR. Furthermore, diesel soot was used as it could help identify when vehicle emissions in airborne ambient PM samples, with unknown sources, were coming from diesel vehicle emissions rather than petrol vehicle emissions.

NIST 2975 Diesel Soot (DS)

NIST Standard Diesel Particulate Matter, 1648a (DS) was purchased from Merck collected from a filtering system designed specifically for diesel-powered forklifts from M.E. Wright of the Donaldson Company, Inc., Minneapolis, MN. DS was used to help identify the PAH ring-size distributions from engine vehicular sources in airborne ambient PM.

Argonne Premium Coal Sample Beulah-Zap Lignite (BZ)

BZ was purchased from Penn State University, Energy Institute of Earth and Mineral Sciences. The material was collected from the Beulah-Zap seam in Mercer County, North Dakota, about eight miles northwest of Beulah, in November 1986. The material is classed as an immature lignite coal. BZ was used to represent a petrogenic material.

Biomass Materials

Charred biomass, laboratory-made charcoals were obtained as proxies for solid particulates emitted from biomass/wood combustion. These samples were of interest, as they could help determine PAH distributions in airborne ambient PM with such sources. Wood and charcoal smoke filters were also analysed.

Charred Biomass (DB and EB)

Miscanthus x giganteus, MxG (DB) and *Miscanthus sinensis* Mx2714/OPM 12 (EB) are perennial C_4 rhizomatous grasses, originating from East Asia. The biomass feedstocks were obtained in pellet form from Aberystwyth University. The

feedstocks were processed in a gasifier which thermochemically extracts useful gases from the feedstock to produce electricity by colleagues in the Engineering department at the University of Glasgow, detailed by Kamble et al. (2019). The gasifier conditions during the DB and EB runs are given in Table 3.1. Samples required homogenisation which was done by placing samples in a stainless-steel compartment with a weighted lid and inducing force with a hammer to pulverise the sample (see Figure 3.1). The DB sample retained some of its biomass structure whilst EB was in a more powdered form.

DB and EB were used as a proxy for solid particulates emitted from biomass combustion to help identify biomass combustion sources in airborne ambient PM samples, with unknown sources, through the use of PAH DRs, PAH ring-size distributions and n-alkane CPIs.

Table 3.1. Gasifier pyrolysis conditions for producing DB and EB.

	DB	**EB**
Air flowrate (L min^{-1})	12.00	14.33
Gasifier pressure (bar)	0.956	0.995
Temperature (°C)		
Drying Zone (T01)	196	218
Pyrolysis Zone (T02)	349	364
Top Reduction Zone (T03)	639	557
Bottom Reduction Zone (T04)	842	846
Below Grate (T05)	438	500
Gasifier Exit (T06)	188	226

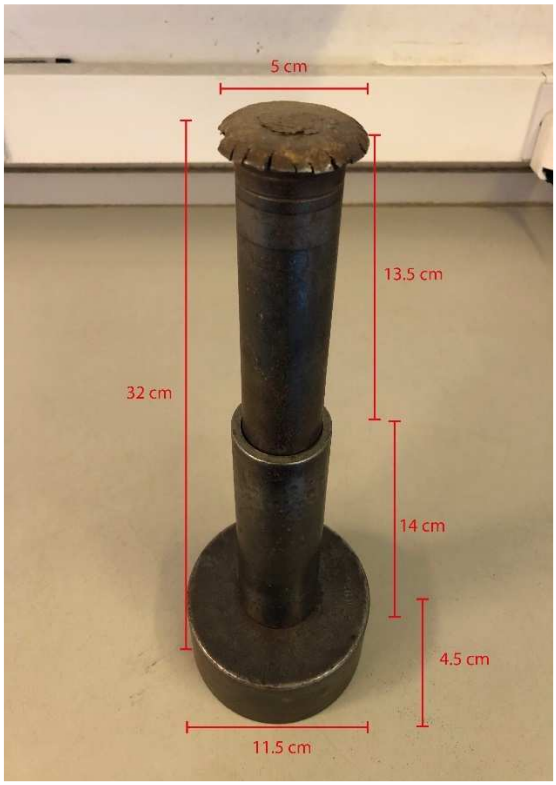

Figure 3.1. Apparatus used to pulverise sample. The sample was placed inside the cylinder, with the weighted lid on top, and hit with a hammer.

Laboratory-made Charcoals

Laboratory-made charcoals were also used as a proxy for solid particulates emitted from wood combustion to help identify wood combustion sources in airborne ambient PM samples. These samples were prepared in previous work and their production methodology is fully described in Ascough et al. (2008). To summarise, the samples consisted of hardwood mangrove (*Rhizophora apiculata* Blume) from north-east Palawan, Philippines, which was pyrolyzed at varying temperatures (300°C or 600°C) and durations (60 and 120 minutes). The entire branch cross-section excluding the bark of mangrove was used to create small 1 cm^3 cubes using a Tema mill for 30 seconds. Mangrove was pyrolyzed in a controlled-atmosphere rotary furnace (Carbolite), under 2% oxygen, to produce charcoal at varying durations and temperatures, which represented those of natural fires. The temperatures were determined with a thermocouple in one of the wood cubes per run. Samples were homogenised by passing the charcoal through a 500 µm sieve with 0.5 M HCl to remove calcitic ash, followed by deionised water. The sample was then passed through another sieve of 63 – 500 µm before drying.

Charcoal Smoke and Wood Smoke Samples

The charcoal smoke and wood smoke samples were provided by a Ph.D. candidate from the University of Strathclyde. The samples were collected from Kalonga village in Chikwawa, Malawi from 08/05/2019 to 25/06/2019 using an SKC Touch or AirLit device (SKC Ltd., Dorset, UK) on quartz filters (QMA, 25 mm diameter, GE Healthcare Life Sciences Whatman). The cookstoves used were 3-stone stoves using wood, Mbaula charcoal burners or improved cookstoves which were more sophisticated in terms of efficiency. The stoves were either used inside the house (kitchen or other room in the house) or outside the house or on the veranda (khondi). The SKC Touch and Airlite were portable pumps fitted with cyclones designed to collect approximate PM_{10} samples. To ensure there was enough sample mass for GC-MS analysis, the filters obtained were grouped into three separate samples according to the fuel type (firewood or charcoal) and whether the combustion occurred indoors or outdoors. Appendix Ia shows details of the samples.

3.2.2. Materials: Airborne Ambient Particulate Matter Samples

Airborne ambient PM consists of particles with an aerodynamic diameter of either ≤10 µm (PM_{10}) or of ≤2.5 µm ($PM_{2.5}$), consisting of a mixture of solid and liquid droplets. Airborne ambient PM collected from GLA-KS and MAN-FF was used within this project so that the sources and the health risks associated to PM-bound PAHs could be determined. The PM samples were collected using gravimetric ambient air samplers. This type of monitoring involves drawing a known volume of ambient air through the sampler inlet with a pump, and then through a filter onto which the particles are captured. The filters were weighed before and after the sampling episode to determine the net mass of particles.

Table 3.2. Number of filters collected from MAN-FF and GLA-KS. GLA-KS samples were provided by Ricardo AEA.

Site	Number of Filters Collected	Sampler Used	Filter Diameter and Type	Sampling Date Range	Filter Change Duration
Glasgow Kerbside (AURN Site ID: Glasgow Kerbside, GLA-KS)	17	Sequential Particulate Sampler MicroPNS LVS16-Split.	47 mm, PALLFLEX membrane filters (PALL Life sciences)	19.01.2020 – 11.02.2021	1 day
University of Manchester (MAN-FF)	14	Digitel HV sampler	150 mm Whatman® QM-A quartz filters	20.11.2019 – 18.12.2019	2 days

A crucial aspect of sample collection was to prevent sample contamination. This was ensured by wearing blue nitrile gloves within the laboratory or when handling the filters within the field. Whenever filters were handled, plastic tweezers were used, which were soaked in deionised water and isopropyl alcohol before first usage, after which, they were wiped with isopropyl lint-free wipes. Laboratory surfaces and equipment were wiped before use to remove dust. The filter holders were cleaned before use in deionised water and isopropyl alcohol and then dried.

Understanding the air mass origins of the sample can help with understanding sources. The air mass back trajectories were plotted using openair R package which used HYSPLIT model to calculate trajectories (Carslaw & Ropkin, 2012; Draxler, 1999; Draxler & Hess, 1997;1998; Stein et al., 2015). The HYSPLIT computes back trajectories through Lagrangian approach using a moving frame of reference for advection and diffusion calculations and Eulerian methodology which uses a fixed three-dimensional grid as a frame of reference to compute air pollutant concentrations (Draxler & Hess, 1997). The air mass back trajectories help with interpretations in the results & discussion section in this chapter.

Glasgow Kerbside (GLA-KS) PM Samples

Glasgow Kerbside is an Automatic Urban & Rural Network monitoring station that is categorised as an urban traffic site. It is situated on Hope Street in Glasgow City Centre, which is a road that restricts vehicles other than buses, taxis, private hires, cycles and goods vehicles from 07:00 to 19:00.

Figure 3.2 shows a map of GLA-KS. GLA-KS is also situated nearby Glasgow Central train station.

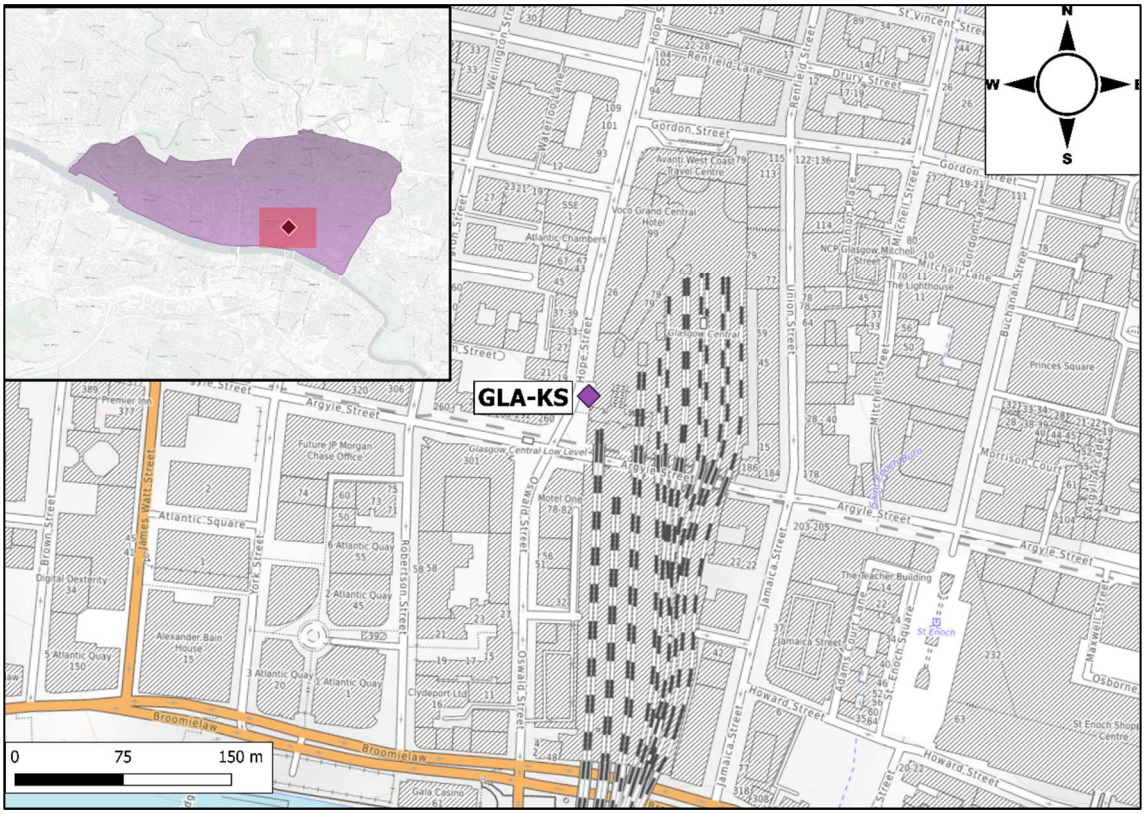

Figure 3.2. Location of GLA-KS sampling site. The map layers used were provided by Esri (Esri Gray light) and OpenTopoMap.

Particulate matter (PM_{10} and $PM_{2.5}$) samples from Glasgow Kerbside were provided by Ricardo AEA. The filters listed in Table 3.3 were collected using a Sequential Particulate Sampler MicroPNS LVS16-Split with a flow rate of 38.5 L min^{-1}. The samples were collected on PALLFLEX membrane filters (PALL Life sciences, Belgium). The filters were collected for a project named "Pilot Research Study to Investigate Particulate Matter Monitoring Techniques in Scotland" to compare different particulate matter monitoring methods against a reference method, by comparing 24-hour PM concentrations. The filters obtained for this project were grouped by dates and PM size fractions into four samples:

4038, 4043, 4046 and 4047 to ensure that PAH concentrations were above the LOD. Table 3.3 shows the grouping of the filters for the samples.

Table 3.3. Collected airborne ambient aerosol PM from Glasgow Kerbside, AURN site.

Sample ID	Filter Number	Inlet Size	Sampling Dates	Mass (mg)	Volume of Air Sampled (m^3)
4038	GLK04	PM_{10}	19.01.2020	1.21	55
	GLK21	PM_{10}	04.02.2020	1.42	55
	GLK23	PM_{10}	06.02.2020	2.26	55
	GLK24	PM_{10}	07.02.2020	2.70	55
4043	GLK72	PM_{10}	23.03.2020	2.19	55
	GLK73	PM_{10}	24.03.2020	1.85	55
	GLK143	PM_{10}	29.05.2020	1.11	55
4046	GLK54	$PM_{2.5}$	06.03.2020	1.12	55
	GLK172	$PM_{2.5}$	25.06.2020	1.02	55
	GLK340	$PM_{2.5}$	29.11.2020	1.30	55
	GLK349	$PM_{2.5}$	07.12.2020	1.26	55
4047	GLK245	PM_{10}	01.09.2020	1.16	55
	GLK263	PM_{10}	18.09.2020	1.63	55
	GLK313	PM_{10}	04.11.2020	2.54	55
	GLK371	PM_{10}	28.12.2020	1.29	55
	GLK381	PM_{10}	06.01.2021	1.44	55
	GLK420	PM_{10}	11.02.2021	1.11	55

A summary of the air mass origins for GLA-KS PM samples can be seen in Table 3.4. These were determined by 96-hour HYSPLIT back trajectories, which were calculated and plotted using Open Air, as seen in Figures 3.3, Figure 3.4., Figure 3.5 and Figures 3.6.

Table 3.4. The summary of air mass origins for each GLA-KS filter.

Sample	Dates	Air Mass Origin Location
4038	19.01.2020	North Atlantic Ocean, Greenland
	04.02.2020	Greenland Sea, Baffin Island
	06.02.2020	North Atlantic Ocean
	07.02.2020	North Atlantic Ocean
4043	23.03.2020	Northern Europe - Scandinavia
	24.03.2020	Northern Europe - Scandinavia
	29.05.2020	North Atlantic Ocean
4046	06.03.2020	North Atlantic Ocean
	25.06.2020	North Atlantic Ocean
	29.11.2020	Scotland, North Atlantic Ocean
	07.12.2020	Eastern Europe, Poland
4047	01.09.2020	North Atlantic Ocean, Norwegian Sea, Iceland
	18.09.2020	North Atlantic Ocean, Norwegian Sea, North Sea, Scotland
	04.11.2020	North Atlantic Ocean, Greenland, Baffin Bay
	28.12.2020	North Atlantic Ocean, Greenland, Baffin Bay
	06.01.2021	Northern Europe - Scandinavia
	11.02.2021	Northern Europe - Scandinavia

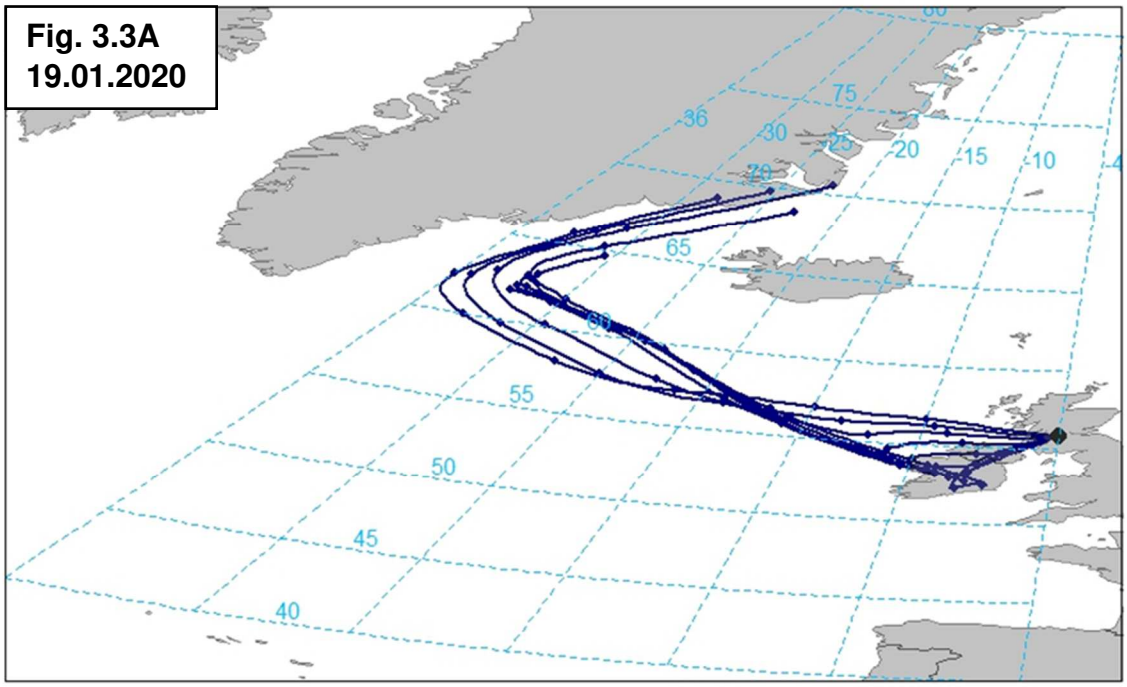

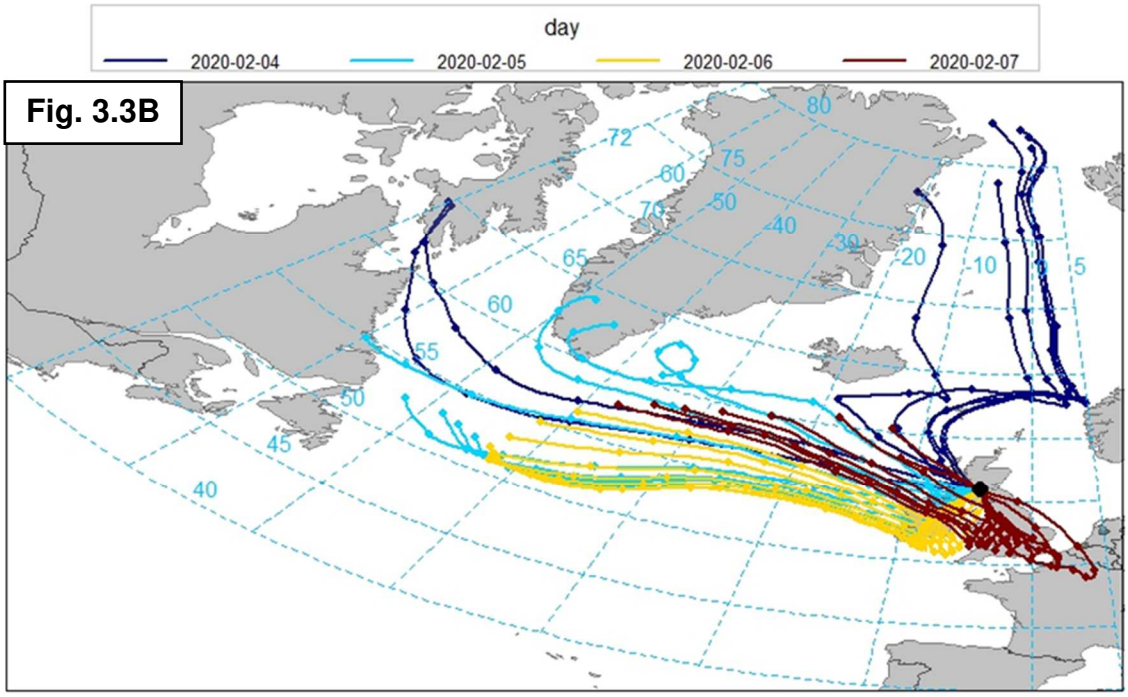

Figures 3.3 A and B. HYSPLIT back trajectories arriving in Glasgow on 19.01.2020 and 04.02.2020 – 07.02.2020. PM_{10} filters that made up sample 4038, were collected on these days. Trajectories for a different date have separate colours.

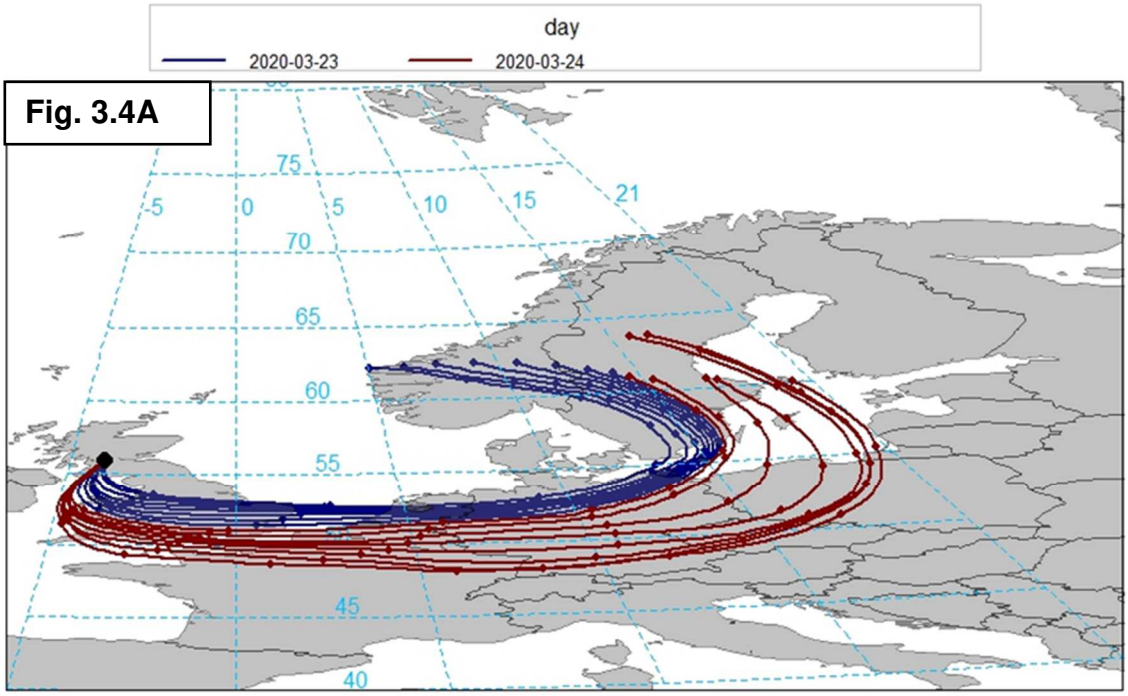

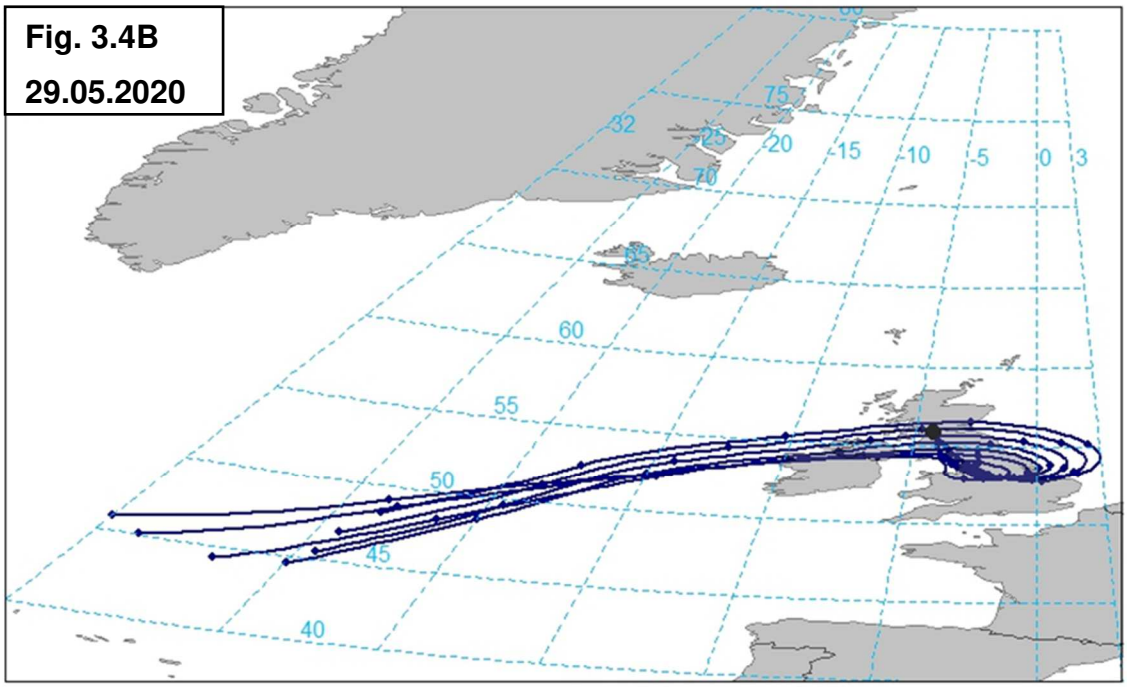

Figures 3.4 A and B. HYSPLIT back trajectories arriving in Glasgow on 23.02.2020, 24.02.2020 and 29.05.2020. PM_{10} filters that made up sample 4043, were collected on these days. Trajectories for more than one date are grouped for each day and coloured accordingly.

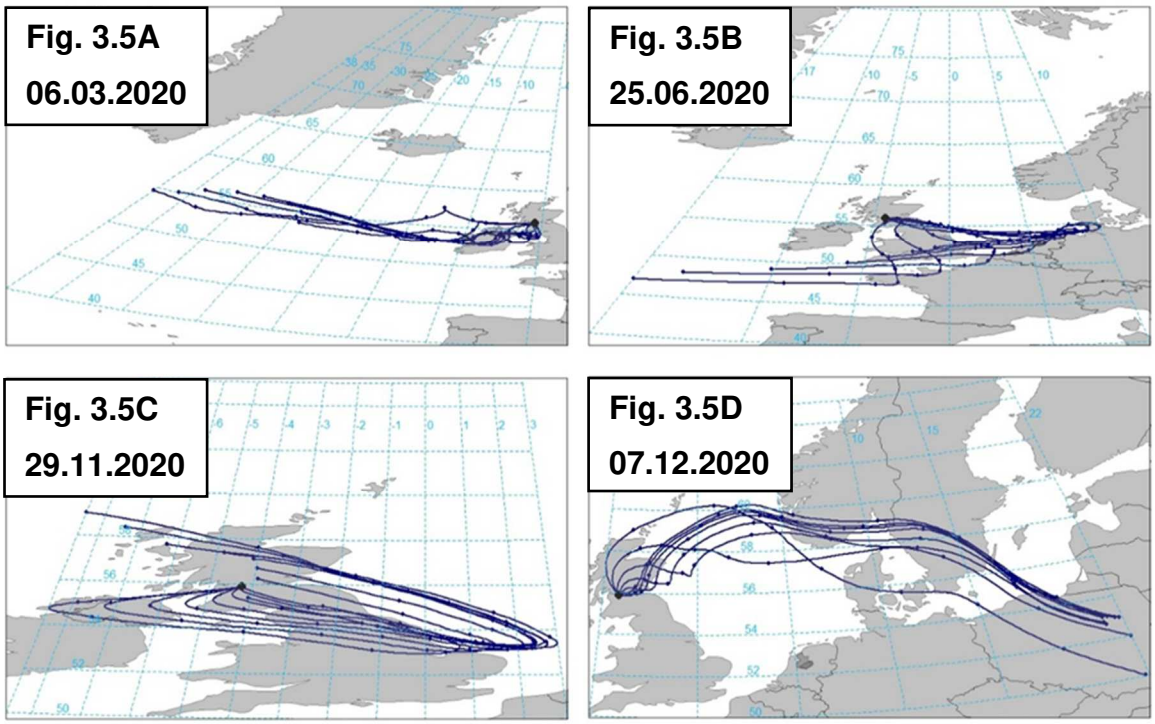

Figure 3.5 A, B, C and D. HYSPLIT back trajectories arriving in Glasgow on 06.03.2020, 25.06.2020, 29.11.2020 and 07.12.2020. $PM_{2.5}$ filters that made up sample 4046, were collected on these days.

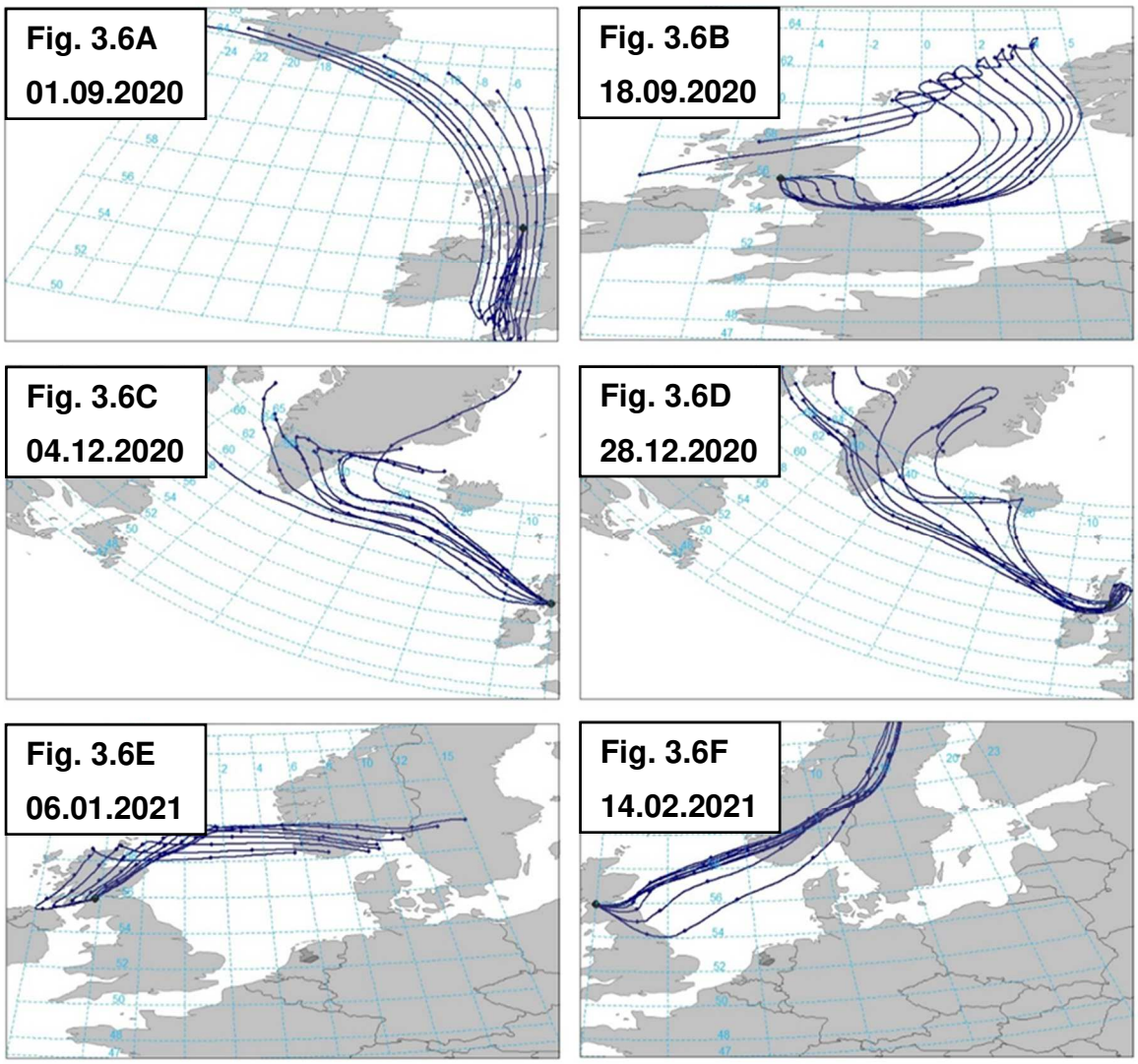

Figures 3.6 A, B, C, D, E and F. HYSPLIT back trajectories arriving in Glasgow on 01.09.2020, 18.09.2020, 04.11.2020, 28.12.2020, 06.01.2021 and 11.02.2021. PM_{10} filters that made up sample 4047, were collected on these days.

Manchester Fallowfield Campus (MAN-FF) PM Samples

MAN-FF is located in Fallowfield to the south of Manchester city centre (Figure 3.7). The sampling area is classified as an urban background site. A Digitel high volume sampler with a $PM_{2.5}$ impactor was used to collect $PM_{2.5}$ at the Manchester Air Quality Super Site at the Environmental Research Station located at Fallowfield Campus. The sampler ran at a flow rate of 1000 L min^{-1} collecting samples on quartz microfibre filters (Whatman™, QMA,150 mm, GE Healthcare Life Sciences). The filters were changed automatically, every two days. The filters collected are detailed in Table 3.5.

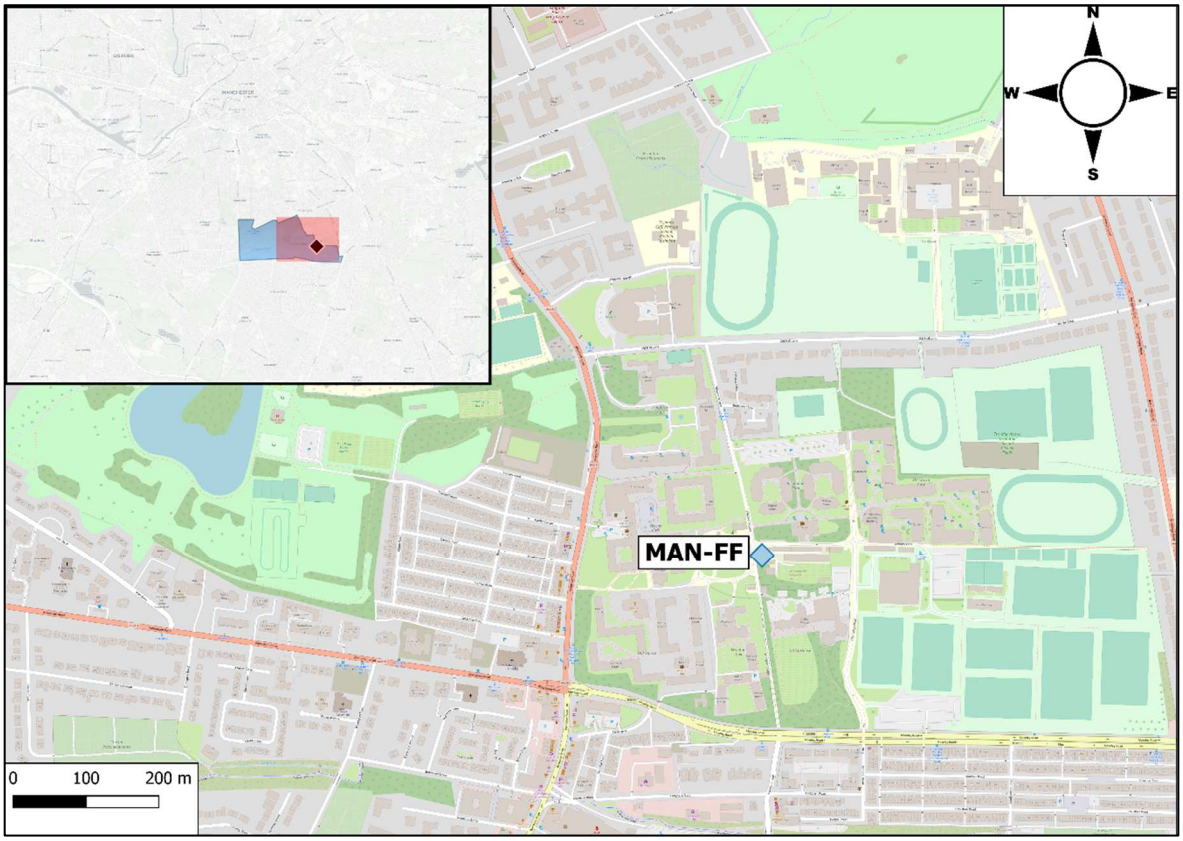

Figure 3.7. Location of MAN-FF sampling site. The map layers used were provided by Esri (Esri Gray light) and OpenTopoMap.

Table 3.5. Filters collected at MAN-FF Campus supersite.

Plate	Sample Code	Date Plate Loaded	Collection Date	Volume of Air Sampled (m^3)
Plate 8	4033	20.11.2019 – 21.11.2019	18.12.2019	1902
Plate 10	4034	24.11.2019 – 25.11.2019	18.12.2019	2880
Plate 11	4035	26.11.2019 –27.11.2019	18.12.2019	2880
Plate 13	4028	30.11.2019 – 01.12.2019	18.12.2019	2880
Plate 14	4036	02.12.2019 – 03.12.2019	18.12.2019	2880
Plate 6	4031	14.12.2019 – 15.12.2019	18.12.2019	2880
Plate 7	4036	16.12.2019 – 18.12.2019	18.12.2019	3706

A summary of the air mass origins for MAN-FF PM samples can be seen in Table 3.6. The 96-hour HYSPLIT back trajectories were calculated and plotted using Open Air, on the dates $PM_{2.5}$ samples were collected from Manchester Fallowfield as seen in the Figure 3.8, Figure 3.9, Figure 3.10, Figure 3.11, Figure 3.12 and Figure 3.13.

Table 3.6. Air mass origins for MAN-FF($PM_{2.5}$) samples.

Sample	Dates	Air Mass Origin Location
4028	30.11.2019 01.12.2019	North Sea
4031	14.12.2019 15.12.2019	Greenland Sea, Barents Sea, North Atlantic Ocean Quebec - Canada
4032	16.12.2019 17.12.2019 18.12.2019	Quebec – Canada, Greenland, North Atlantic Ocean Quebec – Canada, Greenland, Iceland, North Atlantic Ocean Greenland, Iceland, North Atlantic Ocean
4033	20.11.2019 21.11.2019	North Atlantic Ocean
4034	24.11.2019 25.11.2019	Europe Europe, North Atlantic Ocean
4035	26.11.2019 27.11.2019	North Atlantic Ocean
4036	02.12.2019 03.12.2019	North Atlantic Ocean

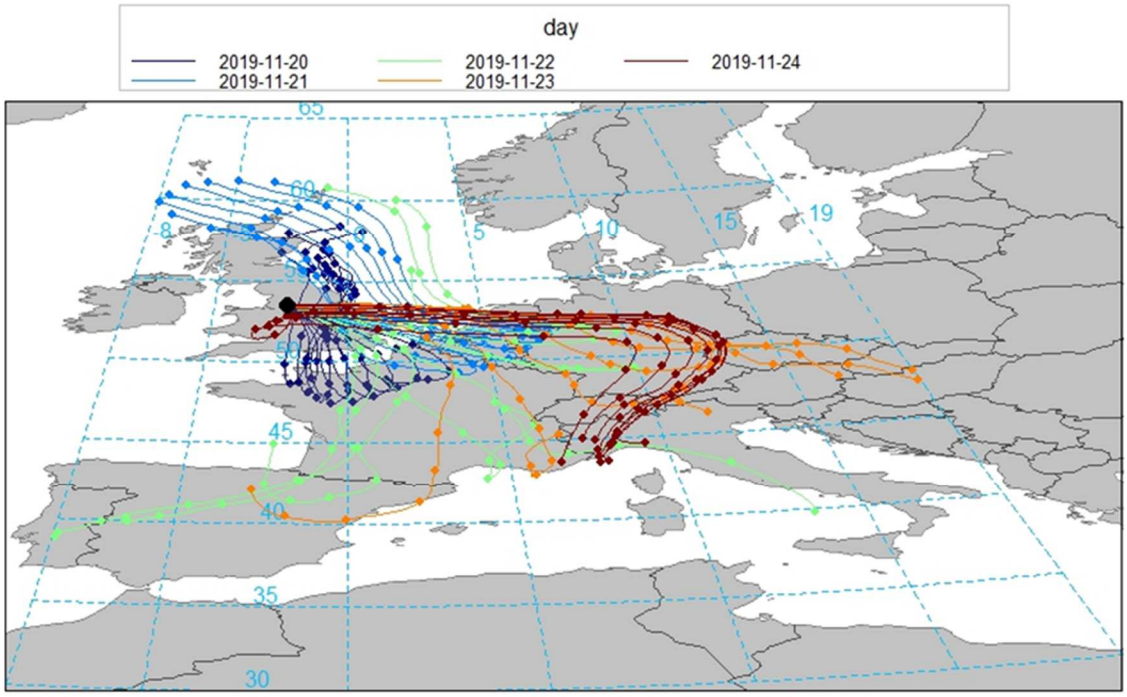

Figure 3.8. 96-hour HYSPLIT back trajectories arriving in Manchester Fallowfield Campus from 20/11/2019 to 24/11/2019. The trajectories are grouped for each day and coloured accordingly.

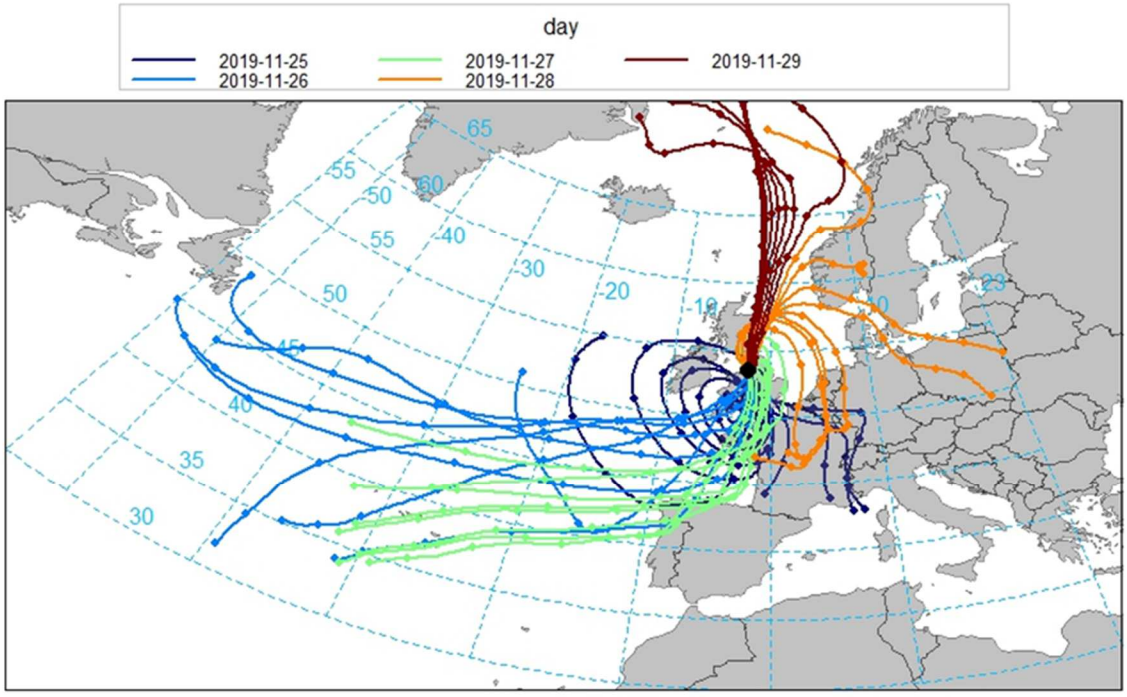

Figure 3.9. 96-hour HYSPLIT back trajectories arriving in Manchester Fallowfield Campus from 25/11/2019 to 29/11/2019. The trajectories are grouped for each day and coloured accordingly.

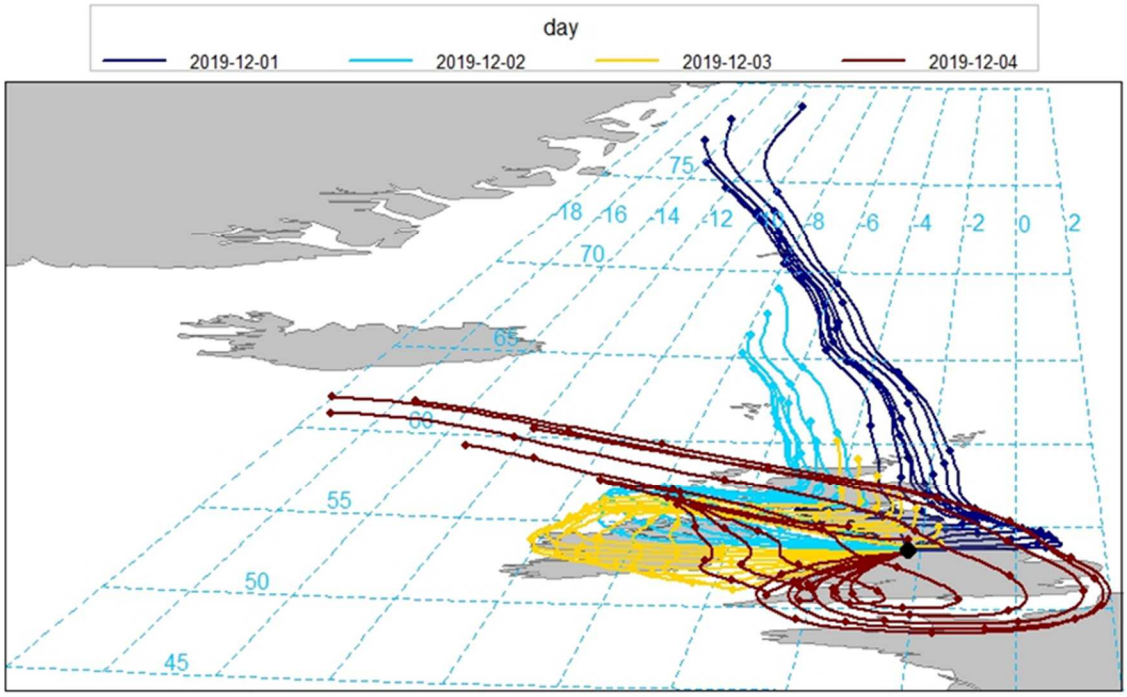

Figure 3.10. 96-hour HYSPLIT back trajectories arriving in Manchester Fallowfield Campus from 01/12/2019 to 04/12/2019. There was not enough data available to plot trajectories for 30/11/2019. The trajectories are grouped for each day and coloured accordingly.

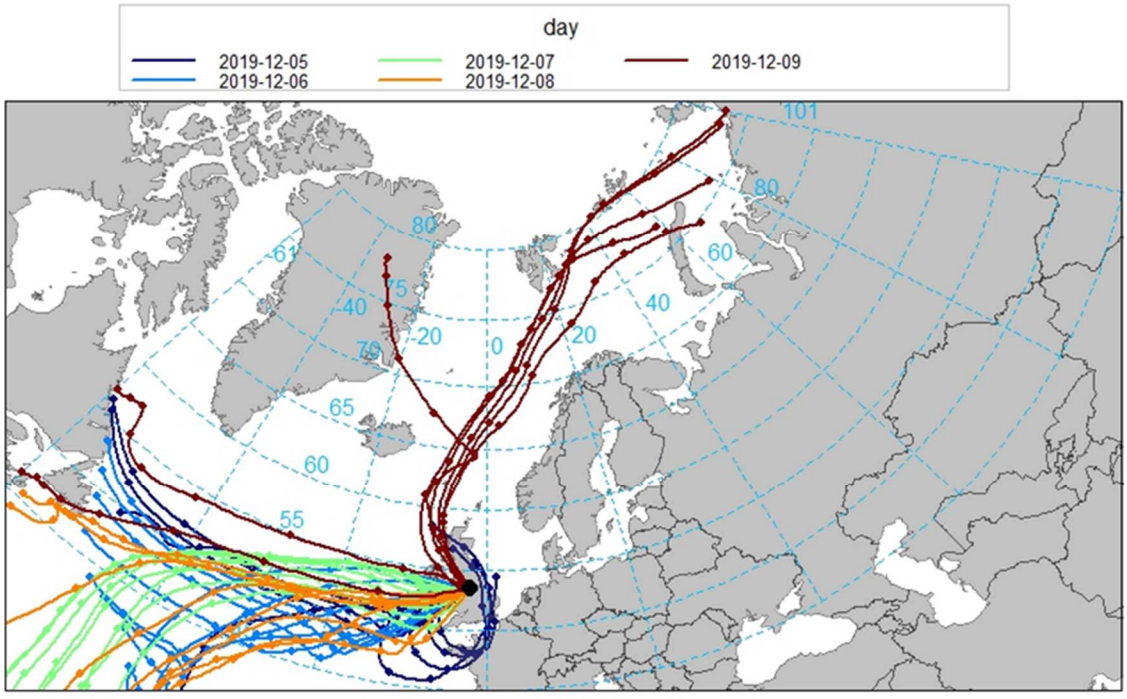

Figure 3.11. 96-hour HYSPLIT back trajectories arriving in Manchester Fallowfield Campus from 05/12/2019 to 09/12/2019. The trajectories are grouped for each day and coloured accordingly.

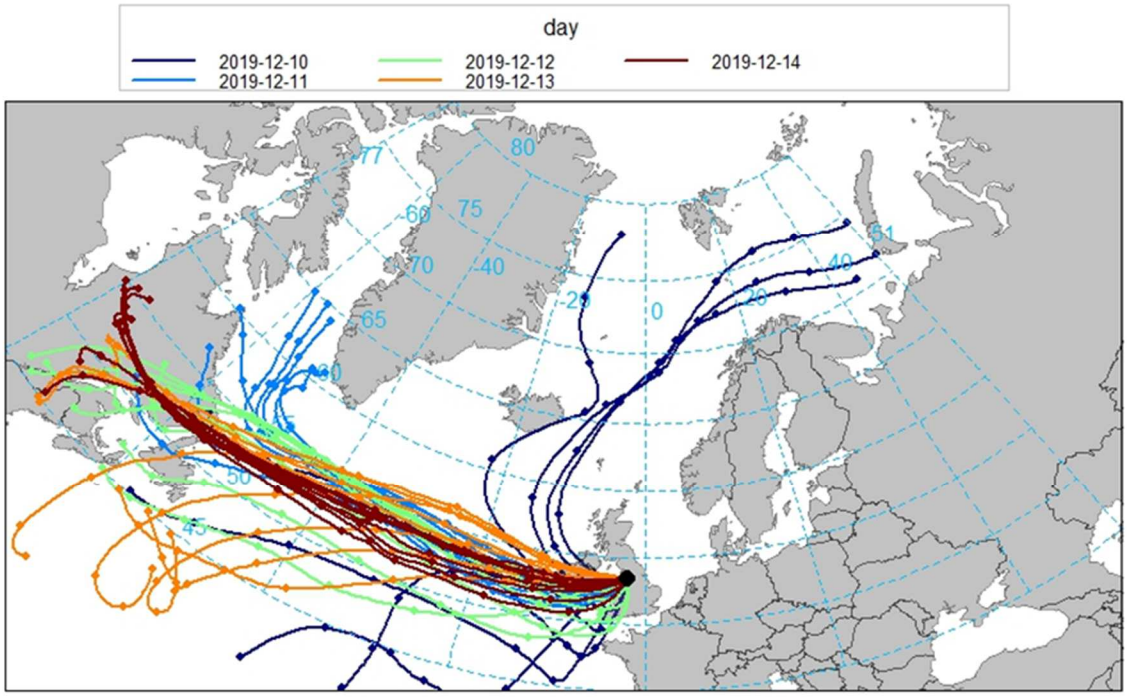

Figure 3.12. 96-hour HYSPLIT back trajectories arriving in Manchester Fallowfield Campus from 10/12/2019 to 14/12/2019. The trajectories are grouped for each day and coloured accordingly.

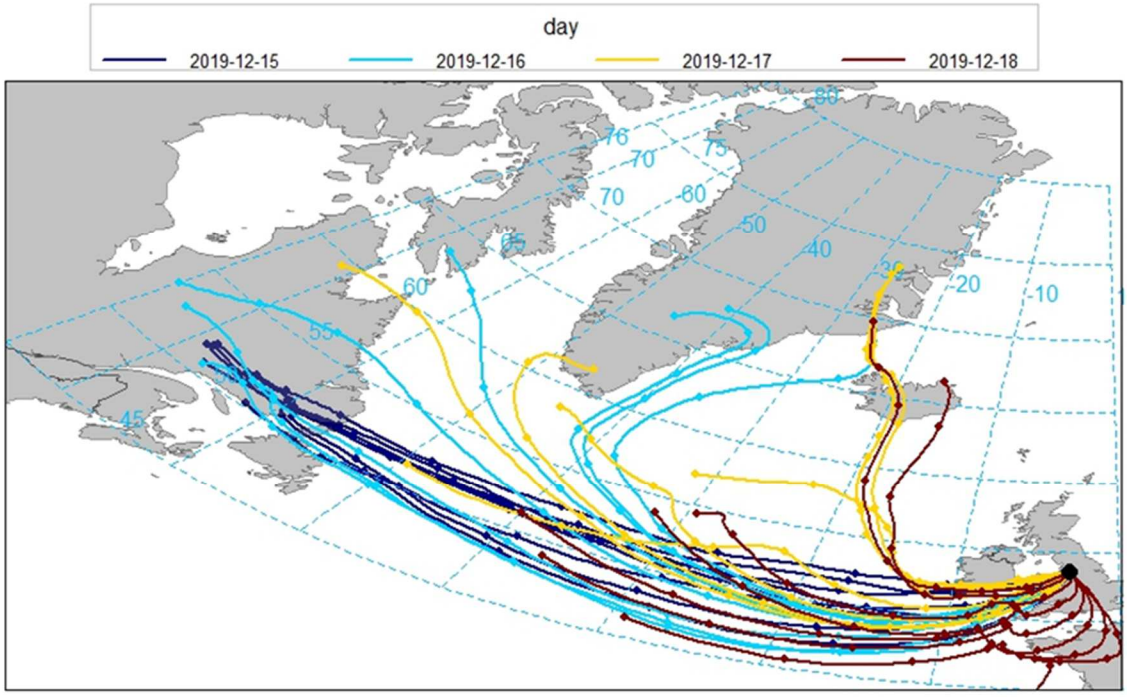

Figure 3.13. 96-hour HYSPLIT back trajectories arriving in Manchester Fallowfield Campus from 15/12/2019 to 18/12/2019. The trajectories are grouped for each day and coloured accordingly.

3.2.3. Materials: GC-MS Analysis Chemicals and Materials

The following organic solvents were utilised for sample preparation as described in Table 3.7: extra pure acetone, dichloromethane (DCM) for HPLC stabilised with amylene, methanol certified AR for analysis, n-hexane ~95 % for HPLC, toluene analytical reagent grade (all reagents were Fisher Scientific, UK).

Table 3.7. The usage of each solvent in the sample preparation process.

Solvent	Use
Acetone	• Accelerated Solvent Extraction • Columns; elution of alcohols and polar compounds (1:1 v/v acetone, methanol)
DCM	• Columns; elution of aromatics • Solvent used for aromatic fraction during analysis
Methanol	• Substitute solvent for aromatic fraction during analysis • Columns; elution of alcohols and polar compounds (1:1 v/v acetone, methanol)
n-Hexane	• Columns; elution of n-alkanes • Solvent used for alkane fraction during analysis
Toluene	Substitute solvent for aromatic fraction during analysis

The Accelerated Solvent Extraction (ASE) caps were lined with glass fibre filters (Thermo Scientific, USA). The void space in the ASE cells was filled with combusted sand (450 ºC for 8 hours), which was extra pure, low iron and 40-100 mesh (Fisher Scientific, UK). Chromatography columns were modified from combusted (450 ºC for 8 hours) borosilicate Pasteur pipettes with fine 4 μm quartz wool used as a filter (Acros Organics, USA). The columns were filled with chromatography grade silica gel with a particle size of 35-70 μm (Fisher Scientific, UK).

A calibration standard containing the 16 priority PAHs was purchased from Merck (Supelco®, 10 μg mL^{-1}, 1 mL in acetonitrile). Two batches of the internal standard 2-methylnapthalene were utilised. The first batch was purchased in solid form, and stock solutions were made up with methanol using volumetric flasks (Alfa Aesar, USA). The second batch was in solution (Merck, Supelco®, 1000 μg mL^{-1}, 1 mL in methanol) and was diluted using a volumetric flask (10 mL) to 100 μg mL^{-1}, producing stock solution A. Stock

solution A was then further diluted to stock solution B (50 μg mL^{-1}) and stock solution C (25 μg $mL^{-1)}$, using volumetric flasks (10 mL).

A calibration standard for alkane analysis was custom made (LGC, UK), from here on it will be referred to as the BECS standard. It contained the following alkanes at a concentration of 10 μg mL^{-1}: n-hexadecane $C_{16}H_{34}$, n-octadecane $C_{18}H_{38}$, n-nonadecane $C_{19}H_{40}$, n-tricosane $C_{23}H_{48}$, n-pentacosane $C_{25}H_{52}$, n-hexacosane $C_{26}H_{54}$, n-octacosane $C_{28}H_{58}$, n-triacontane $C_{30}H_{62}$, n-dotriacontane $C_{32}H_{66}$ and n-heptatriacontane $C_{37}H_{76}$.

3.2.4. Methodology: Gas Chromatography Mass Spectrometry Analysis of Polycyclic Aromatic Hydrocarbons and n-Alkanes

Sample Preparation for n-Alkane and PAH Analysis

Sample Extraction

The sample preparation method was decided through the comparison test which can be found in Appendix Ib. Samples were extracted using the Dionex ASE 350 Accelerated Solvent Extractor. Pre-combusted glass fibre filters were fitted into each cell cap. The pre-weighed sample was transferred into the ASE cell and then filled to the top with combusted sand. Pre-combusted glass vials (60 mL) were placed into the loading tray underneath the ASE cells to collect the total lipid extract (TLE). The ASE instrument settings are listed in Table 3.8.

Table 3.8. Set parameters for ASE.

Solvent	Hexane and acetone 2:1
System Pressure	14 MPa (1500 psi)
Oven Temperature	100 °C
Oven Heat-up Time	5 min
Static Time	5 min
Rinse Volume	60 % cell volume
Nitrogen purge	1 MPa (150 psi) for 60 s
Number of Cycles	2
Cell Type	Stainless Steel
Solvent Saver	Off

Once the TLE collection was complete, the solvent was evaporated completely under nitrogen gas in a Caliper TurboVap LV Evaporator at 30 °C for 15 minutes. The extracted

TLE was then transferred into an 8 mL glass vial with a Pasteur pipette and dried completely using a sample concentrator (Techne Dri-block DB3) which used nitrogen gas and heated blocks at 30 °C to evaporate the solvent. Once the vial had cooled to room temperature the dried TLE was weighed. The mass of the recovered TLE had to be ~10 mg to ensure the column was not over-saturated. If the TLE mass was considerably greater than 10 mg then it was split into two aliquots as follows. First, a known amount of DCM was added and the resulting solution ultrasonicated to ensure the TLE was fully dissolved. This was then split into two aliquots using a Hamilton glass syringe, with one aliquot run through the column and the other archived. The TLE used for the column was dried again and left to reach room temperature, then weighed.

Column Chromatography for Compound Separation

Columns were prepared using combusted Pasteur pipettes. The pipette tips were shortened using a glass cutter so that the capillary tube was around 6 cm long. Glass wool was placed into the pipette as a filter, followed by silica (~4 cm) and combusted sand (~0.5 cm placed at the top). The column was cleaned with hexane (~4 mL) before use. Meanwhile, the TLE was redissolved in hexane (~200 µL, x3) and then pipetted into the column. To elute the aliphatic hydrocarbons, hexane (4 mL) was used. For the aromatics, DCM (4 mL) was used. To elute the alcohols and polar compounds, a 1:1 v/v solution of acetone and methanol was used. The alcohol and polar fractions were not analysed here but were archived.

The eluted alkane and aromatic fractions were dried under nitrogen gas at room temperature. The aromatic fraction was redissolved in DCM (40 µL) and transferred to an insert within a GC vial. An internal standard of 2-methylnapthalene (50 µg mL^{-1},10 µL) was added to each insert giving a total volume of 50 µL. The volumes were changed later in the project to 30 µL DCM and 20 µL 2-methylnapthalene (25 µg mL^{-1}) to reduce the pipetting error of the internal standard by increasing the volume. The solvent was changed to toluene and methanol for certain batches due to a malfunction in the temperature control of the GC-MS laboratory during this work, with the result that a solvent with a greater boiling point was required for these batches. The alkane fractions were transferred to an insert within a GC vial using hexane (50 µL). The GC vials were loaded into the sampling tray before running samples in sequence.

Instrument Conditions

GC-MS Instrument and Conditions

A GC-MS system (Agilent Technologies 7890B GC System coupled with an Agilent Technologies 5977A mass selective detector, U.S.A) equipped with a HP1-MS non-polar 100 % dimethylpolysiloxane capillary column (60 m x 0.25 mm x 0.25 µm) was used for analysis of the aromatic extracts. High purity helium (CP grade 99.99 %) was used as a carrier gas at constant flow 1.2 mL min^{-1}, a temperature program was used to achieve separation of complex mixtures (Appendix Ic). Identification of peaks were based on key fragment ions compared with those in the PAH standard. Selected ion mode (SIM) was used for quantification. Detailed information about the GC-MS parameters is listed in Appendix Ic.

GC-FID Instrument and Conditions

A GC-FID System (Agilent Technologies 7890B GC System coupled with a flame ionisation detector) equipped with an RTX-1 non-polar phase, cross-bonded dimethyl polysiloxane column (60 m x 0.25 mm x 0.25 µm) was used for analysis of the alkane extracts. High purity helium (CP grade 99.99 %) was used as a carrier gas at a constant flow of 1.2 mL min^{-1}. Detailed information about the GC-FID parameters is listed in Appendix Ic. Confirmation and identification of the target compounds was carried out on the GC-FID using the n-alkane calibration standard.

GC-MS and GC-FID Data Analysis

Calibration Curves

Calibration curves were constructed on the day of analysis to avoid any issues associated with any instrumental drift (Denis et al., 2012). Calibration curves for PAHs were constructed using concentrations of 2.0, 4.0, 6.0 and 8.0 µg mL^{-1} of the 16 priority PAHs standard. Co-elution occurred for two PAHs: dibenzo(a,h)anthracene and indeno(1,2,3-c,d)pyrene. However, as the two PAHs had different quantifier ions, separate signals could be obtained by using the extracted ion chromatogram tool on Agilent ChemStation. The linear regression fit to the calibration curve was rearranged to determine the concentration of the unknown. The intercept was set to 0 if the R^2 of the linear regression did not decrease by more than 0.01. Calibration equations and R^2 values per batch are given in Appendix Id. In general, the quality of calibration curves was good, with R^2 values 0.99 for most batches,

but there were instances where R^2 was lower, which meant the uncertainties associated with calculated concentrations for these batches were larger.

An internal standard was used in conjunction with the external calibration curve to increase quantification accuracy by accounting for volume change before analysis and other random variations in the analytical procedure. The calibration curve was formed by dividing the concentrations of the standards by the concentration of the internal standard (10 μg mL^{-1}) and dividing the peak areas of the standards by the peak area of the internal standard (see Equation 3).

$$\frac{Peak\ area\ of\ Calibration\ Standard}{Peak\ area\ of\ I.S.} = Gradient\ \frac{Concentration\ of\ Calibration\ Standard}{Concentration\ of\ I.S.} + intercept \quad (3)$$

Once the equation is rearranged as shown in Equation 4 the concentration of the sample can be calculated.

$$\frac{(\frac{Peak\ area\ of\ Sample}{Peak\ area\ of\ I.S.} - intercept\ ) \times Concentration\ of\ I.S.)}{Gradient} = Concentration\ of\ Sample\ (\mu g\ mL^{-1}) \quad (4)$$

Some samples were re-run due to certain issues such as non-linear calibration curves and a reduction in peak area signals for HMW PAHs caused by accumulation of residue on the GC liner. For samples that were re-run, the internal standard was not used for quantification. This was because the sample initially contained 10 μg mL^{-1} of internal standard during the first run but this compound could have degraded and/or evaporated in storage due to the volatile nature of the internal standard, before it was re-run for a second time. An example chromatogram is shown in Figure 3.14 of the PAH standard at a concentration of 8 μg mL^{-1}.

For n-alkanes, external calibration curves were formed using four concentrations 2.5, 5.0, 7.5 and 10 μg mL^{-1} of the BECS standard. The calibration curves were constructed by selecting signals for 3 out of 10 of the n-alkanes present in the BECS standard ($C_{16}H_{34}$, $C_{23}H_{48}$ and $C_{30}H_{62}$). The $C_{16}H_{34}$ calibration curve was used to quantify n-alkanes in samples

ranging from $C_{16}H_{34}$ – $C_{24}H_{50}$, $C_{23}H_{48}$ was used for alkanes from $C_{25}H_{52}$ – $C_{33}H_{68}$ and $C_{30}H_{62}$ was used for alkanes of $C_{34}H_{70}$ and above. Internal standards were not used for alkane quantification due to the stability of these compounds in comparison to PAH compounds. The intercept was set at 0 for all calibration curves. An example chromatogram is shown in Figure 3.15 of the BECS standard at a concentration of 10 µg mL^{-1}. Calibration equations and R^2 values per batch can be found in Appendix Id. The quality of calibration curves were good, with R^2 values of 0.99 for all batches.

Quantification

Chromatographic peak areas of each analyte were integrated using the Agilent ChemStation software for PAHs and Agilent OpenLab for n-alkanes. Quantification was completed using Microsoft Excel - Office 365 by inputting peak areas and applying linear regression equations from calibration curves to determine PAH and n-alkane concentrations. The peak area was converted into concentrations (µg mL^{-1}) then to µg g^{-1} and ng m^{-3}.

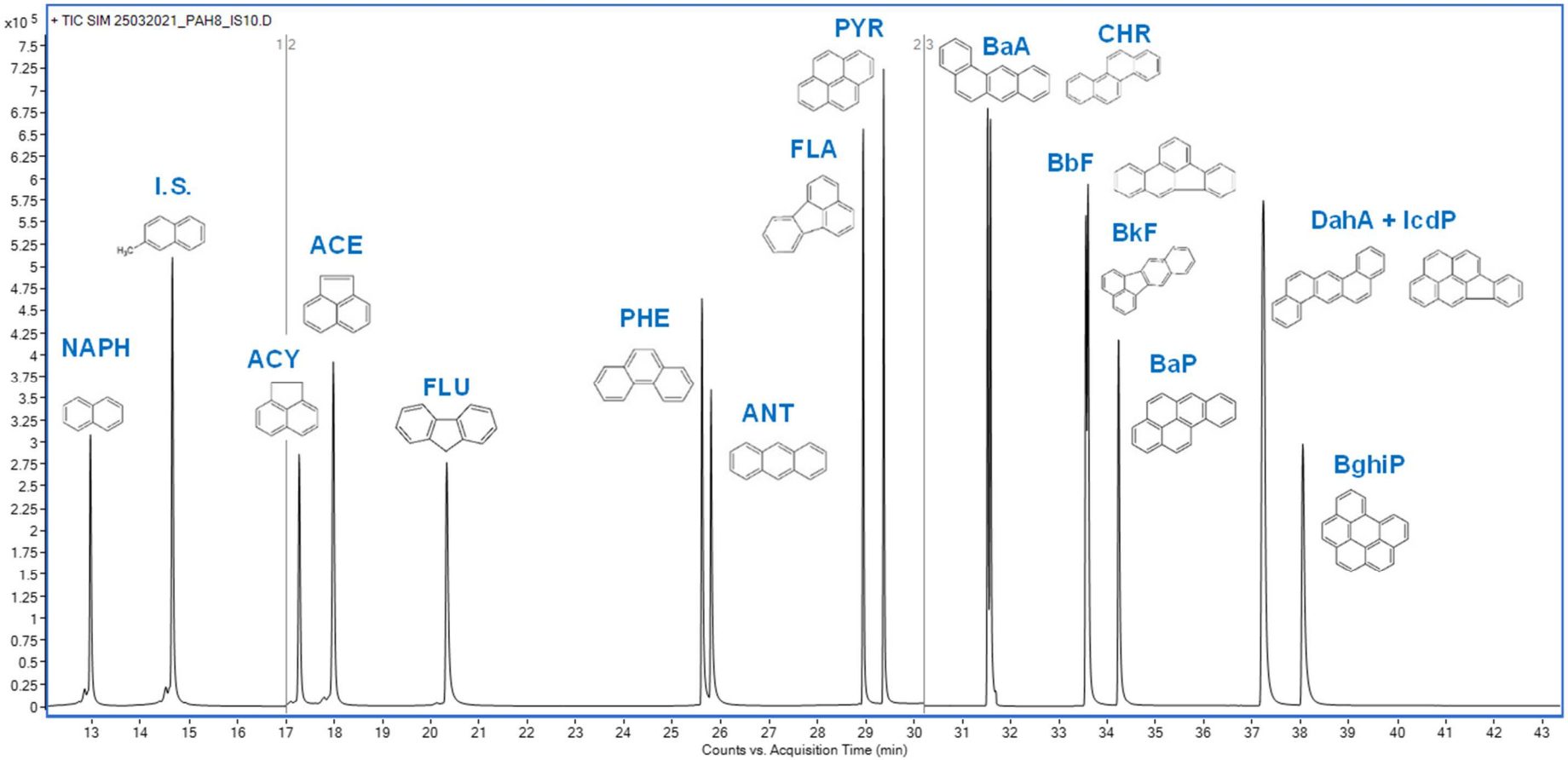

Figure 3.14. Chromatogram of the PAH standard consisting of the 16 priority PAHs (8 µg mL^{-1}) and the internal standard 2-methylnaphthalene (10 µg mL^{-1}).

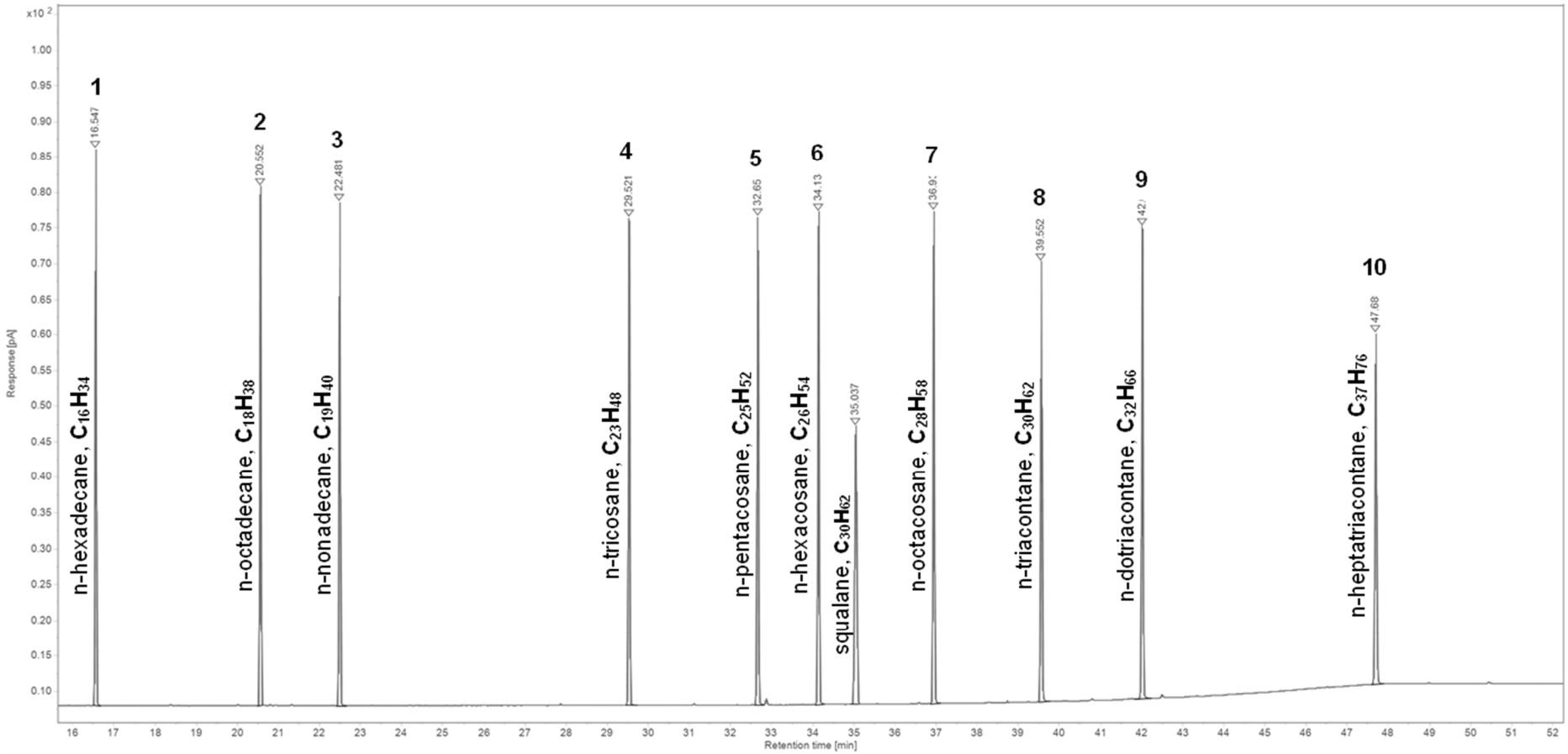

Figure 3.15. Chromatogram of the BECS standard consisting of 10 n-alkanes and squalane at a concentration of 10 µg mL^{-1}.

3.2.5. Methodology: Quality Control of Analytical Procedures

Internal Standard Checks

As described above for PAH calibration curves, an internal standard (IS) was used (details of standard composition as described above). Recovery checks were done using the IS to ensure the calibration curve was returning accurate concentrations. Within each PAH standard (2, 4, 6, 8 µg mL^{-1}) a known concentration of IS was added to the solution using a gas-syringe (10 µg mL^{-1}), which allowed for quality checks to be completed on the calibration curves by using the average IS GC-MS signal per analysis batch. Precision checks were completed by determining the relative standard deviation (RSD%) of the IS GC-MS signal to determine the repeatability as well as the reproducibility. The control chart for the IS GC-MS signals (see Figure 3.16) from the analysis of the PAH calibration standards showed most of the IS signals across batches were within 1 SD of each other. However, batch 9's IS GC-MS signals were beyond the upper control limit (3 SD above the average concentration). Therefore, for this batch the IS was not used, as it could cause positive biases in calculated concentrations. The relative standard deviations of the internal standard were all below 12.3 % except from batch 9 which was at 25.7 %.

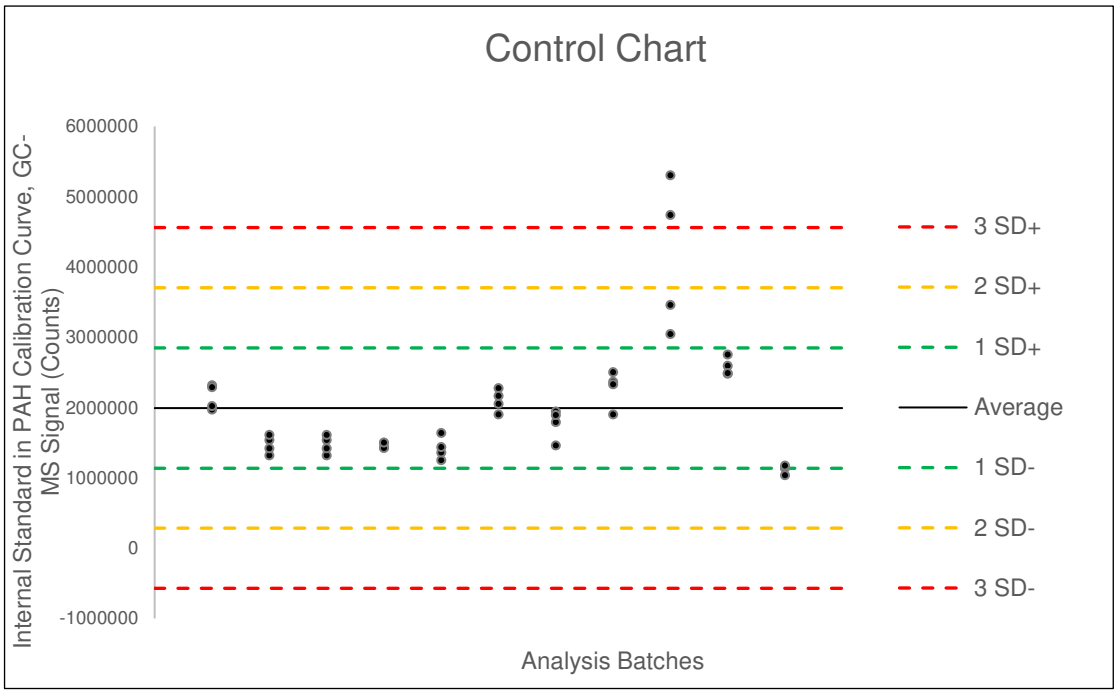

Figure 3.16. A control chart, plotting the I.S. signals in each of the PAH calibration standards, which were run per analysis batch.

Accuracy and Precision

Accuracy and precision checks were conducted on CRMs (DS, FD, UD and UPM) which had similar matrices to airborne ambient PM samples that were collected for analysis.

Table 3.9 shows the recoveries for UD. UD was run four times throughout the analysis period to ensure that the accuracy was periodically checked, in-between different analysis batches. The calculated concentration was divided by the certified reference values for each PAH within each CRM, to determine the recovery of PAHs from the GC-MS method. For precision, the RSD% was calculated for UD measurements made on the same day to assess the repeatability. For reproducibility, the RSD% was calculated for UD measurements made on different days.

Table 3.9. The recoveries (%) for the 3 UD replicates throughout the analysis period. Concentrations reported for LMW PAHs were less accurate than those for MMW and HMW PAHs.

	Urban Dust Recoveries (%)		
	Run 1	Run 2	Run 3
NAPH	8	0	3
ACY	30	0	41
ACE	15	0	0
FLU	0	41	18
PHEN	*Co-eluted	86	11
ANTH	55	66	43
FLA	53	77	70
PYR	50	71	15
BaA	*Co-eluted	*Co-eluted	99
CHRY	36	66	108
BbF	103	*Co-eluted	*Co-eluted
BkF	*Co-eluted	64	79
BaP	115	90	100
DahA	144	108	174
IcdP	55	66	65
BghiP	64	76	82

* "Co-eluted" indicates co-elution of the following pairs of peaks: PHEN & ANTH, BaA & CHR, and BbF & BkF. The recoveries of co-eluted peaks were calculated by comparing the concentration of the co-eluted peak against the sum of the certified concentrations of the two PAHs that co-eluted. Where the recovery is noted as "0.00" the PAH was undetected due to either a small unquantifiable peak or the absence of a peak.

The repeatability was inferred from two replicate UD measurements that were run on the same day by calculating the RSD%. The repeatability was calculated based on 'grouped' concentrations when the following peaks co-eluted: PHEN & ANTH, BaA & CHR and BbF & BkF. FLU was not detected in either replicate thus RSD% could not be calculated. The calculated RSD% values were low for ACY, BbF & BkF, BaP, DahA, IcdP and BghiP, ranging from 6 to 15 % indicating repeatable results. For ACE, ANTH, FLA and PYR the RSD% was higher with a range of 29 – 56 % indicating poor repeatability. The reproducibility was assessed by calculating the RSD% from three different measurements on different days. The reproducibility was acceptable for most PAHs ranging between 8 to 25 %. However, for NAPH, FLU, PHEN, and PYR the RSD% was very high, with a range of 39 – 77 %.

The PAH recoveries for other CRMs (DS, FD and UPM) were calculated (see Table 3.10) DS had low recoveries overall with the LMW PAHs being undetected. The MMW PAHs in DS however were more easily liberated from the sample matrix with recoveries of 35 to 61 %. The HMW PAHs in DS had low recoveries of 0 to 30 %. The recoveries for UPM were similar to UD for example recoveries for LMW PAHs ranged from 0 to 108 %. MMW PAHs had recoveries from 32 to 58 % and for HMW PAHs 63 to 243 %. FD did not contain LMW PAHs NAPH – FLU, but the recovery for PHEN and ANTH was 44 and 57 % For MMW PAHs the recoveries were 46 to 80 % and for HMW PAHs 45 to 127%. This shows that most PAHs especially LMW PAHs, are likely to have underreported concentrations. However, PAHs with recoveries over 100 % are likely to have positive biases in reported concentrations such as BaP.

Table 3.10. The recoveries (%) of the method assessed by the analysis of DS, UPM and FD. The accuracy was calculated by comparing measured concentrations to certified concentrations.

	DS	UPM	FD
NAPH	0	2	-
ACY	-	54	-
ACE	0	10	-
FLU	0	0.00	-
PHEN	30	Co-eluted	44
ANTH	Co-eluted	108	57
FLA	35	57	52
PYR	61	58	46
BaA	Co-eluted	32	74
CHRY	57	Co-eluted	80
BbF	21	138	Co-eluted
BkF	Co-eluted	Co-eluted	82
BaP	0	243	127
DahA	77	156	75
IcdP	44	63	45
BghiP	30	75	47

* "Co-eluted" indicates co-elution of the following pairs of peaks: PHEN & ANTH, BaA & CHR, and BbF & BkF. The recoveries of co-eluted peaks were calculated by comparing the concentration of the co-eluted peak against the sum of the certified concentrations of the two PAHs that co-eluted. Where the recovery is noted as "0.00" the PAH was undetected due to either a small unquantifiable peak or the absence of a peak.

Overall, the method resulted in low recoveries, poor reproducibility and repeatability for LMW PAHs NAPH-ANTH across all standards, with LMW PAHs being undetected in some runs. This could be due to analyte loss during sample preparation steps. LMW PAHs have much higher vapour pressures than MMW and HMW PAHs, so are much more likely to evaporate during preparation steps such as drying and extraction thus leading to low recoveries/accuracies (Bandowe et al., 2014; Elorduy et al., 2018; Tan et al., 2006; Wang et al., 2006). Elorduy et al. (2018), also reported low accuracies in UD recovery for some of the LMW PAHS: NAPH 17 %, ACY 25 %, ACE 31 % and FLU 35 %. The low precision of LMW PAHs (NAPH, ACE, FLU, PHEN, ANTH) can also be explained by the nature of LMW PAHs, leading to inconsistent results. Therefore, use of the method would result in

negative biases in reported LMW PAH concentrations. Recoveries for all other PAHs across all CRMs except DS ranged from 31 % - 96 %. PAHs DahA, BaP and BbF and BkF had high recoveries exceeding 100 %. The peak areas of DahA co-eluted with IcdP, therefore, to determine the peak area, the chromatogram needed to be extracted using the software. This could have led to high uncertainties in peak area, hence resulting in a recovery over 100 %. With regards to BaP, it could have possibly co-eluted with benzo(e)pyrene BeP, which was also present in UPM and had the same ions in the *m*/*z* spectrum. If this was the case, the adjusted recovery for the co-eluted peak would be 84 %, therefore within an acceptable range. BbF & BkF also had higher recoveries which could be caused by co-elution of the peaks causing inaccuracies in quantification.

DS recoveries had lower accuracies, perhaps due to the sample matrix as the PAHs are possibly more strongly bound to the ordered graphitic structure. During ASE, solid particles are supposed to remain in the ASE cell, but because DS contained such fine particles, the particles would be found in the total lipid extract (TLE), meaning difficulties were experienced during solvent extraction. This could be due to the extraction efficiency of the solvents that were used (hexane and acetone 1:1), as Piñeiro-Iglesias et al. (2002) found DCM was more effective at extracting PAHs from diesel PM, as SEM images showed laminar structures after extraction, as opposed to fewer laminar structures and many individual particles, when using 1:1 hexane and acetone. Furthermore, the solvents were unable to extract HMW PAHs, as these had low accuracies. Turrio-Baldassarri et al. (2003) stated that the extraction of PAHs from diesel PM was a demanding task, due to the strength of adsorption of the planar, aromatic structure of these molecules to the carbonaceous semi-graphitic surface of the particles. In their research they utilised high temperatures (180°C), high pressures (15.2 MPa), long extraction times (20 minutes) and unconventional solvents (toluene) to extract HMW PAHs. Despite such severe conditions, the recovery yields of some deuterated standards were below 100 % (Turrio-Baldassarri et al., 2003).

Summary

The quality control activities indicated the analytical method had limitations for LMW PAHs, better suiting MMW and HMW PAHs. The method required optimisation in terms of processing LMW and HMW PAHs differently, potentially by extracting PAHs twice, first by using gentler extraction methods (lower temperatures, pressures, shorter extraction times) which can extract LMW/MMW PAHs, and the second time using harsher extraction methods

to extract MMW/HMW PAHs. The two extracts could also be treated differently in terms of gentler drying conditions for the LMW PAHs. Once analysed, and after data acquisition and quantification, the concentrations of each PAH in the two extracts would be summed to give a total PAH concentration. However, this would increase analysis time and reduce sample throughput. As a result, the uncertainties were taken into account and where PAH concentrations for LMW PAHs were reported, it would be noted that negative biases in LMW PAH concentrations were likely, hence actual PAH concentrations were likely to be higher. With regards to DahA, BaP and BbF/BkF, positive biases could be expected in reported PAH concentrations and were noted alongside uncertainty values. The analytical method showed good repeatability and reproducibility for most MMW and HMW PAHs, therefore it was likely other aspects in the method required optimisation e.g., ASE parameters, solvents used, solvent ratios etc. However, for the scope of this project, the MMW and HMW were more important for determination of health risks associated to inhalation of PM-bound PAHs. Moreover, PAH concentrations were used semi-quantitatively for example PAH ring-size distributions look at the percentage of certain PAHs rather than absolute numbers. Additionally, PAH ratios examine the relative proportions of certain PAHs. Where PAH ratios relied on LMW PAHs, these PAH DRs were not utilised. Therefore, the method was not optimised, and the shortcomings of the method were taken into account and considered during interpretations of results.

3.2.6. Methodology: PAH and n-Alkane Source Indicators

Source Indicators for PAHs

For source identification, a range of PAH diagnostic ratios (DRs) can be used. However, as discussed in Section 3.2.5 the methods used here resulted in low and inconsistent recoveries of LMW PAHs, therefore certain PAH DRs were not used based on the quality control tests. Moreover, LMW PAHs are more susceptible to photochemical oxidation and thermal decomposition (Pehnec et al., 2016). When photochemical reaction rates vary, this can lead to inaccurate PAH DRs. Tobiszewski and Namieśnik (2012) criticized the reliability of the ANTH/PHEN DR due to the reported differential in photochemical reaction rates of the two congeners (Masri et al., 2018). Table 3.11 shows the different PAH DRs and reasons for not using certain PAH DRs; for example, LMW PAHs/HMW PAHs was not used as it specifically included LMW PAHs group for proportion comparisons. The PAH DRs used

were combustion PAHs/total PAHs denoted as PAH-DR-1, IcdP/(IcdP+BghiP) denoted as PAH-DR-2 and BaP/Bghi PAH-DR-3.

Table 3.11. PAH DRs and the sources they can determine. The table includes the reasoning behind certain PAH DRs not being used.

Ratio	Sources	References	Tested Used?
LMW PAHs/HMW PAHs	<1 pyrogenic sources >1 petrogenic sources	Cuadras et al. (2016)	No Takes LMW PAHs group into account
Combustion PAHs/Total PAHs	~1 combustion sources	Ravindra et al. (2008a) Cuadras et al. (2016)	Yes
FLU/(FLU+PYR)	<0.5 petrol >0.5 diesel	Cuadras et al. (2016)	No FLU is a LMW PAH
FLA/(FLA+PYR)	<0.4 petrogenic 0.4 – 0.5 fossil fuel >0.5 grass/wood/coal combustion	Kubo et al. (2020) Alves et al. (2017)	No Low precision for FLA and PYR
ANTH/(ANTH+PHEN)	<0.1 petrogenic >0.1 pyrogenic	Cuadras et al. (2016)	No Co-elution of ANTH and PHEN
BaA/(BaA + CHRY)	<0.2 petrogenic >0.35 combustion	Alves et al. (2017) Sánchez-Piñero et al. (2021)	No Co-elution of BaA and CHRY
IcdP/(IcdP+BghiP)	<0.2 petrogenic 0.2 – 0.5 petroleum combustion >0.5 grass/wood/coal combustion	Kubo et al. (2020) Alves et al. (2017) Brown and Brown (2012) Sánchez-Piñero et al. (2021)	Yes
BaP/BghiP	>0.6 non-traffic <0.6 traffic UK specific >1.1 non-traffic sources <1.1 traffic sources	Sánchez-Piñero et al. (2021) Brown and Brown (2012)	Yes

Source Indicators for n-Alkanes

The CPI diagnostic tool was used for source identification of n-alkanes. This represents a relation of proportionality between alkanes with odd and even carbon chains (Caumo et al., 2020). To determine the CPI value, Equation 5 was applied to n-alkanes with n = 11 and m = 14 (as shown in Equation 6). The n integer was set to be 11 so that higher plant n-alkanes starting from C_{24} were included. This equation was proposed by Marzi et al. (1993) as an alternative equation to the commonly used CPI equation in Bray and Evans (1961) as it prevents overestimation of odd/even carbon preference. n-Alkanes with a non-degraded, higher plant origin tend to have high CPIs (≥3), whilst n-alkanes that have been microbially degraded or emitted from anthropogenic sources show values close to unity (Alves, 2008; Mazurek et al., 1989; Omar et al., 2007; Oros & Simoneit, 2001). Thus, in urban areas, the CPI tends to be around 1 due to the dominant anthropogenic sources, whilst rural areas have CPIs ≥2 due to biogenic influences (Brown et al., 2002; Gupta et al., 2017).

$$CPI = \frac{(\sum_{i=n}^{m} C_{2i+1}) + (\sum_{i=n+1}^{m+1} C_{2i+1})}{2(\sum_{i=n+1}^{m+1} C_{2i})} \quad (5)$$

$$CPI = \frac{(C_{23} + C_{25} + C_{27} + C_{29}) + (C_{25} + C_{27} + C_{29} + C_{31})}{2(C_{24} + C_{26} + C_{28} + C_{30})} \quad (6)$$

The percentage of wax n-alkanes (WNA%) helps provide a quantitative estimate of plant debris contributions to the samples analysed (Simoneit et al., 1991). The WNA% was calculated using Equation 7. The numerator in the equation was calculated from n-alkanes ranging from C_{24} to C_{32}. $\sum C_{total}$ was the sum of all n-alkanes included in the calculations.

$$WNA\% = \frac{\Sigma[C_n - \frac{(C_{n+1} + C_{n-1})}{2}]}{\Sigma C_{total}} \times 100 \quad (7)$$

The C_{max} metric is the most abundant n-alkane within a sample, i.e., it is the n-alkane with the largest concentration. The C_{max} metric can indicate the probable dominant source

contributions of n-alkanes in aerosols (Gupta et al., 2017). The C_{max} calculation included all analysed n-alkanes ranging from C_{16} to C_{33}. Table 3.12. shows the literature interpretations of the sources associated with different C_{max} values.

Table 3.12. C_{max} values found in the literature for a range of sources.

C_{max} value(s)	**Source**
C_{22}, C_{23}	Diesel vehicles and auto engine exhausts (species not burned) (Simoneit, 1984)
C_{23}, C_{25}	Vehicular exhaust (Simoneit, 1989)
≤C_{25}	Anthropogenic emissions, fossil fuel burnings (Omar et al., 2007; Rogge et al., 1993b; Simoneit, 1984; Yadav et al., 2020)
C_{26}	Mixed sources (Caumo et al., 2020)
≥C_{27}	Plant Epicuticular waxes (Hildemann et al., 1996; Rogge et al., 1993b; Simoneit, 1989; Yadav et al., 2020)
C_{24}, C_{25}, C_{27}	Vehicular exhaust and road dust (Gupta et al., 2017)
C_{29}	Road dust *(Rogge et al., 1993d; Yadav et al., 2013b)*

3.2.7. Methodology: Principal Component Analysis

To identify source categories for aerosol constituents, principal component analysis (PCA) was used. PCA was completed using SPSS Statistics.

As mentioned by Harrison et al. (1996) using PCA solely on particle associated PAH data would result in a pattern that would merely reflect the volatility of various PAH species, rather than the sources, therefore PCA was used for n-alkanes and PAHs.

The orthogonal transformation method was used, with Varimax rotation and retention of principal components whose eigenvalues were greater than 1 (Harrison et al., 1996). Only factor loading values with modulus ≥ 0.3 are presented so stronger associations could be observed.

NAPH and FLU were only present in a few samples. Calculations could not be completed due to a higher number of missing values hence NAPH and FLU were removed from the dataset.

3.2.8. Results and Discussion: Measurement of Solvent-Extractable Polycyclic Aromatic Hydrocarbons in Known-Source Materials

The PAH DRs introduced in the preceding Section 3.2.6 were used to identify and apportion the sources of PAHs in known-source materials and airborne ambient PM samples obtained from urban sampling sites in Glasgow and Manchester. The PAH DRs were firstly tested on known-source materials to determine if they could be used accurately to determine sources of PAHs and n-alkanes. The PAH DRs were then applied to airborne ambient PM to build a holistic understanding of sources in airborne ambient PM.

The PAH DRs that were used were: combustion PAHs/total PAHs denoted as PAH-DR-1, IcdP/(IcdP+BghiP) denoted as PAH-DR-2 and BaP/Bghi PAH-DR-3. PAH distributions for all PAHs, 3-4 ring PAHs and 5-6 ring PAHs were also examined, alongside the PAH_{max} to help with source identification in airborne ambient PM.

Biomass Materials PAH Diagnostic Ratios and Ring Size Distributions

PAH DRs were calculated for biomass materials using the data presented in Appendix Ie and are presented in Table 3.13. Low solvent-extracted PAH yields were apparent for charred biomass and laboratory-made charcoal materials, which meant some PAH DRs could not be calculated for these materials due to undetected PAHs.

Table 3.13. PAH DRs for biomass materials.

	PAH-DR-1	PAH-DR-2	PAH-DR-3
DB	0.85	-	-
EB	-	-	-
MC-300-01	-	0.62	-
Indoor wood-smoke	0.92	0.46	1.65
Outdoor wood-smoke	-	-	-
Indoor charcoal-smoke	0.92	0.43	1.48

Charred Biomass PAH Diagnostic Ratios and Ring Size Distributions

Due to low solvent-extracted PAH yield from DB and EB, it was only possible to calculate one PAH DR for DB, where PAH-DR-1 was calculated. No other PAH DRs were possible for DB and EB. The source category for PAH-DR-1 for DB was categorised as combustion sources, hence was consistent with the known source of this material, as DB was pyrolyzed.

Laboratory-made Charcoals PAH Diagnostic Ratios and Ring Size Distributions

Due to low solvent-extracted PAH yield for mangrove char samples some PAH DRs could not be calculated. In general, 1 – 3 PAHs were detected for these samples out of the 16 priority PAHs. This meant inaccuracies affect the use of PAH-DR-1, because this relies on the presence of 9 combustion PAHs for calculation. For example, only one PAH (NAPH) was detected in MC-600-01. For PAH-DR-1 combustion PAHs must be quantified for the calculation. As no combustion PAHs were quantified the PAH-DR-1 ratio for MC-600-01 was 0, hence this result was not included in the Table 3.13. The PAH-DR-2 for MC-300-01 was 0.62 which meant the sources were categorised as grass/wood/coal combustion. This was an accurate source categorisation that was consistent with the known information about the production method of this material, as Mangrove was a wood that had been pyrolyzed.

Charcoal and Wood-smoke PAH Diagnostic Ratios and Ring Size Distributions

PAH DRs were used on charcoal and wood smoke samples as airborne ambient PM samples in the UK may have wood combustion sources as domestic wood combustion was a top contributing source of $PM_{2.5}$ according to the NAEI (2020) . The source categorisations were combustion sources (PAH-DR-1), petroleum combustion (PAH-DR-2) and non-traffic sources (PAH-DR-3). The ratios can be found in Table 3.13. The sources determined by PAH-DR-1 and PAH-DR-3 were accurate, however PAH-DR-2 incorrectly categorised the source of this material when compared to the known information about the production mechanism. However, in the literature, the use of PAH-DR-2 resulted in ratios of 0.44 – 0.60 for wood-smoke (Oanh et al., 1999; Santos Barbosa et al., 2006; Seng et al., 2016). The reported PAH DR for indoor wood-smoke was 0.46 so within the range reported in the literature, despite not falling within the grass/wood/coal sources category.

The PAH ring-size distributions of charcoal and wood-smoke are shown in Figures 3.17 Wood-smoke had a large proportion of 4-ring PAHs (42 %) whereas charcoal had a smaller percentage of 4-ring PAHs (18 %) and a higher percentage of 5-ring PAHs (52 %). For wood-smoke the 3-4 ring distribution constituted of mainly CHRY and BaA and the 5-6 ring distribution constituted mainly of BbF & BkF (co-eluted).

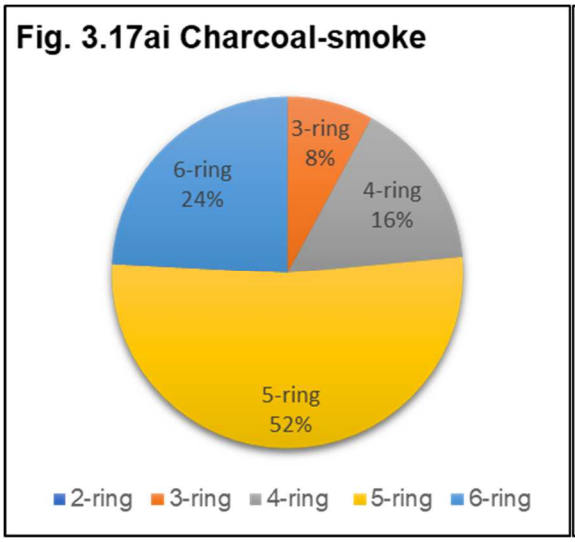

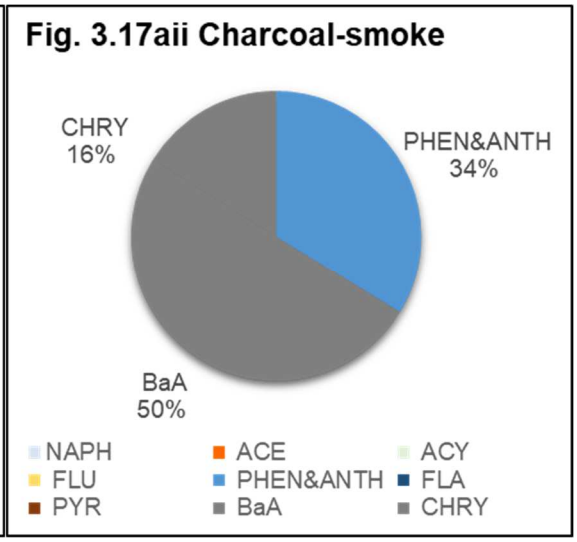

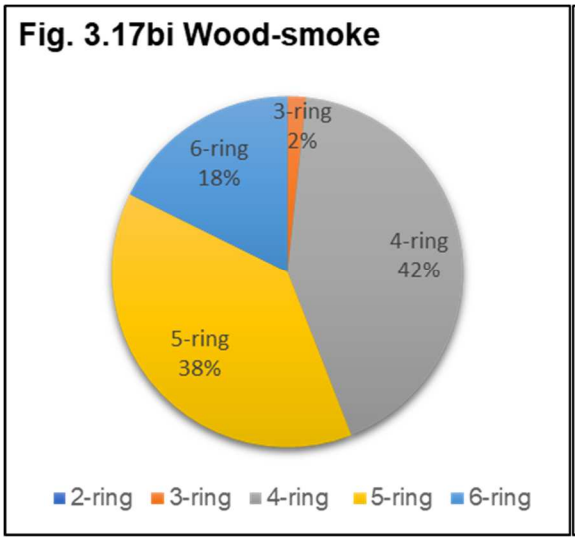

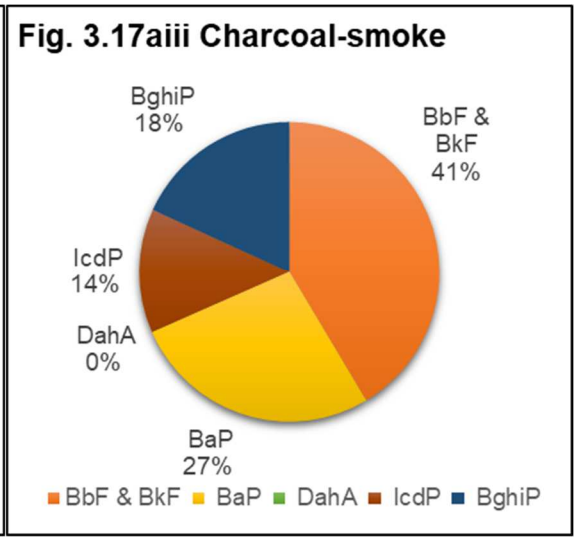

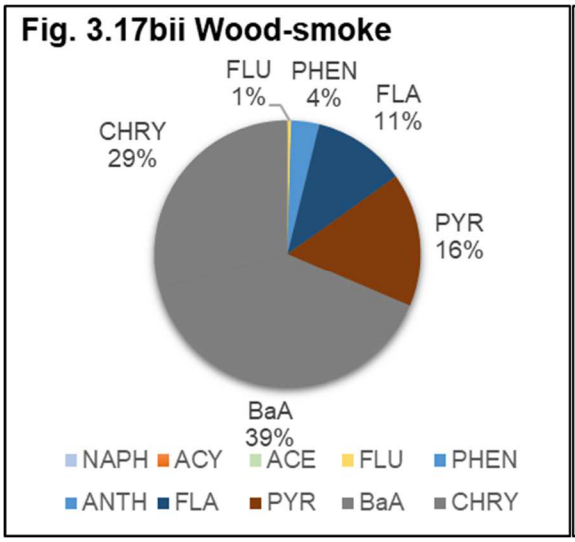

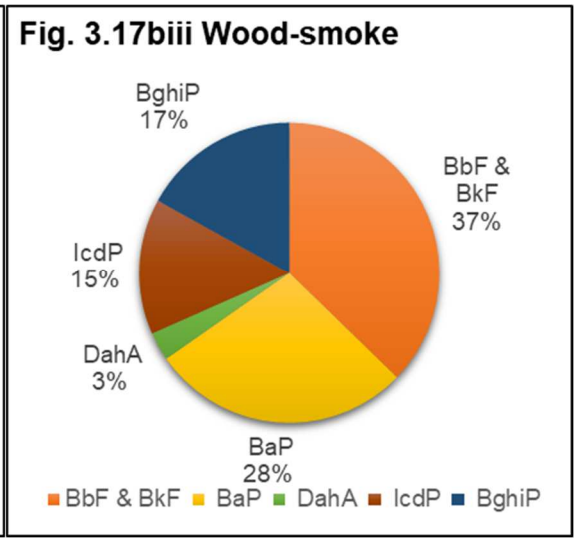

Figures 3.17. PAH ring size distributions for ai) charcoal-smoke total PAHs, aii) charcoal-smoke 3-4 rings, aiii) charcoal-smoke 5-6 rings, bi) wood-smoke total PAHs, bii) wood-smoke 3-4 rings and biii) wood-smoke 5-6 rings.

For charcoal-smoke the 3-4 ring PAHs consisted mainly of BaA and CHRY, whilst 5-6 ring PAHs was similar to wood-smoke and consisted mainly of BbF & BkF and BaP. The PAH_{max} for charcoal and wood-smoke were BbF and BkF (co-eluted), which was in agreement with research that showed 4/5 ring PAHs congeners can indicate biomass combustion sources (Han et al., 2018; Nelson et al., 2021; Yadav et al., 2013a).

Fossil Fuel Materials PAH Diagnostic Ratios and Ring Size Distributions

The PAH DRs were calculated for fossil fuel materials DS and BZ. The results are presented in Table 3.14.

Table 3.14. PAH DRs for fossil fuel materials.

	PAH-DR-1	PAH-DR-2	PAH-DR-3
BZ	0.57	0.28	1.88
DS	0.22	0.27	-

The sources identified for BZ on the basis of PAH DRs were non-combustion sources (PAH-DR-1), petroleum combustion (PAH-DR-2) and non-traffic sources (PAH-DR-3) as seen in Table 3.14. PAH-DR-2 and PAH-DR-3 were able to correctly determine sources however PAH-DR-2 incorrectly categorised PAH sources as petroleum combustion instead of petrogenic. Figures 3.17 shows the PAH ring size distribution for BZ, which had a large 5-ring PAH contribution. The MMW/4-ring percentage of 12 % was rather low in comparison to other studies (59 % MMW PAHs in lignite from USA, 37 % MMW PAHS in lignite from China) whilst the HMW PAHs (5-6 ring PAHs) had higher contributions, 56 % in this study compared to 23.2 % in lignite from USA and 28 % from lignite in China (Gao et al., 2019a; Stout & Emsbo-Mattingly, 2008). These earlier studies utilised DCM rather than hexane for extraction, which could account for the differences in PAH ring-size distributions, as different solvent combinations may lead to different PAH recoveries. Figures 3.17 show BZ had a high proportion of PHEN & ANTH in the 3-4 ring PAH distributions and a high proportion of BbF and BkF in the 5-6 ring distributions. Its PAH_{max} was BbF & BkF.

DS was categorised to have non-combustion sources (PAH-DR-1) and petroleum combustion sources (PAH-DR-2). The source categorisations for PAH-DR-1 were inaccurate, perhaps due to low solvent-extraction efficiencies, as solvent-extracting PAHs from DS has been documented to be a particularly difficult process, which was corroborated by low recoveries for DS in 3.2.5 therefore the absence of certain PAHs due to inadequate

extraction, may have affected the PAH DR results (Turrio-Baldassarri et al., 2003). Figures 3.17 shows DS had a large 4-ring contribution to extracted PAHs, which was consistent with the literature (Zheng et al., 2017). DS had large contributions of FLA in the 3-4 ring PAH distributions and BbF & BkF in the 5-6 ring PAH proportions. The PAH_{max} was FLA for DS, which was characteristic of diesel vehicle emissions (Marr et al., 1999; Miguel et al., 1998; Wang et al., 2021).

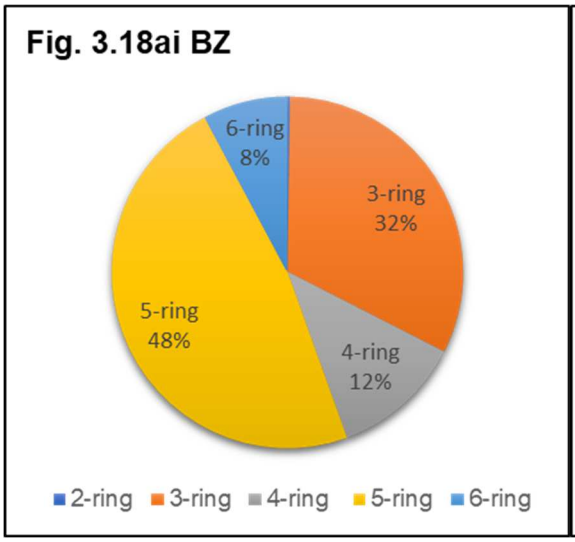

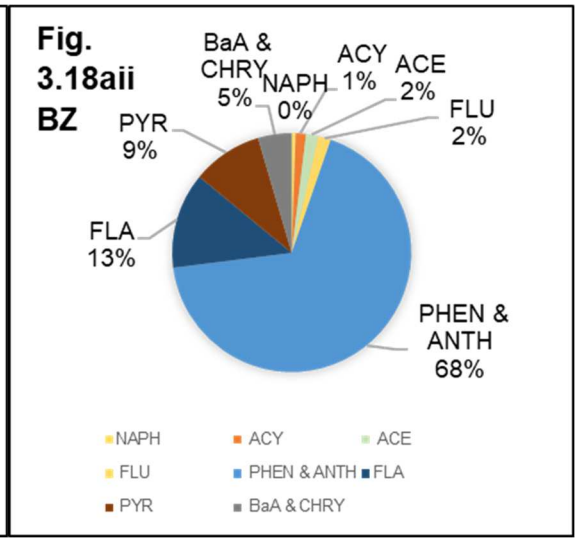

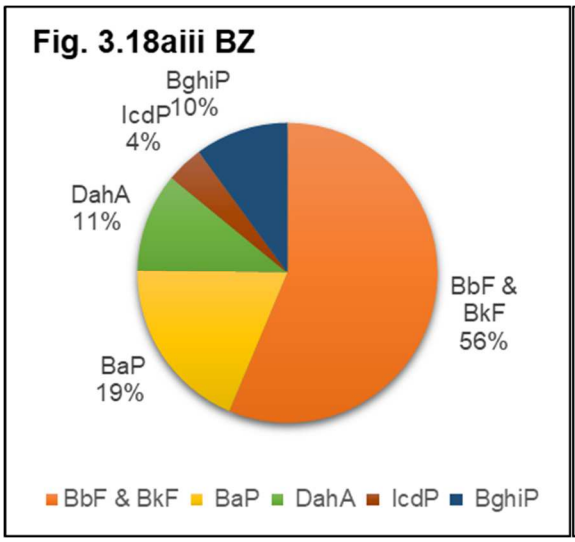

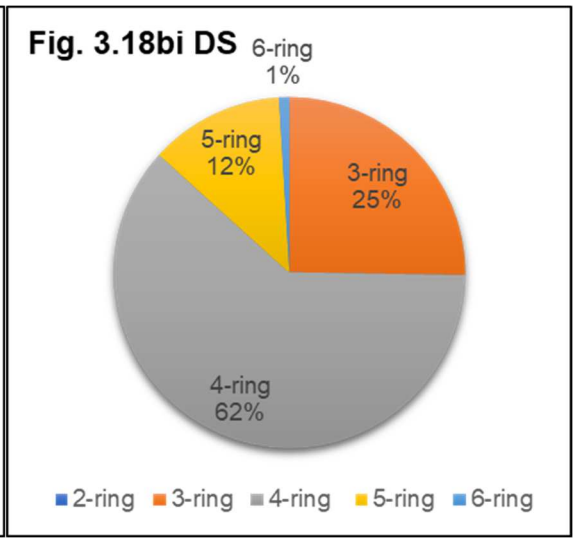

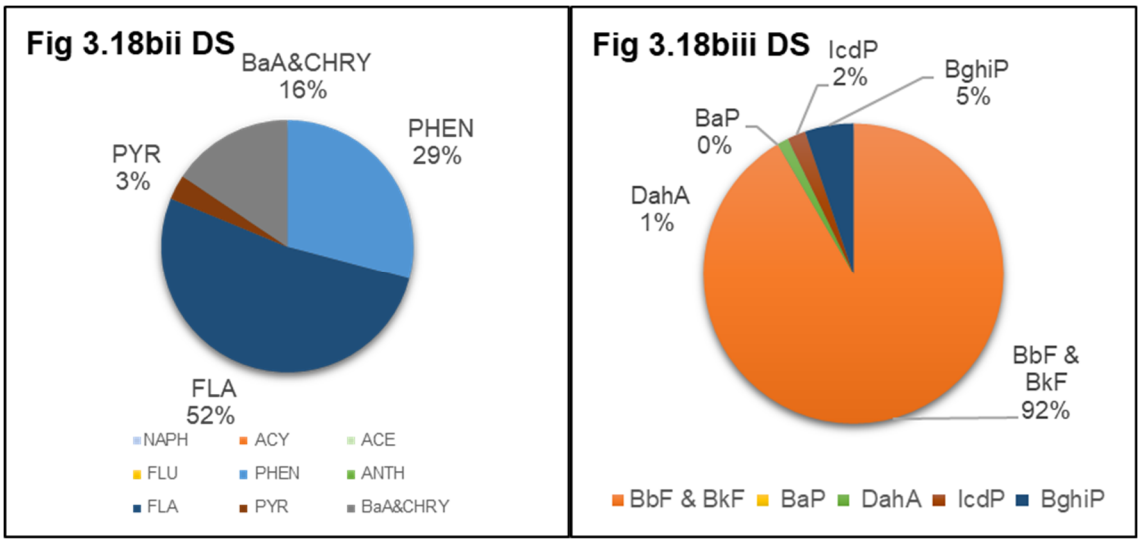

Figures 3.18. PAH ring size distributions for ai) BZ total PAHs, aii) BZ 3-4 rings, aiii) BZ 5-6 rings, bi) DS total PAHs, bii) DS 3-4 rings and biii) DS 5-6 rings.

The results show that difficulties can be experienced when using PAH DRs for source categorisations of solvent-extracted PAHs from fossil fuel materials. PAH-DR-2 was incorrect for BZ whilst PAH-DR-2 was incorrect for DS. This could be due to the materials being extremely condensed, hence causing difficulties in solvent-extraction of PAHs (low extraction efficiencies) hence incorrect source determinations.

To summarise some inaccuracies were observed in using the PAH DR. Wood and charcoal smoke samples were categorised as petroleum combustion instead of wood/grass/coal combustion when using PAH-DR-2. Despite values being in line with those from the literature, the PAH DR categories were inaccurate. Moreover, for fossil fuels PAH-DR-2 deemed lignite as petroleum combustion and PAH-DR-1 was unable to identify that DS was from combustion sources. This means that difficulties may be experienced with determining PAH sources in airborne ambient PM containing diesel soot and uncombusted fossil fuels.

The advantages of PAH DRs are that PAH-DR-1 and PAH-DR-3 worked well in determining combustion and non-traffic sources. However, PAHs in airborne ambient PM in the UK are likely to be mainly from combustion therefore this PAH DR doesn't help to narrow down PAH sources. Another disadvantage of the method is that with matrices where solvent-extraction of PAHs is difficult, e.g., diesel soot and charcoal, PAH concentrations tend to be low, meaning PAH DRs cannot be used. The use of PAH DRs in conjunction with PAH distributions may help with determination of PAH sources. To test this further, the PAH DRs and PAH distribution of aerosol standards were determined.

Aerosol and Dust Materials PAH Diagnostic Ratios and Ring Size Distributions

The PAH DRs for aerosol and dust materials were calculated in order to assess how these related to the known production mechanisms of these materials and contrast with the findings for other materials in this section (described in preceding sections). The PAH DRs can be found in Table 3.15. The results identified that sources of PAHs in UD and UPM were combustion sources (PAH-DR-1), petroleum combustion sources (PAH-DR-2) and non-traffic sources (PAH-DR-3) (Table 3.15). The combustion sources determined for UD, through use of PAH-DR-1 were in line with results from the literature using different PAH DRs (Yim et al., 2005). When PAH DRs were calculated for UD, using reported PAH concentrations from Eiguren-Fernandez and Miguel (2003), the source categorisations for PAH-DR-1 and PAH-DR-3 were found be consistent with those reported here.

Table 3.15. PAH DRs for aerosol and dust materials.

	PAH-DR-1	PAH-DR-2	PAH-DR-3
UD	0.75	0.38	1.11
UPM	0.76	0.41	1.67
FD	0.70	0.37	1.10
BCR-RD	0.28	0.25	1.48
HH-RD	0.74	-	-

UD and UPM were compared to PAHs from the fossil fuel and biomass materials. UD and UPM had similar PAH ring-size distribution patterns to wood-smoke (3-ring 2%, 4-ring 42 %, 5-ring 38 % and 6-ring 18 %) and charcoal-smoke (3-ring 8 %, 4-ring 16 %, 5-ring 52 % and 6-ring 24 %). Like charcoal-smoke, the 3-ring PAHs in UD and UPM were low roughly 10 % of the total PAHs and like wood-smoke the 6-ring PAHs were around 18 % (Figures 3.19a and b). This implies the presence of a combination of wood and charcoal smoke. Previous research found that the aromatic fraction of UD had a %MC of 17 %, with $\%MC_{biomass}$ of 13 % suggesting dominantly fossil PAH sources with a modern component meaning a mixture of coal and charcoal PAH sources could be possible (Currie et al., 2002a).

The 3-4 ring PAH distributions of UPM and UD (Figure 3.20a and b) were not particularly similar to charcoal-smoke or BZ implying the presence of other contributing sources. In UD FLA was the dominant 3-4 ring PAH whilst PHEN & ANTH were the dominant PAHs in UPM. This could imply high temperature wood-burning which can yield similar PAHs such

as PHEN, PYR, FLU and FLA (Hadley et al. 2021). Another possibility is coke PAH emissions as these have shown to have high PHEN, ANTH, FLU and FLA concentrations (Khalili et al., 1995).

The 5-6 ring PAH distributions of UD and UPM (Figure 3.21a and b) were extremely similar to BZ with around 55 % being BbF & BkF and around 19 % BaP. There were also similarities seen between UD and UPM and wood-smoke in terms of the percentages of DahA (3 %), IcdP (15 %) and BghiP (17 %). Previous research by Currie et al. (2002a) found the heavier PAHs in UD such as BghiP had a larger biomass contribution compared to other PAHs suggesting biomass combustion sources.

The PAH_{max} was also BbF & BkF for both UD and UPM which was the same as the PAH_{max} from charcoal-smoke, wood-smoke and BZ. The PAH-DR-3 for UD was 1.1, similar to those in other studies for coal combustion for heating purposes, whilst PAH-DR-3 for UPM was 1.67, more similar to iron and steel industries using coal and heavy oils (Kong et al., 2011; Yang et al., 2002). The USA national emissions inventories show that during the time the standards were collected, around 1975, the dominant sources of PM_{10} sources were "other industrial processes" and "fuel combustion electricity utilities" (USA NEI 1975). Coal was the third top energy source used, after petroleum and gas, in the USA during 1975, with Washington DC using 3.8 % coal or coke and Missouri state using 0.9 % coal or coke (EIA; United States Census Bureau, 2000). Faoro and Manning (1981) reported that the nationwide estimates of BaP emissions were mainly from domestic wood combustion (73 tons/yr) and coke ovens (110 tons/yr). Coal for heat and power generation was said to have declined to 26 tons/yr however coal refuse fires still contributed 50 tons/yr. Faoro and Manning (1981) differentiated sites that contained coke ovens; the urban area where UPM originated from contained coke ovens. This means UPM would have contained PAHs dominantly from coke emissions. UD, however, was likely to contain dominant coal PAH emissions, as a coal plant was nearby Washington DC (Architect of the Capitol, n.d.). It is likely that UPM would also have PAH contributions from coal emissions and UD & UPM would have contributions from vehicle and biomass combustion sources as studies from the USA analysing airborne ambient PM from 1970s, showed a mixture of vehicle sources and domestic fuel burning (including wood-burning) (Dong et al., 1976; Harkov & Greenberg, 1985; Harkov et al., 1984).

The PAH analysis of FD shows the material was most likely derived from combustion sources (PAH-DR-1), petroleum combustion (PAH-DR-2) and non-traffic sources (PAH-DR-3) (see Table 3.15). These sources seem accurate considering FD was collected from a

traffic tunnel. The PAH ring distribution pattern in FD (see Figures 3.19c) was most similar to wood-smoke which contained 2 % 3-ring PAHs, 42 % 4-ring PAHs, 38 % 5-ring PAHs and 18 % 6-ring PAHs. Similar to DS, FD had a high proportion of 4-ring PAHs. The 3-4 ring PAH distributions (see Figure 3.20c) were not particularly similar to one standard, as was the case for UD and UPM. The 5-6 ring PAH distribution (see Figure 3.21c) was similar to wood-smoke which had 3 % DahA, 15 % IcdP and 17 % BghiP. It was also similar to BZ with around 55 % being BbF & BkF and around 19 % BaP. With regards to wood-smoke emissions, 51 % of all households in Poland used heating devices which utilised solid fuels such as coal or wood, in 2009 – close to the 2006 sampling period. These two fuels would be used interchangeably in the same boilers and stoves, with only a small proportion household using only coal or only wood (Kerimraya et al., 2017; Statistics Poland, 2009). Poland's national atmospheric emission inventories showed domestic combustion and power station combustion contributed most to $PM_{2.5}$ emissions during the year the material was collected. Additionally, the largest emission sources for PAHs during the year of material collection was domestic combustion and coke production (The National Centre for Emissions Management - KOBiZE, 2018).

However, these sources are unlikely to be dominant as FD was collected from a traffic tunnel. The PAH_{max} of FD was FLA, which was the same as the PAH_{max} of DS. The literature has shown that LDV diesel vehicle emissions have higher contributions of 4-ring PAHs such as PYR and FLA, so the sources could originate from LDV diesel vehicles (Marr et al., 1999; Miguel et al., 1998; B. Wang et al., 2021). FD material originates from Poland. Poland's household annual average usage for diesel vehicle fuel (1008 L) was larger than that of petrol vehicle fuel (854 L) (Statistics Poland, 2009).

The PAH ring-size distributions for FD were extremely similar to UD and UPM, however the 5-6 ring PAH distribution was more similar to UD (see Figures 3.19, Figure 3.20, Figure 3.21). This suggests possible sources of PAHs are from petrol, coal, and wood combustion. FD had a higher 4-ring proportion than UD and UPM suggesting larger contribution from diesel emissions. Another difference was that FD had a higher contribution of BaA and CHRY making up 26 % of 3-4 ring PAHs compared to 17 – 18 % for UD and UPM. As seen in Figures 3.17 the wood-smoke material BaA and CHRY contributed largely to the 3-4 ring PAHs, thus the differences in 3-4 ring PAH distributions in FD from UD and UPM, could be attributed to a higher proportion of wood burning.

Table 3.15 shows the PAH DRs for BCR-RD which were categorised as non-combustion sources (PAH-DR-1), petroleum combustion (PAH-DR-2) and non-traffic sources (PAH-

DR-3). The sources show a mixture of petrogenic and pyrogenic PAHs which would be expected in a road dust sample, as road dusts have a variety of sources (Majumdar et al., 2012). BCR-RD's PAH distribution pattern (see Figures 3.19d) was unlike any of the other known-source materials discussed here, as it had a large 3-ring proportion making up 57 % of total PAHs, unlike DS, BZ, wood-smoke and charcoal-smoke where 3-ring PAHs made up 25 %, 32 %, 2 % and 8 % of total PAHs respectively. The 3-4 ring PAH distributions seen in Figure 3.20d show large proportion of PHEN & ANTH and FLA which was similar to the findings from analysis of BZ (see Figures 3.18). The similarities could indicate contributions from solid fuel combustion or abrasion of asphalt road surfaces. PAHs could also originate from HDV diesel vehicles which emit 3-ring PAHs (Marr et al., 1999; Miguel et al., 1998; Wang et al., 2021; Yadav et al., 2013a). High temperature wood-burning can also yield 3-4 ring PAHs like PHEN, PYR, FLU and FLA (Hadley et al. 2021).

By looking at the 5-6 ring PAH distribution in Figure 3.21d, it was clear that petrol vehicle emissions were a dominant source due to the large BghiP and BaP proportions (Ravindra et al., 2006; Smith & Harrison, 1998). The non-combustion sources were likely to come from weathered road surfaces. In Austria, 1990, one of the main sources of TSP emissions was resuspended dust from roads (Anderl et al., 2007). Most roads in tunnels >1 km, in Austria are made from concrete materials, due to fire safety considerations (Leitner, 2001). Coal fly ashes are used as a raw material to produce cement in Europe hence it is possible the weathered road surfaces contained PAHs from fly ash incorporated into cement (Alberici et al., 2017; Schorcht et al., 2013). Moreover, the fly ash incorporated into cement can also originate from combustion of lignite which could explain the similarities of the BCR-RD to BZ. Portland cement works as a stabilisation and solidification binder and is used in the cement production process (Schorcht et al., 2013; Shirani, 2011). A study looked at the PAH leach rates from contaminated soil, Portland cement and pulverised fly ash. It was found that 0.154 % of PAHs and 0.113 % total petroleum PAHs leached from the sample after 408 days (Shirani, 2011). Despite this study being centred on contaminated soils incorporated into the Portland cement, alongside the pulverised fly ash, it shows that it is possible for PAHs to leach from the binder. It also showed that the pulverised fly ash itself may contain PAHs, although the individual PAHs were not identified in the study (Shirani, 2011). Other studies have found coal fly ash to contain PAHs, with a higher proportion of 3 and 4-ring PAHs (Li et al., 2014). This would explain the similarities between the 3-4 ring PAH distributions BCR-RD and BZ.

The PAH-DR-3 value of BCR-RD (see Table 3.15) was identical to charcoal-smoke (see Table 3.13), which means the non-traffic PAHs may have been emitted from the energy sector, which was one of the top contributors to PAH emissions and contributed 35 % to TSP emissions in Austria 1990. The energy sector category included small combustion plants, household oven/stoves fired with wood or coke. The similarities to BZ therefore could also be linked to coke combustion sources. Due to the material being collected from a traffic tunnel, it is more likely that the dominant sources originate from weathered road surfaces and vehicle emissions.

Due to extracted PAHs being below the limit of detection (LOD), only PAH-DR-1 could be calculated for HH-RD (see Table 3.15). The result was combustion sources. The PAH ring size distributions can be seen in Figures 3.19e, Figure 3.20e, and Figure 3.21e. HH-RD was most like DS (see Figures 3.18) as it had a high 4-ring proportion at 68 % of total PAHs. HH-RD was compared to street dust from another UK site, in Newcastle and similarly had a high proportion of 4-ring PAHs (Lorenzi et al., 2011). Unlike DS it also had 28 % 5-ring PAHs; this could be from uncombusted petroleum fuels on the road. HH-RD's PAH_{max} was PYR with the 3-4 ring PAHs showing high proportions of PYR and FLA, which are generally emitted from LDV diesel vehicles (Marr et al., 1999; Miguel et al., 1998; Wang et al., 2021). Moreover, DS's PAH_{max} was FLA. The 5-6 ring PAHs were also similar to DS due to the large BbF and BkF contribution, and low BghiP contribution which is emitted from petrol vehicles (Ravindra et al., 2006; Smith & Harrison, 1998). The dominant sources were likely to be diesel vehicle emissions. There were roadworks ongoing at the time of sample collection, with each side of traffic using one road, hence vehicles had to stop at temporary traffic lights. The idling vehicles may have led to increased PAH concentrations in PM, as observed in other studies (Su et al., 2021; Wang et al., 2021). Overall, the dominant sources of HH-RD seemed to be diesel emissions.

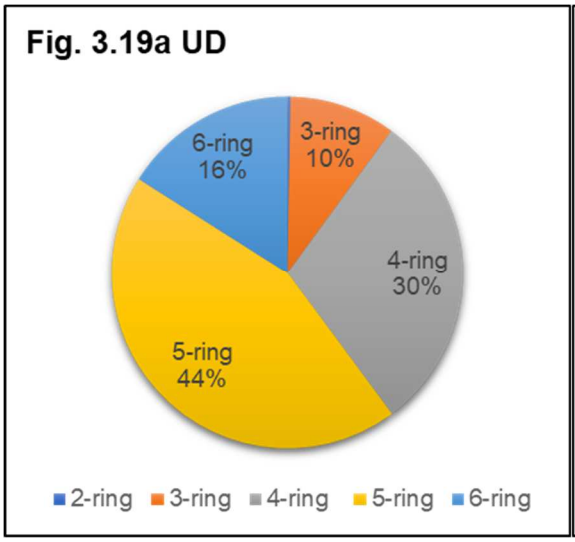

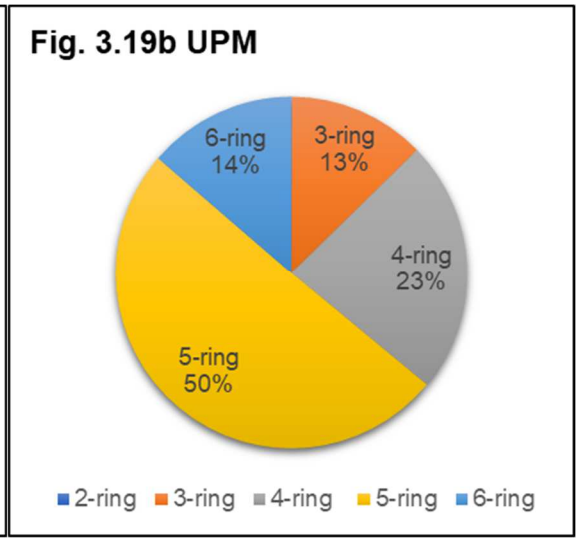

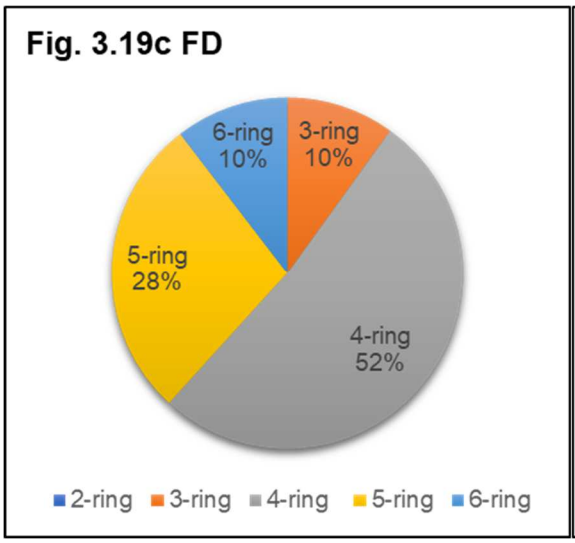

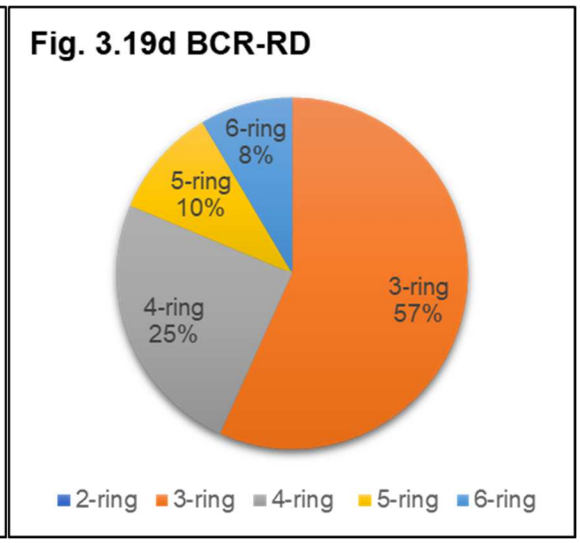

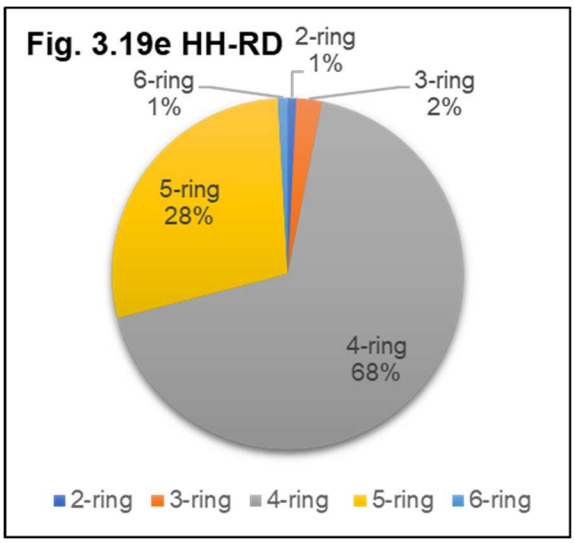

Figures 3.19. The PAH ring size distributions of a) UD b) UPM c) FD d) BCR-RD e) HH-RD.

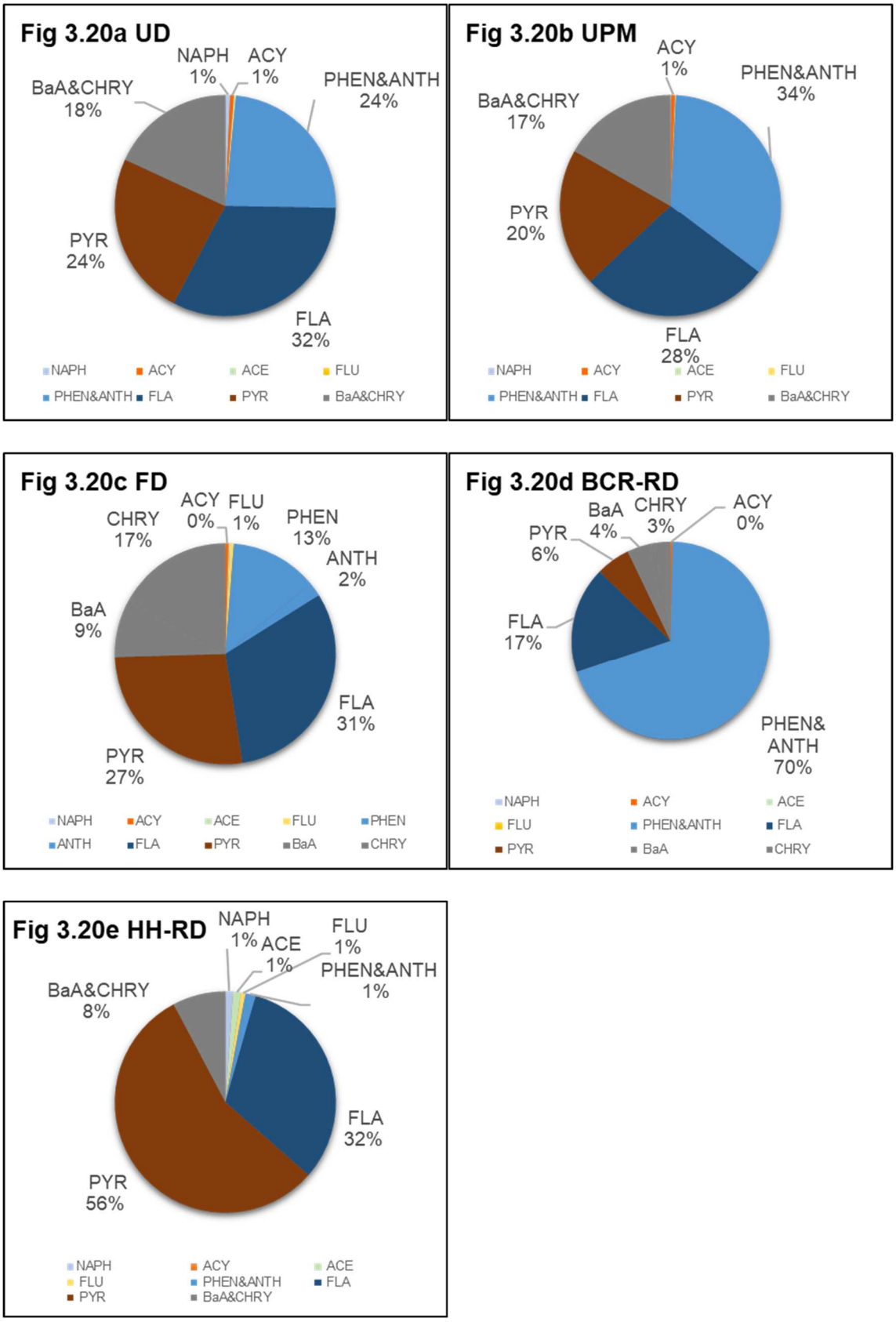

Figure 3.20. Contribution of individual PAHs with 3-4 rings in a) UD, b) UPM, c) FD, d) BCR-RD, and e) HH-RD.

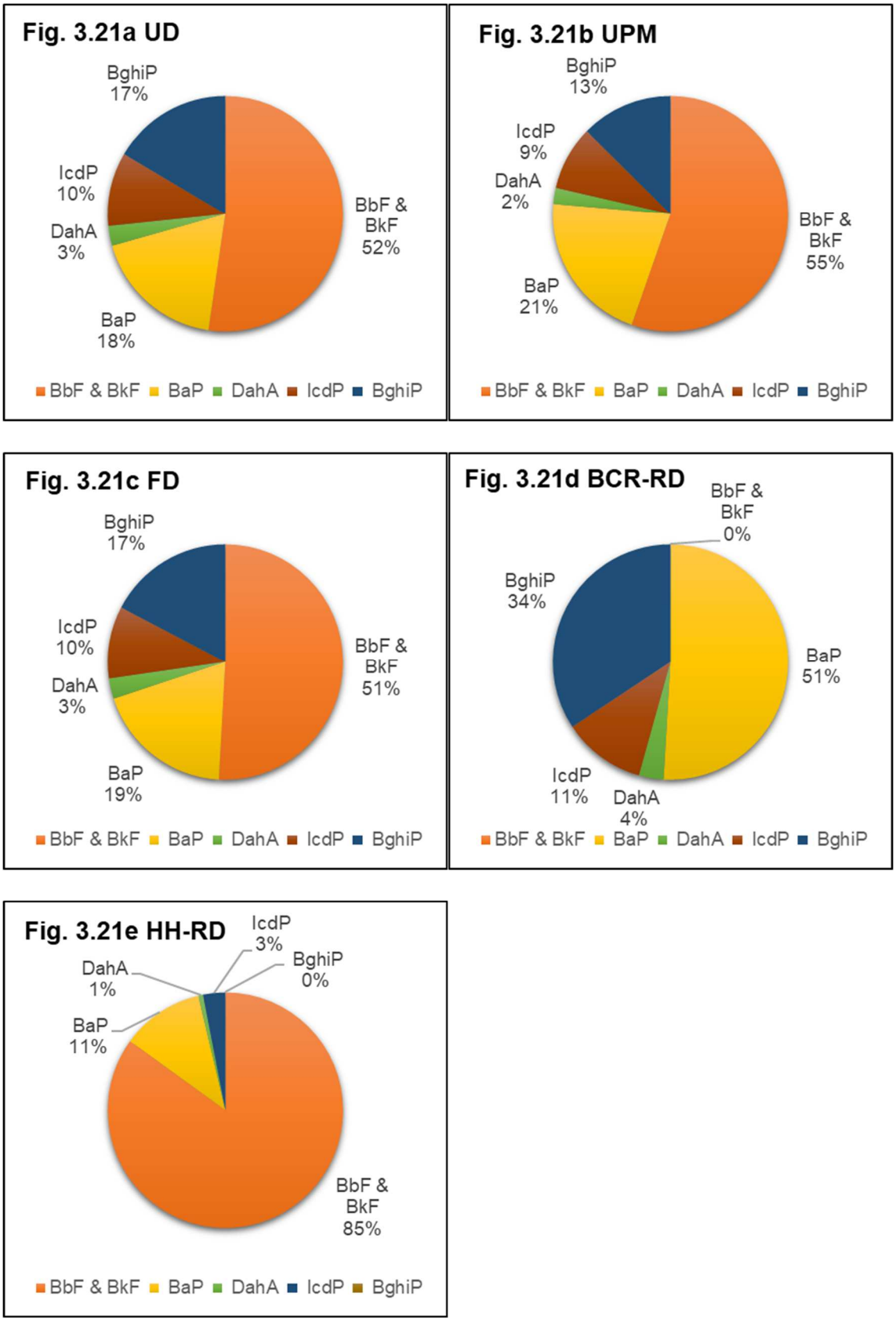

Figure 3.21. Contribution of individual PAHs with 5-6 rings in a) UD, b) UPM, c) FD, d) BCR-RD, and e) HH-RD.

The findings are summarised in Table 3.16. The PAH distributions of UD and UPM were extremely similar implying they had similar PAH sources of coal and coke combustion, wood/charcoal combustion and petrol vehicle emissions. FD had the same sources as UD and UPM except there seemed to be a higher prevalence of diesel vehicle emissions. The two road dust materials BCR-RD and HH-RD had different PAH sources. BCR-RD seemed to have weathered road surface sources, likely from coal fly ash materials incorporated into cements. It also contained petrol and diesel vehicle emissions. HH-RD contained PAHs from diesel emissions.

PAH DRs were useful for determining sources of PAHs when used in conjunction with PAH distributions. This suggests the method could be used on samples with unknown sources. The use of known-source materials was crucial for determining sources, as PAH distribution patterns could be compared. Future working using PAH DRs and distributions for PAH source identification should analyse known-source materials alongside the samples with unknown sources. Individual laboratories may use different extraction methods, extraction solvents, GC columns and so forth. As a result, the method may be better at extracting LMW, MMW or HMW PAHs (as shown from results in Appendix Ib). If comparisons are made between samples and known-source materials analysed in different laboratories, the PAH source identifications could be inaccurate.

Some limitations of this study were:

1) There was no standard for petrol particulates which contribute to PAH emissions in the UK (NAEI 2020).
2) PAH distributions from biomass burning emissions may exhibit variability due to different combustion conditions. For example, Hadley et al. (2021) found high temperature wood burning led to 3-4 ring PAHs however, in the wood-smoke sample analysed, 3-ring PAHs only constituted of 2 % of the total PAHs.
3) Some sources may have similar PAH distributions and/or PAH DRs for example high temperature biomass burning and HDV vehicles both exhibit large LMW PAH contributions (Marr et al., 1999; Miguel et al., 1998; B. Wang et al., 2021; Yadav et al., 2013a; Hadley et al., 2021). Having some local knowledge and/or additional data about the potential sources at the site area, could help guide interpretations.
4) The PAH DR source categorisation thresholds may not be applicable to UK emissions. For example, research by Brown and Brown (2012) for PAH-DR-3 non-traffic emissions were >1.1 rather >0.6 suggested by other studies.

Despite the limitations in determining PAH sources using PAH DRs and distributions, pairing the findings with other source apportionment methods such as ^{14}C analysis can help improve confidence in results.

Table 3.16. Summary of determined PAH sources through use of PAH DR and PAH distributions.

	PAH DR Source Categories	Known-source materials with similar PAH distributions	Urban/dust materials with similar PAH Distributions	PAH Sources
UD	• Combustion (PAH-DR-1) • Petroleum combustion (PAH-DR-2) • Non-traffic (PAH-DR-3)	• BZ • Charcoal-smoke • Wood-smoke	• UPM • FD	• Coal combustion • Wood/charcoal combustion • Dominantly petrol vehicles
UPM	• Combustion (PAH-DR-1) • Petroleum combustion (PAH-DR-2) • Non-traffic (PAH-DR-3)	• BZ • Charcoal-smoke • Wood-smoke	• UD • FD	• Coal and coke combustion • Wood/charcoal combustion • Dominantly petrol vehicles
FD	• Combustion (PAH-DR-1) • Petroleum combustion (PAH-DR-2) • Non-traffic (PAH-DR-3)	• BZ • Charcoal-smoke • Wood-smoke • DS	• UD • UPM	• Coal combustion • Wood/charcoal combustion • Dominantly diesel vehicles
BCR-RD	• Non-combustion sources (PAH-DR-1) • Petroleum combustion (PAH-DR-2) • Non-traffic sources (PAH-DR-3)	• BZ	-	• Weathered road surfaces • Petrol and diesel vehicles
HH-RD	• Combustion (PAH-DR-1)	• DS	-	• Diesel vehicles

3.2.9. Results and Discussion: Measurement of Solvent-Extractable Polycyclic Aromatic Hydrocarbons in Airborne Ambient PM

Airborne Ambient PM from Manchester Fallowfield Site (MAN-FF)

PAHs were analysed from airborne ambient PM collected from MAN-FF using the techniques described in 3.2.4 (listed in Table 3.17 below). Details of PM sample collection can be found in 3.2.2 PAH DRs showed MAN-FF($PM_{2.5}$) to have combustion sources (PAH-DR-1) and petroleum sources (PAH-DR-2). All samples but 4031 and 4034 were found to have traffic sources (PAH-DR-3).

Table 3.17. PAH DRs for PM samples from MAN-FF.

Samples	PAH-DR-1	PAH-DR-2	PAH-DR-3
4028	0.90	0.35	0.90
4031	0.76	0.33	0.42
4032	0.89	0.36	0.79
4033	0.79	0.38	0.82
4034	0.79	0.35	0.41
4035	0.82	0.36	0.67
4036	0.86	0.35	0.75

The ring-size distributions of MAN-FF($PM_{2.5}$) samples, shown in Figures 3.22 and Figures 3.23 were unlike the known-source materials mostly due to the absence of 4-ring PAHs in all samples but 4034. The 3-4 ring PAH distributions for sample 4034 were plotted in Figures 3.22ei. The results of this sample indicated diesel emissions due to presence of FLA, PYR, FLU and PHEN (Abrantes et al., 2004; Zheng et al., 2017). Standardised laboratory tests performed on light duty diesel vehicles running in a chassis dynamometer found NAPH, PHEN, FLA, PYR AND CHRY PAH emissions were detected in all tests. FLU was also detected in some tests (Abrantes et al., 2004). In heavy duty goods vehicles, with mechanical pump fuel injection engines, the most commonly emitted PAHs were PHEN, FLA and PYR (Zheng et al., 2017). The Greater Manchester air quality plan showed that roads nearby Fallowfield campus had high bus usage proportions which could account for the diesel emissions (Transport for Greater Manchester, 2016). Despite this, petrol emissions seemed to be dominant in all other MAN-FF($PM_{2.5}$) samples (see Figures 3.23) as 5-6 ring PAHs contributed highly to these samples, alongside large contributions from BghiP to the 5-6 ring

PAHs, which indicates petrol vehicle emissions. BghiP was also the PAH_{max} for all MAN-FF($PM_{2.5}$) samples. In samples 4031 and 4034 which were predominantly from traffic sources the BaP was lower at 12 % and 15 %, yet BghiP was higher indicating more dominant petrol vehicle emissions.

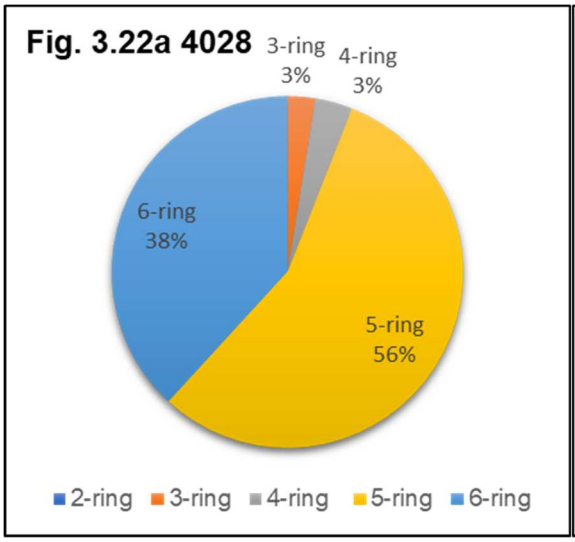

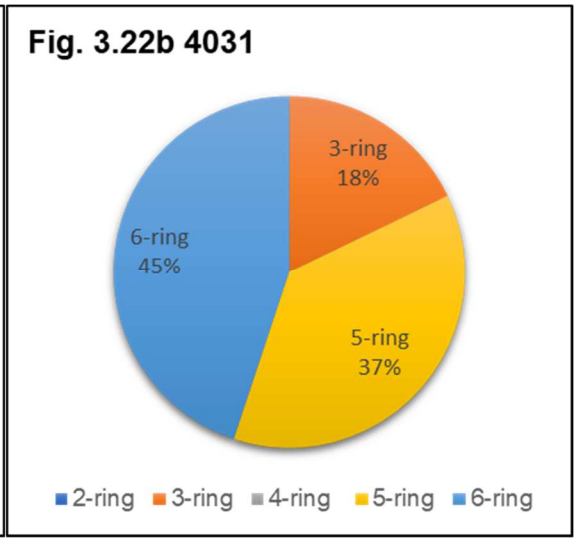

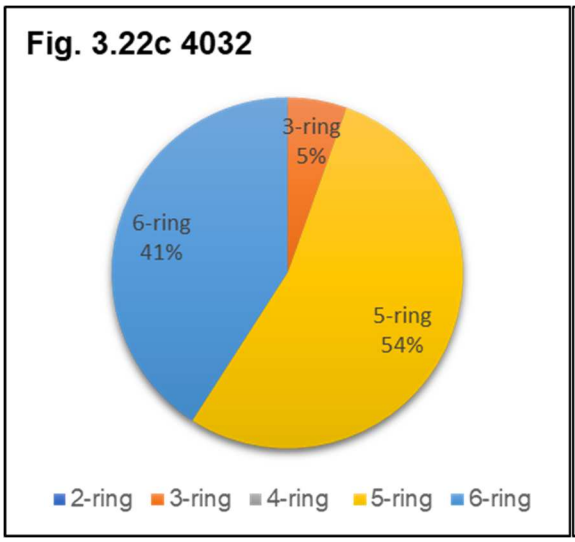

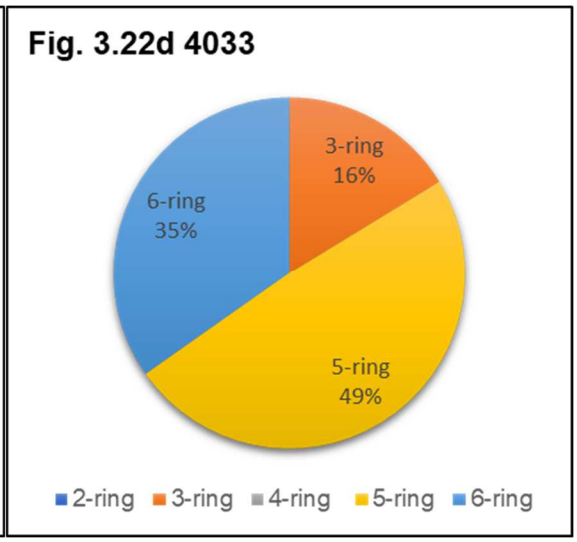

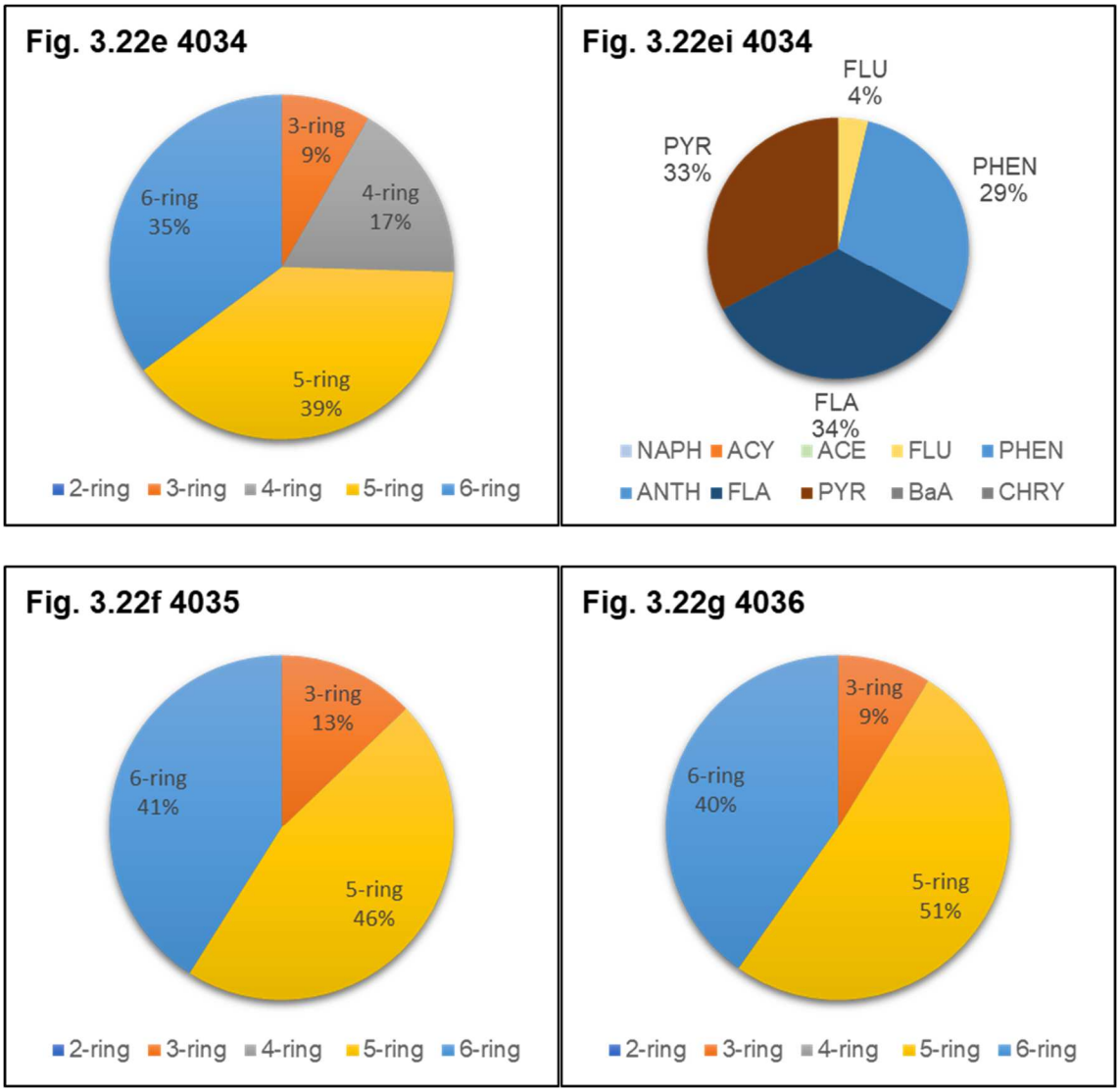

Figures 3.22 PAH ring distributions in MAN-FF samples a) 4028, b) 4031, c) 4032, d) 4033, e) 4034, f) 4035 and g) 4036. PAH 3-4 ring distributions are shown in ei) for 4034.

Fig. 3.23a 4028

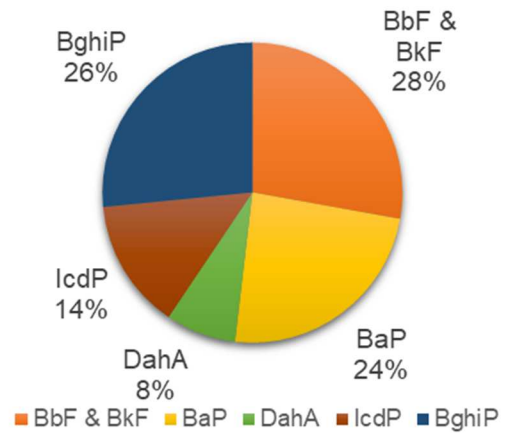

Fig. 3.23b 4031

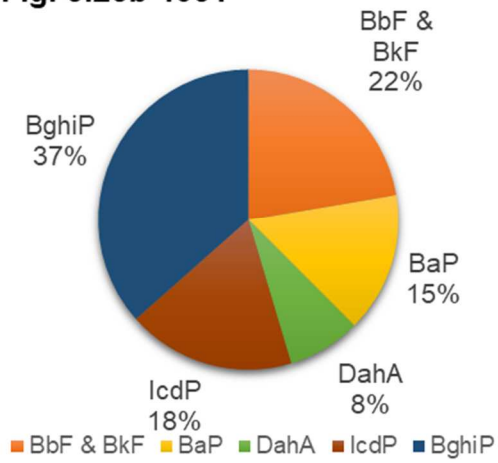

Fig. 3.23c 4032

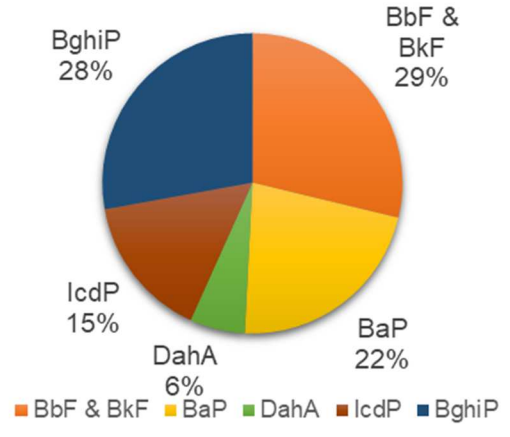

Fig. 3.23d 4033

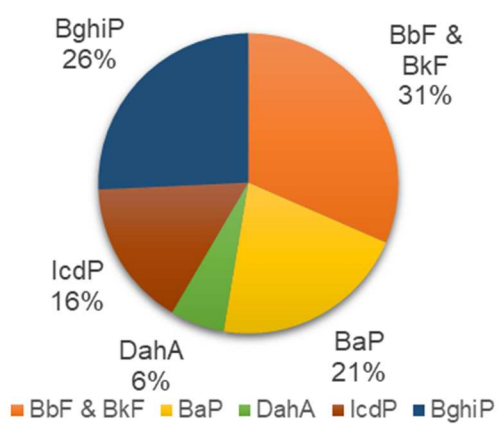

Fig. 3.23e 4034

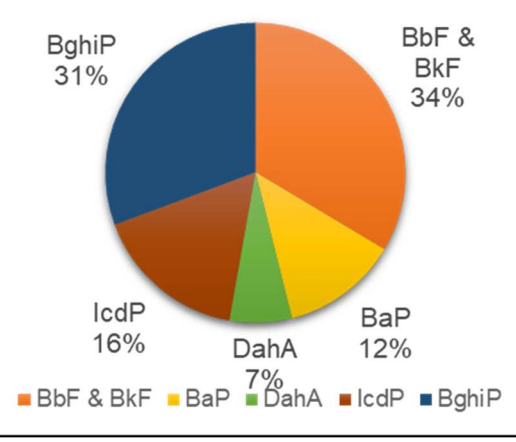

Fig. 3.23f 4035

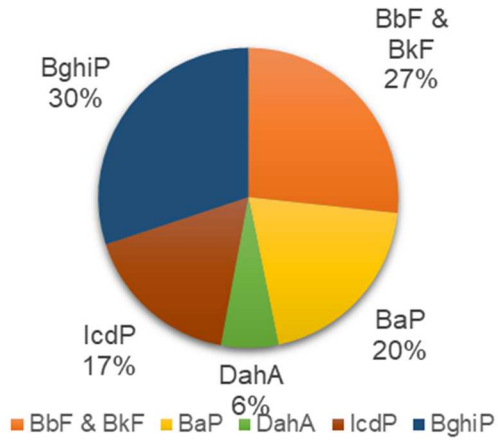

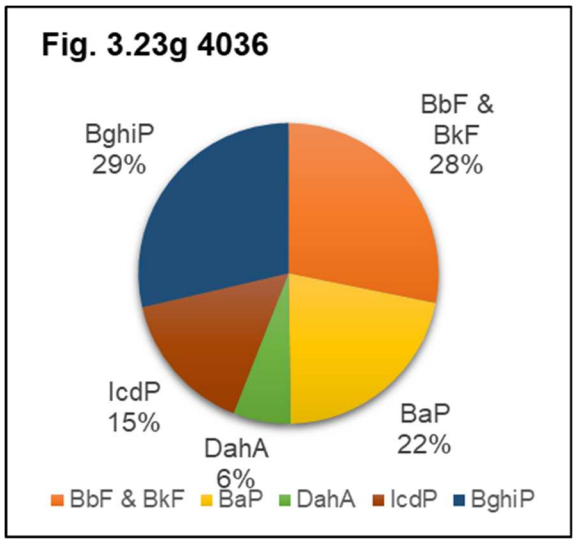

Figures 3.23. PAH 5-6 ring distributions in MAN-FF samples a) 4028, b) 4031, c) 4032, d) 4033, e) 4034, f) 4035 and g) 4036.

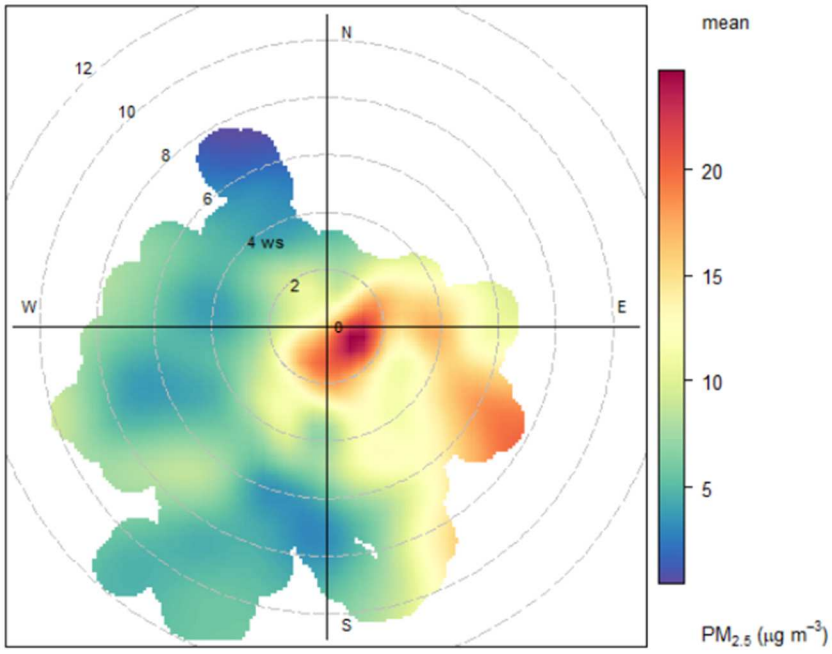

Figure 3.24. Polar plot for $PM_{2.5}$ using data from Manchester Piccadilly AURN site (20.11.2019 – 18.12.2019). Produced using openair package in R.

The PAH-DR-3 values showed traffic sources as the ratio was consistently <1.1 (Table 3.17). However, all samples but 4031 and 4034 showed BaP contributions of around 20 % indicating the presence of non-traffic PAH sources. The 5-6 ring PAH distributions in

Figures 3.23 were similar to wood-smoke emissions (shown in Figures 3.17) as BbF and BkF accounted for 22-28 % of the 5-6 ring PAHs in MAN-FF($PM_{2.5}$), alongside BaP that accounted for 12-24 % of 5-6 ring PAHs. The PAH ring-size distributions differed from wood-smoke however which could be due a mixed source profile or it could imply the presence a non-traffic source, that was not represented by a known-source material. A possible source could be waste incineration sources, as PHEN had high concentrations in all samples which is typical for incineration (Ravindra et al., 2006; Smith & Harrison, 1998). The polar plot, in Figure 3.24, contains data from Manchester Piccadilly AURN site encompassing data from the whole MAN-FF($PM_{2.5}$) sampling period. The plot shows high concentrations of $PM_{2.5}$ occurred with light to gentle breezes from the east/south-east. The high concentrations are therefore being transported from elsewhere. Incinerators to south-east were located 70 miles away (Eastcroft EfW) and 50 miles to the east (Sheffield EfW), suggesting PM-bound PAHs may have originated from long-range transport. Figure 3.24 showed high concentrations of $PM_{2.5}$ from the south-east highlighting the possibility that PM-bound PAHs bound to $PM_{2.5}$ could have been transported from the south-east. Back air mass trajectories in Section 3.2.2 show that the air masses travelled through the Eastcroft EfW area on one or more of the sampling days, for the following samples: 4028, 4033, 4034 and 4035.

Overall, the sources were determined to be dominantly from petrol vehicle emissions but with contributions from diesel vehicles due to the presence of PHEN and ANTH (co-eluted). Waste emissions also contributed to PAHs in MAN-FF samples. In sample 4034, diesel vehicle emissions were clearly seen through the presence of 4-ring PAHs, however petrol was likely to be the dominant source due to BghiP $PAH_{max.}$

Airborne Ambient PM from Glasgow Kerbside AURN Site (GLA-KS)

The sources for aerosol samples obtained from sites in the city of Glasgow (see Table 3.18) were deemed to be combustion sources (DR 2), petroleum combustion (DR 7) and traffic sources (DR 8). The PAH-DR-1 ratio for sample 4043 was 0.61 which suggests contributions from non-combustion PAH sources.

Table 3.18. PAH DRs for PM samples from Glasgow Kerbside.

Sample Code	PAH-DR-1 COMB/PAH	PAH-DR-2 IcdP/(IcdP+BghiP)	PAH-DR-3 BaP/BghiP
4038	0.70	0.33	0.65
4043	0.61	0.37	0.84
4046	0.89	0.36	0.79
4047	0.78	0.34	0.81

PAH ring size distributions of GLA-KS shown in Figures 3.25 differed from the known-source materials and the aerosol and dust materials. The PAH distributions of 4038 and 4043 were comparable to UD (see Figures 3.19) but had smaller 5-ring PAH proportions and higher 3-ring PAH proportions. Samples 4046 and 4047 did not have 4-ring PAHs therefore the PAH ring size distributions were not similar to any known-source material, including HH-RD (see Figures 3.19) which was collected from GLA-HH. Samples 4038 and 4043 had large contributions of 4 and 5-ring PAHs which were almost equal, and similar proportions of 3 and 6-ring PAHs. Sample 4046 and 4047 had a large proportion of 5 and 6-ring PAHs with little 3-ring PAHs.

The 3-4 ring PAH distributions shown in Figures 3.26 were also unlike known-source materials, except sample 4038 which had similar percentages to DS, except it contained a larger proportion of PYR. The 5-6 ring PAH distributions shown in Figures 3.27 were all very similar to wood-smoke known-source material, but with a larger BghiP proportion which could be from vehicle emission contributions. 4038 and 4043 had larger contributions of BghiP and BbF and BkF indicating petrol and diesel vehicle emission mixes as BbF and BkF were detected in high proportions in DS (see Figures 3.18). Samples 4046 and 4047 had larger contributions of BghiP indicating dominant petrol vehicle emissions. The 5-6 ring distributions of GLA-KS samples were most like FD, UD and UPM (Figure 3.21) but with higher BghiP contributions and lower BbF & BkF contributions, indicating dominant petrol sources.

PAH distributions of 4046 and 4047 were similar to those from MAN-FF shown in Figures 3.22 and Figures 3.23. The 3-4 ring PAH distributions of 4043 were similar to 4034. The 5-6 ring PAH distributions of GLA-KS were similar to MAN-FF($PM_{2.5}$).

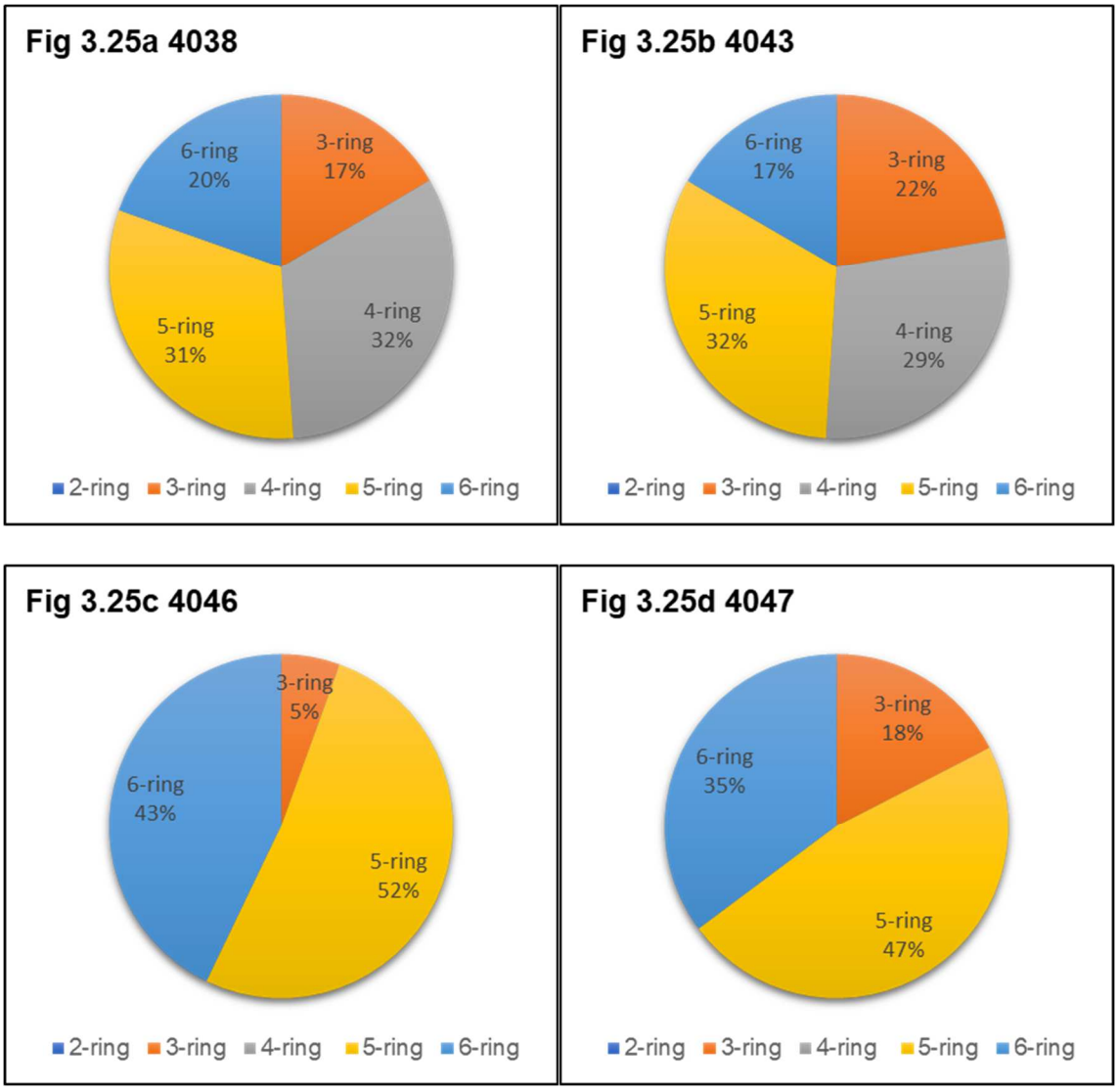

Figures 3.25. PAH distributions in GLA-KS samples a) 4038, b) 4043, c) 4046 and d) 4047.

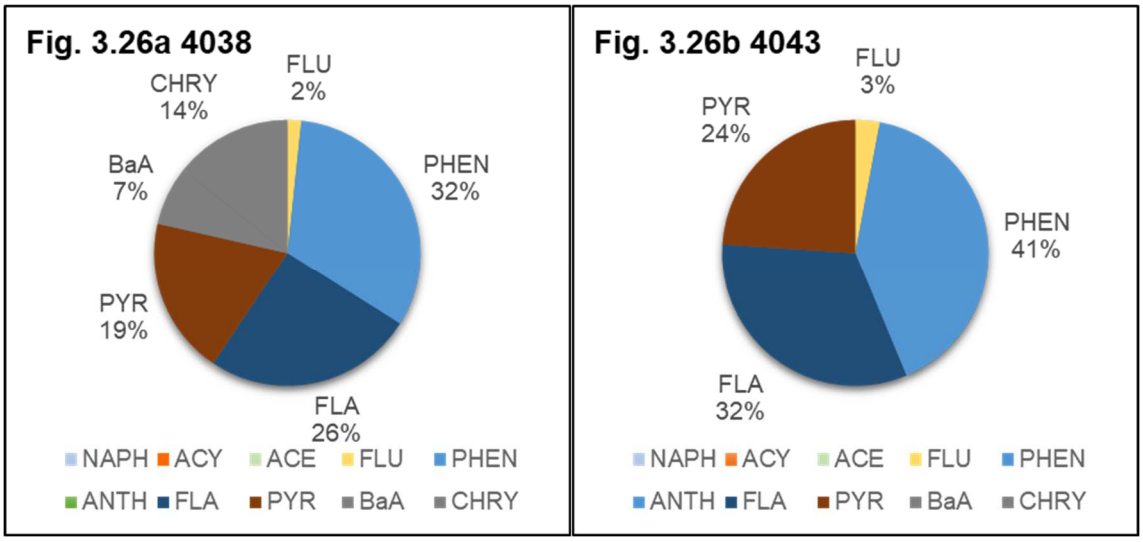

Figures 3.26. PAH distributions for 3-4 ring PAHs in GLA-KS samples a) 4038 and b) 4043.

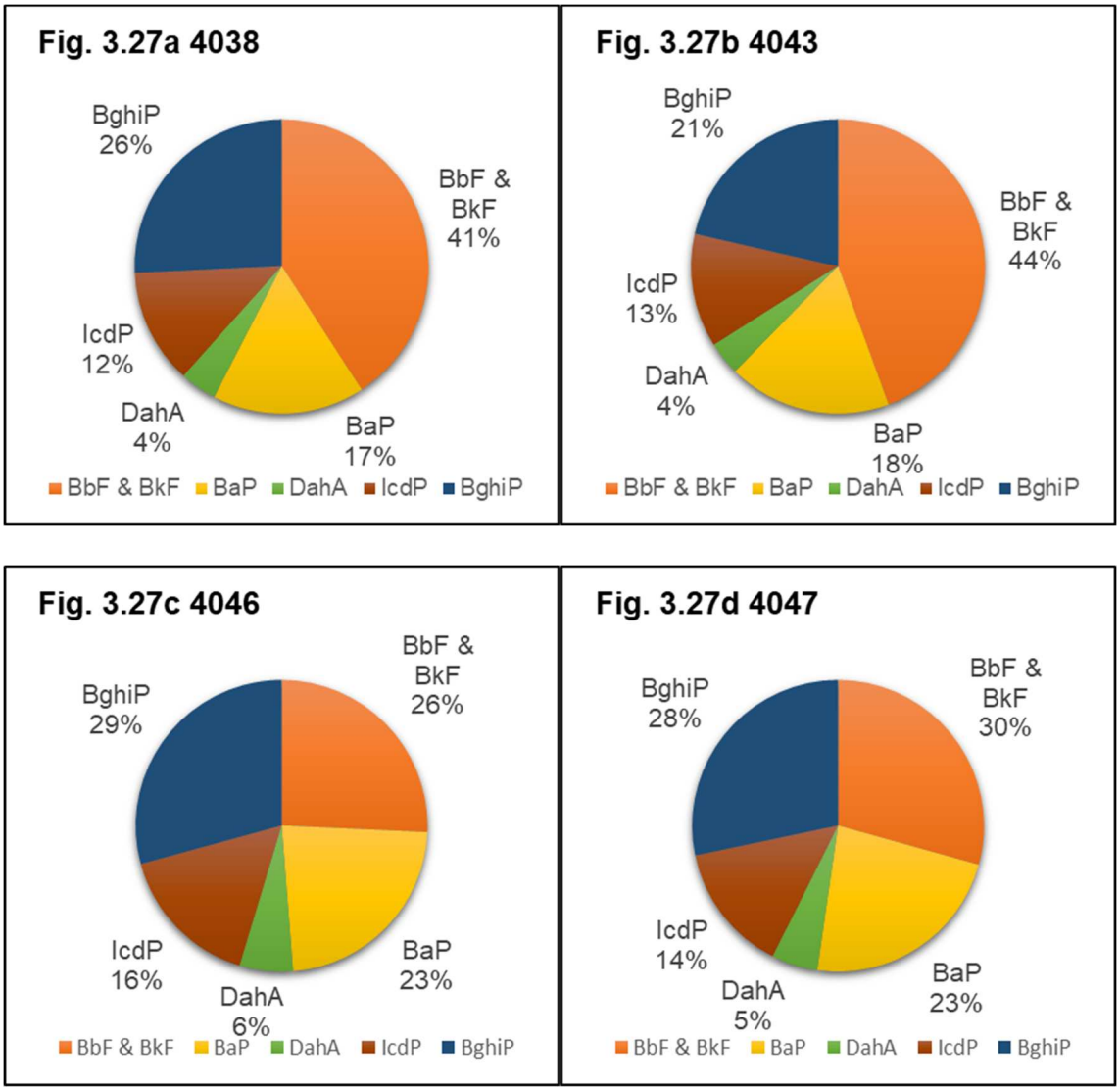

Figures 3.27. PAH 5-6 ring distributions in GLA-KS samples a) 4038, b) 4043, c) 4046 and d) 4047.

A polar plot for $PM_{2.5}$ was produced for Glasgow Townhead in Figure 3.28 which is slightly north of the sampling site where the Glasgow samples were collected. High $PM_{2.5}$ concentrations were found at high wind speeds to the north-west and the south-west. To the north-west, there is the Glasgow canal, where house boats are moored. These houseboats tend to use wood as fuel, which could account for these $PM_{2.5}$-bound PAHs originating from wood-smoke. This suggests small contributions from domestic wood combustion emissions could be transported by high wind speeds to the sampling site. The M8 motorway is also in this direction. Sample 4043 had a similar distribution to that of sample 4038 but with the absence of BaA & CHRY. Despite the lack of BaA and CHRY, high temperature wood burning can yield other PAHs such as 3-4 ring PAHs like PHEN, PYR, FLU and FLA

(Hadley et al. 2021). The city centre is south-west of Glasgow Townhead, accounting for the high $PM_{2.5}$ concentrations at high wind speeds, from that direction. The city centre is a congested area with major bus routes running through it. The sampling site, GLA-KS, only allows buses, taxis and good vehicles through the round 07:00– 19:00, which would account for the diesel vehicle emission contribution. Moreover, the site is nearby a major train station, Glasgow Central, hence diesel emissions from trains could be another source. Transport for Scotland have presented statistics showing that rail contributes to $PM_{2.5}$ emissions (Transport for Scotland, n.d.). Railway emissions come from diesel engine exhaust emissions and electric train emissions (Thornes et al., 2017). In the UK from April 2021 to March 2022, 391 million litres of diesel were used for passenger trains and 161 million litres of diesel were used for freight trains (Office of Rail and Road, 2022). Researchers monitored $PM_{2.5}$ at UK train stations and found $PM_{2.5}$ concentrations of 16 μg m^{-3} (with a range of 2 – 68 μg m^{-3}) at London Paddington (Chong et al., 2015). Moreover, it was found that urban $PM_{2.5}$ concentrations were lower than inside and concourse areas of Edinburgh Waverley and London Kings Cross stations. The concentrations were highest closer to the platforms, especially those with a higher frequency of diesel services (Font et al., 2020).

Diesel source contributions seemed to follow this order: 4038 > 4043 > 4046 > 4047. This could be because sample 4038 was collected before the first National COVID-19 Lockdown whilst sample 4043 contained filters collected around the start of lockdown. Sample 4046 contained filters collected during the first National COVID-19 Lockdown and subsequent local lockdowns which included Glasgow. Sample 4047 contained filters from the local Glasgow lockdowns. Therefore, the reduction in diesel emissions could signify a reduction in public transport services, trains, and buses.

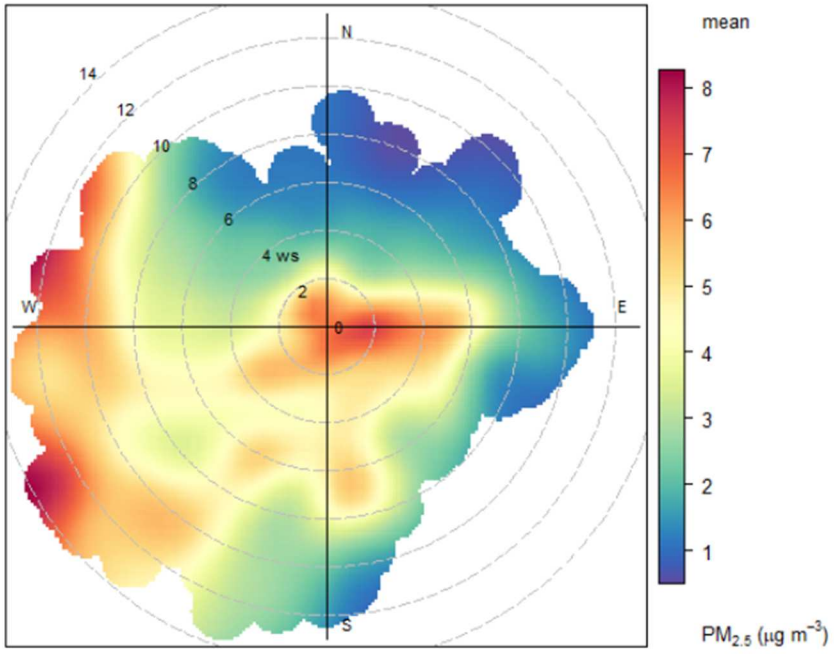

Figure 3.28. Polar plot for $PM_{2.5}$ of Glasgow Townhead AURN data from 19.01.2020 to 11.02.2021. High $PM_{2.5}$ concentrations from high wind speeds from the north-west, west and south-west. Also high concentrations locally and to the east.

Taking the above into consideration, sample 4038 and 4043 seemed to be from a mixture of diesel and petrol emissions, with larger contributions from diesel vehicles which is supported by the PAH_{max} being PHEN, rather than BghiP. Samples 4046 and 4047 had dominant petrol vehicle sources, due to their absence of 4-ring PAHs and a PAH_{max} of BghiP. Biomass burning or wood-smoke emissions seemed plausible as there were similarities between the 5-6 ring size distributions of GLA-KS samples and wood-smoke. This may have been from regional transport.

3.2.10. Results and Discussion: Measurement of Solvent-Extractable n-Alkanes in Known-Source Materials

The sources of n-alkanes were determined in known-source materials and airborne ambient PM samples from GLA-KS and MAN-FF (see Section 3.2.2 for details on sample collection). n-Alkane source indicators such as CPI, WNA and C_{max}, can distinguish anthropogenic and biogenic sources (see Section 3.2.4 for the methodology on calculations). The term 'anthropogenic sources' used in the literature refers to combustion of fossil fuels, wood, agricultural debris or leaves (Boreddy et al., 2018; Caumo et al., 2020; Rogge et al., 1993a). The term 'biogenic sources' includes particles shed from epicuticular waxes of vascular plants, direct suspension of pollen and microorganisms such as bacteria, fungi and fungal spores (Boreddy et al., 2018; Caumo et al., 2020; Rogge et al., 1993a). Biosynthesised n-alkanes exhibit strong odd/even carbon preference. The dominant homologues for epicuticular waxes are C_{29}, C_{31} and C_{33} (Rogge et al., 1993a). These n-alkanes contribute up to 90 % of all paraffins found in plant waxes (Rogge et al., 1993a). The presence of these n-alkanes in airborne ambient PM could help distinguish between fossil fuel combustion and biomass combustion which are both ambiguously included under the 'anthropogenic sources' term. Therefore, the terms 'fossil fuel combustion' and 'biomass combustion' will be used in place of 'anthropogenic sources' to describe n-alkane sources. As not all combustion activities are anthropogenic e.g., natural wildfires, these terms provide more clarity with regards to sources. Considering emissions from biomass combustion may contain epicuticular waxes of vascular plants from the biomass feedstock the term 'natural biogenic sources' will be used to describe natural non-combustion sources such as particles shed naturally from epicuticular waxes of vascular plants, direct suspension of pollen and micro-organisms such as bacteria, fungi and fungal spores.

Biomass Materials

The CPI values, WNA%, and C_{max} of known-source biomass materials are shown in Table 3.19. DB had the highest CPI out of all combusted biomass materials and the laboratory-made charcoals and outdoor wood-smoke had the lowest CPI values. Odd/even carbon preference was observed in DB and EB from C_{27} to C_{33} hence highlighting the presence of epicuticular waxes. This shows that the odd/even carbon preference exhibited by epicuticular waxes remains even after combustion. If particles emitted from biomass burning also exhibit

such patterns, this meant that biomass combustion sources could be identified in airborne ambient aerosols.

Table 3.19. Carbon preference index (CPI), plant wax n-alkanes ratio (WNA%) and C number with the highest concentration (C_{max}) of biomass materials.

Material	Sample ID	CPI	WNA%	C_{max}
DB	*3988*	7.38	74.09	C_{27}
EB	*4005*	1.85	15.29	C_{18}
MC-300-01	*3998*	1.10	10.67	C_{19}
MC-600-01	*3999*	1.13	8.31	C_{26}
MC-300-02	*4007*	1.40	15.72	C_{31}
Wood-smoke (indoors)	*4058*	1.77	23.64	C_{29}
Charcoal-smoke (indoors)	*4059*	2.60	36.49	C_{27}
Wood-smoke (outdoors)	*4060*	1.07	5.36	C_{25}

Charred Biomass

DB had a CPI value of 7.38 which was the highest out of the biomass materials (see Table 3.19Table 3.19). The n-alkane distribution plot in Figures 3.29 shows a distinct odd/even carbon preference for n-alkanes starting from C_{27} to C_{33} with the C_{max} value of C_{27}. This shows that DB has a high proportion of epicuticular wax n-alkanes. The WNA% of 74.1 % corroborated this. The DB sample contained uncharred fragments of biomass. This may have led to a higher CPI than EB (1.85), as non-charred fragments had higher contents of epicuticular plant waxes. EB was more homogenous; it was a powdery substance with no uncharred biomass fragments. The differences in CPI are explained by the thermal breakdown of long-chain n-alkanes, which leads to the dominance of even homologues that decrease the CPI (Kuhn et al., 2010). Thermal breakdown occurs during pyrolytic or combustion processes. EB also exhibited an odd/even carbon preference from C_{27} to C_{33}. However, the pattern was less clear. This showed that combusted biomass particles may retain the epicuticular wax odd/even carbon preference. This suggests that this pattern could be used to identify biomass combustion n-alkane sources in airborne ambient PM. However, the C_{max} of EB was C_{18} and the WNA% was 15.3 %. Low WNA% and C_{max} values of below C_{27} indicating anthropogenic sources. This highlights that observation of the n-alkane

distribution is more informative of biomass combustion sources than other source indicators such CPI, WNA% and C_{max}.

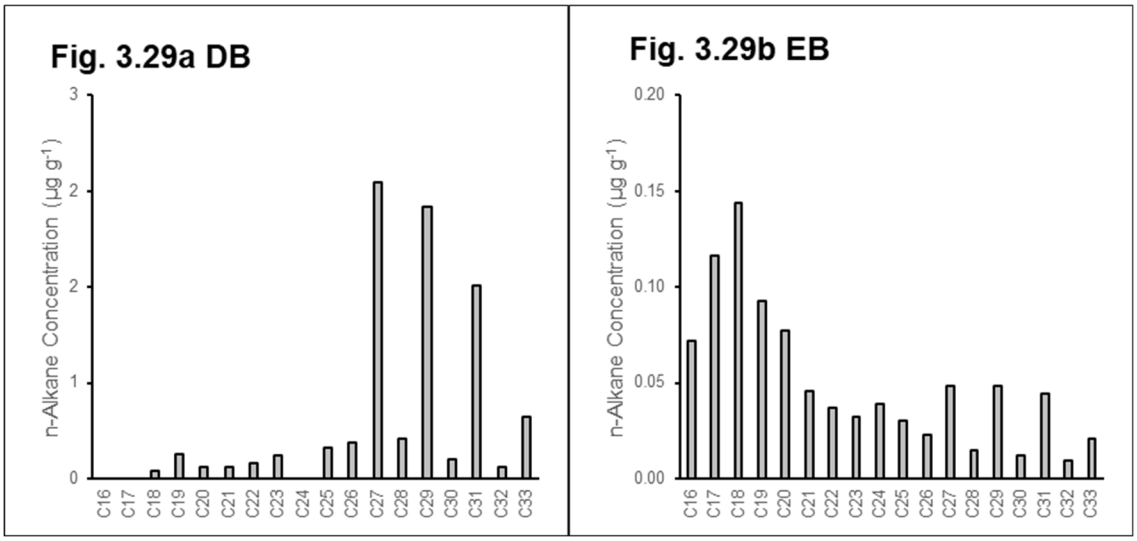

Figures 3.29. n-Alkane distributions of a) DB and b) EB.

Laboratory-made Charcoals

The laboratory-made charcoals MC-300-01 and MC-600-01 had low CPI values slightly above 1 (Table 3.19). This reflected the pyrolytic processes that formed the charcoal. Similar to EB, the WNA% was low, between 8.31 – 15.72 %, indicating a low percentage of epicuticular wax n-alkanes due to pyrolytic processes. The C_{max} for MC-300-01 and MC-600-01 was C_{19} indicating pyrolytic processes. MC-300-02 had higher CPI of 1.40 and C_{max} of C_{31} showing the presence of a dominant homologue for epicuticular waxes. This shows the variability among charcoal materials likely due to heterogeneity. Alternatively, the different charcoal formation conditions (temperature and pyrolysis time) may have affected the n-alkane distributions which are shown in Figures 3.30. This shows that it may be difficult to distinguish between fossil fuel combustion and charcoal combustion as odd/even carbon preference was not exhibited by the charcoals.

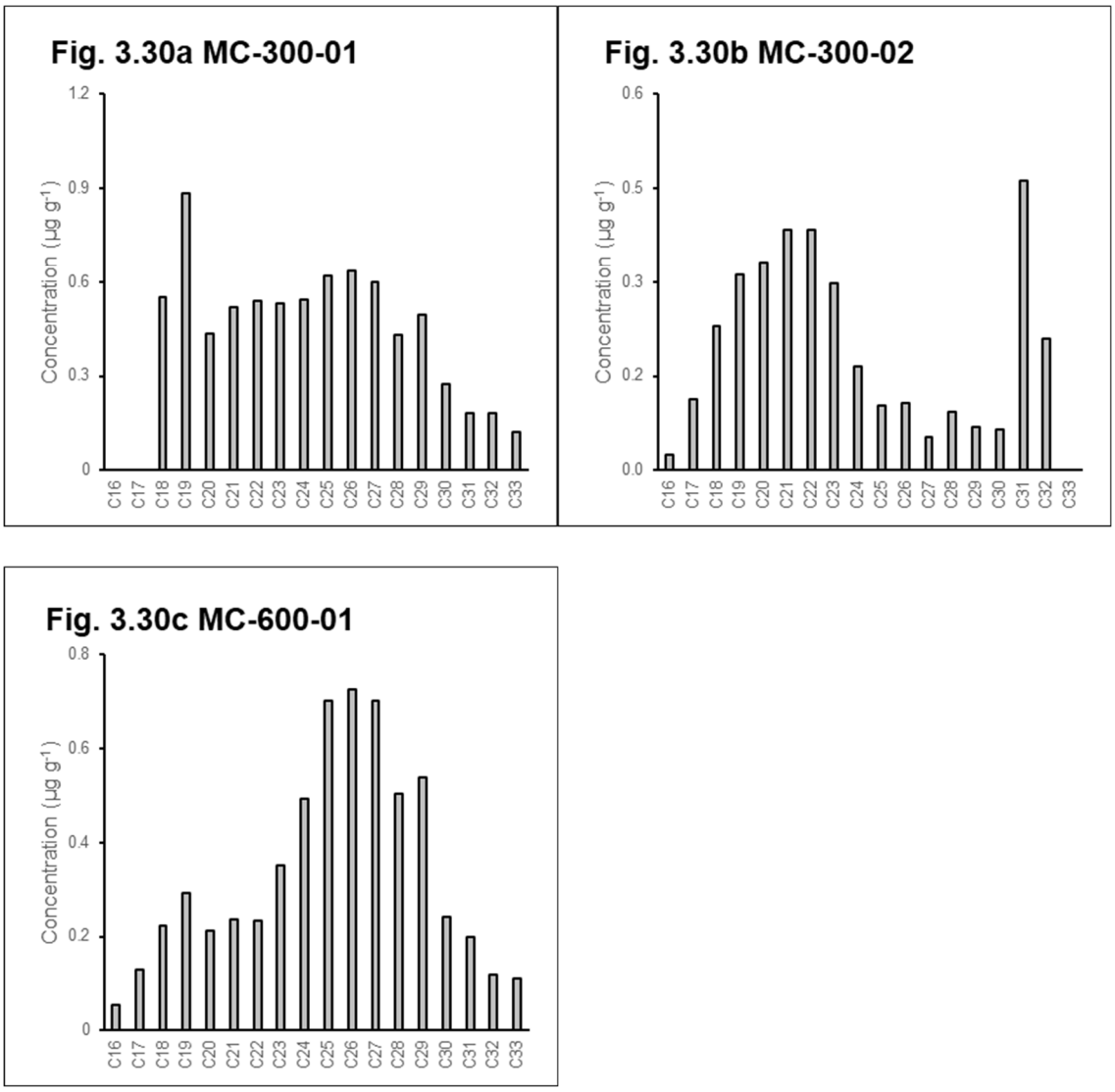

Figures 3.30. n-Alkane distributions of a) MC-300-01, b) MC-300-02 and c) MC-600-01.

Charcoal and Wood-smoke Samples

The CPI value for the indoor wood-smoke sample was 1.77, with a WNA% of 24 % and a C_{max} of C_{29} (see Table 3.19). The n-alkane distribution in Figure 3.31a showed an odd/even carbon preference from C_{25} to C_{29}. This pattern was different to those exhibited by DB and EB. This suggests that odd/even carbon preferences from C_{25} to C_{29} may be indicative of wood combustion emissions. The C_{max} was the same as that of *Celtis australis* twigs, reported in another study (Jambrina-Enríquez et al., 2018).

The outdoor wood-smoke sample had a CPI of 1.07, a WNA% of 5 % and a C_{max} of C_{25} (see Table 3.19). The C_{max} was found to be the same as the C_{max} of *Celtis australis* branches in another study (Jambrina-Enríquez et al., 2018). The outdoor wood-smoke sample had a low

CPI, WNA% and a C_{max} that did not represent epicuticular wax n-alkanes. The n-alkane distribution in Figure 3.31b did not show an odd/even carbon preference. This could be due to wood combustion n-alkanes being dispersed upon emission and mixing with ambient air particles. This shows it may be difficult to determine wood smoke emission n-alkane sources when there are good dispersion conditions. Hence, the use of this methodology may be limited when applied to airborne ambient PM, collected from areas with fewer wood combustion sources.

The charcoal-smoke had the highest CPI of 2.60 with a WNA% of 37 % and a C_{max} of C_{27}. Both the CPI and WNA % were higher than the indoor wood-smoke sample. The n-alkane distribution in Figure 3.31c did exhibit odd/even carbon preference from C_{25} to C_{29}, however the pattern was unclear and different from that of wood-smoke (indoors). This shows that it could be possible to differentiate between charcoal and wood smoke emissions. Conversely, as charcoal can be produced from a range of feedstocks, this cannot be guaranteed, as different feedstocks may exhibit variability. This could explain the difference between charcoal-smoke and charcoals (MC-300-01, MC-300-02 and MC-600-01) analysed. This was apparent also for biomass combustion feedstocks (Iinuma et al., 2007). The wood-smoke n-alkane source indicators reported here differed to those reported by Seng et al. (2007) who found the CPI of wood smoke (seraya wood and kulim wood) to be 1.35 and 1.10 respectively. However, the results here were similar to those reported by He et al. (2010) who analysed airborne ambient PM from Singapore during the regional haze episode due to biomass burning and reported a CPI of 1.59 and WNA% of 35.76 % during October 2006.

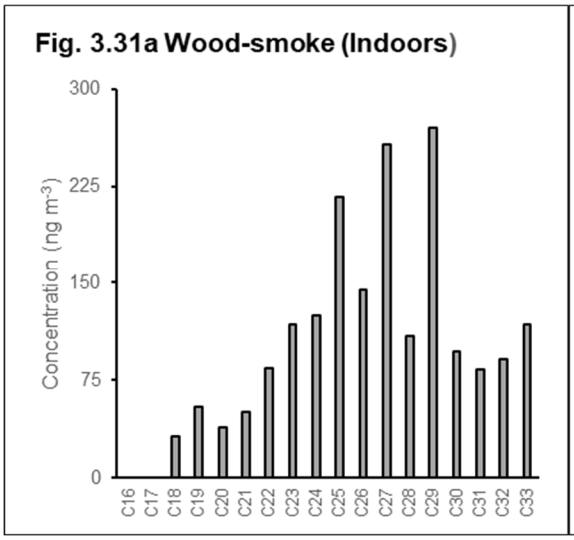

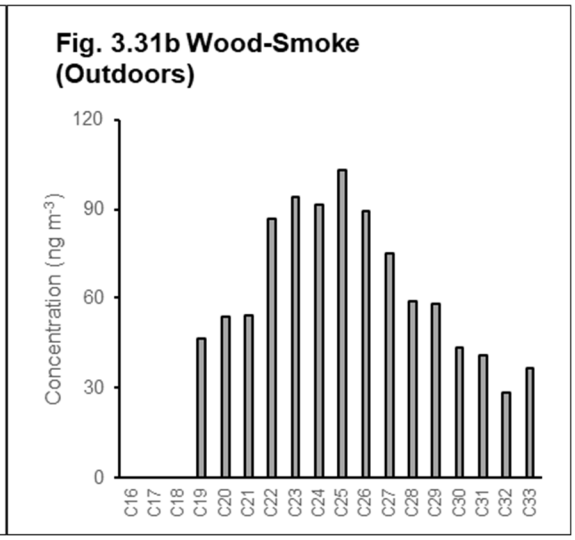

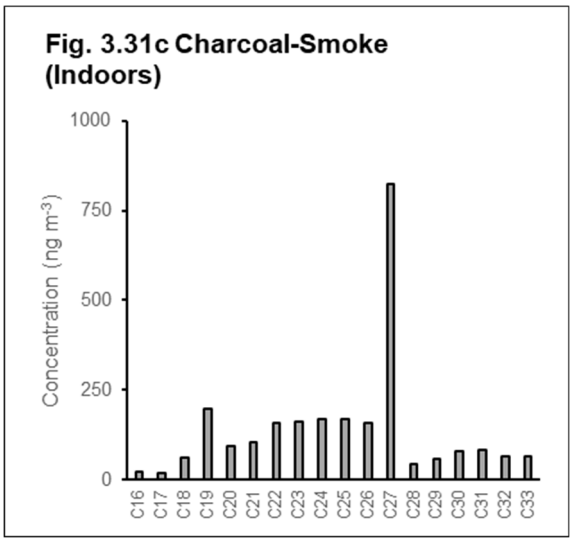

Figure 3.31. n-Alkane distributions in a) wood-smoke (indoors), b) wood-smoke (outdoors) and c) charcoal-smoke (indoors).

Fossil Fuel Materials

The CPI, WNA% and C_{max} for the fossil fuel materials are shown in Table 3.2. In the case of DS, which had replicate n-alkane measurements, the average CPI was calculated through applying Equation 6 (Section 3.2.6), to the average n-alkane concentrations. The C_{max} of the average value was determined through determining the maximum concentration of n-alkanes. DS had lower CPI and WNA% than BZ. The C_{max} values were C_{29} for BZ and C_{19} for DS average.

Table 3.20. CPI, WNA% and C_{max} of fossil fuel materials.

Material	Sample ID	CPI	WNA%	C_{max}
BZ	*3988*	1.65	17.03	C_{29}
DS rep 1	*3992*	1.08	10.27	C_{26}
DS rep 2	*4146*	1.43	23.76	C_{25}
DS rep 3	*4147*	0.49	11.40	C_{26}
DS Average		1.00	15.29	C_{19}

BZ Lignite

The lignite standard, BZ, had a CPI of 1.65, exhibiting an odd/even carbon preference from C_{23} to C_{31} (see Figure 3.32a) indicating natural biogenic sources. The C_{max} was C_{29} indicating presence of epicuticular waxes. The result was within the range of CPI values in other studies that noted lignite samples had a CPI >1 and/or C_{max} values of C_{29} or C_{31} (Del Rio et al., 1992; Havelcová et al., 2012; Jaraula et al., 2013; Paul et al., 2015; Zheng et al., 2020). CPI values of 1 in lignite represent an immature sample without a significant higher plant input, but CPI values of 3 are typical for immature and low rank coals with input from higher plants, leaf cuticles, spores and pollen (Killops & Killops, 2005; Stefanova et al., 2005). The CPI for BZ was between these numbers indicating a moderate input from higher plants, leaf cuticles, spores, and pollen. The WNA% of 17.03 % corroborates this as it was slightly higher than WNA% of DS and lab-made charcoals, which had low WNA% from combustion/pyrolytic processes. This suggests differentiating between uncombusted fossil fuels and biomass combustion may be difficult as BZ exhibited odd/even carbon preference from C_{25} to C_{29} like indoor wood-smoke. Yet, uncombusted fossil fuels are unlikely to be found in airborne ambient $PM_{2.5}$.

DS

DS had the lowest CPI of biomass and fossil fuel materials, ranging between 0.49 – 1.43. The CPI range was wider than those reported for diesel exhaust emissions in the literature (0.99 - 1.02) (Charron et al., 2019; Simoneit, 1984). The WNA% ranged from 10.3 to 23.8 %. It is possible that the replicate yielding 23.8 % WNA% was anomalous, possibly caused by contamination, as the other 2 replicates yielded similar WNA% (10.27 and 11.40 %). The 2 replicates were also in agreement with values from the literature (7 to 17.1 %), from samples likely to be from petrol/diesel emissions (Caumo et al., 2020; Cincinelli et al., 2003; Lin & Lee, 2004). As seen in Figure 3.32b, the C_{max} for DS was C_{19} , which was $\leq C_{25}$, thus within the fossil fuel emissions category. However, for individual replicates the C_{max} was C_{26} and C_{25} with C_{25} representing combustion sources and C_{26} representing mixed sources. Within the literature the C_{max} values for diesel emissions are C_{21} and C_{22} (Simoneit, 1984); however the C_{max} value may be dependent on the diesel fuel used as demonstrated by Caumo et al. (2020) where the C_{max} varied from C_{21} to C_{32}, highlighting the complexity of emissions of different fuels. Charron et al. (2019) also noted the most important n-alkanes in diesel exhaust emissions were C_{19} to C_{26}. DS would be expected to have a relatively low CPI in

comparison to other standards and this was true for 2 out of 3 replicates. The average CPI was less than all other known-source materials. The n-alkane distribution showed no odd/even carbon preference meaning it will be possible to distinguish between biomass combustion and fossil fuel combustion n-alkanes sources in airborne ambient PM.

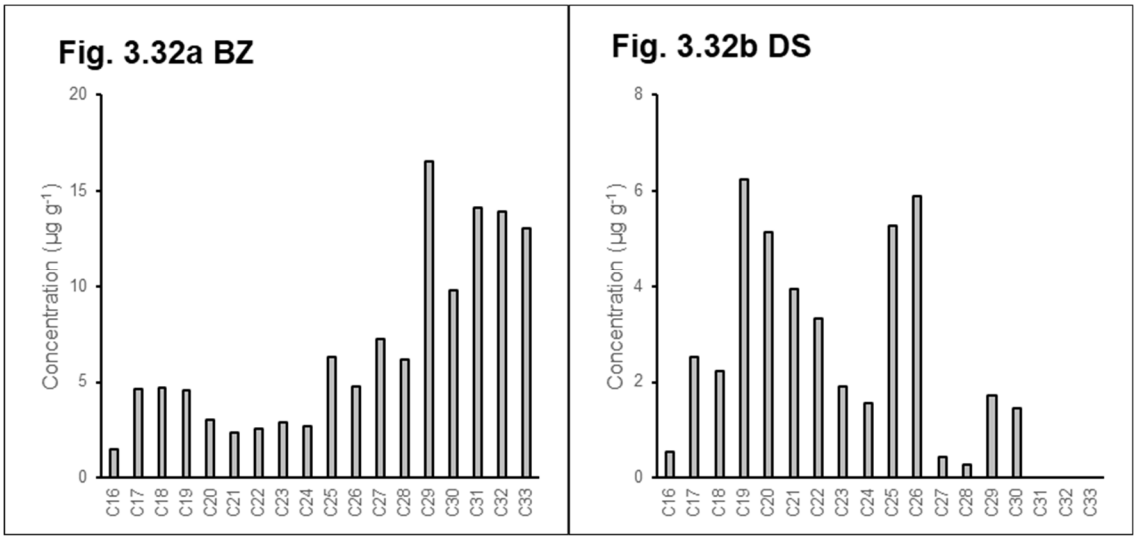

Figure 3.32. n-Alkane distributions of a) BZ and b) DS.

Aerosols and Dusts

The use of source indicators was used on aerosols and dusts to determine if biomass combustion sources were likely. As mentioned previously, it was difficult to distinguish between n-alkane distributions from uncombusted fossil fuels such as lignite and combusted biomass. However, it was unlikely that uncombusted biomass would be present in airborne particles.

HH-RD had the largest CPI value (4.04), see Table 3.21.The CPI of aerosol materials were roughly the same (around 1.43 – 1.46). BCR-RD had an extremely low CPI of 1.12 and WNA% of 4.59 %. FD, HH-RD and BCR-RD had C_{max} values within the range of C_{29} to $C_{31,}$ indicating the presence of epicuticular wax n-alkanes.

Table 3.21. CPI, WNA% and C_{max} of aerosol and dust materials.

	Sample Code	CPI	WNA%	C_{max}
UD	*3983*	1.46	21.41	C_{26}
UPM	*4000*	1.43	21.94	C_{25}
FD	*4003 rep 1*	1.43	12.33	C_{29}
	4004 rep 2	1.47	13.82	C_{29}
	Average	1.45	13.01	C_{29}
HH-RD	*3985*	4.04	56.83	C_{31}
BCR-RD	*4009*	1.12	4.59	C_{33}

Aerosols

The aerosol standards (FD, UD and UPM) had CPI values ranging from 1.43 - 1.46 (see Table 3.21) demonstrating the presence of fossil fuel and biomass combustion sources as the CPI >1. Han et al. (2018) noted that a CPI < 2 was a typical characteristic of urban environments with major contributions from fossil fuel sources such as vehicle exhaust and industrial emissions. Within the literature, urban areas had CPI values ranging from 1.20 – 2.80. (Cincinelli et al., 2003; Lin & Lee, 2004; Simoneit, 1989). As mentioned in Section 3.2.8, UD and UPM likely had coal and coke, wood combustion and vehicular emission sources. Whilst FD was likely to have dominant vehicular emissions. The CPI is in agreement with such sources as it shows the presence of biomass combustion and/or natural biogenic sources likely from resuspended road dusts.

The n-alkane distributions in Figures 3.33 show FD had an odd/even carbon preference from C_{25} to C_{33} . This indicates biomass combustion sources and/or natural biogenic sources such as particles shed from epicuticular waxes of plants or pollen suspension. The C_{max} was C_{29} which could signify road dust sources (Lin & Lee, 2004; Rogge et al., 1993b; Yadav et al., 2013b). Considering FD was collected from Wisłostrada traffic tunnel it is more likely that a C_{max} of C_{29} represents road dust sources, which were resuspended due to vehicle-induced turbulence, that then adhered to the tunnel walls or settled on the tunnel sidewalks, where the material was collected. The WNA% corroborates this as it was lower for FD (12.33 %) than for UD and UPM (21.41 – 21.94 %). Furthermore, the WNA% for FD is line with other literature values, WNA% for TSP and $PM_{2.5}$ collected from traffic tunnels in São Paulo, Brazil, which had a WNA% range of 1 – 25 % with C_{max} values of C_{21}, C_{24} and C_{30} (Caumo et al., 2020).

UD and UPM show a clear odd/even carbon preference from C_{29} to C_{33}. This suggests the presence of epicuticular waxes, most likely from wood combustion. UD and UPM had very similar n-alkane distributions hence were likely to have similar n-alkane sources.

Road Dusts

BCR-RD did not exhibit an odd/even carbon preference, with a low CPI of 1.12 and the lowest WNA% (4.59 %) across all materials (see Table 3.21). This indicates that the n-alkanes in this material were predominantly derived from fossil fuel sources, with little biomass combustion and natural biogenic contributions. BCR-RD is a material that represents traffic tunnel emissions. As the tunnel was physically enclosed, the transportation of soils and pollen into the tunnel would have been hindered thus this may have resulted in lower concentrations of biogenic n-alkanes compared to UD and UPM. This was because of the proportion of n-alkanes from natural biogenic sources were very low compared to the proportion of fossil fuel sources. For BCR-RD the C_{max} value was C_{33}, despite having dominant fossil fuel sources. However, this result could also be from the presence of paraffinic substances, entering the material either from engine exhausts, lubricating oil or the fuel itself (Caumo et al., 2020; Simoneit et al., 2004). Another possibility was that it could represent the forests/grasslands surrounding the tunnel, in Stryia Austria as C_{33} n-alkane typically characterises grasslands, however this is less likely to explain the result, as the tunnel was a fairly closed system, limiting the potential for external carbon sources to enter (Schäfer et al., 2016). BCR-RD had a similar CPI to that found within PM_{10} from urban road dust in Oporto, Portugal, 1.11 ± 0.45 and Serbia, 1.07 – 2.40 (Alves et al., 2018; Flores et al., 2022; Kojić & Šolević Knudsen, 2021).

HH-RD had the second highest CPI across all materials (see Table 3.21). The CPI value was 4.04 which suggested dominant natural biogenic source inputs. The biogenic source was likely to be from vegetative detritus from nearby bushes, trees, and shrubs. The sample was collected in February 2020 during winter, when there was a large amount of plant litter present. Although large fragments of plant debris were removed from the sample during sieving, it was probable smaller particles of plant debris were retained within the sampling after sieving. Additionally, during winter in the UK, high wind speeds are experienced due to the jet stream tracking further south, allowing more Atlantic storms to affect the UK (*Met Office - Where are the windiest parts of the UK? n.d.*). Wind-induced turbulence can dislodge leaf surface waxes directly or by rubbing motions of leaves against each other

alongside resuspension of soil and road dust, that entrains vegetative detritus particles into the atmosphere (Rogge et al., 1993d). Moreover, high winds may displace soils which act as a pool for plant degradation, often having the same n-alkane range as epicuticular plant waxes (Rogge et al., 1993d). Another additional source input could be tree pollen, as the surface waxes contain n-alkanes (Hagenberg et al., 1990). In Scotland from early to mid-February, pollen occurrences are possible from Alder, a native common tree (*University of Worcester - Pollen Forecasting,* n.d.). Alder makes up 7 % of Glasgow's tree population thus it is probable this contributed to n-alkane concentrations (Rumble et al., 2015).

The n-alkane distribution plot in Figures 3.33e showed a clear odd/even carbon preference from C_{23} to C_{33} with a C_{max} of C_{31} which is a dominant homologue of plant epicuticular waxes (Rogge et al., 1993d). The WNA% was 56.8 % indicating roughly half the n-alkanes were derived from plant waxes. Despite being sampled in an urban area, CPI values for HH-RD were not in agreement with the CPI values from the latter publications, indicating dominant biogenic sources. Previous research has shown road dust to have dominant biogenic sources; in an urban area within Athens, Greece, where the coarse particles ($PM_{10-2.5}$) had an average CPI of 7.26. However, the CPI of a sample collected from the same location but in winter (March) rather than summer (August), was much lower (1.03) showing n-alkanes in road dust can exhibit seasonality (Andreou & Rapsomanikis, 2009). This was caused by a larger number of $\leq C_{25}$ homologues in fine and coarse particles, in the colder months, which led an increase in car usage. This was further corroborated by Flores et al. (2022) who found n-alkanes in PM_{10} exhibited a higher CPI of 2.3 in summer. However, HH-RD was collected in winter in the UK, where a large degree of plant debris is present on the roads, as well as high winds which may transport soil to the road that was sampled (Rogge et al., 1993b). Further research would need to be conducted to determine seasonality of n-alkanes in road dust from, through comparison of n-alkanes detected in winter and summer road dust samples.

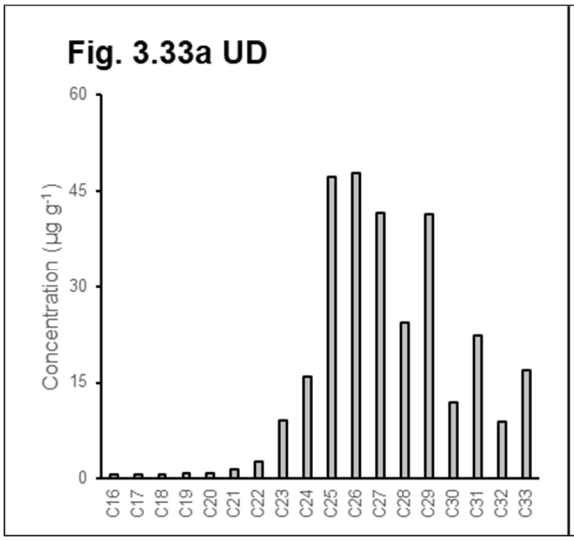

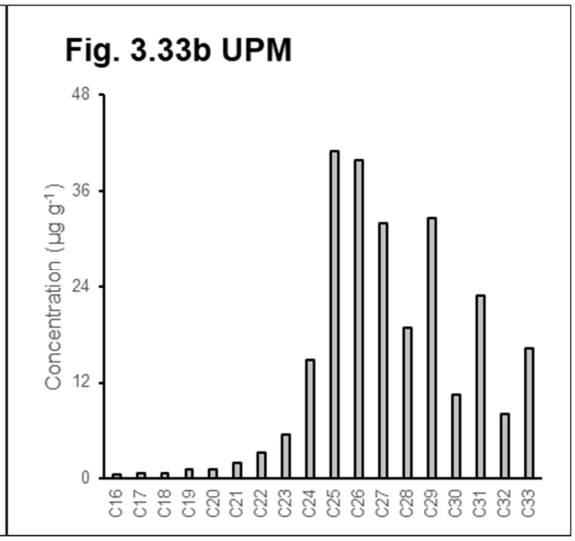

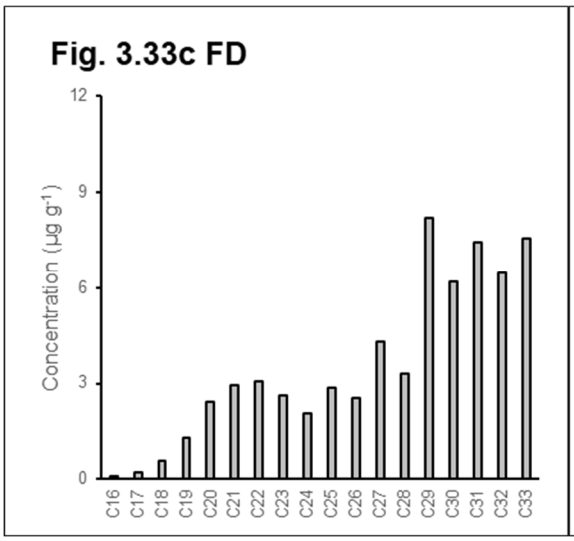

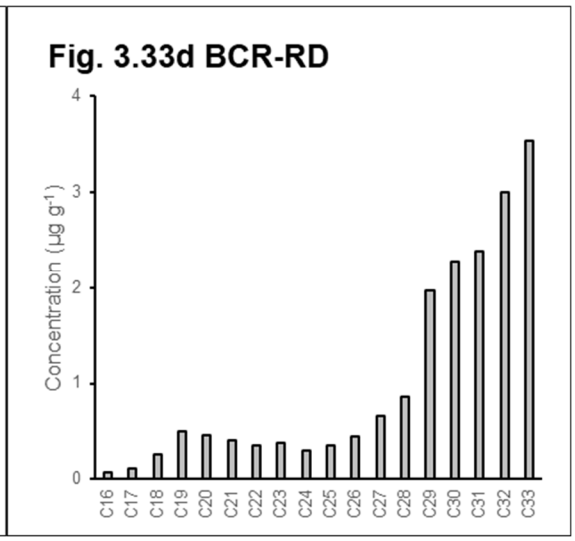

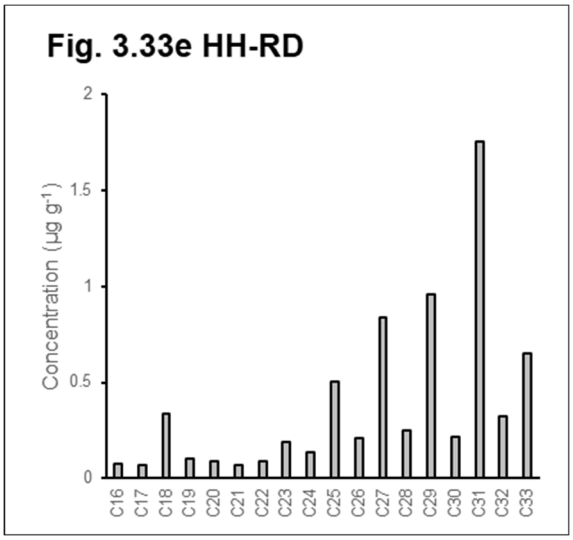

Figures 3.33. Solvent extracted n-alkane distributions in aerosol and dust materials a) UD, b) UPM, c) FD, d) BCR-D and e) HH-RD.

To visualise the sources of n-alkanes from the analysed standards, Figure 3.34 shows CPI values plotted against C_{max} . The plot shows that most of the sources of the standards lie in the 'mixed' category which denotes fossil fuel, biomass combustion and natural biogenic sources. To determine if the differences in CPI value could help distinguish sources, the lower quartile, median and upper quartile were calculated for all standards. The CPI of the standards were then plotted alongside quartile values in Figure 3.35 to determine if CPIs could categorise individual sources more closely, rather than only identifying broad groups within which many categories sit e.g., mixed sources. Figure 3.35 shows that materials in the same category were not always in the same area of the plot e.g., two charcoal samples are around the lower quartile whilst one is between the lower quartile and the median. However, all aerosol materials had CPIs around 1.45, likely representing a mixture of fossil fuel, biomass combustion and natural biogenic sources. CPIs around 1.12 included DS, BCR-RD and charcoals and thus represented anthropogenic sources. It was difficult to distinguish between n-alkanes from fossil fuel combustion and charcoals using CPI ranges from quartiles. It was also difficult to distinguish between uncombusted fossil fuel (BZ lignite) and wood combustion CPIs. Therefore, the use of broad categories was continued for data analysis and interpretation within the thesis. It should be noted that DB and HH-RD were not plotted in Figure 3.35 as their high CPIs meant it would be difficult to discern the other data points visually. These values were however included in the calculation of the statistics.

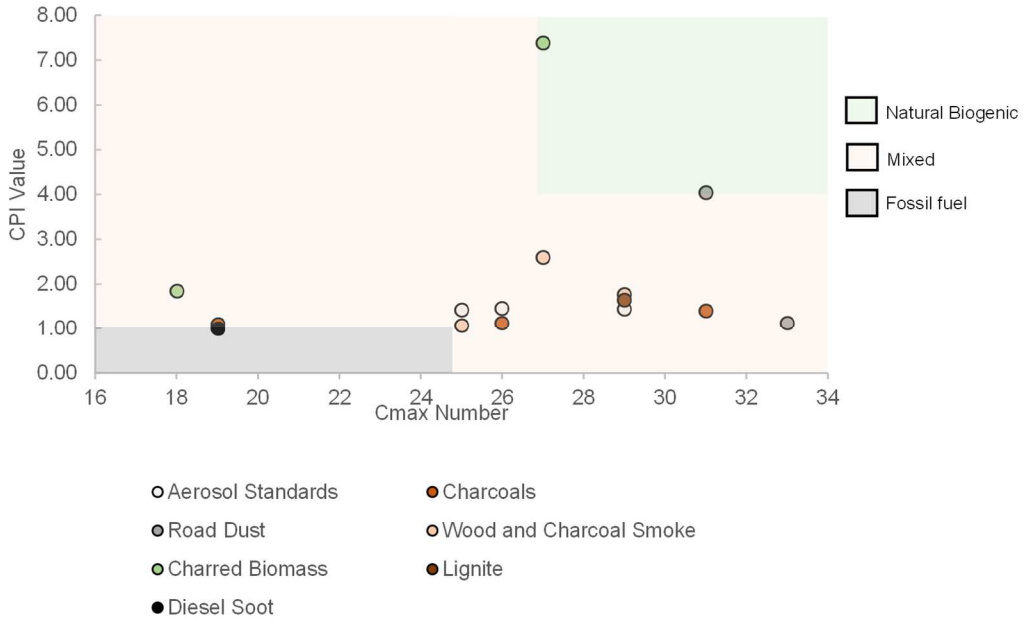

Figure 3.34. Plot of CPI vs. C_{max} number.

Figure 3.35. Visual depiction of CPI values and where they lie in relation to LQ, median and UQ.

3.2.11. Results and Discussion: Measurement of Solvent-Extractable n-Alkanes in Airborne Ambient PM Samples

Airborne Ambient PM from Manchester Fallowfield Site (MAN-FF)

As seen in Table 3.22 the CPI values for MAN-FF samples ranged from 1.29 to 1.84 with a C_{max} of C_{31} in most cases and C_{29} . All samples but 4028 exhibited odd/even carbon preference C29 to C33 (see Figures 3.36 and Figures 3.37). This meant possible sources were biomass combustion. Sample 4028 exhibited odd/even carbon preference from C_{27} to C_{33} indicating resuspended road dust containing vegetative detritus. Sample 4031 had the lowest CPI (1.29), hence was likely to have dominant fossil fuel combustion sources which was corroborated by a WNA% of 16.57 %. Sample 4033 had the highest CPI at 1.84 implying a larger proportion of n-alkanes from biomass combustion. This sample had the highest WNA% of 28.45 % similar to the WNA% of wood and charcoal-smoke.

Table 3.22. CPI, WNA% and C_{max} of MAN-FF($PM_{2.5}$).

	Plate Number	Sample Code	CPI (ng m^{-3})	WNA %	C_{max}
MAN-FF($PM_{2.5}$)	Plate 13	4028	1.34	17.60	C_{29}
	Plate 6	4031	1.29	16.57	C_{31}
	Plate 7	4032	1.66	24.94	C_{31}
	Plate 8	4033	1.84	28.45	C_{31}
	Plate 10	4034	1.42	21.28	C_{31}
	Plate 11	4035	1.40	18.88	C_{31}
	Plate 14	4036	1.65	23.94	C_{31}

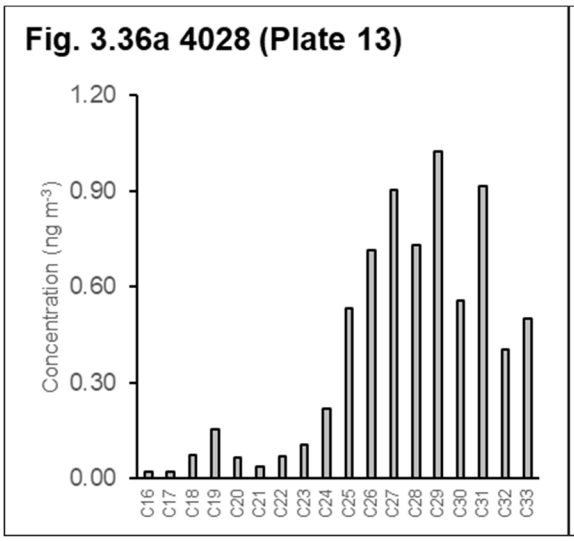

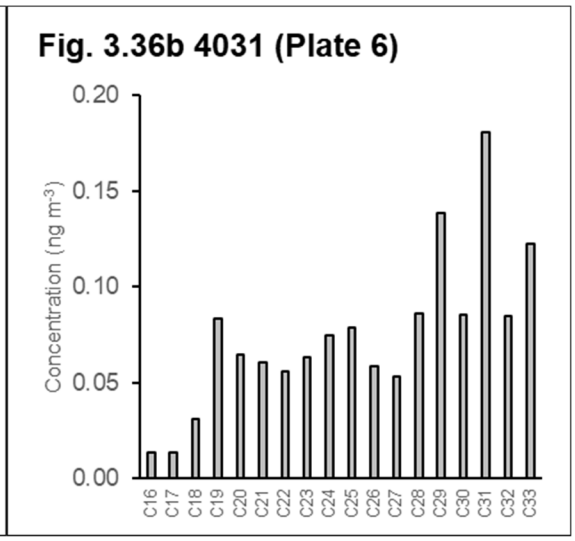

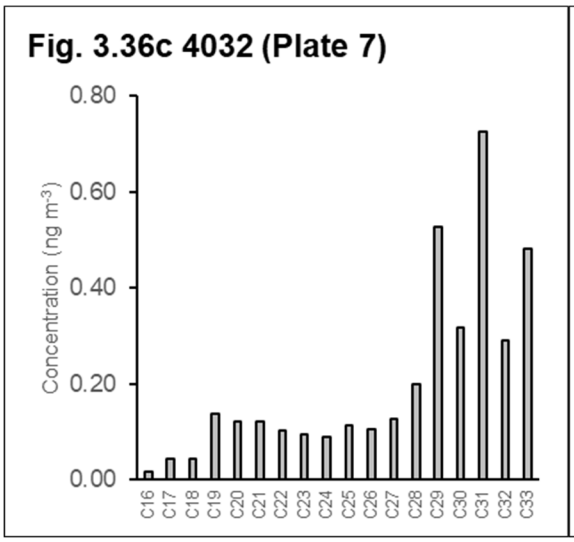

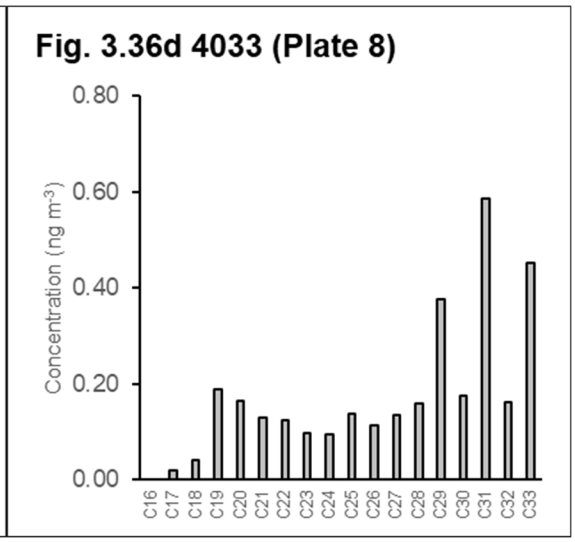

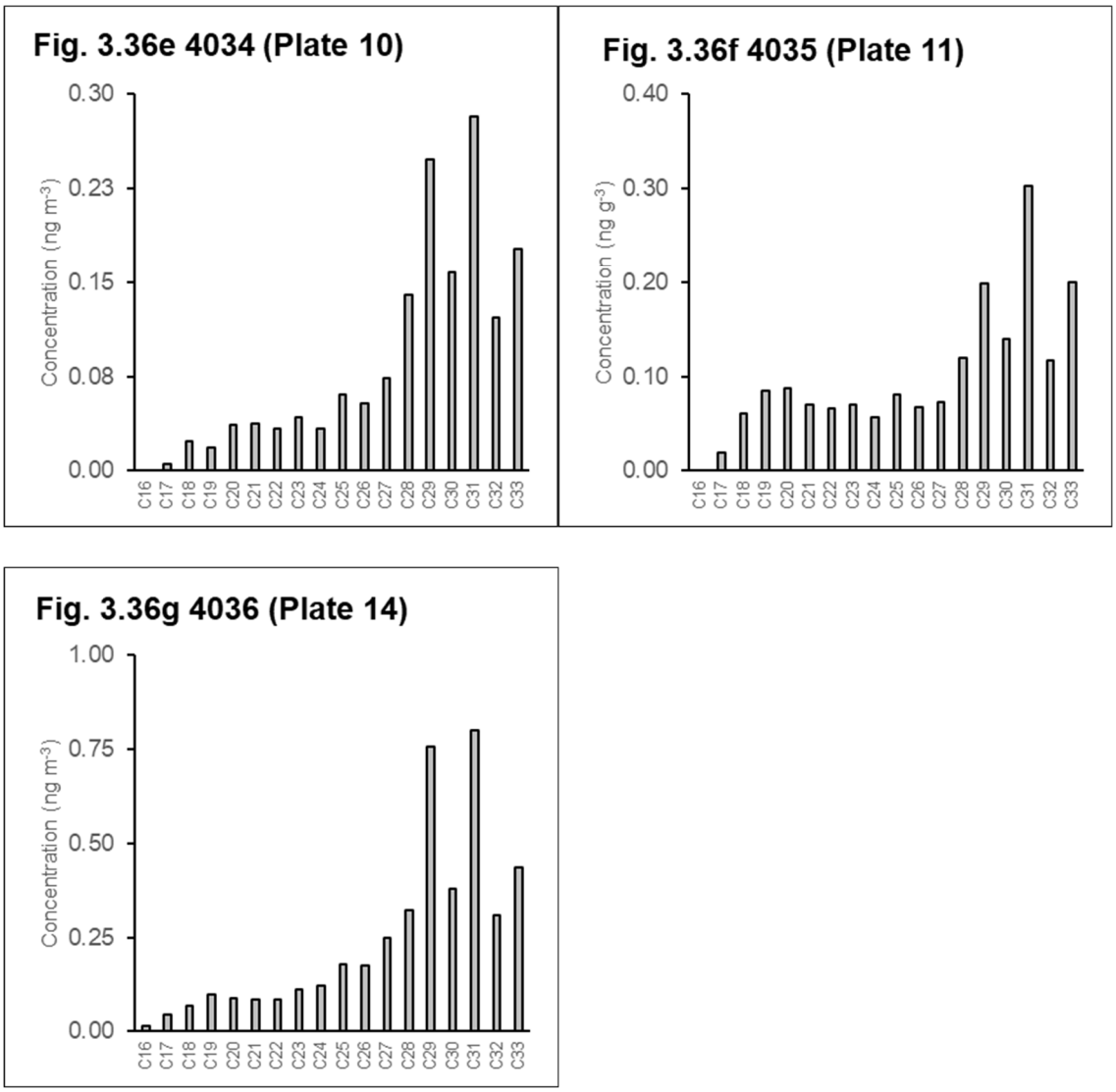

Figures 3.36. N-alkane distributions of MAN-FF($PM_{2.5}$) a) 4028, b) 4031, c) 4032, d) 4033, e) 4034, f) 4035 and g) 4036.

Airborne Ambient PM from Glasgow Kerbside AURN Site (GLA-KS)

As shown in Table 3.23 the CPI values of GLA-KS samples ranged from 1.40 to 1.92 indicating mixed sources. Samples 4038 and 4046 were similar to urban and traffic aerosol materials suggesting similar n-alkane sources. Sample 4038 was collected before COVID-19 lockdown measures hence may represent business-as-usual air pollution sources e.g. higher vehicular emissions and higher $PM_{2.5}$ concentrations (Jephcote et al., 2021). Sample 4046 was collected when COVID-19 lockdown measures were in place (26/03/2020 – 26/04/2021) . Sample 4046 was a $PM_{2.5}$ sample hence contains finer particles likely to be from combustion. However, sample 4043 and 4047 had higher CPI values of 1.63 and 1.92, indicating either biomass combustion and/or natural biogenic n-alkanes. This could be due

to smaller proportion of n-alkanes being released from petrol/diesel vehicular emissions due to COVID-19 restrictions (Jephcote et al., 2021).

Table 3.23. CPI, WNA% and C_{max} of GLA-KS(PM_{10}) and GLA-KS($PM_{2.5}$).

	PM Size Fraction	Sample Code	CPI (ng m^{-3})	WNA %	C_{max}
GLA-KS	PM_{10}	*4038*	1.40	21.94	C_{31}
	PM_{10}	*4043*	1.63	19.07	C_{25}
	$PM_{2.5}$	*4046*	1.40	18.48	C_{31}
	PM_{10}	*4047*	1.92	29.45	C_{31}

The n-alkane distributions shown in Figures 3.37 for 4038, 4043 and 4047 exhibit odd/even carbon preference from C_{25} to C_{33}. For 4046 the odd/even carbon predominance was from C_{27} to C_{33}. The C_{max} was C_{31} across all samples but 4043 hence this indicated presence of epicuticular plant wax n-alkanes. Odd/even carbon preferences from C_{27} to C_{33} correspond to fine particulate vegetative detritus from direct and indirect (resuspension of soil and road dust) release of green, dead, and degraded plant wax material (Rogge et al., 1993d). The odd/even carbon preference for C_{25} in 4038, 4043 and 4047 confirms the vegetative detritus is from resuspended road dusts as C_{25} indicates fossil fuel emissions. The WNA% of 4038, 4043 and 4046 ranged from 18.48 – 21.94 % like the UD and UPM materials WNA% (~22 %). However, sample 4047 had a higher WNA% of 29.45 % which could indicate larger proportions of vegetative detritus either due to increased wind or traffic induced turbulence.

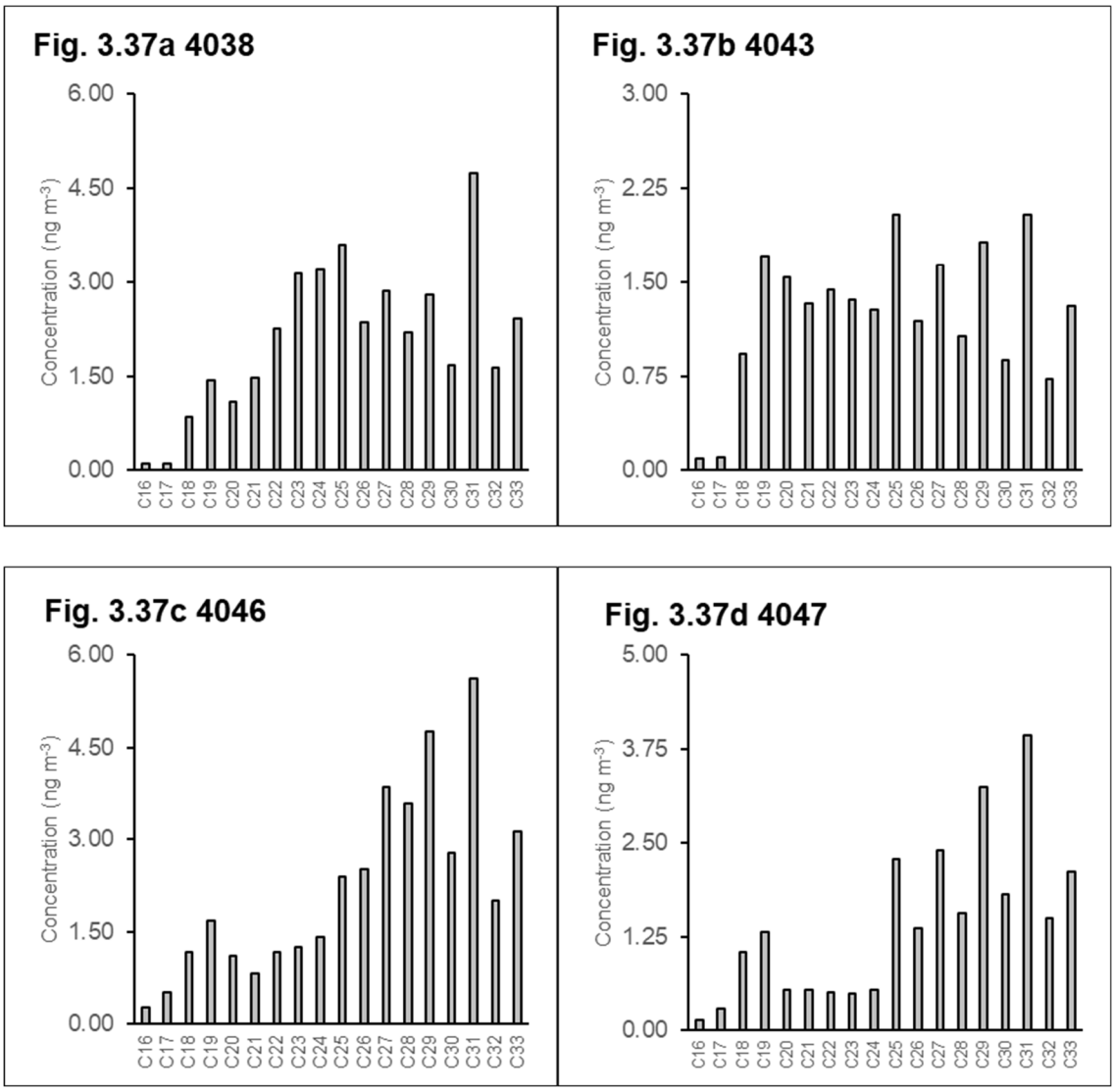

Figures 3.37. n-Alkane distributions of GLA-KS(PM_{10}) a) 4038, b) 4043, d) 4047 and c) GLA-KS($PM_{2.5}$) (4046).

Comparison of GLA-KS and MAN-FF

The C_{max} of GLA-KS and MAN-FF samples was C_{31} except for 2 samples 4043 (GLA-KS) and 4028 (MAN-FF) (see Table 3.22 and Table 3.23). This was similar to MC-300-02 and HH-RD which had a C_{max} of C_{31} showing the presence of epicuticular waxes.

The CPI range of GLA-KS and MAN-FF samples indicated that samples had CPI values within the expected range of urban aerosols (1.20 – 2.80). (Cincinelli et al., 2003; Lin & Lee, 2004; Simoneit, 1989). The CPI was < 2 indicating dominant combustion sources. However, sources likely contained mixtures of fossil fuel combustion, biomass combustion and natural biogenic sources. GLA-KS($PM_{2.5}$) had a lower CPI (1.4) than MAN-FF($PM_{2.5}$) samples and was in the median of the MAN-FF CPI range (1.29 – 1.84) (see Table 3.22 and Table 3.23).

This shows that GLA-KS($PM_{2.5}$) had a higher proportion of fossil fuel combustion sources than MAN-FF, which is expected for an urban traffic site. The GLA-KS(PM_{10}) CPIs were higher than MAN-FF($PM_{2.5}$). This was likely due to the particle sizes being larger in GLA-KS(PM_{10}) samples, as research has shown that the particle size of the airborne ambient aerosol analysed can cause slight variation in the CPI value (Ladji et al., 2014; Marty & Saliot, 1982; Tang et al., 2006). Alves et al. (2000); Tang et al. (2006) found natural biogenic n-alkanes accumulated in larger aerosol whilst combustion sources in the smaller aerosol. This could be due to n-alkanes being co-emitted with BC (and adsorbed to its surface), during fossil fuel combustion. BC would be within the fine fraction of PM (Liang et al., 2005). In the UK, coarse PM ($PM_{10}-PM_{2.5}$) which is a component of PM_{10}, was more closely correlated to road dusts and showed a positive dependence on windspeed (Harrison et al., 1997). This explains the reasoning behind natural biogenic n-alkanes accumulating in larger aerosol as road dusts will contain vegetative detritus. This was corroborated by GLA-KS(PM_{10}) samples having odd/even carbon preference over a larger range from C_{25} to C_{31} compared to GLA-KS($PM_{2.5}$) sample which had an odd/even carbon preference from C_{27} to C_{31} (see Figures 3.37). C_{25} is an indicator of vehicle exhaust emissions therefore an odd/even carbon preference including C_{25} indicates road dust sources (Gupta et al., 2017).

MAN-FF samples had odd/even carbon preference from C_{29} to C_{31} for all samples but 4028 which odd/even carbon predominance from C_{27} to C_{31} (see Figures 3.36). This suggested biomass combustion sources for all samples but 4028. Sample 4028 had contributions from vegetative detritus, from resuspended road dusts.

When comparing the CPI values obtained from MAN-FF and GLA-KS to other UK sites, the CPI values were similar to $PM_{2.5}$, collected in winter, from an urban background site and rural site in the West Midlands (CPI range 1.5 – 1.6) and $PM_{2.5}$ from Elms Road Observatory site, Birmingham, which is situated in an open field (CPI value 1.76) (Pant et al., 2017). The GLA-KS CPIs were close to the reported values as 3 out of 4 samples were PM_{10} samples, hence likely to have a larger contribution from natural biogenic sources, than $PM_{2.5}$. The GLA-KS($PM_{2.5}$) sample was 1.4 hence slightly below the reported CPIs. GLA-KS($PM_{2.5}$) CPI would be expected to be closer to those reported for Regents Park and Marylebone Road, London (1.13 and 1.05) and A38 Queensway Tunnel Birmingham (0.99) (Pant et al., 2017; Xu et al., 2020). This is likely due to GLA-KS($PM_{2.5}$) being collected during COVID-19 restrictions hence less emissions from petrol and diesel vehicles.

Observing the correlation between n-alkanes and PAHs, can help determine n-alkane sources. Polycyclic aromatic hydrocarbons are formed from incomplete combustion. Whilst PAHs

can be emitted from natural sources such as wildfires and volcanic eruptions, these sources are limited in the UK, hence PAHs in the UK likely have dominant anthropogenic combustion sources (Howsam & Jones, 1998). Strong correlations (≥0.8) between total PAH concentrations and total n-alkanes concentrations indicate similar sources from combustion activities (biomass and fossil fuels). As natural biogenic sources would not originate from combustion a weak correlation (≤0.4) implies natural biogenic sources such as vegetative detritus in resuspended road dusts. The total n-alkane concentrations were plotted against total PAH concentrations for each sample, per site, to observe the relationship between the two groups of compounds.

The plot shown in Figure 3.38 of total PAHs vs. total n-alkanes (in $\mu g\ g^{-1}$) for GLA-KS PM_{10} and $PM_{2.5}$ samples shows a strong positive correlation suggesting similar n-alkanes and PAH sources. The R^2 was 0.84. Once the outlier point (GLA-KS($PM_{2.5}$) sample 4046) is removed the correlation becomes much weaker ($R^2 = 0.07$). However, when concentrations of total PAHs and n-alkanes were plotted in ng m^{-3} (see Figure 3.39) a weaker positive correlation is shown ($R^2 = 0.41$). Once the outlier point (GLA-KS($PM_{2.5}$) sample 4046) is removed the correlation becomes much weaker ($R^2 = 0.03$). This suggests that the GLA-KS PAHs and n-alkanes have different sources. This supports that the GLA-KS samples contain vegetative detritus from resuspended road dusts due to the weak correlation once the outlier datapoint was removed.

Figure 3.40 shows a scatterplot of total PAHs vs. total n-alkanes (in ng m^{-3}) for MAN-FF($PM_{2.5}$) showed a strong positive correlation ($R^2 = 0.79$) suggesting similar n-alkane and PAH sources. It is worth noting that when the outlier point in this plot was removed from the scatterplot, a positive correlation between PAHs and n-alkanes remained (R^2 of 0.83). This corroborates with the findings from n-alkane distributions, suggesting biomass combustion sources for all MAN-FF($PM_{2.5}$) samples but 4028 which contained vegetative detritus from road dust resuspension. In the UK domestic wood combustion is a dominant contributor to BaP, PM_{10} and $PM_{2.5}$ emissions according to the National Atmospheric Emission Inventories (NAEI 2020). MAN-FF samples were collected in winter when biomass burning is more likely to occur (Monks et al., 2017). However, Manchester and much of Greater Manchester is a smoke control area (UK Air, n.d.-d), however it is difficult to enforce this as domestic combustion occurs indoors. Moreover, air masses transported to Manchester may originate from non-smoke control areas. The air mass back trajectories for sample 4033, which had the highest CPI, originated from Europe indicating that the plant wax n-alkanes originate from domestic wood burning. For example, Zhang et al. (2020)

found a high contribution of brown carbon to aerosol absorption in France during winter, with the major sources being wood burning emissions from residential heating. The Nantes and Reims sites, which were nearby air mass origin sites in back trajectories for 4033 (see Figure 3.8) had 27 % and 32 % of brown carbon in 2014 – 2015 (Zhang et al., 2020). However, samples 4032 and 4036 also had high CPI values around 1.65, but the air mass did not originate or pass through Europe, indicating local biomass combustion sources. Other potential sources could be biodiesel blends as CPI values for GLA-KS and MAN-FF PM samples were in the range of those from São Paulo, Brazil (1.4 – 3.5) in traffic tunnels where biofuels usage was common (Pereira et al., 2023). However, more research would need to be completed to determine n-alkane distribution patterns from biodiesel emissions.

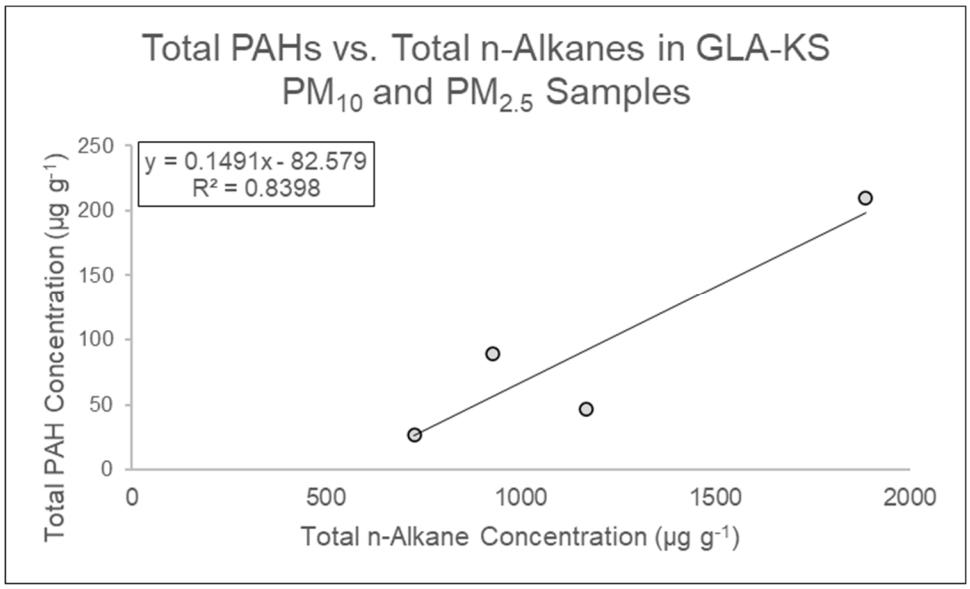

Figure 3.38. Scatterplot of total PAH concentration (µg g^{-1}) against the total alkane concentration (µg g^{-1}) in PM_{10} and $PM_{2.5}$ samples collected from GLA-KS.

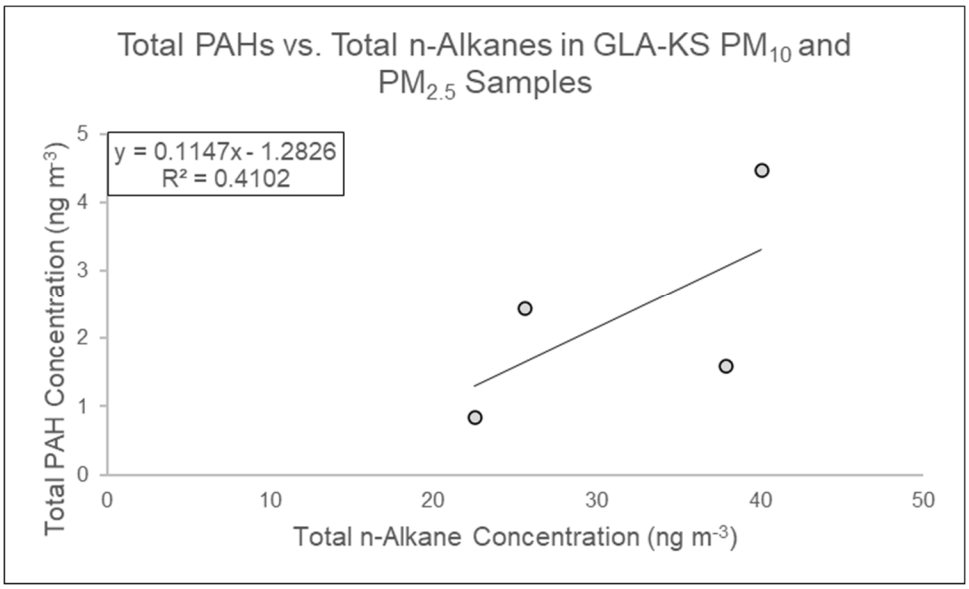

Figure 3.39. Scatterplot of total PAH concentration (ng m^{-3}) against the total n-alkane concentration (ng m^{-3}) in PM_{10} and $PM_{2.5}$ samples collected from GLA-KS.

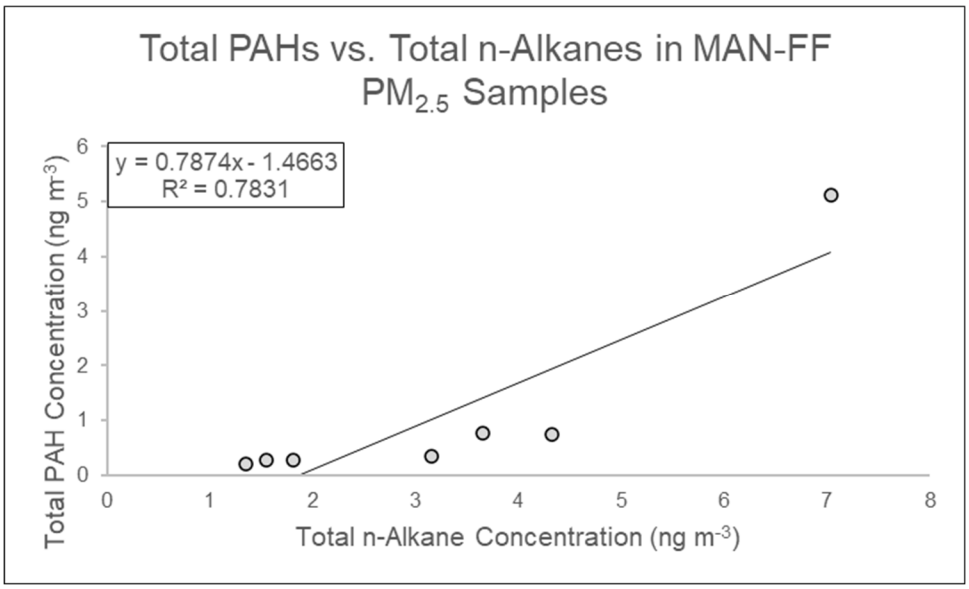

Figure 3.40. Scatterplot of total PAH concentration (ng m^{-3}) against the total n-alkane concentration (ng m^{-3}) in PM_{10} and $PM_{2.5}$ samples collected from MAN-FF.

3.2.12. Results and Discussion: Principal Component Analysis

To help determine biogenic and combustion emission sources in MAN-FF($PM_{2.5}$), GLA-KS($PM_{2.5}$) and GLA-KS(PM_{10}) PCA was undertaken on concentration data of known-source materials, to help identify potential sources for principal components. Then PCA was undertaken on MAN-FF($PM_{2.5}$), GLA-KS($PM_{2.5}$) and GLA-KS(PM_{10}) for source apportionment. PCA had to be conducted separately on known-source materials and airborne ambient PM samples due to unit differences.

The methodology can be seen in Section 3.2.7. However, it should be mentioned again that only factor loading values with modulus ≥ 0.3 are presented. Factor loadings for each principal component (PC) can be found in Appendix If.

Known-Source Materials

In four instances the eigen value was >1 therefore four source groups were identified, accounting for 100 % of the variance (Figure 3.41). PC 4 was not included in the analysis as it only accounted for 3.5 % of the variance, therefore was not a major source component of the analysed samples.

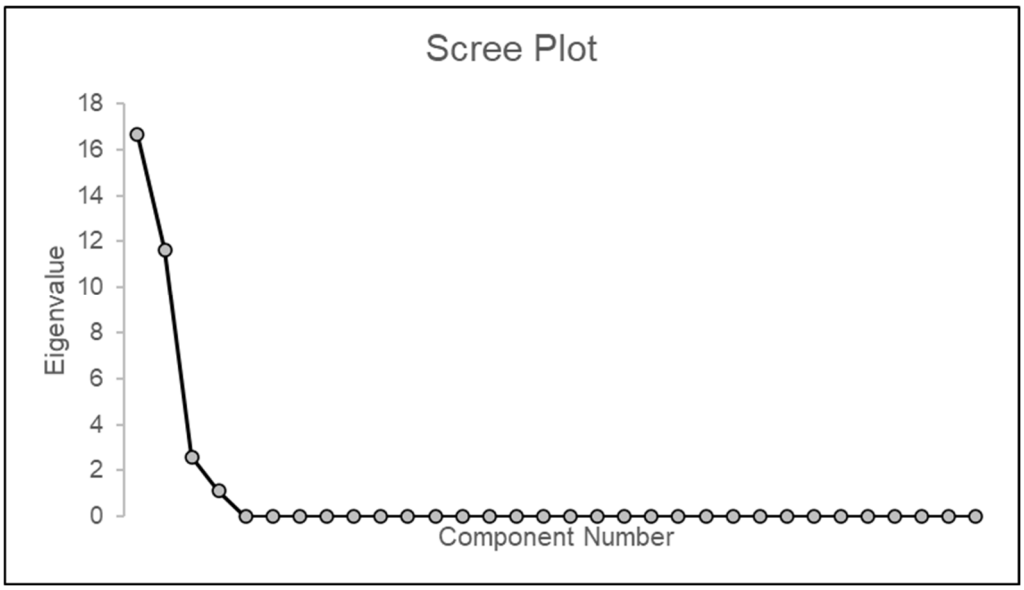

Figure 3.41. Scree plot for standards.

PC 1 in Figure 3.42 accounted for 43.8 % of the variance. The Rotated Component Matrix Loadings (y-axis of Figure 3.42) shows the degree of association between certain PAHs and n-alkanes to the PC.

PC 1 had high loadings for n-alkanes C_{23} to $C_{31,}$ and C_{33} and PAHs BghiP and IcdP. BghiP is strongly linked to vehicular emissions (Harrison et al., 1996; Ravindra et al., 2006; Smith & Harrison, 1998). BaP, BkF, BbF, FLA, PYR and BaA also had moderate loadings. DS showed high proportions of BbF & BkF, FLA, BaA. C_{19}, C_{20} and C_{21} had negative loadings. PC 1 represents vehicular emissions (diesel and petrol) direct and indirect through road dust resuspension. This explains why there are positive loadings for C_{29}, C_{31} and C_{33}, the dominant homologues for epicuticular waxes, due to vegetative detritus in resuspended road dust (Rogge et al., 1993b; Rogge et al., 1993a). Moreover, n-alkanes C_{25} and C_{27} are also linked to road dust emissions (Gupta et al., 2017). n-Alkanes below C_{25} and even n-alkanes such as C_{24}, C_{26}, C_{28} and C_{30} are linked to fossil fuel combustion and general combustion activities (Omar et al., 2007; Rogge et al., 1993b; Simoneit, 1984;1989; Yadav et al., 2020). PC 1 had similar PAHs present in road dust and vehicular emission PCs from Harrison et al. (1996) and Sarti et al. (2017).

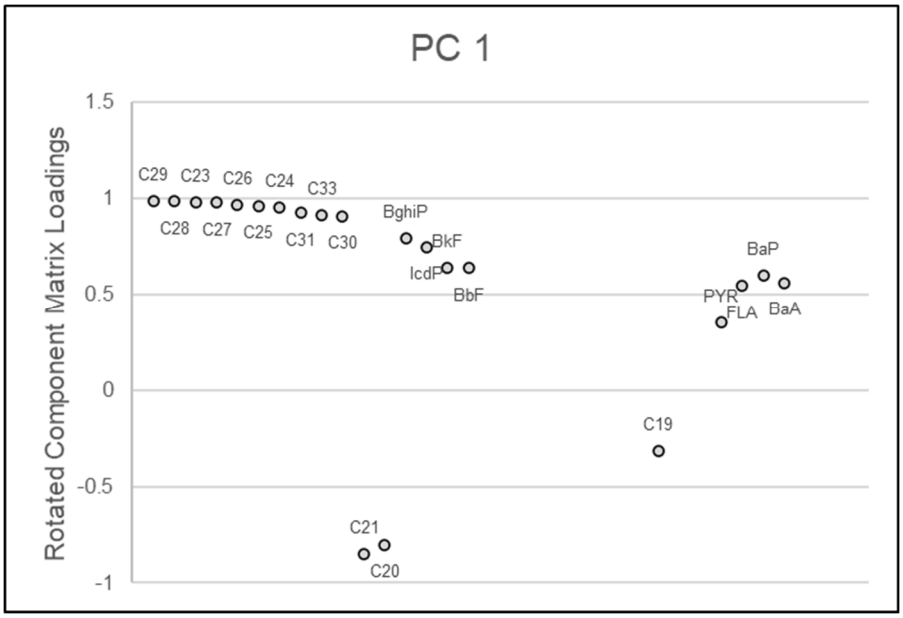

Figure 3.42. Principal component 1 of known-source materials.

PC 2 in Figure 3.43 accounted for 36.4 % of the high loadings for DahA, ACE, ACY, ANTH, PHEN, C_{16}, C_{17}, C_{18} and C_{32}. Moderate loadings were also found for BbF, BkF, C_{20}, C_{30} and

C_{33}. Negative loadings were found for PYR, BaA, CHRY, FLA and C_{22}. All aerosol and dust materials contained DahA, ACY or ACE and PHEN & ANTH. The source represented by PC 2 could therefore be industrial sources as it was found ACE, ACY and ANTH are indicative of cement plant industrial emissions, and DahA has also been detected in different industrial stacks (Ravindra et al., 2008a). Austria (BCR-RD origin), Poland (FD origin), and Missouri, USA (UPM origin) have cement production industries (European Commission, 2001; PCA, 2015; SPC, 2020). In the case of HH-RD, there were construction works happening during sample collection for the 'James McCune Smith Learning Hub' (Glasgow, n.d.). Whilst cement would not have been made on-site, it is likely concrete batching, which uses cement, could have been on-site. Therefore, cement plant emissions could be plausible.

Another additional source represented by PC 2 would be unburned petrogenic sources from accidental spills of unburned liquid fuels which PAHs like ACE, ACY, PHEN have been assigned to in other studies (Amarillo et al., 2017; Jiang et al., 2016; Pilková et al., 2022; Yang et al., 2005). Sources such as these would most likely be found in road dusts, hence are plausible for HH-RD and BCR-RD.

PC 3 in Figure 3.44 represents 8.0 % of the variance and is likely to be from coke, coal and wood combustion as it includes markers for coal combustion (ANTH, PHEN, FLA, PYR and BaA) (Harrison et al., 1996; Jiang et al., 2016; Ravindra et al., 2006) as well as markers for coke combustion (ANTH, PHEN, BaP and BghiP) (Harrison et al., 1996; Ravindra et al., 2006). Wood-smoke also contained the same PAHs in Figures 3.17, with high proportions of BkF and BbF, BaP and BaA. Additionally, Ravindra et al. (2006) found that wood combustion led to positive loadings for FLU, PHEN and ANTH. FLU was not included in PCA however PHEN and ANTH were detected in PC 3. BbF and BkF also had positive loadings. BZ's PAH 5-6 ring distribution showed high levels of BbF and BkF. BkF was also included in the coal PC in Harrison et al. (1996). Using PAH distributions, coal and coke emissions were identified as possible sources in UD, UPM and FD.

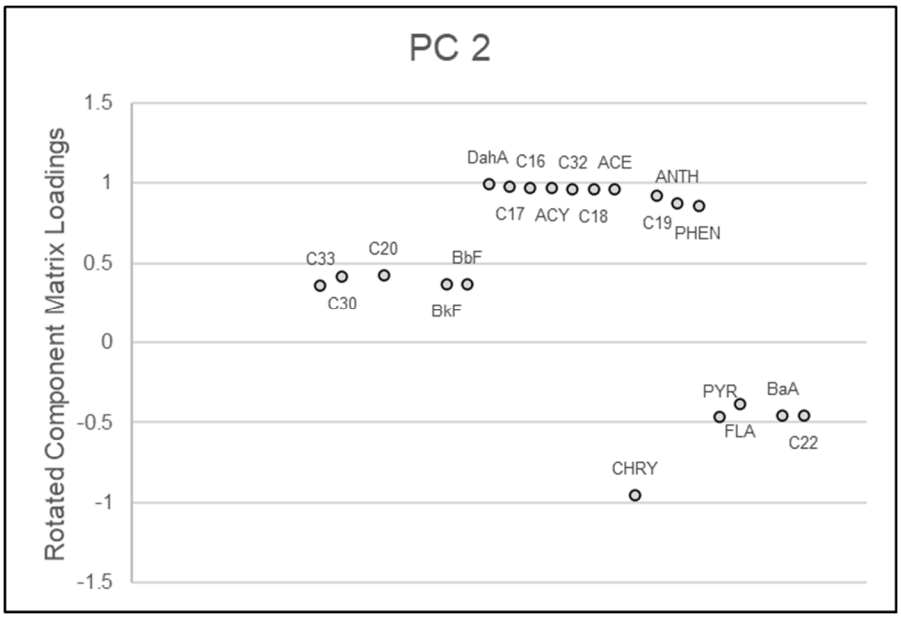

Figure 3.43. Principal component 2 of known-source materials.

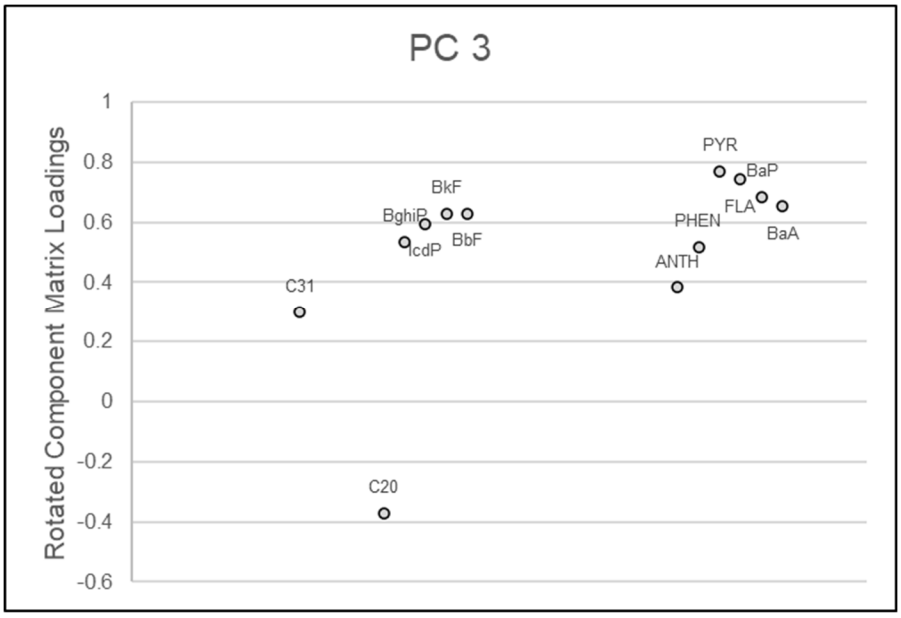

Figure 3.44. Principal component 3 of known-source materials.

Airborne Ambient Aerosols

In two instances the eigen value was above 1 therefore two source groups were identified, accounting for 99.7 % of the variance Figure 3.45. PC 1 consisted of 79.6 % of the variance whereas PC 2 consisted of 20.1 %.

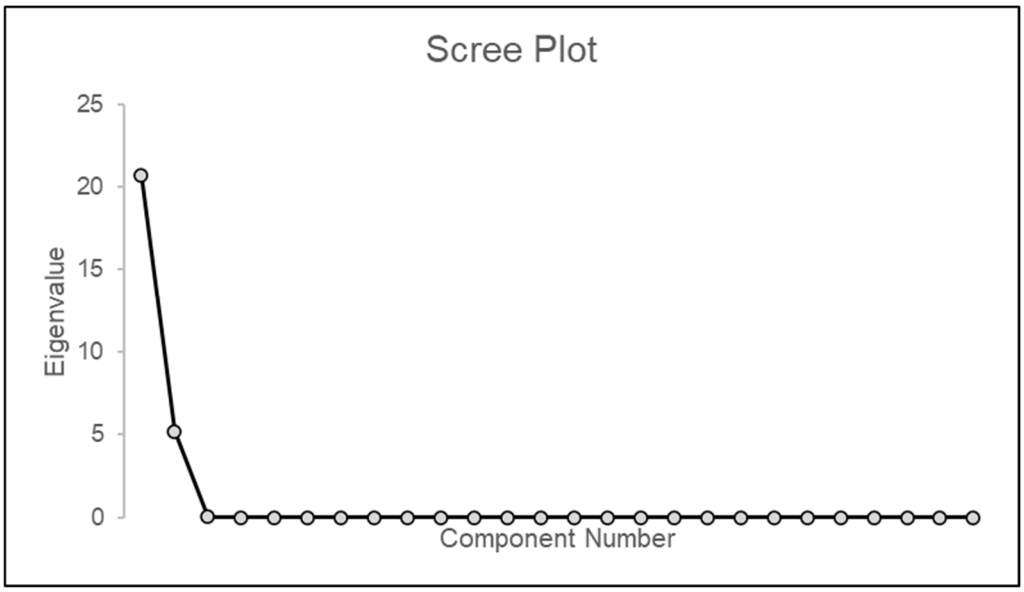

Figure 3.45. Scree plot for airborne ambient PM samples.

PC 1 (Figure 3.46) showed high loadings for most of the n-alkanes as well as PHEN and ANTH. BbF and BkF also had moderate loadings. This group was like PC 2 for the known-source materials. However, as 4-ring PAHs were often not detected in airborne ambient PM, it was difficult to directly compare PC from known-source materials to airborne ambient PM samples, as 4-ring PAHs were missing from the PCA. A possible source could be HDV diesel vehicle emissions as they have large LMW PAH contributions which could explain the high loadings for PHEN and ANTH (Marr et al., 1999; Miguel et al., 1998; B. Wang et al., 2021; Yadav et al., 2013a). Moreover, the DS PAH distribution showed high proportions of BbF and BkF in the 5-6 ring PAHs. Additionally, n-alkanes from C_{16} to C_{23} had the highest loadings which represent n-alkanes emitted from fossil fuel combustion (Omar et al., 2007; Rogge et al., 1993b; Simoneit, 1984; Yadav et al., 2020). It is possible PC 1 also demonstrated wood combustion sources as positive loadings were observed for PHEN and ANTH (Ravindra et al., 2006).

PC 2 (Figure 3.47) showed high loadings of BaP, IcdP, BghiP, BbF and BkF, with moderate loadings for C_{24}, C_{26}, C_{27} and C_{28}. These PAHs are often associated with vehicle emissions and n-alkanes with carbon numbers of C_{24}, C_{25} and C_{27} are associated with resuspended road dust (Gupta et al., 2017). This implies PC 2 represented either direct vehicular emissions or indirect vehicular emissions from resuspended road dusts. PC 2 may include LDV diesel vehicle emissions due to the BbF and BkF positive loadings (as seen in DS Figures 3.18). As 4-ring PAHs were only detected in 2 samples, this is a possibility.

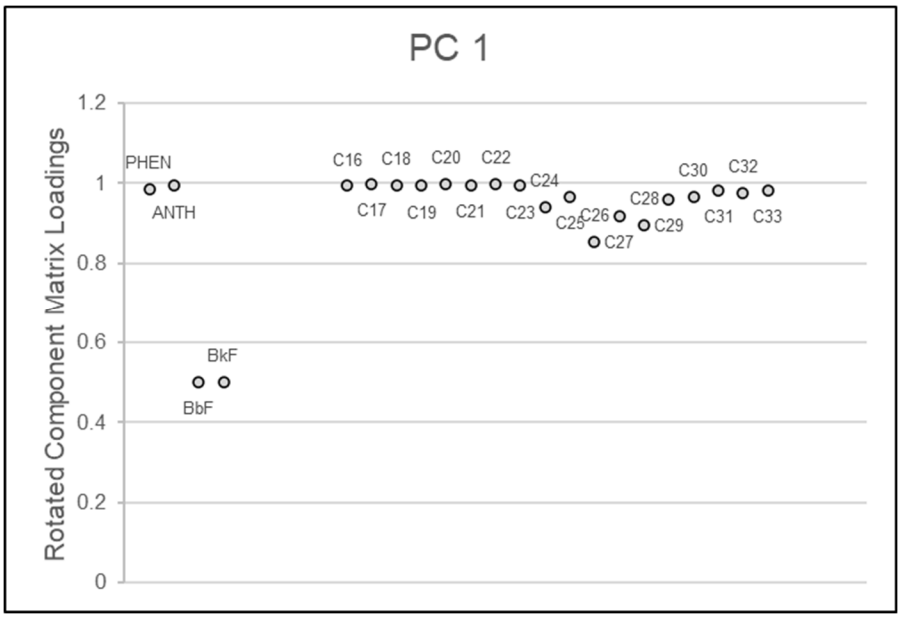

Figure 3.46. Principal Component 1 of airborne ambient PM samples.

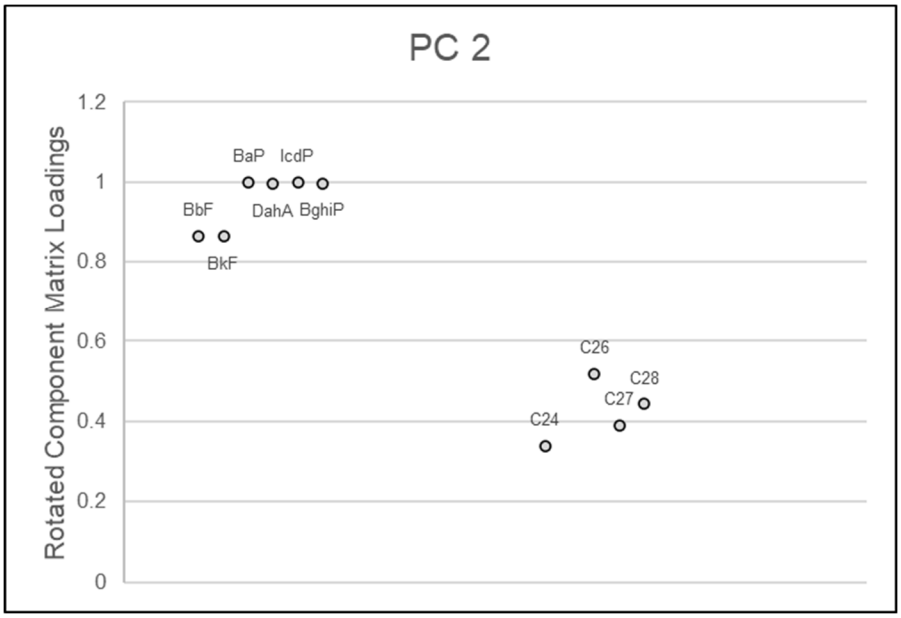

Figure 3.47. Principal component 2 of airborne ambient PM samples.

3.2.13. Conclusions

PAH-DR-1, PAH-DR-2 and PAH-DR-3 were mostly successful in determining sources across all materials. When PAH DRs could be calculated for biomass materials, they generally worked well in the case of MC-300-01, the PAH sources were correctly determined as originating from grass/wood/coal combustion (see Table 3.13. PAH DRs for biomass materials.). PAH sources in aerosol and dust materials agreed with dominant sources reported in national atmospheric emission inventories reported around the year of the materials collection. The source attribution of PAHs in fossil fuel materials were incorrect on two occasions in the work presented above. For example, PAH-DR-2 led to an interpretation of source originating from petroleum combustion instead of petrogenic for BZ. PAH-DR-1 determined sources to be from non-combustion sources in DS (see Table 3.14). This suggests that it may be difficult to differentiate between diesel soot and uncombusted petrogenic sources. Nevertheless, this work has shown that PAH-DR-1, PAH-DR-2 and PAH-DR-3 can be used with confidence to determine PAH sources in airborne ambient PM, when used in conjunction with PAH distribution plots.

The PAH sources of aerosol and dust materials showed a mixture of sources. Values for PAH DRs for aerosol and dust materials can be found in Table 3.15. The aim of these analyses was to determine the dominant source contributions of PAHs in the samples by applying PAH DRs and comparisons of PAH distributions to those of known-source materials. The PAH DRs of UD and UPM were diagnostic of combustion sources (0.75 and 0.76), petroleum combustion (0.38 and 0.41) and non-traffic sources (1.11 and 1.67). Through comparisons of PAH ring-size distributions, it was identified that possible sources of UD and UPM were coke/coal combustion sources likely as result of industrial processes and generation of electricity. Wood-smoke emissions and vehicular emissions were also identified.

The PAH DRs implied combustion (0.70), petroleum combustion (0.37) and non-traffic sources for FD (1.10). The PAH sources for FD were similar to UD and UPM except that a more notable contribution from diesel vehicle emissions was found. Coal combustion and wood-smoke emissions were also detected.

The PAH DRs for BCR-RD showed that this sample is likely to include non-combustion sources (0.28), petroleum combustion sources (0.25) and non-traffic sources (1.48). The sources were deemed to be from petrol and diesel vehicles as well as road dust from

weathered road surfaces. The PAH ring-size distributions were different to DS yet were more similar to those reported for HDV diesel emissions which have high proportions of 3-ring PAHs. The PAH-DR-1 was 0.74 for HH-RD, highlighting combustion PAH sources, as the value was close to 1. PAH-DR-2 and PAH-DR-3 could not be calculated for HH-RD due to PAHs within the calculation being below the limit of detection. HH-RD had a similar PAH distribution to DS, hence was thought to be from indirect diesel emissions.

The results from the known-source materials showed that PAH DRs in conjunction with observation and comparisons of PAH ring size distributions could successfully determine PAH sources. This meant this approach could then be used on airborne ambient PM samples. However, it is not always possible to find and/or produce appropriate known-source materials for some emission sources, hence in these instances identification of such sources can be quite speculative. The use of previous literature values can help to identify such sources but often such values may be indicative of the study area. For example, UK PAH emissions from vehicles may yield different results to emissions from other countries depending on the vehicle technology as well as the fuels used. Therefore, using this data in conjunction with other methods such as PCA and ^{14}C analysis could provide more confidence in the results.

The PAH sources for MAN-FF($PM_{2.5}$) samples were from combustion (PAH-DR-1 0.76 – 0.90), petroleum combustion (PAH-DR-2 0.33 – 0.38), and traffic sources (PAH-DR-3 0.41 – 0.90). PAH DR values per sample can be found in Table 3.17. The dominant sources of PAHs were from petrol vehicle emissions, as the PAH_{max} was BghiP across all samples. For 4034 the 3 – 4 ring PAHs were likely to be from diesel emissions, as the polar plot (Figure 3.24) showed high concentrations from the east/south-east where bus routes were present. The non-traffic sources were difficult to determine as only PHEN & ANTH were present in the samples. However, waste incineration was a possible source, as air mass back trajectories showed air masses travelling through Eastcroft EfW area on >1 of the sampling days. The 5-6 ring PAH distribution was similar to the known-source wood-smoke material analysed in Section 3.2.8. The sources therefore attributed to be dominantly from petrol vehicle emissions as the PAH_{max} was consistently BghiP. However, diesel emissions also contributed to the sources of the samples as PHEN and ANTH (co-eluted) were present indicating diesel emissions, most likely from HDV diesel vehicles such as buses which have large contributions of 3 ring PAHs (Marr et al., 1999; Miguel et al., 1998; B. Wang et al., 2021; Yadav et al., 2013a). Also in sample 4034, diesel vehicle emissions were clearly seen through the presence of 4-ring PAHs. The non-traffic emission source contributed to the

samples, that was likely to be wood-smoke emissions due to the 5 – 6 ring PAH distribution being similar to wood-smoke emissions as BbF and BkF accounted for 22-28 % of the 5-6 ring PAHs and BaP accounted for 12-24 % of 5-6 ring PAHs. It was unknown whether these emissions originated from commercial, institutional, residential, or agricultural sectors. The national atmospheric emissions for 2020 noted domestic wood combustion as the dominant PAH and $PM_{2.5}$ source in the UK 2020, therefore, domestic wood combustion was a probable source, although more research would need to be done to confirm this.

The PAH sources for GLA-KS(PM) samples were also from combustion (PAH-DR-1 0.61 – 0.90), petroleum combustion (PAH-DR-2 0.33 – 0.37), and traffic sources (PAH-DR-3 0.65 – 0.84). Values for each sample are shown in Table 3.18. Samples 4038 and 4043 showed larger diesel contributions. This was through the PAH_{max} which was PHEN for 4038 and 4043 derived from diesel emissions from buses, taxis and goods vehicles in the city centre and wood combustion transported locally and regionally. The PAH_{max} for 4046 and 4047 was BghiP, which is strongly associated to petrol emissions, hence the dominant PAH sources were from petrol emissions (Harrison et al., 1996; Ravindra et al., 2006; Smith & Harrison, 1998).

Overall, it was difficult to determine PAH sources in airborne ambient PM as some samples had low concentrations of 4-ring PAHs, which led to difficulties in source attribution through use of PAH ring-size distributions and PAH DRs.

The CPI values, WNA% and C_{max} gave valuable information about known-source materials, which could then be applied to airborne ambient PM samples. The CPI values for biomass materials ranged from 1.07 to 7.38. DB had the highest CPI value of 7.38 with a C_{max} of C_{27} and WNA% of 74.1 %. DB contained fragments of uncharred biomass. All other biomass materials had a CPI between 1 - 3 demonstrating combustion/pyrolysis processes that thermally breakdown long-chain n-alkanes, leading to the dominance of even homologues that decrease the CPI.

Laboratory-made charcoals had CPI values close to 1 representing the pyrolysis processes utilised to make the charcoals. Moreover, the outdoor wood-smoke sample had the lowest CPI of 1.07, WNA% of 5.36 % and C_{max} of C_{25}. This was likely due to dispersion of emissions from wood-smoke. This showed that it could be difficult to detect wood-smoke emissions in areas with fewer emissions and during periods with good dispersion conditions. DB and EB were the only materials to retain odd/even carbon preference from n-alkane distributions of DB and EB were C_{27} to C_{33}. This shows that some pyrolyzed/combusted

biomass materials do not retain epicuticular waxes, making it difficult to distinguish between fossil fuel and biomass combustion. However, wood-smoke showed a distinct odd/even carbon preference from C_{25} to $C_{29,}$ charcoal smoke had a C_{max} of C_{27} and MC-300-02 charcoal had a C_{max} of C_{31}. These characteristics could help identify combustion of biomass feedstocks.

Comparing the biomass materials to the fossil fuel materials, DS had an average CPI of 1, which was similar CPI and a higher WNA% than 2 of the charcoals (MC-300-01 and MC-600-01). Moreover, BZ, an uncombusted lignite, had a CPI of 1.65, WNA% 17.03 % with a C_{max} of C_{29} indicating a moderate input from higher plants, leaf cuticles, spores and pollen which was in agreement with CPIs from the literature (Del Rio et al., 1992; Havelcová et al., 2012; Jaraula et al., 2013; Paul et al., 2015; Zheng et al., 2020). Therefore, the CPI values were only able to determine if combustion processes had occurred but could not differentiate between biomass and petroleum feedstocks. Nevertheless, BZ represented an uncombusted fossil fuel sample, hence it is unlikely this will be a major source in airborne ambient PM. Furthermore, the n-alkane distribution for DS did not show odd/even carbon preference therefore through use of all n-alkane source indicators and n-alkane distributions, fossil fuel and biomass combustion n-alkane sources could possibly be distinguished.

The aerosol materials had CPIs around 1.43. UD and UPM had WNA% of 21.41 and 21.94 % respectively, with a C_{max} of C_{26} and C_{25} respectively, showing mixed sources. The WNA% of FD was lower, 13.01 %, indicating dominant traffic sources. BCR-RD, like FD represented traffic emissions, and had low WNA% and CPI (4.59 %, 1.12). HH-RD collected from Glasgow, contained a high CPI of 4.04, a WNA% of 56.83 % and a C_{max} of C_{31}. This showed that PM_{10} samples containing resuspended road dust may have large natural biogenic contributions from vegetative detritus.

GLA-KS(PM_{10}) and GLA-KS($PM_{2.5}$) samples CPI ranged from 1.40 to 1.92 (see Table 3.23). This suggested dominant fossil fuel combustion sources. Sample 4043 and 4047 had higher CPI values of 1.63 and 1.92, indicating a larger proportion of n-alkanes from epicuticular waxes. The n-alkane distributions showed odd/even carbon preference from C_{25} to C_{33} for all GLA-KS(PM_{10}) samples. This suggested that source of the epicuticular plant waxes was from resuspended road dust containing vegetative detritus (Gupta et al., 2017). GLA-KS($PM_{2.5}$) had an odd/even carbon preference from C_{27} to C_{33} with the lowest WNA% of 18.48 %. Coarse aerosols tend to contain a higher proportion of n-alkanes from natural biogenic sources; hence this could explain why the WNA% was lower in the GLA-KS($PM_{2.5}$) sample (Alves et al., 2000; Harrison et al., 1997; Tang et al., 2006). There was a weak

correlation between total PAHs and n-alkanes in ng m^{-3} (R^2 = 0.41). Once the outlier point GLA-KS($PM_{2.5}$) was removed the R^2 value was 0.03, hence supporting that epicuticular plant waxes were from vegetative detritus in resuspended road dust, as PAHs and n-alkanes had different sources.

The CPIs ranged from 1.29 to 1.84 for MAN-FF($PM_{2.5}$) samples with a C_{max} of C_{31} in most cases and C_{29} (f). This suggested dominant fossil fuel combustion sources. The n-alkane distributions of MAN-FF samples consistently displayed odd/even carbon preference for C_{29}, to C_{33} indicating the presence of epicuticular wax n-alkanes. The WNA% was close to that of wood-smoke (16.6 % – 28.5 %) indicating biomass combustion sources. Sample 4028 differed from other samples as it had odd/even carbon preference from C_{27} to C_{33} indicating resuspended road dust sources. When plotting the total PAHs against the total n-alkanes, a strong positive correlation was observed (R^2 = 0.79). When the outlier point was removed (sample 4028) the R^2 increased to 0.83. This supports that epicuticular wax n-alkanes (C_{29} to C_{33}) originated from combustion of biomass.

When comparing the CPI of GLA-KS($PM_{2.5}$) to MAN-FF($PM_{2.5}$) GLA-KS was below the median of the CPI range (1.29 - 1.84) therefore it was likely it had a higher proportion of fossil fuel n-alkanes. As GLA-KS is an urban traffic site, these were most likely from vehicular emissions. GLA-KS and MAN-FF samples were generally within CPI ranges from other UK sites including urban background and rural sites with CPI ranges of 1.5 – 1.76 (Pant et al., 2017). The GLA-KS CPIs were close to the reported values as 3 out of 4 samples were PM_{10} samples, hence likely to have a larger contribution from natural biogenic sources, than $PM_{2.5}$. The GLA-KS($PM_{2.5}$) sample was 1.4 hence slightly below the reported CPIs. GLA-KS($PM_{2.5}$) CPI would be expected to be closer to those reported for Regents Park and Marylebone Road, London (1.13 and 1.05) and A38 Queensway Tunnel Birmingham (0.99) (Pant et al., 2017; Xu et al., 2020). This is likely due to GLA-KS($PM_{2.5}$) being collected during COVID-19 restrictions hence fewer emissions from petrol and diesel vehicles (Jephcote et al., 2021).

Four principal components were identified for the known-source materials: PC 1 (43.8 %) indirect (resuspended road dust) and direct vehicle emissions (petrol and diesel), PC 2 (36.4 %) industrial emissions and uncombusted fossil fuels and PC 3 (8 %) coal, coke and wood combustion. PC 4 only accounted for 3.5 % of the variance so was not included. For the airborne ambient aerosols two principal components were identified. PC 1 (79.6 %) represented diesel vehicle emissions and wood combustion whilst PC 2 (20.1 %) represented

vehicular emissions or resuspended road dusts containing particulates from vehicle emissions.

3.3. Determination of the Health Risks of Solvent-Extractable Polycyclic Aromatic Hydrocarbons in $PM_{2.5}$ and PM_{10} from Urban Areas in Glasgow and Manchester

The health risks of PAHs in airborne ambient PM from GLA-KS and MAN-FF were determined through PAH analysis. BaP concentrations were compared against UK National Air Quality Objective (NAQO) for BaP in ambient air which is 0.25 ng m^{-3} published in the UK Air Quality Strategy 2007. The EU Fourth Air Quality Daughter Directive 2004 (FAQDD), which has been transposed into UK law, Air Quality Standards Regulation 2010, sets a target value of 1 ng m^{-3} for BaP in PM_{10} fraction, averaged over the year. As sampling did not represent a full year, the NAQO and FAQDD target values were used as a guideline to identify the level of health risks associated to inhalation of PM-bound PAHs. Additional health risk metrics were used to assess the air quality (with respect to health impacts) of sampled areas, such as BaP toxicity equivalent and the BaP mutagenicity equivalent for the PAH mixture, as well as lifetime excess cancer risk from inhalation of PAHs.

3.3.1. Methods

Analytical methods

PAHs were extracted from airborne ambient PM samples from GLA-KS and MAN-FF. Information on sample collection and the samples analysed can be found in Section 3.2.2, Table 3.3 and Table 3.5. The extracted PAHs were analysed using GC-MS. The sample preparation methods and the instrument conditions in Section 3.2.4 were used here.

Determination of Health Risks Associated with Inhalation of PM

To calculate the toxicity of each of the 16 priority PAHs, a toxicity equivalency factor (TEF_i) was used. This helps to express the toxicity of PAHs relative to BaP, referred to hereon as the BaP toxicity equivalent (BaP_{Teq}) (Gao et al., 2019b). In Equation 8, PAH_i represents the concentration of each the 16 priority parent PAHs detected in the sample using ng m^{-3} units. The TEF_i values used were those suggested by Nisbet and Lagoy (1992), used in a recent

study by Samburova et al. (2017): NAPH, ACE, FLU, PHEN, FLT, PYR (0.001), ANT, CHRY, BghiP (0.01), BaA, BbF, BkF, IcdP (0.1), BaP (1.0) and DahA (5.0). This equation was used to estimate the toxicity of the PAHs in GLA-KS(PM) and MAN-FF($PM_{2.5}$). These values were based on a large amount previous research studies including animal studies investigating the carcinogenicity of PAH mixtures compared to the carcinogenicity of BaP alone (Nisbet & Lagoy, 1992). Nisbet and Lagoy (1992) stated that their TEF_i values reduced uncertainty in PAH risk assessments and would not lead to underestimated risks for mixtures containing high levels of non-carcinogenic PAHs.

$$\sum[BaP_{Teq}] = \sum_{i=1}^{i\,(No.of\ PAHs\ Detected)}([PAHi] \times [TEFi]) \quad (8)$$

The mutagenicity of environmental exposure of PM-bound PAHs was also calculated using Equation 9 for GLA-KS(PM) and MAN-FF($PM_{2.5}$) using the mutagenic equivalent BaP_{Meq} by using their specific MEF_i values obtained from Durant et al. (1996): BaA (0.082), CHRY(0.017), BbF (0.25), BbK (0.11), BaP (1), IcdP (0.31), DahA (0.29) and BghiP (0.19).

$$\sum[BaP_{Meq}] = \sum_{i=1}^{i\,(No.of\ PAHs\ Detected)}([PAHi] \times [MEFi]) \quad (9)$$

The methodology described by Ramírez et al. (2011) and Bandowe et al. (2014) was followed to estimate the lifetime lung cancer risk from inhalation ($ILCR_{inh}$) of PM-bound PAHs in ambient air, using Equation 10. The methodology is based on a procedure from the Office of Environmental Health Hazard Assessment (OEHHA) of the California Environmental Protection Agency and has been used to inform environmental policies (Morello-Frosch et al., 2002). The cancer unit risk factor of IUR_{BaP} is defined as the upper limit of the possibility of contracting cancer for a daily exposure to BaP in air of 1 µg m^{-3} during a 70-year average lifespan (OEHHA, 2005; USEPA, 2011). There are uncertainties when quantifying the cancer risk estimates of PAHs due to the use of IUR_{BaP} values which are not derived from epidemiological studies in the study location e.g., Glasgow or UK. Instead, the three internationally accepted IUR_{BaP} values that are often used in the literature are used here: WHO 8.7 x 10^{-5} (ng m^{-3})$^{-1}$, OEHHA 1.1 x 10^{-6} (ng m^{-3})$^{-1}$ and USEPA 6.0 x 10^{-7} (ng m^{-3})$^{-1}$, denoted as $ILCRinh_{(a)}$, $ILCRinh_{(b)}$ and $ILCRinh_{(c)}$ respectively. (OEHHA, 2005; USEPA, 2017; WHO, 2000). According to the World Health Organisation (WHO) the acceptability of a certain risk should be taken by national authorities (WHO, 2000).

Threshold values for $ILCR_{inh}$ could not be found for the UK or Europe. Thresholds from the literature suggest a value of $ILCR_{inh} \leq 1 \times 10^{-6}$ is negligible or regarded as safe by most institutions and governments formulating safety levels, a value in the range 1×10^{-6} to 1×10^{-4} suggests a potential risk and a value $>1 \times 10^{-4}$ implies a potentially high risk (Cao et al., 2019; Ghanavati et al., 2019; Wang et al., 2011a). These were in line with the thresholds recommended by the WHO for carcinogens in drinking water (1×10^{-5}) and the U.S. EPA risk of 1×10^{-6} were used (Robson & Toscano, 2007; WHO, 2017).

$$ILCR_{inh} = IUR_{BaP} \times \sum BaP_{Teq} \quad (10)$$

The estimated corresponding annual number of lung cancer cases within the population close by the GLA-KS sampling location that could be attributed to PAH inhalation was calculated using Equation 11.

$$\frac{Population\ Exposed\ (number\ of\ inhabitants) \times lifetime\ lung\ cancer\ risk}{70\ (years\ of\ exposure)} \quad (11)$$

Calculations were completed using the population data from the local administration ward in which GLA-KS was situated Anderston, Yorkhill and City.

3.3.2. Results and Discussion of Health Risks

BaP Concentrations

The average BaP concentration for GLA-KS(PM_{10}) was 0.21 ng m^{-3} thus not exceeding the NAQO for BaP (see Table 3.24). However, the GLA-KS($PM_{2.5}$) average BaP concentration did exceed the NAQO concentration by a factor of 4 (0.97 ng m^{-3}) although was still below the FAQDD target value. It is worth noting the calculated BaP concentrations are not annual means. The NAQO and FAQDD are used to protect the populations from adverse health effects of poor air quality as it is the "the largest environmental risk to public health in the UK" (UK Parliament, 2022). As these measurements were above the NAQO and close to the FAQD, this indicates that the health risks associated to BaP concentrations in Glasgow should not be considered negligible. Moreover, BaP concentrations in business-as-usual scenarios are likely to be higher than those observed here, as most of the samples were collected whilst COVID-19 lockdown measures were in place. Glasgow's annual status report (2021) stated that there had been significant reductions in air pollution levels at all monitoring locations in Glasgow, in 2020, due to traffic reduction from COVID-19 restrictions (Glasgow City Council, 2021).

It should be noted that the $PM_{2.5}$ concentration of sample 4046 BaP was considerably higher than the PM_{10} samples' BaP concentrations (see Table 3.24). This could be due to combustion PAHs being more strongly correlated to fine particles, as they are co-emitted with BC, and adsorbed to its surface. The UK PAH network, measures PAHs in the particle phase from the PM_{10} fraction of ambient air (which includes $PM_{2.5}$) rather than solely $PM_{2.5}$. de Kok et al. (2005) found that $PM_{2.5}$ particles had more total and carcinogenic PAHs per µg than PM_{10} particles due to greater surface area (de Kok et al., 2005; Pandey et al., 2012). Moreover, the health effects of $PM_{2.5}$-bound PAHs may be more adverse due to $PM_{2.5}$ and its bound PAHs penetrating into the gas-exchange region of the human lungs. Through this the particles have the ability to pass further through the respiratory barrier, potentially entering the circulatory system and spreading to the whole body. Larger particles, however, are more readily removed by mucociliary clearance (Pinkerton et al., 2000; Wang et al., 2013; Xu et al., 2008). Therefore, focusing on $PM_{2.5}$-bound PAHs may be a better indicator of health effects than PM_{10}-bound PAHs, due to the increased mobility of such particles within the human body.

Table 3.24. Measured BaP concentrations from PM samples collected from GLA-KS and MAN-FF. The mean and median for GLA-KS exclude the $PM_{2.5}$ sample 4046.

Site	Sample ID	Size Fraction	Benzo(a)pyrene (ng m^{-3})	Mean	Median
Glasgow Hope Street	4038	PM_{10}	0.10	0.21	0.10
	4043	PM_{10}	0.05		
	4046	$PM_{2.5}$	0.97		
	4047	PM_{10}	0.48		
Manchester Fallowfield Campus	4028	$PM_{2.5}$	1.16	0.23	0.06
	4031	$PM_{2.5}$	0.03		
	4032	$PM_{2.5}$	0.16		
	4033	$PM_{2.5}$	0.06		
	4034	$PM_{2.5}$	0.03		
	4035	$PM_{2.5}$	0.05		
	4036	$PM_{2.5}$	0.15		

The average BaP concentration in MAN-FF($PM_{2.5}$) was 0.23 ng m^{-3}, which was close to the BaP NAQO (see Table 3.24). However, it should be noted that there was a clear bias in the average caused by sample 4028, which gave values 8 times higher than the sample with the second highest concentration. The inclusion of this sample in the average calculation causes the average to increase. Using the median removes the effect of sample 4028. When using the median value (0.06 ng m^{-3}) the health effects for MAN-FF($PM_{2.5}$) were thought to be negligible as they were below both the NAQO and FAQQD. Samples were collected at this site during the colder months (November – December), due to logistical limitations. The measured BaP concentrations are likely representing the higher end of the BaP concentrations in MAN-FF due to meteorological conditions as well as increased anthropogenic activities. During winter months solar radiation is reduced causing lower temperatures, alongside a more stable planetary boundary layer and frequent thermal inversions that trap pollutants in the boundary layer, preventing dispersion and causing higher concentrations of air pollutants (Masiol et al., 2012). Additionally, there is a larger demand for domestic heating in the winter months in the UK, thus more PAHs are emitted from combustion (Masiol et al., 2012). As a result, it is likely that the 2019 annual mean at this site, which would include the BaP concentrations from summer months, would also be below the NAQO guideline value. This is shown in the latest UK PAH Monitoring and Analysis Network by Conolly and Carpenter (2021). PAHs from urban background and urban traffic sites within the UK, showed higher concentrations in winter months.

Comparing the medians of both sites (see Table 3.24) shows that GLA-KS(PM_{10}) had a higher BaP median concentration than MAN-FF($PM_{2.5}$). The GLA-KS($PM_{2.5}$) sample BaP concentration was almost 4 times that of the MAN-FF($PM_{2.5}$) BaP average. It cannot be stated definitively that BaP concentrations from GLA-KS($PM_{2.5}$) are generally higher than that of MAN-FF($PM_{2.5}$) due to the small sample subset. However, the GLA-KS(PM_{10}) BaP average was similar to that of MAN-FF($PM_{2.5}$), as well as the GLA-KS(PM_{10}) median being higher than that of MAN-FF($PM_{2.5}$). As there are likely to be higher concentrations of BaP in $PM_{2.5}$ due to the PAHs being associated more strongly to finer particles, it was reasonable to assume that BaP concentrations in GLA-KS may be generally higher than that of MAN-FF (de Kok et al., 2005).

Figure 3.48 shows a plot of average BaP concentrations from December 2019 – January 2021 from urban sites within the UK PAH network (UK Air, Air Information Source). This period represented the sampling dates of both GLA-KS and MAN-FF samples, hence the data included measured BaP concentrations from the PAH network, for the period during COVID-19 measures. Comparing GLA-KS(PM_{10}) BaP concentrations to other sites in the Scotland, GLA-KS(PM_{10}) BaP concentrations were higher than Edinburgh St. Leonards, but lower than Kinlochleven. Research using PAH DRs showed that solid fuel was used in Kinlochleven, therefore this could have contributed to the higher BaP levels (Brown & Brown, 2012).

When comparing BaP concentrations from GLA-KS to other sites in the UK, GLA-KS concentrations were above the median (0.18 ng m^{-3}) but below the upper quartile value (0.28 ng m^{-3}). Sites in England that were above the upper quartile value were Scunthorpe and Royston. These sites are classified as urban industrial; therefore, the monitoring stations was deliberately placed in these locations to monitor potential industrial PAH emissions. In Northern Ireland, all three sites were above the median and in Wales one site, Port Talbot Margam. However, Port Talbot Margam was also classified an urban industrial site, nearby Port Talbot steelworks, thus represents a PAH emission hotspot (Brown & Brown, 2012). Also, in Northern Ireland, the three PAH network sites are known to be areas where solid fuel is extensive hence explaining why BaP concentrations are higher (Brown & Brown, 2012). This highlights the influences of different sources on PAH emissions. Considering GLA-KS has predominantly traffic sources for PAHs, this may explain why PAH concentrations are lower in GLA-KS. However, GLA-KS had higher BaP concentrations than sites in London (UT), Birmingham (UB), Nottingham (UB), Leeds (UB), Liverpool (UI) and had similar BaP concentrations to urban background sites in Sheffield, Bristol, Cardiff

and Swansea. London Marylebone road had an average BaP concentration of 0.12 ng m^{-3}, with a pre-COVID average concentration of 0.16 ng m^{-3} (December 2018 to January 2020). The low BaP concentrations could be attributed to the ultra-low emission zone which deters certain vehicle types from entering the zone, with fines being distributed to drivers of non-compliant vehicles. The explanation for the 2019 average of 0.12 ng m^{-3} during COVID measures could be due to changes in transport modes within London. Transport for London found that in April – June 2020, the share of very short trips (≤1 km) increased from ~33 % to 42 % whilst the share of trips between 1 km and 2 km increased from to 15 to 18 %. Mid-length trips between 2 and 5 km reduced from 21 % to 18 % and ≥5km trips reduced from 31 % to 22 %. They also found an increase in walking and cycling; estimated mode shares went from 29.4 % pre-COVID (January – March 2020) to 46.4 % April – June 2020. (*Transport for London: Travel in London*, 2021).

It should be noted that there are limitations to these comparisons as most sites, except London Marylebone Road, were classified as either urban background or urban industrial, thus more meaningful comparisons could be made against BaP concentrations from sites that are more similar to GLA-KS and represent urban traffic.

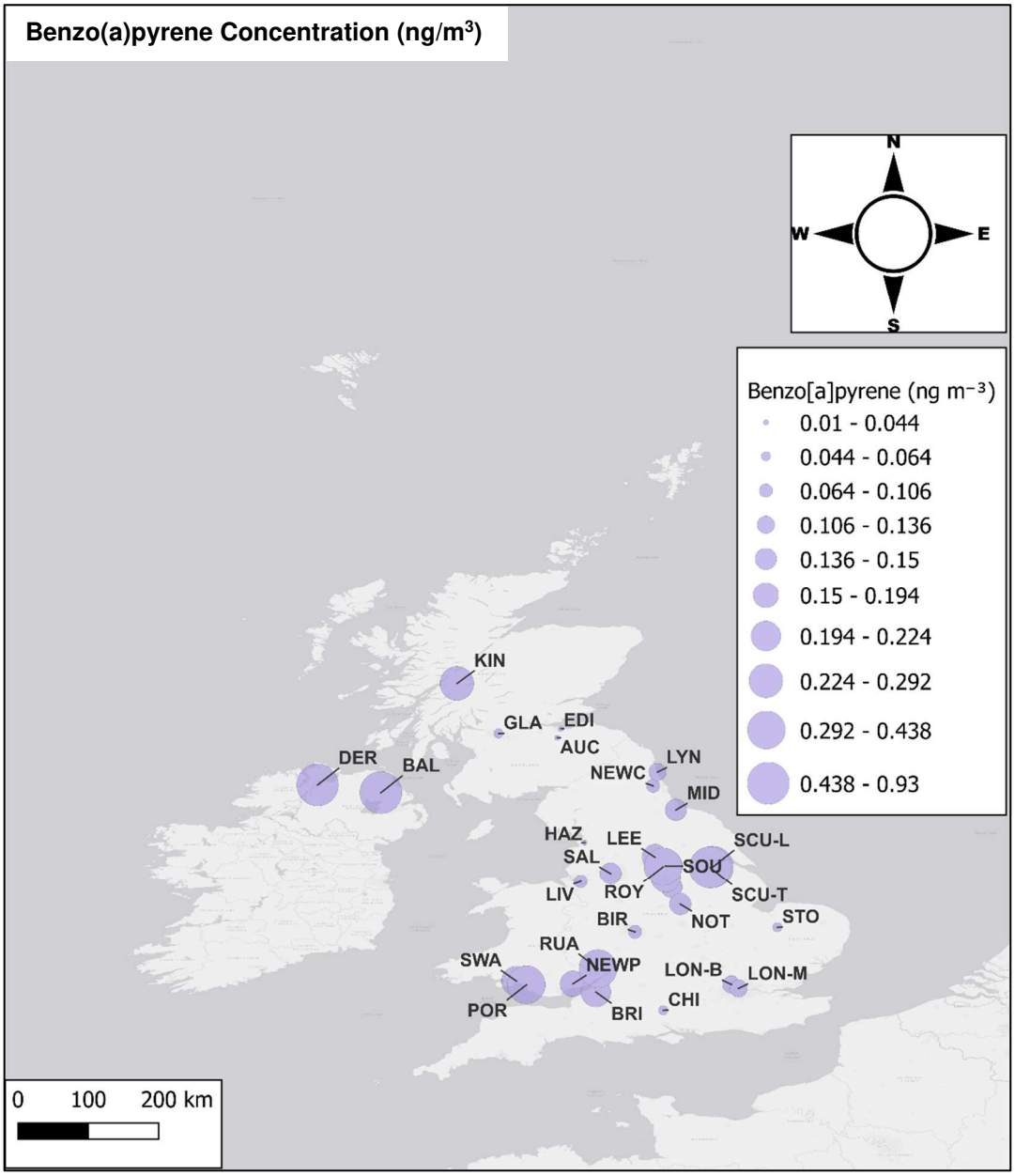

Figure 3.48. Average PM_{10}-bound BaP concentrations (ng m^{-3}) from December 2019 – January 2021 from urban sites around the UK within the PAH Network (Conolly & Carpenter, 2021). Urban sites include urban background, urban traffic, and urban industrial. The larger the size of the dot the higher the BaP concentration. The map layer was provided by Esri.

Exposure Assessment and Health Risk Assessment

The BaP mutagenicity and toxicity equivalent concentrations and the lifetime lung cancer risk from inhalation ($ILCR_{inh}$) were calculated using Equations 8, 9 and 10. This was used to determine the excess lung cancer risk from inhalation of PAHs, to develop a clearer understanding of the associated health risks of PAHs.

Table 3.25 shows the calculated $ILCR_{inh}$ values. The $ILCR_{inh(a)}$ calculated from the average concentration of PAHs in GLA-KS(PM_{10}) was 4.6×10^{-5}, $ILCR_{inh(b)}$ 5.8×10^{-7} and $ILCR_{inh(c)}$ 3.2×10^{-7} . For PAHs in GLA-KS($PM_{2.5}$) $ILCR_{inh(a)}$ was 2.1×10^{-4}, $ILCR_{inh(b)}$ 2.7×10^{-6} and $ILCR_{inh(c)}$ 1.4×10^{-6}. For PM_{10} samples the risk was negligible except from the calculated $ILCR_{inh(a)}$ value which indicated a potential risk. For $PM_{2.5}$ samples the risk was deemed a potential risk from calculated $ILCR_{inh(b+c)}$ and deemed a high risk from $ILCR_{inh(a)}$. There was a large deviation across different $ILCR_{inh}$ values due to the different IUR_{BaP} values being used, thus leading to inconsistent interpretations. Consequently, interpretations have been provided as ranges to include values from $ILCR_{inh(a,b,c)}$.

Table 3.25. BaP toxicity equivalent PAH concentrations, BaP mutagenicity equivalent PAH concentrations and incremental lifetime cancer risk for PM-bound PAHs collected from GLA-KS and MAN-FF PM.

	Sample Code	**BaP_{Teq}**	**BaP_{Meq}**	**WHO $ILCR_{inh(a)}$**	**OEHHA $ILCR_{inh(b)}$**	**USEPA $ILCR_{inh(c)}$**
GLA-KS (PM_{10},$PM_{2.5}$)	*4038*	0.33	0.23	2.84×10^{-5}	3.60×10^{-7}	1.96×10^{-7}
	4043	0.13	0.10	1.16×10^{-5}	1.46×10^{-7}	7.97×10^{-8}
	4046	2.41	1.61	2.09×10^{-4}	2.65×10^{-6}	1.44×10^{-6}
	4047	1.11	0.78	9.61×10^{-5}	1.22×10^{-6}	6.63×10^{-7}
	PM_{10} Average	0.53	0.37	4.60×10^{-5}	5.80×10^{-7}	3.17×10^{-7}
MAN-FF ($PM_{2.5}$)	*4028*	3.20	1.87	2.79×10^{-4}	3.52×10^{-6}	1.92×10^{-6}
	4031	0.10	0.05	8.51×10^{-6}	1.08×10^{-7}	5.87×10^{-8}
	4032	0.41	0.27	3.53×10^{-5}	4.47×10^{-7}	2.44×10^{-7}
	4033	0.16	0.11	1.42×10^{-5}	1.80×10^{-7}	9.80×10^{-8}
	4034	0.11	0.06	9.43×10^{-6}	1.19×10^{-7}	6.50×10^{-8}
	4035	0.13	0.09	1.16×10^{-5}	1.47×10^{-7}	8.00×10^{-8}
	4036	0.39	0.25	3.36×10^{-5}	4.25×10^{-7}	2.32×10^{-7}
	Average	0.64	0.39	5.60×10^{-5}	7.09×10^{-7}	3.87×10^{-7}

Therefore, the estimated average lifetime lung cancer risk for inhaled PAHs from GLA-KS(PM_{10}) and GLA-KS($PM_{2.5}$) was $3.7 \times 10^{-7} - 4.6 \times 10^{-5}$ and $1.4 \times 10^{-6} - 2.1 \times 10^{-4}$ respectively (Table 3.25).

This equates to an additional 0.37 – 46 and 1.4 – 209 cases per 1,000,000 people exposed to PM_{10}-bound and $PM_{2.5}$-bound PAHs respectively. This represents the estimated risk above the baseline lifetime lung cancer risk in the absence of atmospheric PAH exposure. The maximum $ILCR_{inh}$ was applied to the population of individuals living in Anderston, City, Yorkhill using Equation 11. The population was 30,184 inhabitants in 2015, in the ward where GLA-KS samples were collected. Assuming homogenous exposure of inhabitants this resulted in around 1 and 6 annual cases of lung cancer can be attributed to exposure from PM_{10}-bound and $PM_{2.5}$-bound PAHs, respectively. Overall risks may be lower as it is unlikely that residents in the Anderston, City and Yorkhill ward would be continuously exposed to PAH concentrations equal to those at the GLA-KS site. However, calculated risks do not include major indoor sources such as tobacco smoking, cooking fumes residential heating which may in turn elevate the $ILCR_{inh}$ value (Spengler et al., 2001). Furthermore, other studies have found the contribution of gas-phase PAHs to total BaP_{Teq} values to be substantial, in which case overall $ILCR_{inh}$ values may be underestimated as gas-phase PAHs were not analysed thus not included in the BaP_{Teq} calculations (Ramírez et al., 2011; Santos et al., 2020).

The reported values for MAN-FF($PM_{2.5}$) in Table 3.25 were $ILCR_{inh(a)}$ 5.1×10^{-5}, $ILCR_{inh(b)}$ 7.1×10^{-7} and $ILCR_{inh(c)}$ 3.9×10^{-7}. $ILCR_{inh(b+c)}$ were negligible but $ILCR_{inh(a)}$ was deemed a potential risk. This equates to 0.39 – 51 excess lung cancer cases per 1 million people exposed to $PM_{2.5}$-bound PAHs. These values were lower than that from GLA-KS($PM_{2.5}$) but higher than GLA-KS(PM_{10}). As $PM_{2.5}$ samples are more comparable between the two locations, GLA-KS had a higher $ILCR_{inh}$ than MAN-FF. In terms of sampling locations, this could be explained by GLA-KS samples being obtained from an extremely busy road within Glasgow city centre, which is utilised by many major bus routes and vehicles, whilst MAN-FF is not within the inner-city and by student accommodation (see map of sampling site in Figure 3.7). Therefore, it is important that the results are interpreted within this context, as the situation of the GLA-KS site is not representative of the conditions to which overall population of Glasgow is exposed to. Moreover, the $ILCR_{inh}$ values for MAN-FF and GLA-KS were not completely comparable as most of the GLA-KS samples were collected during COVID-19 restrictions/lock-down which may have led to reduced PAH concentrations. Therefore, results from MAN-FF and GLA-KS should not be compared directly due to such differences.

The $ILCR_{inh,}$ BaP_{Teq} and BaP_{Meq} values for GLA-KS(PM_{10},$PM_{2.5}$) and MAN-FF($PM_{2.5}$) were compared to values reported in the literature for other locations. As seen in Table 3.26, GLA-

KS(PM_{10}) average $ILCR_{inh}$ was lower than $ILCR_{inh}$ values found in PM_{10} from A Coruña, Spain but higher than those in Medellin, Colombia for main roads and side roads with traffic. GLA-KS($PM_{2.5}$) was higher than $ILCR_{inh}$ from $PM_{2.5}$-bound PAHs from Thessaloniki urban traffic site during the warm and cold periods in 2011-2012 ($2.2 \times 10^{-7} – 1.6 \times 10^{-6}$), various areas in Pakistan which calculated $ILCR_{inh}$ from gas and solid PAHs in 2014 (8.28×10^{-7} - 2.09×10^{-5}), Rio de Janeiro which calculated $ILCR_{inh}$ from gas and solid PAHs in 2017-2018 (4.3×10^{-5}), Heraklion in 2012-2014 ($3.4 \times 10^{-8} – 8.3 \times 10^{-8}$), Limassol 2012-2014 ($3.5 \times 10^{-8} – 8.4 \times 10^{-8}$), Bangi in 2013-2014 ($5 \times 10^{-5}$), Florence urban background site and Athens suburban area in 2013-2014 which included azaarenes, nitro-PAHs and oxygenated PAHs in the calculations (8.8×10^{-5} and 2.59×10^{-5}). Sites with higher or similar $ILCR_{inh}$ than GLA-KS($PM_{2.5}$) were North-eastern Italy in 2012-2013 (2.4×10^{-4}) and Porto traffic site which included azaarenes, nitro-PAHs and oxygenated PAHs in the calculations (2.06×10^{-4}). The $ILCR_{inh}$ calculation for GLA-KS($PM_{2.5}$) did not include azaarenes, nitro- and oxy-PAHs, indicating that the parent PAH concentrations may be higher than those in Porto. Further research would need to be done to confirm this, however.

Table 3.26. Details from research in literature about $ILCR_{inh}$, BaP_{Teq} and BaP_{Meq} in various countries.

Sampling Location	Sample	Sampling Period	$ILCR_{inh}$	BaP_{Teq} ($ng\ m^{-3}$)	BaP_{Meq} ($ng\ m^{-3}$)
A Coruña, Spain (Sánchez-Piñero et al., 2021)	PM_{10}	January 2017 to December 2017	2.40×10^{-4}, 3.00×10^{-6}, 1.60×10^{-6} (WHO, OEHHA, USEPA IUR values respectively).	Average: 2.7	Average: 1.4
Medellin, Colombia a- Traffic (Main Road) b- Traffic (Main Road) c- Traffic (Side Road) d- Traffic (Side Road) e- Traffic (Motorway) f- Industrial (Mueller et al., 2019)	PM_{10}	October 2015	a- 1.62×10^{-4} b- 8.5×10^{-5} c- 2.75×10^{-5} d- 5.32×10^{-5} e- 7.86×10^{-5} f- 1.39×10^{-4} (Using WHO 2000, IUR)	-	-
Beijing and Shijiazhuang Urban Areas (Shi et al., 2020)	$PM_{2.5}$	November 2017 – July 2018	-	3.0 – 50.4 Average: 13.6	-
Thessaloniki, Greece a- Urban Traffic Site b- Urban Background Site	$PM_{2.5}$	Feb–March 2012 (Cold Period) July–Sept 2011 (Warm Period)	a- 1.6×10^{-6} (cold) 2.2×10^{-7} (warm) b- 1.5×10^{-6} (cold)	a- 1.50 (cold) <0.4 (warm) b- 1.40 (cold) <0.4	a- 2.0 (cold) <0.4 (warm) b- 1.8 (cold)

(Manoli et al., 2016)			1.4 x 10^{-6} (warm) (Using USEPA, IUR)	(warm)	<0.4 (warm)
North-Eastern Italy (Belluno, Conegliano, Vicenza, Venezia Mestra, Padua, Rovigo) (Khan et al., 2018)	$PM_{2.5}$	April 2012 – March 2013	Annual average: 2.4 x 10^{-4} Winter average: 4.4 x 10^{-4} Summer average: 7.0 x 10^{-5} (WHO IUR used)	Regional average: 2.7	Regional average: 3.6
Southern European Cities a- Porto, Portugal (Traffic Site) b- Florence (Urban Background) c- Athens (Suburban) (Alves et al., 2017)	$PM_{2.5}$ Analysis included azaarenes, nitro-PAHs and oxygenated PAHs in calculations	January 2013 – February 2014	a- 2.06 x 10^{-4}, 2.61 x 10^{-6} b- 8.80 x 10^{-5}, 1.11 x 10^{-6} c- 2.59 x 10^{-5}, 3.28 x 10^{-7} (WHO, OEHHA IUR respectively)	Annual Average: a- 2.37 b- 1.01 c- 0.30	-
Pakistan a- Peshawar (Urban, Residential and Commercial) b- Faisalabad (Urban, Agricultural) c- Mutlan (Urban, Commercial) d- Lahore (Urban, Commercial) e- Rawalpindi (Urban, Commercial) f- Quetta (Rural, Commercial)	$PM_{2.5}$ and gaseous PAHs on PUF samplers	July – September 2014	8.28 x 10^{-7} to 2.09 x 10^{-5} (Using WHO IUR)	a- 0.24 b- 0.17 c- 0.16 d- 0.14 e- 0.11 f- 0.09 g- 0.08 h- 0.01	-

g- Karachi (Suburban) h- Gilgit (Rural, Residential) (Ishtiaq et al., 2021)					
Rio de Janeiro, RJ, Brazil (Santos et al., 2020)	$PM_{2.5}$ and gaseous PAHs on PUF	May 2017 – April 2018	4.3×10^{-5} (Using WHO, IUR)	Annual Average: 0.49	-
Venice-Mestre, Italy Urban Background (Masiol et al., 2012)	$PM_{2.5}$	March, June, July, October, December 2009, and January 2010.	-	Annual Average: 1.9	Annual Average: 2.1
Bangi, Malaysia (Khan et al., 2015)	$PM_{2.5}$	June – September 2013 (South-West monsoon) January – February 2014 (North-East Monsoon)	Average: 5.0×10^{-5} (Using WHO IUR)	Average: 0.57	-
a- Heraklion, Island of Crete (Greece) b- Limassol (Cyprus) (Iakovides et al., 2019)	$PM_{2.5}$	April 2012 – February 2014	a- 3.4×10^{-8} to 8.3×10^{-8} b- 3.5×10^{-8} to 8.4×10^{-8} (Using USEPA IUR)	Average a- 0.056 b- 0.057 (PM_{10} 0.060)	-

GLA-KS($PM_{2.5}$) BaP_{Teq} was compared to the calculated BaP_{Teq} from PAHs bound to $PM_{2.5}$ from Beijing and Shijiazhuang, collected from November 2017 – July 2018. The average value was 13.61 ng m^{-3} whereas Glasgow's was 2.41 ng m^{-3}. Glasgow's BaP_{Teq} concentration is extremely low compared to that from Beijing and Shijiazhuang, which is expected considering Beijing and Shijiazhuang are megacities. Manchester BaP_{Teq} concentrations are low in comparison, considering they were collected during winter where other studies have noticed PAH concentrations to be higher than other seasons. Other areas with higher BaP_{Teq} concentrations than GLA-KS were A Coruña (PM_{10}, 2.7), Venice-Mestre ($PM_{2.5}$, 1.9) and

North-Eastern Italy ($PM_{2.5}$, 2.7). However, the BaP_{Meq} of Thessaloniki (2.0), Northern Italy (3.6) and Venice-Mestre (2.1) were higher than GLA-KS($PM_{2.5}$) BaP_{Meq}.

The PM_{10}-bound PAHs GLA-KS $ILCR_{inh}$ values, shown in Figure 3.49, were in a similar range to other urban traffic sites and the GLA-KS $PM_{2.5}$-bound PAHs were also in the same range as an urban traffic site (Porto, Portugal), showing good agreement between $ILCR_{inh}$ values from the same type of site. However, an urban background site (Northern Italy) showed a similar concentration to GLA-KS($PM_{2.5}$) $ILCR_{inh}$ value (Figure 3.50). This could either be due to Northern Italy having higher PAH concentrations than Glasgow, or this could be due to PAH concentrations in Glasgow being lower during pandemic times. Additionally, the MAN-FF $ILCR_{inh}$ values were also within the range of other suburban sites and urban background sites, once again showing good agreement between $ILCR_{inh}$ values from similar site types.

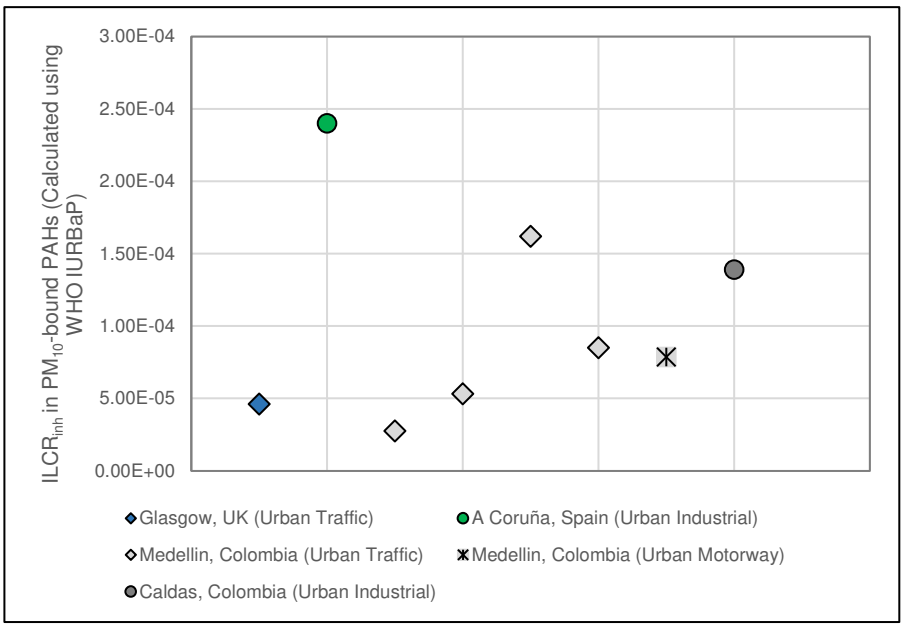

Figure 3.49. $ILCR_{inh}$ of PM_{10}-bound PAHs found within the literature and from the studies listed in Table 3.26.

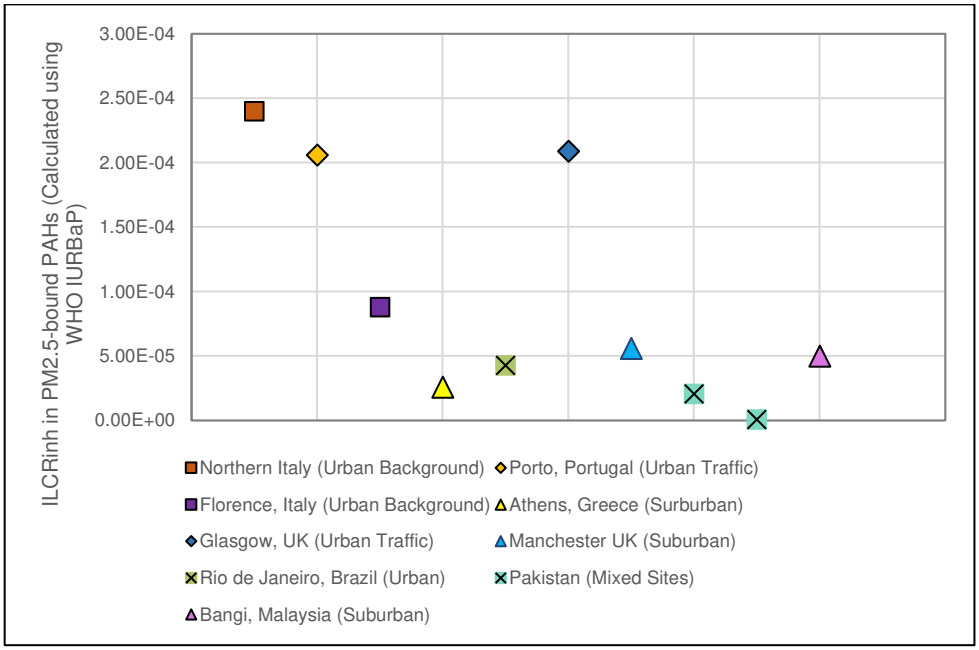

Figure 3.50. $ILCR_{inh}$ of $PM_{2.5}$-bound PAHs found within the literature and from the studies listed in Table 3.26.

To determine whether the $ILCR_{inh}$ values for Glasgow samples analysed were representative of business-as-usual scenarios, the PAH trends within the UK before and after COVID-19 are shown in Figure 3.51. BaP, BghiP and BkF concentrations in 2019 were significantly higher than concentrations during 2020 COVID-19 restriction period during the months of January, February, and November. As mentioned previously PAH concentrations tend to be higher in winter months (Conolly & Carpenter, 2021), which is shown clearly in Figure 3.51. However, the November 2020 BaP, BkF and BghiP concentrations are consistently lower than 2019.

Table 3.27 shows the annual average concentrations of BaP, BghiP and BkF from Glasgow Townhead in 2019 and 2020. The 2019 annual average BaP and BbF concentrations were almost double those in 2020. BkF and BghiP also had higher concentrations in 2019 than 2020. Therefore, it is logical to assume that both PAH concentrations and calculated BaP_{Teq}, BaP_{Meq} and $ILCR_{inh}$ values at GLA-KS were not representative of usual PAHs concentrations from this site, indicating the health risk could be higher than stated. Interestingly, the PAH concentrations in December 2020 seem to be higher than December 2019, this could be due to increased wood-burning due to more individuals being indoors due to COVID-19 restrictions. Alternatively, this may have been caused by meteorological conditions.

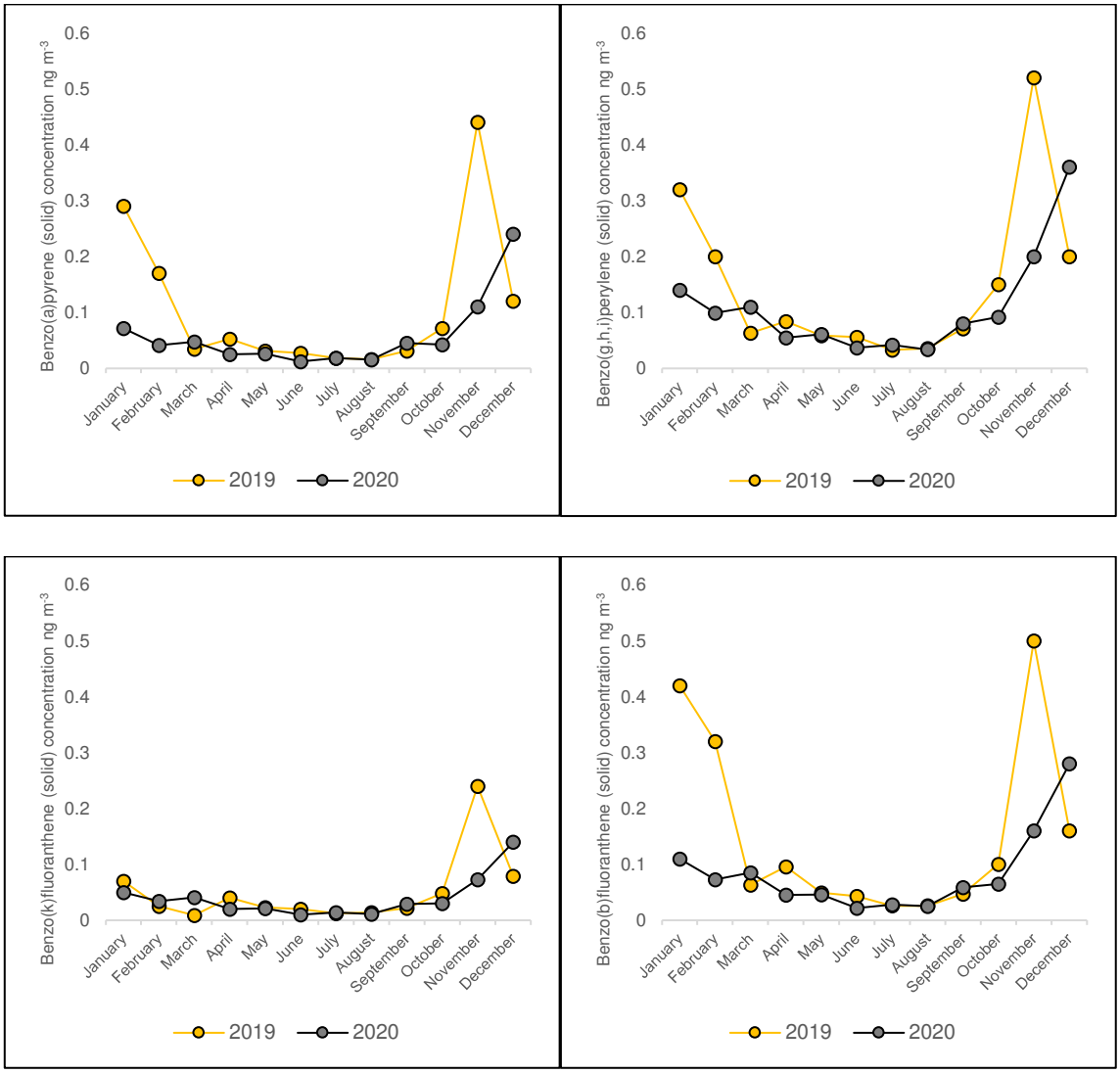

Figure 3.51. Monthly BaP, BghiP, BbF and BkF concentrations, from 2019 and 2020, measured at Glasgow Townhead by PAH network.

Table 3.27. Average Concentrations of BaP, BghiP, BbF and BkF from 2019 and 2020, from PAH Network site Glasgow Townhead, UK.

Townhead – Glasgow				
Average Concentrations (ng m^{-3})				
	BaP	BghiP	BbF	BkF
2019	0.11	0.15	0.15	0.05
2020	0.06	0.11	0.08	0.04

In order to decrease the lifetime excess cancer risk from inhalation, it is important to understand the sources of PAHs. The PAHs which were most dominant within the GLA-KS(PM_{10}+$PM_{2.5}$) average were BbF/BkF (co-eluted), BaP and BghiP. Sources linked to these PAHs have been discussed in Section 3.2.8, 3.2.9 and 3.2.12.

3.3.3. Conclusions

The toxicity, mutagenicity and lifetime excess cancer risk of PM-bound PAHs were calculated for GLA-KS(PM) and MAN-FF($PM_{2.5}$). The results showed that the average BaP concentrations from GLA-KS(PM_{10}) and GLA-KS($PM_{2.5}$) were 0.21 ng m^{-3} and 0.97 ng m^{-3} respectively. GLA-KS($PM_{2.5}$) exceeded the NAQO and FAQDD proposed annual mean concentrations of 0.25 ng m^{-3} and 1 ng m^{-3} for BaP. It is worth noting the target values were solely used as a guideline to determine potential adverse health effects as samples analysed were not representative of annual means due to sampling limitations. The exceedance of GLA-KS($PM_{2.5}$) indicates the potential for increased health risks associated to inhalation of PM-bound PAHs in Glasgow. MAN-FF($PM_{2.5}$) had an average BaP concentration of 0.23 ng m^{-3} in November – December 2019 and did not exceed any target values despite being close to the NAQO annual target. The difference in BaP concentration can be attributed to different site characteristics, i.e., MAN-FF is an urban background site, but also different proportions of BaP emissions and different sources. For example, in Section 3.2.9 wood combustion was denoted to be a possible source in most MAN-FF samples but only in one GLA-KS sample. This indicates that health risks associated to PAH inhalation may be lower of the region surrounding the site of from MAN-FF compared to that for the region surrounding GLA-KS. In relation to other sites in the UK PAH Network, GLA-KS(PM_{10}) BaP concentrations were similar to Bristol, Cardiff, Sheffield and Swansea but higher than Birmingham, Leeds, Liverpool, London and Nottingham (UK Air, Air Information Source). It is worth noting that most PAH network sites aforementioned were classified as urban background, whilst GLA-KS is classified as an urban traffic site so is likely to have higher BaP concentrations because of proximity to vehicular emissions. Comparisons with sites classified as urban traffic or roadside would have been more valuable had they been available.

The largest contributors to total PAH concentrations in GLA-KS across all samples varied between samples. For samples 4038 and 4043: BbF and BkF (co-eluted) 22 – 23 %, PHEN 16 – 21 %, FLA 12 – 16 % and BghiP 10 – 14 %. For samples 4046 and 4047: BghiP 20 –

27 %, BaP 16 – 22 % and BbF and BkF 21 – 24 %. The largest contributors in GLA-KS average ($PM_{2.5}$ and PM_{10}) combined were BbF & BkF (co-eluted), 23 %, BghiP, 22 % and BaP, 17 %.

The average BaP_{Teq} for GLA-KS(PM_{10}), GLA($PM_{2.5}$) and MAN-FF($PM_{2.5}$) were 0.53, 2.41 and 0.64 ng m^{-3}. GLA-KS(PM_{10}) was lower than A Coruna (2.7 ng m^{-3}) and GLA($PM_{2.5}$) was similar to European urban sites such as Venice-Mestre (1.9 ng m^{-3}), North-eastern Italy (2.7 ng m^{-3}) and Porto (2.37 ng m^{-3}) (Khan et al., 2018; Manoli et al., 2016; Masiol et al., 2012; Sánchez-Piñero et al., 2021). The BaP_{Meq} for GLA-KS(PM_{10}), GLA($PM_{2.5}$) and MAN-FF($PM_{2.5}$) were 0.37, 1.61 and 0.39 ng m^{-3}.

The average BaP_{Meq} for GLA-KS(PM_{10}), GLA($PM_{2.5}$) and MAN-FF($PM_{2.5}$) were 0.37, 1.61 and 0.39. As seen in studies the mutagenicity is higher in finer particles GLA-KS($PM_{2.5}$) > GLA-KS(PM_{10}) (de Kok et al., 2005; Pandey et al., 2012). MAN-FF($PM_{2.5}$) had a lower BaP_{Meq} than GLA-KS($PM_{2.5}$) but similar to GLA-KS(PM_{10}). Compared to other sites in Europe GLA-KS BaP_{Meq} was lower than BaP_{Meq} calculated from annual average PAH concentrations from A Coruna, Spain, Venice-Mestre Italy, North-Eastern Italy and cold seasons in Thessaloniki urban traffic and background sites (Khan et al., 2018; Manoli et al., 2016; Masiol et al., 2012; Sánchez-Piñero et al., 2021). This indicates the potential risks posed by mutagenicity of PAHs at the study sites presented here was lower than most of Europe, although this could be due to the samples being collected during COVID-19 lockdown/restriction periods. This result contrasts with findings from Alam et al. (2014) who found concentrations of PAHs in air masses originating from Southern England and mainland UK were larger than those from Eastern Europe and the North Atlantic. It also contrasts with findings from Prevedouros et al. (2004) which showed PAH contamination at rural Scandinavian sites were 1-2 orders lower than those at urban UK sites. However, these studies observed PAH concentrations rather than the mutagenicity of the PM-bound PAH mixtures. More research is required here; the application of this method on PM collected from the UK, post-pandemic, could determine whether mutagenicity of PAHs was lower in the UK compared to Europe.

The estimated lung cancer risk for the study area GLA-KS($PM_{2.5}$), 2.09×10^{-4}, was higher than the 10^{-5} the upper-bound excess lifetime cancer risk recommended by the World Health Organisation (WHO) for carcinogens in drinking water and higher than the U.S. EPA risk of 10^{-6} (Robson & Toscano, 2007; WHO, 2017).

This is still considered to be a potential medium risk especially considering these values were calculated from samples obtained during COVID-19 restrictions/lock-downs in 2020 where annual PAH concentrations were lower than the previous year (2019). Considering, gas-phase PAHs were not analysed the $ILCR_{inh}$ for GLA-KS may have been higher. Furthermore, the $ILCR_{inh}$ in this study does not include nitrogenated or oxygenated PAHs. Nitro- and oxy-PAHs have been found to be more detrimental to human health than parent PAHs due to their direct mutagenic potency (Environmental Health Criteria (EHC), 2003; Lara et al., 2022; Niu et al., 2017; Traversi et al., 2011). Therefore, further research determining the health risk of inhalation of PAHs, oxy-PAHs and nitro-PAHs in Glasgow, Manchester and additional UK sites would be useful, as it would assist in obtaining more accurate $ILCR_{inh}$ calculations. There are several limitations and uncertainties to be considered about the $ILCR_{inh}$ approach as mentioned in Alves et al. (2017) i) TEFs were measured from animal studies ii) BAP_{IUR} was extrapolated from results of epidemiological studies with exposures to high concentrations, therefore can be biased, iii) the sampling sites may not be representative of entire urban areas under evaluation, iv) the point-estimate approach assumes additive cancer risk, but different isomers in conjunction with other pollutants may increase or decrease toxicity through possible synergistic and/or antagonistic effects with other existing compounds. Despite the uncertainties, this research gives a general evaluation of health risks associated to PAH inhalation of PM from urban areas in the UK, Glasgow and Manchester. The findings indicated that inhalation of PM-bound PAHs from GLA-KS may be a public health concern. Based upon this research it is recommended that PAHs in $PM_{2.5}$ should be monitored instead of, or as well as, PM_{10}. Finer particles can penetrate more deeply into the human body due to size; thus higher risks are posed to health (Pinkerton et al., 2000; Wang et al., 2013; Xu et al., 2008). Research has found finer particles contain PAHs with high mutagenicity and carcinogenicity risks (de Kok et al., 2005; Pandey et al., 2012). This was also demonstrated in this research where toxicity and mutagenicity of GLA-KS(PM_{10}) was lower than GLA-KS($PM_{2.5}$).

4. Exploration of Hydropyrolysis as a Method to Isolate BC in Airborne Ambient PM

4.1. Introduction

BC measurements are useful as they can provide a basis for mitigation measures for climate change and the understanding of the role of BC in the carbon cycle (Bond et al., 2013; IPCC, 2018; Masiello, 2004). They are also crucial to understanding the health risks associated to BC in PM (Achilleos et al., 2017; Grahame et al., 2014; Janssen et al., 2012; Janssen et al., 2011). Current legislation in the UK focuses on reducing $PM_{2.5}$ mass (Environment Act, 2021). However, it is thought that BC is a better indicator for human health effects of particulate substances from combustion sources, than undifferentiated PM mass (WHO, 2012). By measuring BC in $PM_{2.5,}$ it could be determined whether particle mass is acting as a surrogate for BC in epidemiological studies (UK Government, 2022b). However, difficulties have been experienced when measuring BC in environmental matrices including aerosols (Hammes et al., 2007). Currie et al. (2002a) found large variations in reported BC/TC% ratios (6.9 – 52 % BC/TC) in NIST SRM 1649a, when using 13 different BC measurement techniques. This was thought to be from operational definitions of BC (as stated in Section 1.2.1), as there is an absence of a universally recognised structural definition of BC (Currie et al., 2002a; Hammes et al., 2007; Meredith et al., 2012). The uncertainties in BC concentrations acts as a barrier to progression of climate models, monitoring of BC in the environment and uncovering the adverse health effects directly associated to BC rather than to PM. There highlights the need for a method that can reproducibly separate a consistent portion of BC in airborne ambient PM.

Hydropyrolysis is a thermal technique utilising high hydrogen pressures to reductively remove the semi-labile organic carbon from PM. The semi-labile organics are then retained on a silica trap, leaving behind the hypy residue, which is then termed BC_{hypy} (Meredith et al., 2012). Hypy utilises one consistent thermal protocol. Unlike other thermal techniques hypy yields minimal charring artefacts and reproducible BC_{hypy} determinations. Hypy also retains the BC_{hypy} and the non-BC_{hypy} segments, which can then be chemically characterised for further analysis (Meredith et al., 2012). Whilst hypy has been used for the determination and separation of BC in many different sample types such as charcoals, biochar, soils, and sediments (Ascough et al., 2009; Ascough et al., 2010; Foereid et al., 2015; Meredith et al.,

2013; Wurster et al., 2012; Wurster et al., 2013), it has been used less widely on airborne ambient PM. Meredith et al. (2012) analysed urban dust standard (NIST 1649b) using hypy, but as this is just one aerosol material. As mentioned previously airborne ambient PM samples may have varying compositions due to different source contributions. To ensure hypy can be used effectively to measure BC in airborne ambient PM, further analysis on a wider range of BC-containing aerosol and dust materials is required. Zhang et al. (2019a) used hypy on airborne ambient PM from China for source apportionment of BC using ^{14}C analysis, however it is yet to be used on UK airborne ambient PM which are likely to have different composition to PM from China. Zheng et al. (2017) did not analyse any standards such as urban dust (NIST 1649b) for quality assurance purposes. This meant the consistency of hypy measurements for aerosol materials across different laboratories could not be determined. This is fundamental to determining accuracy and reproducibility of the technique, hence its suitability to measure BC in PM. Therefore, there is a need for inter-laboratory comparisons for BC/TC% measurements made by hypy.

The objectives in this chapter were:

1) To analyse urban dust (NIST 1649b) using hypy, to compare against BC/TC% measurements from hypy and other measurement techniques.
2) To analyse a wider range of aerosol and dust standards that are representative of varying emission sources to test the suitability of hypy as a separation technique for airborne ambient PM.
3) Obtain a set of BC/TC% values for readily-available standards, that can be compared against in future studies utilising hypy for BC/TC% measurements in airborne ambient PM.

4.2. Hydropyrolysis Methodology

4.2.1. Materials

Two end member materials Diesel soot (NIST 2975) and Beulah Zap were used. Diesel soot (DS) is a BC-rich material, whilst Beulah Zap (BZ) is a lignite that should contain little or no BC. When analysing BZ using hypy, a conversion close to 100 % non-BC_{hypy} is expected (Love et al., 1995; Meredith et al., 2012; Robert et al., 1995). This means that the BC/TC% would be zero or very low. Contrastingly, a high BC/TC% would be expected for DS. Analysis of these materials confirmed that there were no issues with the hypy instrumentation and that it was working correctly. Five other aerosol and road dust materials were used as they represented potential end members. Charred biomass was also included as proxy of particles originating from biomass combustion. BC_{hypy} measurements on the range of materials aforementioned, were completed to determine if hypy could be used effectively on aerosol/dust from different sources as aerosols vary widely in composition due to sources. Materials that were readily available i.e., could be purchased, were prioritised, so that if hypy proved suitable for aerosol BC measurements, the BC/TC% values in this section could be compared against in future studies using hypy, for quality control purposes. However, where an appropriate standard could not be purchased, materials were created in-house such charred biomass samples DB and EB (see Section 3.2.1. for more information) and road dust from Hillhead, Glasgow UK (see Section 3.2.1. for more information).

BC End Members

Beulah-Zap Lignite (BZ)

BZ was used as a reference material as it should contain little BC meaning it should have a conversion close to 100 % thermally labile material (Love et al., 1995; Meredith et al., 2012; Robert et al., 1995). A low BC/TC% is expected, therefore running this material ensures the hypy instrumentation is in good working order. BZ has been used in previous hypy work by Meredith et al. (2012). More information on BZ can be found in Section 3.2.1.

NIST 2975 Diesel Soot (DS)

DS was used as an end-member due to its high proportion of BC and low proportion of thermally labile material. Hammes et al. (2007) recommended the use of this material to help

with method evaluation for novel analytical approaches that quantify BC in environmental samples. This was due to the material being well-characterised, environmentally relevant, and readily-accessible. More information on DS can be found in Section 3.2.1.

Charred Biomass

DB and EB

Charred biomass DB and EB were used in this chapter to represent particulate matter originating from biomass combustion. More information on DB and EB can be found in Section 3.2.1.

Aerosols and Road Dust Materials

UD and UPM

UD and UPM were used to represent a typical urban ambient airborne aerosol. UD has been analysed using hypy in Meredith et al. (2012) and using other BC methods in Hammes et al. (2007), thus BC/TC% determinations in this standard can be compared to BC/TC% from other measurement techniques and laboratories. More information on UD and UPM can be found in Section 3.2.1.

FD and BCR-RD

FD and BCR-RD was used to typify airborne ambient PM emitted from vehicular traffic as both materials were collected from traffic tunnels. More information on FD and BCR-RD can be found in Section 3.2.1.

HH-RD

HH-RD was used as resuspended road dusts contribute to airborne ambient PM. Moreover, it represented a real-world sample from the UK hence was representative of the BC contents in the sampling area. It was important to determine the variability in BC/TC% in real-world samples that are likely to be less homogenous than purchased standards.

4.2.2. Instrumentation

Carbon analysis

Carbon analysis is crucial for the determination of BC. The %C of the sample is measured before hypy and after hypy to determine the BC/TC%. The %C was measured using the elemental analyser (IsoLink™ IRMS System, Thermofisher Scientific). An internationally recognised standard, L-glutamic acid, USGS40 was used for %C determination. This was purchased from USA Geological Survey in Reston California. The calibration curves were made by plotting the area of the C peak of the USGS40 against the mass of the standard. Four masses were used to construct the calibration curve, which always resulted in a R^2 of >0.99. The linear regression equation was used to calculate the mass of C in a sample from its C peak area. The measurement uncertainty was calculated for the calibration curve using 95 % confidence limits. The overall measurement uncertainty was determined to be ± 0.01 mg C.

Hypy Sample Preparation

Hypy was used to measure BC in the materials mentioned in previously. Samples required a catalyst coating to facilitate the separation of BC_{hypy} from non-BC_{hypy}. The sulfided molybdenum catalyst was made by adding ammonium molybdate tetrahydrate [$(NH_4)_6Mo_7O_{24}$] (Merck, 2 g) to an ammonium sulphide solution (20 % in water, 9 mL) in a conical flask. A magnetic stirrer and glass rod were used to break any lumps that form, to ensure the solid dissolved. Once dissolved, the conical flask was placed into an ice bath on top of the stirrer for roughly 30 minutes, until a bright orange precipitate formed. The precipitate was separated from the excess solution via vacuum filtration with a Buchner funnel with a side arm conical flask to connect to the vacuum pump. The solid was recovered on the filter paper and dried in a vacuum oven at 50 °C for ~1 hour. Lumps were broken up with a clean spatula.

The glass vials and amber glass vials were used to contain samples, hypy crucibles, and hypy product on silica. These were pre-combusted at 450 °C, for 3 – 4 hours. The sample was loaded with an amount of catalyst, which was estimated using the TC of a sample as an indicator of how much BC was present. The TC of the sample was determined as described above, where the TC was not already known. A catalyst mass of 5 % the sample weight was used if the TC of the sample was less than 10 %. If the TC was more than 10 %, 10 % of the

sample weight was used. The dry catalyst was placed on top of the sample in a pre-combusted 20 mL glass vial. A solution of distilled water and 20 % methanol was poured into a measuring cylinder that had been rinsed with distilled water three times. This solution dissolved the catalyst forming an aqueous/methanol solution of ammonium dioxydithiomolybdate [$(NH_4)_2MoO_2S_2$]. The solution was placed on a hotplate at 80 °C, for 2 hours, to evaporate the solvent. Once the solvent had evaporated, and the catalyst had been coated homogenously onto the sample, the glass vial was then placed in the freezer for a minimum of 1 hour. The sample was then placed in a freeze drier (Christ Alpha, Germany) overnight with a filter placed on top of the glass vial. The samples were transferred into pre-combusted hypy crucibles which were 10 mm long and had glass frits at the bottom (see Figure 4.1). The samples were transferred using a metal spatula that had been wiped with a lint-free tissue and cleaned with a flame torch to prevent contamination. The hypy crucibles were plugged at each end with pre-cleaned quartz filter punches (450 °C, 8 hr) with the catalyst coated sample in the middle as shown in Figure 4.1.

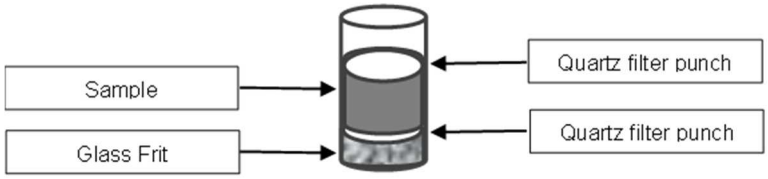

Figure 4.1. Schematic of a hypy crucible containing a glass fit at the bottom, with a quartz filter punch on both ends of the sample to keep it contained within the crucible during the hypy run.

Operating Conditions and Procedures

The setup of the hypy can be seen in Figure 4.2. The hypy crucibles were placed towards the bottom of the reactor. One hypy crucible was placed in the reactor for high carbon samples such as BZ, DS, FD, UD and UPM. However, for BCR-RD, DB, EB and HH-RD three hypy crucibles were put into the reactor per run, to ensure there was enough carbon after hypy for a C % measurement. Each hypy crucible inside the hypy was considered a replicate measurement. The silica trap was prepared by inserting a small sample of steel wool (approx. 0.5 g) to the bottom of the silica trap. Silica gel was cleaned through two rounds of Soxhlet extraction which were left overnight. One round used n-hexane and the other used

DCM/methanol (93:7 v/v) to ensure any organic material was removed. Once complete the silica was placed on a ceramic dish and heated in the furnace at 600 °C for 6 hr and then stored in a pre-combusted beaker (450 °C, 8 hr) within a desiccator. Silica (~ 2 g) was loaded into the silica trap, and a compressed air duster used to remove any silica gel from the seal of the trap, which could cause leaks in the hypy system.

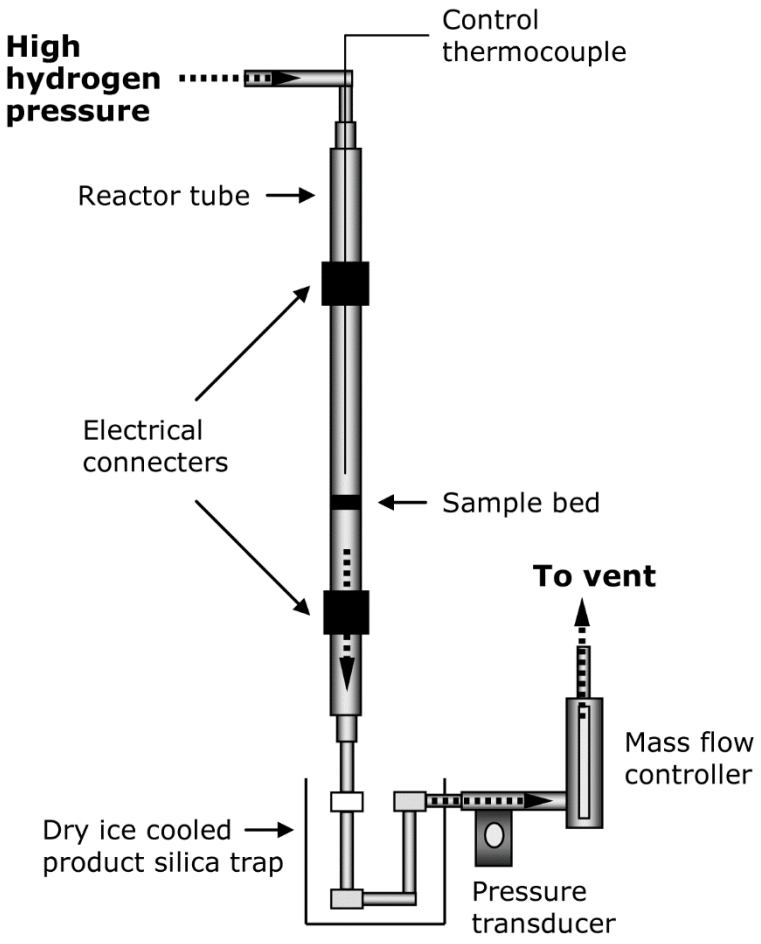

Figure 4.2. A schematic of the HyPy instrumentation which shows the flow of hydrogen gas sweeping through the reactor tube where the HyPy crucibles are placed, through to the silica trap where the non-BC_{hypy} adsorbs to the silica gel. Reprinted from Hydropyrolysis as a new tool for radiocarbon pre-treatment and the quantification of black carbon, volume 4, Ascough et al., 140-147, Copyright (2009), with permission from Elsevier.

The final pressure was 150 bar with a sweep flow of 5 L min^{-1}. The pyrolysis resistive heating programme went from 50 °C to 250 °C at 300 °C min^{-1}, and then from 250 °C to 550 °C at 8 °C min^{-1}, before being held at the final temperature for 2 min, all under a hydrogen

pressure of 15 bar. The flow rate, heating rate, heating output and gauge pressures were checked throughout the run.

Carbon Content Calculation

The BC_{hypy} content of each sample was derived by submitting the material for elemental analysis of %C content before and after hypy. The resulting proportion of the total carbon (TC) that was BC was then calculated and expressed as BC/TC% using Equation 12. The sample before hypy contains the catalyst as does the sample after hypy, however in this case the catalyst is spent. The calculations account for the catalyst weight as a proportion of the total sample. By comparing the OC content before and after HyPy, this can reveal the BC to OC percentage.

$$BC_{hypy}\left(\frac{BC}{TC}\%\right) = \frac{Residual\ \ BC\ (mg\ C\ in\ hypy\ residue\ with\ spent\ catalyst)}{Initial\ TC\ (mg\ C\ in\ sample\ with\ catalyst)} \times 100 \qquad (12)$$

4.2.3. Results and Discussion

The BC/TC% for BZ was 2 ± 0.48 % (see Table 4.1) which was slightly lower than the value in a previous study, 4.2 ± 0.6 % (Meredith et al., 2012). The presence of BC was thought to be from ancient fire occurrences incorporated during deposition (Meredith et al., 2012). This standard was expected to have a low amount of BC. The lower value was probably an indication of less contamination either during preparation steps or in between hypy runs. Nonetheless, the BC/TC% were similar, despite the standard deviations not overlapping. This showed that the hypy was working well, as almost 100 % conversion of thermally labile organic material occurred. Gustafsson et al. (2001) also reported a low BC/TC% of 0.031 % for BZ. The result was lower than the hypy BC/TC% likely due to the method that was used – the CTO-375 method with pre-treatment to remove carbonates – which generally underestimates BC. This is because of the aggressive removal of labile carbon, which leave only the most condensed forms of BC (Hammes et al., 2007; Meredith et al., 2012). Other methods TOT/R, UV and BPCA when applied to the BZ standard reported higher values

(23.4 – 50.2 %) showing they could not distinguish between BC and petrogenic materials with similar structures, thus overestimated BC (Hammes et al., 2007).

The BC/TC% for the BC-rich material, DS, had a value of 106 ± 0.76 % (see Table 4.1). This value was over 100 % meaning the %C was higher after hypy compared to before hypy, which indicates weighing errors. This could have happened during the preparation of the hypy insert, when weighing the sample submitted for %C and/or the weighing of the post-hypy sample due losses in glass wool during hypy. Nonetheless, the hypy BC/TC% indicated DS had zero OC contribution. Using a thermal-optical technique, with pre-treatment of carbonates and minerals Han et al. (2007) reported BC/TC % of 92.9 % for DS. Gustafsson et al. (2001) reported a 78.2 % BC/TC%, lower than the hypy result due to a negative bias of the CTO-375 method.

The charred biomass standards had BC/TC% of 15.1 ± 0.1 % for DB and 62.5 ± 0.6 % for EB. The gasifier pyrolysis conditions varied slightly (see Section 3.2.1) which could have led to different BC/TC% as well as the feedstocks being different. Moreover, the EB material was more homogenous whilst DB contained fragments of charred biomass and was more heterogenous. This could explain the differences in BC/TC%. EB exhibited more variability in BC/TC% this was likely due to the low %C of the sample and the uncertainty of %C values increasing with smaller masses outside of the calibration curve.

The results showed that urban aerosols UD and UPM had similar BC/TC% of 28 ± 0.1 % and 25 %, respectively (see Table 4.1). FD also had a similar BC/TC% of 26 ± 0.4 %, despite having dominant vehicle emission sources. The SE for aerosol standards were low and showed little variability between replicate measurements. BCR-RD, collected from traffic tunnel roads, had a higher BC/TC% of 41 ± 1.3 %, than the aerosol standards. When comparing HH-RD to BCR-RD, a road dust collected in urban area Glasgow, UK, the BC/TC% was much lower at 14 ± 0.7 %. This could be from the presence of vegetative detritus in the samples, since, as reported in Chapter 3, these samples had high CPI for n-alkanes. The SE value shows that HH-RD, which was a real-world sample likely to be more heterogenous than BCR-RD, exhibited less variability in determined BC/TC%. The SE of HH-RD was similar to BZ, DS and EB showing hypy could be suitable for real-world samples which are likely to be less homogenous. BCR-RD had the highest variability out of all standards. Despite this, the variability of replicate BC/TC% measurements were still low with a SE of 1.3 %, showing hypy is a reproducible method when used on aerosols and road dusts, although road dusts exhibited more variability between replicate measurements.

Table 4.1. Hypy-derived BC/TC % of reference materials.

	BC/TC %	N (replicates)	SD	SE
UD	27.8	2	0.2	0.1
UPM	24.8	1	-	-
FD	26.1	2	0.6	0.4
BCR-RD	40.9	6	3.1	1.3
HH-RD	14.2	3	2.0	0.7
DB	15.1	6	0.6	0.1
EB	62.5	9	5.3	0.6
Beulah Zap	2.4	2	0.8	0.4
Diesel Soot	105.9	2	1.1	0.6

The BC/TC% of UD within this study was 27.8 ± 0.2 % thus very similar to that reported by Meredith et al. (2012); 27.9 ± 0.6 %. This shows there is good reproducibility between measurements made at different laboratories. The reported UD result was approximately in the middle of the range reported by Currie et al. (2002a), 6.9 – 52.0 % (BC/TC) derived using 19 different chemical and thermal methods. Considering some of these methods are known to over-estimate or under-estimate BC due to different thermal and pre-treatment protocols, being in the middle of the range is promising. The BC/TC% value from hypy was comparable to the BC/TC% values from multi-element scanning thermal analysis (24.6 ± 5.7 %), thermal oxidation methods (22.7 ± 0.78 %) and some results from thermal optical methods using IMPROVE or IMPROVE_A protocol (24.02 and 22.82 % respectively) (Hsieh & Bugna, 2008; Mannino & Harvery, 2004; Zhan et al., 2013). The higher value reported by hypy was likely due to the lack of acid pre-treatment steps for the removal of carbonates and minerals. Without acid pre-treatment inorganic C is present in the sample and the BC_{hypy} residue. The measured %C before and after hypy therefore may be higher due to the contribution of carbonates to the sample mass and C content, increasing the BC/TC%. The hypy BC/TC% was higher than other methods such as the CTO-375 method where Reddy et al. (2002) reported 8 % BC/TC%, the thermalcoulombimetric method where Alvarez-Ospina et al. (2016) reported 11 % BC/TC% and the dichromate oxidation method used by Meredith et al. (2012) which had 11.8 % BC/TC% (Alvarez-Ospina et al., 2016; Meredith et al., 2012; Reddy et al., 2002). The explanation for this could be that these

methods are harsher due to aggressive oxidation, leading to underestimations in BC during heating (Hammes et al., 2007; Meredith et al., 2012). One method that yielded higher BC/TC% than hypy was the thermogravimetric differential scanning calorimetry method (TG-DSC). Hammes et al. (2007) reported 58.9% BC/TC% in UD. This method exhibits positive biases as it measures the total weight loss during the heating profile, so samples with mineral impurities that lose water contribute to the weight loss upon heating (Hammes et al., 2007). However, it has been noted that calcites can be differentiated from BC due to decomposition at higher temperatures (Manning et al., 2005).

The UPM BC/TC% values measured in this study were higher than values in the literature; for example a thermal-coulombimetric method reported 14 % BC/TC% (Alvarez-Ospina et al., 2016). The thermal-coulombimetric method was most similar to thermal oxidation and thermal-optical combustion methods e.g.CTO-375, hence displayed negative biases.

There was no BC/TC% measurements found in the literature for FD and BCR-RD.

4.2.4. Conclusions

BC determinations were made on range of aerosol and dust and biomass char standards, using hypy. The BC/TC% determined by hypy had minimal variation across replicates. The highest reported SD reported was 5.3 for the in-house standard EB, and the highest SE was 1.3 for BCR-RD, a purchased standard. HH-RD, had a lower SD and SE than BCR-RD, showing hypy yields precise BC determinations in real-world samples, which may be more heterogeneous than purchased standards. The variation across replicates was generally low, proving hypy may be a suitable method for BC determinations in airborne ambient PM with a variety of compositions and from various emission sources.

Hypy BC/TC% values for BZ and UD were in agreement with those from Meredith et al. (2012), showing that hypy yielded reproducible results as there was agreement in BC determinations from two different laboratories. BC/TC% results from hypy were above reported BC/TC% from methods that usually underestimate BC and were lower than methods that overestimate BC. This was observed in UD and UPM, however for DS hypy over-estimated the BC/TC%, as it was over 100 %. The BC/TC% of DS from other studies was reported to be 92.9 % (TOT/R) and 78.2 % (CTO-375). The overestimation in BC content from hypy for DS was thought to be from weighing errors.

A set of BC/TC% values were obtained for a range of readily available aerosol and dust standards such as BCR-RD, FD, UD and UPM. BZ and DS can be used as end-member standards to ensure the hypy yielding accurate results for samples with low and high BC contents.

5. Source Apportionment of Particulate Matter and Black Carbon Using ^{14}C Analysis

5.1. Introduction

The radioisotope ^{14}C ('radiocarbon') is an ideal tracer for source apportionment of airborne ambient PM, due to its ability to distinguish between fossil and modern carbon (Heal et al., 2011). The background of ^{14}C analysis was discussed in Section 1.4. The ^{14}C isotope decays with a half-life of 5370 years so fossil carbon (i.e., >50,000 years old) has virtually no ^{14}C and is referred to as '^{14}C-dead' making it isotopically very distinct from 'modern' carbon, where the latter refers to carbon that has been recently fixed from the atmosphere, e.g., in recently-formed plant and animal tissues. The low natural abundance of ^{14}C (with a typical 'modern' $^{14}C/^{12}C$ ratio of 1×10^{-12}) and the highly sensitive measurement techniques available to measure these low abundances (i.e., Accelerator Mass Spectrometry), mean it is possible to use ^{14}C to establish the proportion of 'modern' versus 'fossil' carbon in a sample to a very high level of accuracy and precision using an isotope mass balance approach (Schuur et al., 2016). Therefore, ^{14}C analysis is a powerful tool when used for source apportionment of carbonaceous components in airborne ambient PM (Currie, 2000; Heal et al., 2011; Hou et al., 2021; Lim et al., 2022; Perron et al., 2010; Szidat et al., 2004a). For example, total carbon (TC), which is the sum of BC (usually referred to as EC in the aerosol science community, but for consistency referred to as BC throughout the chapter) and OC, constitutes about one third of the mass of $PM_{2.5}$ in the UK. This means that source apportionment of such components is of central importance to efforts seeking to mitigate airborne pollution and improve air quality (Air Quality Expert Group, 2012;2015; Yin & Harrison, 2008).

As shown in Figure 5.1 modern sources of BC and OC include biomass combustion, biogenic secondary organic aerosol (SOA), primary biological particles. Fossil sources of BC and OC include fossil fuel combustion and anthropogenic SOA (Heal, 2013). Research has evidenced the toxicity of $PM_{2.5}$ from coal- and traffic-related emissions (Thurston et al., 2021). This was due to their association with cardiovascular mortality in both short- and long-term exposure studies. Research has also shown human health effects of wood-smoke (Erlandsson et al., 2020). Wood-smoke emissions caused cytotoxicity and disrupted proliferation in exposed placenta cells, as well as structural damage to mitochondria and

endoplasmic reticulum. This suggested that wood smoke particles can have detrimental effects early in pregnancy by disrupting normal placenta development and function. This shows that having an understanding of the sources of $PM_{2.5}$ is important in shaping policy efforts to reduce the abundance of these pollutants. These efforts will only be successful if they are appropriately targeted to the correct sources of the problem.

Separate ^{14}C determinations of BC and OC,, are also a useful approach to obtaining more detailed information on the source apportionment of TC in airborne ambient PM. Heal et al. (2011) adopted this approach when separating BC and OC using thermal methods and were able to determine source attributions of BC and OC components such as $BC_{biomass}$ and BC_{fossil} for BC and $OC_{biogenic}$, $OC_{biomass}$ and OC_{fossil} for OC using results from the thermal method and radiocarbon analysis. However, difficulties have been experienced in various studies when separating BC and OC, which are both methodologically defined by the thermal or thermochemical/optical protocol used to separate them (Andreae & Gelencsér, 2006). When separating BC and OC for ^{14}C analysis, different approaches and instruments are used across studies, each with varying protocols and conditions, which leads to inconsistent determinations of both BC abundance, and the ^{14}C value of the isolated BC, as each method may isolate a different part of the BC 'continuum', and thus have differing positive and negative artifacts (Currie et al., 2002a; Currie et al., 2002b; Hammes et al., 2007; Meredith et al., 2012). This was found in an interlaboratory comparison for ^{14}C analysis of carbonaceous aerosol samples and standards, which showed there was good agreement for ^{14}C determinations of TC and OC but for BC there were considerable discrepancies between the laboratories with standard deviations of up to 79 % of the measured ^{14}C(BC) value (Szidat et al., 2013). A more recent study by Zenker et al. (2017) found poor agreement in BC mass concentration after using a two-step protocol referred to as '2stepCIO' on a custom-built aerosol combustion system and a thermal protocol on a Sunset OC-BC analyser. This showed BC recovery was sensitive to temperature steps and instrument specific parameters such as heating rates. The pre-treatment of a PM sample was also shown to be important as untreated samples yielded underestimations in BC concentrations by 20 – 45 % compared to water-extracted samples using the same EUSAAR_2 protocol. Inconsistent method-dependant separation of BC for ^{14}C analysis complicates the comparison between studies and sites and leads to methodological artifacts that potentially produce misleading conclusions as to the true proportions of carbon originating from modern and fossil biomass sources. This highlights the need for a method that yields reproducible results for BC content and subsequent ^{14}C source apportionments independent of laboratory, operator or sample matrix.

Hydropyrolysis (hypy) is a novel technique used to separate BC from TC in a variety of environmental matrices. Unlike other thermal techniques, the hypy process results in minimal charring as well as the isolation of relatively consistent portions of the BC continuum from a wide range of environmental matrices (Meredith et al., 2012). Meredith et al. (2012) found the BC_{hypy} values for BC-containing materials fell within the BC/TC% ranges from an interlaboratory comparison using different BC measurement methods reported in Hammes et al. (2007). The BC_{hypy} value for aerosols was similar to those from UV photo-oxidation and, like CTO-375, it could discriminate refractory soot-like BC from more labile char-BC contents derived from vegetation burning such as two agricultural soils (Hammes et al., 2007). Research by Zhang et al. (2019a) showed that hypy could successfully separate a consistent form of BC in airborne ambient PM samples from China. The temperature programme used in a previous hypy study by Meredith et al. (2012) on NIST 1649b UD was shown to be applicable to ambient aerosols from China (Meredith et al., 2012). Considering airborne ambient PM composition may vary geographically, this provides good evidence that the hypy method provides consistent separation of BC_{hypy} and non-BC_{hypy} in airborne ambient PM with varying compositions. The percentage of modern carbon (%MC) in BC_{hypy} from Beijing were in between that of CTO-375 – an under-estimating BC %MC method – and a thermal-optical method which tends to be an over-estimating BC %MC method (Zhang et al., 2019a). Apart from the two aforementioned studies, there is limited literature on use of hypy as a separation method for BC and OC for ^{14}C analysis in airborne ambient PM, thus there is a lack of literature to provide comparative BC_{hypy} %MC values for the purpose of quality assurance.

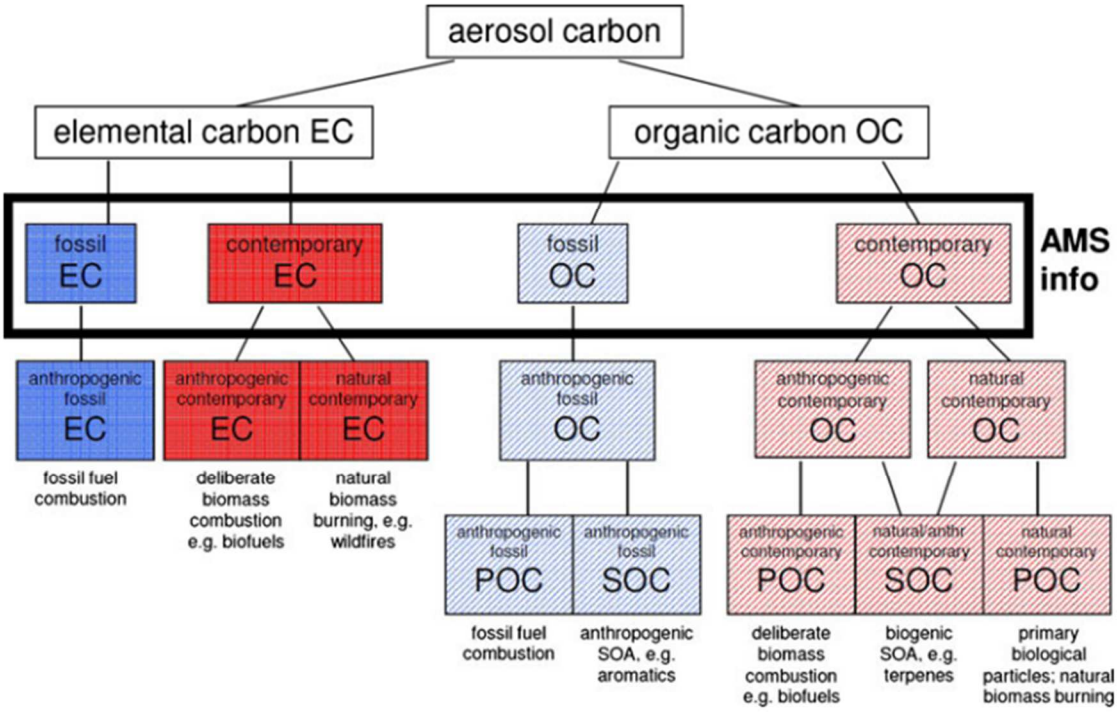

Figure 5.1. The demonstration of the subgroups of aerosol carbon TC into its subsequent fractions and their origin. Reprinted by permission from Springer Nature Customer Service Centre GmbH: Springer, Analytical and Bioanalytical Chemistry, the application of carbon-14 analyses to the source apportionment of atmospheric carbonaceous particulate matter: a review, Mathew R. Heal, Copyright 2013.

The research aims of the work presented in this chapter were:

1. Explore a methodology in which hypy can be used to isolate BC_{hypy} from TC for the purpose of ^{14}C measurements on these components, obtaining a set of ^{14}C values that can be used for quality assurance purposes of future studies.
2. Apply ^{14}C to a range of UK urban airborne ambient PM samples to identify the proportion of fossil versus modern biomass carbon sources contributing to the sampled PM TC at different sites, and the within-site variability.
3. Develop a methodology for the application of ^{14}C measurements to TC, BC_{hypy} and non-BC_{hypy} and explore how the results could inform air quality improvement measures in UK urban environments.

These acronyms will be frequently used throughout this chapter hence are provided below.

5.2. Methodology for ^{14}C, HyPy and $\delta^{13}C$ Measurements

The established standard operating procedures of the National Environmental Isotope Facility (NEIF) Radiocarbon laboratory were utilised for ^{14}C analysis of both TC and BC_{hypy}. A flowchart summarising the key steps within the method is shown below in Figure 5.2. Throughout all preparation steps particular care was taken to avoid carbon contamination for the ^{14}C work, due to the low natural abundance of ^{14}C.

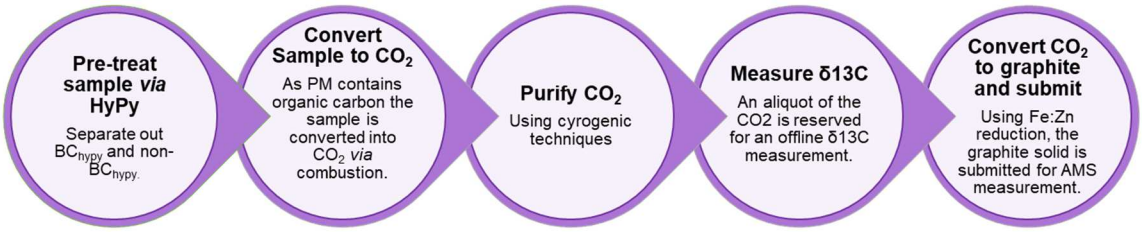

Figure 5.2. A flow chart denoting the steps required to prepare a PM sample for 14C. The first pre-treatment step is only applicable if the PM needs to be separated into BC_{hypy} or non-BChypy for separate analyses of these components.

5.2.1. Hydropyrolysis for BC separation

For ^{14}C measurement of sample TC, hydropyrolysis was not required, as the object was to measure the ^{14}C value for the entire (BC and non-BC) carbon on the sample. However, for ^{14}C analysis of the sample BC, hydropyrolysis was used to separate BC_{hypy} from non-BC_{hypy}. This was achieved for all samples according to the methodology that is described in full in Section 4.2.2 in Chapter 5.

5.2.2. Conversion of sample to CO_2 and subsequent purification

Before preparation for ^{14}C analysis, samples were freeze-dried either before combustion to CO_2 (TC samples) or before the hypy process (BC_{hypy} samples) to remove water from the samples and enable accurate mass measurements. The carbon within the prepared samples

(whether TC or BC_{hypy}) was converted into CO_2 through combustion in sealed quartz tubes that were pre-cleaned in air at 850 °C. For the TC measurements, whole PM samples on filter papers were folded with flame-cleaned tweezers and placed inside pre-cleaned quartz tubes. The tubes also contained 0.5 g copper oxide (CuO) and a small piece of silver wire that removed halides which could in later steps prevent the conversion of CO_2 to C (Buchanan and Corcoran, 1959). The tubes were numbered and evacuated on a vacuum line before being flame sealed. Sample combustion was achieved through the heating of tubes at 850 °C for 8 h in a muffle furnace, after which they were cooled slowly and attached to a vacuum line for CO_2 collection. The sample gas was released by cracking in a sealed, evacuated cracking unit that was attached to a vacuum rig for CO_2 purification (see below).

The sample CO_2 formed via the sealed tube combustion was purified using a high vacuum custom-built vacuum rig to prevent introduction of atmospheric CO_2, a potential contaminant, to the sample. The use of cryogenic purification techniques was utilised to separate non-carbonaceous gases from the sample CO_2. Water vapour was removed at -78 °C in a spiral trap surrounded by solid CO_2/ethanol, following which the gaseous sample was passed through a spiral trap surrounded by liquid N_2 (-196 °C), where non-condensing gaseous contaminants were removed by pumping under vacuum while the CO_2 was frozen with liquid N_2. The purified CO_2 sample yield was measured with a strain gauge and three aliquots were taken. The first aliquot was for graphitisation of the sample CO_2 to graphite for AMS measurement of the sample ^{14}C. The second aliquot was for off-line $\delta^{13}C$ analysis (see below). The final aliquot was retained as an archive of any remaining sample gas once the two latter aliquots had been isolated. In practice, some samples yielded very small amounts of CO_2 (<1 mL). A separate aliquot for off-line $\delta^{13}C$ analysis was not taken for these samples to ensure all carbon was converted to graphite and to maximise the chance of a successful AMS measurement. In these cases, the $\delta^{13}C$ value for normalisation of the sample $^{14}C/^{12}C$ ratios was obtained on-line in the AMS and is not reported.

5.2.3. $\delta^{13}C$ analysis

The ThermoFisher Delta V isotope ratio mass spectrometer was used in dual inlet mode, to analyse the stable isotopes of carbon to obtain the isotopic signature, $\delta^{13}C$, of the sample. $\delta^{13}C$ is calculated as detailed in Equation 13.

$$\mathrm{d}^{13}\mathrm{C}\ (‰) = \left[\frac{\frac{^{13}\mathrm{C}}{^{12}\mathrm{C}}(\mathrm{Sample})}{\frac{^{13}\mathrm{C}}{^{12}\mathrm{C}}(\mathrm{Standard})} - 1 \right] \times 1000 \quad (13)$$

Determination of the $\delta^{13}C$ using offline measurements could only be completed if the sample had 0.1 – 0.5 mg C to produce enough CO_2 for a measurement. Where samples had low CO_2 volumes, an online measurement for $\delta^{13}C$ was used, which was obtained by the AMS instrument. This was done to ensure there was enough mg C for the AMS measurement. Online measurements are not representative of the original $\delta^{13}C$ of the sample material, due to fractionation that occurs in the AMS, during measurement. Although this approach produces a $\delta^{13}C$ value that is suitable for normalisation of the sample $^{14}C/^{12}C$ ratio, these 'on-line' values are not reported by convention, to minimise the possibility they are inadvertently used as a proxy for other information (e.g. source apportionment).

$\delta^{13}C$ values are of interest as they can retain information about the sources of aerosols due to an isotopic difference in the $^{13}C/^{12}C$ of different potential sources, particularly fossil fuels versus biomass (Cao et al., 2011; Reiffarth et al., 2016). The $\delta^{13}C$ of ambient aerosol is assumed to be identical to the raw source material, e.g., wood, but processes forming the particles can result in isotopic fractionation of the material, hence why inventories of different sources $\delta^{13}C$ values can help with source apportionment of aerosols (Dempster et al., 1997; Gauchotte et al., 2009; O'Sullivan & Kalin, 2008; Smallwood et al., 2001). Hypy was deemed to be a robust technique for estimating the $\delta^{13}C$ of pyrogenic carbon across a range of materials such as biochar, coal, sediments, and soils (Mcrae et al., 1998; Wurster et al., 2012; Wurster et al., 2013). As BC is thought to be chemically inert once formed, the $\delta^{13}C$ signature of BC should closely reflect the signature of the ambient aerosol sources. OC, however, undergoes atmospheric reactions such as photochemical processing which may affect the $\delta^{13}C$ signature (Huang et al., 2006; Kirillova et al., 2013; Zenker et al., 2020). The offline $\delta^{13}C$ values were also used to help with source apportionment. More negative $\delta^{13}C$ values indicate a lower $^{13}C/^{12}C$ ratio whereas more positive $\delta^{13}C$ values indicate the reverse. The $\delta^{13}C$ of a mixed-source sample is a mass balance of its components. Hence, in a mixture between biomass and fossil fuel sources, the $\delta^{13}C$ value will become increasingly negative with a higher proportion of fossil carbon sources (Schuur et al., 2016).

5.2.4. Conversion of sample CO_2 to C

The 2 mL of purified sample CO_2 was converted to filamentous C (graphite) first through reduction to CO using 0.06 g of zinc (Zn) as a reaction catalyst at 400 °C then by reduction to C with 0.003 g iron (Fe) catalyst at 600 °C, following the method of Slota et al. (1987). The reactions occurred on a graphitisation unit under vacuum, consisting of 2 mL sample of CO_2 and two pre-cleaned Pyrex tubes containing catalyst surrounded by a small furnace. The pressure within the reaction vessel was continuously monitored by a computer-controlled pressure transducer. The measured pressure was converted to a digital value, and this value (input) was displayed on-screen, plotted as a function of time (hours). As pressure within the reaction vessel fell, the yield of graphite increased. Upon completion of the reaction, the sample graphite was collected and pressed into an aluminium sample holder to produce a target suitable for AMS analysis.

5.2.5. Accelerator Mass Spectrometry (AMS)

The prepared graphite targets larger than 0.5 mg carbon were inserted into an AMS sample source and measured at the Scottish Universities Environmental Research Centre (SUERC). The SUERC AMS facility is a NEC 5 MV terminal voltage instrument operated at 4.5 MV, with carbon in 4^+ charge state. The sample measurement proceeded for 40,000 counts of ^{14}C to give a 3‰ measurement uncertainty.

Samples generating <0.5 mg of carbon were measured on the Keck Carbon Cycle Accelerator Mass Spectrometry Facility at the University of California, Irvine, USA (KCCAMS/UCI; Southon et al. 2004).

5.2.6. Determination of the Fraction Modern Carbon

^{14}C is expressed as the fraction modern F ^{14}C which reports the $^{14}C/^{12}C$ ratio of the sample relative to the international standard Oxalic Acid II (NIST). Anthropogenic activities cause perturbations in the atmospheric abundance of ^{14}C which is why F ^{14}C is calculated against a standard reference value that is unaffected by these perturbations. Notable events include spikes in ^{14}C from nuclear bomb tests and reductions in ^{14}C through the release of CO_2 from

fossil fuel burning. At the SUERC AMS laboratory the ratio of ^{14}C to ^{13}C is typically measured in practice due to the high currents generated by ^{12}C, and the use of offline $\delta^{13}C$ values for normalisation of measured sample ratios Xu et al. (2004).

The radiocarbon primary standard, Oxalic Acid II, was used for normalisation of the sample $^{14}C/^{13}C$ ratios. The normalisation scheme was verified by measurements of secondary standards of Bulk Belfast Cellulose and Bulk TIRI Barleymash. Ascough (2006) highlighted why these known age standards (Oxalic acid and TIRI Barleymash) became established in international radiocarbon comparisons.

"The aim of the intercomparisons was to provide ^{14}C laboratories with an independent and objective assessment of the quality of their analytical data. Laboratories that took part in the exercise undertook measurements of several core and optional samples. This resulted in the production of reference (consensus) values for the measured samples, which could then be used as known age standards in ^{14}C measurement. The known age standards measured along with unknown age samples that were included in this study were: 1. Modern reference standard. Oxalic acid II produced by the National Institute of Standards and Technology for 14C age calculation and obtained from a 1977 sugar beet molasses harvest. 2. Modern Barley mash. This was a core sample in the TIRI exercise and is a by-product from malt whisky production, provided by Glengoyne Distillery. The sample was taken from a single fermentation vat and was well mixed during the industrial process. The sample was force dried and physically mixed before being provided as a TIRI sample (Scott, 2003). Standards were produced by combusting a bulk sample of the barley mash to produce a bulk bottled gas, from which aliquots were taken for measurement."

The fraction modern ($F^{14}C$) for a sample is the ratio of measured ^{14}C activities for the sample ($^{14}A_S$) and the oxalic acid standard ($^{14}A_{OX}$) (Ascough, 2006). Equation 14 shows how $F^{14}C$ has been presented throughout this chapter.

$$\%MC = 100 \times F^{14}C \quad (14)$$

5.3. Data Analysis

A simple mixing model was applied (see Figure 5.3) to determine the percentage fossil carbon (%FC) in airborne ambient PM samples. Mixing models are the tools used to convert isotopic data into estimates of source proportions (Levin & Hesshaimer, 2000; Phillips, 2012). The internal blank for the NEIF Radiocarbon Laboratory where the measurements

were made was used to represent the value for a theoretical sample with 100% fossil fuel composition. This was plotted against the northern hemisphere ^{14}C data for 2019 – where biomass-derived C was assumed to be from, as the samples analysed were first collected in 2019. The value for the atmosphere in 2019 was used to represent a theoretical 100% 'modern' carbon contribution to the samples. The linear equation was applied to $F^{14}C$ to convert to %FC.

There are currently no values for tropospheric $^{14}CO_2$ in 2020 from Levin and Hesshaimer. However, using extrapolation of previous values, an assumption that a fall of 0.004 $F^{14}C$ per year occurs. This leads to 1.005 $F^{14}C$ for 2020. When this value was applied to the data there was either no difference in resultant %FC values or a difference of 1 %FC when rounded up to 0 decimal places. As there was not a large difference, the tropospheric $^{14}CO_2$ value for 2019 was used.

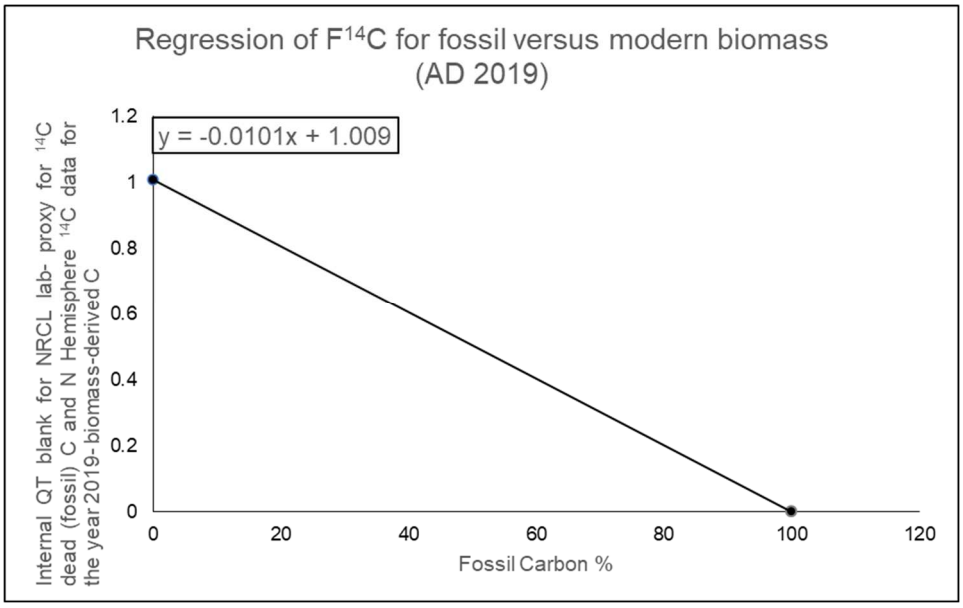

Figure 5.3. Regression of $F^{14}C$ for fossil versus modern biomass (AD 2019).

Chi-squared tests at 0.05 level of significance, were undertaken to determine if the differences between replicate ^{14}C measurements were significantly different and could be included in the weighted average.

The openair R package was utilised to calculate and plot air-mass back-trajectory frequencies as well as gridded and smoothed back trajectory concentrations showing mean $PM_{2.5}$ concentrations using the Concentration Weighted Trajectory approach (Seibert et al., 1994).

5.4. Method Testing and Development

The proposed method in Figure 5.4 details an exhaustive outline of the different potential method steps that could be applied to the airborne ambient PM in order to analyse various carbon fractions, and the subsequent products and data that could be obtained. The boxes in red show where ^{14}C analysis can be used for source apportionment of the carbon components found in particulate matter. Application of all proposed method steps in the Figure 5.4 would require large amounts of material to achieve all these analyses on one individual sample. Additionally, ^{14}C analysis at The SUERC AMS facility requires at least 0.5 mg of C within the sample to ensure accurate analysis for a 'routine' measurement, which is desirable as larger samples experience a smaller measurement uncertainty. In this project, a low volume air sampler (LVAS) was used for the collection of airborne ambient PM from Glasgow. Unlike high volume air samplers (HVAS) which can sample 1000 L min^{-1}, the LVAS used in this project sampled a lower volume of air (5 L min^{-1}) hence in comparison required longer sampling times to collect the same PM mass as a HVAS. Since one LVAS was available for use in this project, it was important to conduct calculations to determine how much airborne ambient PM was required for all analyses detailed in Figure 5.4 and whether collecting this amount of airborne ambient PM was possible within the project timeframe.

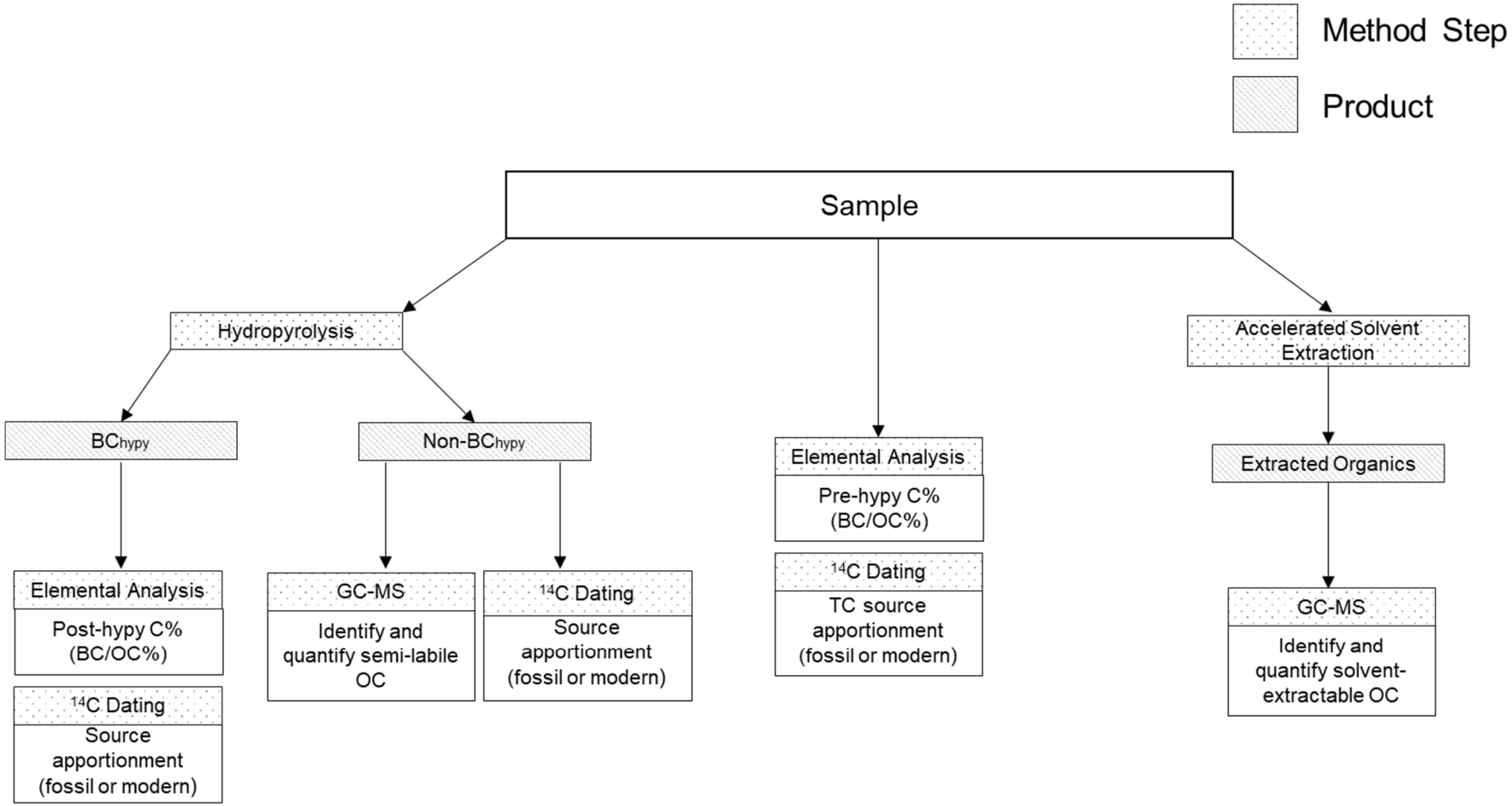

Figure 5.4. A flow chart showing the proposed method steps, products and potential results obtained, applied to the airborne ambient PM.

5.4.1. Hypy Mass Considerations for Airborne Ambient PM for ^{14}C Analysis

In the work presented in this section, the hypy methodology was explored to test whether ^{14}C measurement could be completed for TC, BC_{hypy} and non-BC_{hypy} in airborne ambient aerosols using this approach, with the aim of determining sources for each carbonaceous component of PM. Samples submitted for ^{14}C measurements to the SUERC AMS facility ideally should have at least 0.5 mg C within the sample. Smaller measurements down to 0.1 mg C are possible, but it is difficult to identify before processing whether aerosol samples will yield sufficient C for measurement, particularly for BC isolated by hypy. Therefore, a target of 0.5 mg C was set as the amount of material to aim for to ensure ^{14}C analysis would be feasible. It was hoped that this would allow for sample processing losses to result in a final sample measurement of ^{14}C that was between 0.1 – 0.5 mg C.

When submitting PM samples for TC ^{14}C measurements, the ideal scenario would be to submit a single filter, which would be representative of a certain period, typically one to two weeks. It would also be ideal to obtain the BC_{hypy} residue from a single PM filter. However, as mentioned in Section 4.2.2 in Chapter 5. hypy removes semi-labile OC, which adsorbs onto a silica trap, hence the %C of the BC_{hypy} residue is lower than the %C of the initial PM sample, as BC comprises a sub-fraction of the TC in the sample. The lower %C equates to a lower absolute value of carbon available for analysis in terms of mg C per sample of BC_{hypy} residue. Therefore, it was important to conduct calculations to determine what quantity of airborne ambient PM would be required not only for the TC ^{14}C measurement but also for the BC_{hypy} and non-BC_{hypy} measurements to establish approximate lower limits on the amount of sample material that would be required for a successful ^{14}C measurement.

The proposed method plan in Figure 5.4 shows that some method steps are interdependent. Before a quantitative value for the sources of BC in a sample can be determined through ^{14}C analysis, the BC/TC% of a sample should be determined through pre-hypy and post-hypy %C measurements. It is possible to calculate the proportion of fossil and non-fossil carbon in a sample based on a linear mixing model (i.e. based only on ^{14}C measurement of the individual sample and solving using a two end-member approach). However, for mass balance approaches, for example, to solve for a component of the sample that was not directly measured, then a measurement of the BC/TC% is necessary. When submitting a sample for the pre-hypy %C, relatively small amounts of sample (0.1 – 0.3 mg) can be submitted to ensure the samples mg C is within the calibration range for elemental analysis (usually 0.14 – 0.5 mg C). After hypy, the sample loses a portion of mg C as hypy separates

out recalcitrant carbon from semi-labile carbon. When a sample has a lower amount of mg C, larger sample masses need to be submitted for %C analysis and ^{14}C analysis, to ensure enough mg C is present for an accurate measurement. As post-hypy C% measurements occur before ^{14}C analysis this means there is a risk that the mg C of the sample submitted for ^{14}C may be insufficient for a measurement. A potential solution could be %C measurements using gaseous C (in form of CO_2), which are manometrically measured as part of the routine processing prior to ^{14}C analysis of the BC_{hypy}, hence helping ensure sufficient mg C for ^{14}C measurements. However, this raises logistical issues as gaseous %C techniques are time-consuming and laborious compared to measurement in an elemental analyser and require a separate set-up for standards and quality control of %C determinations, which is not routine during ^{14}C preparation due to the lower requirement for highly accurate and precise %C values during this process. It is also important to note that the two measurement techniques require rigorous quality assurance protocols to ensure inter-comparability of measurements made using the two approaches. The overall issue is ensuring that sufficient C (in mg C) is collected in the initial bulk sample to enable enough C to be collected at each processing step for %C and/or ^{14}C measurements of the individual sample fractions to all be successful. Overall, it is preferable to measure the samples using one approach, and ideally in a single batch, or as few batches as possible.

Materials

UD was used for this work as the standard was representative of urban aerosols hence was representative of mg C likely to be present in urban airborne ambient PM. More information on UD can be found in 3.2.1. Varying masses (approximately 50, 100 and 200 mg) of UD were used as the initial hypy mass. UD had 17 %TC, therefore calculations were made assuming collected airborne ambient PM would have the same amount of TC; however, in reality the %TC could be up to 33 % for airborne ambient PM in the UK (AQEG, 2012).

Results and Discussion of Hypy Mass Considerations for Airborne Ambient PM

Table 5.1 showed that if the TC was 17 % C for 46 mg of catalyst-free UD, the amount of carbon present would be 7.6 mg pre-hypy. Calculations were made to determine the

minimum sample mass required for ^{14}C analysis. The C mass was divided by the minimum C mass required for ^{14}C analysis.

Table 5.1. Calculations for BC/TC% of UD before and after hypy.

Sample weight (mg)	Catalyst-free weight (mg)	Catalyst-free Pre-hypy Sample C (%)	Sample C (mg)	Catalyst-free residue (mg)	Catalyst-free post-hypy sample C (%)	Residue C (mg)	BC/TC (%)
51.3	46.0	16.6	7.6	28.9	7.2	2.1	27.2
95.3	85.4	16.6	14.2	47.8	7.8	3.7	26
212.0	190.2	16.6	31.5	125.3	6.7	8.3	26

The catalyst-free starting mass used (46 mg of UD) was divided by the result of Equation 15(15), giving the minimum sample mass required for raw ^{14}C analysis, provided the sample has 17 % TC. The result is shown in Equation 16.

$$\frac{7.6\ mg\ of\ C}{0.5\ mg\ of\ C} = 15.2 \tag{15}$$

$$\frac{46\ mg\ of\ sample\ (TC = 17\%\ C)}{15.2} = 3.0\ mg \tag{16}$$

Lower-end limits were calculated in case the TC % was lower than 17 % (see Equation 17(17) and 18). A TC % of 10 % was used to represent the lower-end of TC present in an airborne ambient PM sample from the UK.

$$\frac{17\ \%\ TC}{10\ \%\ TC} = 1.7 \tag{17}$$

$$3.0\ mg\ \times 1.7 = 5.1\ mg \tag{18}$$

Based on these calculations a starting sample mass of 3.0 – 5.1 mg of PM for TC ^{14}C was required. These calculations also could be used to provide a basis for calculating the initial hypy starting masses of standards analysed using ^{14}C.

Post-hypy 29 mg of catalyst-free UD was left over after (hypy residue), with 2.1 mg of C present. For ^{14}C analysis, roughly around 0.5 mg of C is required for accurate results, therefore if 46 mg of airborne ambient aerosol was collected, with a C content of 17 % this would be enough for ^{14}C analysis. Calculations were made to determine the minimum amount of airborne ambient PM required:

$$\frac{2.1\ mg\ of\ C}{0.5\ mg\ of\ C} = 4.2 \tag{19}$$

$$\frac{46\ mg\ (catalyst\ free\ PM)}{4.2} = 11.0\ mg\ of\ catalyst\ free\ PM \tag{20}$$

Based on the calculations above, the minimum mass required for 0.5 mg C post-hypy of airborne ambient PM containing 17 % C, would be 11.0 mg.

Lower-end limits were calculated in Equation 21 and 22 assuming lower TC values of 10 % TC.

$$\frac{17\ \%\ TC}{10\ \%\ TC} = 1.7 \tag{21}$$

$$11.0\ mg\ \times 1.7 = 18.7\ mg\ of\ catalyst\ free\ PM \tag{22}$$

The calculations showed that if TC of airborne ambient aerosol was 10 % TC, then 18.7 mg of catalyst-free PM would be required for one hypy run whereas if the TC was 17 %, then 11.0 mg of catalyst-free PM would be required for one hypy run.

For the non-BC_{hypy}, calculations were made to ensure enough C was present within the sample for a ^{14}C measurement (Equation 23, 24 and 25(23)).

$$7.6\ mg\ TC - 2.1\ mg\ BC_{hypy} = 5.5\ mg\ non - BC_{hypy}\ C \tag{23}$$

$$\frac{5.5\ mg\ C}{0.5\ mg\ C} = 11.0 \tag{24}$$

$$\frac{46\ mg\ C\ catlayst\ free\ PM}{11.0} = \ 4.18\ mg\ of\ catalyst\ free\ PM \tag{25}$$

The calculations show that with 4.2 mg initial sample mass of PM would result in 0.5 mg C of non-$BC_{hypy.}$ Due to the high hydrogen pressures during hypy, it is unlikely that there would be 100 % recovery of the non-BC_{hypy}, due to loss of volatile components, removed by the hydrogen sweep gas. Moreover, 100 % recovery of the non-BC_{hypy} would require 100 % recovery and desorption of semi-labile organics from the silica in the hypy trap. The %MC of non-BC_{hypy} can also be achieved through mass balance calculations shown in Equation 26(26).

$$\frac{\left[\%\mathrm{MC(TC)} \times \mathrm{C\ mass\ (\%)} - \ \%\mathrm{MC}(\mathrm{BC}_{hypy}) \ \times \%\mathrm{BC/TC}\right]}{(100 - \%\mathrm{BC/TC})} = \%\mathrm{MC}(\mathrm{non} - \mathrm{BC}_{hypy}) \tag{26}$$

To check whether single filters could be used for TC, BC_{hypy} and non-BC_{hypy} ^{14}C measurements, a $PM_{2.5}$ sampling test was conducted at GLA-CC on 01/02/2019 to 08/02/2019. The $PM_{2.5}$ mass collected was 0.5 mg. As reported in AQEG (2012) around one-third of $PM_{2.5}$ can constitute of carbonaceous material. As levels of carbonaceous components may vary during sampling, a lower bound percentage of carbonaceous material in $PM_{2.5}$ was denoted as 11 %. This meant 0.055 mg – 0.165 mg of C could be collected per

week. Based on these calculations it was clear that a single filter could not be used for TC, BC_{hypy} and non-BC_{hypy} measurements.

Conclusions

The findings showed that several filters would need to be combined for a TC ^{14}C measurement from the same sampling location. $PM_{2.5}$ sampling test runs showed that 0.5 mg could be collected per week at GLA-CC. However, at least 3.0 – 5.1 mg of PM with a %TC of 10 – 17 %, would be required for one measurement TC ^{14}C measurement. As mentioned in the UK, up to one-third of $PM_{2.5}$ consists of carbonaceous components, therefore it was likely that these calculations were overestimating the mass of $PM_{2.5}$ required for a TC ^{14}C measurement. These calculations were useful as they act as a basis for determining the required mass for other standards/samples with known %C values that were analysed using ^{14}C. Moreover, they helped shape the $PM_{2.5}$ sampling approach. As more filters were required for the analyses, this meant that $PM_{2.5}$ sampling could not be as spatially representative as initially hoped.

The findings also highlighted that several filters, separate to those for TC ^{14}C measurements, would need to be combined to obtain the BC_{hypy} ^{14}C measurement. The calculations showed that 11.0 mg of PM with a %TC of 17 % or 18.7 mg of PM with a %TC of 10 % would be required per hypy run. Ultimately, the mass required is dependent on the %TC of the PM sample. In UD, the BC content was 27 % of TC, however in $PM_{2.5}$ in the UK, it has been stated that BC makes up 11 – 16 % of $PM_{2.5}$ (AQEG, 2012). This means potentially larger masses of $PM_{2.5}$ would be required than those calculated. Therefore, it was decided that a large volume of PM filters would need to be firstly run on hypy to isolate BC, then the residues would be combined for ^{14}C measurements. This would ensure ^{14}C measurements could be obtained as the BC_{hypy} would have sufficient mg C (0.1 – 0.5 mg). To enable GC-MS analysis of the non-BC_{hypy} of $PM_{2.5}$ samples, it was decided that the %MC of non-BC_{hypy} would be done through the difference of TC and BC_{hypy} measurements. This was necessary due to the time constraints of $PM_{2.5}$ sampling with the LVAS. With this in mind, it became clear that sampling would have to be conducted in one location to ensure the non-BC_{hypy} %MC could be calculated by difference. Considering large masses were required for one measurement, it was evident that a lower number of hypy-^{14}C analyses could be completed, due to the LVAS used in this project.

5.4.2. Exploration of Hypy Methodology to Isolate BC for ^{14}C Measurements

Before the hypy methodology was applied to airborne ambient PM it was necessary to ensure that hypy could be used to reproducibly separate BC_{hypy} from $PM_{2.5.}$ This was done by testing the hypy methodology on known-source materials that could contribute to airborne ambient $PM_{2.5.}$ The replicate BC_{hypy} ^{14}C measurements of known-source materials could be compared to determine the precision of the hypy methodology. It was also important to ensure the results were in line with other literature therefore analysis of widely available aerosol standards was completed. As these aerosol standards had reported %MC for BC in the literature, it allowed for comparisons to be made.

Method and materials

The materials used in this section are listed below. The materials did not undergo acid pre-treatment, as acid fumigation may introduce errors in source apportionment through reaction with other carbonaceous components in the sample. Moreover, as these ^{14}C values could be used for quality assurance purposes for future studies, differences may occur in reported ^{14}C values due to differences in acid pre-treatment methods and in operators. Therefore, to ensure comparability, it was decided that acid pre-treatment was not necessary, considering that airborne ambient PM contains a negligible number of carbonates.

Aerosol and Dust Materials

As the hypy methodology was being developed to determine the sources of BC in PM, it was important to test the methodology on the same environment matrix. The particles in PM vary greatly in terms of composition depending on their sources hence it was important to test a range of aerosol materials (Long et al., 2013). UD and UPM represented aerosols with sources typical in urban areas whilst FD represented vehicular emissions as it was collected in a traffic tunnel. UD has also been analysed in previous studies therefore comparisons between BC ^{14}C measurements could be made. Road dust contributes to PM in the form of exhaust and non-exhaust emissions. The UK NAEI found tyre wear, brake wear and road wear emissions increased from 26 % of road traffic $PM_{2.5}$ emissions in 2000 to 67 % in 2018

(AQEG, 2019). Therefore, road dust materials BCR-RD and HH-RD were analysed. More information on these materials, their sources and composition is given in Section 3.2.1.

Charred Biomass

DB and EB were charred biomass samples used as ^{14}C standards to signify the age of solid particulates emitted from biomass combustion. These standards were used as end members for anthropogenically-produced ^{14}C-modern carbon within the sample, which was useful as industrial biomass burning and domestic wood combustion are the top two contributors to $PM_{2.5}$ in the UK (NAEI, 2020). For more information on these materials see Section 3.2.1.

Fossil Fuel Materials

BZ, a lignite, and DS, a solid particulate emitted from combustion of diesel, a fossil fuel, were used as ^{14}C standards to signify the results obtained from analysis of both non-combusted fossil fuels, and particulates emitted from combusted fossil fuels. These acted as end members for petrogenic fossil sources and pyrogenic fossil sources. For more information on these materials see Section 3.2.1.

Total Carbon ^{14}C Analysis

The ^{14}C results in Table 5.2 showed that the fossil carbon end members had extremely low %MC, whilst the modern carbon end members had high %MC. This is in line with expectations, due to the geological age of the carbon in the fossil carbon end members. Aerosols and road dusts had values in between the two end members, demonstrating a mixture of modern and fossil carbon. There was no significant difference between petrogenic and pyrogenic fossil fuel end members, but there was a difference between TIRI Barley Mash and the charred biomass, which could have been due to the year of the fixing of the carbon from the atmosphere to form the plant tissues that comprised these two individual samples.

Table 5.2. Results from total carbon ^{14}C analysis for the following standards: BZ, DS, DB, EB, HH-RD, BCR-RD, UD, UPM, FD and radiocarbon standards. Additional data $\delta^{13}C$ and %C is included.

Material ID	$\delta^{13}C$ ‰ (TC)	%MC	%MC error	%C
Fossil Fuel Materials				
BZ	-24.14	0.1	0.00	57.3
DS	-28.42	0.2	0.01	81.1
Biomass Materials				
DB-1	-12.90	103	0.5	57.1
DB-2	-13.10	103	0.5	62.7
EB	-15.12	97	0.4	1.9
Aerosol and Dust Materials				
HH-RD-1	-24.21	24	0.1	4.8
HH-RD-2	-24.65	23	0.1	4.7
HH-RD-3	-24.59	23	0.1	4.7
BCR-RD-1	-23.1	19	0.1	14.0
BCR-RD-2	-23.0	19	0.1	14.0
UD	-25.87	53	0.2	17.7
UPM	-24.1	64	0.3	13.5
FD	-24.9	20	0.1	10.5
Radiocarbon Standards				
Anthracite	-23.1	0.2	0.00	91.3
Anthracite-1	-23.34	0.1	0.00	91.3
TIRI Barleymash	-27.04	116	0.5	47.0

* Error represents the ^{14}C measurement uncertainty

Aerosol and Dust Standards ^{14}C(TC)

The ^{14}C measurement of UD, UPM and FD gave %MC (TC) values of 53, 64 and 20 % respectively. These %MC (TC) values represent mixed sources which are expected from airborne ambient aerosols. FD had a lower %MC (TC) value, compared to the other standards, most likely because FD was collected from a traffic tunnel in Warsaw, Poland, meaning PM constitutes dominantly from vehicular emissions, which have fossil sources, hence has a lower %MC value.

Previous studies have reported ^{14}C results for UD. The values obtained here were compared to those from the literature in Figure 5.5. The %MC (TC) value from this study for UD was 53 % (see Table 5.2) which was extremely similar to those reported by Szidat et al. (2004b) (number 2 on the graph 52 %, NIST certificate 2007 (number 3 and 4, 51 % and 52 %), Heal et al. (2011) single combustion (number 5 on the graph, 52 %) and Bonvalot et al. (2016)

(number 8 on the graph 54 %). The value in this study was not within the error bars of Currie et al. (1984) or Heal et al. (2011) two-step combustion method, however measurement 3, 4, 5 and 8 were also not within the error bars of these measurements.. The agreement between the value in this research and those from previous research provides assurance that the quality of the measurements was, to a good standard, producing reproducible results.

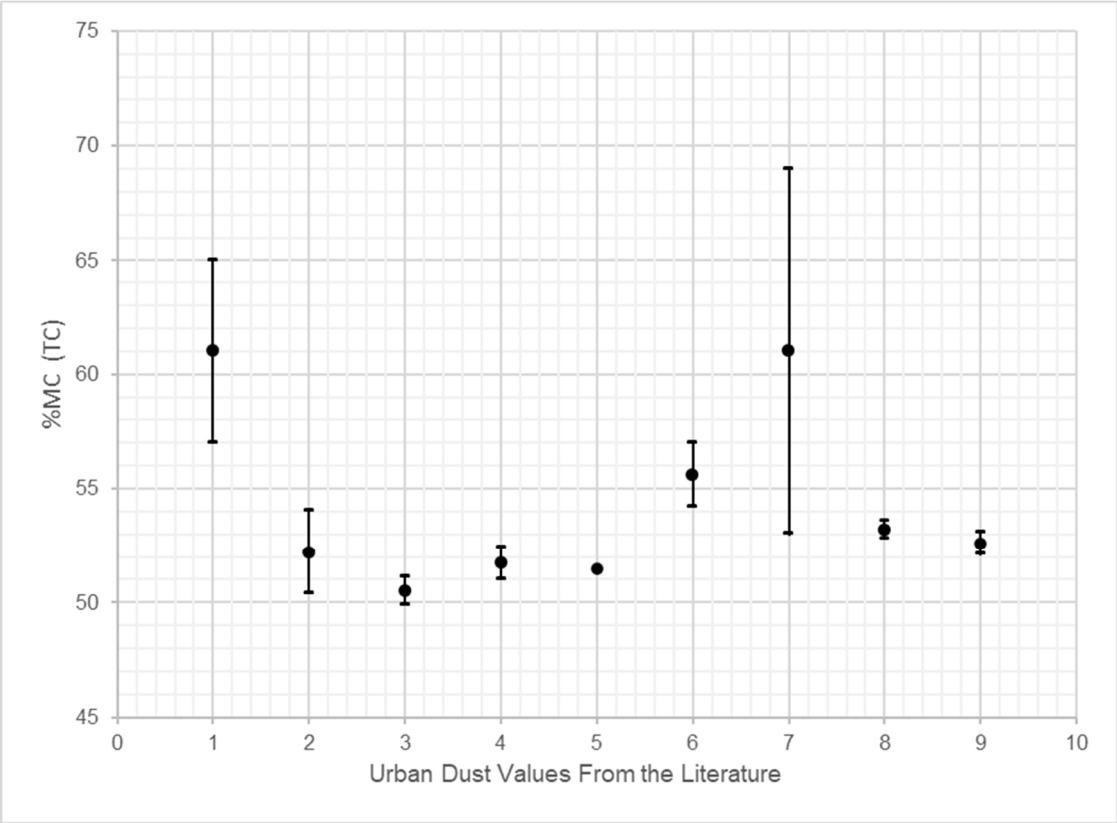

Figure 5.5. A graph showing the %MC (TC) of NIST 1649 and the associated errors, from the literature and this work. References: Currie et al. (1984) (1), Szidat et al. (2004b) (2), NIST 2007 Certificate H_3PO_4-combustion-manometry method (3) combustion-GC method (4), Heal et al. (2011) single combustion method (5), Heal et al. (2011) two-step combustion method (6), NIST 2007 Certificate Combustion manometry method (7), Bonvalot et al. (2016) Solid Source Method (8) and this work. (9).

There are few ^{14}C (TC) measurements on UPM within the literature. Weissenbok et al. (1998) reported a value of 60.9 ± 1.7 %MC (TC) for a UPM sample, whilst Kaplan and Gordon (1994) reported 62.1 ± 0.9 % and 62.4 ± 0.4 % and Currie et al. (1984) reported 60 ± 3 % through beta counting method. Results from this study were 63.56 ± 0.56 % (see Table 5.2). The error bars from Kaplan and Gordon (1994) and Currie et al. (1984) overlapped with the ^{14}C measurement from this study. This meant results from this study were close to prior measurements. The measurement in this study was higher than those in other studies.

BCR-RD had %MC (TC) values of 19 % and HH-RD had %MC values of 23 – 24 % (see Table 5.2). The low %MC (TC) values in comparison to the aerosol standards UD and UPM could be due to a larger proportion of fossil fuel sources contributing to the total carbon in this sample as BCR-RD was collected from roads in a traffic tunnel in Austria, thus vehicular emissions from petroleum or diesel fuel combustion may contribute more highly to the road dust, hence yielded a lower %MC (TC) relative to HH-RD. HH-RD was collected from an open road in Glasgow, University Avenue, with potential sources from vegetative detritus, airborne soil and traffic emissions hence explaining the higher %MC (TC) value. To check whether the replicate values for each road dust standard could be combined into a weighted average, the values and their associated errors were plotted (Figure 5.6 and Figure 5.7).

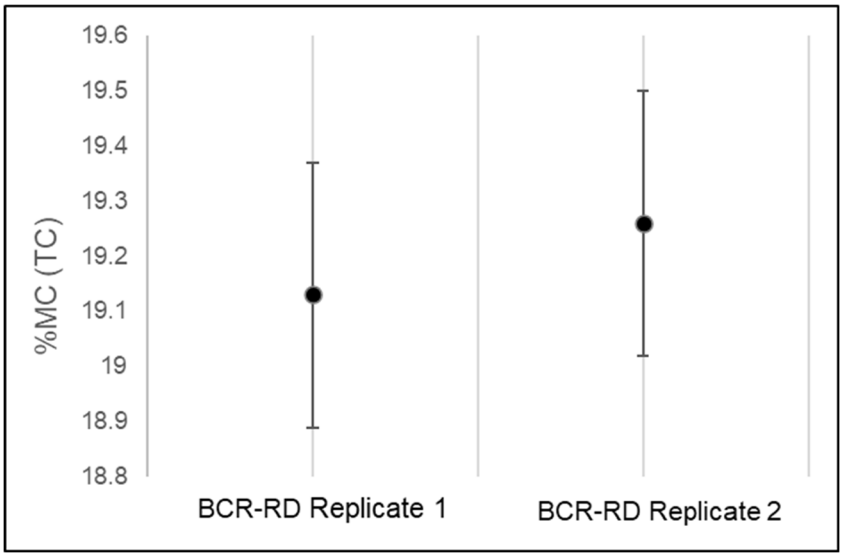

Figure 5.6. The %MC (TC) values for BCR-RD replicates, with the error bars used representing the ^{14}C measurement uncertainty.

As seen in Figure 5.6 BCR-RD replicates were extremely similar with overlapping error bars, therefore these measurements can be combined to form %MC (TC) weighted average of 19.2 % round to 19 %. The HH-RD replicate 1 did not overlap with replicate 2 and 3 and a chi-squared test confirmed that there was a statistical difference between the three replicates RD [X^2 (2, N = 3) = 5.99, p = 0.00]. However, as the difference was less than 1 %MC (TC) this deviation would not make a significant difference to the interpretations. The variations may be a result of sample heterogeneity despite sample homogenisation via sieving; road dust in general contains different components e.g., vegetative detritus, PM, crustal minerals etc. The weighted average %MC (TC) calculated using the three replicates was 23.21 ± 0.34 % rounded to 23 %.

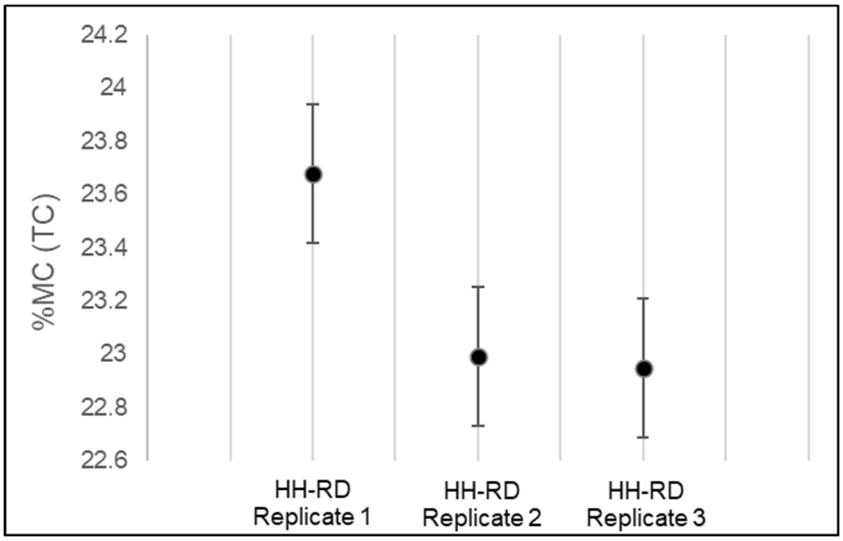

Figure 5.7. The %MC (TC) values for HH-RD replicates, with the error bars used representing the ^{14}C measurement uncertainty.

UD had the most negative $\delta^{13}C$ (-25.87 ‰) in the aerosol materials indicating larger fossil fuel contributions, compared to FD (-24.9 ‰) and UPM (-24.1 ‰). HH-RD had a more negative $\delta^{13}C$ value (-24.5 ‰) than BCR-RD (-23.1 ‰) indicating a larger fossil fuel contribution BCR-RD.

Charred Biomass and Biomass Ash Standards ^{14}C(TC)

The %MC (TC) values of DB and EB were 103 and 97 %. As expected, these standards had a high %MC due to their biogenic origins. Both standards had lower %MC (TC) values than the TIRI Barley Mash standard, implying the biomass was either fixed after the time of collection of the TBM standard (due to declining atmospheric %MC values over this time), or a contribution from lab-derived fossil carbon sources. It was less likely that the biomass carbon was fixed on the upward limb of the atmospheric ^{14}C bomb curve (i.e. c.1950s), as the material used in the processes from which EB and DB were obtained from material that was sourced over the past few years. The fossil fuel sources could be attributed to contamination in the laboratory where the samples were run. The most likely explanation for DB is that the biomass relates to a period over the past couple of decades, and for EB the result that is <100 %MC is strongly indicative of a fossil fuel component. The latter could

be the result of inadequate cleaning of the combustion chamber in between tests of different fuel materials which included fossil-fuel sources. The DB replicates yielded similar %MC (TC) as seen in Figure 5.8.

The $\delta^{13}C$ values were -13 ‰ for DB and -15.12 ‰ for EB. These high values represent C_4 plants, such as aquatic plants, desert plants, salt marsh plants and, relevant to these samples, tropical grasses. They were also within the range of other studies-19.0 to -6.0 ‰ for C_4 plants (Deines, 1980; Medina et al., 1999).

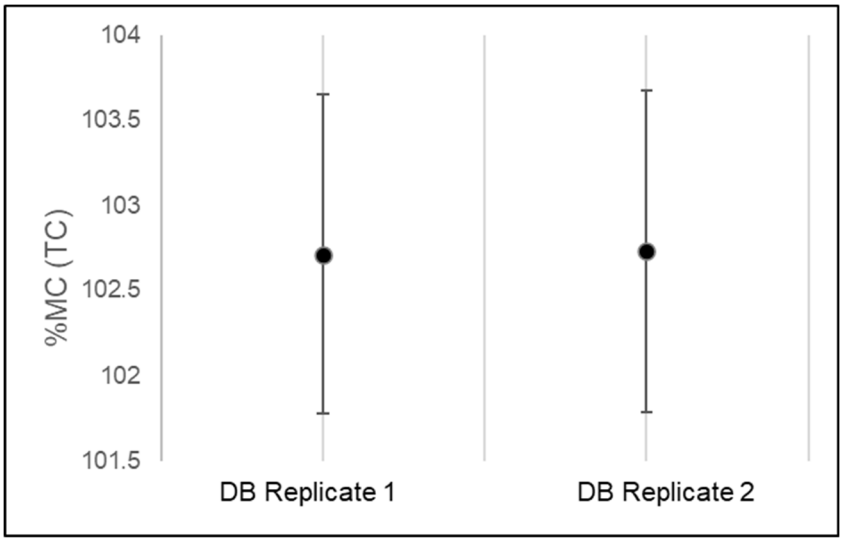

Figure 5.8. The %MC (TC) values for DB replicates, with the error bars used representing the ^{14}C measurement uncertainty.

Fossil Fuel Standards ^{14}C(TC)

The DS and BZ materials had %MC (TC) values of 0.1 % and 0.2 % respectively. These values overlapped at 2 sigma with the NEIF radiocarbon laboratory process background (anthracite) which has a long-term average %MC value of 0.17 % and are hence indistinguishable from the laboratory ^{14}C background. BZ is a lignite, hence has petrogenic sources whereas DS has pyrogenic sources produced from combusted diesel fuel. Low %MC values are expected as these standards contain fossil carbon which is ^{14}C 'dead'. The $\delta^{13}C$ (TC) for DS was -28.42 ‰ and for BZ -24.14 ‰. The DS $\delta^{13}C$ (TC) was more negative than all other materials showing fossil fuel contributions whilst the BZ $\delta^{13}C$ (TC) was more similar to anthracite.

Figure 5.9 summarises the %MC (TC) measured for the standards. DS and BZ had almost 0 %MC (TC) similar to the anthracite radiocarbon standard. Road dust standards and FD had lower %MC (TC) values indicating contributions from vehicular emissions of petroleum and diesel combustion or coal combustion. UD and UPM had a larger contribution from modern sources as opposed to fossil carbon. DB and EB were similar to the Barleymash radiocarbon standard.

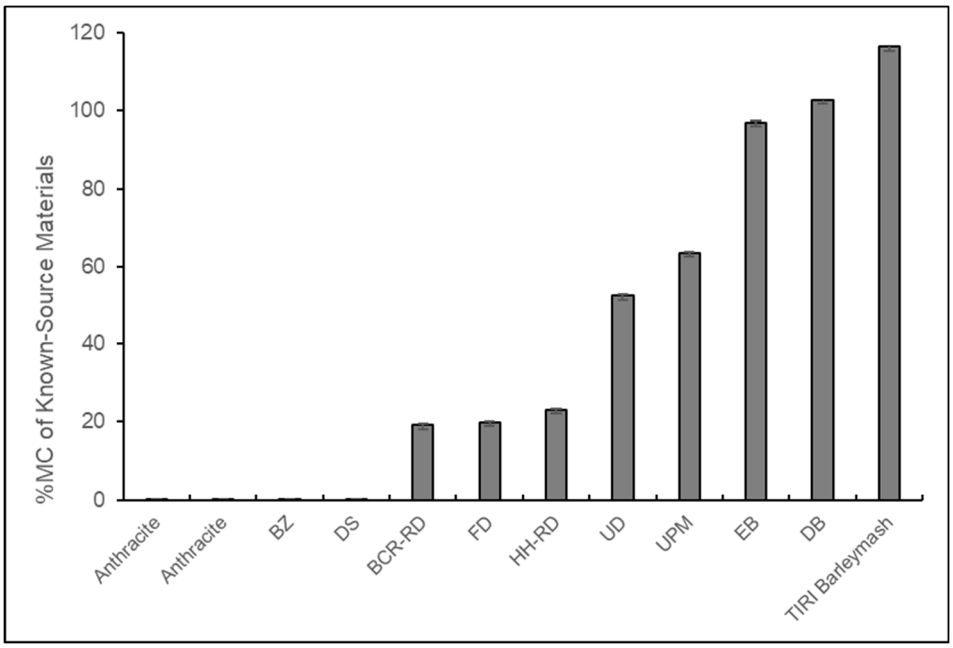

Figure 5.9. The %MC for radiocarbon standards and biomass, fossil fuel, aerosol and dust materials.

^{14}C Analysis Measurements for BC_{hypy}

^{14}C analysis was performed on the BC_{hypy} component of the known-source materials mentioned in the previous section. The %MC (non-BC_{hypy}) was calculated on a mass balance basis using the %MC of TC and BC_{hypy} of the sample (Equation 26). A negative result was obtained for DS it had a BC/TC% over 100 %. Table 5.3 shows the results from the BC_{hypy} ^{14}C analysis which includes $\delta^{13}C$ results.

Table 5.3. Results from BC_{hypy} ^{14}C analysis for the following standards: BZ, DS, DB, EB, HH-RD, BCR-RD, UD, UPM, FD and radiocarbon standards. Additional $\delta^{13}C$ data is included. The non-BC_{hypy} %MC was calculated as described in Equation 26.

Material ID	%MC (TC)	BC/TC %	$\delta^{13}C$ (BC_{hypy})	%MC (BC_{hypy})	%MC Error (BC_{hypy})	%MC (non-BC_{hypy})
DS	0.1	105.9	-28.9	0.14	0.01	-0.9
DB-1	103	15.1	-13.2	103	0.47	103
DB-2	103	15.1	-13.4	103	0.47	
EB-1	97	62.5	-14.0	102	0.47	89
EB-2	97	62.5	-13.9	101	0.46	
BCR-RD-1	19	40.9	-23.4	8	0.10	28
BCR-RD-2	19	40.9	-21.8	6	0.10	
UD	53	27.8	-25.4	6	0.10	70
UPM	64	24.8	-24.5	12	0.11	81
FD-1	20	26.1	-22.1	9	0.10	24
FD-2	20	26.1	-21.8	9	0.11	
Anthracite	0.1	-	-23.4	0.25	0.01	-

* Error represents the ^{14}C measurement uncertainty

Aerosol and dust standards

The %MC (BC_{hypy}) of UD, UPM and FD was 6, 12 and 9 %, respectively, and of the %MC (non-BC_{hypy}) of UD, UPM and FD was 70, 81 and 24 % (see Table 5.3). Figure 5.10 shows that the BC/TC% of all aerosol standards were extremely similar with UD 28 % BC/TC%, UPM 25 % BC/TC% and FD 26 % BC/TC%. However, the proportion of fossil versus modern carbon was different in the BC_{hypy} and the non-BC_{hypy} components, suggesting different emission sources for each of the components. The BC_{hypy} component in the aerosol materials comprised mainly of fossil carbon. FD had the lowest %MC (BC_{hypy}) which was expected due to it representing traffic emissions. UPM had the highest %MC (BC_{hypy}) hence suggests there was a larger contribution of modern BC sources from biomass combustion. The fossil sources in UD and UPM were likely to be from coal combustion as the USA National Emission Inventories showed that in 1975 when the material was collected, that the dominant sources of PM_{10} were fuel electricity utilities and other industrial processes (USA NEI 1975). The %MC (non-BC_{hypy}) was highest in UPM. The proportions of %MC (non-

BC_{hypy}) differed from that of %MC (BC_{hypy}) suggesting biogenic sources. This was also observed in UD and FD. However, in FD %MC (non-BC_{hypy}) had approximately 15 % difference.

BCR-RD %MC (BC_{hypy}) value was 6 – 8 % and %MC (non-BC_{hypy}) 28 %. The %MC (BC_{hypy}) and %MC (non-BC_{hypy}) was similar to FD which was also collected from a traffic tunnel. Despite this the BC/TC% of BCR-RD and FD were different; 41% and 26 % respectively (see Figure 5.10). This could suggest differences in vehicle fleet composition, perhaps with BCR-RD having a higher proportion of diesel to petroleum emission sources than FD. The %MC (non-BC_{hypy}) of BCR-RD was similar to FD. HH-RD could not be analysed as the mg C was too low after hypy, therefore a measurement could not be obtained.

The %MC (BC_{hypy}) and %MC (non-BC_{hypy}) were used to determine sources of BC and OC, using equations reported in Heal et al. (2011) that were applied to provide a source apportionment of carbonaceous $PM_{2.5}$ in Birmingham, UK. Here the use of this method was utilised on aerosol standards to determine if hypy could be used in conjunction with ^{14}C analysis to allow for further source apportionment beyond BC and OC categories. Figure 5.11 show the source categories per aerosol and dust standard. Terms BC_{fossil} and $BC_{biomass}$ refer to fossil fuel combustion and biomass combustion sources of BC. Terms OC_{fossil}, $OC_{biomass}$ and $OC_{biogenic}$ imply fossil fuel sources, biomass combustion sources and natural biogenic sources.

UD and UPM had extremely similar source profiles which was expected as they were sampled around the same time, from different cities in the USA. The BC_{fossil} was higher in UD whilst $OC_{biomass}$ was higher in UPM, as mentioned previously. BCR-RD and FD had very similar source profiles with the main difference being BCR-RD had a larger proportion of BC_{fossil} than FD, whilst FD had a larger OC_{fossil} contribution, perhaps highlighting a larger contribution of diesel emissions to petrol emissions, in BCR-RD. FD and BCR-RD did not have biogenic sources, this is likely to be because traffic tunnels are closed environments. In contrast, UD and UPM had biogenic OC contributions. All analysed materials contained small contributions of $BC_{biomass}$ and $OC_{biomass}$ indicating the presence of biomass burning. As mentioned in Section 3.2.8, the domestic combustion of wood was common in Austria in 1990, when BCR-RD material was collected and also was common in Poland during the time FD was collected.

The $\delta^{13}C$ (BC_{hypy}) for UD, UPM, and FD were -25.87 ‰, -24.1 ‰ and -24.9 ‰. UD was the lowest, hence this material was likely to have had a larger contribution of fossil sources

than FD then UPM. This is in agreement with the %MC (BC_{hypy}) results. The $\delta^{13}C$ (BC_{hypy}) of UPM was lower than $\delta^{13}C$ (TC) by 0.4 ‰ whereas FD and UD increased by 2.95 ‰ and 0.46 ‰ respectively. This shows that the removal of non-BC_{hypy} removed a portion of $OC_{biogenic}$ or $OC_{biomass}$ in UD. However, in FD and UPM, the OC_{fossil} was removed causing the change in $\delta^{13}C$ signatures. As seen in Figure 5.11, the TC of FD constituted of 64 % of OC_{fossil} hence its removal had an impact on the $\delta^{13}C$ signatures. In Figure 5.11 UD and UPM are very similar, however the higher $\delta^{13}C$ (BC_{hypy}) in UPM can be explained by a smaller proportion of BC_{fossil} (23 % compared to 27 % in UD) and a slightly larger proportion of $BC_{biomass}$ (2 % compared to 1 % in UD) hence the removal of OC_{fossil} caused a slight increase in $\delta^{13}C$ (BC_{hypy}).

The average $\delta^{13}C$ (BC_{hypy}) of BCR-RD was -22.6 ‰ compared to $\delta^{13}C$ (TC) of -23.1 ‰. The BC_{hypy} therefore was higher likely due to the removal of OC_{fossil} which made up 50 % of TC (see Figure 5.11).

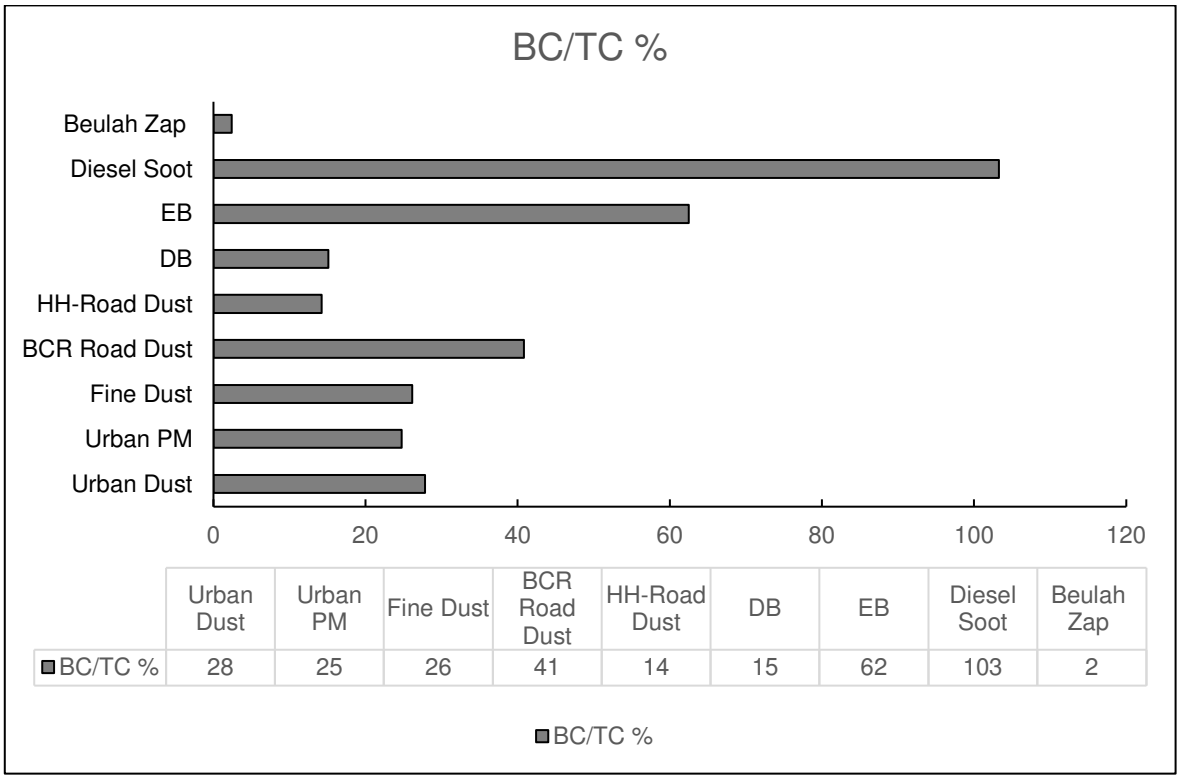

Figure 5.10. The BC/TC % of all standards analysed.

Fossil fuel standards

The %MC (BC_{hypy}) for DS was 0.1 %. The BC/TC % ratio was 106 %. DS had a small OC contribution, which was also observed during solvent extraction through the TLE mass and the n-alkane and PAH concentrations after GC-MS analysis in Chapter 3. The %MC (non-BC_{hypy}) gave negative values. This implied that there was no evidence for the presence of ^{14}C carbon. The $\delta^{13}C$ (BC_{hypy}) values of DS (-28.9 ‰) were similar $\delta^{13}C$(TC) values (-28.42 ‰).

Charred Biomass

The %MC (BC_{hypy}) were 103 % for DB and 101 – 102% for EB. The %MC (BC_{hypy}) showed a slight increase compared to %MC (TC); EB %MC (BC_{hypy}) increased by ~ 5 % whereas for DB the increase was less than 1 % therefore the increase was within the measurement uncertainty. The increase in %MC (BC_{hypy}) in EB could be due to the cleaving of chemical compounds within the OC_{fossil} segment, via hypy, and inhomogeneities in the sample composition. For example, material that was grown at slightly differing time periods being more or less susceptible to polyaromatisation, and hence slightly differing %MC values for the highly polyaromatic (BC_{hypy}) fraction of the sample, versus the TC. The non-BC_{hypy} for DB consisted of 103 %MC and EB consisted of 89 %MC.

The $\delta^{13}C$ (BC_{hypy}) values for DB and EB were -13.2 to – 13.4 ‰ and -13.9 to – 14.0 ‰. The changes in DB were likely to be negligible as they were similar to the uncertainty errors exhibited across replicate measurements (0.1 – 0.3 ‰). However, EB had lower $\delta^{13}C$ (BC_{hypy}) than the $\delta^{13}C$(TC) -15.12 ‰, which could be from the cleaving and removal of modern chemical components during hypy.

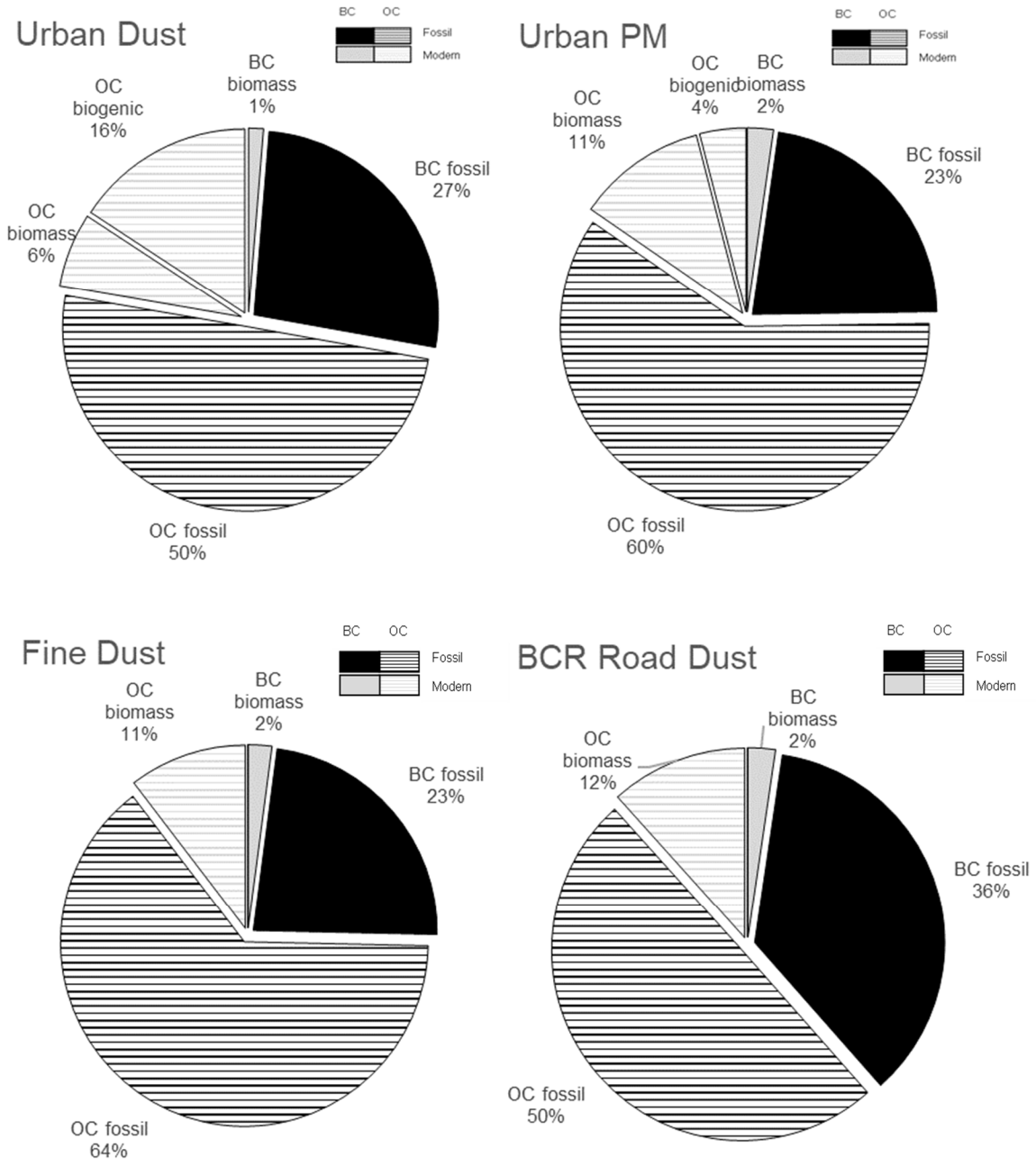

Figure 5.11. Source apportionment of BC and OC components within aerosol and dust standards.

Conclusions

In summary, the %MC (TC) of the known-source materials showed that the method was reproducible and accurate when compared to other literature %MC values. UD (53 %MC) and UPM (64 %MC) results obtained were similar to those in the literature. Urban aerosols UD had roughly equal contributions from ^{14}C-dead (i.e. fossil) and ^{14}C-modern sources whilst UPM had a larger proportion of ^{14}C-modern sources indicating biogenic SOA and/or biomass combustion. The road dusts and aerosol collected from traffic tunnel had lower %MC (TC) values (BCR-RD 19 %, FD 20 %, and HH-RD 23 % MC TC) indicating fossil sources from vehicular emissions and potentially erosion of asphalt road surfaces. Both FD and BCR-RD had very similar %MC (TC). When HH-RD was collected the road was being resurfaced, so the fossil contributions could be from asphalt and vehicular emissions whilst the modern carbon could have been from vegetative detritus as there were many larger fragments of plant litter present in the sample before sieving. The fossil fuel standards exhibited ^{14}C dead signatures whilst the charred biomass exhibited modern signatures.

The use of hypy successfully separated BC_{hypy} from TC, thus permitting the determination of the %MC (BC_{hypy}) component as well as of the non-BC_{hypy} component through mass balance calculations. The %MC (BC_{hypy}) of DS was 0.1 %MC, the same as the %MC (TC). The %MC (TC) was 0.2 % for BZ. Hypy was not conducted on BZ however as it was a non-BC containing material. The BC_{hypy} of DB and EB were around 100 % MC (BC_{hypy}).

Standards FD, UD, UPM had %MC (BC_{hypy}) values ranging from 6 – 12 %MC (BC_{hypy}). The %MC (BC_{hypy}) was low in comparison to the %MC (TC). This indicates that the sources contributing to BC were mainly fossil sources however, there were clearly some modern BC sources as the %MC (BC_{hypy}) was above DS 0.1 %MC (BC_{hypy}). The modern contribution to BC_{hypy} was from biomass combustion. UPM had the highest %MC (BC_{hypy}), indicating that it had a larger contribution from biomass combustion. The %MC (non-BC_{hypy}) was highest in UPM (81 %) indicating a large proportion of biogenic SOA. UD had 70 %MC (non-BC_{hypy}) indicating there were also biogenic sources as the proportions of %MC in BC_{hypy} and non-BC_{hypy} differed. FD had the lowest %MC (non-BC_{hypy}) with the contributions from BC_{hypy} and non-BC_{hypy} being similar which indicated a large proportion of $OC_{fossil.}$ BCR-RD had a low %MC (BC_{hypy}) at 5.53-7.85 % and MC (non-BC_{hypy}) at 10.2-14.3%. The relatively low %MC (non-BC_{hypy}) indicated a higher proportion of $OC_{fossil.}$

The source attribution of UD and UPM showed significant biogenic SOA contributions as well as biomass contributions for BC and OC. FD and BCR-RD did not have biogenic

contributions but had biomass combustion contributions to BC and OC, and high OC_{fossil} which explained why the %MC (non-BC_{hypy}) was low. FD had the highest OC_{fossil} contribution which suggested that petroleum vehicle emissions were dominant in FD whilst in BCR-RD diesel vehicle emissions were more dominant as there was a higher BC_{fossil} contribution. This shows that hypy can be used for source apportionment of airborne ambient PM as well as road dusts. Moreover, the source attribution of BC_{hypy} and non-BC_{hypy} can be very useful for determination of different categories of BC (fossil and biomass) and OC (fossil, biomass and biogenic). Changes in $\delta^{13}C$ values could be explained by the source attribution of the aerosol and dusts materials. This shows that $\delta^{13}C$ signatures can also be used alongside ^{14}C measurements for source apportionment.

5.4.3. Pre-treatment of Airborne Ambient Samples using Acid Fumigation

Carbonates contain fossil C, albeit formed through different mechanisms to coal and oil. Due to carbonates and coal and oil all being '^{14}C dead', the presence of carbonates in a sample can reduce the 'apparent' ^{14}C content of the sample, lowering the overall %MC (and increasing the ^{14}C age) (Bench, 2004). Carbonates can also interfere with hypy BC/TC determinations as, after separation of BC from TC, any remaining carbonates will incorrectly be denoted as BC during the post-hypy %C analysis. There is no consensus in the literature on whether carbonates must be removed from aerosols prior to ^{14}C analysis or BC/TC determinations. In a UK report on PM (AQEG, 2005), it was assumed that inorganic carbonates make negligible contribution to carbon in UK $PM_{2.5}$ compared with OC and BC. Studies in the literature corroborated this suggestion; Szidat et al. (2013) showed there was no difference between the TC %MC of acid-fumigated and non-acid-fumigated ambient airborne aerosols and aerosol standards. Górka et al. (2020) also found acid fumigation made no difference to $\delta^{13}C$ values of PM_{10} in Poland meaning significant amounts of carbonates were not removed, as this would change the $\delta^{13}C$ of the sample, as carbonates have significantly different $\delta^{13}C$ source signatures to other carbonaceous components in PM. A study analysing OC and BC in airborne ambient aerosols in Sweden, removed carbonates when using the CTO-375 method, and thermograms obtained by thermo-optical analysis confirmed the absence of carbonates in the samples (Zencak et al., 2007). To conclude, it was unclear whether acid fumigation is necessary for airborne ambient PM before ^{14}C

analysis and BC/TC separation via hypy, so the purpose of this work was to determine if acid pre-treatment was a necessary step for ^{14}C source apportionment of PM. This was done through ^{14}C analysis of acid fumigated and non-acidified aerosol and dust materials. The comparison of the results helps to inform whether carbonates were present in the sample and whether their removal effected the source apportionment significantly. The results of this investigation are presented in the sections below.

Materials and Method

Acid fumigation was conducted on aerosol materials FD and UPM and one road dust material BCR-RD (more information is provided on these sample types, their source and composition in 3.2.1). Samples were treated with a standard method that is commonly used in the aerosol literature for carbonate removal. This comprised 24-h of HCl fumigation. This was achieved by adding a small volume of Milli-Q water to 20 mL sample vials, ensuring the sample was fully dampened, after which the vials were placed inside a desiccator. Concentrated HCl (50 mL) was poured into the beaker (100 mL), over the sink with water running, then transferred into the desiccator with the sample. The desiccator lid was closed, ensuring an airtight seal, and then enclosed in a black polythene bag to exclude light, within a fume cupboard. After 24 h, the HCl within the desiccator was discarded into the appropriate waste container, whilst the sample vial was placed into an evaporating dish with potassium hydroxide covering the bottom (25 g) in order to neutralise the sample. This was left in the sealed desiccator for 3 days. The sample was then freeze-dried, followed by the quartz tube combustion method of CO_2 generation. Measurements were made of ^{14}C, $\delta^{13}C$ and %C on the samples both before and after the acid fumigation treatment using the methods described in Section 5.2. These results were then compared to identify whether the acid fumigation treatment resulted in a measurable removal of carbonate contaminants.

Results and Discussion

The ^{14}C, $\delta^{13}C$ and %C results for acid fumigation and non-acid fumigation are shown in Table 5.4. The %C results for the standards decreased after acid fumigation, which demonstrated a loss in carbon content: BCR-RD 14.0 %C to 10.2% C; FD 10.5 %C to 9.0 %C; UPM 13.5 %C to 12.1 %C. The greatest carbon loss was from BCR-RD. The %MC values (Figure 5.12) were lower after acid-fumigation for aerosol standards UPM and FD, however for BCR-RD the %MC values were higher after acid-fumigation. To determine if these changes were significant a chi-square test of independence was performed to test the

null hypothesis that acid fumigation does not make a significant difference to %MC value. The null hypothesis was rejected; acid fumigation made a statistically significant difference to the %MC value for BCR-RD [χ^2 (1, N = 2) = 3.84, Test Statistic = 31.1, p = 0.00] and UPM [χ^2 (1, N = 2) = 3.84, Test Statistic = 4.2, p = 0.04]. However, for FD the null hypothesis was accepted [X^2 = 0.02, N = 2) = 3.84, Test Statistic = 0.02, p = 0.84]. Despite statistical differences for UPM, the plots in Figure 5.12 show that the error bars overlap for acid fumigated and non-acidified conditions which indicates that despite the difference in %MC being statistically significant, the small difference could be attributed to uncertainty in measurements such as instrument variation, sample heterogeneity, weather conditions on the day and/or the operator. Therefore, acid fumigation makes a very small difference to the %MC values in the context of source apportionment of airborne PM. In the case of BCR-RD the error bars did not overlap, but the %RSD was around 3.1 % indicating the difference in %MC across acid-fumigated and non-acidified conditions were negligible.

Table 5.4. ^{14}C analysis results alongside $\delta^{13}C$ and %C results, for aerosol and dust standard acid fumigated and non-acid fumigated.

	Material ID	**$\delta^{13}C$ ‰ (TC)**	**%MC**	**%MC error**	**%C**
Acid Fumigation	UPM replicate 1	-25.04	62.00	0.29	11.8
	UPM replicate 2	-24.68	62.92	0.29	12.3
	UPM Average	-24.86	62.46	0.46	12.1
	FD replicate 1	-27.69	19.57	0.12	9.0
	FD replicate 2	-27.68	20.00	0.12	8.9
	FD Average	-27.69	19.79	0.22	9.0
	BCR-RD replicate 1	-26.53	19.92	0.13	10.1
	BCR-RD replicate 2	-26.55	20.16	0.12	10.2
	BCR-RD Average	-26.54	20.05	0.12	10.2
Non-acidified	UPM	-24.10	63.56	0.28	13.5
	FD	-24.90	19.84	0.13	10.5
	BCR-RD replicate 1	-23.10	19.13	0.12	-
	BCR-RD replicate 2	-23.00	19.26	0.12	-
	BCR-RD Average	-23.05	19.20	0.09	14.0

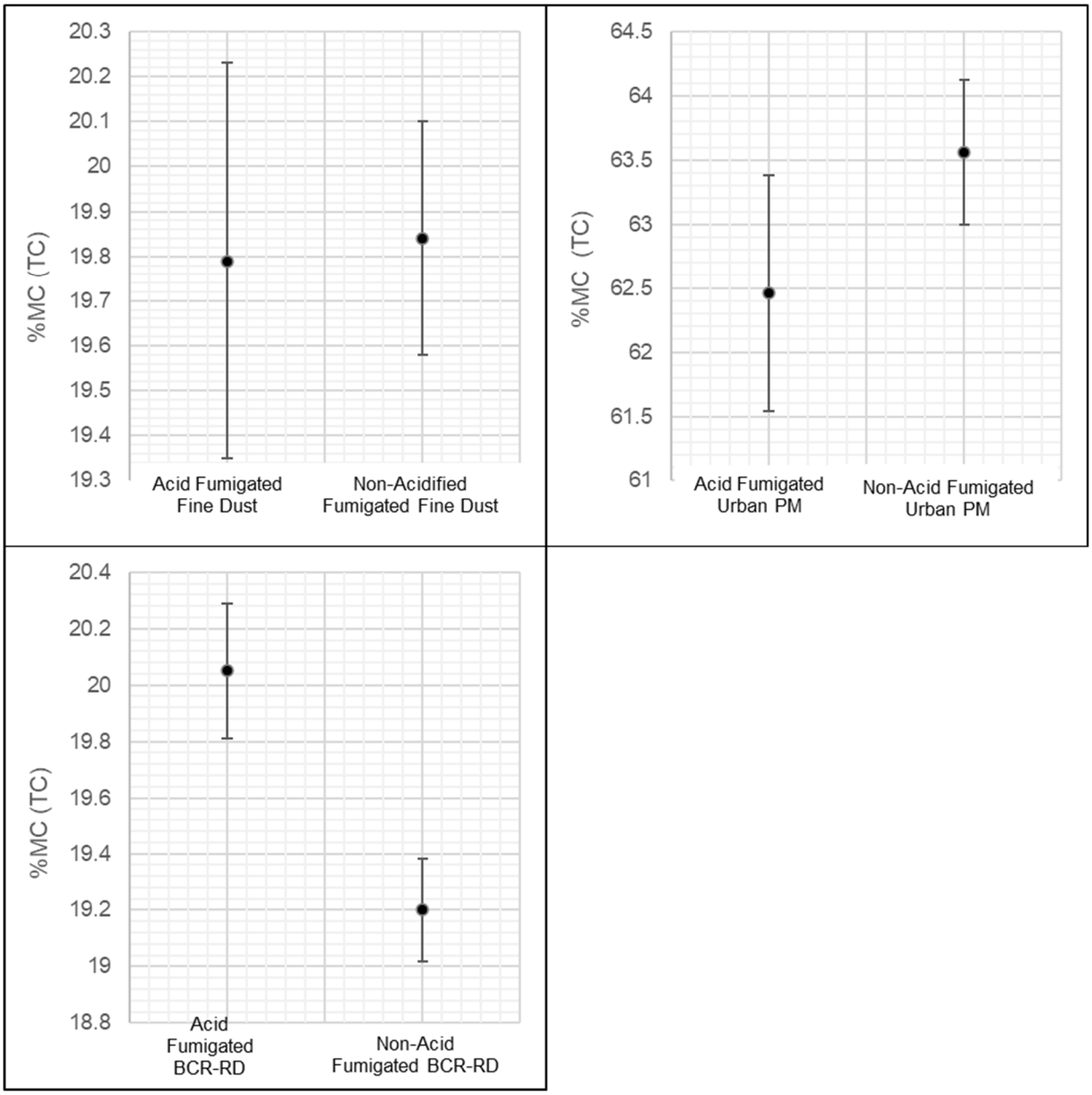

Figure 5.12. The %MC (TC) values of acid fumigated and non-acid fumigated aerosol and road dust standards. The error bars show the measurement uncertainty. The average %MC was used.

The $\delta^{13}C$ values before and after acid fumigation were compared. For UPM, $\delta^{13}C$ values went from -24.1 to -24.86, for FD -24.9 to -27.69 and for BCR-RD -23.05 to -26.54. All standards $\delta^{13}C$ values decreased when undergoing acid fumigation. The decrease in %C across all standards after acid-fumigation implies their carbon content had decreased. However, this alone could not confirm that carbonates were removed as other carbonaceous components may have been removed. The radiocarbon results showed that %MC (TC) of standards FD and UPM were lower than non-acidified FD and UPM. This implies there were zero carbonates present within the samples, as removal of carbonates should lead to increased %MC (TC). The possibility of 'modern' pedogenic carbonate contamination is

considered very unlikely as ^{14}C-modern pedogenic carbonates are not generally formed in temperate locations, and the overwhelming sources of carbonates in the UK are geological age (Kim et al., 2020). The decrease in %MC values suggest acid fumigation removed chemically labile OC. This is feasible as HCl can react with organic matter, as demonstrated by Bao et al. (2019) who found that fumigation by HCl degrades young and labile components of OC in sediments, leaving more refractory organic parts. However, BCR-RD had higher %MC values after acid fumigation which indicates that carbonates were removed alongside organics with larger carbonate concentrations led to a net increase in %MC. Another potential explanation is that geological-age OC components were removed somehow in the treatment. Considering BCR-RD is a road dust material, carbonates may be present due to erosion of concrete road surfaces and components of crustal materials from erosion of sedimentary rocks that contain limestone and dolomite. Also, construction activities such as cement and stone working, may contribute to carbonate concentrations in road dusts.

The $\delta^{13}C$ of FD, UPM and BCR-RD became more negative which suggests modern labile OC was removed. The depletions were larger in FD and BCR-RD. However, a study using acid fumigation pre-treatment for aquatic and terrestrial samples found large within-sample and between-sample variability in $\delta^{13}C$ values, thus concluded acid fumigation could not produce consistently reliable results (Brodie et al., 2011). Lorrain et al. (2003) stated that acid fumigation significantly decreased $\delta^{13}C$ values in filters of suspended particulate organic matter collected from sea water, when compared to non-acidified samples. No data could be found on the effect of acid fumigation on $\delta^{13}C$ values in aerosols. However, considering all standards $\delta^{13}C$ values decreased, this suggests acid-fumigation may yield inaccurate results for airborne ambient PM samples also.

Limitations of this experiment were that the materials used were not directly representative of carbonate concentrations in UK airborne PM. However, the aerosol and dust materials were representative of urban areas hence the results provided useful insights.

Conclusions

Acid-fumigated aerosol and dust materials, UPM and BCR-RD, showed statistically significant differences for %MC values, at 95% confidence to the non-acidified condition for UPM and BCR-RD. In the case of UPM, the differences were only just exceeding the 95 % statistical significance. For FD the difference in %MC was statistically insignificant

between the two conditions. Despite the statistically significant differences for UPM and BCR-RD, the actual difference in %MC values were less than 1 % for all standards. Therefore, it was concluded that acid fumigation was not necessary for ^{14}C source apportionment of PM. BCR-RD showed the largest deviation in %MC between the two conditions, with an increased %MC value after acid fumigation indicating the presence of carbonates. Aerosol standards showed a slight increase in fossil carbon after fumigation, which suggests a portion of modern labile OC was altered with the use of acids. Alternatively, the deviations could also be down to measurement uncertainty, in this case it was most likely from inhomogeneity of the materials. As the error bars of acidified and non-acidified aerosol standards overlapped, this indicated that there was little difference between the %MC values, and that the 'true' value lies somewhere within those uncertainties. The $\delta^{13}C$ values differed between the two conditions, showing a depletion in BCR-RD, FD and UPM indicating the removal of modern carbon through use of acid fumigation. This corroborated %MC results which showed a decrease in %MC for FD and UPM. However, a slight increase in %MC was observed for BCR-RD, which suggests both modern OC and carbonates were removed in this material.

In view of the data and interpretations, although there is evidence that the acid fumigation treatment can remove carbonates where these are present in samples, it was decided that acid fumigation was not required as a pre-treatment step for ^{14}C analysis of airborne ambient PM in this study. There is a risk of modern OC being removed from samples, as seen for UPM and FD, where carbonates were not present or present in small quantities. This in turn can affect the %MC as well as the $\delta^{13}C$ values yielding inaccurate source apportionment data. Although there was a significant difference in %MC in UPM before and after acidification, the error bars between both conditions overlapped indicating the difference could be attributed to the measurement uncertainty.

5.5. Application of ^{14}C to Ambient Airborne PM from Sites in the UK to Identify the Variability in Proportion of Fossil versus Modern Biomass Carbon Sources

^{14}C TC measurements were conducted on ambient airborne PM from different sites across the UK to determine the variability in the proportion of fossil carbon versus modern biomass carbon sources.

5.5.1. Materials and methods

$PM_{2.5}$ samples from locations in the UK were analysed. $PM_{2.5}$ samples from GLA-CC and GLA-HH were collected on 47 mm filters, whilst MAN-FF samples were collected with 150 mm filters. Samples on 47 mm filters were collected using a LVAS so had to be grouped to ensure sufficient carbon for a successful measurement. Table 5.7 gives information on collection periods of the grouped filters. MAN-FF $PM_{2.5}$ samples on 150 mm diameter filters were collected using a HVAS which provided sufficient sample mass on each filter for measurement. See Section 3.2.2 for more information on sample collection of MAN-FF.

Glasgow Sampling Sites

Glasgow City – George Street

A low volume air sampler, BGI Omni ™ FT Ambient-Air Sampler (Mesa Labs, Lakewood, Colorado, USA) was used to collect $PM_{2.5}$, PM_{10} and TSP samples from Glasgow City - George Street (Figure 5.13). The sampler was housed at the University of Strathclyde, Royal College building, which is located by a busy road, George Street, which is nearby public transport connections as well as the city centre. The sampler was placed at this entrance behind the large gates, which sheltered the sampler from adverse weather (rain/wind) but enabled outdoor sampling. The sampler operated at 5 L min^{-1}. The filter paper was changed manually, and samples were stored in the freezer after collection. Initially the filters were changed on a weekly basis but subsequently they were changed fortnightly. The purpose of this was to increase particle mass filter loading as this would help with sample

introduction/preparation for samples being run on hypy. The list of filters collected is shown in Table 5.5.

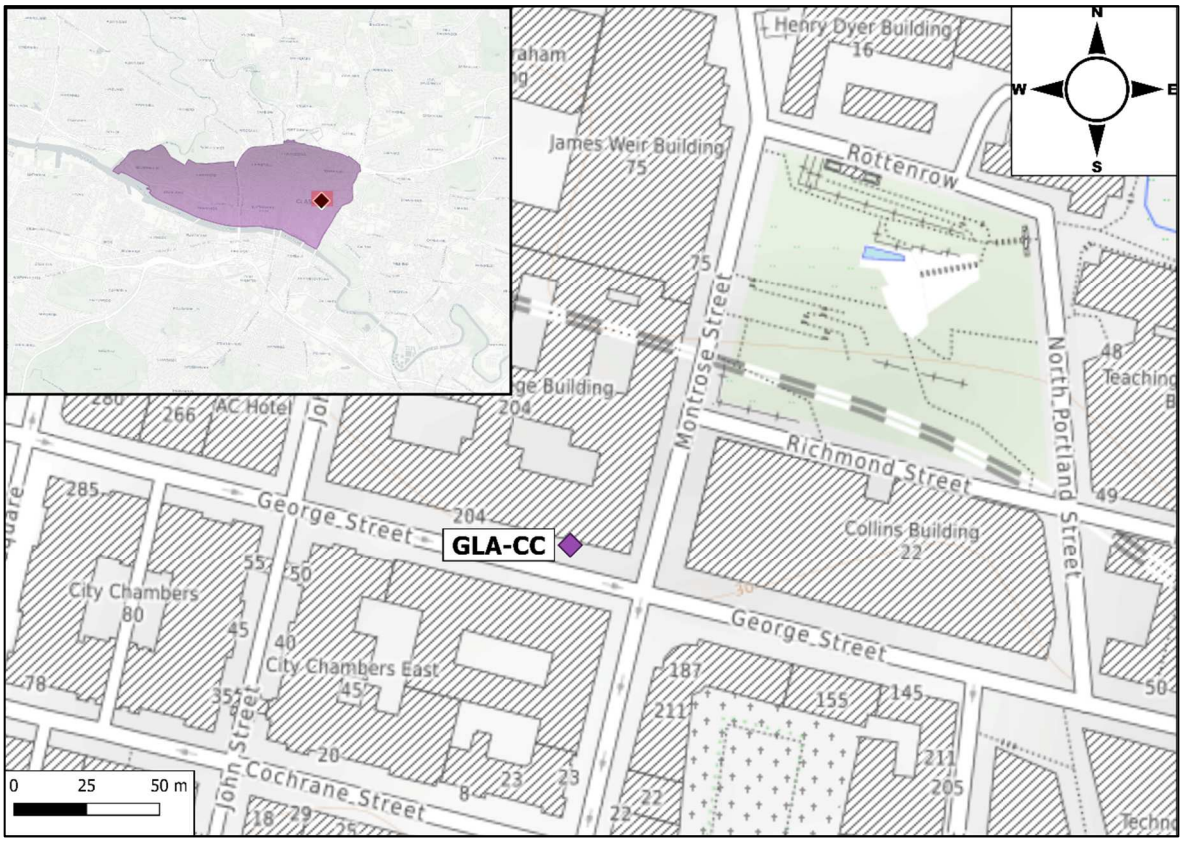

Figure 5.13. A map showing the sampling point, GLA-CC. The map layers used were provided by Esri (Esri Gray light) and OpenTopoMap.

Table 5.5. Airborne ambient PM samples collected in Glasgow City – George Street. Samples with a * were collected by another LVAS named the EcoTech. There were issues with this sampler; it was unable to properly shield/house the filters from moisture hence only two samples were collected. A negative mass was experienced, due to the tearing of a filter due to the moisture.

Filter Number	Inlet Size	Sampling Dates	Mass (mg)	Volume of Air Sampled (m^3)	Analysis Completed
Filter 06	TSP	18/01/2019 – 25/01/2019	0.97	50	^{14}C Raw Analysis
Filter 04	$PM_{2.5}$	25/01/2019 – 08/02/2019	1.40	101	^{14}C Raw Analysis
Filter 01	$PM_{2.5}$	08/03/2019 – 15/03/2019	1.07	50	^{14}C Raw Analysis
Filter 02	$PM_{2.5}$	29/03/2019 – 05/04/2019	1.20	50	^{14}C Raw Analysis
Filter 34	PM_{10}	25/10/2019 – 31/10/2019	1.25	43.2	^{14}C Raw Analysis
Filter 17	PM_{10}	06/11/2019 – 12/11/2019	1.48	46	^{14}C Raw Analysis
Filter 18	PM_{10}	15/11/2019 – 21/11/2019	1.96	44	^{14}C Raw Analysis
Filter 19	$PM_{2.5}$	29/11/2019 – 05/12/2019	1.49	43	^{14}C Raw Analysis
Filter 20*	$PM_{2.5}$	29/11/2019 – 05/12/2019	-0.55	26	^{14}C Raw Analysis
Filter 22	$PM_{2.5}$	28/02/2020 – 10/03/2020	1.53	79	^{14}C Raw Analysis
Filter 23*	$PM_{2.5}$	28/02/2020 – 10/03/2020	0.88	48	^{14}C Raw Analysis

Glasgow Hillhead – University Avenue

A low volume air sampler, BGI Omni™ FT Ambient-Air Sampler (Mesa Labs, Lakewood, Colorado, USA) was used to collect $PM_{2.5}$ samples from Glasgow Hillhead – University Avenue (Figure 5.14). The sampler was placed in a cage by University Avenue, near the Boyd Orr building. The sampler operated at 5 L min^{-1}. The sampling site changed on 07.10.2020 due to safety concerns as construction was occurring by the sampling site. The alternative sampling site was also situated on University Avenue but located on the other

side of the road, roughly opposite to the initial site. The list of filters collected is shown in Table 5.6.

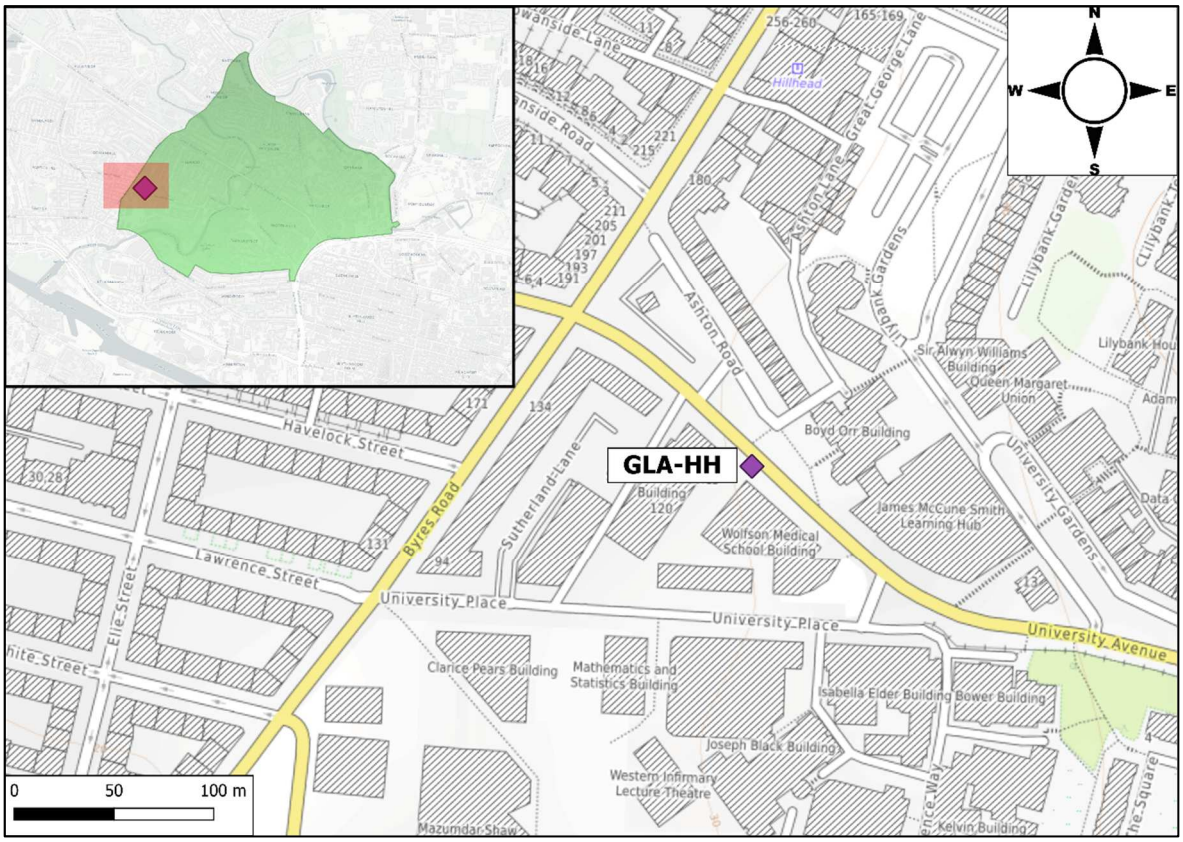

Figure 5.14. A map showing the sampling point, GLA-HH. The map layers used were provided by Esri (Esri Gray light) and OpenTopoMap.

Table 5.6. Airborne ambient PM samples collected from Glasgow Hillhead – University Avenue. Samples with a * were collected by another LVAS named the EcoTech. There were issues with this sampler; it was unable to properly shield/house the filters from moisture hence only two samples were collected. A negative mass was experienced, due to the tearing of a filter due to the moisture.

Filter Number	Inlet Size	Sampling Dates	Mass (mg)	Volume of Air Sampled (m^3)	Analysis Completed
Filter 03	$PM_{2.5}$	18/06/2019 – 24/06/2019	0.47	43	HyPy then GC-MS & ^{14}C
Filter 28	$PM_{2.5}$	07/10/2020 – 22/10/2020 *	2.00	108	^{14}C Raw Analysis
Filter 24	$PM_{2.5}$	22/10/2020 – 05/11/2020	0.84	101	HyPy then GC-MS & ^{14}C
Filter 25	$PM_{2.5}$	05/11/2020 – 19/11/2020	2.24	100	^{14}C Raw Analysis
Filter 26	$PM_{2.5}$	19/11/2020 – 30/11/2020	1.18	86	^{14}C Raw Analysis
Filter 29	$PM_{2.5}$	22/01/2021 – 04/02/2021	1.11	86	^{14}C Raw Analysis
Filter 30	$PM_{2.5}$	04/02/2021 – 18/02/2021	1.17	101	HyPy then GC-MS & ^{14}C
Filter 31	$PM_{2.5}$	18/02/2021 – 04/03/2021	1.53	101	HyPy then GC-MS & ^{14}C
Filter 32	$PM_{2.5}$	04/03/2021 – 18/03/2021	1.23	101	HyPy then GC-MS & ^{14}C
Filter 33	$PM_{2.5}$	18/03/2021 – 29/03/2021	1.27	79	HyPy then GC-MS & ^{14}C
Filter 35	$PM_{2.5}$	01/04/2021 – 16/04/2021	0.97	107	^{14}C Raw Analysis
Filter 36	$PM_{2.5}$	16/04/2021 – 29/04/2021	0.93	94	^{14}C Raw Analysis
Filter 38	$PM_{2.5}$	29/04/2021 – 14/05/2021	-2.40	108	HyPy then GC-MS & ^{14}C
Filter 39	$PM_{2.5}$	14/05/2021 – 27/05/2021	0.03	244	HyPy then GC-MS & ^{14}C
Filter 37	$PM_{2.5}$	27/05/2021 – 17/06/2021	1.63	151	HyPy then GC-MS & ^{14}C
Filter 40	$PM_{2.5}$	17/06/2021 – 24/06/2021	0.80	51	HyPy then GC-MS & ^{14}C
Filter 41	$PM_{2.5}$	24/06/2021 – 15/07/2021	0.80	152	HyPy then GC-MS & ^{14}C
Filter 42	$PM_{2.5}$	15/07/2021 – 30/07/2021	0.73	109	HyPy then GC-MS & ^{14}C
Filter 02	$PM_{2.5}$	30/07/2021 – 12/08/2021	1.07	92	HyPy then GC-MS & ^{14}C

Filter 05	$PM_{2.5}$	12/08/2021 – 26/08/2021	0.83	101	HyPy then GC-MS & ^{14}C
Filter 43	$PM_{2.5}$	26/08/2021 – 09/09/2021	0.80	101	HyPy then GC-MS & ^{14}C

Shared $PM_{2.5}$ Samples from Other UK Sites

$PM_{2.5}$ samples on 47 mm filters from AURN sites Auchencorth Moss, London Marylebone Road, London Honor Oak Park and Chilbolton Observatory (see Figure 5.15) were received from the National Physics Laboratory. Chilbolton Observatory, London Marylebone Road, and London Honor Oak filters were changed daily; Auchencorth Moss filters were changed weekly due to extremely low air pollutant concentrations at this rural background site. The filters were collected during the COVID-19 pandemic, therefore the results for samples from AURN sites were not directly comparable to GLA-CC, GLA-HH and MAN-FF due to different sampling periods.

Groupings of filters collected from GLA-CC, GLA-HH, MAN-FF and Other UK sites can be seen in Table 5.7.

Figure 5.15. Locations of sampling sites plotted on a map of the UK using www.datawrapper.de.

Table 5.7. Details of the sample groupings per ^{14}C measurement of TC airborne ambient aerosol in the UK. Sample masses with a * may be incorrect due to samples being collected by another LVAS named the EcoTech. There were issues with this sampler; it was unable to properly shield/house the filters from moisture hence only two samples were collected. A negative mass was experienced, due to the tearing of a filter due to the moisture.

Material ID	Sampling Site	Description	Mass (mg)	Collection Dates	Sampler Type	Notes
GLA-CC1	Glasgow George St.	Filter0004 Filter0001	2.47	25.01.2019 – 08.02.2019 08.03.2019 – 15.03.2019	LVAS, Omni, $PM_{2.5}$	-
GLA-CC2	Glasgow George St.	Filter0034 Filter0017 Filter0018	4.96	25.10.2019 – 31.10.2019 06.11.2019 – 12.11.2019 15.11.2019 – 21.11.2019	LVAS, Omni, PM_{10}	Did not generate sufficient CO_2 for measurement.
GLA-CC3	Glasgow George St.	Filter0019 Filter0020	1.49*	29.11.19 – 05.11.19	LVAS, Omni and Ecotech, $PM_{2.5}$	Combined with GLA-C4_2 and submitted for small sample measurement.
GLA-CC4	Glasgow George St.	Filter0022 Filter0023	2.41	28.02.2020 – 10.03.2020	LVAS, Omni and Ecotech, $PM_{2.5}$	Combined with GLA-C4_1 and submitted for small sample measurement.
GLA-HH1	Glasgow, University Avenue	Filter00025 Filter00026 Filter00028	5.42	05.11.2020 – 19.11.2020 19.11.2020 – 30.11.2020 07.10.2020 – 22.10.2020	LVAS, Omni, $PM_{2.5}$	-
GLA-HH2	Glasgow, University Avenue	Filter00029 Filter0035 Filter0036	3.01	22/01/2021 – 04/02/2021 01/04/2021 – 16/04/2021 16/04/2021 – 29/04/2021	LVAS, Omni, $PM_{2.5}$	Did not generate sufficient CO_2 for measurement.

MAN-FF1	Manchester, Fallowfield Campus	Manchester Filter Plate 2	20.0*	06.12.19, 00:00 – 07.12.19, 23:59	HVAS, Digitel, $PM_{2.5}$	
MAN-FF2	Manchester, Fallowfield Campus	Manchester Filter Plate 3	9.00*	08.12.19, 00:00 – 09.12.19, 23:59	HVAS, Digitel, $PM_{2.5}$	
MAN-FF3	Manchester, Fallowfield Campus	Manchester Filter Plate 4	29.8*	10.12.19, 00:00 – 11.12.19, 23:59	HVAS, Digitel, $PM_{2.5}$	
MAN-FF4	Manchester, Fallowfield Campus	Manchester Filter Plate 5	20.4*	12.12.19, 00:00– 13.12.19, 23:59	HVAS, Digitel, $PM_{2.5}$	-
MAN-FF5	Manchester, Fallowfield Campus	Manchester Filter Plate 9	16.6*	22.11.19, 00:00 – 23.11.19, 23:59	HVAS, Digitel, $PM_{2.5}$	-
MAN-FF6	Manchester, Fallowfield Campus	Manchester Filter Plate 12	24.5*	28.11.19, 00:00 – 29.11.19, 23:59	HVAS, Digitel, $PM_{2.5}$	-
MAN-FF7	Manchester, Fallowfield Campus	Manchester Filter Plate 15	8.20*	04.12.19, 00:00 – 05.12.19 23:59	HVAS, Digitel, $PM_{2.5}$	-
AUC-MOS	Auchencorth Moss	2/889 2/895 2/896 2/897	1.25	21.03.2020 – 27.03.2020 04.04.2020 – 10.04.2020 11.04.2020 – 17.04.2020 18.04.2020 – 24.04.2020	HVAS, Digitel, $PM_{2.5}$	-
CHI-OBS	Chilbolton Observatory	CH5285 CH5286 CH5287 CH5368	1.41	06.11.2020 07.11.2020 08.11.2020 27.11.2020	HVAS, Digitel, $PM_{2.5}$	-
LON-HON	London, Honor Oak Park	HO5351 HO5352 HO5353 HO5354	1.24	05.11.2020 06.11.2020 07.11.2020 08.11.2020	HVAS, Digitel, $PM_{2.5}$	-

LON-MAR	London, Marylebone Road	MY5336 MY5337 MY5338 MY5339	1.02	05.11.2020 06.11.2020 07.11.2020 08.11.2020	HVAS, Digitel, $PM_{2.5}$	-

* As filter was not weighed before sampling, the sample mass was estimated by subtracting the average blank filter weight (n = 10) from the post-conditioned sample weight (sample + filter).

Large Point Sources

Point sources of $PM_{2.5}$ emissions were plotted for Glasgow and Manchester can be seen in Figure 5.16 and Figure 5.17. These were plotted using NAEI 2020 data. The NAEI receives data on individual sources in the industrial and commercial sector called point sources. These figures were used for interpretations.

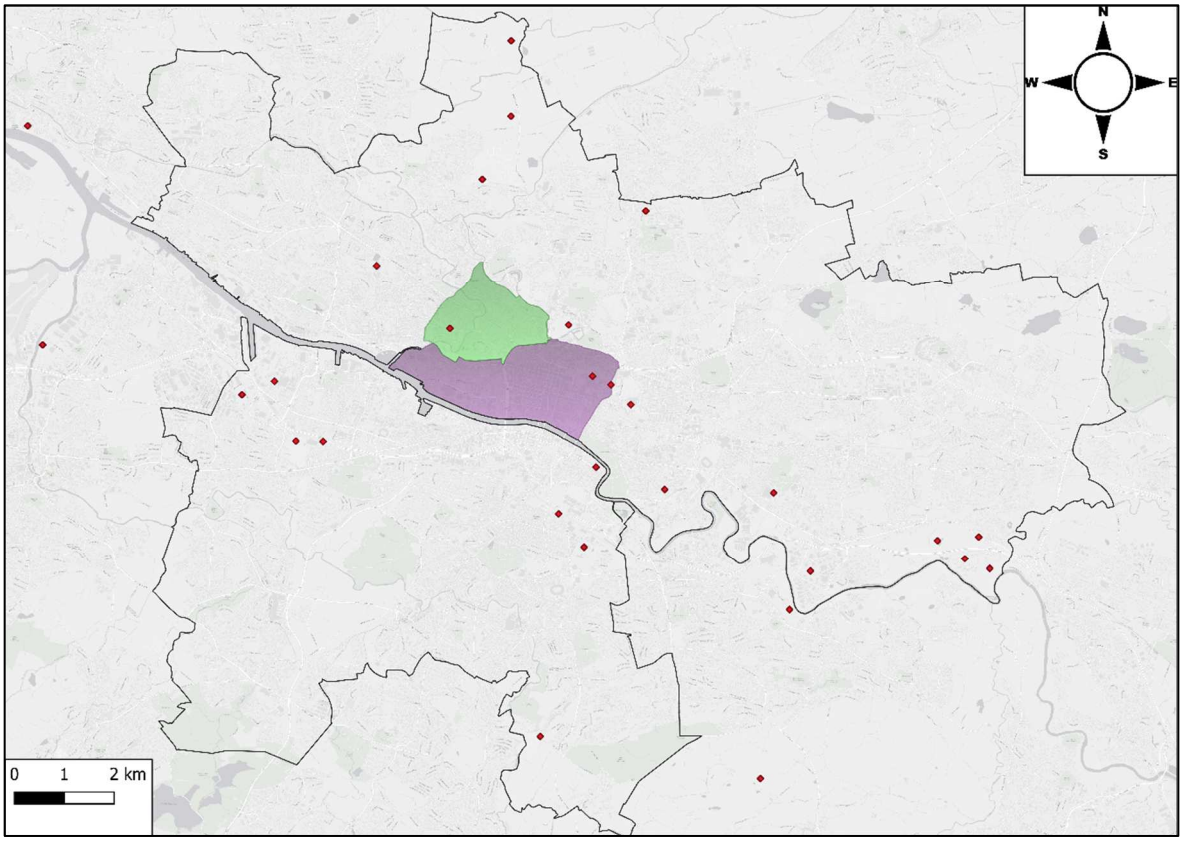

Figure 5.16. Current large point sources of $PM_{2.5}$ emissions in Glasgow. Data obtained from th National Atmospheric Emissions Inventories for 2020. The green shape highlights Glasgow Hillhead ward and the purple shape highlights Anderston, City and Yorkhill ward. The map layer used was provided by Esri (Esri Gray light).

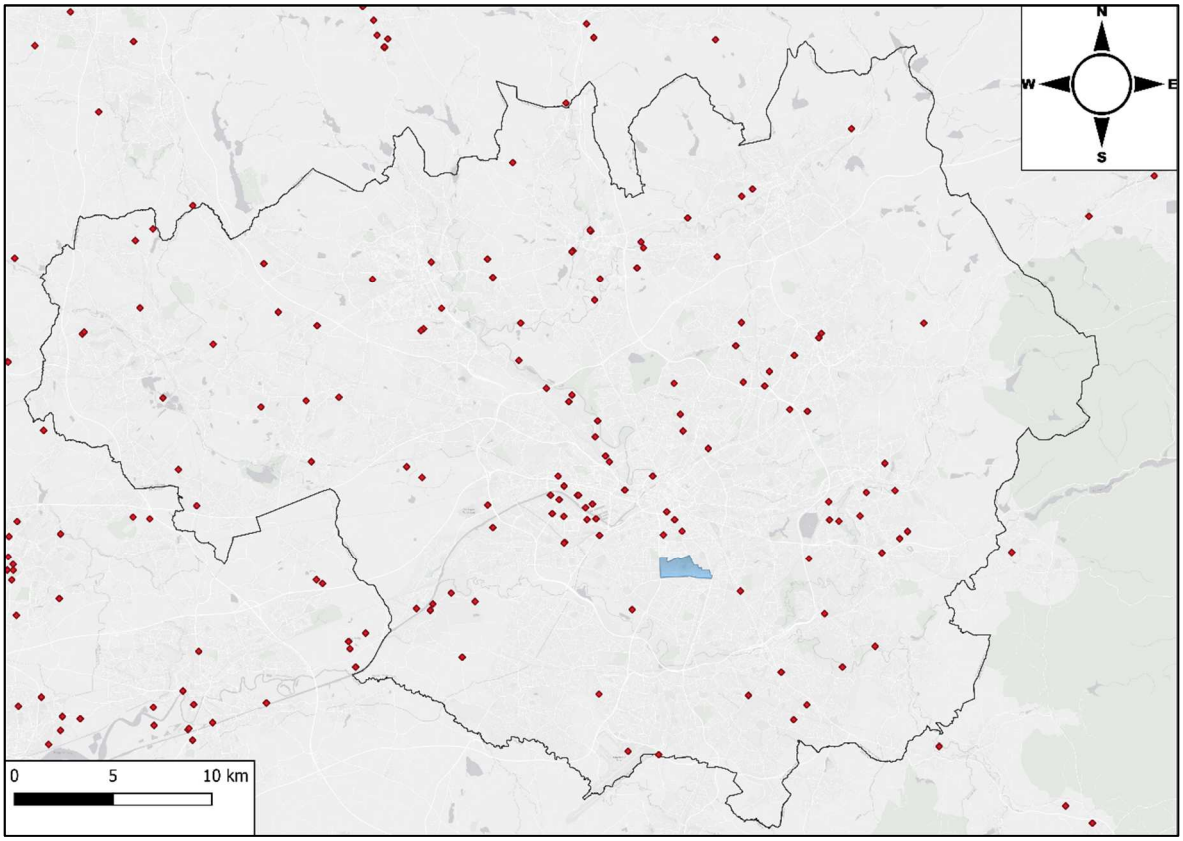

Figure 5.17. Current large point sources of $PM_{2.5}$ emissions in Greater Manchester. Data obtained from the National Atmospheric Emissions Inventories for 2020. The blue shape highlights Manchester Fallowfield ward. The map layer used was provided by Esri (Esri Gray light).

5.5.2. Results and Discussion

The ^{14}C and $\delta^{13}C$ results are shown in Table 5.8.Where there is no data for $\delta^{13}C$, an offline measurement could not be made so as to conserve the CO_2 generated from the sample during processing, as the sample had low mg C. Figure 5.18 spatially exhibits the %MC values for the $PM_{2.5}$ samples across the UK. The %FC was calculated using the simple mixing model mentioned in Section 5.3.

Table 5.8. Data obtained from ^{14}C analysis for TC airborne ambient aerosol in the UK.

Material ID	Sampling Period	$\delta^{13}C$	%MC	%MC Error	%FC
GLA-CC1	25.01.2019 – 15.03.2019	-	45	0.21	55
GLA-CC3+4	29.11.19 – 10.03.2020	-	47	0.21	54
GLA-HH1	07.10.2020 – 30.11.2020	-	47	0.23	54
MAN-FF1	06/12/2019 – 07/12/2019	-27.58	74	0.34	27
MAN-FF2	08/12/19 – 09/12/19	-27.69	60	0.28	41
MAN-FF3	10/12/19 – 11/12/19	-29.46	65	0.30	36
MAN-FF4	12/12/19 – 13/12/19	-28.85	65	0.28	36
MAN-FF5	22/11/19 – 23/11/19	-27.48	67	0.31	33
MAN-FF6	28/11/19 – 29/11/19	-27.75	49	0.23	52
MAN-FF7	04/12/19 – 05/12/19	-27.99	134	0.61	-
AUC-MOS	21.03.2020 – 24.04.2020	-26.6	93	0.42	8
CHI-OBS	06.11.2020 – 27.11.2020	-27.4	83	0.36	18
LON-HON	05.11.2020 – 08.11.2020	-27.4	85	0.39	15
LON-MAR	05.11.2020 – 08.11.2020	-27.5	193	0.88	-

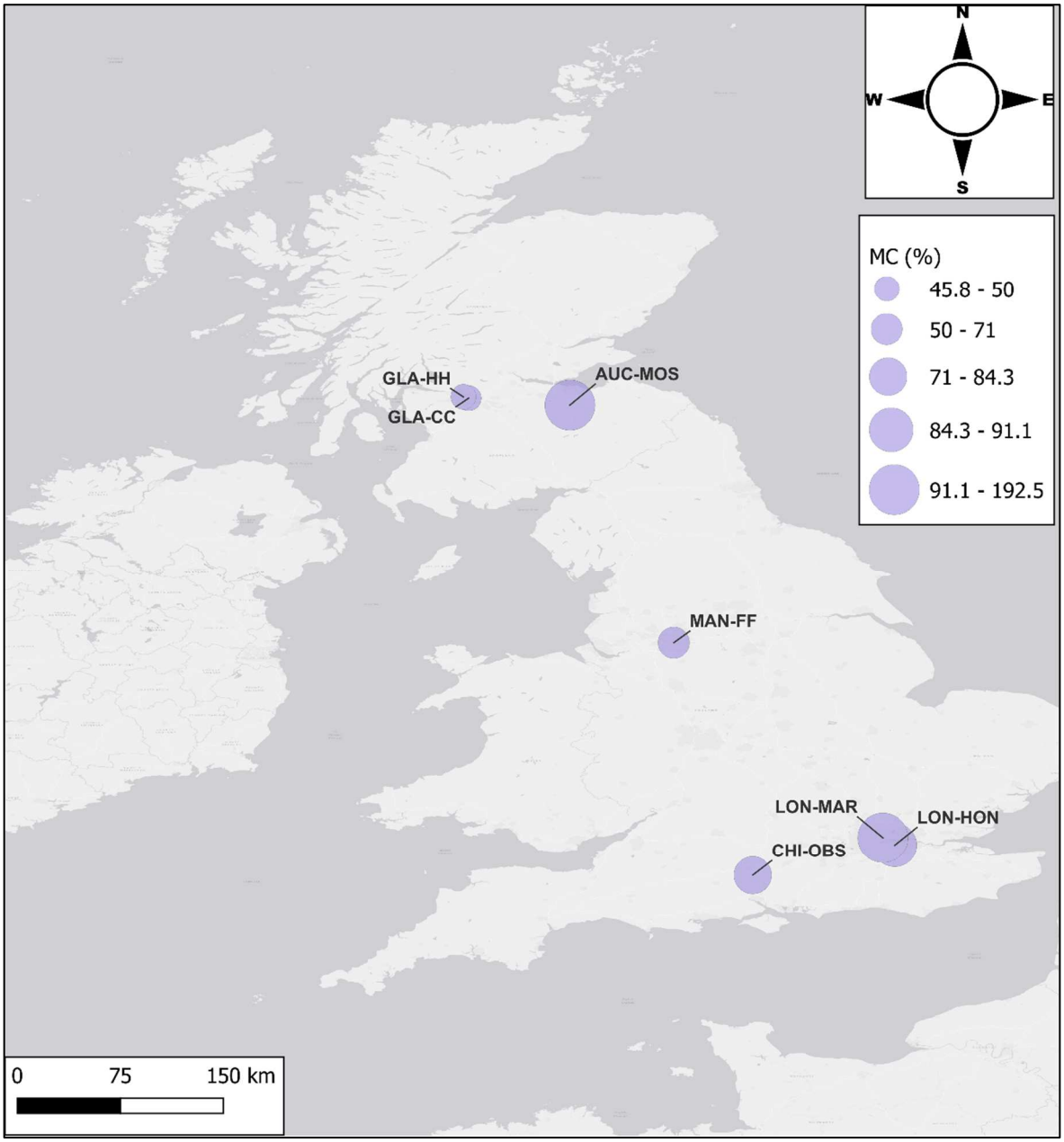

Figure 5.18. The %MC values of $PM_{2.5}$ from UK sites. The size of the circle represents the average %MC value of the individual $PM_{2.5}$ samples analysed at each location; the larger the circle, the higher its %MC value. The map layer was provided by Esri.

TC ^{14}C Analyses – Glasgow $PM_{2.5}$

Glasgow city sample GLA-CC3 did not generate enough CO_2 for a ^{14}C (TC) measurement, so CO_2 generated from GLA-CC3 was combined with that from GLA-CC4. Based on a mass balance calculation of modern and fossil radiocarbon end members, GLA-CC1 and GLA-CC3+4 had %MC (TC) values of 45 ± 0.21 % and 47 ± 0.21 %, therefore, with use of the

mixing model this means 55 % and 54 % %FC (TC), respectively. This split indicates roughly half the sources of C are fossil and the other half are modern.

Glasgow Hillhead sample, GLA-HH2 did not generate enough CO_2 for a measurement therefore only one sample was analysed from Glasgow Hillhead, GLA-HH1. GLA-HH1, had a %MC (TC) value of 47 ± 0.23 %, with 54 % %FC (TC), similar to GLA-CC3+4, and GLA-CC1.

Figure 5.16 shows a map of large industrial and commercial $PM_{2.5}$ point sources near sampling sites. The map shows that GLA-CC1, GLA-CC3+4 and GLA-HH2 local $PM_{2.5}$ emissions have contributions from the public administration commercial sector from University of Strathclyde and Glasgow Royal Infirmary for GLA-CC1 and GLA-CC3+4 and University of Glasgow for GLA-HH2. GLA-CC1 and GLA-CC3+4 may also have contributions from distilleries nearby. Polar plots were made for $PM_{2.5}$ using Glasgow Townhead AURN data which was nearby to GLA-CC sites (Figure 5.19). The polar plot for GLA-CCI showed high $PM_{2.5}$ contributions from local sources and moderate $PM_{2.5}$ concentrations from the south-east. For GLA-CC3+4 $PM_{2.5}$ concentrations were higher from the south-east than locally. The contributions from the south-east were likely to be from traffic from the city centre or the M8 motorway. A windrose was plotted for GLA-HH using Glasgow Airport meteorological data (Figure 5.19). The windrose showed high wind speeds originated from the north-east and south-west. This could mean traffic contributions from Great Western Road and the A814. Other possible contributing sources could have been from 4 large point sources from the south-west (hospital, metal fabricators, crematorium and other industries) and 1 large point source from the north-east (hospital).

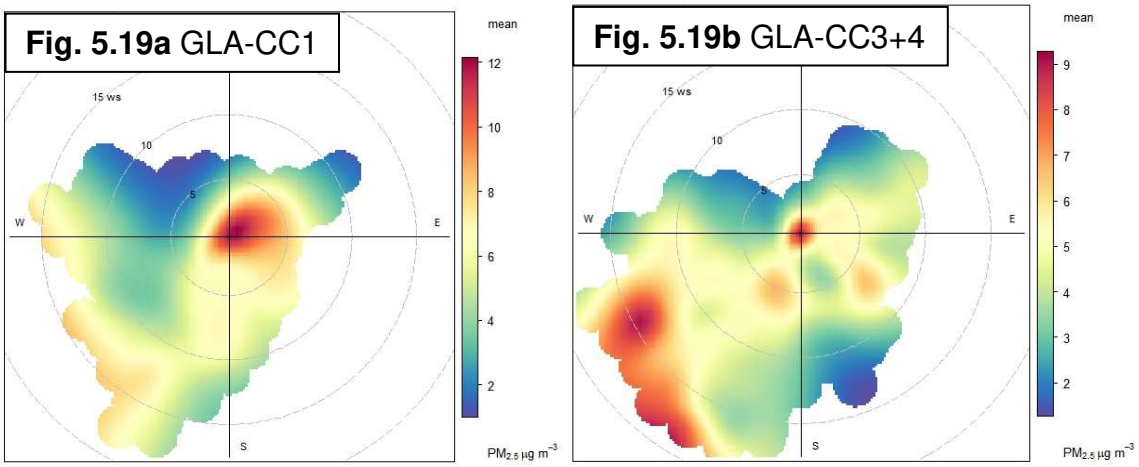

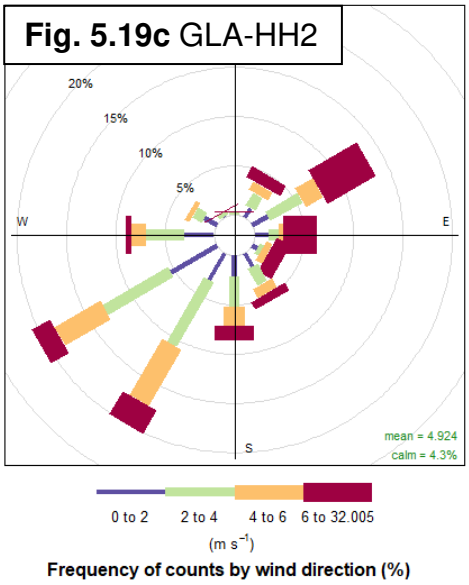

Figure 5.19. Polar plots for $PM_{2.5}$ concentrations from Glasgow Townhead for sampling dates of a) GLA-CC1, b) GLA-CC3+4 and windrose plots for sampling dates of c) GLA-HH2 using Glasgow Townhead AURN data and Glasgow Airport meteorological data. The plots use data from the sampling period of GLA-CC1, GLA-CC3+4 and GLA-HH2.

The SEPA work mentioned in Section 2.2.4 used measured AADT's and Defra's emission factor toolkit to determine the traffic fleet composition for GLA-CC and GLA-HH shown in Figure 5.20. The sampling sites had modelled AADT counts of 4118 (GLA-CC) and 9345 (GLA-HH). The roads were used predominantly by private passenger cars. GLA-CC had a slightly higher proportion of buses and heavy goods vehicles (HGVs) compared to GLA-HH perhaps accounting for the lower %MC (TC).

Additionally, GLA-HH may have had a higher proportion of modern sources. The modern sources of C could originate from vegetative detritus or transported air masses containing woodsmoke from rural areas and biogenic SOA, as well as particles formed from cooking oils as all sites were in close proximity to restaurants. All samples had low CO_2 levels <1 mL during sample preparation, meaning insufficient CO_2 for off-line $\delta^{13}C$ values. Considering GLA-CC1 and GLA-CC3+4 were collected during different time periods, the %MC values showed that the sources did not change much from Jan-March 2019 and Nov 2019 – March 2020.

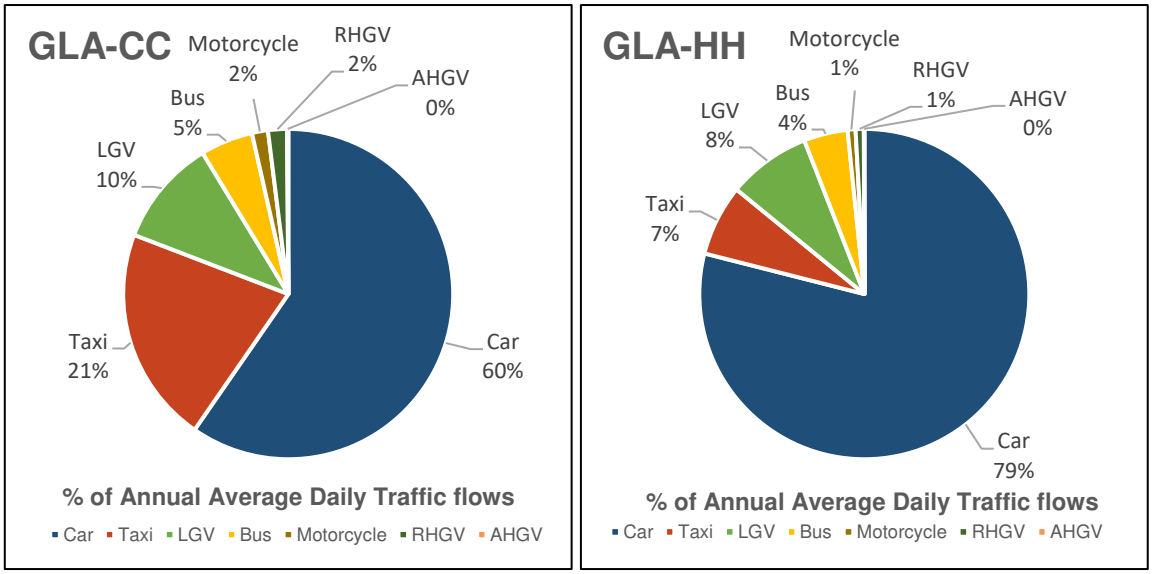

Figure 5.20. Percentage of annual average daily traffic flows (AADT) per vehicle category on roads in GLA-CC and GLA-HH. Data supplied by SEPA.

TC ^{14}C Analyses – Manchester $PM_{2.5}$

The measured %MC (TC) range for seven samples collected from Manchester Fallowfield Campus was 49 – 74 %, representing a sampling period of November – December 2019. One sample, MAN-FF7, had an anomalously high %MC (TC) of 134 ± 0.61 %. When calibrated with CALIBOMB the age returned was AD 1962 – AD 1978 with a 95 % confidence interval. This result could imply that the combustion of biomass containing carbon fixed from this period was the dominant source. However, the likelihood of this is low considering the low likelihood of carbon sources of this age. Additionally, the results for other MAN-FF samples gave substantially lower %MC values. Therefore, an alternative explanation could be that the combustion material contained a ^{14}C 'spike'. Potential sources

of this could include incinerated biomedical waste where ^{14}C has been used as a diagnostic in a hospital setting which has been observed in UK urban environments (Reimer et al., 2004; Waters et al., 2015). A clinical waste incinerator was located in Manchester at Royal Oldham hospital, operated by Stericycle (SRCL), therefore the anomalous result could be explained by waste being incinerated at this site. However, a windrose plot was constructed using data from Manchester Piccadilly AURN site to understand which direction wind speeds were coming from during the sampling period for MAN-FF7. Figure 5.21 shows that the high wind speeds came from the south-west. Although Manchester Piccadilly was not the sampling site, a pollution rose plot was also constructed to determine if $PM_{2.5}$ concentrations were correlated to high wind speeds from the south-east. Figure 5.22 confirms high wind speeds from south-west were correlated with high $PM_{2.5}$ concentrations. Possible $PM_{2.5}$ point sources from the south-west of MAN-FF, that could have contributed to a ^{14}C spike were Manchester crematorium and Trafford crematorium. In the south-west there are parks and greenery which could explain the higher %MC (TC) contributions. The A6010 road is also to the south-west of MAN-FF and could account for fossil contributions.

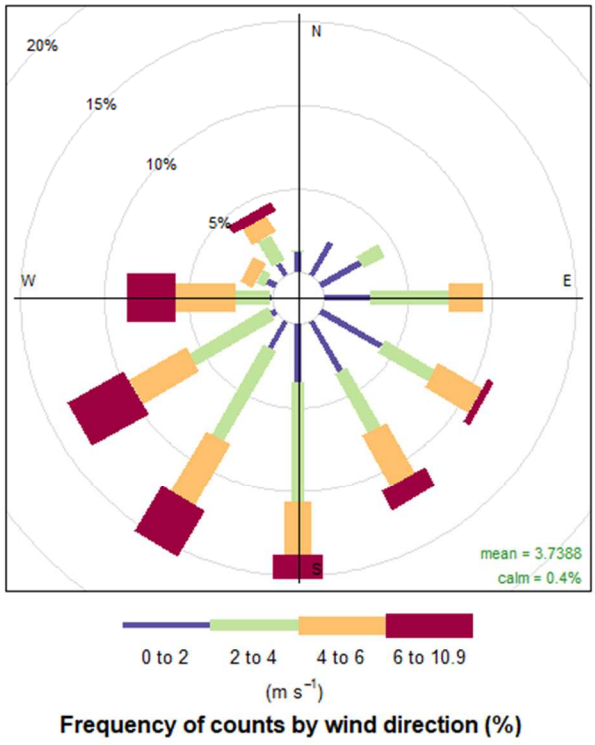

Figure 5.21. Windrose plot using Manchester meteorological data from 20.11.2019 to 18.12.2019.

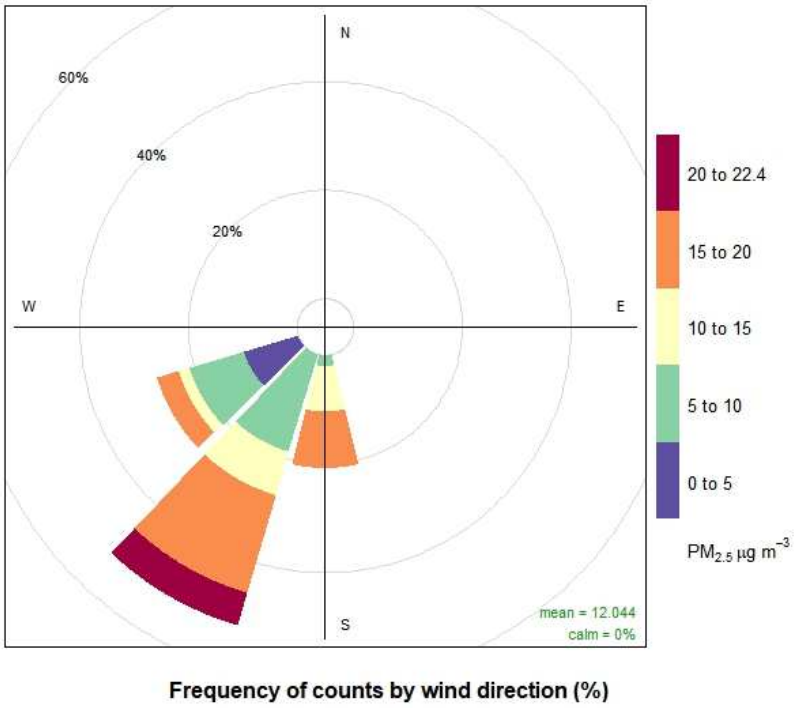

Figure 5.22. Pollution rose plot for $PM_{2.5}$ from Manchester Piccadilly AURN site on 04.12.19 to 05.12.19.

The $\delta^{13}C$ values for the samples ranged between -27.48 ‰ and -29.46 ‰. This $\delta^{13}C$ signature range includes those seen for of C_3 plants -34 to -24 ‰, signatures and for DS TC, -28.42 ‰ (from this study) (Deines, 1980). The results suggest generally higher contributions from modern carbon except for sample MAN-FF6.

The %FC (TC) ranged from 27 to 52 % based on the linear regression, with an average of 37 % fossil carbon. There was good consistency amongst 4 of the 6 samples which ranged from 33 – 41 % fossil carbon. Calculating %FC in this manner assumes that the non-fossil component of OC on the filters is composed of material fixed into biomass in 2019. Clearly, the non-fossil component is likely to include material fixed before this date, however it is likely that the bulk of non-fossil OC is represented by biomass carbon fixed over the past 5 years with a diminishing component beyond this. The absence of non-fossil OC load in the sampling meant that 2019 region was selected as the representative point for non-fossil OC in this study.

TC ^{14}C Analyses – London $PM_{2.5}$

London Honor Oak Park had a %MC (TC) value of 85 % whereas London Marylebone Road had an extremely high %MC (TC) value of 193 %, which could be an enriched source of ^{14}C, similar to that of M15 sample. There are a few hospitals and waste incinerator plants in the surrounding area of LON-MAR (SELCHP Energy Recovery Facility, Edmonton EcoPark Energy from Waste , Hillingdon Hospital and Veterinary Laboratories Agency) which could have incinerator clinical waste which can find its way into the samples. In general, the samples from London had high modern contributions, which could be due to the sampling period being during the second National Lockdown during the COVID-19 pandemic, meaning traffic flows were likely to be reduced significantly, removing fossil contributions. $\delta^{13}C$ TC signatures of both samples were -27.4 ‰ and -27.5 ‰ within the range of C_3 plants -34 to -24 ‰.

TC ^{14}C Analyses – Rural Background Sites

Samples from Auchencorth Moss and Chilbolton show a contribution of 93 % and 83 %MC (TC), so 8 % and 18 %FC (TC). Auchencorth Moss and Chilbolton are both rural background sites, so the high modern contributions to the TC could be due to the distance from urban areas, and fossil sources like vehicular emissions. Auchencorth Moss shows the lowest fossil carbon content of any sample at 8 %FC (TC).

Comparison Between Sites

The %MC (TC) for GLA-CC and GLA-HH were similar, giving results of 45 to 46 %MC. Compared to all other sites in the UK Glasgow had a higher fossil contribution, which is likely to be from vehicular emissions, as in Scotland there is a huge reliance on private passenger cars, due to lack of public transport infrastructure like trams. MAN-FF had higher %MC (TC) values than Glasgow with an average of 63 %.

The sources of MAN-FF($PM_{2.5}$) were mixed showing a slightly higher contribution from modern sources, as the average %MC (TC) was 63.20 %. Road-transport is a major contributor to $PM_{2.5}$ in the UK so it was likely that fossil sources in Manchester were from vehicular emissions (ApSimon et al., 2021). The lower %FC value could be explained by MAN-FF being an urban background site, with less vehicular traffic generating fossil-fuel aerosol loads than Glasgow sites. Furthermore, Fallowfield campus is surrounded by trees and greenery therefore biogenic SOA contributions could be probable.

A study in 2008, found $PM_{2.5}$ collected from an urban background site in Birmingham UK had 27 – 66 %MC, with a mean of 50 %MC (Heal et al., 2011). It would be expected that the vehicle emissions would have declined since this study. The MAN-FF %MC (TC) showed this was the case with %MC (TC) ranges of 48.5 – 73.7 %MC (TC) and a mean of 63.2 %MC. However, GLA-CC and GLA-HH samples were 45.1 - 46.8 %MC (TC). Results were similar to %MC (TC) from background sites in Hungary which had 50 – 78 %MC in $PM_{2.5}$ collected in 2017-2018 (Major et al., 2022).

The modern sources of $PM_{2.5}$ from the UK could be from domestic combustion of wood – the top contributor to UK $PM_{2.5}$ emissions according to NAEI 2020 – however most UK cities, including Glasgow and Manchester, are within smoke control areas, which should in theory prevent the domestic combustion of wood in such areas. However, the domestic combustion of wood in these areas is still possible alongside small-scale biomass residential heating appliances i.e., biomass boilers, which could contribute to the modern sources. Industrial biomass combustion could also contribute to $PM_{2.5}$ as the NAEI shows industrial biomass fuels to be increasing and to have contributed 18 % of UK $PM_{2.5}$ emissions in 2020 (NAEI 2020). Globally, biomass supplied 600 TWh of electricity in 2019 more than double of the amount supplied in 2009 (Tomlin, 2021). Usage of biomass power generation is dominated by Europe and Asia and is likely to increase in the UK as stated in "UK Net Zero Strategy – Build Back Greener" report that biomass will become a key energy carrier to support low carbon fuel production (*Net Zero Strategy: Build Back Greener*, 2021; Tomlin, 2021). Considering the health effects of different components of $PM_{2.5}$ are poorly understood, research that determines the chemical components of wood-smoke and biomass-burning emissions is extremely important to prevent the global health burdens, from the transition to biomass fuels. Domestic wood combustion is the main source of toxic PAHs such as BaP, therefore $PM_{2.5}$ emitted from biomass and wood could be extremely toxic to human health (NAEI 2020). A study using the UK Integrated Assessment Model (UKIAM) which was applied to $PM_{2.5}$ concentrations in UK during 2016, found domestic wood-burning to be a dominant source, on a national scale as well as in urban and rural environments, so domestic wood combustion could also be prominent in Glasgow and Manchester despite being in smoke control areas (ApSimon et al., 2021). Houseboats parked on Glasgow canals combust wood for heating so these emissions could also contribute to the modern sources. Another explanation could be long-range imported modern contributions from other countries which were found to be important in the UKIAM study (ApSimon et al., 2021). Natural biomass burning sources e.g., wildfires, are likely to be negligible in the UK and also occur in the summer months therefore were unlikely to contribute to the samples analysed.

London sites had high %MC (TC) values with London Honor Oak Park having a %MC (TC) of 85 % and London Marylebone Road had a %MC of 193 %. Both sites in London exhibited high %MC compared to Glasgow and Manchester; LON-MAR had extremely high %MC (TC) values, thus this could have been from enriched ^{14}C sources emitted from incineration of clinical waste. However, LON-HON also had high %MC values. Considering the samples were taken during the second national lockdown during the COVID-19 pandemic, the contribution of fossil sources was low as vehicular traffic was extremely reduced, which could have in turn led to high %MC (TC) values. A plausible source contributing to high %MC (TC) was domestic combustion of wood and cooking emissions. Previous research confirmed biomass smoke in London had regional source contributions which were overlaid by local domestic burning emissions (Crilley et al., 2015). Correlations were found across central London and two sites in surrounding rural areas, between concentrations of levoglucosan, EC, OC and K^+. Biomass was found to be a source of OC and EC and domestic heating was a major contributing local source in London as there were similar ratios of BrC to BC and peaks of levoglucosan and K^+ concentrations during low ambient temperature. However, at all sites, biomass burning was the smallest of the major sources of OC, with secondary biogenic organic aerosols, and primary biogenic and cooking sources of OC dominating.The lack of fossil sources was likely from a decrease in traffic including public transport, thus decrease in vehicular emissions during COVID-19 second national lockdown. In the 'Travel in London' report, there was an estimated 20.3 million daily trips on an average day in 2020, which showed a 24.8 % decrease compared to daily trips on an average day in 2019 (TfL, 2021). This could have increased %MC contributions, thus the results do not represent 'normal' source contributions in London, due to the period of time the $PM_{2.5}$ was collected.

Source apportionment studies in Europe also found modern sources, such as a study in France in 2013 which found high concentrations of biomass burning marker levoglucosan in winter, with synchronous temporal patterns indicating emissions at a regional scale. Source of primary organic aerosol indicated that contributions of wood burning to OC were high with an average level of 90 % at some rural sites (Golly et al., 2019). Biomass burning was the second most important source of $PM_{2.5}$ in Milan and Porto (Amato et al., 2016). Similarly, the ICARUS EU2020 project examined sources of $PM_{2.5}$ in 5 European cities and found biomass burning contributed around 22 % at traffic sites, 30 % at urban background and 28 % at rural sites. Furthermore, in the majority of the cases, traffic, biomass burning, fuel oil combustion and sea salt sources revealed a clear dependence on the wind direction indicating regional sources (Saraga et al., 2021). In Athens, Greece 44 % of $PM_{2.5}$ was

attributed to a mixed source of secondary formation and biomass burning in August 2016 – July 2017. However, the OC/EC ratios were low, as were K^+ levels, suggesting the biomass burning emissions were related to transport of wildfire smoke plumes rather than local biomass burning for residential heating (Diapouli et al., 2022). This shows there may be regional scale biomass burning emissions that affect contributions within the UK. A study in Gothenburg found around 50 % of $PM_{2.5}$ was from long-range transported pollution (Molnár et al., 2017). This was observed in a study conducted in London, that found that regionally influenced S-rich and solid fuel factors were affected by many anthropogenic point sources and were influenced by emissions not only in and around London but also from elsewhere in the UK and northern Europe. They were restricted to smaller size fractions of PM and had similar concentrations throughout the day and across larger regions (Visser et al., 2015).

To explore the effect of regional sources on %MC (TC) values of samples from AURN sites, 96 h air-mass back trajectories were linked to $PM_{2.5}$ concentrations from AURN sites using openair R package. In the case of Auchencorth Moss, air masses from the east coast of the UK and North Sea were generally associated with higher $PM_{2.5}$ concentrations as seen in Figure 5.23. The local air masses exhibit lower $PM_{2.5}$ concentrations.

For Chilbolton, the $PM_{2.5}$ concentrations linked to air-mass back trajectories showed $PM_{2.5}$ concentrations were higher when originating from the south-east of England, as well as some parts in north-western Europe such as north of France, Belgium and mid-west Germany (Figure 5.24). This shows the presence of UK and regional sources in Chilbolton samples.

In London, during the period of time LON-HON and LON-MAR samples were collected, the air masses originated from Europe, as shown in Figure 5.25. The $PM_{2.5}$ concentrations could not be linked to the air-mass back trajectories due to an insufficient $PM_{2.5}$ dataset therefore it cannot be said if regional sources affected the %MC in these samples. However, considering the air quality in south of England is often impacted by air masses from Europe, regional sources cannot be ruled out.

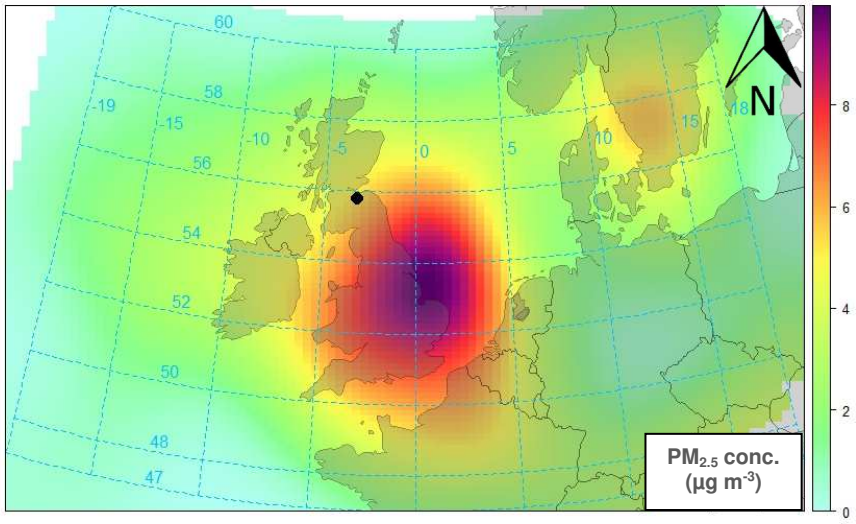

Figure 5.23. Auchencorth moss $PM_{2.5}$ concentrations linked to air-mass back trajectories.

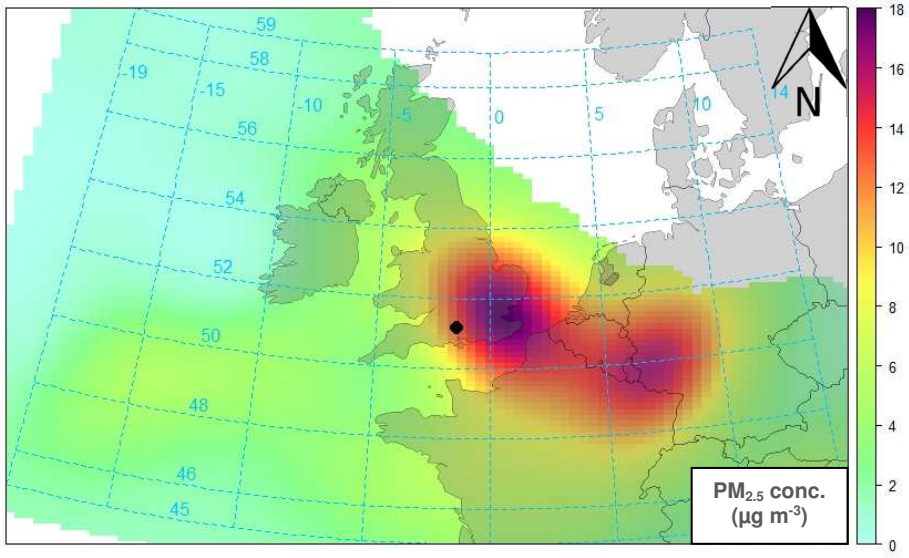

Figure 5.24. Chilbolton $PM_{2.5}$ concentrations linked to air-mass back trajectories. The scale of the map is 1:24900820.

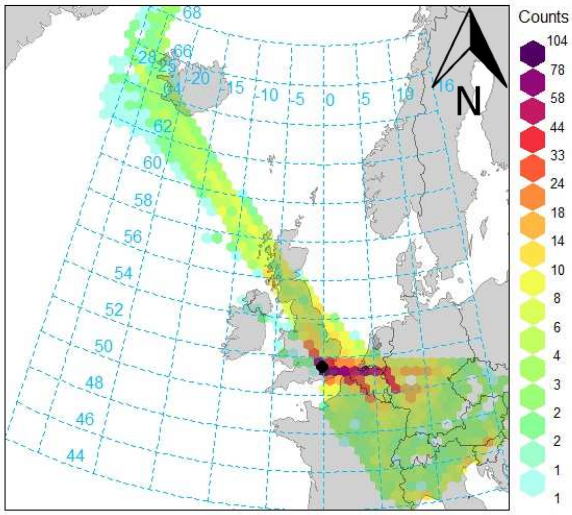

Figure 5.25. Air-mass back-trajectory frequencies for London.

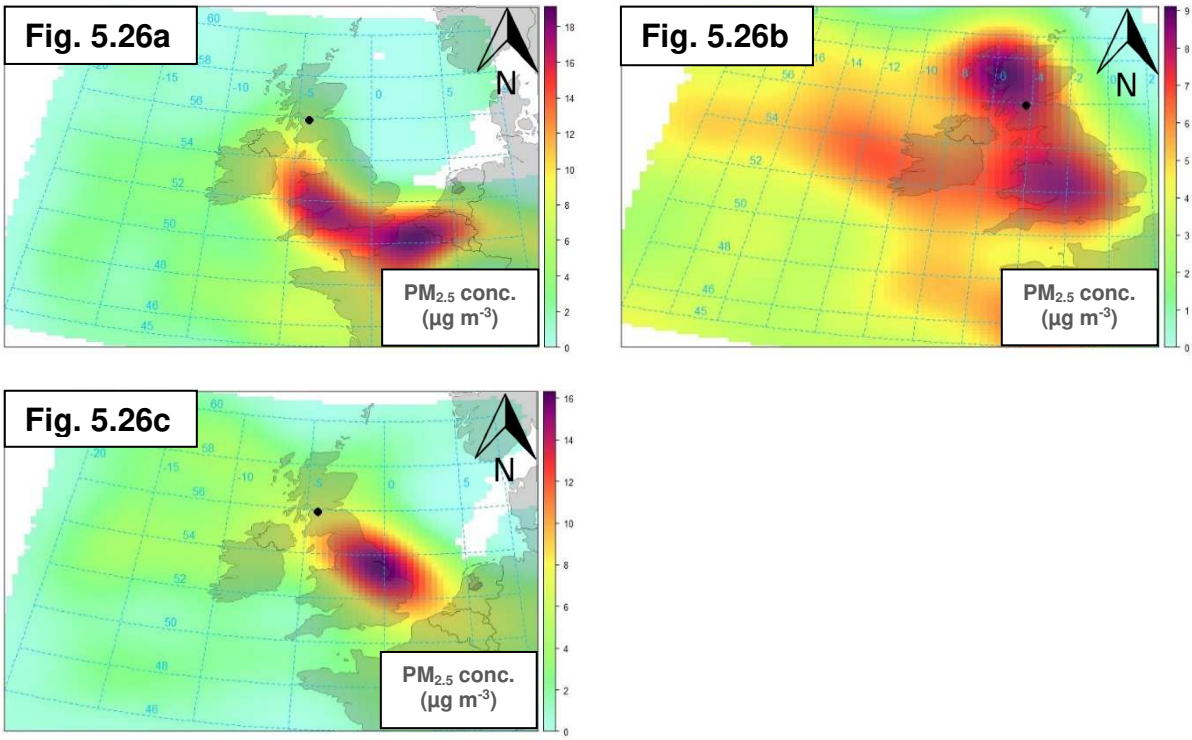

Figures 5.26. Glasgow Townhead $PM_{2.5}$ concentrations linked to air-mass back-trajectories for a) GLA-CC1, b) GLACC3+4 and c) GLA-HH1.

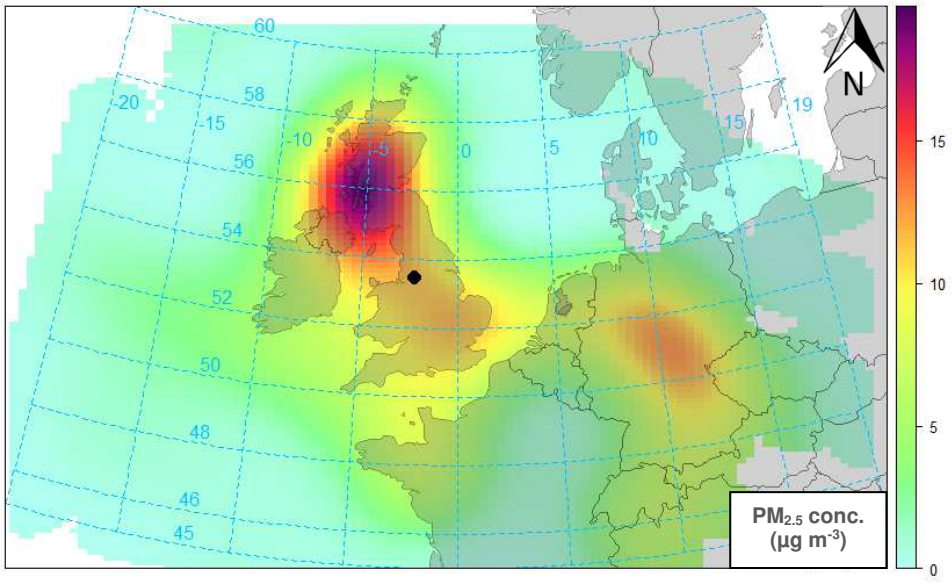

Figure 5.27. Manchester Piccadilly $PM_{2.5}$ concentrations linked to air-mass back trajectories.

The air-mass back trajectories when GLA-CC1 filters were collected, were mainly from Europe, and the North Atlantic, crossing over Ireland, whilst when GLA-CC3+4 filters were collected, the air masses originated mainly from the Atlantic, crossing over Ireland. For GLA-HH1, air masses originated from the North of Scotland, from the North Atlantic Ocean, as well as from the West, with air mass crossing over Ireland. The $PM_{2.5}$ concentrations from Glasgow Townhead linked to the air-mass back trajectories showed high $PM_{2.5}$ concentrations in Glasgow when GLA-CC3+4 was collected indicating local sources could contribute to the fossil and modern sources of GLA-CC3+4 (Figures 5.26).

The air-mass back-trajectory frequencies from Manchester seemed to be localised to the UK however, there are high frequencies from the North of France and Germany. The $PM_{2.5}$ concentrations show high concentrations linked to the back trajectories in west of Scotland and central Germany (Figure 5.27). This shows that $PM_{2.5}$ concentrations likely had dominant UK contributions rather than transboundary sources. The relatively high %MC (TC) values for Manchester samples could be explained by the air masses originating from the north, which consists of cleaner air and relatively less fossil fuel sources and more regional biogenic background C.

The %MC (TC) results from Glasgow and Manchester show that fossil sources are still prevalent in UK. This was corroborated by research that found road traffic was still a significant source of $PM_{2.5}$ in London and urban areas in the UK (ApSimon et al., 2021). This was also supported by research in Europe which showed traffic exhaust contributions

to $PM_{2.5,}$ were 23.3 % at traffic sites, 13.3 % at urban background sites and 8.8 % at rural sites (Saraga et al., 2021).

5.5.3. Conclusions

The ^{14}C analysis showed that, before COVID-19, GLA-HH and GLA-CC had 46%:54% MC:FC proportions, whilst MAN_FF had about 63%:37% MC:FC proportions. This meant that there was more fossil carbon present in GLA-CC and GLA-HH samples, and more modern carbon present in MAN-FF samples. This could be explained by heavy reliance on road transport within Scotland.

Manchester %MC values also had a big contribution from fossil sources, most likely due to road transport. Legalisation and regulations should continue to target fossil sources. It is important to note the specificity of the sampling sites, due in part to COVID restrictions on the number of samples that could be collected. This means that there were a low number of individual sampling sites and the period of time over which samples were collected was restricted. This limits the interpretation of, for example, longer-term trends in ^{14}C sources over time, or inter-comparability of sites.

Samples collected during the COVID-19 pandemic, showed that modern sources dominated UK $PM_{2.5}$ samples at the sampling sites during the (limited) period of time samples were collected during this time. The dominant contributions of modern sources for rural background site Auchencorth moss was most likely biogenic SOA sources from oxidation of isoprene and monoterpene emissions, background cooking aerosol emissions, background wildfire/prescribed fire emissions and local and regional wood-smoke emissions. In Chilbolton there were likely to be UK and transboundary $PM_{2.5}$ sources. London sites were likely to have emissions domestic and regional wood combustion sources as well as cooking oils. The southern parts of the UK are more susceptible to transboundary long-range transport of $PM_{2.5}$ from Europe, therefore this could explain the high %MC values in London and Chilbolton (DEFRA National Statistics, 2022).

It was difficult to come to any conclusions about MC%:FC% contributions at London sites due to potential contamination at LON-MAR site. LON-HON however had a large modern contribution likely due to COVID restrictions during the pandemic. Generally, it was difficult to compare sites due to the small number of samples and the samples being collected at different time periods. As mentioned, some samples were representative of sources during

the COVID pandemic therefore did not represent business-as-usual scenarios. Further work would be needed to fully establish the spatial difference in sources across the UK, however this work provides an insight into the sources of UK aerosols using ^{14}C dating which is based on isotopic signatures as opposed to the use of multivariate models.

The results show that fossil sources still contribute largely to airborne ambient PM in urban areas within the UK such as Glasgow and Manchester, and that dependence on fossil fuel combustion still needs to be addressed and reduced. Modern sources were dominant in LON-HON as it was collected during COVID restrictions. This could represent the reduction in fossil sources, however due to small number of samples such interpretations cannot be made. Modern sources of airborne ambient PM should be monitored, considering the UK strategy to transition to carbon-neutral fuels as well as the rise in $PM_{2.5}$ emissions from domestic wood combustion. Recommendations for future work include analysis of the same sites, over a longer sampling period to compare to results reported here, to determine the effect of COVID-19 restrictions on the sources of airborne ambient PM at the sampling sites. Moreover, sampling across sites should occur simultaneously to enable the comparisons of %MC and %FC between sites. To monitor modern sources of carbon in airborne ambient PM, source attributions such as $OC_{biomass}$ and $OC_{biogenic}$ should also be investigated.

5.6. Application of 14C measurements to TC and BChypy of UK Urban Airborne Ambient PM

Section 5.4.2 showed that hypy could successfully separate BC_{hypy} from TC and determine non-BC_{hypy} %MC values through subtraction of BC_{hypy} from TC. Therefore, the method was applied to UK urban airborne ambient $PM_{2.5}$, to gain more information on the sources of carbonaceous components within $PM_{2.5}$.

5.6.1. Method Development: Insertion of Airborne Ambient PM into Hypy System

Samples are introduced into the hypy system using quartz tubes, which can then be combusted for ^{14}C analysis. As few studies have used hypy to separate BC_{hypy} and non-BC_{hypy} in airborne ambient PM, trial and error was needed to determine how to transfer the $PM_{2.5}$ filters into the hypy system. A concern in this project was low sample mass/low carbon mass, so the method utilised needed to take this into consideration to ensure measurements could be made on the samples. Contamination of samples during insertion into the hypy system was also considered.

Method and Results

Several hypy sample insertion methods were trialled, see Table 5.9. Method 1 was recently reported by Zhang et al. (2019a). All tests were undertaken on blank quartz filters to preserve $PM_{2.5}$ samples for analyses.

Table 5.9. Methods for inserting airborne ambient PM on a filter into the hypy instrumentation.

	Method	Results
1	Peel top layer of filter Grind the filter with pestle and mortar. Transfer into quartz insert with a spatula	Difficult to peel top layer uniformly. Could lead to sample losses due to $PM_{2.5}$ disintegrating Allows more sample to be packed into the quartz insert meaning fewer sub-samples required
2	Make filter punches (6 mm diameter) Load into quartz insert using spatula and tweezers	Intricate method Time-consuming
3	Roll whole filters. Insert into the hypy reactor	Quick sample introduction to the reactor Difficulty experienced when retrieving filters from the reactor. Could jeopardise subsequent ^{14}C analysis if filters disintegrate upon retrieval
4	Cut filters with a scalpel. Roll the filter segments. Transfer into the quartz insert with spatula and tweezers	Quick method Requires a few sub-samples.

When testing Method 1 it became apparent that it was difficult to peel the top layer off uniformly. Also, the grinding process could lead to sample loss, due to fine particles. However, this method has the advantage of enabling more sample to be packed into the hypy quartz insert, meaning less sub-samples and fewer hypy runs. Additionally, sample contamination is minimal as the pestle, mortar and spatula can be cleaned with solvents.

Method 2 was intricate and time-consuming, as it required obtaining filter punches for the whole filter alongside the loading of these filter punches into the quartz insert. However, this method has minimal contamination as a new punching tool can be used for each preparation. The tweezers can also be cleaned with lint-free wipes, solvents and high temperature blow torch.

For Method 3, rolling the filter and inserting it into the reactor was a quick process, but its subsequent retrieval was difficult because parts of it disintegrated upon retrieval. A longer and thinner tweezer-type tool might permit successful retrieval of the filter sample, but no such tool was available during testing. The method has minimal contamination as the hypy reactor was continually cleaned in-between runs, but sample loss could occur once the filter was retrieved post-hypy due to the filter disintegrating when removed from the hypy reactor.

The process for method 4 was relatively quick, compared to methods 1 and 2. The method has minimal contamination as the cutting board and the scalpel can be cleaned with solvents,

gloves are worn when rolling the filters, and the tweezers used to insert the filter into the quartz insert were cleaned with lint free wipes, solvents and high temperatures using a blow torch. The disadvantage of this method is that several sub-samples are required; for a 47 mm filter, the filter was cut into quarters and put into four different quartz inserts.

Conclusions

In summary, method 4 was chosen because preparation and sample insertion into the quartz tube is relatively quick compared to methods 1 and 2. All methods can minimise contamination via cleaning of apparatus used. The main issue with methods 1 and 3 is sample preservation. For this project, sample losses during preparation, insertion into hypy and retrieval of the sample from the hypy need to be minimal. However, for method 1 sample loss during grinding is possible, whilst for method 3 sample loss during retrieval of the filter is possible. Method 2 was not considered further because it is time consuming.

5.6.2. Method

As described in Section 4.2.2, 10 mL aqueous/methanol solution of ammonium dioxydithiomolybdate [$(NH_4)_2MoO_2S_2$] was prepared in a 20 mL pre-combusted glass vial. The filters were placed in pre-combusted foil filter holders. The entire catalyst solution was pipetted onto the PM filter. The filters were kept in their foil filter holders and placed on top of a hot plate to dry the samples at 80 °C. Once filters were dried, they were freeze-dried then weighed before running on hypy as seen in Figure 5.28. Freeze drying was important to remove water so that accurate masses were recorded for the mass balance calculations. The freeze-dried 47 mm filters were split into quarters with a pre-cleaned scalpel and cutting board. Each quarter was rolled and placed into a separate quartz insert (10 mm). All four inserts were placed into the hypy reactor and run at the same time (see Figure 5.29). This was completed 8 times for 8 different filters (see Table 5.10). The post-hypy quartz inserts were combusted into separate quartz tubes. The quartz tubes were sequentially cracked on a vacuum cracking unit where the CO_2 for all filters from a single sample were combined for measurements. Section 5.2 details the method of purification of CO_2 and graphitisation.

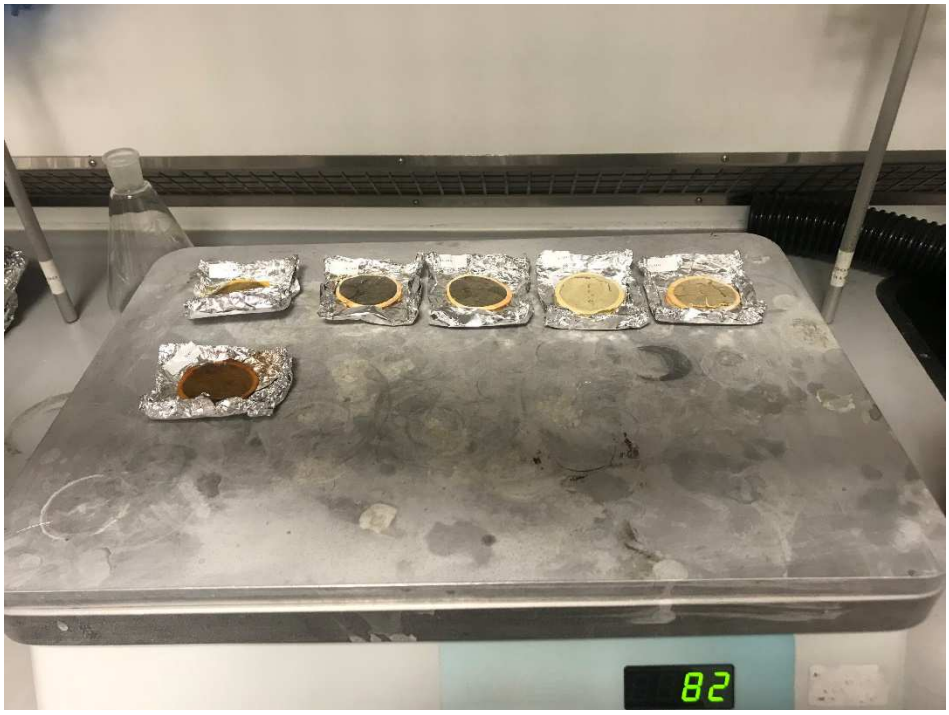

Figure 5.28. Drying process for airborne ambient PM deposited on filters with catalyst, within pre-combusted (at 450 °C) aluminium foil holders.

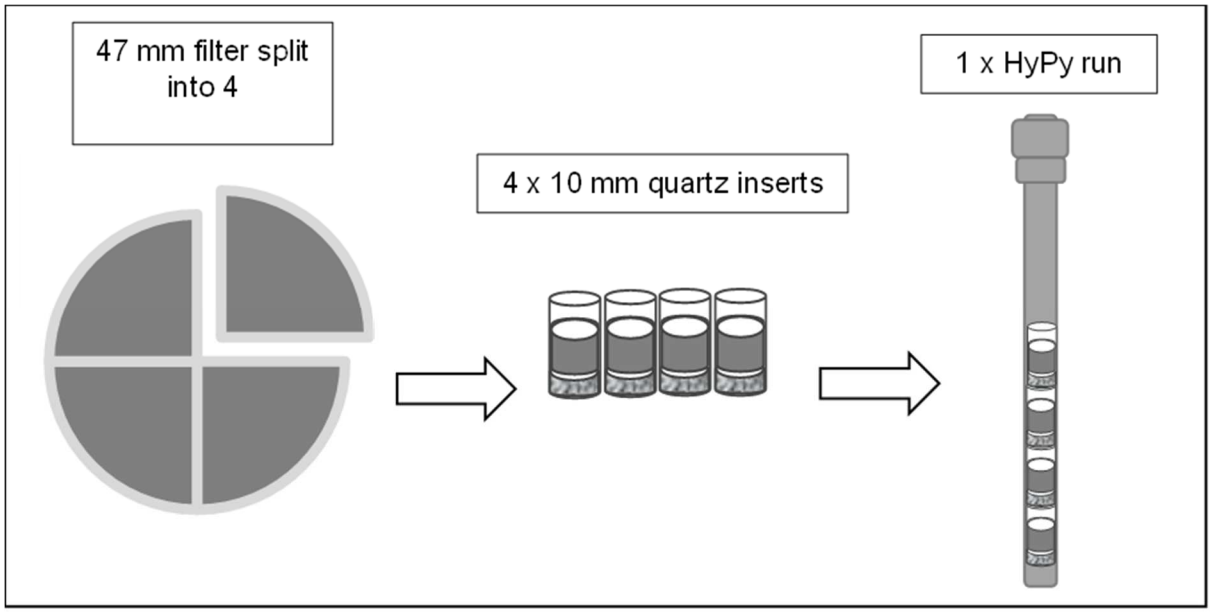

Figure 5.29. Method of sample introduction to hypy instrumentation, for 47 mm filters.

The method was slightly different for the 150 mm filters on which the Manchester samples were collected. Due to the large size of the filter, 30 mm quartz inserts had to be used for hypy combustions. The filters were divided into sixteenths using a pre-cleaned scalpel and

cutting board as only $^{1}/_{16}$ of a filter could fit into a 30 mm quartz insert. In total $^{3}/_{8}$ of a filter was put into 6 separate 30 mm quartz inserts. The rest of the filter was kept for GC-MS analysis and %C analysis.

Table 5.10. Details of the sample groupings per ^{14}C measurement of BC_{hypy} airborne ambient aerosol in the UK.

Material ID	Sampling Site	Description	Mass before hypy (mg)	Collection Dates	Sampler Type	Notes
GLA-HH(BC_{Hypy})	Glasgow University Avenue	Filter0002 Inserts 1,2,3,4 Filter0003 Inserts 1,2,3,4 Filter 0005 Inserts 1,2,3,4 Filter 0037 Inserts 1,2,3,4 Filter0040 Inserts 1,2,3,4 Filter0041 Inserts 1,2,3,4 Filter0042 Inserts 1,2,3,4 Filter0043 Inserts 1,2,3,4	7.1	30.07.2021 – 12.08.21 18.06.2019 – 24.06.2019 12/08/2021 – 26/08/2021 27/05/2021 – 17/06/2021 17/06/2021 – 01/07/2021 01/07/2021 – 15/07/2021 15/07/2021 – 30/07/2021 26/08/2021 – 09/09/2021	LVAS, Omni, $PM_{2.5}$	All samples generated low levels of CO_2 therefore the samples had to be bulked together to generate enough CO_2 for a single small sample ^{14}C measurement.
MAN-FF13_1 (BC_{Hypy})	Manchester Fallowfield Campus	Plate 13 Inserts 1,2,3	9.7*	30/11/2019 – 02/12/2019	HVAS, Digitel, $PM_{2.5}$	Sub-samples 1 to 3 of Plate 13 were combined for a single ^{14}C measurement due to the amounts of CO_2 generated

MAN-FF13_2 (BC_{Hypy})	Manchester Fallowfield Campus	Plate 13 Inserts 4,5,6	9.7*	30/11/2019 – 02/12/2019	HVAS, Digitel, $PM_{2.5}$	Sub-samples 4 to 6 of Plate 13 were combined for a single ^{14}C measurement due to the amounts of CO_2 generated
MAN-FF14(BC_{Hypy})	Manchester Fallowfield Campus	Plate 14 Inserts 1,2,3,4,5,6	13.8*	02/12/2019 – 04/12/2019	HVAS, Digitel, $PM_{2.5}$	All sub-samples of Plate 14 were combined for a single ^{14}C measurement due to the amounts of CO_2 generated

* As filter was not weighed before sampling, the sample mass was estimated by subtracting the post-conditioned sample weight (filter and sample) from the average blank filter weight (n = 10), then calculating $^{3}/_{8}$ of the sample weight.

5.6.3. Results and Discussion

It was not possible to obtain BC/TC% values for the samples processed as described above. This was due to difficulties in obtaining accurate pre- and post-hypy sample weights for the %C analysis. These arose partly because of the need to combust the entire sample to obtain sufficient CO_2 for a successful ^{14}C measurement, due to low mg C in the samples, particularly after the hypy process. The BC/TC% requires a sub-sample of material both pre- and post-hypy for separate %C measurements and this was at odds with the need to use all of the sample for ^{14}C. A further difficulty was the accuracy of pre- and post-hypy %C measurements, given that it would not have been possible to analyse an identical sample for these values; instead different sections of the filter would have had to be used, with potentially different catalyst distributions, and inhomogeneities in the sample itself. Finally, there were difficulties with obtaining an accurate value for the weight loss during hypy, because of the very high ratio of filter paper to sample that comprised the material in the hypy crucible. For the Manchester samples, filters were not weighed before sample collection, therefore the %C could not be accurately calculated, as the mass of the sample was unknown. This led to difficulties in obtaining the %MC value through mass balance, as %C measurements were required for this. Instead, the %MC (non-BC_{hypy}) was obtained by subtracting the %MC (TC) from the %MC (BC_{hypy}) (see Table 5.11). Other issues included a lack of ^{14}C measurements for GLA-HH2 due to low amounts of sample CO_2 being

generated; therefore GLA-HH1 had to be used as the TC value from which to subtract the GLA-HH(BC_{hypy}) value so as to determine GLA-HH %MC (non-BC_{hypy}). However, as seen in Section 5.5.2, %MC (TC) values did not differ much from 2019 to 2020 for GLA-CC1 and GLA-CC3+4 samples, therefore the same could be assumed for 2020 to 2021. Considering both samples were collected during times when COVID-19 measures were in place, the samples could be comparable. Overall, there may be errors associated with this method so the results will be treated with caution. For MAN-FF samples, the average %MC (TC) was used for the non-BC_{hypy} calculation. Although the samples were not from the exact same sampling date, they were collected during the same sampling period, so errors are likely to be minimal for the Manchester %MC (non-BC_{hypy}) values.

Table 5.11. Data obtained from ^{14}C analysis for TC airborne ambient aerosol in the UK.

Material ID	Sampling Period	δ13C ‰ (BC_{hypy})	%MC (BC_{hypy})	%MC Error	%FC (BC_{hypy})	%MC (non-BC_{hypy}) *
GLA-HH(BC_{Hypy})	27/05/2021 – 09/09/2021	-	24	0.15	76	23
MAN13_1-FC(BC_{Hypy})	30/11/2019 – 02/12/2019	-26.4	25	0.14	76	40
MAN13_2-FC(BC_{Hypy})	30/11/2019 – 02/12/2019	-28.1	25	0.14	76	
MAN14-FC(BC_{Hypy})	02/12/2019 – 04/12/2019	-26.2	20	0.12	80	

* %MC (non-BC_{hypy}) was determined through subtraction of %MC (TC) from % MC (BC_{hypy}), not through mass balance calculations.

As seen in Table 5.11, the BC_{hypy} measurement for the GLA-HH sample had 24 ± 0.15 %MC (BC_{hypy}) with 76 %FC(BC_{hypy}). The BC_{hypy} %MC value was roughly half of the %MC (TC) value for GLA-HH1. This implies the BC_{hypy} has dominant fossil source contributions with modern source contributions such as biomass combustion, as the %MC value was higher than for FD and BCR-RD which were predominantly from vehicular emissions. GLA-HH %MC (BC_{hypy}) was higher than the UD and UPM aerosol standard BC_{hypy} values of 9 – 12 %, meaning there could be a larger contribution of $BC_{biomass}$ in GLA-HH samples due to modern nature of the BC_{hypy}. The non-BC_{hypy} was 23 %MC (non-BC_{hypy}) indicating modern

sources, such as biomass combustion and biogenic SOA, with dominant OC_{fossil} contributions.

The %MC (BC_{hypy}) for MAN13_1, MAN13_2 and MAN14 had 25 %, 25 % and 20 %MC values, respectively. The %FC was 80 % for MAN13_1 and MAN13_2 and 76 % for MAN14. The duplicate MAN13 runs yielded almost identical %MC (BC_{hypy}) values, 24.57 and 24.59 %MC (BC_{hypy}), which indicates consistency in repeat measurements. The $\delta^{13}C$ signatures for samples Plate13_3 and Plate13_6 differed slightly, by 1.7‰, with the uncertainty of the measurements being ± 0.5‰. The M14 measurement had a different %MC (BC_{hypy}) value than the M13 measurements of 20.20 %. This is likely to represent emission source fluctuations across different sampling days rather than inconsistencies from instrumentation. This was also seen in the %MC (TC) for MAN-FF samples, which showed variation in modern to fossil C proportions. The MAN-FF results showed dominant fossil contributions for %MC (BC_{hypy}) but a large proportion of the %MC (non-BC_{hypy}) was from modern sources indicating biogenic SOA contributions, as if it were from biomass combustion the %MC (BChypy) and %MC (non-BChypy) would be more similar. This was seen in standards UD and UPM which had higher non-BC_{hypy} values than $BC_{hypy,}$ and their source attributions showed significant contributions from $OC_{biogenic}$.

The %MC (BC_{hypy}) of GLA-HH and MAN-FF showed mixed sources with a %MC of 24.14 % and 20.20 - 24.59 % respectively. The %MC (BC_{hypy}) were similar across GLA-HH and MAN-FF. The BC_{hypy} had modern contributions which was likely to be from industrial biomass combustion and domestic wood combustion across the region. This indicates fossil sources have dominant contributions to BC_{hypy} over modern sources. Nevertheless, there are clearly $BC_{biomass}$ sources as the DS BC_{hypy} value was 0.05 %. Diesel blends in the UK now incorporate biodiesel so the modern sources could be vehicular emissions. The $\delta^{13}C$ values of Manchester samples were -28.1 ‰ to -26.2 ‰. This indicated that the BC_{hypy} was derived from biomass combustion due to the values being more consistent with northern hemisphere terrestrial plants (Deines, 1980).

The results in this study are consistent with those from Liu et al. (2014) who categorised BC aerosols in London during 2012 using PMF and HR-AMS and found that, although traffic sources dominated, non-traffic solid-fuel combustion sources were also important in winter. A review paper identified 50 BC + EC source apportionment studies in Europe since 2003 and found fossil fuel combustion was the dominant BC source but biomass contributions during winter at non-urban locations had significant contributions (Briggs & Long, 2016). Due to recent general increases in emissions from domestic wood-burning, urban areas such

as Glasgow and Manchester are also affected. In Italy, biomass burning also contributed to BC in Milan and Bareggio, and peaks were seen at night-time when wood burning would be used for residential heating. The lowest $BC_{biomass}$ contributions were during the day (Mousavi et al., 2019). In a ^{14}C study in Naples, Italy, BC was 34 %MC whilst OC was 77 %MC(Sirignano et al., 2019). BC values here were similar to those in Naples however, the non-BC_{hypy} values were much lower.

5.6.4. Conclusions

Hypy was used for the first time on airborne ambient $PM_{2.5}$ samples from the UK and was successful in separating BC_{hypy} and non-BC_{hypy} and in ^{14}C analysis on the BC_{hypy} component. A method was established for the insertion of airborne ambient PM into the hypy system which included pipetting catalyst solution on top of the filter paper and drying it and cutting the filter paper into segments and rolling it, in order to fit it into a quartz insert for hypy.

The BC_{hypy} of GLA-HH2 and MAN-FF samples had dominant fossil sources. The %MC (BC_{hypy}) of GLA-HH2 and MAN-FF(13+14) were higher than the standards that represented traffic emissions (FD and BCR-RD) and urban areas (UD and UPM). This shows that the BC_{hypy} segment likely has $BC_{biomass}$ contributions. With domestic wood combustion being the top contributor of primary $PM_{2.5}$ emissions in the UK, this is unsurprising (NAEI 2020). However, the sources could also be from industrial combustion of biomass, which is the top emission source for BC (NAEI 2020). The %MC (BC_{hypy}) for GLA-HH2 and MAN-FF13 were extremely similar (24 %MC and 25 %MC respectively). MAN14 had more fossil carbon (20 %MC) but was still similar to the other samples. The similarities show that BC sources in urban areas of the UK are similar, with dominant fossil sources but modern contributions from $BC_{biomass}$. Other potential contributions could be biodiesel emissions and transported emissions from nearby areas. In comparison with the %MC (TC) of GLA-HH2 and MAN-FF the BC_{hypy} had a stronger fossil carbon contributions showing that the non-BC_{hypy} is largely from $OC_{biogenic}$ and $OC_{biomass}$.

The non-BC_{hypy} of GLA-HH samples were roughly the same as the %MC (BC_{hypy}) thus like BCR-RD and FD likely had low $OC_{biogenic}$ contributions with large OC_{fossil} contributions from vehicular emissions. However, MAN-FF samples like UD and UPM had a more modern non-BC_{hypy} than BC_{hypy}, so these samples were likely to have natural $OC_{biogenic}$ contributions, especially considering Manchester Fallowfield campus is surrounded by trees and greenery.

This shows that different approaches are required to mitigate against the different components of $PM_{2.5.}$ It is difficult to disentangle natural sources from anthropogenic sources when looking at just $PM_{2.5}$ (%MC of TC) therefore this shows the importance of BC as an additional marker for detrimental health effects. Although BC is monitored in the UK there is currently no legislation focusing on reduction of BC itself. Current legislation focuses on reducing $PM_{2.5}$ levels on a mass basis without regarding that the health effects of different components of $PM_{2.5}$ vary. This study has shown that monitoring and aiming to reduce BC exclusively would reduce the fossil components of $PM_{2.5}$ which are most detrimental to human health. This means air quality management should continue to focus on the reduction of fossil fuel combustion through traffic management schemes, transition to e-mobility and endorsement of active travel. As the BC_{hypy} had a significant modern contribution this also highlights that there should be a focus on reducing domestic combustion of wood and industrial biomass combustion. Recent legislation in England is already trying to tackle this issue through the 'Ready to burn' certification scheme. However, to monitor the effect of this ^{14}C analysis in conjunction with analysis of chemical markers such as levoglucosan or K^+ could be used to confirm the modern contribution is from wood burning.

A limitation of this work was that low sample masses led to a small number of %MC (BC_{hypy}) measurements. Recommendations have been made below on how to best use hypy for on $PM_{2.5}$ samples for future BC_{hypy} source apportionment research.

5.6.5. Recommendations for Hypy Preparation Steps for ^{14}C analysis of TC and BC_{hypy}

When using hypy in conjunction with ^{14}C to analyse aerosols, it is likely that samples will need to be pooled due to low sample masses. Therefore, it is recommended that before filters are pooled, they are split in 2, with one half going for TC ^{14}C analysis and the other half into 2 x 10 mm quartz inserts. This allows for direct comparisons to be made between TC and BC_{hypy} and non-BC_{hypy} %MC values even if filters are pooled together. Gaseous C % analysis should be done before ^{14}C analysis on both TC and BC_{hypy} to obtain C % for BC/TC% to help with source attributions. More filters should be added to pooled samples to ensure enough CO_2 is generated for successful ^{14}C and $\delta^{13}C$/C % measurements.

From an analytical perspective, HVAS are recommended for sample collection so that larger amounts of PM can be collected and in shorter collection times. However, the portability of LVAS enables sample collection from a range of sites. For example, in this study samples were collected from the city centre and west end of Glasgow, each representing different types of areas in Glasgow, with the west end being more residential. If using LVAS then it is preferable to have 47 mm filters as this enables more accurate mass determinations to be made. The filters can be easily cut into quarters, and 1 x ¼ of 47 mm filter can fit into 1 x 10 mm quartz insert, with 3 x 10 mm quartz inserts being able to fit into the hypy reactor resulting in the analysis of an area of 13.01 cm^2. On the other hand, when using 150 mm filters, only 1 x $^1/_{16}$ of the filter can fit into 1 x 30 mm quartz insert, with only 1 x 30 mm quartz insert being able to fit into the reactor resulting in the analysis of an area of 11.04 cm^2. Furthermore, cutting $^1/_{16}$ of a filter can lead to larger mass uncertainties of the filter allowing for accurate BC/TC% calculations post-hypy.

For PM samples, a mass range of 14.0 – 23.8 mg is suggested to complete both raw ^{14}C analysis as well as ^{14}C analysis of both post-hypy products, for samples with a TC% of approximately 17 %. However, this is likely to vary depending on season of sample collection. If HVAS are being used it is recommended that prior to ^{14}C analysis a %C value is derived for the smallest mass (or lightest filter by eye) and the largest mass (darkest) filter, as the C% can be used to estimate the range in C content of collected PM.

Depending on research purposes, the non-BC_{hypy} can be submitted for ^{14}C analysis if no further analysis is to be completed on the non-$BC_{hypy.}$ This may not be possible for all sample types, if samples have low non-BC_{hypy} C content. In such cases, the non-BC_{hypy} %MC value can be obtained via mass balance.

5.7. Key Findings

Method development – Mass Considerations

- Calculations were conducted to determine a hypy initial sample mass for $PM_{2.5}$ samples to ensure all subsequent analyses could be completed. By doing so, a method was developed for simultaneous ^{14}C analysis of BC_{hypy}, GC-MS analysis of non-BC_{hypy} and determination of BC/TC % of $PM_{2.5}$.

Method development - Exploration of Hypy methodology to isolate BC for ^{14}C Measurements.

- ^{14}C TC values of UD and UPM in line with previous literature which proves the measurements are yielding accurate results (UD 53 % MC, UPM 64 % MC). Additionally, the difference between replicate measurements were small, with overlapping error bars, which showed the data had good precision.
- Aerosols standards UD and UPM had roughly equal contributions of modern and fossil sources, however road dust standards had dominant fossil sources.
- BC_{hypy} of all standards had dominant fossil sources (6 – 12 % MC) whilst the non-BC_{hypy} was more modern (70 % and 81 %). This shows that the BC_{hypy} and non-BC_{hypy} have different proportions of modern: fossil carbon indicating different sources. This highlights BC measurements are a better human health indicator for fossil carbon. Furthermore, UD and UPM had high $OC_{biogenic}$ contributions which were estimated using source attributions. This also shows that it is difficult to disentangle natural and anthropogenic sources in the non-BC_{hypy} hence monitoring of BC_{hypy} or BC more generally can provide direct insight to whether anthropogenic emissions have increased or decreased, as opposed to $PM_{2.5.}$
- $\delta^{13}C$ values of TC and BC_{hypy} were similar which showed that $\delta^{13}C$ interpretations of sources for BC_{hypy} would still be representative of original sources. FD BC_{hypy} was the only sample that showed a large deviation to TC $\delta^{13}C$ value. The BC_{hypy} had lower values than the TC $\delta^{13}C$ value likely to be from the removal of OC_{fossil} which contributed to 64 % of TC.

Method Development – Acid fumigation

- Acid fumigation tests showed fumigation removes carbon as C % values decreased, however for FD and UPM, the %MC also decreased, showing that modern labile OC was destroyed through acid fumigation pre-treatment step. As this could yield inaccurate %MC values, the step was not deemed necessary, as there was little difference between acidified and non-acidified samples; for FD and UPM the error bars overlapped indicating the differences could be down to natural variation. However, for BCR-RD there was a significant difference between acidified and non-acidified samples yet the RSD% of both conditions was low therefore acid fumigation was deemed an unnecessary step.

TC ^{14}C Analysis on $PM_{2.5}$ Samples in the UK

- $PM_{2.5}$ samples from Glasgow had a %MC (TC) range of 45 – 47 % and Manchester samples had a %MC range of 49 – 74 % (excluding an anomalous result of 134 %). This showed that Glasgow samples had a higher proportion of fossil C compared to Manchester samples. There was more variability in the MAN-FF samples however this could have been due to the measurements representing shorter time resolution (2 days) whereas Glasgow $PM_{2.5}$ filters were grouped together covering roughly a month period. The sites varied with MAN-FF having a more modern contribution, likely due to it being a suburban site. This shows the health risks associated with inhalation of $PM_{2.5}$ in Glasgow may be more adverse.
- London, Chilbolton and Auchencorth moss had dominant modern contributions to $PM_{2.5}$, however London and Chilbolton samples were collected during the second national lockdown when traffic sources were reduced, thus fossil source contributions were extremely low. London Marylebone road had extremely high %MC 193 % which was speculated to be from emissions of enriched ^{14}C e.g., incineration of biomedical waste.
- The fossil fuel sources were most likely from vehicular emissions and resuspended road dust.
- The modern sources were likely to be local and regional domestic wood combustion. Glasgow samples were likely to have contributions from cooking oils whereas Manchester, London Honor Oak and rural background sites were likely to have

natural biogenic sources also. Chilbolton and London most likely had $PM_{2.5}$ contributions from south-east UK and Europe.

- ^{14}C (TC) measurements from London Honor Oak, London Marylebone and Chilbolton Observatory were unlikely to represent business-as-usual modern to fossil contributions. However, the results demonstrated the modern to fossil proportions during the COVID pandemic were high possibly due to the reduction in vehicle usage.

Application of ^{14}C measurements to TC and BC_{hypy} to Urban UK Airborne Ambient PM

- A method was developed for insertion of airborne ambient PM into hypy system. Catalyst was added by putting the catalyst into a solution then pipetting it onto the filter and allowing the filter to dry at 80 °C in a pre-cleaned foil filter holder. The filter was freeze-dried then split using a scalpel (47 mm into quarters, 150 mm into sixteenths) and rolled, then put into quartz inserts.
- Hypy-^{14}C was used for first time on UK aerosols, to our knowledge. The %MC (BC_{hypy}) measurements for $PM_{2.5}$ samples from Glasgow and Manchester had higher %MC (BC_{hypy}) than the aerosol and dust standards, showing a contribution of $BC_{biomass.}$ This shows that domestic combustion of wood and industrial biomass combustion are anthropogenic activities that should be focused on in terms of air quality management as well as fossil fuel combustion. More research should be conducted into the human health effects of $BC_{biomass}$. The modern to fossil contributions of the BC_{hypy} were similar in Glasgow and Manchester, unlike the %MC (TC). This shows that BC_{hypy} or BC more generally, is a better indicator of anthropogenic emissions.
- Manchester %MC (non-BC_{hypy}) had $OC_{biogenic}$ contributions as the non-BC_{hypy} was more modern than the BC_{hypy}. This shows that there were natural SOA contributions to the non-BC_{hypy} highlighting $PM_{2.5}$ is not the best indicator of human health effects, as it is difficult to disentangle natural and anthropogenic sources of carbon.
- More information could have been obtained with BC/TC% values of samples, as this would enable further source apportionment into consequent categories; OC_{fossil}, $OC_{biomass}$, $OC_{biogenic}$, $BC_{biomass}$ and BC_{fossil}. However, due to limited sample mass, submitting part of the sample for post-hypy %C could have jeopardised the ^{14}C measurements, as there were some instances with the ^{14}C (TC) measurements where there was not enough C in the sample for a ^{14}C measurement.

Recommendations for Hypy Preparation Steps for ^{14}C analysis of TC and BC_{hypy}

- 47 mm filters should be used as they fit into 10 mm inserts, and four of these can be fit into the hypy per run, which increases sample throughput.
- Half of the $PM_{2.5}$ filter should be submitted for a TC measurement (pooled with other filters) and the other half of the $PM_{2.5}$ filter should be submitted for hydropyrolysis to separate BC_{hypy} from non-$BC_{hypy.}$
- Gaseous C % analysis should be done before hypy on the TC sample and after hypy on the BC_{hypy} sample. To ensure these measurements can be made more filters should be pooled together.
- HVAS should be used to obtain larger sample masses over a shorter sampling period, however LVAS should be used for spatial representativeness if long periods of time can be dedicated to sample collection.
- Analysis of non-BC_{hypy} is not necessary as can be done by difference (TC – BC_{hypy}) but if non-BC_{hypy} is not needed for other analyses, it could be submitted too.

6. Discussion

6.1. Abundance and Spatial Variation of BC in Glasgow

BC increments taken by the roadside, referred to as BC 'mobile' measurements (BC_m) were measured in four electoral wards withing Glasgow. The results showed that the BC increments varied across the four wards. The city centre having the highest BC increments. Baillieston, a residential ward, on the outskirts of city, had the lowest BC increments. This shows that variation in BC increments has spatial characteristics. BC_m increments showed consistent trends for morning and mid-morning sampling campaigns whereas fixed BC measurements from a microAethalometer (BC_f) were less consistent. This suggests that 'mobile' measurements closer to the roadside are more representative of local air quality due to their proximity to vehicle emissions. Population, population density and socioeconomic factors were good indicators of BC pollution levels. Epidemiological studies frequently use central site monitoring data to represent air pollutant levels in an area (Fann et al., 2011); however, it has been shown here that central site monitoring data does not represent air pollution levels in other areas of the city with different site characteristics. Recent studies have suggested new approaches for epidemiological studies using multiple monitoring sites, air quality sensors and modelling approaches (Brokamp et al., 2019; Gómez-Losada et al., 2019). The use of sensors or portable instruments, such as the microAethalometer, would be useful in epidemiological studies, as it has been shown here that they are able to register short but elevated exposures to air pollutants due to proximities to the source.

The spatial variation in BC increments leads to recommendations with regards to land-use in Glasgow. Housing developments should be spread out across the city, rather than concentrated in particular wards, to reduce hotspots of BC. Along with better active travel and public transport links, this could lead to a reduction in exposure to BC with consequent positive health outcomes for affected populations.

Mid-morning median BC increments were higher than morning median increments but only those for BC_m were significantly different. Once again this shows that mobile measurements are better at capturing changes to local air pollution, due to proximity to roads. Absolute BC concentrations showed the opposite trend, showing that background BC may make a significant contribution to morning BC concentrations. This shows that the use of BC increments over BC concentrations can help improve understanding of local pollution events,

through removing background influences. Future monitoring studies should report both BC concentrations and increments and interpret increments to understand local air pollution.

A strong correlation was observed between bus/HGV AADTS and BC increments of stopping sites. This was also observed by Wu et al. (2015) in Edinburgh, Scotland, where BC emissions were thought to be linked to heavy goods vehicles (HGV). The most recent UK BC report showed lower BC concentrations at the weekend at Glasgow High Steet. This was thought to be from a reduction in traffic including HGVs (Ciupek et al., 2021). This suggests local policies could focus on controlling HGV emissions. Such measures that could tackle such emissions include bus retrofits, electrification of bus fleets, retrofitting existing diesel freight engines, research into electrification of freight vehicles and research into low emission last mile delivery operations, which could help to lower the total BC emissions in congested areas (Local Government Association, 2022).

Glasgow has worked on improving the emission standards of buses through the low emission zone (Glasgow City Council, 2021). It was reported that more than 60 % bus journeys through the city centre meet this emission standard (Glasgow City Council, 2021). The enforcement of the second phase of the LEZ is on 1st June 2023 and will apply to all vehicle types, meaning the number of compliant vehicles is expected to increase (Glasgow City Council, 2021). Additionally, the Glasgow ECO Stars Fleet Recognition Scheme is being promoted by Glasgow City Council (Glasgow City Council, 2021). The purpose of this is to help fleet operators improve efficiency, reduce fuel consumption and emissions whilst making cost savings (Eco Stars, n.d.).

6.2. Health Risks of PM-Bound PAHs

As discussed in Chapter 3, Section 3.3, exposure to PAHs with PM can cause detrimental human health effects. The UK currently measures BaP as a marker for carcinogenic risk of PAHs in ambient air. However, the carcinogenic potential of BaP in PAH mixtures varies depending on its proportion to the total PAHs present in the PM. The sole use of BaP to determine health risks rather than the collective risk of the PAH mixture may lead to underestimations in overall health risks associated to PM-bound PAHs. This possibility led to an assessment of the health risks associated to the inhalation of PM-bound PAH mixtures from urban (Glasgow Kerbside site, GLA-KS) and suburban areas (Manchester Fallowfield site, MAN-FF) in the UK. PAHs co-emitted with BC are thought to be trapped in the micro-

porous structure of BC. Therefore, PAH analysis was conducted on samples collected from Anderston, City and Yorkhill ward which were found to have the highest BC concentrations compared to other investigated wards (Hillhead, Partick East/Kelvindale and Baillieston) in Chapter 2.

The PAH-associated mutagenicity (BaP_{Meq}), toxicity (BaP_{Teq}) and lifetime lung cancer risk from inhalation ($ILCR_{inh}$) were calculated. The results are presented in Chapter 3, Section 3.3.2.

The average BaP concentrations were 0.21 ng m^{-3} for the 3 GLA-KS(PM_{10}) samples and 0.97 ng m^{-3} for 1 GLA-KS($PM_{2.5}$) sample. The GLA-KS($PM_{2.5}$) sample concentration exceeded the UK NAQO for BaP of 0.25 ng m^{-3} (as an annual mean) and was close to exceeding the FAQDD for BaP of 1 ng m^{-3}. As the COVID pandemic and restrictions interrupted the PM sampling, samples were obtained from Ricardo as discussed in Chapter 3, Section 3.2.2. A batch of samples were obtained which did not comprise of the whole year. The filters were grouped to create 4 samples in total (see Section 3.2.2, Table 3.3). Overall, the 4 samples included filters sampled between 19/01/2020 – 11/02/2021. Despite the samples not being representative of business-as-usual scenarios, due to samples 4043, 4046 and 4047 being collected during COVID-19 restrictions), the values show that GLA-KS PAHs could be associated with potential detrimental health effects such as lung cancer and age-related diseases, including Alzheimer's disease and Parkinson's disease (Armstrong et al., 2004; Fritsch et al., 2020).

MAN-FF samples were representative of the winter/cold season as they were collected between 20.11.19 – 18.12.19. This meant they represented a worst case scenario for PM-bound PAH concentrations as these are generally higher in the colder months within the UK, due to increase in domestic combustion and other sources (Conolly & Carpenter, 2021). The average BaP concentration was 0.23 ng m^{-3} which does not exceed either the NAQO or FAQDD. This suggests population exposure to PAHs in suburban areas had lower associated health risks than compared to inner-city urban areas, which has negative implications as inner-city areas tend to have high population densities. This means larger populations will experience exposure to PM-bound PAHs. This finding should be taken into consideration when planning land-use in cities. For example, Glasgow City Council could prioritise housing developments outside of the city centre to lower the overall population exposure to PM-bound PAHs. Glasgow City Council has mentioned some of the challenges the city faces in its City Development plan through phrases such as "tackling congestion and improving air quality" and "the need to address health levels and health inequalities across the city"

(Glasgow City Council, 2017). The city council has recognised that student accommodation, which is characterised by houses in multiple occupation, is largely centred around universities or the city centre. The Council currently supports purpose-built student accommodation in or adjacent to main campuses (Glasgow City Council, 2017). However, as mentioned, the inner-city areas expose the population to higher PM-bound PAHs. Glasgow could follow the example of Manchester and locate student accommodation in areas outside of the inner-city. Therefore, new policies focusing on the development of student accommodation in outskirt areas of the city, with good transport links (cycle routes and bus/train links), could lower students' exposure to PM-bound PAHs. A limitation of this finding is PM-bound PAHs from different parts of Glasgow were not compared in this study. Future work could determine PM-bound BaP concentrations as well as the toxicity and mutagenicity of PAH mixes in different Glasgow wards, to provide support for these new policies that could be implemented into the City's development plans.

To further investigate the health effects of PM-bound PAHs, their mutagenicity (BaP_{Meq}) and toxicity (BaP_{Teq}) were calculated. The BaP_{Meq} and BaP_{Teq} for GLA-KS(PM_{10}) were 0.37 of 0.53 respectively (see Chapter 3, Section 3.3.2). These values were compared with European cities to determine the similarities and differences in PAHs mutagenicity and toxicity. GLA-KS(PM_{10}) had lower values than A Coruña, Spain (1.4 BaP_{Meq} and 2.7 BaP_{Teq}) (Sánchez-Piñero et al., 2021). Populations in both Spain and the UK were not exposed to annual BaP levels higher than EU standards in 2019, so it would be expected that BaP_{Meq} and BaP_{Teq} would be similar. However, Sánchez-Piñero et al. (2021) stated that shipping, as well as road traffic, emitted PAHs in A Coruña. Glasgow has different PAH sources (see Chapter 3, Section 3.2.11), hence this shows that different emission activities lead to different quantities of toxic and mutagenic PAHs in PM_{10}.

The BaP_{Meq} and BaP_{Teq} were 1.6 and 2.4 for GLA-KS($PM_{2.5}$) respectively. The average BaP_{Meq} and BaP_{Teq} for MAN-FF were 0.39 and 0.64. This was lower than GLA-KS($PM_{2.5}$) but higher than GLA-KS(PM_{10}). This shows that PM_{10} and $PM_{2.5}$-bound PAHs have different levels of mutagenicity and toxicity. This is consistent with other studies that found $PM_{2.5}$ to have more total and carcinogenic PAHs per µg than PM_{10} (de Kok et al., 2005; Pandey et al., 2012). It is also in agreement with Jahedi et al. (2021) who found that as PM size decreased, the proportion of 5 to 6-ring PAHs (which are considered to be more toxic than LMW and MMW PAHs) to the total PAHs increased. The UK PAH Network currently measures PAHs in PM_{10} rather than $PM_{2.5}$. Considering the mutagenicity and toxicity of

$PM_{2.5}$ was higher than PM_{10} this shows that measurement of PAHs in $PM_{2.5}$ may be a better indicator of associated health risks.

The BaP_{Meq} and BaP_{Teq} of $PM_{2.5}$-bound PAHs in GLA-KS were compared to other European cities. GLA-KS($PM_{2.5}$) was comparable to other urban sites in Thessaloniki (0.4 - 2.0 BaP_{Meq} and 0.4 - 1.5 BaP_{Teq}), Porto (2.37 BaP_{Teq}) and Venice (2.1 BaP_{Meq} and 1.9 BaP_{Teq}) (Alves et al., 2017; Manoli et al., 2016; Masiol et al., 2012). Italy had approximately 52,000 premature deaths caused by $PM_{2.5}$ with 2.6 % and 16.3 % of the population in 2019 and 2020, respectively, exposed to BaP concentration above the EU standard (European Environment Agency, n.d.-a). GLA-KS($PM_{2.5}$) had similar BaP_{Meq} and BaP_{Teq} values to Italy. Considering the UK had exposed 0 % of the population exposed to BaP annual concentrations above the EU standard in 2019, it was surprising that GLA-KS($PM_{2.5}$) had similar values to Venice, especially considering GLA-KS($PM_{2.5}$) was collected during COVID pandemic and associated restrictions on transport/travel, commercial, and industrial activities (European Environment Agency, n.d.-b). This could be attributed to different $PM_{2.5}$ sources. In 2020 Italy's commercial, institutional, and residential combustion sector was the main source of $PM_{2.5}$ (66 %) whilst in 2020 the UK's manufacturing and extractive industry was the dominant source for $PM_{2.5}$ emissions (39 %) (European Environment Agency, n.d.-a;n.d.-b). This shows the importance of calculating BaP_{Meq} and BaP_{Teq} as although the BaP exceedances for Italy were higher, the BaP_{Meq} and BaP_{Teq} were comparable to the UK, due to different $PM_{2.5}$ sources.

The increased lung cancer risk through inhalation of PAHs ($ILCR_{inh}$) was calculated through use of three different inhalation cancer unit risk factor (IUR_{BaP}) values (Chapter 3, Section 3.3.2.). The highest $ILCR_{inh}$ values were calculated using the IUR_{BaP} value from the World Health Organization (denoted $ILCR_{inh(a)}$) with 2.09×10^{-4} for GLA-KS($PM_{2.5}$) and 4.60×10^{-5} for GLA-KS(PM_{10}). The thresholds used here were used in other studies and were in line with thresholds recommended by the WHO for carcinogens in drinking water (1×10^{-5}) and the U.S. EPA thresholds (1×10^{-6}).

A value of $ILCR_{inh} \leq 1 \times 10^{-6}$ was deemed negligible or regarded as safe, a value in the range 1×10^{-6} to 1×10^{-4} suggests a potential risk and a value $>1 \times 10^{-4}$ implies a potentially high risk (Cao et al., 2019; Ghanavati et al., 2019; Robson & Toscano, 2007; Wang et al., 2011b; WHO, 2017). GLA-KS($PM_{2.5}$) $ILCRinh_{(a)}$ was within the potentially high-risk category, translating to 209 excess lung cancer cases per 1,000,000 people exposed to this level of PM-bound PAHs. When applied to the Anderston/City/Yorkhill ward population this translates to 6 excess annual cases of lung cancer, assuming continuous and homogenous

exposure of inhabitants. For MAN-FF the $ILCR_{inh(a)}$ was highest (5.60×10^{-5}) which was deemed to be a potential risk , equating to roughly 56 excess cases of lung cancer per 1,000,000 people (Cao et al., 2019; Ghanavati et al., 2019; Wang et al., 2011a). As these samples were collected in the colder winter months, where PAH concentrations in the UK are generally higher, it is likely that the values for MAN-FF would be lower if calculated using annual averages of PAHs (Conolly & Carpenter, 2021). On the other hand, actual risks calculated for both MAN-FF and GLA-KS samples could be higher than reported because:

GLA-KS samples were collected during COVID-19 where restrictions in place were shown to lower PAH emissions across the UK (see Chapter 3, Section 3.2.2).

The $ILCR_{inh}$ was calculated solely from outdoor pollution. It does not include indoor PM-bound PAH pollution (home and work environments) or additional sources such as cigarette smoking (Vardoulakis et al., 2020). Other possible sources include use of household products, domestic burning, and cooking (Harrison et al., 2008; Vardoulakis et al., 2020). Studies in the UK did not find significant differences between indoor and outdoor PAH concentrations (Hernandez, 2015; Kingham et al., 2000). However, indoor PM-bound PAH concentrations are likely to be extremely variable and dependent on many factors subject to the occupants' behaviours/the dwellings facilities such as usage of fume hoods, frequency of window opening and usage of fire places (Shrubsole et al., 2012; Vardoulakis et al., 2020).

Photodecomposition of PAHs occurs when they are exposed to solar UV light. In the atmosphere PAHs can react with other pollutants (ozone, sulfur dioxide and nitrogen oxides) to form nitrogenated (nitro-) and oxygenated (oxy-) PAHs (Nowakowski et al., 2022). Nitro- and oxy-PAHs would likely be within the semi-polar fractions of PM extracts (Keyte et al., 2016). Research has shown higher direct acting mutagenicity, associated with this fraction (Jariyasopit et al., 2014a; Jariyasopit et al., 2014b; Keyte et al., 2016; Umbuzeiro et al., 2008; Wang et al., 2011b). These PAHs were not quantified in this study therefore it is likely that the associated mutagenicity and toxicity of PM-bound PAHs is higher than is concluded based on the results presented.

PAHs in ambient air exist in gaseous form as well as particulate form (Kim et al., 2013). Only PM-bound PAHs were analysed in this study therefore associated mutagenicity and toxicity of PAHs in ambient air could be higher than presented, as it does not account for the inhalation of gaseous PAHs.

When the $ILCR_{inh(a)}$ of $PM_{2.5}$-bound PAHs from GLA-KS and MAN-FF were compared to other countries with different sampling site classifications (urban, urban background, urban traffic, suburban), the site types generally had similar $ILCR_{inh(a)}$ values. For example, urban traffic sites GLA-KS and Porto had similar values, whilst suburban sites had similar values (MAN-FF, Bangi – Malaysia, Athens – Greece) (Alves et al., 2017; Khan et al., 2015). Some sites did not follow the trend such as Northern Italy which was an urban background site but had similar levels to urban traffic sites (Khan et al., 2018). Also, Rio de Janeiro urban sites were similar to suburban and mixed sites (Santos et al., 2020). This could be due to the site being classified as 'urban' instead of 'urban background' or 'urban traffic'. It could be difficult to categorise sites from different countries into the same classifications because of variations in land-use, activities in the area, and other factors. Generally, the $ILCR_{inh(a)}$ followed this order of decreasing $ILCR_{inh(a)}$: urban traffic > urban background > suburban > mixed sites. This was also observed by Aquilina and Harrison (2023) who found the $ILCR_{inh(a)}$ to be the following: traffic roads > urban background > rural background, independent of the country (Aquilina & Harrison, 2023).

To reduce exposure to PM-bound PAHs in Glasgow, Glasgow City Council should focus on awareness campaigning and behaviour change with regards to health considerations of air pollution exposure. The most recent action plan and annual status report mentions using of signage of the low emission zone to increase awareness of air pollution, advertising campaigns to raise awareness of unnecessary vehicle idling and the Glasgow ECO Stars Fleet Recognition Scheme (Glasgow City Council, 2009;2021). In the Chief Medical Officer's annual report 2022 it was suggested that "the training of healthcare staff on the health effects of air pollution, including communication with patients" could help with raising awareness about the health effects of air pollution (UK Government, 2022a). In a project in Islington, GPs were taught causes and health impacts of air pollution (Global Action Plan, 2022). GPs shared leaflet and materials with participants. Additionally, a borough-wide communications campaign, outlining harms of air pollution, was implemented. Post-project analysis showed that GPs felt they understood the health impacts of air pollution better and felt more confident in talking to their patients about air pollution and reducing their exposure to it. This is an example of an approach that Glasgow City Council could take to further improve awareness of air pollution health effects.

The limitations of the study performed within this thesis are that annual averages of PAH concentrations were not used to calculate BaP_{Meq}, BaP_{Teq} and $ILCR_{inh}$. The sample sizes were small (4 GLA-KS samples and 6 MAN-FF samples), which meant they were not

representative of the whole calendar year or seasonal range, with different samples representing different periods in the year. This meant it was difficult to generalise the results beyond the sampling periods. Another limitation is that this study only examines health effects associated with the inhalation of PM-bound parent PAHs rather than other components such as PAH derivatives and transition metals which have been linked to oxidative stress potential (Ayres et al., 2008). Oxidative stress potential has been linked to pro-inflammatory effects in the nose, lung and cardiovascular system (Ayres et al., 2008). However, this was beyond the scope of the study. Future research in Glasgow could look into the health effects associated with nitro- and oxy-PAHs and transition metals to estimate the cumulative health effects of all toxic component of PM.

Recent research has revealed the presence of BC particles as a part of combustion-derived PM on the foetal side of human placentae (Bové et al., 2019), potentially causing detrimental early-life health effects. Other research that quantified BC in prenatal and postnatal biological matrices found that BC was associated with the composition and diversity of the childhood intestinal microbiome, which plays an essential role in human health (Van Pee et al., 2023). This shows that other components of $PM_{2.5}$, specifically BC exposure during pregnancy and early life, can affect human health. It is unknown whether BC itself is toxic or if BC is toxic because it acts as a carrier of toxic compounds adsorbed to BC such as PAHs. In general, very little is known about how BC is metabolised in the body; whether BC breaks down into smaller constituents or remains intact and is excreted. BC breaking down would be alarming as BC comprises condensed polyaromatic structures, and PAHs are extremely toxic to human health. Therefore, more research is required to determine the health effects of inhalation of $PM_{2.5}$ from all toxic components. The hypy methodology could help progress toxicological research by disentangling the health effects of BC and semi-labile organic compounds. The BC_{hypy} residue could be used in place of carbon black which is used as a proxy of BC in toxicological studies such as in Pozzi et al. (2003) (see Chapter 4 for the hypy methodology). Unlike other methods, hypy retains the semi-labile organic compounds, therefore the total toxicity of both the BC_{hypy} residue, non-polar fraction (PAHs) and semi-polar fraction (nitro- and oxy-PAHs) of the PM extract, could be added to culture media in toxicological studies.

6.3. Use of Hypy for BC Measurements and Source Apportionment

6.3.1. BC/TC% Measurements

The aim of this work was to determine if the hypy methodology was suitable for separation of BC_{hypy} in airborne ambient aerosols with the purpose of understanding the variation of sources contributing to airborne ambient PM and subsequent source apportionment of $BC_{hypy.}$. Hypy has been previously utilised on urban aerosol standard urban dust (NIST 1649b) for BC/TC% measurements (Meredith et al., 2012). However, to ensure hypy can be used effectively on airborne ambient aerosols, it was important to test the methodology on a range of materials with different BC sources, as BC particles are extremely variable in composition and morphology. The objectives were:

1. Compare BC/TC% from this study to other BC/TC% measurements to determine if hypy consistently and reproducibly isolates BC in aerosol and dust materials.
2. Obtain BC/TC% measurements for a range of BC-containing materials with different sources to evaluate 'end members' for BC formation the ability of hypy to consistently isolate BC despite differences in BC composition, properties, and morphology.
3. Observe the variation between different BC-containing materials with respect to the assumption that lignite and charred biomass have low BC/TC%, aerosol and dust materials have mid-range BC/TC% due to mixed sources, and DS has a high BC/TC%. This was important to achieve to ensure that hypy can discriminate refractory material with >7 aromatic rings (BC_{hypy}) from semi-labile organic structures, hence ensuring the method was not over-estimating BC.

The BC/TC% results, shown in Chapter 4, Section 4.2.3, for UD (NIST 1649b) (27.8 % ± 0.1 %) were in agreement with the values for BC content from this standard material presented in previous work, including Meredith et al. (2012) who used hypy (27.9 ± 0.6 %) and Zhang et al. (2023) who used hypy (~28 %). This provides confidence that hypy can consistently isolate BC in aerosol and dust materials as three BC/TC% measurements for UD across different laboratories yielded very similar results. Whilst this is a success, there are limitations with the study, as only two other hypy-derived BC/TC% measurements have been published (Meredith et al., 2012; Zhang et al., 2023). To increase confidence in the use of hypy as a means of routinely determining BC/TC% in airborne ambient PM, it is important that more aerosol and dust materials are analysed across laboratories and

compared to other BC measurement techniques via comprehensive intercomparison studies. Hammes et al. (2007) conducted intercomparison studies for BC measurements applying different methodologies, and variations in applying a single methodology, on a range of environmental matrices (sediments, soils and aerosols) and Currie et al. (2002a) conducted an intercomparison study on urban dust (1649a) using different measurement techniques. A new intercomparison study could be useful, as it could incorporate existing BC measurement techniques as well as new BC measurement techniques such as hypy. The intercomparison study should solely analyse aerosol and dust materials, including readily accessible materials that have emerged since the previous analyses in Hammes et al. (2007) and Currie et al. (2002a), such as fine dust (ERMCZ100 Fine Dust PM10-like with PAHs), urban particulate matter (NIST 1648a), BCR-723 Road dust and diesel soot (NIST 2975). The importance of the work done for this thesis is that it analysed a range of aerosol and dust standards, against which future hypy research can be compared.

The methodology for obtaining hypy-derived BC/TC% measurements from airborne ambient PM has been developed in this project. The use of 47 mm filters over 100 mm filters is encouraged because the former can be split into quarters with a scalpel whereas the latter need to be split into sixteenths then cut down into smaller sections to fit into a 30 mm hypy crucible. The latter leads to higher uncertainties in the PM mass before and after hypy. This methodology can be used in toxicological research to determine the toxicity of carbonaceous components in airborne ambient $PM_{2.5}$. Pozzi et al. (2003) used carbon black instead to determine if the toxicity was due to adsorbed OC or BC itself. By separating the BC_{hypy} and non-$BC_{hypy,}$ the toxicity of BC alone can be disentangled from OC. It should be noted that BC_{hypy} contains not only carbonaceous components but all other components of $PM_{2.5}$ not reductively removed through the hypy process, such as metals and minerals, therefore these variables would have to be controlled in the toxicological research.

The hypy-derived BC/TC% measurements for UD were also comparable to BC/TC% measurements derived from other measurement techniques such as Mannino and Harvery (2004) who used thermal oxidation methods (22.7 ± 0.78 %), Hsieh and Bugna (2008) who used multi-elemental scanning thermal analysis (24.6 ± 5.7 %) and Zhan et al. (2013) who used thermal optical methods IMPROVE and IMPROVE_A protocols (24.02 and 22.82 % respectively). As discussed in Meredith et al. (2012), it was once again found that the BC/TC% results obtained for UD were higher than methods that use more aggressive oxidation, which lead to underestimations in BC due to unselective removal of carbonates, such as Reddy et al. (2002) who used the CTO-375 method (8 % BC/TC), Alvarez-Ospina et al. (2016) who

used the thermal-coulombimetric method (11 % BC/TC) and Meredith et al. (2012) who used the dichromate method (11.8 % BC/TC). The same was observed for UPM, where the BC/TC% of 25 % was higher than a more aggressively oxidising thermal-coulombimetric method (14 %) (Alvarez-Ospina et al., 2016). Hypy yielded higher BC/TC% values than these methods likely due to the absence of aggressive oxidising conditions and the ability to detect a wide range of aromatic structures as BC. The values obtained for UD in this study were in the middle of the range reported by Currie et al. (2002a) for UD (6.9 – 52 %) where 19 different chemical and thermal methods were used, some of which were methods that led to underestimations due to aggressive oxidation and others that led to overestimations due to assigning OC as BC. As hypy was in the middle of the range of underestimating and overestimating methods, it provides confidence that hypy values are closer to the 'true' value of BC. These findings were in agreement with Meredith et al. (2012) who found that BC_{hypy} values fell within the range of BC contents reported in the BC ring trial intercomparison study by Hammes et al. (2007). As reported in Meredith et al. (2012), the BC_{hypy} values were generally higher than oxidising methods and similar to results from thermal optical methods.

The implications of the research are that it enables this methodology to be used in future work looking to determine BC/TC% with minimal instrument artefacts. Currently, different methodologies result in a wide range of reported BC in aerosol standards, which leads to problems in monitoring and modelling BC for example it leads to inaccuracies in BC emission factors used in specialised models such as chemical transport models for source apportionment (Rönkkö et al., 2023). This inaccuracy stems from use of different BC measurement techniques to calculate emission factors and issues in calibrating different BC methods. Hypy-derived BC/TC% measurements could therefore be used to improve the accuracy of future emission inventories, and subsequent source apportionments determined from this. These measurements could also be used on airborne ambient PM in the UK to compare against current aethalometer-derived BC measurements to determine if any new insights can be found using the hypy methodology with regards to the accuracy of these methods. As hypy is an offline method, it is more time-consuming, hence expensive, than online methods like the aethalometer making it better suited as a routine measurement that is completed seasonally (4 times in a year) or annually. Unlike aethalometers it would need to be applied to samples collected over longer time resolutions of >1 week to ensure enough mg C for the post hypy %C measurement. A particular focus on intra and inter-site comparisons would be useful, to determine if there were large variations in BC/TC% across different site classifications (e.g., urban background, urban traffic, urban industrial, suburban and rural background) within towns/cities and across different towns/cities.

As the BC/TC% measurements were comparable to other hypy-derived BC/TC% measurements and other techniques such as thermal optical methods and multi-elemental scanning thermal analysis, the next step was to obtain BC/TC% measurements in a range of BC-containing materials from different sources (Chapter 4, Section 4.2.3). BC/TC% measurements were obtained for charred biomass samples (DB and EB), which represent solid particulates emitted from biomass burning, aerosols, road dusts and diesel soot. One of the charred biomass materials, DB, had a relatively low BC/TC% of 15.1 ± 0.1 %. This material was less homogenous than that of EB. EB had a higher BC/TC% of 62.5 ± 0.6 %. This could be due to the pyrolysis temperatures being higher than that of DB as well as a higher air flow rate, gasifier pressure and different species. This shows the wide variation in BC/TC% of pyrolyzed biomass materials, caused by varying pyrolysis conditions. The effect of pyrolysis conditions of laboratory-made charcoals was further researched (Appendix II). The results showed that the BC/TC% varied depending on species and pyrolysis temperature. The BC/TC% of the three aerosols materials, UD, UPM and FD, were extremely similar. FD represented traffic emissions from a road tunnel, yet its BC/TC% was still within the range of UD and UPM. UD and UPM represented highly polluted areas, as they were collected in 1970s, hence pollution levels would have been higher due to less efficient industrial and vehicle technologies, as well as fewer air pollution legislation and policies. Therefore, as all standards represented highly polluted environments, this was not an unexpected result.

The road dust material (BCR-RD) had a higher BC content than aerosols at 40.9 ± 1.3 %. This could be due to BC settling on the roads within the tunnel, due to it being a closed environment, hence preventing dispersion. However, there could also be additional source inputs from carbon black from tyres, which is used as a reinforcing compound (Youn et al., 2020). The release of carbon black from tyre-wear particles is often overlooked due to the particles being tightly bound to the rubber matrix (Kim et al., 2021). To determine whether carbon black particles could be released from tyres, Kim et al. (2021) ground the surface of a passenger car tyre, to obtain tyre wear particles. The tyre-wear particles were subject to ball-milling which was used to represent the weathering effect and surface abrasion of tyres on the road. The experiment showed that carbon black particles were released from the tyre-wear particles. Kim et al. (2022) then went on to quantify carbon black particles from tyre-wear particles in road dusts. The results showed that road dust in closed sites exhibited 21.5 times higher tyre-wear particles and 5.1 times higher carbon black content compared to open sites (Kim et al., 2022). This could contribute to the higher BC/TC% of BCR-RD (closed traffic tunnel) compared with HH-RD (open road in Glasgow). Moreover, the site where HH-RD was collected likely had less traffic flow than the traffic tunnel where BCR-RD

standard was collected. Other potential contributors to BCR-RD could be carbonates from tyre fillers and road erosion (Harrison et al., 2021). This reinforces the need for more research into non-exhaust traffic-associated particles, such as carbon black, to understand the proportion of its contributions to $PM_{2.5}$ in the UK. Overall, hypy was able to determine the BC/TC% in a range of BC-containing materials that represented different sources of airborne ambient aerosols showing that hypy can consistently isolate a consistent portion of the BC continuum in airborne ambient aerosols with mixed sources. The ordering of the BC/TC% from lowest to highest was:

Charred biomass (DB) < Aerosols < Road dust (BCR-RD) < Charred biomass (EB) < Diesel Soot (DS)

These findings were consistent with Meredith et al. (2012) who also found that hypy was able to discriminate between relatively labile materials (in this case charred biomass DB and BZ) and more refractory high BC_{hypy} samples (in this case DS). With regards to the aerosol materials hypy reported similar BC/TC% for UD, UPM and FD (see Chapter 4, Section 4.2.3). As all standards represented highly polluted environments, this was not an unexpected result. Hypy was able to distinguish between road dusts from highly polluted areas, BCR-RD, reporting higher BC/TC% values, and road dusts from less polluted areas (HH-RD), reporting lower BC/TC% values.

The limitations of hypy are its inability to distinguish BC from carbon black or carbonates. If the contribution is small, it could be negligible and may not affect the BC/TC%; however, this would need to be tested further through understanding the proportions of non-exhaust particles, and their subcategories e.g., tyre-wear particles, to $PM_{2.5}$ in the UK. In general, having a broad understanding of the sources of $PM_{2.5}$ and its constituents is extremely important for mitigation. It is better to take a preventative approach to air pollutant emissions, targeting sources, rather than taking actions for remediation. Different components of $PM_{2.5}$ may have different sources; therefore, it is important to obtain a holistic overview of the sources by understanding the sources of each of these components.

6.3.2. ^{14}C Measurements

To determine the sources of TC, BC an OC in $PM_{2.5}$ samples from GLA-CC, GLA-HH and MAN-FF, ^{14}C measurements were obtained. Hypy was used as the method for BC/OC separations (see Chapter 5).

Firstly, it was important to determine whether airborne ambient PM samples required acid fumigation to remove carbonates, which could affect the ^{14}C source apportionment (see Section 5.4.3). Tests were carried out on aerosols and dust materials BCR-RD, FD and UPM. The %C results of all materials showed a decrease demonstrating carbon was removed. The %MC values were examined as a loss of carbonates should equate to a loss in fossil carbon, therefore higher %MC. The %MC values in FD and UPM decreased and increased in BCR-RD. The chi-squared test of independence showed the difference between acidified and non-acidified samples was significant. Despite this, for UPM the error bars of acidified and non-acidified samples overlapped. Whilst they did not overlap for BCR-RD, the difference in acidified and non-acidified BCR-RD was <1 %MC (TC).

The decrease in %MC indicated that there were no carbonates present in UPM and FD. Unless modern pedogenic carbonates were present in these samples, the acid fumigation may have attacked modern labile OC components leaving more refractory OC components (Bao et al., 2019). The possibility of 'modern' pedogenic carbonate contamination in UPM and FD was low as the materials originated from areas that were not arid or semi-arid (Fernández et al., 2022).

BCR-RD had higher %MC values after acid-fumigation implying the presence of carbonates or the removal of geological-age OC components. Considering BCR-RD is a road dust material then carbonates could be present due to weathering of concrete road surfaces.

Acid fumigation was not applied to airborne ambient aerosols for the following reasons:

1. It was difficult to know what exactly the acid fumigation removed, as it is a non-selective process it could remove 'modern' labile OC, fossil OC, 'modern' carbonates and fossil carbonates. This would therefore lead to inaccurate %MC.
2. Whilst BCR-RD most likely contained carbonates and the chi-squared test showed significant differences between acidified and non-acidified samples, the differences in %MC before and after acid-fumigation were <1 %MC which is extremely low.
3. Unless 'modern' carbonates were present in FD and UPM, it was likely that 'modern' labile OC was removed, due to decreases in %MC (TC) of acidified FD and UPM. This

would therefore lead to inaccurate %MC. The differences between acidified and non-acidified samples were <2 %MC for UPM and FD.

The findings suggest that acid-fumigation is an unnecessary pre-treatment step for ^{14}C analysis of airborne ambient PM and road dusts. A limitation of this finding however is that it may not be generalisable as the proportion of carbonates in airborne ambient PM from different locations may vary. Therefore, researchers utilising ^{14}C analysis for source apportionment in airborne ambient PM in future work, may need to complete their own acid fumigation tests to ensure the step is unnecessary for their site of interest. Another way to determine if a sample has carbonates is to acid fumigate the BC_{hypy} rather than the $PM_{2.5}$. As the hypy process should remove labile OC, the acid fumigation should theoretically only react with carbonates as BC consists of refractory and non-labile carbon. A set of experiments could be completed to determine the carbonate content in airborne ambient PM through comparing %MC (BC_{hypy}) of acidified BC_{hypy} and non-acidified BC_{hypy} samples.

To determine the proportions of fossil and modern carbon in $PM_{2.5}$ samples from the UK, ^{14}C measurements for aerosol standards were compared with those in the literature for quality assurance (see Section 5.4.2). The %MC (TC) values for UD (53 %) were in agreement with those from other studies such as Szidat et al. (2004b) 52 %, NIST certificate 2007 51-53 %, Heal et al. (2011) single combustion 52 % and Bonvalot et al. (2016) 54 %. However, the error bars did not overlap with two measurements reported by Currie et al. (1984) 61 % and Heal et al. (2011) 51.5 %. The %MC (TC) values for UPM (64 %) was in agreement with those reported by Kaplan and Gordon (1994), 62.1 and 62.4 % and Currie et al. (1984) 60 % through beta counting method. The measurement was close to the value reported by Weissenbok et al. (1998), 60.9 %MC (TC), however the error bars did not overlap. The agreement with previous research provided assurance that the quality of the measurements were at a good standard.

Another step taken to ensure the quality of the measurements was to analyse known-source materials that represented potential sources of airborne ambient PM with varying ^{14}C(TC) content. The fossil fuel standards had low %MC (TC) (BZ 0.1 % and DS 0.2 %) and the charred biomass standards had high %MC (TC) (DB 102.7 % and EB 96.9 %). The aerosol standards exhibited variation in ^{14}C contents, due to mixed sources. UD consisted of roughly equal modern and fossil sources (52.6 %MC), whilst UPM had slightly more modern sources (63.6 %MC). FD however had a higher proportion of fossil sources (19.8%MC) due to dominant sources being vehicles with petroleum combustion engines. The road dusts, BCR-RD and HH-RD had similar %MC (TC) values of 19.1 – 19.3 % and 23.0 – 23.8 %. This

showed that ^{14}C measurements could be used to determine fossil/modern contributions in airborne ambient PM with low to high ^{14}C contents. The findings suggested that materials with similar sources had similar %MC (TC) as BCR-RD and FD, both collected from traffic tunnels had similar %MC (TC). UD and UPM which had similar sampling environments also had similar %MC (TC). This shows that ^{14}C measurements can be useful in identifying areas with similar source contributions.

The fossil/modern proportions were determined for several locations in the UK (see Figure 5.15 for sampling locations). The ^{14}C measurements across the different sampling sites in the UK were then compared. AUC-MOS and CHI-OBS, both rural background sites had %MC (TC) of 93 and 83 % respectively. Whilst LON-HO and the average for MAN-FF, urban background sites had %MC (TC) of 85 and 62 %. LON-MA had extremely high ^{14}C contents (193 %), which was deemed anomalous as it was an urban traffic site. GLA-HH and the average for GLA-CC had the lowest %MC (TC) of 46 and 47 %. The rural background sites differed by about 10 %, whilst the urban background sites differed by 23 %. This is likely due to closer proximity to local emissions sources, which exhibit spatiotemporal variation. Urban traffic sites could not be compared due to the high ^{14}C contents of the LON-MA sample. The results showed sites with the same environment type exhibited large variations in %MC (TC) hence had differing source contributions. The variations could represent differences in biogenic SOA across the sites. However, as these samples were taken during different times of the year, with LON-MA, LON-HO, AUC-MOS, CHI-OBS and GLA-HH1 being collected during COVID-19 restrictions it was difficult to compare %MC (TC) values and generalise the findings beyond the dates of sample collection. GLA-HH1 exhibited similar %MC (TC) to GLA-CC1 and GLA-CC3+4 despite being collected during COVID-19 restrictions. During this time in Scotland hospitality sector was operational but with a 10 pm curfew, hence the %MC (TC) was similar to GLA-CC1 and GLA-CC3+4 which represented emission sources in business-as-usual scenarios. However, around the time LON-MA, LON-HO and CHI-OBS were collected, a second national lockdown in England was enforced meaning business-as-usual %MC (TC) may be higher than reported here. AUC-MOS may also have higher %MC (TC) values as it was collected during the first national lockdown for the whole of the UK. Future work could repeat these measurements in the present day to determine the inter-site variability in fossil/modern proportions across different environment type e.g., urban traffic, urban background, and urban industrial. As the work completed on aerosol and dust standards showed that standards with similar environments had similar %MC (TC), it would be interesting to see if this was similar for airborne ambient PM from the UK.

To obtain ^{14}C measurements for BC_{hypy} and non-BC_{hypy} for samples from Glasgow and Manchester, ^{14}C measurements BC_{hypy} and non-BC_{hypy} were first obtained from a range of BC-containing materials which represented end members of ^{14}C content (See Section 5.4.2.). This step was used as means of quality assurance. The result for UD %MC (BC_{hypy}) was 6.31 % which was consistent with literature values derived from other BC/OC separation techniques such as those reported by Szidat et al. (2004b) (6.6 %) and NIST 2007 certificate (6.5 %). The result was also within the range reported by Zhang et al. (2023) for UD using hypy, (3.8 % - 15.3 %MC (BC_{hypy}).This provides assurance that the results are reliable hence can determine sources of BC_{hypy} accurately. However, there is a need for more $^{14}C(BC_{hypy})$ measurements from the research community, for a range of aerosol and dust standards, to determine confidence in reproducibility across laboratories for more than one aerosol material.

Other materials were analysed such as charred biomass, diesel soot and road dusts. Some of these materials (BCR-RD, FD and DS) are readily available, which allows for comparisons with future measurements that use hypy or other BC/OC% separation methods prior to ^{14}C analysis, as a means of quality assurance.

The %MC (BC_{hypy}) values for charred biomass samples DB and EB were 103.0 – 103.1 %MC and 101.3 – 102.0 %. Both samples had a higher %MC (BC_{hypy}) than %MC (TC) indicating there was some OC_{fossil} within the sample. This could have been contamination from the gasifier set-up such as rotary pumps (referred to as the air flow pump in Kamble et al. (2019) which are lubricated with oil (Gaines et al., 2021; Laurenson et al., 1998). The non-BC_{hypy} for both DB and EB had a lower ^{14}C content than %MC (TC) indicating fossil sources. EB had higher levels of contamination as the %MC (non-BC_{hypy}) was 89.1 %. Despite the BC/TC of EB being larger than DB, the sources of BC were $BC_{biomass}$ hence this shows the value of using ^{14}C measurements on BC_{hypy} as it can differentiate between the fossil and biomass BC. There was no difference between the %MC (BC_{hypy}) and %MC (TC) of DS.

The ^{14}C content of the non-BC_{hypy} was consistently higher than the BC_{hypy} in BCR-RD, FD, UD and UPM. This suggests the labile OC had different sources to BC. As the BC_{hypy} ^{14}C content was quite low, this suggests dominant fossil sources, from fossil fuel combustion. The non-BC_{hypy} ^{14}C contents of BCR-RD and FD were lower than UD and UPM. Aerosol aging is where each individual particle in an aerosol population mixes with other chemical species, due to Brownian coagulation among particles, condensation of gaseous phase chemical and heterogenous chemical reactions on particles surface (Bondy et al., 2018;

Ching & Kajino, 2018). The lower non-BC_{hypy} contents of BCR-RD and FD could be due to a lesser degree of aerosol aging, as BCR-RD and FD were sampled from closed traffic tunnels. The same effect was observed by Hou et al. (2018) where atmospheric processing of aerosols in tunnels was less than that of urban areas. UD and UPM had higher %MC (non-BC_{hypy}) likely due to aerosol aging. This could be from internal mixing with natural biogenic SOA. UPM %MC (BC_{hypy}) was almost double the %MC (BC_{hypy}) of BCR-RD, FD and UD. This suggests biomass combustion, most likely for domestic combustion purposes.

A part of the BC_{hypy} and non-BC_{hypy} must have originated from biomass combustion due to the %MC (BC_{hypy}) values being above that of DS (0.14 %) which was composed mainly of fossil carbon. These particulates likely were dispersed from nearby emission sources such as domestic combustion of wood. The findings showed that BC and OC in aerosols and dusts had different source contributions. This shows that the source apportionment of the BC_{hypy} is a better indicator of anthropogenic emission sources, as it removes labile OC that may have been externally and internally mixed, with BC. Through monitoring the ^{14}C content of BC_{hypy} progress towards curtailing fossil fuel combustion can be monitored directly and give a clear indication of progress made to policymakers.

This method was applied to UK airborne ambient PM from GLA-HH and MAN-FF and the %MC (BC_{hypy}) was 24.1 % and 24.6 % respectively. The BC_{hypy} values were extremely similar despite being sampled from different locations at different dates. Moreover, the BC_{hypy} values had lower ^{14}C contents than the TC. This is likely due to the removal of natural 'modern' sources such as biogenic SOA. This shows that determination of sources in BC_{hypy} gives a better indication of anthropogenic sources that can be mitigated through policies and regulations. The BC_{hypy} had higher ^{14}C contents than aerosol and dust standards analysed. This suggests there is an increase in non-fossil combustion sources such as wood or biodiesel.

6.3.3. Sources of TC, OC (PAHs and n-alkanes) and BC in PM Samples

The sources of $PM_{2.5}$ TC, BC_{hypy}, non-BC_{hypy}, PAHs and n-alkanes were determined in aerosols from Glasgow City Centre and Glasgow Hillhead (GLA-CC and GLA-HH). GLACC1, GLA-CC3+4, and GLA-HH1 had %MC (TC) values of 45– 46 %. This meant that fossil and modern sources were roughly equal in Glasgow for $PM_{2.5}$. The GLA-HH %MC (BC_{hypy}) was 24 %. This implies that the anthropogenic sources of carbon are dominantly from fossil sources as the samples had low ^{14}C contents. The fossil sources were

most likely from vehicular emissions. This is corroborated by Glasgow having the largest number of vehicles licensed in Scotland, 239,008 vehicles, at the end of 2021 (Transport Scotland, 2022). Moreover, polar plots from Glasgow Townhead in Section 3.2.9 show that the wind direction during days of high pollution came from the north-west and south-west which was in the direction of motorways and congested traffic areas. This was corroborated by PAH data from a nearby site, Glasgow Kerbside (GLA-KS), where PAH-DR-1, -2, and -3 categorised PAH sources to be from combustion, petroleum combustion and traffic sources. Examination of PAH profiles and ring-size distributions from GLA-KS showed that diesel and petrol emissions were present due to high proportions of BbF, BkF and BghiP. This was unsurprising considering the fleet composition had a high contribution from buses, with the older buses using diesel fuel. Moreover, the site is in close proximity to a large train station, Glasgow Central, where diesel is used to power trains. The CPIs of n-alkanes were 1.4 for GLA-KS($PM_{2.5}$) and 1.4 – 1.92 for GLA-KS(PM_{10}) meaning n-alkanes were dominated by combustion sources. Overall, the source apportionment data from ^{14}C measurements, PAH and n-alkane analysis were in agreement. However, GLA-KS's vehicle fleet composition differed slightly to GLA-CC and GLA-HH. GLA-CC and GLA-HH fleet consisted mainly of private cars, taxis and LGVs. GLA-KS also consisted of private cars and taxis but the AADT of buses were higher than LGVs, hence GLA-KS PAH sources may not be entirely representative of those from GLA-CC and GLA-HH. Zonal statistics are a tool in QGIS which can calculate statistics (for example mean, median and sum) for specified zones. Using a shapefile for the Glasgow Hillhead ward, the zonal sums were calculated from NAEI 2020 BC spatial atmospheric emission raster files, for Glasgow Hillhead ward (Figure 6.1). Road transport was the dominant BC source as it contributed to 49 % of BC emissions. This corroborates with the findings of this study.

There was a modern contribution in the GLA-HH BC sample; %MC (BC_{hypy}) 23 %. This could be from domestic wood combustion which could be transported by air masses travelling through rural areas of England or Scotland, to Glasgow. However, the zonal sums for NAEI BC emissions from Glasgow Hillhead show 0 % contributions from domestic and industrial combustion but large contributions from waste (19 %). This suggests that the domestic combustion contributions to GLA-HH BC/$PM_{2.5}$ may be small. The modern contributions could originate from the waste sector which includes waste incineration, cremation, and municipal waste incineration. High wind speeds were correlated to high $PM_{2.5}$ concentrations coming from the north-east and south-west. This means the source most likely to cause modern BC contributions would be a crematorium to the south-west of

GLA-HH. It is also likely that biodiesel blends either from road vehicles or trains (other transport category) contribute to the modern nature of BC_{hypy}.

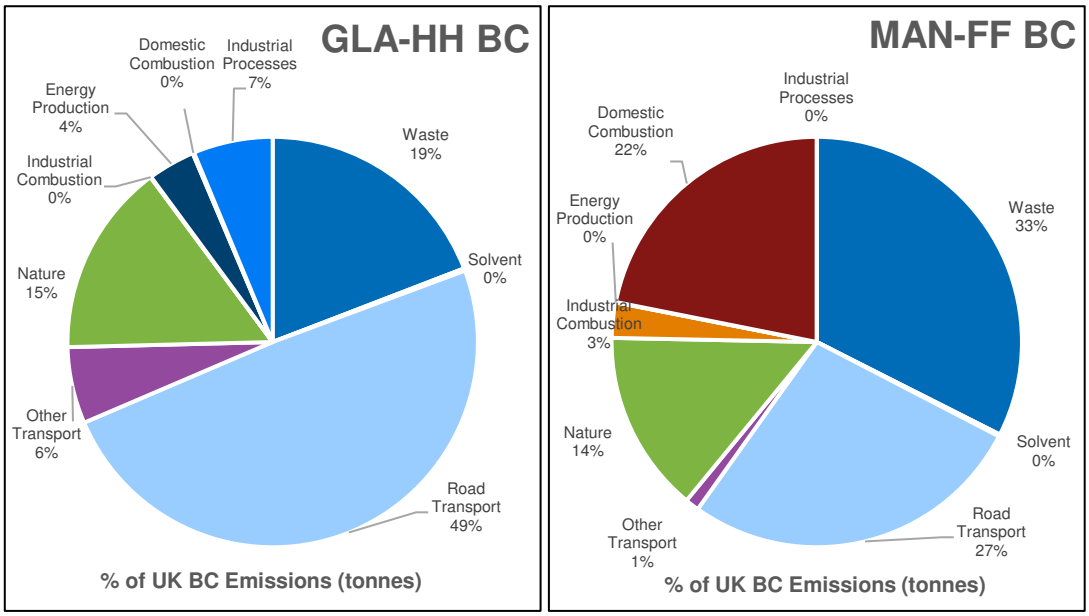

Figure 6.1. Zonal sums for UK BC emissions in tonnes, calculated for Hillhead ward, Glasgow and Fallowfield, Manchester, using NAEI 2020 data.

The sources of $PM_{2.5}$ TC, BC_{hypy}, non-BC_{hypy}, PAHs and n-alkanes were also determined in aerosols from Manchester Fallowfield Campus (MAN-FF). MAN-FF samples had a %MC (TC) range of 39 – 74 % (average 37.5 %) and %MC (BC_{hypy}) range of 20 – 25 % (average 23 %). Compared to Glasgow samples (GLACC1, GLA-CC3+4, and GLA-HH1) there was more variation in the samples collected from sites in Manchester; however, this is likely caused by the different sampling durations; MAN-FF samples were sampled over 2-days whereas Glasgow samples, were sampled over 2 – 3 weeks. The day-to-day variation was likely to be averaged out in Glasgow samples, however as each MAN-FF sample represented a 2-day period, the daily variation was more pronounced. The %MC (TC) average was higher than that of Glasgow samples. This could be attributed to differences in site characteristics as MAN-FF was a suburban site, surrounded by greenery, hence likely to have a larger contribution of biogenic SOA. Moreover, MAN-FF samples back trajectories showed air masses originated from Scotland/northern regions of UK, which consists of cleaner air, which could lead to lower fossil contribution, hence a higher %MC (TC), in

$PM_{2.5.}$ The windrose plots showed that high wind speeds often originated from the south-west. In this direction there were traffic emission sources such as the A6010 and a large point source from a crematorium. One sample had a particularly high %MC (TC) of around 134 %MC. The windrose plots showed high wind speeds from the north-east in the direction of Oldham hospital, on the date this sample was collected. Oldham hospital incinerates clinical waste, which could lead to elevated ^{14}C content in samples, due to the presence of material from highly 14C-enriched clinical tracer materials. The dominant sources were likely to be from traffic as corresponding PAH DRs for PAH-DR-1, -2, and -3 categorised the PAH sources to be from combustion, petroleum combustion and traffic sources. Examination of PAH profiles and ring-size distributions showed that petrol emissions were present due to high proportions of BghiP. Diesel emissions also seemed probable as PHEN & ANTH were present, indicating HDV diesel vehicles. The CPI of n-alkane data had a range of 1.34 – 1.84 which indicated dominant combustion sources. Overall, the source apportionment data from ^{14}C measurements, PAH and n-alkane analysis were in agreement.

The zonal sums in Figure 1.1 calculated from the NAEI 2020 spatial atmospheric emissions for MAN-FF, show 27 % of BC emissions were from road transport, 33 % were from waste and 22 % from domestic combustion. The results from this study differed from the zonal sums of NAEI 2020 spatial atmospheric emissions of BC. The proportion of emissions from domestic combustion and waste emission suggested in Figure 1.1 would likely result in higher ^{14}C content than reported. However, the ^{14}C content of BC_{hypy} was on average around 22 %. The pollution rose in Figure 5.22 showed that during the MAN-FF sample collection dates high winds from the north-east, south-east, south and south-west are correlated with high $PM_{2.5}$ concentrations. The waste sources from the latter directions (crematoriums and waste collection, treatment & disposal) were around 8 – 12 km away from the sampling site. The contributions were more likely to be from domestic combustion from residential areas.

There are a limited number of ^{14}C measurements within the literature from the UK, therefore this limits comparisons between data presented here and results from other studies in these and other study areas. A study collected $PM_{2.5}$ in Birmingham in 2008 and found the %MC (TC) to be between 27 – 66 %, with a mean of 50 % (Heal et al., 2011). Vehicle emissions would be expected to decrease since 2008 due to stricter emission standards and development of advanced end-of-pipe control technologies. This is reflected by the UK's downward trend, between 1990 to 2020, in $PM_{2.5}$ emissions from road transport (UK Government, 2022c). Therefore, sources of carbon in $PM_{2.5}$ may have higher ^{14}C content. As expected, the ^{14}C(TC) measurements had a higher ^{14}C content here with MAN-FF %MC

(TC) average of 62 % close to the maximum of the range and GLA-CC and GLA-HH samples %MC (TC) values of 45 – 46 %, typically in the middle of the range in Heal et al. (2011). The mean %MC (BC) from Heal et al. (2011) was 11 % which was much lower than the %MC (BC_{hypy}) of GLA-HH and MAN-FF (Heal et al., 2011). This shows a decrease in fossil carbon in BC, due to the decline in fossil-fuel derived BC as well as increasing BC emissions from biomass combustion. The increase biomass combustion has been highlighted in both domestic and industrial settings since 2011 (National Statistics, 2023). The %MC (BC_{hypy}) of MAN-FF and GLA-HH were compared to %MC (BC_{hypy}) from Beijing, China 23 %FC(BC_{hypy}) and Guangzhou China, 35% MC (BC_{hypy}), reported by Zhang et al. (2019a). The main sources of carbonaceous particles from both cities were described to be biomass burning, coal combustion and traffic emissions. Interestingly GLA-HH and MAN-FF BC_{hypy} fossil carbon proportions were similar to that of Beijing (22 % and 25 % respectively).

The %MC (BC_{hypy}) of samples from Manchester and Glasgow were similar. This shows similarities in the ^{14}C content between the two sites, likely due to similar proportions of BC from the same sources. This is supported by a study that found the diurnal trends exhibited by BC were linked to periods of high traffic 'rush hour' hence closely linking BC to road transport sources (Singh et al., 2018). Another study investigating the sources of UFP in London and Europe found that the sources of UFP in London were strongly correlated to BC concentrations (Rivas et al., 2020). The UFP were mostly from fresh traffic (41 %), traffic nucleation (12 %), urban sources (41 %), secondary aerosols (5 %) and photonucleation (1 %). As the UFP were strongly correlated to BC concentrations, this shows that the sources of BC were likely to be similar to UFP, hence dominantly from traffic (Rivas et al., 2020). This corroborates with the %FC(BC_{hypy}) in this study of 76 % for GLA-HH and 78 % average for MAN-FF. Moreover, a review paper found that the top contributing source of BC in Europe were transport emissions (Briggs & Long, 2016).

In this study the high ^{14}C contents in the non-BC_{hypy} could not be attributed to specific sources; however possible sources could include vegetative detritus, biogenic SOA, and transported air masses from rural areas in UK that combust wood domestically. GLA-HH had a %MC (non-BC_{hypy}) of 23 % similar to the %MC (BC_{hypy}) implying the sources were not from biogenic SOA. The PAH DRs confirmed that the majority of the PAHs were from combustion sources. Therefore, if strong correlations were observed through plotting the PAHs against the n-alkanes, it would imply that the n-alkanes had similar combustion sources (Kang et al., 2020). There were weak correlations (R^2 = 0.41) for GLA-KS PM samples indicating n-alkanes sources were not from combustion sources. Once the outlier

point GLA-KS(PM2.5) was removed the R^2 decreased to 0.03. The n-alkane data showed that GLA-KS(PM_{10}) and GLA-KS($PM_{2.5}$) samples had epicuticular waxes present, with an odd/even carbon preference from C_{25} to C_{33} for GLA-KS(PM_{10}) and C_{27} to C_{33}. Research has shown that such patterns arise from road dusts (Gupta et al., 2017; Rogge et al., 1993b; Rogge et al., 1993a). Moreover, as coarse particles have a higher proportion of biogenic n-alkanes, this shows that the epicuticular plant waxes are from vegetative detritus in resuspended road dusts (Alves et al., 2000; Tang et al., 2006). The HH-RD road dust sample also showed a high proportion of vegetative detritus from sampling sit GLA-HH. Fine vegetative detritus may have contributed to GLA-KS($PM_{2.5}$) alongside regional biomass combustion sources.

In MAN-FF samples there was a strong correlation ($R^2 = 0.79$) between total PAHs and total n-alkanes indicating biomass combustion sources. The n-alkane distributions showed an odd/even carbon predominance from C_{29} – C_{33} indicating epicuticular wax n-alkanes. The %MC (non-BC_{hypy}) of MAN-FF samples was 40 % which was more modern than the BC_{hypy} indicating the presence of biogenic SOA. This is expected as MAN-FF is a suburban area surrounded by nearby greenery. The biomass combustion sources could be from domestic combustion of wood which were shown to be the most prevalent modern sources of BC in the UK (NAEI, 2020) . Another possible source could be biodiesel blends, as several studies have shown that biodiesel can cause shifts to a more modern ^{14}C signature, which could explain the modern contributions to BC_{hypy} (Bennett et al., 2008; Cheng et al., 2003).

The PCA results for PAHs and n-alkanes in GLA-KS and MAN-FF samples showed 79.6 % of the PAHs and n-alkanes could be attributed to principal component 1 (PC 1) which was thought to be diesel vehicle and biomass combustion emissions. The 20.1 % to principal component 2 (PC 2) was thought to be from indirect (resuspended road dust) and direct petrol vehicular emissions and/or resuspended dusts. PC 1 explained the higher ^{14}C contents in the BC_{hypy} of GLA-HH and MAN-FF. Another possibility is that PC 1 reflects a combination of diesel, biodiesel and wood-burning, as a study found biodiesel in buses emitted 3-ring PAHs such as PHEN and ANTH like DS and wood combustion (Tzillah, 2009; Zhang et al., 2019b).

The implications of the data help to inform regulations and local policies, to focus on reduction of fossil sources of BC mainly through regulating vehicle emissions. Useful schemes include clean air zones, and low emission zones, as these help with the phasing out of older more polluting vehicles. Glasgow's fleet composition showed private vehicles

contributed largely to the fleet meaning electric vehicle government subsidies or incentives could have a positive impact through increasing the uptake of electric vehicles, which would help to reduce exhaust emissions. This would also need to be supported by a more expansive electric vehicle charging infrastructure. Another method includes promotion and incentivising of active travel. Glasgow has an existing bike-sharing scheme and Manchester has recently started a new scheme. However, improvements need to be made in the cycling infrastructure through more bicycle lanes, bicycle parking and better cycling routes from residential areas to the city centre. Moreover, such routes need to be signposted through some sort of web or app platform with clear markings of roads with cycle lanes and road speed limits. Greater Manchester currently has an online map which shows road speed limits and route characteristics (Transport for Greater Manchester, 2023). Other strategies could focus on improving public transport in Glasgow such as investment in electric trams or widening of the subway network, to promote a reduction in private passenger cars. Glasgow's AQAP for NO_2 and PM_{10} AQMA in the city centre and for NO_2 in Byres Road/Dumbarton Road mentions some of the above measures such as promotion of active travel, increasing EV charging points and implementing low emission zones (Glasgow City Council, 2009). Other measures mentioned include reducing bus congestion and reducing taxi and private hires emissions (Glasgow City Council, 2009). This implies that road transport sources are already focused on in terms of policies and mitigation measures. The annual status report shows that a LEZ was implemented, with the second phase being implemented in June 2023, a cycling infrastructure project in underway, a bus partnership, retrofit scheme for taxis, more cycle racks and more electric charging points (Glasgow City Council, 2021). This shows that Glasgow City Council is making progress to reaching its goals in reducing air pollution emissions from transport emissions. Manchester's AQAP mentioned measures on introducing clean air zones, 20 mph roads, reduced taxi emissions, improved green infrastructure, freight measures, reducing bus emissions and improving cycling routes and infrastructure (Transport for Greater Manchester, 2016). Improvements have since been made to Manchester's cycling infrastructure and electric vehicle charging points, as well as preparatory steps towards reducing bus emissions (Transport for Greater Manchester, 2021).

Some limitations of the study include low time resolution of some measurements; for example, Glasgow samples were obtained from 3-weeks of sampling. However, Manchester samples were obtained from 2 days of sampling. This also limited the comparability of the measurements due to them being collected during different years, seasons, and timeframes. For Glasgow samples, the PAH and n-alkane analysis was not completed on samples from

GLA-CC and GLA-HH but rather GLA-KS meaning there is an assumption that GLA-KS represents such sites. Most of these aforementioned limitations of the study were largely caused by the limitations of the sampling equipment used as well as COVID-19 which meant the sampling had to be paused whilst the University was closed as restrictions were in place. This also led to a small number of $^{14}C(BC_{hypy})$ measurements due to the collection of fewer $PM_{2.5}$ samples than originally planned for the study. This meant the generalisability of the results is limited. Future work using this methodology should use a high-volume air sampler and split pooled filters for $^{14}C(TC)$, $^{14}C(BC_{hypy})$, PAH and n-alkane analysis as stated in the recommendations in Section 5.6.5. This will allow for comparability between measurements. Future work could include collecting $PM_{2.5}$ from various locations in the UK simultaneously and completing ^{14}C measurements to determine the variation in fossil/modern carbon sources (TC and BC_{hypy}). This could help monitor changes in anthropogenic sources across the UK over time hence determining the success of air pollution mitigation measures in AQAPs. Seasonal measurements should also be included to determine the seasonality of fossil/modern proportions. If the BC_{hypy} values are similar across the UK, chemical characterisation could be done to determine the emission sources for example K^+ and levoglucosan can be used for biomass burning. More research needs to be completed to determine markers for biodiesel to understand its contribution to the samples, as the BC in GLA-HH and MAN-FF were more modern than aerosol and dust standards with dominant vehicular emissions.

7. Conclusions and Future Work

7.1. Conclusions

7.1.1. BC hotspots and spatiotemporal variation in Glasgow

Spatiotemporal variation in BC was determined in Glasgow. BC increments showed spatial variation amongst the wards investigated exhibiting the following trend for 'mobile' measurements (BC_m) that were closer to the roadside:

City > Partick > Hillhead > Baillieston.

The city centre was a hotspot whilst Baillieston, a residential ward, on the outskirts of city, had the lowest BC increments. The population, population densities and socio-economic data could be used as valuable BC indicators to determine other BC hotspots in Glasgow and beyond.

Temporal variation was observed as mid-morning (10:30 – 11:30) median BC increments were higher than morning (08:00 – 09:00) median increments. BC_m increments were significantly different at a 0.05 level of significance. Absolute BC concentrations showed the opposite trend showing that background BC contributes highly to morning BC concentrations. This also showed that the use of BC increments over absolute BC concentrations can help improve understanding of local pollution events by removing background influences. Future monitoring studies should report both BC concentrations and increments and interpret increments to understand local air pollution. Moreover, the use of BC_m measurements is recommended as proximity to the road led to more consistent trends in spatiotemporal variation. Such measurements are more representative of local air quality and human exposure to BC. The use of microaethalometers to determine BC concentrations could be useful in epidemiological studies, as it has been shown here that they are able to register short but elevated exposures to air pollutants due to proximities to the source.

BC increments were correlated strongly with NOx concentrations and bus/HGV AADTs at the sampling sites. This showed that Glasgow City Council could focus local air quality measures towards reducing emissions from bus/HGV vehicles.

7.1.2. Health risks associated with inhalation of PM-bound PAHs

The health risks associated with samples collected in the hotspot Anderston/City/Yorkhill ward were determined. GLA-KS BaP concentrations exceeded the UK NAQO of 0.25 ng m^{-3} and were close to the FAQDD limit value of 1 ng m^{-3}. This implied that inhalation of $PM_{2.5}$ from GLA-KS could be associated with potential health effects such as lung. MAN-FF samples did not exceed the NAQO or FAQQD. This suggested that health risks in suburban areas had lower associated health risks than inner-city areas.

Toxicity equivalent factors (TEFi) were used to determine BaP toxicity (BaP_{Teq}) and mutagenicity (BaP_{Meq}) equivalents for PAH mixtures in PM. GLA-KS samples had lower BaP_{Teq} and BaP_{Meq} compared to those calculated from European cities. This could be due to differences in emissions sources and proportions of emissions. Alternatively, as samples did not represent business-as-usual scenarios due to the COVID-19 pandemic, this may have led to lower BaP_{Teq} and BaP_{Meq}. GLA-KS($PM_{2.5}$) had higher BaP_{Teq} and BaP_{Meq} GLA-KS(PM_{10}). Therefore, it is recommended that the UK PAH Network, which currently measures PAHs in PM_{10}, to measure PAHs solely in $PM_{2.5}$.

The increased lung cancer risk through inhalation ($ILCR_{inh}$) was calculated for PM-bound PAHs. The $ILCR_{inh}$ using the World Health Organization IUR_{Bap} value resulted in $ILCR_{inh}$ of 2.09 x 10^{-4} for GLA-KS($PM_{2.5}$) and 4.60 x 10^{-5} for GLA-KS(PM_{10}). This equated to 209 excess lung cancer cases per 1,000,000 people for $PM_{2.5}$ and 46 excess lung cancer cases per 1,000,000 people for PM_{10}. When applied to the Anderston, City and Yorkhill ward population this translated to 6 excess annual cases of lung cancer, assuming continuous and homogenous exposure of inhabitants. As actual $ILCR_{inh}$ could be higher due GLA-KS samples being collected during COVID-19 restrictions, the $ILCR_{inh}$ only representing outdoor pollution rather than indoor pollution, $ILCR_{inh}$ not being calculated for gaseous PAHs, oxy- and nitro- PAHs. This shows that health risks posed to those living in Anderston/City/Yorkhill ward is not negligible and should be improved through $PM_{2.5}$ reductions.

$ILCR_{inh}$ across different studies with sampling locations outside of the UK, showed that sampling site classifications generally had similar $ILCR_{inh}$ with MAN-FF fitting into the suburban site values and GLA-KS with the urban traffic sites. Whilst some sites did not follow the trends, the general trend observed was:

Urban traffic > Urban background > Suburban > Mixed sites.

This shows that health risks are correlated with traffic emissions.

7.1.3. Hypy Methodology

The hypy methodology was developed and tested on materials that represented potential sources of BC, as well as aerosol and dust materials. The BC/TC% values were determined for end members of BC showing BC could be determined in samples containing high and low BC contents. The ordering of the BC/TC% from lowest to highest was:

Charred biomass (DB) < Urban Aerosols < Road dust (BCR-RD) < Charred biomass (EB) < Diesel Soot (DS)

As all aerosol and road materials standards represented highly polluted environments, this was not an unexpected result. Hypy was able to distinguish between road dusts from highly polluted areas, BCR-RD, reporting higher BC/TC% values, and road dusts from less polluted areas (HH-RD), reporting lower BC/TC% values. These reported BC/TC% values can be used for quality assurance checks in any future studies using the hypy methodology for BC/TC% determination.

The BC results for NIST1649b standard were in agreement with those from other studies using hypy and other thermal methods. Hypy-derived BC/TC% values were consistently higher than those measured using aggressive oxidising conditions suggesting hypy has less measurement artefacts than other methods. The results assured that hypy could be used successfully to determine BC/TC% in airborne ambient PM.

A methodology for obtaining hypy-derived BC/TC% measurements from airborne ambient PM was developed in this project and can be used for future studies using hypy methodology for BC/TC% determination. The use of 47 mm filters rather than 150 mm filters is encouraged when collecting PM for hypy determination.

7.1.4. ^{14}C Measurements

TC ^{14}C and BC ^{14}C measurements for NIST 1649b were in agreement with those from other studies. TC ^{14}C measurements for sites in the UK showed fossil/modern proportions varied across the UK. The %MC followed this order:

AUC-MOS > LON-HON > CHI-OBS > MAN-FF > GLA-CC > GLA-HH

The variation between rural background sites (AUC-MOS and CHI-OBS) was smaller than that of urban background sites (LON-HO and MAN-FF) due to the sites' closer proximity to local emissions sources, which exhibit spatiotemporal variation. As samples were collected during COVID-19 they are not representative of business-as-usual scenarios. However, during COVID-19 restrictions Glasgow %MC were lowest compared to all UK sites.

%MC (BC_{hypy}) was determined for MAN-FF and GLA-HH sites. The results were 24.6 % and 24.1 % respectively. The BC_{hypy} values were similar despite being sampled from different locations at different dates. Moreover, the BC_{hypy} values had lower ^{14}C contents than the TC. This is likely due to the removal of natural 'modern' sources such as biogenic SOA. This shows that determination of sources in BC_{hypy} gives a better indication of anthropogenic sources that can be mitigated through policies and regulations. The BC_{hypy} had higher ^{14}C contents than aerosol and dust standards analysed. This suggests there is an increase in non-fossil combustion sources such as wood or biodiesel and a decrease in fossil fuel combustion sources.

Sources of Carbonaceous Components of Airborne Ambient PM

The fossil and modern sources in Glasgow were roughly equal as the %MC (TC) was 45 – 46 %. The GLA-HH %MC (BC_{hypy}) was 24 %. This suggested dominant fossil sources for BC, most likely from vehicular emissions. PAH and n-alkane sources were determined to be dominantly from fossil fuel combustion. The n-alkane distributions however showed epicuticular waxes with odd/even carbon preference from C_{25} to C_{33}. The contributions were thought to be from vegetative detritus in GLA-KS samples. The PAHs showed diesel sources in one GLA-KS(PM_{10}) sample (4043) and GLA-KS($PM_{2.5}$). This was unsurprising considering the fleet composition had a high contribution from buses, with the older buses using diesel fuel. Moreover, the site is in close proximity to a large train station, Glasgow

Central, where diesel is used to power trains. However, there was a modern element to GLA-HH BC_{hypy} suggesting biomass combustion sources. These were thought to be from biodiesel and industrial/domestic combustion of wood.

The modern sources were more prominent in MAN-FF with %MC (TC) range of 39 – 74 % (average 62 %) and %MC (BC_{hypy}) range of 20 – 25 % (average 23 %). This could be attributed to site characteristics as MAN-FF was a suburban site, surrounded by greenery, hence likely to have a larger contribution of biogenic SOA. Moreover, MAN-FF samples back trajectories showed air masses originated from Scotland/northern regions of UK, which consists of cleaner air with lower fossil contribution, hence a higher %MC (TC), in $PM_{2.5.}$ The dominant PAH and n-alkane sources were combustion sources likely from vehicular traffic. Examination of PAH profiles and ring-size distributions showed that petrol emissions were present due to high proportions of BghiP. Diesel emissions also seemed probable as PHEN & ANTH were present, indicating HGV diesel vehicles. The n-alkane data showed epicuticular waxes with odd/even carbon preference from C_{29} to $C_{33,}$ indicating biomass combustion sources.

The PCA results for PAHs and n-alkanes in GLA-KS and MAN-FF samples showed 79.6 % of the PAHs and n-alkanes could be attributed to principal component 1 (PC 1) which was interpreted to be diesel vehicle and biomass combustion emissions. The 20.1 % to principal component 2 (PC 2) was thought to be from indirect (resuspended road dust) and direct petrol vehicular emissions and/or resuspended dusts. PC 1 explained the higher ^{14}C contents in the BC_{hypy} of GLA-HH and MAN-FF. Another possibility is that PC 1 reflects a combination of diesel, biodiesel and wood-burning, as a study found biodiesel in buses emitted 3-ring PAHs such as PHEN and ANTH like DS and wood combustion. The PCA confirmed the deviation in sources between OC and BC.

A previous UK study that collected $PM_{2.5}$ in Birmingham in 2008 found the %MC (TC) to be between 27 – 66 %, with a mean of 50 % (Heal et al., 2011). As expected, the ^{14}C(TC) measurements were higher here with MAN-FF %MC (TC) average of 62 % close to the maximum of the range and GLA-CC and GLA-HH samples %MC (TC) values of 45 – 46 %, typically in the middle of the range of Heal et al. (2011). The mean %MC (BC) from Heal et al. (2011) was 11 % which was much lower than the %MC (BC_{hypy}) of GLA-HH and MAN-FF (Heal et al., 2011). This shows that over time the proportion of fossil contributions to BC have decreased as vehicle emissions have decreased, but biomass combustion sources have increased.

7.2. Future work

7.2.1. Health risks associated inhalation to PM-bound PAHs

The use of BaP equivalent toxicity and mutagenicity and the increased lung cancer risk through inhalation could be used to determine the differences in health risks in different wards of Glasgow. The PAH analysis could include gaseous, nitro- and oxy- PAHs. This could help develop tailored air quality management plans based on the health risks associated with air pollution rather than concentration data.

As hypy removes semi-labile organics from PM, these hypy-extracted PAHs could be used to determine the health effects associated with the inhalation of BC. Toxicological experiments could be conducted on the non-BC_{hypy} as well as the BC_{hypy} to determine which fraction is more toxic to human health.

7.2.2. Sources of Carbonaceous Components of Airborne Ambient PM

The $^{14}C(TC)$ and $^{14}C(BC_{hypy})$ measurements in this thesis could be repeated to determine inter-site variability in fossil versus modern proportions across the UK incorporating sites with different classifications such as urban traffic, urban background, and urban industrial. As the work here was undertaken on samples collected during COVID-19 restrictions, the normal fossil and modern proportions were not realised. Routine measurements could monitor the sources of BC more closely and better inform local and national policies. Samples should be collected simultaneously to allow for direct comparisons.

Appendices

Appendix I.

Appendix Ia. Charcoal and wood smoke sample details and grouping details.

BECS Sample ID	Filter ID	Household ID	Area	Date	Start	End	Device	Mean Flow Rate (L min^{-1})	Fuel	Stove Type
4058	1Q	HH1	Kitchen	08/05/2019	11:15:00	13:37:00	SKC Touch	1.25	Firewood	3-stone
	2Q	HH1	Kitchen	09/05/2019	11:00:00	12:39:00	SKC Touch	1.10	Firewood	3-stone
	5Q	HH3	House	15/05/2019	11:14:00	12:57:00	SKC Touch	0.95	Firewood	3-stone
	6Q	HH3	House	16/05/2019	10:30:00	12:27:00	SKC AirLit	1.00	Firewood	3-stone
	7Q	HH3	House	16/05/2019	12:27:00	12:53:00	SKC AirLit	1.01	Firewood	3-stone
	12Q	HH7	House	06/06/2019	11:05:49	12:40:45	SKC Touch	1.01	Firewood	Improved
	14Q	HH10	Kitchen	19/06/2019	11:11:22	12:09:27	SKC Touch	1.00	Firewood	Improved
4059	11Q	HH5	Khondi	30/05/2019	10:42:32	12:32:20	SKC Touch	0.99	Firewood	3-stone
	13Q	HH8	Outside	11/06/2019	09:34:00	12:48:00	SKC AirLit	1.00	Firewood	3-stone
	15Q	HH11	Khondi	20/06/2019	12:02:00	13:11:00	SKC AirLit	0.97	Firewood	Improved
	16Q	HH12	Outside	24/06/2019	11:56:00	13:41:00	SKC AirLit	1.01	Firewood	Improved
	17Q	HH12	Outside	25/06/2019	10:31:00	12:26:00	SKC AirLit	0.97	Firewood	Improved
4060	3Q	HH2	Kitchen	13/05/2019	10:46:00	12:53:00	SKC Touch	0.97	Charcoal	Mbaula
	4Q	HH2	Kitchen	14/05/2019	10:39:00	12:50:00	SKC Touch	1.00	Charcoal	Mbaula
	8Q	HH4	House	27/06/2019	12:42:29	13:11:09	SKC Touch	0.96	Charcoal	Mbaula
	9Q	HH4	House	28/05/2019	11:01:24	12:35:12	SKC Touch	1.02	Charcoal	Mbaula
	10Q	HH4	House	29/05/2019	08:39:00	09:54:00	SKC AirLit	1.01	Charcoal	Mbaula

Appendix Ib. Method Development

To undertake PAH analysis in known-source materials, airborne ambient PM and their non-BC_{hypy} with organic compounds adsorbed onto silica, certain method development steps were required.

Sample Preparation – Extraction and Clean-Up Methods

There is a plethora of extraction and clean-up methods in the literature for PAH analysis using GC-MS, as illustrated in Table 1, however the literature is particularly limited on extraction for non-BC_{hypy} starting materials. Within the literature, the extraction and clean-up methods for non-BC_{hypy} tend to be more simplistic than those for environmental matrices that have not undergone hypy beforehand (Brocks et al., 2003; Meredith et al., 2013; Sephton et al., 2005). This could be due to hypy being considered as an extraction method in itself, as it separates labile organic matter from a solid environmental matrix, through the cleaving weak bonds. Therefore, the use of less intensive extraction methods could be deployed post-hypy. Within this project, known-source materials and airborne ambient PMs undergo PAH analysis before hypy and after hypy, therefore, to enable meaningful comparisons between the two conditions, it was critical to adopt a consistent sample preparation method for both conditions. Two suitable sample preparation methods for PAH analysis, that were not previously used on non-BC_{hypy} samples, were identified in Toney et al. (2010) and Coyle 2015.

The sample preparation method in Toney et al. (2010), referred to as method 1, is used as the standard operating procedure within the BECS organic geochemistry laboratory. The method has been used for PAH analysis in sediments in Denis et al. (2012). The sample preparation method used in Coyle 2015, referred to as method 2, was adapted from the Scottish Environment Protection Agency (SEPA) standard method for PAH analysis in soils and sediments. The method was adapted to use ASE instead of Soxhlet for extraction of organic compounds, to improve sample throughput. The method was then used to analyse PAH sediments from Luce Bay in Dumfries and Galloway, with the results being published in the form of a dissertation.

A quantitative comparison of the PAHs extracted using sample preparation methods by Toney et al. (2010) and Coyle 2015 was conducted to choose the most suitable method. The differences in the sample preparation methods can be seen in Table 1. Results were also

compared to a commonly used sample preparation method for non-BC_{hypy} samples, referred to as method 3, mentioned in Meredith et al. (2013) in Table 1. This was used as a control, to compare the results to.

The analysis was conducted on the non-BC_{hypy} of BZ. BZ was used as an in-house standard, chosen specifically because it was readily available in large quantities and known to have a high quantity of PAHs in the non-BC_{hypy}, due to previous hydropyrolysis work conducted on this material by Meredith et al. (2012). This was advantageous as it would ensure the PAHs would be above the LOD and LOQ enabling quantitative comparisons between the different methods. Furthermore, it allowed for qualitative comparisons between the GC-MS chromatograms and spectra from the previous work and from this experiment.

The method used to prepare and run the BZ are mentioned in Chapter 3. Approximately 100 mg of catalyst-loaded BZ was used per insert. The BZ inserts were run separately in the reactor and not combined. This was to ensure that the non-BC_{hypy} of each sample was not combined, hence allowing comparisons between the PAH results from each sample preparation method. The ASE cell was filled with the BZ non-BC_{hypy} adsorbed onto silica and filled with combusted sand. The following ASE conditions were used for SEPA method (Table 3) and BECS method (Table 3). The sample preparation method in Meredith et al. (2012) did not utilise ASE so the silica gel was poured straight into a column. Three replicates were completed per method.

The sample preparation methods PAH yields were compared as higher PAH yield would be beneficial as the method would be used on airborne ambient PM, which generally will have lower PAH concentrations than BZ. Therefore, the method with higher yields is more likely to ensure quantification of PAHs from airborne ambient PM before and after hypy. Moreover, the sample preparation method that exhibits better precision, will be more reproducible and consistent method overtime, hence will allow for meaningful comparisons to be made between conditions.

Table 1. Details of extraction and clean-up methods used for PAH analysis using GC-MS.

Author	Sample Matrix	Extraction Technique Used	Column Materials	Solvents used to Elute Target Analytes	Additional Details/Steps
Alves et al. (2017)	$PM_{2.5}$ on quartz microfibre filter	ASE 1. DCM 2. Acetone and DCM (2:1 v/v)	Silica gel (10 % deactivated)	-Hexane:DCM (15 ml) 5:1 v/v for PAHs - DCM (8 ml) then acetone (5ml) for NPAHs, OPAHs, AZAs	Three drops of toluene added to each fraction
Yagoh et al. (2006)	Activated-carbon fibre filter paper with PAHs adsorbed onto it	ASE 1. Toluene	Silica solid-phase extraction (SPE) cartridges	DCM (10 ml)	Acetone solution (2 uL) containing 0.5 % polyethylene glycol added to eluent
Wei et al. (2019)	$PM_{2.5}$ sampling filter on quartz fibre filter	ASE 1. Acetone and DCM (1:1 v/v)	Sodium sulphate, silica gel and alumina	- Hexane (15 ml) - Hexane:DCM (3:7 v/v, 70 ml)	Add 0.5 g copper powders and 2 g diatomite to ASE
Rombolà et al. (2016)	Biochar from pine wood, beech wood and corn digestate	Soxhlet Acetone and cyclohexane (1:1 v/v)	Solid phase extraction with silica cartridge	- Hexane/DCM (1:1 v/v, 10 ml)	Used on non-$BC_{hypy.}$ n-nonane (1 ml) added to prevent the extraction solution being reduced to dryness with loss of analytes
Grotheer et al. (2015)	PAH standard adsorbed to silica	DCM (40 ml)	-	-	Used on non-$BC_{hypy.}$ HCl-activated copper turnings were added to remove sulphur
Brocks et al. (2003)	Non-BC_{hypy} of kerogens	DCM and methanol (4:1 v/v)	-	-	Used on non-$BC_{hypy.}$ HCl-activated copper turnings were

					added to remove sulphur
Sephton et al. (2005)	Non-BC_{hypy} of meteorites	DCM	-	-	Used on non-$BC_{hypy.}$ HCl-activated copper turnings were added to remove sulphur
Meredith et al. (2013)	Non-BC_{hypy} of soil	n-hexane (10 mL) and DCM (10 mL), then eluents were combined	-	-	Evaporated to 1 mL under nitrogen at room temperature
Toney et al. (2010)	Sediments	ASE DCM and Methanol (9:1 v/v)	Two columns, one to separate out acid and neutral fraction, second for the neutral fraction 1. **L**C-NH_2-SPE 2. Silica gel	1. DCM:isopropyl alcohol (2:1 v/v) followed by ether with 4 % acetic acid (v/v) 2. for alkanes n-hexane, alkenones DCM, alcohol ethyl acetate:n-hexane (1:3 v/v), polar methanol.	To remove alkenoates, alkenone fractions were saponified in 5 % KOH in methanol with 3 % water and heated overnight at 75 °C, acidified and extracted using n-hexane.
Coyle 2015	Sediments	ASE 1. Hexane: Acetone (2:1 v/v)	Silica gel	- Hexane:DCM (2:1, 1:1 v/v, 6 ml)	The column was topped with sodium sulphate and HCl-activated copper turnings to remove water content and sulphur

Table 2. A description of the preparation methods used.

	Toney et al. (2010)	Coyle (2015)	Meredith et al. (2012)
Sample Matrix Method is Usually Used For	Sediments/lake sediments	Soils and sediments	Non-BC_{hypy} from a range of environmental matrices
Sample Analysed	Non-BC_{hypy} of BZ (adsorbed to silica gel)	Non-BC_{hypy} of BZ (adsorbed to silica gel)	Non-BC_{hypy} of BZ (adsorbed to silica gel)
Solvents used in ASE Process	2: 1 DCM, Methanol	2: 1 Hexane, Acetone	-
Solvents for n-Alkane Elution	Hexane (4 mL)	Hexane (6 mL)	Hexane (15 mL)
Solvents Used for Aromatic Elution	DCM (4 mL)	2:1 Hexane/DCM (6 mL)	3:2 Hexane, DCM (15 mL)
Additional Details	Combusted sand placed on the top of columns.	Activated copper turnings and sodium sulphate placed at the tops of columns to remove sulphur containing compounds and alkenes.	The column consists solely of the non-BC_{hypy} extract adsorbed onto silica gel, and the solvents wash through the column to elute compounds.

Table 3. The ASE conditions used for preparation method 1 and 2.

	Toney et al. (2010)	Coyle (2015)
Solvent	DCM: Methanol 9:1	Hexane: Acetone 2:1
System Pressure	14 MPa (1500 psi)	14 MPa (1500 psi)
Oven Temperature	120 °C	100 °C
Oven Heat-up Time	6 minutes	5 minutes
Static Time	5 minutes	5 minutes
Rinse Volume	60 % cell volume	60 % cell volume
Nitrogen purge	1 MPa (150 psi) for 100 seconds	1 MPa (150 psi) for 60 seconds
Number of Cycles	2	2

GC-MS Instrument Conditions

The details of the GC-MS were run in SCAN mode, as the SIM method was not yet made.

Table 4. The GC-MS instrument conditions used for this experiment.

Washes and Injection Volume	
Solvent A (TMP) Wash	Pre-injection = 3 Post injection = 6
Solvent B (MeOH) Wash	Pre-injection = 3 Post injection = 6
Injection volume	1 µL
Inlet	
Mode	Split-less
Temperature	300 °C
Pressure	33.6 psi
Purge Flow	3 mL/min
Total Flow	55.3 mL/min
Gas Saver	On
Column	
Flow	2.3 mL/min
Pressure	33.6 psi
Average Velocity	39 cm/second
Oven Temperature Programme	
55 °C, 10 minutes initial	
55 °C - 180 °C at 10 °C/min	
Hold at 180 °C for 10 minutes	
180 °C – 320 °C at 30 °C/min	
Hold at 320 °C for 10 minutes	
MS Settings	
Transfer Line Heater	320 °C
MS Source	230 °C
MS Quad	150 °C
Solvent Cut Time	6 minutes

Data Analysis

Calibration curves were produced. Co-elution occurred for BaA & CHR and BbF & BkF, thus a combined calibration curve was made for the co-eluting PAHs.

The PAHs were identified by matching the retention times of each peak in the sample's chromatogram to those within a 16 priority PAH certified reference material (Supelco, 10 µg/mL acetonitrile). The external standard method was used for PAH quantification using standard mixtures of 1.0, 2.0, 4.0, 6.0, 8.0 and 10.0 µg mL^{-1} per PAH.

Results and Discussion

The average concentrations were calculated per PAH from the three replicates per method, alongside the relative standard deviation (Table 5). Table 5 shows the concentrations of PAHs per replicate.

Table 5. The average concentration and standard deviation per 16 PAHs (n=3), for each sample preparation method.

	Average PAH Concentrations (µg/g)					
	Sample Preparation Method 1		Sample Preparation Method 2		Sample Preparation Method 3	
	Average	RSD %	Average	RSD %	Average	RSD %
NAPH	-	-	-	-	-	-
ACE	-	-	-	-	26 ± 11	41
ACY	-	-	-	-	-	-
FLU	18 ± 9	47	12 ± 0	2	14 ± 11	77
PHEN	10 ± 4	35	10 ± 1	6	24 ± 3	11
ANTH	16 ± 6	37	12 ± 1	9	14 ± 1	6
FLA	45 ± 13	28	15 ± 3	20	23 ± 3	12
PYR	29 ± 9	31	14 ± 2	14	33 ± 3	8
BaA & CHR	141 ± 25	18	132 ± 30	22	68 ± 10	15
BbF & BkF	81 ± 19	23	92 ± 19	20	40 ± 6	14
BaP	54 ± 14	25	19 ± 5	25	28 ± 4	16
DahA	174 ± 65	37	222 ± 49	22	145 ± 7	5
IcdP	261 ± 72	28	351 ± 81	23	188 ± 6	3
BghiP	216 ± 56	26	267 ± 90	34	106 ± 6	6

Table 6. The concentrations of the 16 priority PAHs calculated for each sample preparation technique. Each sample preparation technique had three replicates, to assess the repeatability of each technique.

	PAH Concentrations (µg/g)								
	Sample Preparation Technique 1			Sample Preparation Technique 2			Sample Preparation Technique 3		
	Replicate 1	Replicate 2	Replicate 3	Replicate 1	Replicate 2	Replicate 3	Replicate 1	Replicate 2	Replicate 3
NAPH	-	-	-	-	-	-	-	-	-
ACE	-	-	-	-	-	-	37	-	15
ACY	-	-	-	-	-	-	-	-	-
FLU	31	13	12	12	12	12	29	8	5
PHEN	15	7	8	10	9	11	27	24	21
ANTH	25	13	12	12	10	12	14	15	13
FLA	61	45	30	13	19	12	26	20	21
PYR	42	23	23	11	16	13	37	32	31
BaA & CHR	151	166	106	91	149	157	80	66	56
BbF & BkF	89	99	55	72	88	117	48	37	36
BaP	65	61	35	21	24	12	32	22	30
DahA	264	145	114	224	161	280	144	154	138
IcdP	343	270	168	351	252	450	196	187	182
BghiP	260	251	138	284	150	367	102	115	101

The results indicated that sample preparation method in Toney et al. (2010) yielded the highest average concentration for 6 PAHs (FLU, ANTH, FLA, BaA, CHR, and BaP). The sample preparation method in Coyle (2015) had the highest average concentration for five HMW PAHs (DahA, IcdP, BbF, BkF and BghiP). The Meredith et al. (2012) method had the highest concentration for three PAHs (ACY, PHEN and PYR). ACY was only detected in one out of three replicates.

The relative standard deviations for the total PAH concentrations were 31 % for method 1, 24 % for method 2 and 7 % for method 3. The variability of each sample preparation method could be explained by the number of processing steps. Method 1 had an extra column clean-up step to separate total acid and total neutral fractions, whilst method 2 did not include this step and method 3 had the least processing steps. This suggests that the use of ASE and/or its subsequent preparation steps such as evaporating the solvent from the TLE with nitrogen, may lead to a loss in analytes either through degradation or volatilisation. As a result, method 3 had the best repeatability.

The PAH distributions per sample preparation method are shown in Figure 1. A non-parametric Friedman statistical test was conducted to determine if there was a significant different between the conditions. There was not a statistically significant difference in PAH concentrations depending on which type sample preparation method was used , $\chi^2(2) = 2.21$, $p = 0.332$. The ring-size distributions were similar across each method except for method 3 which had a higher proportion of LMW PAHs, whilst method 2 seemed to have a higher proportion of HMW PAHs.

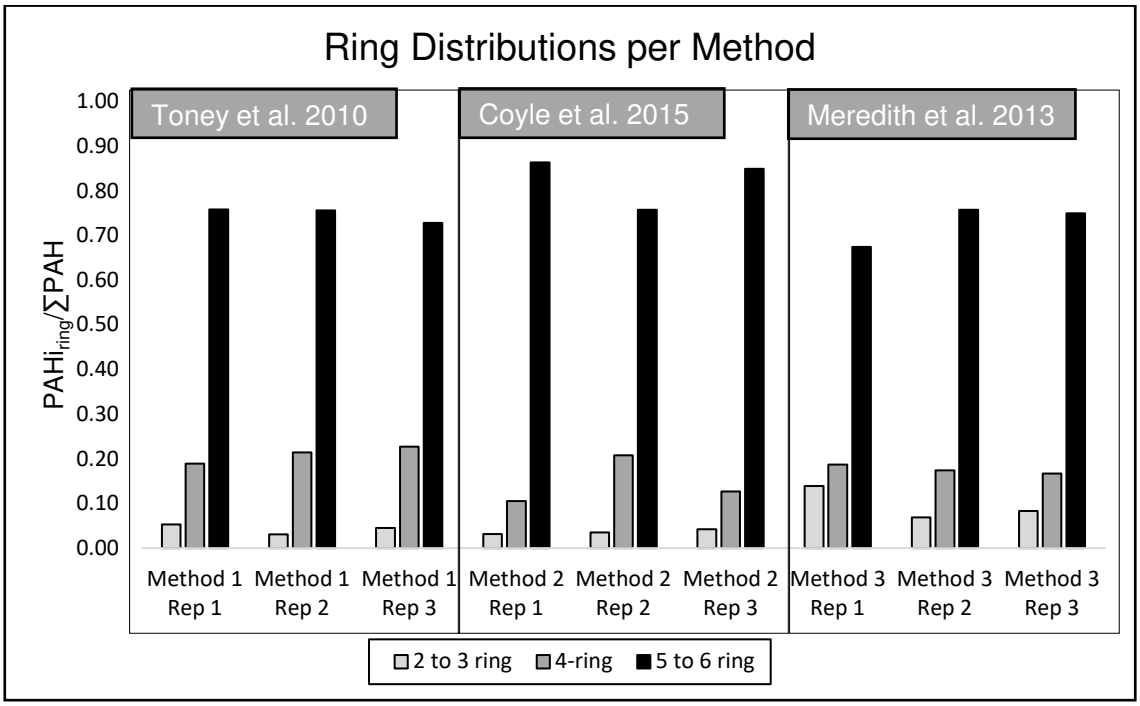

Figure 1. The PAH ring size distributions per replicate per method by dividing the individual PAH (PAH$_i$) present in per ring size category by the total concentration of PAHs.

A qualitative comparison of chromatograms from replicate 1 of method 1, 2 and 3 was conducted by overlaying chromatograms as seen in figure 2. The peak distributions seem similar across different methods. However, method 3 seemed to have larger peaks from 12 – 18 minutes in the chromatogram of replicate 1. The chromatogram from previous research in Meredith et al. (2012) can be seen in figure 3. The LMW PAHs seem to have tall peaks as in the chromatogram for method 3, with smaller peaks for the HMW PAHs.

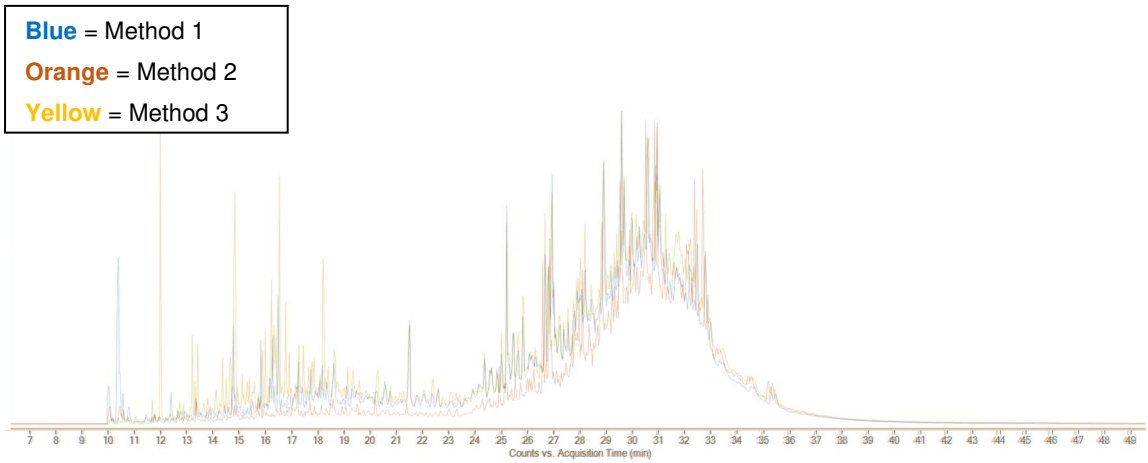

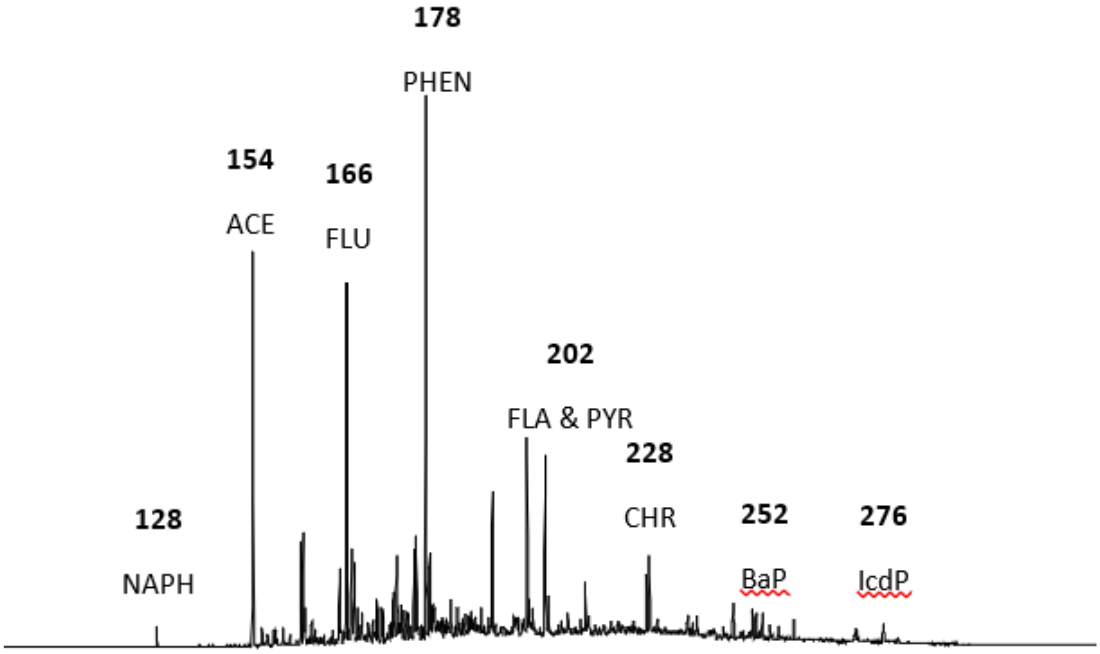

Figure 3. Chromatograms from BZ runs by Meredith et al. 2012.

The PAHs which had the lowest concentrations were LMW PAHs. Some PAHs such as NAPH, ACY and ACE were undetected in almost every run per preparation method. Chimjarn et al. (2021) investigated PAHs in Strasbourg, France and found LMW PAHs (2-ring and 3-ring) and moderate molecular weight (MMW) (4-ring) PAHs contribute dominantly to the gas phase, while the particulate phase is associated with MMW (4-ring) and high molecular weight (HMW) (5-6 ring) PAHs (Chimjarn et al., 2021). This could explain why the concentrations for LMW PAHs were below the LOD, and why HMW PAHs had higher concentrations. The concentrations of LMW PAHs in method 3 were higher than method 1 and 2. Method 3 did not undergo ASE or clean-up steps. Therefore, the LMW PAHs could have been lost during extraction and column-clean up steps. Drying steps within this process could cause evaporation of LMW PAHs.

HMW PAHs tend to have higher associated health risks such as carcinogenicity and acute toxicity to human health (Huang et al., 2019; Zhang et al., 2016). According to the carcinogenicity classifications verified by the EPA Carcinogenicity Risk Assessment Endeavor Work Group which shows that BaA, BbF, BkF, BaP, CHRY and DahA are considered to be probable human carcinogens whereas ACY, ANTH, BghiP, FLU, PHEN, PYR and FLA are not classified to pose the same health risk (EPA 1994). Part of the project

is most concerned with the health risks of PAHs. Additionally, HMW PAHs are more closely linked to BC. Hence sample preparation methods that have high HMW yields are more important than LMW PAHs, which are less crucial.

There was no significant statistical differences between the sample preparation methods therefore all methods were suitable. As HMW PAHs were of interest, due to the health risks associated to the inhalation of PM-bound HMW PAHs, method 2 was chosen, as it yielded higher concentrations of HMW PAHs.

Limitations

Some calibration curves had R^2 values below 0.9, such as PYR, BaA & CHRY, BbF & BkF,, BaP, IcdP and DahA. However, absolute concentrations were not of interest here, rather semi-quantitative comparisons between three different sample preparation methods, therefore the conclusions were still valid. The comparisons between sample preparation methods would have been more useful if applied to both airborne ambient PM filter samples and non-BC_{hypy} of airborne ambient PM. However, when the experiment was conducted, aerosol sampling had not commenced. Moreover, due to financial constraints PM filter standards could not be purchased. Archived filter samples from Auchencorth Moss were obtained from NPL (Teddington, UK). However, during a test run where two filters underwent PAH analysis using GC-MS, the concentrations were below the LOD. Additionally, the methodology for hypy of airborne ambient PM filters was not yet developed to run them on hypy and analyse the non-BC_{hypy} in the sample preparation method comparisons.

Conclusions

To summarise the PAH concentrations from the three sample preparation methods were comparable, with no statistically significant differences at 95 % confidence limits. The repeatability in total PAH concentration across different methods was at an acceptable level for all methods (method 1 – 31 %, method 2 – 24 %, method 3 – 7 %). The higher RSD% for method 1 could be attributed to the extra column step in the method. The PAH ring size distributions varied per method. Method 1 seemed to have a higher proportion of MMW PAHS, method 2 had a higher proportion of HMW PAHs and method 3 a higher proportion

of LMW PAHs. Sample preparation method 2 was chosen the higher proportion of HMW PAHs, which are of interest in this project due to the health risks associated with inhalation of PM-bound HMW PAHs.

Appendix Ic. Instrument Conditions

GC-MS Conditions

1. Front Injector

1.1. Injection

	Volume
Syringe Size	10 µL
Injection Volume	1 µL

1.2. Sample Depth

Enabled to 5 mm

1.3. Injection Type

Standard – L1 air gap 0.2 µL

2. Inlet

Liner used:

	Set Point	Actual
Heater	300 °C	298.5 °C
Pressure	24.261 psi	24.3 psi
Total Flow	54.2 mL min^{-1}	54.2 mL min^{-1}
Septum Purge Flow	3 mL min^{-1}	3 mL min^{-1}
Mode	Standard	

Splitless Mode – Purge Flow to Split Vent 50 mL min^{-1} at 0.75 min

3. Columns

HP1-MS column (60 m x 250 µM x 0.25 µM), operational temperature range -60 °C – 325 °C (Agilent, USA).

Control mode was on and set to constant flow.

	Set Point	Actual
Flow	1.2 mL min^{-1}	1.2 mL min^{-1}
Pressure	24.261 psi	23 psi
Average Velocity	22.505 cm sec^{-1}	
Holdup Time	4.4436 min	

4. Oven

Oven temperature was set to 55 °C with a maximum oven temperature of 325 °C. The equilirbation time was 0.5 min.

4.1. Oven Temperature Programme

	Rate (°C Min^{-1})	Value (°C)	Hold Time (Min)	Run Time (Min)
Initial		55	1.000	1.00
Ramp 1	10	180	10.00	23.5
Ramp 2	30	320	21.83	50.0

4.2. Aux Heaters

Thermal Aux 2 MSD Transfer line set to 320 °C (actual temperature 320.4 °C).

5. Events

5.1. Deans Switch

A phthalate contaminant peak was present in samples thus the method was adapted to turn on the valves at a particular retention time, so the contaminant did not reach the detector and affect the ion source.

Time (min)	Event Type	Position	Set Point
0	Valve	Valve 1	On
10	Valve	Valve 1	Off
31.7	Valve	Valve 1	On
33.3	Valve	Valve 1	Off
49	Valve	Valve 1	On

5.2. Tuning

Tune Type: EI
Tune EMV: 1603

5.3. Ion Source

	Actual (°C)	Set Point (°C)
MS Source	230	230
MS Quad	160	160

Solvent Delay: 10 min

5.4. Detector Setting

EM Setting	Gain Factor
Gain Factor	1.00
Applied Voltage	1478

5.5. Selected Ion Monitoring Mode Method

Time (min)	Group Name	Number of Ions	Total Dwell Time (ms)	Cycle time (Hz)	Resolution	Calculated EMV
10	Naphthalene – 2-methyl naphthalene	4	200	4.4937	High	1478
17	Acenapthene – Pyrene	9	450	2.0971	High	1478
30.20	Remaining PAHs	7	350	2.6584	High	1478

PAH	**m/z**	**Dwell Time (min)**
Naphthalene	127	50
	128	50
2-Methylnaphthalene	141	50
	142	50
Acenaphthylene	152	50
Acenapthene	153	50
	154	50
Fluorene	165	50
	166	50
	178	50

Phenanthrene and Anthracene	179	50
Fluoranthene and Pyrene	202	50
	203	50
Benz[a]anthracene and Chrysene	228	50
	226	50
Benzo[b]fluoranthene and Benzo[k]fluoranthene	252	50
	126	50
Benzo[a]pyrene	252	50
Dibenz[a,h]anthracene	278	50
Indeno[1,2,3-c,d]pyrene	276	50
	138	50
Benzo[g,h,i]perylene	276	50
	138	50

GC-FID Conditions

1. Front Injector

1.1. Injection

	Volume
Syringe Size	10 µL
Injection Volume	1 µL

1.2. Sample Depth

Enabled to 5 mm

1.3. Injection Type

Standard – L1 air gap 0.2 µL

2. Inlet

Liner used:

	Set Point	Actual
Heater	320 °C	320 °C
Pressure	13.38 psi	13.40 psi

Total Flow	54.2 mL min^{-1}	54.2 mL min^{-1}
Septum Purge Flow	3 mL min^{-1}	3 mL min^{-1}
Mode	Standard	

Splitless Mode – Purge Flow to Split Vent 50 mL min^{-1} at 0.75 min

3. Columns

RTX-1 column (60 m x 250 µM x 0.25 µM), operational temperature range 0 °C – 325 °C (Restek, USA).

Control mode was on and set to constant flow.

	Set Point	Actual
Flow	1.2 mL min^{-1}	1.2 mL min^{-1}
Pressure	13.38 psi	13.40 psi
Average Velocity	30.418 cm sec^{-1}	
Holdup Time	3.2875 min	

4. Oven

Oven temperature was set to 60 °C with a maximum oven temperature of 350 °C. The equilirbation time was 3.0 minutes.

4.1. Oven Temperature Programme

	Rate (°C Min^{-1})	Value (°C)	Hold Time (Min)	Run Time (Min)
Initial		60	2	2
Ramp 1	30	120	0	4
Ramp 2	5	330	15	61

Post-Run: 50 °C

5. Detectors

Flame Ionisation Detector		
	Set-Point	Actual
Heater	250 °C	250 °C
Air Flow	400 mL min^{-1}	400 mL min^{-1}

H_2 Air Flow	40 mL min^{-1}	40 mL min^{-1}
Makeup Flow	25 mL min^{-1}	25 mL min^{-1}
Carrier Gas Correction		
Column Flow: H_2 Constant makeup and fuel flow	1.2 mL min^{-1}	1.2 mL min^{-1}
Flame	-	8.1 Pa

Appendix Id. PAH and n-Alkane Linear Regression Equations

Table 1. PAH calibration curve equations and R^2. Where the internal standard was not used a * is designated by the sample batch range.

Sample Batch Range		NAPH	ACY	ACE	FLU	PHEN	ANTH	FLA	PYR	BaA	CHRY	BbF	BkF	BaP	DahA	IcdP	BghiP
3983 - 3992	m	0.8755	0.9412	1.3292	1.0894	0.9961	0.9047	1.052	1.1052	0.8773	1.0164	0.817	1.0778	0.8815	0.7491	1.263	1.0159
	c																
	R^2	0.9997	0.9996	0.9998	0.9996	0.9985	0.9988	0.9987	0.9986	0.9969	0.9971	0.9984	0.9966	0.9973	0.9959	0.9969	0.9971
	Vol. (mL)																
3998 - 4001	m	0.8446	0.9525	1.3293	1.0651	0.9987	0.9081	1.0486	1.1108	0.9117	1.0031	0.8215	1.1065	0.8761	0.7434	1.2447	1.0113
	c																
	R^2	0.9973	0.9998	0.9999	0.9985	0.9983	0.9986	0.9983	0.9984	0.9968	0.9965	0.9983	0.9964	0.9977	0.9951	0.9974	0.9977
	Vol. (mL)																
4003 - 4010	m	0.7801	0.7016	1.144	0.9623	0.939	0.8318	1.0463	1.0955	0.9181	1.1522	0.877	1.2412	0.9411	0.9589	1.447	1.1443
	c																
	R^2	0.9954	0.9986	0.9997	0.9981	0.9951	0.9975	0.9967	0.997	0.9904	0.9974	0.9907	0.9961	0.988	0.994	0.9938	0.9916
	Vol. (mL)																
4011 - 4019	m	0.7948	0.7068	1.1308	0.9221	0.9953	0.9112	1.0342	1.0664	0.8359	0.8449	0.4177	0.5714	0.3478	0.1339	0.2104	0.1771
	c									-0.1278		-0.074	-0.0812	-0.054			
	R^2	0.9981	0.9956	0.9992	0.9975	0.9955	0.9967	0.9964	0.9968	0.9941	0.9875	0.9861	0.9947	0.9946	0.99	0.9896	0.991
	Vol. (mL)																
	m	0.9262	0.6792	1.3575	1.0118	1.0094	0.9504	1.2449	1.3604	0.8044	1.4459	0.83	1.4885	0.9076	1.0383	1.5867	1.2649

4068 - 4072, 4077 not inc. 4073-4076	**c**																
	R^2	0.9952	0.9873	0.9992	0.9994	0.9972	0.996	0.9962	0.9931	0.9857	0.9894	0.9844	0.9909	0.9924	0.9935	0.9931	0.9942
	Vol. (mL)																
4073-4076, 4078-4089 inc. 4073-4076	**m**	1.0191	0.7719	1.3	1.0052	0.8151	0.8982	1.0238	1.1071	0.6732	1.1289	0.655	1.3062	0.8403	0.7867	1.2716	0.9547
	c																
	R^2	0.999	0.9962	0.9996	0.9968	0.9813	0.9946	0.9916	0.9941	0.9809	0.9936	0.9816	0.9975	0.9933	0.9937	0.9949	0.9925
	Vol. (mL)	7.5															
4028-4036, 4058-4060 *	**m**	147224	139985	213686	170313	147401	131083	161090	169504	127188	186320	112561	193837	143207	137640	228604	171099
	c																
	R^2	0.9808	0.9987	0.9944	0.9961	0.9988	0.9976	0.9981	0.998	0.99	0.9954	0.9912	0.999	0.9946	0.9968	0.9973	0.9975
	Vol. (mL)																
4141-4147	**m**	0.9311	0.8546	1.3463	1.0637	0.9168	0.8022	1.0169	1.0721	0.7671	1.2029	0.6687	1.2076	0.8782	0.8598	1.4296	1.0698
	c																
	R^2	0.999	0.9861	0.9962	0.9948	0.9835	0.9726	0.9812	0.9828	0.9499	0.9884	0.9546	0.9855	0.9611	0.9699	0.9725	0.9733
	Vol. (mL)																
4063 - 4067	**m**	0.9492	0.8195	1.2276	1.0138	0.7136	0.7317	0.8186	0.8962	0.598	0.8205	0.5391	0.9198	0.7081	0.6411	1.1173	0.8061
	c																
	R^2	0.9974	0.9949	0.9921	0.9963	0.9942	0.997	0.9965	0.9981	0.9969	0.9979	0.9904	0.9995	0.9991	0.9969	0.997	0.9945
	Vol. (mL)																
4038 – 4043 *	**m**	247652	223215	327878	248549	232233	241049	301925	291207	217990	290840	206490	316648	242320	227019	375267	280035
	c																
	R^2	0.9878	0.9716	0.9789	0.9641	0.9648	0.9825	0.9592	0.9765	0.9704	0.9845	0.9687	0.9831	0.9703	0.9657	0.9658	0.9649
	Vol. (mL)																

4046 - 4047	**m**	0.7724	0.6526	1.0107	0.7162	0.6707	0.7804	0.8768	0.9483	0.6028	0.9747	0.5978	1.0194	0.7158	0.6553	1.0952	0.8436
	c																
	R^2	0.9989	0.9978	0.9997	0.9926	0.9931	0.9986	0.999	0.9992	0.9877	0.999	0.9885	0.9991	0.994	0.9964	0.9967	0.9972
	Vol. (mL)																
4214 - 4224	**m**	0.8832	0.9584	1.3152	1.1154	0.9689	1.0729	1.2127	1.2492	1.052	1.5695	1.127	1.5295	1.0617	0.912	1.4367	1.141
	c									-0.1997		-0.2165					
	R^2	0.9978	0.991	0.9986	0.9921	0.9865	0.9969	0.9929	0.9961	0.9802	0.9975	0.9769	0.9983	0.9855	0.9865	0.9878	0.9882
	Vol. (mL)																

Table 2. n-Alkane calibration curve equations and R^2.

Sample Batch Range		**C16**	**C23**	**C30**
3983 - 4018	m	13.425	13.377	12.993
	c	-	-	-
	R^2	0.9986	0.9988	0.9988
	volume (mL)	0.1		
3992 and 4004	m	13.425	13.189	-
	c	-	-	-
	R^2	0.9986	0.9987	
	volume (mL)	0.15		
4003, 4028-4029	m	10.553	10.717	9.5693
	c	-	-	-
	R^2	0.9969	0.9966	0.9939

	volume (mL)	0.1		
4031 - 4037	m	12.361	12.472	12.3
	c	-	-	-19.75
	R^2	0.9996	0.9986	0.9973
	volume (mL)	0.05		
4038, 4043, 4046-4047	m	13.251	12.185	11.692
	c	-	-	-
	R^2	0.9993	0.999	0.9993
	volume (mL)	0.05		
4141 - 4147	m	13.482	12.766	12.17
	c	-	-	-
	R^2	0.9991	0.9991	0.9991
	volume (mL)	0.15		
4058 - 4089	m	13.547	13.252	12.957
	c	-	-	-
	R^2	0.9998	0.9998	0.9998
	volume (mL)	0.15		
4214 - 4224	m	15.647	14.868	13.688
	c			
	R^2	0.9995	0.9994	0.9994
	volume (mL)	0.05		

Appendix Ie. PAH Concentrations for Samples and Standards

Table 1. PAH Concentrations for Known-Source Materials and Airborne Ambient PM (μg g^{-1}).

	NAPH	ACY	ACE	FLU	PHEN	ANTH	FLA	PYR	BaA	CHRY	BbF	BkF	BaP	DahA	IcdP	BghiP
UD1	-	0.05	0.04	-	2.85	3.14	4.71	3.87	2.16	1.86	7.62	5.77	2.40	0.45	1.69	2.91
UD2	0.07	0.06	0.02	-	1.57	1.73	1.96	1.09	-	-	8.59	6.51	3.27	0.39	1.46	2.20
HH-RD1	0.00	-	0.00	-	-	-	-	-	-	-	0.10	0.08	0.01	-	-	-
HH-RD1	-	-	0.002	0.001	0.008	0.003	0.061	0.107	0.012	0.015	0.032	0.025	0.005	0.001	0.002	-
DB	-	-	-	-	-	-	-	-	-	-			-	0.00	0.01	-
BZ1	0.05	0.15	0.14	-	9.32	10.26	1.70	0.97	-	-	9.89	7.50	3.33	2.65	0.34	1.84
BZ2	0.07	0.16	0.23	0.19	4.27	4.70	1.16	1.13	0.58	0.50	5.64	4.28	1.87	0.30	0.76	0.93
DS1	-	-	-	-	3.03	1.51	1.14	-	-	-	0.42	0.42	-	0.03	0.04	-
DS2	-	-	-	-	3.40	-	13.46	-	1.47	1.47	1.01	1.01	-	-	-	0.15
DS3	-	-	-	-	6.27	-	13.53	0.57	1.34	1.34	0.86	0.86	-	-	0.07	0.14
UPM1	0.02	0.10	0.04	-	4.68	5.15	7.93	5.95	2.60	2.36	15.63	11.61	6.26	0.71	2.82	3.97
UPM2	0.02	0.09	0.01	-	5.77	6.34	1.29	0.82	2.98	2.71	17.18	12.75	6.21	0.60	2.41	3.49
FD1	-	0.03	0.01	0.02	0.57	0.11	1.87	1.29	0.64	1.24	0.90	0.90	0.96	0.17	0.57	0.97
FD2	-	0.05	0.02	0.06	1.41	0.21	3.00	2.89	0.71	1.35	0.82	0.82	0.86	0.10	0.39	0.68
EB1	-	-	-	-	0.005	-	0.002	-	-	-	-	-	-	-	-	-
EB2	-	-	-	-	0.006	-	0.002	-	-	-	-	-	-	-	-	-
MC-300-01	-	-	-	-	-	-	-	-	-	-	-	-	-	0.05	0.04	0.03
MC-600-01	-	-	-	-	-	-	-	-	-	-	-	-	-	-	-	-
MC-300-02	-	-	-	0.04	0.04	0.03	-	-	-	-	-	-	-	-	-	-
BCR-RD1	-	-	0.02	-	-	5.89	6.65	1.66	0.58	0.34	0.27	-	-	1.13	0.07	0.24
BCR-RD2	-	-	0.03	-	-	4.57	5.16	1.31	0.37	-	-	-	-	0.86	0.06	0.21

MAN-FF 4028	-	0.20	-	-	4.64	4.64	-	-	6.37	6.37	48.68	48.68	84.09	26.51	49.04	92.93
MAN-FF 4031	-	-	-	-	3.65	3.65	-	-	-	-	3.75	3.75	5.09	2.64	6.07	12.27
MAN-FF 4032	-	-	-	-	1.70	1.70	-	-	-	-	8.43	8.43	12.94	3.49	9.05	16.33
MAN-FF 4034	-	-	-	0.27	2.08	-	2.44	2.33	-	-	3.50	3.50	2.61	1.40	3.45	6.40
MAN-FF 4035	-	-	-	-	2.42	-	-	-	-	-	2.19	2.19	3.29	1.01	2.78	4.93
MAN-FF 4036	-	-	-	-	1.88	1.88	-	-	-	-	5.49	5.49	8.43	2.41	6.01	11.17
GLA-KS 4038	-	-	-	0.38	7.32	-	5.76	4.35	1.64	3.23	4.85	4.85	3.98	0.96	2.99	6.12
GLA-KS 4043	-	-	-	0.41	5.58	-	4.42	3.28	-	-	2.92	2.92	2.36	0.48	1.65	2.82
GLA-KS 4046	-	-	-	-	11.60	-	-	-	-	-	25.56	25.56	45.72	11.74	31.99	58.09
GLA-KS 4047	-	-	-	-	6.82	6.82	-	-	-	-	11.01	11.01	17.23	3.84	10.75	21.24

Table 2. n-Alkane Concentrations for Known-Source Materials and Airborne Ambient PM (μg g^{-1}).

	C16	C17	C18	C19	C20	C21	C22	C23	C24	C25	C26	C27	C28	C29	C30	C31	C32	C33
UD	0.62	0.62	0.69	0.83	0.96	1.47	2.63	9.19	16.01	47.22	47.94	41.62	24.36	41.42	11.91	22.44	8.92	16.95
HH-RD	0.08	0.07	0.34	0.10	0.09	0.07	0.09	0.19	0.13	0.50	0.21	0.84	0.25	0.96	0.21	1.75	0.32	0.65
DB	-	-	0.06	0.20	0.10	0.09	0.12	0.18	-	0.24	0.28	2.32	0.31	2.13	0.15	1.51	0.10	0.49
BZ	1.49	4.62	4.72	4.59	3.06	2.38	2.55	2.93	2.72	6.32	4.78	7.25	6.17	16.57	9.80	14.15	13.93	13.07
DS	0.06	0.10	0.16	0.28	0.36	0.40	0.22	0.27	0.26	0.52	0.55	0.44	0.28	0.09	-	-	-	-
DS	-	4.32	3.22	10.39	7.86	5.97	5.20	2.77	1.66	11.04	8.93	-	-	4.52	1.24	-	-	-
DS	1.04	3.11	3.30	8.07	7.24	5.45	4.57	2.68	2.79	4.27	8.20	-	-	0.52	1.65	-	-	-

UPM	0.60	0.67	0.71	1.14	1.25	1.91	3.20	5.56	14.81	41.00	39.84	32.06	18.81	32.73	10.50	22.88	8.02	16.26
FD	0.11	0.21	0.61	1.60	2.76	3.30	3.35	2.94	2.37	3.13	2.78	4.63	3.59	8.87	6.70	7.88	7.00	8.25
FD	0.11	0.19	0.51	1.02	2.10	2.58	2.74	2.34	1.76	2.57	2.30	4.01	3.02	7.55	5.71	7.00	5.95	6.84
EB	0.07	0.12	0.14	0.09	0.08	0.05	0.04	0.03	0.04	0.03	0.02	0.05	0.01	0.05	0.01	0.04	0.01	0.02
MC-300-01	-	-	0.55	0.88	0.43	0.52	0.54	0.53	0.54	0.62	0.64	0.60	0.43	0.50	0.27	0.18	0.18	0.12
MC-600-01	0.05	0.13	0.22	0.29	0.21	0.24	0.23	0.35	0.49	0.70	0.73	0.70	0.51	0.54	0.24	0.20	0.12	0.11
MC-300-02	0.02	0.11	0.23	0.31	0.33	0.38	0.38	0.30	0.17	0.10	0.11	0.05	0.09	0.07	0.06	0.46	0.21	0.00
BCR-RD	0.07	0.12	0.25	0.50	0.46	0.41	0.36	0.39	0.29	0.35	0.45	0.66	0.86	1.98	2.28	2.39	3.00	3.54
MAN-FF 4028	1.43	1.48	5.35	11.12	4.63	2.72	4.92	7.64	15.90	38.41	51.90	65.48	52.98	74.37	40.14	66.37	29.19	36.34
MAN-FF 4031	2.79	2.73	6.31	16.82	13.07	12.22	11.31	12.79	15.06	15.94	11.83	10.76	17.35	28.11	17.24	36.62	17.07	24.79
MAN-FF 4032	1.28	3.54	3.67	11.29	9.97	9.83	8.40	7.60	7.21	9.23	8.54	10.29	16.13	43.04	25.80	59.28	23.58	39.35
MAN-FF 4034	-	0.53	2.31	1.86	3.56	3.73	3.28	4.20	3.34	6.04	5.32	7.34	13.90	24.63	15.61	27.97	12.11	17.57
MAN-FF 4035	-	1.27	4.15	5.76	5.98	4.78	4.52	4.75	3.84	5.48	4.65	4.93	8.17	13.54	9.52	20.74	7.96	13.64
MAN-FF 4036	0.89	2.56	3.93	5.73	5.07	4.94	4.98	6.36	7.05	10.39	10.18	14.45	18.54	43.81	21.88	46.23	17.78	25.15
GLA-KS 4038	3.16	2.96	24.52	40.59	30.93	42.14	64.13	89.38	91.37	102.48	33.42	47.41	60.82	143.77	71.80	151.69	58.34	82.52
GLA-KS 4043	3.06	3.28	29.85	54.89	49.36	42.59	46.08	43.46	41.13	65.63	38.24	52.72	34.28	58.42	28.10	65.39	23.27	42.04
GLA-KS 4046	13.56	25.78	57.17	82.20	54.75	40.10	57.59	61.94	69.31	118.04	123.35	189.89	177.06	233.86	136.55	276.37	98.86	154.21
GLA-KS 4047	6.64	13.13	47.68	59.83	24.71	24.20	22.91	22.24	24.41	103.25	62.04	108.79	70.72	147.20	82.53	179.01	67.58	96.03

Table 3. PAH Concentrations for Known-Source Materials and Airborne Ambient PM (ng m^{-3}).

	FLU	PHEN	ANTH	FLA	PYR	BaA	CHRY	BbF	BkF	BaP	DahA	IcdP	BghiP
MAN-FF 4028	-	0.06	0.03	-	-		0.18	0.34	0.34	1.16	0.37	0.68	1.28
MAN-FF 4031	-	0.02	0.01	-	-		-	0.01	0.01	0.03	0.01	0.03	0.06
MAN-FF 4032	-	0.02	0.01	-	-		-	0.05	0.05	0.16	0.04	0.11	0.20
MAN-FF 4033	-	0.03	0.01	-	-		-	0.02	0.02	0.06	0.02	0.05	0.08
MAN-FF 4034	0.00	0.02	-	0.02	0.02		-	0.02	0.02	0.03	0.01	0.03	0.06
MAN-FF 4035	-	0.04	-	-	-		-	0.02	0.02	0.05	0.01	0.04	0.07
MAN-FF 4036	-	0.03	0.03	-	-		-	0.05	0.05	0.15	0.04	0.10	0.19
GLA-KS 4038	0.01	0.25	-	0.20	0.15	0.06	0.11	0.08	0.08	0.14	0.03	0.10	0.21
GLA-KS 4043	0.01	0.17	-	0.14	0.10	-	-	0.09	0.09	0.07	0.01	0.05	0.09
GLA-KS 4046	-	0.25	-	-	-	-	-	0.54	0.54	0.97	0.25	0.68	1.23
GLA-KS 4047	-	0.44	0.38	-	-	-	-	0.30	0.30	0.48	0.11	0.30	0.59
Woodsmoke indoors	4.44	33.13	-	109.69	158.08	382.58	283.61	229.80	229.80	345.60	37.84	180.88	209.24
Woodsmoke outdoors	-	16.62	12.89	-	-	-	-	-	-	-	-	-	-
Charcoal-smoke indoors	-	8.66	8.66	-	-	25.71	8.26	34.56	34.56	45.00	-	22.42	30.31

Table 4. n-Alkane Concentrations for Known-Source Materials and Airborne Ambient PM (ng g^{-1}).

	C16	C17	C18	C19	C20	C21	C22	C23	C24	C25	C26	C27	C28	C29	C30	C31	C32	C33
MAN-FF 4028	0.02	0.02	0.07	0.15	0.06	0.04	0.07	0.11	0.22	0.53	0.72	0.90	0.73	1.03	0.55	0.91	0.40	0.50
MAN-FF 4031	0.01	0.01	0.03	0.08	0.06	0.06	0.06	0.06	0.07	0.08	0.06	0.05	0.09	0.14	0.09	0.18	0.08	0.12
MAN-FF 4032	0.02	0.04	0.04	0.14	0.12	0.12	0.10	0.09	0.09	0.11	0.10	0.13	0.20	0.53	0.32	0.73	0.29	0.48
MAN-FF 4033	-	0.02	0.04	0.19	0.16	0.13	0.12	0.10	0.09	0.14	0.11	0.13	0.16	0.38	0.17	0.59	0.16	0.45
MAN-FF 4034	-	0.01	0.02	0.02	0.04	0.04	0.03	0.04	0.03	0.06	0.05	0.07	0.14	0.25	0.16	0.28	0.12	0.18
MAN-FF 4035	-	0.02	0.06	0.08	0.09	0.07	0.07	0.07	0.06	0.08	0.07	0.07	0.12	0.20	0.14	0.30	0.12	0.20
MAN-FF 4036	0.02	0.04	0.07	0.10	0.09	0.09	0.09	0.11	0.12	0.18	0.18	0.25	0.32	0.76	0.38	0.80	0.31	0.44
GLA-KS 4038	0.11	0.10	0.86	1.42	1.08	1.48	2.25	3.13	3.20	3.59	2.35	2.85	2.20	2.80	1.67	4.74	1.63	2.42
GLA-KS 4043	0.10	0.10	0.93	1.71	1.54	1.33	1.44	1.35	1.28	2.05	1.19	1.64	1.07	1.82	0.88	2.04	0.73	1.31
GLA-KS 4046	0.28	0.52	1.16	1.67	1.11	0.82	1.17	1.26	1.41	2.40	2.51	3.86	3.60	4.75	2.78	5.62	2.01	3.13
GLA-KS 4047	0.15	0.29	1.05	1.32	0.54	0.53	0.50	0.49	0.54	2.27	1.37	2.40	1.56	3.24	1.82	3.94	1.49	2.12
Woodsmoke indoors	-	-	31.51	54.28	39.01	50.55	84.45	117.60	125.08	216.39	144.72	257.27	108.75	269.70	97.04	82.87	91.29	118.00

Woodsmoke outdoors	-	-	-	46.33	53.80	54.37	86.95	94.18	91.35	103.18	89.46	75.23	58.91	58.04	43.55	40.97	28.30	36.67
Charcoal-smoke indoors	22.11	20.43	62.02	196.49	94.44	104.13	157.26	161.71	168.13	169.15	158.10	823.89	45.71	58.16	79.32	83.89	65.12	64.60

Table 5. PAH Concentrations for Laboratory-Made Charcoals (μg g^{-1}).

	NAPH	ACY	ACE	FLU	PHEN	ANTH	FLA	PYR	BaA	CHRY	BbF	BkF	BaP	DahA	IcdP	BghiP
PC-400-01	11	-	762	4247	5581	1269	2204	2452	1887	1066	162	1503	1837	650	1494	1705
PC-500-01	19	-	926	8074	16028	1835	6989	8170	5236	3043	549	4238	4908	1624	3809	4978
PC-600-01	-	-	227	2529	8332	99	2216	5815	579	880	2377	1192	1050	223	1099	2774
PC-400-02	20	-	816	4439	9300	1253	3695	4326	2656	1707	5916	2967	2795	847	2475	3385
PC-500-02	-	-	1285	8534	14032	1240	5405	6110	3443	2481	7563	3792	3413	1721	4097	5822
PC-600-02	-	-	279	4517	15118	114	3272	9899	544	1144	292	2197	1896	379	2193	6799
PC-600-03	-	-	-	199	4899	7	1036	5401	55	244	-	256	48	19	160	636
MC-400-02	18	-	723	2767	4233	801	1759	2270	1338	752	189	1668	2215	668	1791	2300
MC-500-02	58	-	359	2506	4354	251	1539	3103	1153	923	2698	1353	1308	332	979	1403
MC-600-02	3	-	88	590	1550	14	379	1496	40	95	14	105	213	11	93	373
MC-500-01	39	-	400	2176	3482	241	1209	1622	707	490	109	1015	977	254	728	997
MC-600-01	-	-	33	937	4147	17	653	2780	28	84	235	118	203	12	70	196

Appendix If. Principal Component Analysis: Matrix Loadings

Table 1. Rotated Component Matrix for Known-Source Materials. Extraction Method: Principal Component Analysis. Rotation Method: Varimax with Kaiser Normalization. Rotation converged in 13 iterations. Only factor loading values with modulus ≤ 0.3 are not shown as they were not included in the results.

	PC 1	PC 2	PC 3	PC 4
C_{29}	0.987			
C_{28}	0.985			
C_{23}	0.979			
C_{27}	0.979			
C_{26}	0.965			
C_{25}	0.962			
C_{24}	0.952			
C_{31}	0.924		0.3	
C_{33}	0.914	0.36		
C_{30}	0.909	0.417		
C_{21}	-0.851			0.418
C_{20}	-0.801	0.427	-0.371	
BghiP	0.795		0.536	
IcdP	0.747		0.595	
BkF	0.637	0.369	0.63	
BbF	0.637	0.369	0.63	
DahA		0.995		
C_{17}		0.976		
C_{16}		0.972		
ACY		0.97		
C_{32}		0.963		
C_{18}		0.96		
ACE		0.959		
CHRY		-0.953		
C_{19}	-0.318	0.919		
ANTH		0.876	0.383	
PHEN		0.854	0.518	
PYR	0.35	-0.469	0.771	
FLA	0.546	-0.385	0.744	
BaP	0.6		0.685	
BaA	0.56	-0.457	0.653	
C_{22}		-0.46		0.852

Table 2. Rotated Component Matrix for Airborne Ambient PM from GLA-KS and MAN-FF. Extraction Method: Principal Component Analysis. Rotation Method: Varimax with Kaiser Normalization. A Rotation converged in 3 iterations. Only factor loading values with modulus ≤ 0.3 are not shown as they were not included in the results.

	PC 1	PC 2
PHEN	0.986	
ANTH	0.993	
BbF	0.502	0.864
BkF	0.502	0.864
BaP		0.999
DahA		0.996
IcdP		0.998
BghiP		0.997
C_{16}	0.993	
C_{17}	0.999	
C_{18}	0.995	
C_{19}	0.993	
C_{20}	0.997	
C_{21}	0.996	
C_{22}	0.998	
C_{23}	0.994	
C_{24}	0.939	0.338
C_{25}	0.967	
C_{26}	0.853	0.519
C_{27}	0.919	0.391
C_{28}	0.894	0.443
C_{29}	0.96	
C_{30}	0.965	
C_{31}	0.983	
C_{32}	0.976	
C_{33}	0.983	

Appendix II. Determination of BC/TC % and PAHs in Laboratory-Made Charcoals Produced under Varying Conditions.

Introduction

Hypy has been shown to be a useful tool for quantification of BC in environmental matrices as well as for the isolation of BC for reliable decontamination of pyrogenic carbon samples prior to radiocarbon analysis (Ascough et al., 2009; Meredith et al., 2012). The advantage of hypy is that when isolating BC the semi-labile organics (non-BC_{hypy}) are conserved hence can undergo further analysis (Ascough et al., 2009; Meredith et al., 2012).

The formation of BC depends on the fuel, temperature, and oxygen availability (Ascough et al., 2008). This has also been highlighted in previous hypy studies where the BC/TC% has been shown to vary in charcoals formed from different feedstocks and under different conditions (Rombolà et al., 2016; Wurster et al., 2012; Wurster et al., 2013). The aim of this study was to investigate the change in BC_{hypy}, in laboratory-made charcoal produced using different wood species, temperatures and pyrolysis durations. The PAHs in the non-BC_{hypy} would also be identified and quantified to determine the effect of wood species, temperature and pyrolysis durations on semi-labile PAHs ring size concentrations and distributions.

Method

Materials

The charcoals used in this study were obtained from existing material. The information on the production of the material is published in Ascough et al. (2008). Extract 1, 2 and 3 were taken from Ascough et al. (2008) to describe what wood species the charcoals were produced from, how the materials were homogenised and the pyrolysis conditions.

Extract 1:

"Two woods were used in the study; a sample of Scots Pine (Pinus sylvestris L.), obtained from Tentsmuir Forest, Fife in November 2005, and a sample of mangrove (Rhizo-phora apiculata Blume), collected in North East Palawan, Philippines, in February 2006… Bulk lipids were extracted from the woods by accelerated solvent extraction of 1 g of ground wood, using 500 ml of 2:1 (v/v) dichloromethane/methanol, following which the δ13C values and carbon weight percent (%C) for the extracts were determined as described below."

Extract 2:

"…all charcoal was produced from a single, homogenized initial sample from both species, obtained from an individual branch of either wood type. For pine this was the outermost 15 rings of the branch, and for mangrove this was the entire branch cross-section, excluding the bark of the tree in both cases. The wood samples were processed to a larger and a smaller sample size, first by cutting to 1 cm3 cubes, which formed the larger size sample, and then by grinding in a Tema mill for 30 s to produce a 1- to 2-mm fraction, which formed the smaller sample size."

Extract 3:

"Charcoal was produced in a controlled-atmosphere rotary furnace (Carbolite) for periods of either 60- or 120-min duration with an initial heating rate of 10 °C $min^{-}1$. Four temperatures were used, between 300 and 600 °C, covering a range representative of natural fires (e.g. Swift et al., 1993), in which significant changes in structure are observed (Williams and Besler, 1996). Temperature was determined via a thermocouple inserted into one of the wood cubes in each run…The second sample suite was produced under identical conditions, but with 2% O_2 mixed with the purge gas prior to introduction to the furnace…After the heating interval was complete, the samples were allowed to cool to room temperature (20 °C) under the same gas flow, and the mass loss of the sample was determined by comparison of the pre- and post-charcoal production sample weights. Each charcoal sample was then ground to pass a 500 µm sieve before treatment with 0.5 M HCl for 24 h to remove calcitic ash. Following the HCl treatment the samples were neutralized with deionised H2O and wet-sieved to 63–500 µm before drying."

Methodology

The samples were prepared and processed using hypy using the methodology descried in Chapter 4. The %C before and after hypy was calculated as described in Chapter 4. and the BC/TC% was determined. The non-BC_{hypy} was analysed as detailed in Appendix Ib. Sixteen parent PAHs were identified and quantified as described in Chapter 3.

Effect of different pyrolysis temperatures and time on BC_{hypy} content

Charcoals formed at different temperatures and times were analysed to determine which conditions yielded lower BC/TC% ratios.

The results showed a large range of BC/TC% values for mangrove charcoal (45.7 – 94.1 %) and pine charcoal (15.5 – 77.6 %) at different combustion conditions (see Table 1). The BC/TC% of mangrove charcoal was generally higher than that of pinewood char under the same conditions (temperature and pyrolysis time), which showed that the plant species influenced BC content (see Figure 1). Longer pyrolysis times increased the BC content of pinewood char at 400°C, 500°C and 600°C when pyrolyzed for 60 and 120 minutes, yet there was not much difference between pine pyrolyzed at 600 °C for 120 minutes and 180 minutes (see Figure 1). This mean the pine charcoal chemical structures had a less condensed aromatic structure at lower formation temperature, but charcoals formed at 600 °C were more condensed hence leading to higher BC/TC%. Longer pyrolysis times did not increase BC content in mangrove charcoal with the average BC/TC% being similar for MC-500-01 (mangrove at 500°C/60 minutes), 68.7 % and MC-500-02 (mangrove at 500°C/120 minutes), 74.4 %, and for MC-600-01 (mangrove at 600°C/60 minutes) 94.1 % and MC-600-02 (mangrove at 600°C/120 minutes) 93.6 %. Increased temperature increased BC content in pine charcoal from 400 to 500°C, however from 500 to 600°C BC content increased but by smaller amounts, less than 10 % (see Figure 1). However, for mangrove increased pyrolysis temperature from 400 to 600°C increased BC/TC% significantly by around 20 %.

Samples PC-400-01, PC-400-02 and PC-600-01 exhibited more variability than other samples as seen in see Figure 1. This was likely to be due to cracked hypy crucibles post-hypy causing the BC_{hypy} contents to leak. With lower BC_{hypy} masses the variation in %C is more likely to increase.

The results were in line with those of Rombolà et al. (2016), McBeath et al. (2015) and Wurster et al. (2013), as the BC/TC% increased with the charcoal formation temperature, due to a rapid increase in the aromatic domains with average cluster sizes between 7 and 14, which become resistant to hypy. PAHs with ring-sizes below 7 are removed via hypy, lignocellulose materials, and any initial products formed via depolymerisation/fragmentation of lignin to monomeric phenols and alcohols or cellulose degradation (Wurster et al., 2013). The pine charcoal BC/TC% was similar to those reported by Rombolà et al. (2016) at 340 – 400 °C had a BC/TC% of 15.7 ± 0.54%, however the BC/TC% at 600 °C was reported to be 95.9 ± 0.7% which was higher than the result here.

However, this could be due to the pyrolysis time which was not described in Rombolà et al. (2016).

Table 1. BC/TC% of mangrove and pinewood charcoals formed at different temperatures, with different pyrolysis times.

	BC/TC%	SE	Number of Replicates
PC-400-01	15.5	8.2	2
PC-500-01	36.1	1.1	3
PC-600-01	44.0	4.4	3
PC-400-02	35.3	6.0	3
PC-500-02	73.0	2.5	2
PC-600-02	74.8	1.8	3
PC-600-03	77.6	1.2	3
MC-500-01	68.7	2.5	3
MC-600-01	94.1	1.5	3
MC-400-02	45.7	1.8	3
MC-500-02	74.4	1.2	3
MC-600-02	93.6	1.9	3

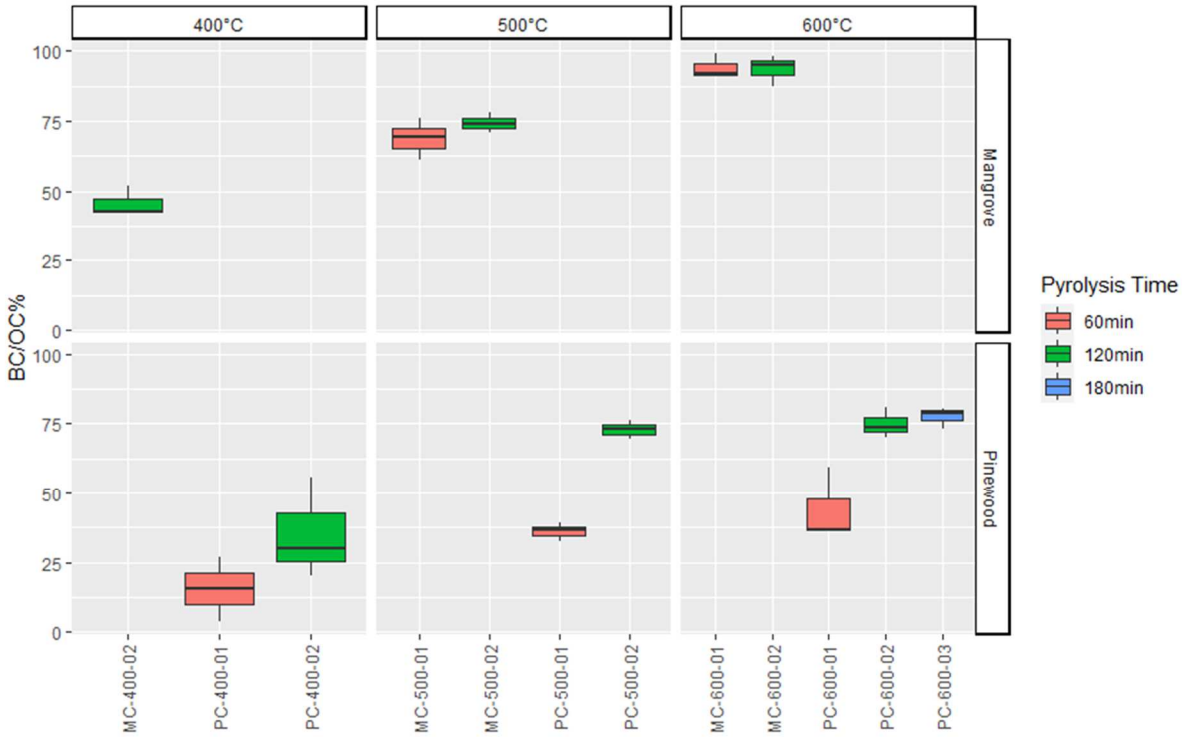

Figure 2. Box plots of each charcoal sample, separated by pyrolysis temperature, time and species.

Effect of different pyrolysis temperatures and time on PAH distributions and concentrations

Larger PAH concentrations were observed for charcoals produced at 60min/500°C for pine and mangrove charcoal, and 120min/500°C for pine (see Figures 2). This suggests at this temperature a higher proportion of the organic components in the feedstock are transforming into polycyclic aromatic structures after dehydration (McBeath et al., 2015). The PAH ring sizes that generally had the highest concentrations amongst the different formation temperatures were 3 and 4-ring PAHs which was in accordance with results from Rombolà et al. (2016).

PAH concentrations were generally lower at 400 °C and 600 °C except for mangrove charcoal 120min/400°C which had higher PAH concentrations than 120min/500°C, suggesting the pyrolysis duration can affect the PAH concentrations. Overall, pine charcoal 120min/500 °C had the highest PAH concentrations. Pine charcoal generally had higher PAH concentrations than mangrove perhaps due to it being denser (a hard wood) and therefore containing less lignin (Ascough et al., 2008).

The PAH distributions remained fairly stable in all conditions for pine with larger contributions from 3- and 4-ring PAHs. However, there seemed to be a lack of 5-ring PAHs

at 600 °C for both species. This was especially evident for pine 180 min/600°C, where the 5-ring and 6-ring PAHs were extremely low. This shows that 5-ring PAH structures may have reacted with other radicals to form larger condensed PAH structures that form BC, as BC/TC% highest for pine 180 min/600°C.

When BC/TC% were lowest in mangrove, the PAH concentrations were highest. This was not the case with pine which had higher PAH concentrations at 500 °C, where the BC/TC% was higher than that of pine charcoal formed at 400 °C.

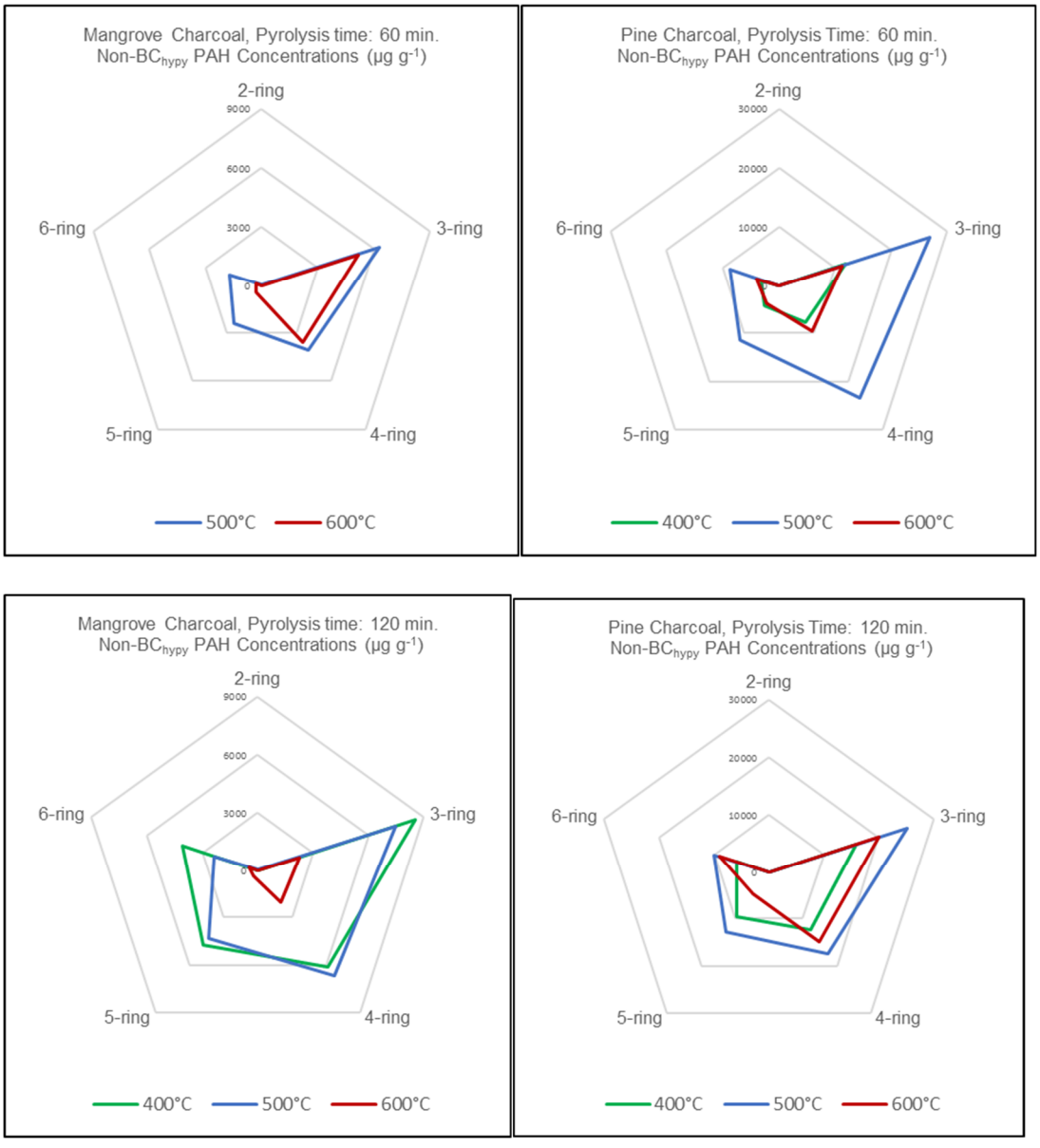

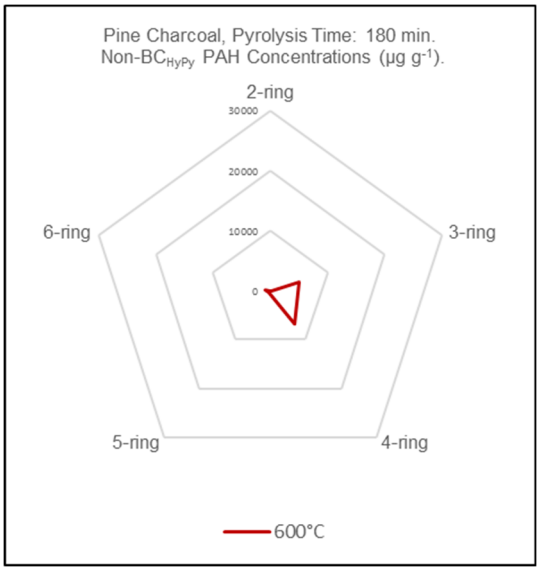

Figures 2. PAH ring-distributions in non-BC$_{hypy}$ for the charcoals.

Summary of Findings

To summarise, pyrolysis temperature and pyrolysis time affected mangrove and pinewood differently. In general, increased temperatures increased BC/TC% but the extent of the increase varied between the two different wood species. There was a larger increase in BC/TC% in mangrove between 500 °C and 600 °C, in comparison with pine. Pyrolysis time did not affect the BC/TC% of mangrove charcoal but did affect the BC/TC% of pine charcoal, as it increased with increased pyrolysis duration.

PAHs with the highest concentrations in the non-BC$_{hypy}$ were 3 and 4-ring PAHs. It was observed that charcoals formed at 500 °C had the highest PAH concentrations. The exception to this was mangrove 400°C/120min which had higher concentrations than mangrove 500°C/120min. As mangrove 400°C/60min was not analysed cannot be concluded that PAH concentrations were higher at charcoals formed at 500 °C. However, for pine, PAH concentrations were highest at 500 °C.

References

Abrantes, R., Assunção, J. V., & Pesquero, C. R. (2004). Emission of polycyclic aromatic hydrocarbons from light-duty diesel vehicles exhaust. *Atmospheric Environment, 38*(11), 1631-1640. doi:10.1016/j.atmosenv.2003.11.012

Achilleos, S., Kioumourtzoglou, M., Wu, C., Schwartz, J. D., Koutrakis, P., & Papatheodorou, S. I. (2017). Acute effects of fine particulate matter constituents on mortality: A systematic review and meta-regression analysis. *Environment International, 109*, 89-100. doi:10.1016/j.envint.2017.09.010

Air Quality Expert Group. (2005). *Particulate Matter in the United Kingdom.* Retrieved from London:

Air Quality Expert Group. (2012). *Fine Particulate Matter (PM2.5) in the United Kingdom*. Retrieved from https://uk-air.defra.gov.uk/assets/documents/reports/cat11/1212141150_AQEG_Fine_Particulate_Matter_in_the_UK.pdf

Air Quality Expert Group. (2015). Mitigation of United Kingdom PM2.5 Concentrations. Retrieved from https://uk-air.defra.gov.uk/assets/documents/reports/cat11/1508060903_DEF-PB14161_Mitigation_of_UK_PM25.pdf

The Air Quality Strategy for England, Scotland, Wales and Northern Ireland. (2007). Retrieved from https://assets.publishing.service.gov.uk/government/uploads/system/uploads/attachment_data/file/69336/pb12654-air-quality-strategy-vol1-070712.pdf

Akhter, M. S., Chughtai, A. R., & Smith, D. M. (1984). The structure of hexane soot — I. Spectroscopic studies. *Appl. Spectrosc., 39*(1), 143–153.

Akhter, M. S., Chughtai, A. R., & Smith, D. M. (1985). The structure of hexane soot — II. Extraction studies. *Applied Spectroscopy, 39*(1), 154-167.

Alam, M. S., Delgado-Saborit, J. M., Stark, C., & Harrison, R. M. (2014). Investigating PAH relative reactivity using congener profiles, quinone measurements and back trajectories. *Atmospheric Chemistry and Physics, 14*, 2467–2477. doi:10.5194/acp-14-2467-2014

Alberici, S., de Beer, J., van der Hoorn, I., & Staats, M. (2017). *Fly ash and blast furnace slag for cement manufacturing*. Retrieved from https://assets.publishing.service.gov.uk/government/uploads/system/uploads/attachment_data/file/660888/fly-ash-blast-furnace-slag-cement-manufacturing.pdf

Alexis, N., Barnes, C., Bernstein, L., Nel, A., Peden, D., Diaz-Sanchez, D., . . . Williams, P. B. (2004). Health effects of air pollution. *Journal of Allergy and Clinical Immunology, 114*(5), 1116-1123. doi:10.1016/j.jaci.2004.08.030

Alvarez-Ospina, H., Peralta, O., Castro, T., & Saavedra, M. I. (2016). Optimum quantification temperature for total, organic, and elemental carbon using thermal-coulombimetric analysis. *Atmospheric Environment, 145*, 74-80. doi:10.1016/j.atmosenv.2016.08.080

Alves, C., Pio, C. A., & Duarte, A. C. (2000). Particulate Size Distributed Organic Compounds in a Forest Atmosphere. *Environmental Science & Technology, 34*, 4287-4293. doi:10.1021/es000028a

Alves, C. A. (2008). Characterisation of solvent extractable organic constituents in atmospheric particulate matter:

An overview. *Anais da Academia Brasileira de Ciências 80*(1), 21-82. doi:10.1590/S0001-37652008000100003

Alves, C. A., Evtyugina, M., Vicente, A. M. P., Vicente, E. D., Nunes, T. V., Silva, P. M. A., . . . Querol, X. (2018). Chemical profiling of PM10 from urban road dust. *Science of the Total Environment, 634*, 41-51. doi:10.1016/j.scitotenv.2018.03.338

Alves, C. A., Vicente, A. M., Custódio, D., Cerqueira, M., Nunes, T., Pio, C., . . . Bandowe, B. A. M. (2017). Polycyclic aromatic hydrocarbons and their derivatives (nitro-PAHs, oxygenated PAHs, and azaarenes) in PM2.5 from Southern European cities. *Science of the Total Environment, 595*, 494-504. doi:10.1016/j.scitotenv.2017.03.256

Amarillo, A. C., Mateos, A. C., & Carreras, H. (2017). Source Apportionment of PM10-Bound Polycyclic Aromatic Hydrocarbons by Positive Matrix Factorization in Córdoba City, Argentina. *Archives of Environmental Contamination and Toxicology, 72*, 380–390. doi:10.1007/s00244-017-0384-y

Amato, F., Lucarelli, F., Nava, S., Calzolai, G., Karanasiou, A., Colombi, C., & Querol, X. (2016). *Airborne Particulate Matter: Sources, Atmospheric Processes and Health*. Croydon, UK: Royal Society of Chemistry.

Anderl, M., Kampel, E., Köther, T., Muik, B., Schodl, B., Poupa, S., & Wieser, M. (2007). *Austria's Annual Emission Inventory 1980-2005*. Retrieved from Vienna, Austria https://www.umweltbundesamt.at/fileadmin/site/publikationen/REP0072.pdF

Anderson, H. R., Bremner, S. A., & Atkinson, R. W. (2001). Particulate matter and daily mortality and hospital admissions in the west midlands conurbation of the United Kingdom: associations with fine and coarse particles, black smoke and sulphate. *Occupational and Environmental Medicine, 58*, 504-510. doi:10.1136/oem.58.8.504

Andersson, A., Sheesley, R. J., Kruså, M., Johansson, C., & Gustafsson, O. (2011). 14C-Based source assessment of soot aerosols in Stockholm and the Swedish EMEP-Aspvreten regional background site. *Atmospheric Environment, 45*(1), 215-222. doi:10.1016/j.atmosenv.2010.09.015

Andreae, M. O., & Gelencsér, A. (2006). Black carbon or brown carbon? The nature of light-absorbing carbonaceous aerosols. *Atmos. Chem. Phys., 6*(10), 3131–3148. doi:10.5194/acp-6-3131-2006

Andreou, G., & Rapsomanikis, S. (2009). Origins of n-alkanes, carbonyl compounds and molecular biomarkers in atmospheric fine and coarse particles of Athens, Greece. *Science of the Total Environment, 407*(21), 5750-5760. doi:10.1016/j.scitotenv.2009.07.019

ApSimon, H., Oxley, T., Woodward, H., Mehlig, D., Dore, A., & Holland, M. (2021). The UK Integrated Assessment Model for source apportionment and air pollution policy applications to PM2.5. *Environment International, 153*. doi:10.1016/j.envint.2021.106515

Apte, J. S., Kirchstetter, T. W., Reich, A. H., Deshpande, S. J., Kaushik, G., Chel, A., . . . Nazaroff, W. W. (2011). Concentrations of fine, ultrafine, and black carbon particles in auto-rickshaws in New Delhi, India. *Atmospheric Environment, 45*(26), 4470-4480. doi:10.1016/j.atmosenv.2011.05.028

AQEG. (2005). *Particulate Matter in the United Kingdom.* Retrieved from London:

AQEG. (2012). *Fine Particulate Matter (PM2.5) in the United Kingdom*. Retrieved from https://uk-air.defra.gov.uk/assets/documents/reports/cat11/1212141150_AQEG_Fine_Particulate_Matter_in_the_UK.pdf

AQEG. (2019). *Non-Exhaust Emissions from Road Traffic*. Retrieved from

Aquilina, N. J., & Harrison, R. M. (2023). Evaluation of the cancer risk from PAHs by inhalation: are current methods fit for purpose? *Environment International*. doi:10.1016/j.envint.2023.107991

Arbex, M. A., de Souza Conceição, G. M., Cendon, S. P., Arbex, F. F., Lopes, A. C., Moysés, E. P., . . . Braga, A. L. F. (2009). Urban air pollution and chronic obstructive pulmonary disease-related emergency department visits. *J Epidemiol Community Health, 63*(10), 777-783. doi:10.1136/jech.2008.078360

Architect of the Capitol. (n.d.). Capitol Power Plant. Retrieved from https://www.aoc.gov/explore-capitol-campus/buildings-grounds/capitol-power-plant

Armstrong, B., Hutchinson, E., Unwin, J., & Fletcher, T. (2004). Lung Cancer Risk after Exposure to Polycyclic Aromatic Hydrocarbons: A Review and Meta-Analysis. *Environmental Health Perspectives, 112*(9), 970–978. doi:10.1289/ehp.6895

Ascough, P. L. (2006). *Holocene variations in the North Atlantic marine radiocarbon reservoir effect.* University of Edinburgh, Retrieved from https://ethos.bl.uk/OrderDetails.do?uin=uk.bl.ethos.641093

Ascough, P. L., Bird, M. I., Brock, F., Higham, T. F. G., Meredith, W., Snape, C. E., & Vane, C. H. (2009). Hydropyrolysis as a new tool for radiocarbon pre-treatment and the quantification of black carbon. *Quaternary Geochronology, 4*(2), 140-147. doi:10.1016/j.quageo.2008.11.001

Ascough, P. L., Bird, M. I., Meredith, W., Wood, R. E., Snape, C. E., Brock, F., . . . Apperley, D. C. (2010). Hydropyrolysis: Implications for Radiocarbon Pretreatment and Characterization of Black Carbon. *Radiocarbon, 52*, 1336–1350. doi:10.1017/S0033822200046427

Ascough, P. L., Bird, M. I., Wormald, P., Snape, C. E., & Apperley, D. (2008). Influence of production variables and starting material on charcoal stable isotopic and molecular characteristics. *Geochimica et Cosmochimica Acta, 72*, 6090-6102. doi:10.1016/j.gca.2008.10.009

Ayres, J. G., Borm, P., Cassee, F. R., Castranova, V., Donaldson, K., Ghio, A., . . . Froines, J. (2008). Evaluating the toxicity of airborne particulate matter and nanoparticles by measuring oxidative stress potential - A workshop report and consensus statement. . *Inhalation Toxicology, 20*, 75-99. doi:10.1080/08958370701665517

Balci, M. (2005). *Basic 1H- and 13C-NMR Spectroscopy*: Elsevier.

Baldock, J. A., & Smernik, R. J. (2002). Chemical composition and bioavailability of thermally altered Pinus resinosa (Red pine) wood. . *Organic Geochemistry, 33*(9), 1093–1109. doi:doi.org/10.1016/S0146-6380(02)00062-1

Ballester, F., Rodríguez, P., Iñíguez, C., Saez, M., Daponte, A., Galán, I., . . . Toro, S. (2006). Air pollution and cardiovascular admissions association in Spain: results within the EMECAS project. *J Epidemiol Community Health, 60*(4), 328-336. doi:10.1136/jech.2005.037978

Ban-Weiss, G. A., McLaughlin, J. P., Harley, R. A., Lunden, M. M., Kirchstetter, T. W., Kean, A. J., . . . G.R., K. (2008). Long-term changes in emissions of nitrogen oxides and particulate matter from on-road gasoline and diesel vehicles. *Atmospheric Environment, 42*(2), 220-232. doi:10.1016/j.atmosenv.2007.09.049

Bandowe, B. A. M., Meusel, H., Huang, R., Ho, K., Cao, J., Hoffman, T., & Wilcke, W. (2014). PM2.5-bound oxygenated PAHs, nitro-PAHs and parent-PAHs from the atmosphere of a Chinese megacity: Seasonal variation, sources and cancer risk assessment. *Science of the Total Environment, 473-474*, 77-87. doi:10.1016/j.scitotenv.2013.11.108

Bao, R., McNichol, A. P., Hemingway, J. D., Gaylord, M. C. L., & Eglinton, T. I. (2019). Influence of Different Acid Treatments on the Radiocarbon Content Spectrum of Sedimentary Organic Matter Determined by RPO/Accelerator Mass Spectrometry. *Radiocarbon, 61*(2), 395 - 413. doi:10.1017/RDC.2018.125

Belch, J. J., Fitton, C., Cox, B., & Chalmers, J. D. (2021). Associations between ambient air pollutants and hospital admissions: more needs to be done. *Environmental Science and Pollution Research 28*, 61848–61852. doi:10.1007/s11356-021-16544-0

Belis, C. O., Larsen, B. R., Amato, F., El Haddad, I., Favez, O., Harrison, R. M., & Viana, M. (2014). *European guide on Air Pollution Source Apportionment with Receptor Models*. Retrieved from

Bench, G. (2004). Measurement of Contemporary and Fossil Carbon Contents of PM2.5 Aerosols: Results from Turtleback Dome, Yosemite National Park. *Environ. Sci. Technol., 38*(8), 2424-2427. doi:10.1021/es035161s

Bennett, M., Volckens, J., Stranglmaier, R., McNichol, A. P., Ellenson, W. D., & Lewis, C. W. (2008). Biodiesel effects on particulate radiocarbon (14C) emissions from a diesel engine. *Journal of Aerosol Science, 39*(8), 667-678. doi:10.1016/j.jaerosci.2008.04.001

Beramendi-Orosco, L. E., Castro-Díaz, M., Snape, C. E., Vane, C. H., & Large, D. J. (2004). Application of catalytic hydropyrolysis for the rapid preparation of lignin concentrates from wood. *Organic Geochemistry, 35*(1), 61-72. doi:10.1016/j.orggeochem.2003.07.001

Bernardoni, V., Calzolai, G., Chiari, M., Fedi, M., Lucarelli, F., Nava, S., & Vecchi, R. (2013). Radiocarbon analysis on organic and elemental carbon in aerosol samples and source apportionment at an urban site in Northern Italy. *Journal of Aerosol Science, 56*, 88-99. doi:10.1016/j.jaerosci.2012.06.001

Beverland, I. J., Tunes, T., Sozanska, M., Elton, R. A., Agius, R. M., & Heal, M. R. (2000). Effect of long-range transport on local PM 10 concentrations in the UK. *International Journal of Environmental Health Research, 10*(3), 229-238. doi:10.1080/09603120050127176

Bond, T. C., Doherty, S. J., Fahey, D. W., Forster, P. M., Berntsen, T., DeAngelo, B. J., . . . Zender, C. S. (2013). Bounding the role of black carbon in the climate system: A scientific assessment. *Journal of Geophysical Research: Atmospheres, 118*(11), 5380-5552. doi:doi.org/10.1002/jgrd.50171

Bondy, A. L., Bonanno, D., Moffet, R. C., Wang, B., Laskin, A., & Ault, A. P. (2018). The diverse chemical mixing state of aerosol particles in the southeastern United States. *Atmos. Chem. Phys., 18*, 12595–12612. doi:10.5194/acp-18-12595-2018

Bonvalot, L., Tuna, T., Fagault, Y., Jaffrezo, J.-L., Jacob, V., Chevrier, F., & Bard, E. (2016). Estimating contributions from biomass burning, fossil fuel combustion, and biogenic carbon to carbonaceous aerosols in the Valley of Chamonix: a dual approach based on radiocarbon and levoglucosan. *Atmos. Chem. Phys., 16*, 13753–13772. doi:10.5194/acp-16-13753-2016

Boreddy, S. K. R., Haque, M. M., Kawamura, K., Fu, P., & Kim, Y. (2018). Homologous series of n-alkanes (C19-C35), fatty acids (C12-C32) and n-alcohols (C8-C30) in atmospheric aerosols from central Alaska: Molecular distributions, seasonality and source indices. *Atmospheric Environment, 184*, 87-97. doi:10.1016/j.atmosenv.2018.04.021

Boucher, O. (2015). *Atmospheric Aerosols: Properties and Climate Impacts*: Springer.

Bové, H., Bongaerts, E., Slenders, E., Bijnens, E. M., Saenen, N. D., Gyselaers, W., . . . Nawrot, T. S. (2019). Ambient black carbon particles reach the fetal side of human placenta. *Nature Communications, 10*. doi:10.1038/s41467-019-11654-3

Bray, E. E., & Evans, E. D. (1961). Distribution of n-paraffins as a clue to recognition of source beds. *Geochimica et Cosmochimica Acta, 22*, 2-15. doi:10.1016/0016-7037(61)90069-2

Briggs, N. L., & Long, C. M. (2016). Critical review of black carbon and elemental carbon source apportionment in Europe and the United States. *Atmospheric Environment, 144*, 409-427. doi:10.1016/j.atmosenv.2016.09.002

Brocks, J. J., Love, G. D., Snape, C. E., Logan, G. A., Summons, R. E., & Buick, R. (2003). Release of bound aromatic hydrocarbons from late Archean and Mesoproterozoic kerogensvia hydropyrolysis. *Geochimica et Cosmochimica Acta, 67*(8), 1521-1530. doi:10.1016/S0016-7037(02)01302-9

Brodie, C. R., Leng, M. J., Casford, J. S. L., Kendrick, C. P., Lloyd, J. M., Yongqiang, Z., & Bird, M. I. (2011). Evidence for bias in C and N concentrations and δ13C composition of terrestrial and aquatic organic materials due to pre-analysis acid preparation methods. *Chemical Geology, 282*(3-4), 67-83. doi:10.1016/j.chemgeo.2011.01.007

Brodowski, S., Rodionov, A., Haumaier, L., Glaser, B., & Amelung, W. (2005). Revised black carbon assessment using benzene polycarboxylic acids. *Organic Geochemistry, 36*(9), 1299-1310. doi:10.1016/j.orggeochem.2005.03.011

Brokamp, C., Brandt, E. B. B., & Ryan, P. H. (2019). Assessing exposure to outdoor air pollution for epidemiological studies: Model-based and personal sampling strategies. *Journal of Allergy and Clinical Immunology, 143*(6), 2002-2006. doi:10.1016/j.jaci.2019.04.019

Bronk Ramsey, C. (2008). Radiocarbon Dating: Revolutions in Understanding. *Archaeometry, 50*(2), 249-275. doi:10.1111/j.1475-4754.2008.00394.x

Brook, R. D., Franklin, B., Cascio, W., Hong, Y., Howard, G., & Lipsett, M. (2004). A Statement for Healthcare Professionals From the Expert Panel on Population and Prevention Science of the American Heart Association. *Air Pollution and Cardiovascular Disease, 109*(21). doi:10.1161/01.CIR.0000128587.30041.C8

Brook, R. D., Rajagopalan, S., PopeIII, C. A., Brook, J. R., Bhatnagar, A., Diez-Roux, A. V., & Holguin, F. (2010). Particulate Matter Air Pollution and Cardiovascular Disease. *Circulation, 121*(21). doi:10.1161/CIR.0b013e3181dbece1

Brown, A. S., & Brown, R. J. C. (2012). Correlations in polycyclic aromatic hydrocarbon (PAH) concentrations in UK ambient air and implications for source apportionment. *Journal of Environmental Monitoring, 14*(8). doi:10.1039/C2EM10963H

Brown, S. G., Herckes, P., Ashbaugh, L., Hannigan, M. P., Kreidenweis, S. M., & Collet, J. L. (2002). Characterization of organic aerosol in Big Bend National Park, Texas. *Atmospheric Environment, 36*(38), 5807–5818. doi:10.1016/S1352-2310(02)00578-2

Burtscher, H. (2005). Physical characterization of particulate emissions from diesel engines: a review. *Aerosol Science, 36*, 896-932. doi:10.1016/j.jaerosci.2004.12.001

Bytnerowicz, A., Omasa, K., & Paoletti, E. (2007). Integrated effects of air pollution and climate change on forests: A northern hemisphere perspective. *Environmental Pollution, 147*(3), 438-445. doi:10.1016/j.envpol.2006.08.028

Callén, M. S., de la Cruz, M. T., López, J. M., & Mastral, A. M. (2011). PAH in airborne particulate matter.: Carcinogenic character of PM10 samples and assessment of the energy generation impact. *Fuel Processing Technology, 92*(2), 176-182. doi:10.1016/j.fuproc.2010.05.019

Cao, J. J., Chow, J. C., Tao, J., Lee, S. C., Watson, J. G., Ho, K. F., . . . Han, Y. M. (2011). Stable carbon isotopes in aerosols from Chinese cities: influence of fossil fuels. *Atmospheric Environment, 45*, 1359-1363. doi:10.1016/j.atmosenv.2010.10.056

Cao, Z., Wang, M., Chen, Q., Zhu, C., Jie, J., Li, X., . . . Bu, Q. (2019). Spatial, seasonal and particle size dependent variations of PAH contamination in indoor dust and the

corresponding human health risk. *Science of the Total Environment, 653*, 423–430. Retrieved from 10.1016/j.scitotenv.2018.10.413

Carslaw, D. C., & Ropkin, K. (2012). openair - An R package for air quality data analysis." Environmental Modelling & Software. *Environmental Modelling & Software, 27–28*, 52–61. doi:10.1016/j.envsoft.2011.09.008.

Caumo, S., Bruns, R. E., & Vasconcellos, P. C. (2020). Variation of the Distribution of Atmospheric n-Alkanes Emitted by Different Fuels' Combustion. *Atmosphere, 11*(6). doi:10.3390/atmos11060643

Caumo, S., Vicente, A., Custódio, D., Alves, C., & Vasconcellos, P. (2018). Organic compounds in particulate and gaseous phase collected in the neighbourhood of an industrial complex in São Paulo (Brazil). *Air Quality, Atmosphere & Health, 11*, 271-283. doi:10.1007/s11869-017-0531-7

Chakrabarty, R. K., Moosmuller, H., Chen, L. W. A., Lewis, K., Arnott, W. P., Mazzoleni, C., . . . Kreidenweis, S. M. (2010). Brown carbon in tar balls from smoldering biomass combustion. *Atmos. Chem. Phys., 10*(13), 6363-6370. doi:10.5194/acp-10-6363-2010

Chakraborty, M., Giang, A., & Zimmerman, N. (2023). Performance evaluation of portable dual-spot micro-aethalometers for source identification of black carbon aerosols: application to wildfire smoke and traffic emissions in the Pacific Northwest. *Atmospheric Measurement Techniques, 16*(9). doi:10.5194/amt-16-2333-2023

Chang, S. G., Brodzinsky, R., Gundel, L. A., & Novakov, T. (1982). Chemical and catalytic properties of elemental carbon. In G. T. Wolff & R. L. Klimisch (Eds.), *Particulate Carbon: Atmospheric Life Cycle* (pp. 159–181). New York: Plenum Press.

Chang, Z., Tian, L., Li, F., Zhou, Y., Wu, M., Steinberg, C. E. W., . . . Xing, B. (2018). Benzene polycarboxylic acid - A useful marker for condensed organic matter, but not for only pyrogenic black carbon. *Science of the Total Environment, 626*, 660-667. doi:10.1016/j.scitotenv.2018.01.145

Charron, A., Polo-Rehn, L., Besombes, J., Golly, B., Buisson, C., Chanut, H., . . . Jaffrezo, J. (2019). Identification and quantification of particulate tracers of exhaust and non-exhaust vehicle emissions. *Atmos. Chem. Phys., 19*(7), 5187–5207. doi:10.5194/acp-19-5187-2019

Cheng, A. S., Buchholz, B. A., & Dibble, R. W. (2003). Isotopic Tracing of Fuel Carbon in the Emissions of a Compression-Ignition Engine Fueled with Biodiesel Blends. *Journal of Fuels and Lubricants, 112*, 2015-2020. Retrieved from https://www.jstor.org/stable/44742421

Chimjarn, S., Delhomme, O., & Millet, M. (2021). Temporal Distribution and Gas/Particle Partitioning of Polycyclic Aromatic Hydrocarbons (PAHs) in the Atmosphere of Strasbourg, France. *Atmosphere, 12*(3). doi:10.3390/atmos12030337

Ching, J., & Kajino, M. (2018). Aerosol mixing state matters for particles deposition in human respiratory system. *Sci Rep., 8*(8864). doi:10.1038/s41598-018-27156-z

Chong, U., Swanson, J. J., & Boies, A. M. (2015). Air quality evaluation of London Paddington train station. *Environmental Research Letters, 10*(9). doi:10.1088/1748-9326/10/9/094012

Chughtai, A. R., Kim, J. M., & Smith, D. M. (2002). The effect of air/fuel ratio on properties and reactivity of combustion soots. *Journal of Atmospheric Chemistry, 43*, 21-43.

Cincinelli, A., Mandorlo, S., Dickhut, R. M., & Lepri, L. (2003). Particulate organic compounds in the atmosphere surrounding an industrialised area of Prato (Italy). *Atmospheric Environment, 37*(22), 3125-3133. doi:10.1016/S1352-2310(03)00298-X

Ciupek, K., Butterfield, D., Quincey, P., Sweeney, B., Lilley, A., Bradshaw, C., . . . Font, A. (2021). *2019 Annual Report For The UK Black Carbon Network.* Retrieved from https://eprintspublications.npl.co.uk/9278/1/ENV38.pdf

Clark, J. S., & Patterson, W. A. I. (1997). *Background and local charcoal in sediments: scales of fire evidence in the paleorecord* (Vol. 51). Berlin: Springer-Verlag.

Claxton, L. D., Matthews, P. P., & Warren, S. H. (2004). The genotoxicity of ambient outdoor air, a review: Salmonella mutagenicity. *Mutation Research/Reviews in Mutation Research, 567*(2-3), 347-399. doi:10.1016/j.mrrev.2004.08.002

COMEAP. (2010). *The Mortality Effects of Long-Term Exposure to Particulate Air Pollution in the United Kingdom.* Retrieved from

Conolly, C., & Carpenter, S. (2021). *UK PAH Monitoring and Analysis Network.* Retrieved from https://uk-air.defra.gov.uk/assets/documents/reports/cat09/2209290923_2021_PAH_Annual_Report_Issue_1.html#33_other_pahs_monthly_concentrations

Cornelissen, G., Gustafsson, O., Bucheli, T. D., Jonker, M. T. O., Koelmans, A. A., & Van Noort, P. C. M. (2005). Extensive sorption of organic compounds to black carbon, coal, and kerogen in sediments and soils: mechanisms and consequences for distribution, bioaccumulation, and biodegradation. *Environ. Sci. Technol., 39*(18), 6881-6895. doi:doi/10.1021/es050191b

Crilley, L. R., Bloss, W. J., Yin, J., Beddows, D. C. S., Harrison, R. M., Allan, J. D., . . . Mohr, C. (2015). Sources and contributions of wood smoke during winter in London: assessing local and regional influences. *Atmos. Chem. Phys., 15*, 3149-3171. doi:10.5194/acp-15-3149-2015

Cuadras, A., Rovira, E., Marcé, R. M., & Borrull, F. (2016). Lung cancer risk by polycyclic aromatic hydrocarbons in a Mediterranean industrialized area. *Environ. Sci. & Pollut. Res., 23*, 23215–23227. doi:10.1007/s11356-016-7566-4

Currie, L. A. (2000). Evolution and Multidisciplinary Frontiers of 14C Aerosol Science. *Radiocarbon, 42*(1), 115 - 126. doi:10.1017/S003382220005308X

Currie, L. A., Benner, B. A., Kessler, J. D., Klinedinst, D. B., Klouda, G. A., Marolf, J. V., & Slater, J. F. (2002a). A Critical Evaluation of Interlaboratory Data on Total, Elemental, and Isotopic Carbon in the Carbonaceous Particle Reference Material, NIST SRM 1649a. *Journal of Research of the National Institute of Standards and Technology,, 107*(3), 279–298. doi:10.6028/jres.107.022

Currie, L. A., Benner, B. A., Kessler, J. D., Klinedinst, D. B., Klouda, G. A., Marolf, J. V., . . . Schmid, H. (2002b). A Critical Evaluation of Interlaboratory Data on Total, Elemental, and Isotopic Carbon in the Carbonaceous Particle Reference Material, NIST SRM 1649a. *Journal of Research of the National Institue of Standards and Technology, 107*(3), 279–298. doi:10.6028/jres.107.022

Currie, L. A., Klouda, G. A., & Voorhees, K. J. (1984). Atmospheric carbon: The importance of accelerator mass spectrometry. *Nucl. Instrum. Meth. B., 5*, 371–379. doi:10.1016/0168-583X(84)90544-5

Dargie, G. C. (2010). *Assessing the Use of Hydrogen Peroxide Oxidation to Quantify Black Carbon in Amazonian Soils.* (Masters). University of Newcastle,

Dat, N.-Y., & Chang, M. B. (2017). Review on characteristics of PAHs in atmosphere, anthropogenic sources and control technologies. *Science of the Total Environment, 609*, 682-693. doi:10.1016/j.scitotenv.2017.07.204

de Kok, T. M., Hogervorst, J. G., Briedé, J. J., Herwijnen, M. H., Maas, L. M., Moonen, E. J., . . . Kleinjans, J. C. (2005). Genotoxicity and physicochemical characteristics of traffic-related ambient particulate matter. *Environmental and Molecular Mutagenesis, 46*(2), 71-80. doi:10.1002/em.20133

De Prins, S., Dons, E., Van Poppel, M., Panis, L. I., Van de Mieroop, E., Nelen, V., . . . Koppen, G. (2014). Airway oxidative stress and inflammation markers in exhaled breath from children are linked with exposure to black carbon. *Environment International, 73*, 440-446. doi:10.1016/j.envint.2014.06.017

Decesari, S., Fuzzi, S., Facchini, M. C., Mircea, M., Emblico, L., & Cavalli, F. (2006). Characterization of the organic composition of aerosols from Rondonia, Brazil, during the LBA-SMOCC 2002 experiment and its representation through model compounds. *Atmos. Chem. Phys., 6*, 375–402. doi:10.5194/acp-6-375-2006

Defra. (2023). *Emissions of air pollutants in the UK – Nitrogen oxides (NOx)*. Retrieved from https://www.gov.uk/government/statistics/emissions-of-air-pollutants/emissions-of-air-pollutants-in-the-uk-nitrogen-oxides-nox

DEFRA National Statistics. (2022). Concentrations of particulate matter (PM10 and PM2.5). Retrieved from https://www.gov.uk/government/statistics/air-quality-statistics/concentrations-of-particulate-matter-pm10-and-pm25

Deines, P. (1980). *The isotopic composition if reduced organic carbon* (Vol. 1). Dordrecht: Elsevier.

Del Rio, J. C., Gonzalez-Vila, F. J., & Martin, F. (1992). Variation in the content and distribution of biomarkers in two closely situated peat and lignite deposits. *Organic Geochemistry, 18*(1), 67-78. doi:10.1016/0146-6380(92)90144-M

Dempster, H. S., Sherwood-Lollar, B., & Feenstra, S. (1997). Tracing organic contaminants in groundwater: a new methodology using compound-specific isotopic analysis. *Environ. Sci. Technol., 31*, 3193-3197. doi:10.1021/es9701873

Denis, E. H., Toney, J. L., Tarozo, R., Anderson, R. S., Roach, L. D., & Huang, Y. (2012). Polycyclic aromatic hydrocarbons (PAHs) in lake sediments record historic fire events: Validation using HPLC-fluorescence detection. *Organic Geochemistry, 45*, 7-17. doi:10.1016/j.orggeochem.2012.01.005

Diapouli, E., Fetfatzis, P., Panteliadis, P., Spitieri, C., Gini, M. I., Papagiannis, S., . . . Eleftheriadis, K. (2022). PM2.5 Source Apportionment and Implications for Particle Hygroscopicity at an Urban Background Site in Athens, Greece. *Atmosphere, 13*(10). doi:10.3390/atmos13101685

Directive 2004/107/EC of the European Parliament and of the Council of 15 December 2004 relating to arsenic, cadmium, mercury, nickel and polycyclic aromatic hydrocarbons in ambient air. (2005). Retrieved from https://eur-lex.europa.eu/legal-content/EN/TXT/?uri=CELEX%3A32004L0107

Dong, M., Locke, D. C., & Ferrand, E. (1976). High Pressure Liquid Chromatographic Method for Routine Analysis of Major Parent Polycyclic Aromatic Hydrocarbons in Suspended Particulate Matter. *Analytical Chemistry, 48*(2). doi:10.1021/ac60366a049

Draxler, R. R. (1999). *HYSPLIT4 user's guide*. Silver Spring, MD.: NOAA Air Resources Laboratory.

Draxler, R. R., & Hess, G. D. (1997). *Aust. Met. Mag., 47*, 295-308. Retrieved from https://www.arl.noaa.gov/documents/reports/MetMag.pdf

Draxler, R. R., & Hess, G. D. (1998). An overview of the HYSPLIT_4 modeling system of trajectories, dispersion, and deposition. *Aust. Meteor. Mag., 47*, 295-308.

Durant, J. L., Busby, W. F., Lafleur, A. L., Penman, B. W., & Crespi, C. L. (1996). Human cell mutagenicity of oxygenated, nitrated and unsubstituted polycyclic aromatic hydrocarbons associated with urban aerosols. *Mutation Research/Genetic Toxicology, 371*(3-4), 123-157. doi:10.1016/S0165-1218(96)90103-2

Eco Stars. (n.d.). What is Eco Stars? Retrieved from https://www.ecostars-uk.com/about-eco-stars/introduction/

EIA. (10/06/2022). U.S. Energy Facts Explained. *Consumption & Production.* Retrieved from https://www.eia.gov/energyexplained/us-energy-facts/

Eiguren-Fernandez, A., & Miguel, A. H. (2003). Determination of Semi-volatile and Particulate Polycyclic Aromatic Hydrocarbons in SRM 1649a and PM2.5 Samples by HPLC-Fluorescence. *Polycyclic Aromatic Compounds, 23*, 193-205. doi:10.1080/10406630390208756

Elorduy, I., Durana, N., García, J. A., Gómez, M. C., & Alonso, L. (2018). Optimization and Validation of Thermal Desorption Gas Chromatography-Mass Spectrometry for the Determination of Polycyclic Aromatic Hydrocarbons in Ambient Air. *J Anal Methods Chem.* doi:10.1155/2018/8734013

(2021).

Environmental Health Criteria (EHC). (2003). Selected Nitro- and Nitrooxy Policyclic Aromatic Hydrocarbons. In J. Kielhorn, U. Wahnschaffe, & I. Mangelsdorf (Eds.). Hanover.

Erlandsson, L., Lindgren, R., Nääv, Å., Krais, A. M., Standberg, B., Lundh, T., . . . Malmqvist, E. (2020). Exposure to wood smoke particles leads to inflammation, disrupted proliferation and damage to cellular structures in a human first trimester trophoblast cell line. *Environmental Pollution, 264*. doi:10.1016/j.envpol.2020.114790

European Commission. (2001). *Reference Document on Best Available Techniques in the Cement and Lime Manufacturing Industries*. Retrieved from https://eippcb.jrc.ec.europa.eu/sites/default/files/2020-03/superseded_clm_bref_1201.pdf

European Environment Agency. (n.d.-a). ltaly - Air pollution country fact sheet. Retrieved from https://www.eea.europa.eu/themes/air/country-fact-sheets/2021-country-fact-sheets/italy

European Environment Agency. (n.d.-b). United Kingdom - Air pollution country fact sheet. Retrieved from https://www.eea.europa.eu/themes/air/country-fact-sheets/2021-country-fact-sheets/united-kingdom

Ezani, N. E. B. (2017). *Development of novel methods for extended exposure assessment of combustion-related air pollutants in indoor and outdoor locations.* (Ph.D.). University of Strathclyde University of Strathclyde (T14756)

Famiyeh, L., Chen, K., Xu, J., Sun, Y., Guo, Q., Wang, C., . . . He, J. (2021). A review on analysis methods, source identification, and cancer risk evaluation of atmospheric polycyclic aromatic hydrocarbons. *Science of the Total Environment, 789.* doi:10.1016/j.scitotenv.2021.147741

Fann, N., Bell, M. L., Walker, K., & Hubbell, B. (2011). Improving the Linkages between Air Pollution Epidemiology and Quantitative Risk Assessment. *Environmental Health Perspectives, 119*(12), 1671–1675. doi:10.1289/ehp.1103780

Faoro, R. B., & Manning, J. A. (1981). Trends in Benzo(a)Pyrene, 1966-77. *Journal of Air Pollution Control Association, 31*(1), 62-64. doi:10.1080/00022470.1981.10465188

Fernandes, M. B., Skjemstad, J. O., Johnson, B. B., Wells, J. D., & Brooks, P. (2003). Characterization of carbonaceous combustion residues. I. Morphological, elemental and spectroscopic features. *Chemosphere, 51*, 785-795. doi:10.1016/S0045-6535(03)00098-5

Fernández, D. V., Rebolledo, E. S., Sedov, S., & Pustovoitov, K. (2022). Provenance, and environment context of pedogenic carbonates formation from MIS 3 to MIS 1 in the Teotihuacan Valley, Mexico. *Quaternary International, 618*, 52-69. doi:10.1016/j.quaint.2021.03.019

Flores, R. M., Özdemir, H., Ünal, A., & Tayanç, M. (2022). Distribution and sources of SVOCs in fine and coarse aerosols in the megacity of Istanbul. *Atmospheric Research, 271*. doi:10.1016/j.atmosres.2022.106100

Foereid, B., Lehmann, J., Wurster, C. M., & Bird, M. I. (2015). Presence of black carbon in soil due to forest fire in the New Jersey Pine Barrens. *Journal of Earth Science and Engineering, 5*, 91-97. doi:10.17265/2159-581X/2015.02.001

Folinsbee, L. J. (1993). Human health effects of air pollution. *Environmental Health Perspectives, 100*, 45-56. doi:10.1289/ehp.9310045

Font, A., Tremper, A. H., Lin, C., Priestman, M., Marsh, D., Woods, M., . . . Green, D. C. (2020). Air quality in enclosed railway stations: Quantifying the impact of diesel trains through deployment of multi-site measurement and random forest modelling. *Environmental Pollution, 262*. doi:10.1016/j.envpol.2020.114284

Fritsch, C., Gout, J.-F. , Haroon, S., Towheed, A., Chung, C., LaGosh, J., . . . Vermulst, M. (2020). Genome-wide surveillance of transcription errors in response to genotoxic stress. *PNAS, 118*(1). doi:10.1073/pnas.2004077118

Gaines, J. R., Healy, M. D., & Rankin, L. (2021). Backstreaming of pump oil vapors in vacuum systems. *Vakuum, 33*(1), 28-32. doi:10.1002/vipr.202100755

Gao, B., Feng, Q., Zhou, L., Wu, H., & E., A. (2019a). Distributions of Polycyclic Aromatic Hydrocarbons in Coal in China. *Pol. J. Environ. Stud., 28*(3), 1665-1674. doi:10.15244/pjoes/89899

Gao, P., Liu, D., Guo, L., He, C., Lin, N., Xing, Y., . . . Hang, J. (2019b). Ingestion bioaccessibility of indoor dust-bound PAHs: Inclusion of a sorption sink to simulate passive transfer across the small intestine. *Science of the Total Environment, 659*, 1546-1554. doi:10.1016/j.scitotenv.2018.12.459

Gauchotte, C., O'Sullivan, G., Davis, S., & Kalin, R. M. (2009). Development of an advanced on-line position-specific stable carbon isotope system and application to methyl tert-butyl ether. *Rapid Communications in Mass Spectrometry, 23*(19), 3183 - 3193.

Ghanavati, N., Nazarpour, A., & Watts, M. J. (2019). Status, source, ecological and health risk assessment of toxic metals and polycyclic aromatic hydrocarbons (PAHs) in street dust of Abadan, Iran. *CATENA, 177*, 246–259. doi:10.1016/j.catena.2019.02.022

Gillespie, J., Masey, N., Heal, M. R., Hamilton, S., & Beverland, I. J. (2017). Estimation of spatial patterns of urban air pollution over a 4-week period from repeated 5-min measurements. *Atmospheric Environment, 150*. doi:10.1016/j.atmosenv.2016.11.035

Glaser, B. H., L., Guggenberger, G., & Zech, W. (1998). Black carbon in soils: the use of benzenecarboxylic acids as specific markers. *Organic Geochemistry, 29*(4), 811-819. doi:10.1016/S0146-6380(98)00194-6

Glasgow City Council. (2009). *Air Quality Action Plan*. Retrieved from https://www.glasgow.gov.uk/CHttpHandler.ashx?id=32447&p=0

Glasgow City Council. (2017). *Glasgow City Development Plan*. Retrieved from https://www.glasgow.gov.uk/CHttpHandler.ashx?id=35882&p=0

Glasgow City Council. (2021). *Air Quality Annual Progress Report (APR) for Glasgow City Council*. Retrieved from https://glasgow.gov.uk/CHttpHandler.ashx?id=54895&p=0

Glasgow, U. o. (n.d.). Campus Development. Retrieved from https://www.gla.ac.uk/myglasgow/campusdevelopment/jamesmccunesmithlearninghub/#buildinginfo

Global Action Plan. (2022). *Educating Islington health professionals for action on air pollution*. Retrieved from https://www.islington.gov.uk/-/media/sharepoint-

lists/public-records/environmentalprotection/information/adviceandinformation/20232024/health-professionals-air-quality-training-project-report.pdf
Goldberg, E. D. (1985). *Black Carbon in the Environment* (Vol. 21). New York: Wiley.
Golly, B., Waked, A., Weber, S., Samake, A., Jacob, V., Conil, S., . . . Jaffrezo, J.-L. (2019). Organic markers and OC source apportionment for seasonal variations of PM2.5 at 5 rural sites in France. *Atmospheric Environment, 198*, 142-157. doi:10.1016/j.atmosenv.2018.10.027
Gómez-Losada, A., Santos, F. M., Gibert, K., & Pires, J. C. M. (2019). A data science approach for spatiotemporal modelling of low and resident air pollution in Madrid (Spain): Implications for epidemiological studies. *Computers, Environment and Urban Systems, 75*, 1-11. doi:10.1016/j.compenvurbsys.2018.12.005
Gordon, A. J. E., Halliday, J. A., Blankschien, M. D., Burns, P. A., Yatagai, F., & Herman, C. (2009). Transcriptional Infidelity Promotes Heritable Phenotypic Change in a Bistable Gene Network. *PLOS Biology, 7*(2). doi:10.1371/journal.pbio.1000044
Górka, M., Kosztowniak, E., Lewandowska, A. U., & Widory, D. (2020). Carbon isotope compositions and TC/OC/EC levels in atmospheric PM10 from Lower Silesia (SW Poland): Spatial variations, seasonality, sources and implications. *Atmospheric Pollution Research, 11*(7), 1099-1114. doi:10.1016/j.apr.2020.04.003
Gout, J. F., Li, W., Fritsch, C., Li, A., Haroon, S., Singh, L., . . . Vermulst, M. (2017). The landscape of transcription errors in eukaryotic cells. *Science Advances, 3*(10). doi:10.1126/sciadv.1701484
Goyal, N., Karra, M., & Canning, D. (2019). Early-life exposure to ambient fine particulate air pollution and infant mortality: pooled evidence from 43 low- and middle-income countries *International Journal of Epidemiology, 48*(4), 1125–1141. doi:10.1093/ije/dyz090
Grahame, T. J., Klemm, R., & Schlesinger, R. B. (2014). Public health and components of particulate matter: The changing assessment of black carbon. *Journal of the Air & Waste Management Association, 64*(6), 620-660. doi:10.1080/10962247.2014.912692
Grotheer, H., Robert, A. M., Greenwood, P. F., & Kliti, G. (2015). Stability and hydrogenation of polycyclic aromatic hydrocarbons during hydropyrolysis (HyPy) - Relevance for high maturity organic matter. *Organic Geochemistry, 86*, 45-54. doi:10.1016/j.orggeochem.2015.06.007
Gupta, S., Gadi, R., Mandal, T. K., & Sharma, S. K. (2017). Seasonal variations and source profile of n-alkanes in particulate matter (PM10) at a heavy traffic site, Delhi. *Environmental Monitoring and Assessment, 187*. doi:10.1007/s10661-016-5756-7
Gustafsson, O., Bucheli, T. D., Kukulska, Z., Andersson, M., Largeau, C., Rouzaud, J.-N., . . . Eglinton, T. I. (2001). Evaluation of a protocol for the quantification of black carbon in sediments. *Global Biogeochemical Cycles, 15*, 881-890. doi:10.1029/2000GB001380
Hadley, O., Cutler, A., Schumaker, R., & Bond, R. (2021). Wildfires and wood stoves: Woodsmoke toxicity and chemical characterization study in the north-western United States. *Atmospheric Environment, 253*. doi:10.1016/j.atmosenv.2021.118347
Hagenberg, S., Wehling, K., & Wiermann, R. (1990). n-Alkanes - Common Surface Constituents of Pollen from Gymno- and Angiosperms. *Z. Naturforsch, 45*(11-12), 1090-1092. doi:10.1515/znc-1990-11-1203
Hammes, K., Schmidt, M. W. I., Smernik, R. J., Currie, L. A., Ball, W. P., Nguyen, T. H., . . . Ding, L. (2007). Comparison of quantification methods to measure fire-derived (black/elemental) carbon in soils and sediments using reference materials

from soil, water, sediment and the atmosphere. *Global Biogeochemical Cycles, 21*(3). doi:10.1029/2006GB002914

Han, D., Fu, Q., Gao, S., Li, L., Ma, Y., Qioa, L., . . . Cheng, J. (2018). Non-polar organic compounds in autumn and winter aerosols in a typical city of eastern China: size distribution and impact of gas–particle partitioning on PM2.5 source apportionment. *Atmos. Chem. Phys., 18*(13), 9375–9391. doi:10.5194/acp-18-9375-2018

Han, Y., Cao, J., An, Z., Chow, J. C., Watson, J. G., Jin, Z., . . . Liu, S. (2007). Evaluation of the thermal/optical reflectance method for quantification of elemental carbon in sediments. *Chemosphere, 69*, 526-533. doi:10.1016/j.chemosphere.2007.03.035

Harkov, R., & Greenberg, A. (1985). Benzo(a)pyrene in New Jersey—Results from a Twenty-Seven-Site Study. *Journal of the Air Pollution Control Association, 35*(3), 238-243. doi:10.1080/00022470.1985.10465906

Harkov, R., Greenberg, A., Darack, F., Daisey, J. M., & Lloy, P. J. (1984). Summertime Variations in Polycyclic Aromatic Hydrocarbons at Four Sites in New Jersey. *Environ. Sol. Technol., 18*, 287-291. doi:10.1021/es00122a015

Harrison, R. M., Allan, J., Carruthers, D., Heal, M. R., Lewis, A. C., Marner, B., . . . Williams, I. (2021). Non-exhaust vehicle emissions of particulate matter and VOC from road traffic: A review. *Atmospheric Environment, 262*. doi:10.1016/j.atmosenv.2021.118592

Harrison, R. M., Deacon, A. R., Jones, M. R., & Appleby, R. S. (1997). Sources and processes affecting concentrations of PM10 and PM2.5 particulate matter in Birmingham (U.K.). *Atmospheric Environment, 31*(24), 4103-4117. doi:10.1016/S1352-2310(97)00296-3

Harrison, R. M., Delgado-Saborit, J. M., Baker, S. J., Aquilina, N., Meddings, C., Harrad, S., . . . Anderson, H. R. (2008). *Measurement and Modeling of Exposure to Selected Air Toxics for Health Effects Studies and Verification by Biomarkers*. Retrieved from https://www.um.edu.mt/library/oar/handle/123456789/58169

Harrison, R. M., Smith, D. J. T., & Luhana, L. (1996). Source apportionment of atmospheric polycyclic aromatic hydrocarbons collected from an urban location in Birmingham, UK. *Environ. Sci. Technol., 30*. doi:10.1021/es950252d

Harrison, R. M., & Yin, J. (2010). Chemical speciation of PM2.5 particles at urban background and rural sites in the UK atmosphere. *Journal of Environmental Monitoring, 12*(7), 1404–1414. doi:10.1039/C000329H

Havelcová, M., Sýkorová, I., Trejtnarová, H., & Šulc, A. (2012). Identification of organic matter in lignite samples from basins in the Czech Republic: Geochemical and petrographic properties in relation to lithotype. *Fuel, 99*, 129-142. doi:10.1016/j.fuel.2012.03.025

Hays, M. D., & Vander Wal, R. L. (2007). Heterogeneous Soot Nanostructure in Atmospheric and Combustion Source Aerosols. *Energy Fuels, 21*(2), 801–811. doi:doi.org/10.1021/ef060442h

He, J., Zielinska, B., & Balasubramanian, R. (2010). Composition of semi-volatile organic compounds in the urban atmosphere of Singapore: influence of biomass burning. *Atmos. Chem. Phys., 10*, 11401–11413. doi:10.5194/acp-10-11401-2010

Heal, M. R. (2013). The application of carbon-14 analyses to the source apportionment of atmospheric carbonaceous particulate matter: a review. *Analytical and Bioanalytical Chemistry, 406*, 81-98. doi:10.1007/s00216-013-7404-1

Heal, M. R., Naysmith, P., Cook, G. T., Xu, S., Raventós Duran, T., & Harrison, R. M. (2011). Application of 14C analyses to source apportionment of carbonaceous PM2.5 in the UK. . *Atmospheric Environment, 45*(14), 2341-2348. doi:doi.org/10.1016/j.atmosenv.2011.02.029

Healy, R. M., Sofowote, U., Su, Y., Debosz, J., Noble, M., Jeong, C. H., . . . Munoz, A. (2017). Ambient measurements and source apportionment of fossil fuel and biomass burning black carbon in Ontario. *Atmospheric Environment, 161*, 34–47. doi:10.1016/j.atmosenv.2017.04.034

Heaton, T. J., Bard, E., Bronk Ramsey, C., Butzin, M., Köhler, P., Muscheler, R., . . . Wacker, L. (2021). Radiocarbon: A key tracer for studying Earth's dynamo, climate system, carbon cycle, and Sun. *Science, 374*. doi:10.1126/science.abd7096

Hedges, J. I., Eglinton, G., Hatcher, P. G., Kirchman, D. L., Arnosti, C., Derenne, S., & Evershed, R. P. (2000). The molecularly-uncharacterized component of nonliving organic matter in natural environments. *Organic Geochemistry, 31*(10). doi:10.1016/S0146-6380(00)00096-6

Hernandez, B. A. M. (2015). *Influence of indoor nicroenvironments and personal activities on the inhalation dose and personal exposure to PM2.5, PAH, oxy-PAH, VOC and BC air pollutants.* (Doctor of Philosophy). University of Birmingham, University of Birmingham. Retrieved from https://etheses.bham.ac.uk/id/eprint/7731/

Hildemann, L. M., Rogge, W. F., Cass, G. R., Mazurek, M. A., & Simoneit, B. R. T. (1996). Contribution of primary aerosol emissions from vegetation-derived sources to fine particle concentrations in Los Angeles. *Journal of Geophysical Research: Atmospheres, 101*, 19541-19549. doi:10.1029/95JD02136

Hoffer, A., Gelencsér, A., Guyon, P., Kiss, G., Schmid, O., Frank, G. P., . . . Andreae, M. O. (2006). Optical properties of humic-like substances (HULIS) in biomass-burning aerosols. *Atmos. Chem. Phys., 6*(11), 3563–3570. doi:doi.org/10.5194/acp-6-3563-2006

Hou, C., Shao, L., Hu, W., Zhang, D., Zhao, C., Xing, J., . . . Hu, M. (2018). Characteristics and aging of traffic-derived particles in a highway tunnel at a coastal city in southern China. *Science of the Total Environment, 619-620*, 1385-1393. doi:10.1016/j.scitotenv.2017.11.165

Hou, S., Liu, D., Xu, J., Vu, T. V., Wu, X., Srivastava, D., . . . Shi, Z. (2021). Source apportionment of carbonaceous aerosols in Beijing with radiocarbon and organic tracers: insight into the differences between urban and rural sites. *Atmos. Chem. Phys., 21*(10), 8273–8292. doi:10.5194/acp-21-8273-2021

Houck, M. M., & Siegel, J. A. (2010a). *Chapter 5 - Light and Matter* (2 ed.): Academic Press.

Houck, M. M., & Siegel, J. A. (2010b). *Chapter 6 - Separation Methods* (2 ed.): Academic Press.

Howsam, M., & Jones, K. C. (1998). Sources of PAHs in the Environment. In A. H. Neilson (Ed.), *PAHs and Related Compounds* (pp. 137–174). Berlin, Heidelberg: Springer.

Hsieh, Y. P., & Bugna, G. C. (2008). Analysis of black carbon in sediments and soils using multi-element scanning thermal analysis (MESTA). *Organic Geochemistry, 39*, 1562-1571. doi:10.1016/j.orggeochem.2008.07.015

Huang, L., Brook, J. R., Zhang, W., Li, S. M., Graham, L., Ernst, D., . . . Lu, G. (2006). Stable isotope measurements of carbon fractions (OC/EC) in airborne particulate: A new dimension for source characterization and apportionment. *Atmospheric Environment, 40*(15), 2690-2705. doi:10.1016/j.atmosenv.2005.11.062

Huang, X., Deng, X., Li, W., Liu, S., Chen, Y., Yang, B., & Liu, Q. (2019). Internal exposure levels of polycyclic aromatic hydrocarbons in children and adolescents: A systematic review and meta-analysis. *Environ. Health. Prev. Med, 24*. doi:10.1186/s12199-019-0805-9

Hübschmann, H.-J. (2009). *Handbook of GC/MS: Fundamentals and Applications* (2 ed.): Wiley.

Hwang, H.-M., Wade, T. L., & Sericano, J. L. (2003). Concentrations and source characterization of polycyclic aromatic hydrocarbons in pine needles from Korea, Mexico, and United States. *Atmospheric Environment, 37*, 2259-2267. doi:10.1016/S1352-2310(03)00090-6

Iakovides, M., Stephanou, E. G., Apostolaki, M., Hadjicharalambous, M., Evans, J. S., Koutrakis, P., & Achilleos, S. (2019). Study of the occurrence of airborne Polycyclic Aromatic Hydrocarbons associated with respirable particles in two coastal cities at Eastern Mediterranean: Levels, source apportionment, and potential risk for human health. *Atmospheric Environment, 213*, 170-184. doi:10.1016/j.atmosenv.2019.05.059

Iinuma, Y., Brüggemann, E., Gnauk, T., Müller, K., Andreae, M. O., Helas, G., . . . Herrmann, H. (2007). Source characterization of biomass burning particles: The combustion of selected European conifers, African hardwood, savanna grass, and German and Indonesian peat. *Journal of Geophysical Research: Atmospheres, 112*(D8). doi:10.1029/2006JD007120

IPCC. (2018). *Global Warming of 1.5 ºC*. Retrieved from

Ishtiaq, J., Syed, J. H., Jadoon, W. A., Hamid, N., Chaudhry, M. J. I., Shahnawaz, M., . . . Zhangi, G. (2021). Atmospheric polycyclic aromatic hydrocarbons (PAHs) at urban settings in Pakistan: Spatial variations, sources and health risks. *Chemosphere, 274*. doi:10.1016/j.chemosphere.2021.129811

Jahedi, F., Rad, H. D., Goudarzi, G., Birgani, Y. T., Babaei, A. A., & Angali, K. A. (2021). Polycyclic aromatic hydrocarbons in PM1, PM2.5 and PM10 atmospheric particles: identification, sources, temporal and spatial variations. *J Environ Health Sci Eng. , 19*(1), 851–866. doi:10.1007/s40201-021-00652-7

Jambrina-Enríquez, M., Herrera-Herrera, A. V., & Mallo, C. (2018). Wax lipids in fresh and charred anatomical parts of the Celtis australis tree: Insights on paleofire interpretation. *Organic Geochemistry, 122*, 147-160. doi:10.1016/j.orggeochem.2018.05.017

Janssen, N. A. H., Gerlofs-Nijland, M. E., Lanki, T., Salonen, R. O., Cassee, F., & Kryzanowski, M. (2012). *Health effects of black carbon.* Retrieved from https://apps.who.int/iris/handle/10665/352615

Janssen, N. A. H., Hoek, G., Simic-Lawson, M., Fischer, P., van Bree, L., ten Brink, H., . . . Cassee, F. R. (2011). Black carbon as an additional indicator of the adverse health effects of airborne particles compared with PM10 and PM2.5. *Environmental Health Perspectives, 119*(12), 1691-1699. doi:10.1289/ehp.1003369

Jaraula, C., Schwark, L., Moreau, X., Grice, K., & Bagas, L. (2013). *Molecular marker and stable carbon isotope analyses of carbonaceous Ambassador uranium ores of Mulga Rock in Western Australia*. Paper presented at the American Geophysical Union.

Jariyasopit, N., McIntosh, M., Zimmerman, K., Arey, J., Atkinson, R., Cheong, P., . . . Simonich, S. L. M. (2014a). Novel Nitro-PAH Formation from Heterogeneous Reactions of PAHs with NO2, NO3/N2O5, and OH Radicals: Prediction, Laboratory Studies, and Mutagenicity. *Environmental Science & Technology, 48*(1), 412-419. doi:10.1021/es4043808

Jariyasopit, N., Zimmerman, K., Schrlau, J., Arey, J., Atkinson, R., Yu, T.-W., . . . Simonich, S. L. M. (2014b). Heterogeneous Reactions of Particulate Matter-Bound PAHs and NPAHs with NO3/N2O5, OH Radicals, and O3 under Simulated Long-Range Atmospheric Transport Conditions: Reactivity and Mutagenicity. *Environmental Science & Technology, 48*(17), 10155-10164. doi:10.1021/es5015407

Jephcote, C., Hansell, A. L., Adams, K., & Gulliver, J. (2021). Changes in air quality during COVID-19 'lockdown' in the United Kingdom. *Environmental Pollution, 272*. doi:10.1016/j.envpol.2020.116011

Jiang, Y., Yves, U. J., Sun, H., Hu, X., Zhan, H., & Wu, Y. (2016). Distribution, compositional pattern and sources of polycyclic aromatic hydrocarbons in urban soils of an industrial city, Lanzhou, China. *Ecotoxicology and Environmental Safety, 126*, 154-162. doi:10.1016/j.ecoenv.2015.12.037

Kamble, P., Khan, Z., Gillespie, M., Farooq, M., McCalmont, J., Donnison, I., & Watson, I. (2019). Biomass gasification of hybrid seed Miscanthus in Glasgow's downdraft gasifier testbed system. *Energy Procedia, 158*, 1174-1181. doi:10.1016/j.egypro.2019.01.303

Kampa, M., & Castanas, E. (2008). Human health effects of air pollution. *Environmental Pollution, 151*(2), 362-367. doi:10.1016/j.envpol.2007.06.012

Kang, M., Kim, K., Choi, N., Kim, Y. P., & Lee, J. Y. (2020). Recent Occurrence of PAHs and n-Alkanes in PM2.5 in Seoul, Korea and Characteristics of Their Sources and Toxicity. *Int. J. Environ. Res. Public Health 17*(4). doi:10.3390/ijerph17041397

Kaplan, I. R., & Gordon, R. J. (1994). Non-Fossil-Fuel Fine-Particle Organic Carbon Aerosols in Southern California Determined During the Los Angeles Aerosol Characterization and Source Apportionment Study. *Aerosol Science and Technology, 21*(4), 343-359. doi:10.1080/02786829408959720

Karanasiou, A. A., Sitaras, I. E., Siskos, P. A., & Eleftheriadis, K. (2007). Size distribution and sources of trace metals and n-alkanes in the Athens urban aerosol during summer. *Atmospheric Environment, 41*(11), 2368-2381. doi:10.1016/j.atmosenv.2006.11.006

Keyte, I. J., Albinet, A., & Harrison, R. M. (2016). On-road traffic emissions of polycyclic aromatic hydrocarbons and their oxy- and nitro- derivative compounds measured in road tunnel environments. *Science of the Total Environment, 566-567*, 1131-1142. doi:10.1016/j.scitotenv.2016.05.152

Khalili, N. S., Scheff, P. A., & Holsen, T. M. (1995). PAH source fingerprints for coke ovens, diesel and, gasoline engines, highway tunnels, and wood combustion emissions. *Atmospheric Environment, 29*(4), 533-542. doi:10.1016/1352-2310(94)00275-P

Khan, B., Hays, M. D., Geron, C., & Jetter, J. (2012). Differences in the OC/EC Ratios that Characterize Ambient and Source Aerosols due to Thermal-Optical Analysis. *Aerosol Science and Technology, 46*(2), 127-137. doi:10.1080/02786826.2011.609194

Khan, B., Masiol, M., Bruno, C., Pasqualetto, A., Formenton, G. M., Agostinelli, C., & Pavoni, B. (2018). Potential sources and meteorological factors affecting PM2.5-bound polycyclic aromatic hydrocarbon levels in six main cities of northeastern Italy: an assessment of the related carcinogenic and mutagenic risks. *Environmental Science and Pollution Research, 25*, 31987–32000. doi:10.1007/s11356-018-2841-1

Khan, M., F., Latifa, M. T., Lim, C. H., Amil, N., Jaafar, S. A., Dominick, D., . . . Tahir, N. M. (2015). Seasonal effect and source apportionment of polycyclic aromatic hydrocarbons in PM2.5. *Atmospheric Environment, 106*, 178-190. doi:10.1016/j.atmosenv.2015.01.077

Killops, S., & Killops, V. (2005). *Introduction to Organic Geochemistry* (2 ed.). Oxford: Blackwell Publishing.

Kim, J., Wi, E., Moon, H., Son, H., Hong, J., Park, E., . . . Kim, Y. (2022). Quantitative analysis of the concentration of nano-carbon black originating from tire-wear

particles in the road dust. *Science of the Total Environment, 842*. doi:10.1016/j.scitotenv.2022.156830
Kim, J., Yang, S. I., Moon, H., Hong, J., Hong, J., Choi, W., . . . Kim, Y. (2021). Potential release of nano-carbon black from tire-wear particles through the weathering effect. *J. Ind. Eng. Chem., 96*, 322-329. doi:10.1016/j.jiec.2021.01.036
Kim, J. H., Jobbágy, E. G., Richter, D. D., Trumbore, S. E., & Jackson, R. B. (2020). Agricultural acceleration of soil carbonate weathering. *Global Change Biology, 26*(10), 5988-6002. doi:10.1111/gcb.15207
Kim, K.-H., Jahan, S. A., Kabir, E., & Brown, R. J. C. (2013). A review of airborne polycyclic aromatic hydrocarbons (PAHs) and their human health effects. *Environment International, 60*, 71-80. doi:10.1016/j.envint.2013.07.019
Kim, S. Y., Peel, J. L., Hannigan, M. P., Dutton, S. J., Sheppared, L., Clark, M. L., & Vedal, S. (2012). The Temporal Lag Structure of Short-Term Associations of Fine Particulate Matter Chemical Constituents and Cardiovascular and Respiratory Hospitalizations. *Environmental Health Perspectives, 120*(8), 1094-1099. doi:10.1289/ehp.1104721
Kingham, S., Briggs, D., Elliot, P., Fischer, P., & Lebret, E. (2000). Spatial variations in the concentrations of traffic-related pollutants in indoor and outdoor air in Huddersfield, England. *Atmospheric Environment, 34*(6), 905-916. doi:10.1016/S1352-2310(99)00321-0
Kirchstetter, T. W., & Novakov, T. (2007). Controlled generation of black carbon particles from a diffusion flame and applications in evaluating black carbon measurement methods. *Atmospheric Environment, 41*(9), 1874-1888. doi:10.1016/J.ATMOSENV.2006.10.067
Kirillova, E. N., Andersson, A., Sheesley, R. J., Kruså, M., Praveen, P. S., Budhavant, K., . . . Gustafsson, O. (2013). 13C- and 14C-based study of sources and atmospheric processing of water-soluble organic carbon (WSOC) in South Asian aerosols. *Journal of Geophysical Research: Atmospheres, 118*(2).
Kittelson, D. B. (1998). Engines and nanoparticles: a review. *J. Aerosol Sci., 29*, 575-588.
Knicker, H., Müller, P., & Hilscher, A. (2007). How useful is chemical oxidation with dichromate for the determination of “Black Carbon” in fire-affected soils? *Geoderma, 142*(1-2), 178-196. doi:10.1016/j.geoderma.2007.08.010
Kocbach, A., Li, Y., Yttri, K. E., Cassee, F. R., Schwarze, P. E., & Namork, E. (2006). Physicochemical characterisation of combustion particles from vehicle exhaust and residential wood smoke. *Particle and Fibre Toxicology, 3*. doi:10.1186/1743-8977-3-1
Kocbach Bølling, A., Pagels, J., Yttri, K. E., Barregard, L., Sallsten, G., Schwarze, P. E., & Boman, C. (2009). Health effects of residential wood smoke particles: the importance of combustion conditions and physicochemical particle properties. *Particle and Fibre Toxicology, 6*(29). doi:10.1186/1743-8977-6-29
Kojić, I., & Šolević Knudsen, T. (2021). *Compounds in Street Dust Samples, Pančevo, Serbia.* Paper presented at the European Meeting on Environmental Chemistry, Novi Sad, Serbia.
Kubo, T., Bai, W., Nagae, M., & Takao, Y. (2020). Seasonal fluctuation of polycyclic aromatic hydrocarbons and aerosol genotoxicity in long-range transported air mass observed at the western end of Japan. *Int. J. Environ. Res., 17*(4). doi:10.3390/ijerph17041210
Kuhn, T. K., Krull, E. S., Bowater, A., Grice, K., & Gleixner, G. (2010). The occurrence of short chain n-alkanes with an even over odd predominance in higher plants and soils. *Organic Geochemistry, 41*(2), 88-95. doi:10.1016/j.orggeochem.2009.08.003

Kuo, L., Herbert, B. E., & Louchouarn, P. (2008). Can levoglucosan be used to characterize and quantify char/charcoal black carbon in environmental media? *Organic Geochemistry, 39*(10), 1466-1478. doi:10.1016/j.orggeochem.2008.04.026

Kurt, O. K., Zhang, J., & Pinkerton, K. E. (2016). Pulmonary Health Effects of Air Pollution. *Curr Opin Pulm Med., 22*(2), 138-143. doi:10.1097/MCP.0000000000000248

Lack, D. A., Moosmüller, H., McMeeking, G. R., Chakrabarty, R. K., & Baumgardner, D. (2014). Characterizing elemental, equivalent black, and refractory black carbon aerosol particles: a review of techniques, their limitations and uncertainties. *Analytical and Bioanalytical Chemistry, 406*, 99–122. doi:10.1007/s00216-013-7402-3

Ladji, R., Yassaa, N., Balducci, C., & Cecinato, A. (2014). Particle size distribution of n-alkanes and polycyclic aromatic hydrocarbons (PAHS) in urban and industrial aerosol of Algiers, Algeria. *Environmental Science and Pollution Research, 21*, 1819–1832. doi:10.1007/s11356-013-2074-2

Lara, S., Villanueva, F., Martín, P., Salgado, S., Moreno, A., & Sánchez-Verdú, P. (2022). Investigation of PAHs, nitrated PAHs and oxygenated PAHs in PM10 urban aerosols. A comprehensive data analysis. *Chemosphere, 294*. doi:10.1016/j.chemosphere.2022.133745

Laurenson, L., Hickman, S., & Livesey, R. G. (1998). Rotary pump backstreaming: An analytical appraisal of practical results and the factors affecting them. *Journal of Vacuum Science & Technology*, 238–242. doi:10.1116/1.575434

Leitner, A. (2001). The fire catastrophe in the Tauern Tunnel: experience and conclusions for the Austrian guidelines. *Tunnelling and Underground Space Technology, 16*(3), 217-223. doi:10.1016/S0886-7798(01)00042-6

Levin, I., & Hesshaimer, V. (2000). Radiocarbon – A Unique Tracer of Global Carbon Cycle Dynamics. *Radiocarbon, 42*, 69-80. doi:10.1017/S0033822200053066

Levy, I., Mihele, C., Lu, G., Narayan, J., & Brook, J. R. (2014). Evaluating Multipollutant Exposure and Urban Air Quality: Pollutant Interrelationships, Neighborhood Variability, and Nitrogen Dioxide as a Proxy Pollutant. *Environmental Health Perspectives, 122*(1), 65–72. doi:10.1289/ehp.1306518

Li-bin, L., Yan, L., Jin-Ming, L., Ning, T., Kazuichi, H., & Tsuneaki, M. (2007). Development of analyticalmethods for polycyclic aromatic hydrocarbons (PAHs) in airborne particulates: A review. *Journal of Environmental Sciences, 19.* doi:10.1016/S1001-0742(07)60001-1

Li, B., Mitchell, S. C., & Snape, C. E. (1996). Effect of heating rate on normal and catalytic fixed-bed hydropyrolysis of coals. *Fuel, 75*(12), 1393-1396. doi:10.1016/0016-2361(96)00095-6

Li, H., Liu, G., & Cao, Y. (2014). Content and Distribution of Trace Elements and Polycyclic Aromatic Hydrocarbons in Fly Ash from a Coal-Fired CHP Plant *Aerosol and Air Quality Research, 14*, 1179–1188. doi:10.4209/aaqr.2013.06.0216

Liang, F., Lu, M., Keener, T. C., Liu, Z., & Khang, S.-J. (2005). The organic composition of diesel particulate matter, diesel fuel and engine oil of a non-road diesel generator. *Journal of Environmental Monitoring, 7*(10), 983-988. doi:10.1039/B504728E

Lim, S., Hwang, J., Lee, M., Czimczik, C. I., Xu, X., & Savarino, J. (2022). Robust Evidence of 14C, 13C, and 15N Analyses Indicating Fossil Fuel Sources for Total Carbon and Ammonium in Fine Aerosols in Seoul Megacity. *Environmental Science & Technology, 56*(11), 6894-6904. doi:10.1021/acs.est.1c03903

Lin, J. J., & Lee, L. (2004). Characterization of n-alkanes in urban submicron aerosol particles (PM1). *Atmospheric Environment, 38*(19), 2983-2991. doi:10.1016/j.atmosenv.2004.02.048

Lin, L., Lee, M. L., & Eatough, D. J. (2010). Review of Recent Advances in Detection of Organic Markers in Fine Particulate Matter and Their Use for Source Apportionment. *Journal of the Air & Waste Management Association, 60*(1), 3-25. doi:10.3155/1047-3289.60.1.3

Liu, C., Wang, B., Liu, S., Li, S., Zhang, K., Luo, B., & Yang, A. (2021). Type 2 diabetes attributable to PM2.5: A global burden study from 1990 to 2019. *Environment International, 156*. doi:10.1016/j.envint.2021.106725

Liu, D., Allan, J. D., Young, D. E., Coe, H., Beddows, D., Fleming, Z. L., . . . Zotter, P. (2014). Size distribution, mixing state and source apportionment of black carbon aerosol in London during wintertime. . *Atmospheric Chemistry and Physics, 14*(18), 10061–10084. doi:10.5194/acp-14-10061-2014

Local Government Association. (2022). The future of last-mile deliveries: Understanding the local perspective. Retrieved from https://www.local.gov.uk/publications/future-last-mile-deliveries-understanding-local-perspective

Long, C. M., Nascarella, M. A., & Valberg, P. A. (2013). Carbon black vs. black carbon and other airborne materials containing elemental carbon: Physical and chemical distinctions. *Environmental Pollution, 181*, 271-286. doi:doi.org/10.1016/j.envpol.2013.06.009

Lorenzi, D., Entwistle, J. A., Cave, M., & Dean, J. R. (2011). Determination of polycyclic aromatic hydrocarbons in urban street dust: Implications for human health. *Chemosphere, 83*(7), 970-977. doi:10.1016/j.chemosphere.2011.02.020

Lorrain, A., Savoye, N., Chauvaud, L., Paulet, Y.-M., & Naulet, N. (2003). Decarbonation and preservation method for the analysis of organic C and N contents and stable isotope ratios of low-carbonated suspended particulate material. *Analytica Chimica Acta, 491*(2), 125-133. doi:10.1016/S0003-2670(03)00815-8

Love, G. D., McAulay, A., & Snape, C. E. (1997). Effect of Process Variables in Catalytic Hydropyrolysis on the Release of Covalently Bound Aliphatic Hydrocarbons from Sedimentary Organic Matter. *Energy and Fuels, 11*(3), 522-531. doi:10.1021/ef960194x

Love, G. D., Snape, C. E., Carr, A. D., & Houghton, R. C. (1995). Release of covalently-bound alkane biomarkers in high yields from kerogen via catalytic hydropyrolysis. *Organic Geochemistry, 23*, 981-986. doi:10.1016/0146-6380(95)00075-5

Lyu, R., Zongbo, S., Alam, M. S., Wu, X., Liu, D., Vu, T. V., . . . Harrison, R. M. (2019). Alkanes and aliphatic carbonyl compounds in wintertime PM2.5 in Beijing, China. *Atmospheric Environment, 202*, 244-255. doi:10.1016/j.atmosenv.2019.01.023

Madronich, S., Sulzberger, B., Longstreth, J. D., Schikowski, T., Andersen, M. P., Solomon, K. R., & Wilson, S. R. (2023). Changes in tropospheric air quality related to the protection of stratospheric ozone in a changing climate. *Photochemical & Photobiological Sciences, 22*, 1129–1176. doi:10.1007/s43630-023-00369-6

Major, I., Molnár, M., Futó, I., Gergely, V., Bán, S., Machon, A., . . . Varga, T. (2022). Detailed Carbon Isotope Study of PM2.5 Aerosols at Urban Background, Suburban Background and Regional Background Sites in Hungary. *Atmosphere, 13*(5). doi:10.3390/atmos13050716

Majumdar, D., Rajaram, B., Meshram, S., & Rao, C. V. C. (2012). PAHs in Road Dust: Ubiquity, Fate, and Summary of Available Data. *Critical Reviews in Environmental Science and Technology 42*(12). doi:10.1080/10643389.2011.556550

Manning, D. A. C., Lopez-Capel, E., & Barker, S. (2005). Seeing soil carbon: use of thermal analysis in the characterization of soil C reservoirs of differing stability. *Mineralogical Magazine, 69*(4). doi:10.1180/0026461056940260

Mannino, A., & Harvery, H. R. (2004). Black carbon in estuarine and coastal ocean dissolved organic matter. *Limnol. Oceanogr., 49*(3), 735-740. doi:10.4319/lo.2004.49.3.0735

Manoli, E., Kouras, A., Karagkiozidou, O., Argyropoulos, G., Voutsa, D., & Samara, C. (2016). Polycyclic aromatic hydrocarbons (PAHs) at traffic and urban background sites of northern Greece: source apportionment of ambient PAH levels and PAH-induced lung cancer risk. *Environmental Science and Pollution Research, 23*, 3556–3568. doi:10.1007/s11356-015-5573-5

Marr, L. C., Kirchstetter, T. W., Harley, R. A., Miguel, A. H., Hering, S. V., & Hammond, S. K. (1999). Characterization of polycyclic aromatic hydrocarbons in motor vehicles fuels and exhaust emissions. *Environ. Sci. Technol., 33*, 3091-3099.

Marty, J., & Saliot, A. (1982). Aerosols in equatorial Atlantic air: n-alkanes as a function of particle size *Nature, 298*, 144-147.

Marzi, R., Torkelson, B. E., & Olson, R. K. (1993). A revised carbon preference index. *Organic Geochemistry, 20*(8). doi:10.1016/0146-6380(93)90016-5

Masiello, C. (2004). New directions in black carbon organic geochemistry. *Marine Chemistry, 92*, 201-213. doi:10.1016/j.marchem.2004.06.043

Masiello, C., Druffel, E. R. M., & Currie, L. A. (2002). Radiocarbon measurements of black carbon in aerosols and ocean sediments. *Geochimica et Cosmochimica Acta, 66*(6), 1025-1036. doi:10.1016/S0016-7037(01)00831-6

Masiol, M., Hofer, A., Squizzato, S., Piazza, R., Rampazzo, G., & Pavoni, B. (2012). Carcinogenic and mutagenic risk associated to airborne particle-phase polycyclic aromatic hydrocarbons: A source apportionment. *Atmospheric Environment, 60*, 375-382. doi:10.1016/j.atmosenv.2012.06.073

Masri, S., Li, L., Dang, A., Chung, J. H., Chen, J.-C., Fan, Z.-H., & Wu, J. (2018). Source characterization and exposure modeling of gas-phase polycyclic aromatic hydrocarbon (PAH) concentrations in Southern California. *Atmospheric Environment, 177*, 175-186. doi:10.1016/j.atmosenv.2018.01.014

Mazurek, M. A., Cass, G. R., & Simoneit, B. R. T. (1989). Interpretation of High-Resolution Gas Chromatography and High-Resolution Gas Chromatography / Mass Spectrometry Data Acquired from Atmospheric Organic Aerosol Samples. *Aerosol Science and Technology, 10*(2), 408-420. doi:10.1080/02786828908959280

Mazurek, M. A., & Simoneit, B. R. T. (1984). *Characterization of biogenic and petroleum-derived organic matter in aerosols over remote, rural, and urban areas. In: Keith LH (ed) Identification and analysis of organic pollutants in air*. Woburn, Massachusetts: Ann Arbor Science.

McBeath, A. V., Wurster, C. M., & Bird, M. I. (2015). Influence of feedstock properties and pyrolysis conditions on biochar carbon stability as determined by hydrogen pyrolysis. *Biomass & Bioenergy, 73*, 155-173. doi:10.1016/j.biombioe.2014.12.022

Mcrae, C., Snape, C. E., & Fallick, A. E. (1998). Variations in the stable isotope ratios of specific aromatic and aliphatic hydrocarbons from coal conversion processes. *Analyst, 123*, 1519-1523. doi:10.1039/A801899E

Medina, E., Martinelli, L. A., Barbosa, E., & Victoria, R. L. (1999). Natural abundance of 13C in tropical grasses from the INPA, Instituto Nacional de Pesquisas da Amazônia, herbarium. *Brazillian Journal of Botany, 22*(1). doi:10.1590/S0100-84041999000100007

Meredith, W., Ascough, P. L., Bird, M. I., Large, D. J., Snape, C. E., Song, J., . . . Tilston, E. L. (2013). Direct evidence from hydropyrolysis for the retention of long alkyl

moieties in black carbon fractions isolated by acidified dichromate oxidation. *Journal of Analytical and Applied Pyrolysis, 103*, 232-239. doi:10.1016/j.jaap.2012.11.001

Meredith, W., Ascough, P. L., Bird, M. I., Large, D. J., Snape, C. E., Sund, Y., & Tilston, E. L. (2012). Assessment of hydropyrolysis as a method for the quantification of black carbon using standard reference materials. *Geochimica et Cosmochimica Acta, 97*, 131-147. doi:10.1016/j.gca.2012.08.037

Miguel, A. H., Kirchstetter, T. W., Harley, R. B., & Hering, R. A. (1998). On-road emissions of particulate polycyclic aromatic hydrocarbons and black carbon from gasoline and diesel vehicles. *Environ. Sci. Technol., 32*, 450-455.

Molnár, P., Tang, L., Sjöberg, K., & Wichmann, J. (2017). Long-range transport clusters and positive matrix factorization source apportionment for investigating transboundary PM2.5 in Gothenburg, Sweden. *Environ. Sci: Processes Impacts, 19*, 1270-1277. doi:10.1039/C7EM00122C

Monks, P., Carruthers, D., Carslaw, D., Dore, C., Harrison, R. M., Heal, M. R., . . . Gowers, A. (2017). *The potential air quality impacts from biomass combustion.* Retrieved from

Monks, P. S., Granier, C., Fuzzi, S., Stofl, A., Williams, M. L., Akimoto, H., & von Glasow, R. (2009). Atmospheric composition change – global and regional air quality. *Atmospheric Environment, 43*(33), 5268-5350. doi:10.1016/j.atmosenv.2009.08.021

Mordukhovich, I., Wilker, E., Suh, H., Wright, R., Sparrow, D., Vokonas, P. S., & Schwartz, J. (2009). Black Carbon Exposure, Oxidative Stress Genes, and Blood Pressure in a Repeated-Measures Study. *Environmental Health Perspectives, 117*(11), 1767-1772. doi:10.1289/ehp.0900591

Morello-Frosch, R. A., Woodruff, T. J., Axelrad, D. A., & Caldwell, J. C. (2002). Air Toxics and Health Risks in California: The Public Health Implications of Outdoor Concentrations. *Risk Analysis, 20*(2), 273-292. doi:10.1111/0272-4332.202026

Mostert, M. M. R., Ayoko, G. A., & Kokot, S. (2010). Application of chemometrics to analysis of soil pollutants. *Trends in Analytical Chemistry, 29*, 430-435. doi:10.1016/j.trac.2010.02.009

Mousavi, A., Sowlat, M. H., Lovett, C., Rauber, M., Szidat, S., Boffi, R., . . . Sioutas, C. (2019). Source apportionment of black carbon (BC) from fossil fuel and biomass burning in metropolitan Milan, Italy. *Atmospheric Environment, 203*, 252-261. doi:10.1016/j.atmosenv.2019.02.009

Mueller, A., Ulrich, N., Hollmann, J., Sanchez, C. E. Z., Rolle-Kampczyk, U. E., & Bergenad, M. (2019). Characterization of a multianalyte GC-MS/MS procedure for detecting and quantifying polycyclic aromatic hydrocarbons (PAHs) and PAH derivatives from air particulate matter for an improved risk assessment. *Environmental Pollution, 255*. doi:10.1016/j.envpol.2019.112967

Müller, J. O., Su, D. S., Wild, U., & Schlogl, R. (2007). Bulk and surface structural investigations of diesel engine soot and carbon black. *Phys. Chem. Chem. Phys., 9*, 4018-4025. doi:10.1039/B704850E

Murray, I. P., Love, G. D., Snape, C. E., & Bailey, N. (1998). Comparison of covalently-bound aliphatic biomarkers released via hydropyrolysis with their solvent-extractable counterparts for a suite of Kimmeridge clays. *Organic Geochemistry, 29*(5-7), 1487-1505. doi:10.1016/S0146-6380(98)00162-4

NAEI. (2020). Retrieved from https://naei.beis.gov.uk/data/data-selector?view=pms

National Statistics. (2023, 22/03/2023). Emissions of air pollutants in the UK – Particulate matter (PM10 and PM2.5). Retrieved from

https://www.gov.uk/government/statistics/emissions-of-air-pollutants/emissions-of-air-pollutants-in-the-uk-particulate-matter-pm10-and-pm25
Nelson, J., Chalbot, M. G., Tsiodra, I., Mihalopoulos, N., & Kavouras, I. G. (2021). Physicochemical Characterization of Personal Exposures to Smoke Aerosol and PAHs of Wildland Firefighters in Prescribed Fires. *Exposure and Health, 13*, 105–118. doi:10.1007/s12403-020-00366-5
Net Zero Strategy: Build Back Greener. (2021). Retrieved from https://assets.publishing.service.gov.uk/government/uploads/system/uploads/attachment_data/file/1033990/net-zero-strategy-beis.pdf
Niranjan, R., & Thakur, A. K. (2017). The Toxicological Mechanisms of Environmental Soot (Black Carbon) and Carbon Black: Focus on Oxidative Stress and Inflammatory Pathways. *Front Immunol, 8*(763), 1-20 doi:10.3389/fimmu.2017.00763
Nisbet, I., & Lagoy, P. (1992). Toxic Equivalency Factors (TEFs) for Polycyclic Aromatic Hydrocarbons (PAHs) *Regulatory Toxicology and Pharmacology, 16*(3), 290-300. doi:10.1016/0273-2300(92)90009-X
Niu, X., Ho, S. S. H., Ho, K. F., Huang, Y., Sun, J., Wang, Q., . . . Cao, J. (2017). Atmospheric levels and cytotoxicity of polycyclic aromatic hydrocarbons and oxygenated-PAHs in PM2.5 in the Beijing–Tianjin–Hebei region. *Environmental Pollution, 231*, 75-1084. doi:10.1016/j.envpol.2017.08.099
Novakov, T., & Corrigan, C. E. (1995). Thermal characterization of biomass smoke particles. *Microchimica Acta, 119*, 157–166. doi:doi.org/10.1007/BF01244864
Nowakowski, N., Rykowska, I., Wolski, R., & Andrezejewski, P. (2022). Polycyclic Aromatic Hydrocarbons (PAHs) and their Derivatives (O-PAHs, N-PAHs, OH-PAHs): Determination in Suspended Particulate Matter (SPM) – a Review. *Environmental Processes, 9*(2). doi:10.1007/s40710-021-00555-7
O'Sullivan, G., & Kalin, R. M. (2008). Investigation of the Range of Carbon and Hydrogen Isotopes Within a Global Set of Gasolines. *Environ. Forensics, 9*, 166-176. doi:10.1080/15275920802119037
Oanh, N. T. K., Reutergardh, L. B., & Dung, N. T. (1999). Emission of polycyclic aromatic hydrocarbons and particulate matter from domestic combustion of selected fuels. *Environmental Science and Technology, 33*, 2703-2709.
OEHHA. (2005). *Air Toxics Hot Spots Program Risk Assessment Guidance, Part II - Technical Support document for describing available cancer potency factors*. . Retrieved from https://oehha.ca.gov/media/downloads/crnr/may2005hotspots.pdf
Office of Rail and Road. (2022). *Rail emissions: April 2021 to March 2022*. Retrieved from https://dataportal.orr.gov.uk/statistics/infrastructure-and-emissions/rail-emissions/
Ogren, J. A., & Charlson, R. J. (1983). Elemental carbon in the atmosphere: cycle and lifetime. *Tellus B, 35*(4), 241-254. doi:10.1111/j.1600-0889.1983.tb00027.x
Oliveira, C., Martins, N., Tavares, J., Pio, C., Cerqueira, M., Matos, M., . . . Camões, F. (2011). Size distribution of polycyclic aromatic hydrocarbons in a roadway tunnel in Lisbon, Portugal. *Chemosphere, 83*(11), 1588-1596. doi:10.1016/j.chemosphere.2011.01.011
Omar, N. Y. M. J., Abas, M. R. B., Rahman, N. A., Tahir, N. M., Rushdi, A. I., & Simoneit, B. R. T. (2007). Levels and distributions of organic source tracers in air and roadside dust particles of Kuala Lumpur, Malaysia. *Environmental Geology, 52*, 1485-1500. doi:10.1007/s00254-006-0593-6
Oros, D. R., & Simoneit, B. R. T. (2001). Identification and emission factors of molecular tracers in organic aerosols from biomass burning Part 1. Temperate climate

conifers. *Applied Geochemistry, 16*, 1513-1544. doi: 10.1016/S0883-2927(01)00021-X

Pandey, P., Patel, D. K., Khan, A. H., Barman, S. C., Murthy, R. C., & Kisku, G. C. (2012). Temporal distribution of fine particulates (PM2.5, PM10), potentially toxic metals, PAHs and Metal-bound carcinogenic risk in the population of Lucknow City, India. *Journal of Environmental Science and Health, 48*(7). doi:10.1080/10934529.2013.744613

Pant, P., Shi, Z., Pope, F. D., & Harrison, R. M. (2017). Characterization of Traffic-Related Particulate MatterEmissions in a Road Tunnel in Birmingham, UK: Trace Metals and Organic Molecular Markers. *Aerosol and Air Quality Research, 17*(1), 117–130. doi:10.4209/aaqr.2016.01.0040

Paul, M. C. (2012). *Soot: Sources, Formation and Health Effects* (M. C. Paul Ed.): Nova Science Publishers Incorporated.

Paul, S., Sharma, J., Singh, B. D., Saraswati, P. K., & Dutta, S. (2015). Early Eocene equatorial vegetation and depositional environment: Biomarker and palynological evidences from a lignite-bearing sequence of Cambay Basin, western India. *International Journal of Coal Geology, 149*, 77-92. doi:10.1016/j.coal.2015.06.017

PCA. (2015). Missouri Cement Industry. Retrieved from https://www.cement.org/docs/default-source/ga-pdfs/cement-industry-by-state-2015/missouri.pdf

Pehnec, G., Jakovljević, I., Šišović, A., Bešlić, I., & Vađić, V. (2016). Influence of ozone and meteorological parameters on levels of polycyclic aromatic hydrocarbons in the air. *Atmospheric Environment 131*, 263-268. doi:10.1016/j.atmosenv.2016.02.009

Pereira, G. M., Nogueira, T., Kamigauti, L. Y., dos Santos, D. M., Nascimento, E. Q. M., Martins, J. V., . . . Andrade, M. F. (2023). Particulate matter fingerprints in biofuel impacted tunnels in South America's largest metropolitan area. *Science of the Total Environment, 856*. doi:10.1016/j.scitotenv.2022.159006

Pérez, I. A., García, A., Sánchez, S., Pardo, N., & Fernández-Duque, B. (2020). Key Points in Air Pollution Meteorology. *Int. J. Environ. Res. Public Health, 17*(22). doi:10.3390/ijerph17228349

Perron, N., Szidat, S., Fahrni, S., Ruff, M., Wacker, L., Prévôt, A. S. H., & Baltensperger, U. (2010). Towards On-Line 14C Analysis of Carbonaceous Aerosol Fractions *Radiocarbon, 52*(2), 761 - 768. doi:10.1017/S003382220004577X

Petzold, A., Ogren, J. A., Fiebig, M., Laj, P., Li, S. M., Baltensperger, U., . . . Zhang, X. Y. (2013a). Recommendations for reporting "black carbon" measurements. *Atmos. Chem. Phys., 13*(16), 8365-8379. doi:10.5194/acp-13-8365-2013

Petzold, A., Ogren, J. A., Fiebig, M., Laj, P., Li, S. M., Baltensperger, U., . . . Zhang, X. Y. (2013b). Recommendations for reporting “black carbon” measurements. *Atmos. Chem. Phys., 13*, 8365–8379. doi:10.5194/acp-13-8365-2013

Phillips, D. L. (2012). Converting isotope values to diet composition: the use of mixing models. *Journal of Mammology, 93*(2), 342-352. doi:10.1644/11-MAMM-S-158.1

Phuah, C. H., Peterson, M. R., Richards, M. H., Turner, J. H., & Dillner, A. M. (2009). A Temperature Calibration Procedure for the Sunset Laboratory Carbon Aerosol Analysis Lab Instrument. *Aerosol Science and Technology, 43*(10), 1013-1021. doi:10.1080/02786820903124698

Piascik, M., Perez, E. P., & A., H. (2010). *The Certification of the Mass Fractions of Selected Polycyclic Aromatic Hydrocarbons (PAHs) in Fine Dust (PM10-like Matrix) - Certified Reference Material ERM®-CZ100*. Retrieved from Luxembourg: https://publications.jrc.ec.europa.eu/repository/handle/JRC61262

Pilková, Z., Hiller, E., Filová, L., & Jurkovič, L. (2022). Sixteen priority polycyclic aromatic hydrocarbons in roadside soils at traffic light intersections (Bratislava,

Slovakia): concentrations, sources and influencing factors. *Environmental Geochemistry and Health, 44*, 3473-3492. doi:10.1007/s10653-021-01122-7
Piñeiro-Iglesias, M., López-Mahía, P., Vázquez-Blanco, E., Muniategui-Lorenzo, S., & Prada-Rodríguez, D. (2002). Problems in the Extraction of Polycyclic Aromatic Hydrocarbons from Diesel Particulate Matter. *Polycyclic Aromatic Compounds, 22*(2), 129-146. doi:10.1080/10406630211460
Pinkerton, K. E., Green, F. H., Saiki, C., Vallyathan, V., Plopper, C. G., Gopal, V., . . . Schenker, M. B. (2000). Distribution of particulate matter and tissue remodeling in the human lung. *Environmental Health Perspectives, 108*(11). doi:10.1289/ehp.001081063
Pöschl, U. (2005). Atmospheric Aerosols: Composition, Transformation, Climate and Health Effects. *Angewandte Chemie International Edition, 44*(46), 7485-7647. doi:10.1002/anie.200501122
Pozzi, R., De Berardis, B., Paoletti, L., & Guastadisegni, C. (2003). Inflammatory mediators induced by coarse (PM2.5–10) and fine (PM2.5) urban air particles in RAW 264.7 cells. *Toxicology, 183*(1-3), 243-254. doi:10.1016/S0300-483X(02)00545-0
Prevedouros, K., Brorström-Lundén, E., Halsall, C. J., Jones, K. C., Lee, R. G. M., & Sweetman, A. J. (2004). Seasonal and long-term trends in atmospheric PAH concentrations: evidence and implications. *Environmental Pollution, 128*(1-2), 17-27. doi:10.1016/j.envpol.2003.08.032
Provost, E. B., Louwies, T., Cox, B., Op't Roodt, J., Solmi, F., Dons, E., . . . Nawrot, T. S. (2016). Short-term fluctuations in personal black carbon exposure are associated with rapid changes in carotid arterial stiffening. *Environment International, 88*, 228-234. doi:10.1016/j.envint.2015.12.023
Public Health England. (2018). *Estimation of costs to the NHS and social care due to the health impacts of air pollution*. Retrieved from
Ramírez, R., Cuadras, A., Rovira, E., Marcé, R. M. M., & Borrull, F. (2011). Risk Assessment Related to Atmospheric Polycyclic Aromatic Hydrocarbons in Gas and Particle Phases near Industrial Sites. *Environmental Health Perspectives, 119*(8). doi:10.1289/ehp.1002855
Ravindra, K., Bencs, L., Wauters, E., Hoog, J., Deutsch, F., Roekens, E., . . . Van Grieken, R. (2006). Seasonal and site-specific variation in vapour and aerosol phase PAHs over Flanders (Belgium) and their relation with anthropogenic activities. *Atmospheric Environment, 40*(4), 771-785. doi:10.1016/j.atmosenv.2005.10.011
Ravindra, K., Sokhia, R., & Van Grieken, R. (2008a). Atmospheric polycyclic aromatic hydrocarbons: Source attribution, emission factors and regulation. *Atmospheric Environment, 42*(13), 2895-2921. doi:10.1016/j.atmosenv.2007.12.010
Ravindra, K., Wauters, E., & Van Grieken, R. (2008b). Variation in particulate PAHs levels and their relation with the transboundary movement of the air masses. *Science of the Total Environment, 396*, 100-110. doi:10.1016/j.scitotenv.2008.02.018
Reddy, C. M., Pearson, A., Xu, L., McNichol, A. P., Benner, B. A., Wise, S. A., . . . Eglinton, T. I. (2002). Radiocarbon as a Tool To Apportion the Sources of Polycyclic Aromatic Hydrocarbons and Black Carbon in Environmental Samples. *Environ. Sci. Technol., 36*, 1774-1782. doi:10.1021/es011343f
Reid, J. S., Koppmann, R., Eck, T. F., & Eleuterio, D. P. (2005). A review of biomass burning emissions. Part II. Intensive physical properties of biomass burning particles. *Atmos. Chem. Phys. Discuss., 5*, 799–825. doi:10.5194/acp-5-799-2005
Reiffarth, D. G., Petticrew, E. L., Owens, P. N., & Lobb, D. A. (2016). Sources of variability in fatty acid (FA) biomarkers in the application of compound-specific

stable isotopes (CSSIs) to soil and sediment fingerprinting and tracing: A review. *Science of the Total Environment, 565*, 8-27. doi:10.1016/j.scitotenv.2016.04.137

Reimer, P. J., Brown, T. A., & Reimer, R. W. (2004). Discussion: Reporting and Calibration of Post-Bomb 14C Data. *Radiocarbon, 46*(3), 1299–1304. doi:10.1017/S0033822200033154

Rivas, I., Beddows, D., Amato, F., Green, D. C., Järvi, L., Hueglin, C., . . . Kelly, F. (2020). Source apportionment of particle number size distribution in urban background and traffic stations in four European cities. *Environment International, 135*. doi:10.1016/j.envint.2019.105345

Robert, M. J., Snape, C. E., & Mitchell, S. C. (1995). *Hydropyrolysis: fundamentals, two-stage processing and PDU operation*. Dordecht.

Robson, M. G., & Toscano, W. A. (2007). *Risk Assessment for Environmental Health*. San Francisco: Jossey-Bass.

Rocha, J. D., Luengo, C. A., & Snape, C. E. (1999). The scope for generating bio-oils with relatively low oxygen contents via hydropyrolysis. *Organic Geochemistry, 30*(12), 1527-1534. doi:10.1016/S0146-6380(99)00124-2

Rogge, W. F., Hildemann, L. M., Mazurek, M. A., Cass, G. R., & Simoneit, B. R. T. (1993b). Sources of Fine Organic Aerosol. 3. Road Dust, Tire Debris, and Organometallic Brake Lining Dust: Roads as Sources and Sinks. *Environ. Sci. Technol., 27*(9), 1892-1904.

Rogge, W. F., Hildemann, L. M., Mazurek, M. A., Cass, G. R., & Simoneit, B. R. T. (1993c). Sources of fine organic aerosol. 2. Noncatalyst and catalyst-equipped automobiles and heavy-duty diesel trucks. *Environ. Sci. Technol., 27*, 636–651.

Rogge, W. F., Hildemann, L. M., Mazurek, M. A., Cass, G. R., & Simoneit, B. R. T. (1993d). Sources of Fine Organic Aerosol 4. Particulate Abrasion Products from Leaf Surfaces of Urban Plants. *Environ. Sci. Technol., 28*, 2700–2711.

Rogge, W. F., Mazurek, M. A., Hildemann, L. M., Cass, G. R., & Simoneit, B. R. T. (1993a). Quantification of urban organic aerosols at a molecular level: identification, abundance and seasonal variation. . *Atmospheric Environment, 27*(8), 1309–1330. doi:10.1016/0960-1686(93)90257-Y

Rombolà, A. G., Fabbri, D., Meredith, W., Snape, C. E., & Dieguez-Alonsoc, A. (2016). Molecular characterization of the thermally labile fraction of biochar by hydropyrolysis and pyrolysis-GC/MS. *Journal of Analytical and Applied Pyrolysis, 121*, 230-239. doi:10.1016/j.jaap.2016.08.003

Rönkkö, T., Saarikoski, S., Kuittinen, N., Karjalainen, P., Keskinen, H., Järvinen, A., . . . Timonen, H. (2023). Review of black carbon emission factors from different anthropogenic sources. *Envionmental Research Letters, 18*. doi:10.1088/1748-9326/acbb1b

Rumble, H., Rogers, K., Doick, K., Albertini, A., & Hutchings, T. (2015). *Assessing the Ecosystem Services of Glasgow"s Urban Forest: A Technical Report*. Retrieved from https://cdn.forestresearch.gov.uk/2015/07/glasgow_technical_report_v5.1_final.pdf

Samburova, V., Zielinska, B., & Khlystov, A. (2017). Do 16 polycyclic aromatic hydrocarbons represent PAH air toxicity? *Toxics, 5*(3). doi:10.3390/toxics5030017

Sánchez-Piñero, J., Moreda-Piñeiro, J., Turnes-Carou, I., Fernández-Amado, M., Muniategui-Lorenzo, S., & López-Mahía, P. (2021). Polycyclic aromatic hydrocarbons in atmospheric particulate matter (PM10) at a Southwestern Europe coastal city: status, sources and health risk assessment. *Air Quality, Atmosphere & Health volume, 14*, 1325–1339. doi:10.1007/s11869-021-01022-w

Santos Barbosa, J. M. D., Re-Poppi, N., & Santiago-Silva, M. (2006). Polycyclic aromatic hydrocarbons from wood pyrolysis in charcoal production furnaces. *Environmental Research, 101*, 304-311.

Santos, R. R., Cardeal, Z. L., & Menezes, H. C. (2020). Phase distribution of polycyclic aromatic hydrocarbons and their oxygenated and nitrated derivatives in the ambient air of a Brazilian urban area. *Chemosphere, 250*. doi:10.1016/j.chemosphere.2020.126223

Saraga, D., Maggos, T., Degrendele, C., Klánová, J., Horvat, M., Kocman, D., & Gotti, A. (2021). Multi-city comparative PM2.5 source apportionment for fifteen sites in Europe: The ICARUS project. *Science of the Total Environment, 751*. doi:10.1016/j.scitotenv.2020.141855

Sarti, E., Pasti, L., Scaroni, I., Casali, P., Cavazzini, A., & Rossi, M. (2017). Determination of n-alkanes, PAHs and nitro-PAHs in PM2.5 and PM1 sampled in the surroundings of a municipal waste incinerator. *Atmospheric Environment, 149*, 12-13. doi:10.1016/j.atmosenv.2016.11.016

Saxowsky, T. T., Meadows, K. L., Klungland, A., & Doetsch, P. W. (2008). 8-Oxoguanine-mediated transcriptional mutagenesis causes Ras activation in mammalian cells. *PNAS, 105*(48), 18877-18882. doi:10.1073/pnas.0806464105

Schäfer, I. K., Lanny, V., Franke, J., Eglinton, T. I., Zech, M., Vysloužilová, B., & Zech, R. (2016). Leaf waxes in litter and topsoils along a European transect. *Soil, 2*, 551–564. doi:10.5194/soil-2-551-2016

Schauer, J. J., Rogge, W. F., Hildemann, L. M., Mazurek, M. A., Cass, G. R., & Simoneit, B. R. T. (1996). Source apportionment of airborne particulate matter using organic compounds as tracers. *Atmospheric Environment, 30*(22), 3837-3855. Retrieved from 10.1016/1352-2310(96)00085-4

Schneider, M., Smittenberg, R., Dittmar, T., & Schmidt, M. W. I. (2011). Comparison of gas with liquid chromatography for the determination of benzenepolycarboxylic acids as molecular tracers of black carbon. *Organic Geochemistry, 42*(3), 275-282. doi:10.1016/j.orggeochem.2011.01.003

Schorcht, F., Kourti, I., Scalet, B. M., Roudier, S., & Sancho, L. D. (2013). *Best Available Techniques (BAT) Reference Document for the Production of Cement, Lime and Magnesium Oxide*. Retrieved from Luxembourg: https://eippcb.jrc.ec.europa.eu/sites/default/files/2019-11/CLM_Published_def_0.pdf

Schuur, E. A. G., Druffel, E. R. M., & Trumbore, S. E. (2016). *Radiocarbon and Climate Change: Mechanisms, Applications and Laboratory Techniques* (E. A. G. Schuur, E. R. M. Druffel, & S. E. Trumbore Eds.). Switzerland: Springer.

Scott, E. M. (2003). Part 2: The Third International Radiocarbon Intercomparison (TIRI). *Radiocarbon, 45*(2), 293-328.

Seibert, P., Kromp-Kolb, H., Baltensperger, U., Jost, D. T., & Schwikowski, M. (1994). *Air Pollution Modeling and Its Application X: Trajectory Analysis of High-Alpine Air Pollution Data* (Vol. 18).

Seng, T. H., Abas, M. R., & Tahir, N. M. (2016). Characterization of Hydrocarbons in Smoke Aerosols from Burning of Three Tropical Wood Species. *Sains Malaysiana, 45*(3), 365–371.

Seng, T. H., Tahir, N. M., & Abas, M. R. B. (2007). Aliphatic and PAHs Emissions from Open Burning of Selected Tropic Woods. *The Malaysian Journal of Analytical Sciences, 11*(1), 36-41.

Sephton, M. A., Love, G. D., Meredith, W., Snape, C. E., Sun, C., & Watson, J. S. (2005). Hydropyrolysis: A new technique for the analysis of macromolecular material in

meteorites. *Planetary and Space Science, 53*, 1280-1286. doi:10.1016/j.pss.2005.06.008
Sergides, C. A., Jassim, J. A., Chughtai, A. R., & Smith, D. M. (1987). The structure of hexane soot: Part III. Ozonation studies. *Applied Spectroscopy, 41*(3), 482-492.
Shi, J. P., Mark, D., & Harrison, R. M. (2000). Characterization of particles from a current technology heavy-duty diesel engine. *Environmental Science & Technology, 34*, 748-755. doi:10.1021/es990530z
Shi, M., Zhang, R., Wang, Y., Zhang, Y., Zhang, Y., & Zhang, Y. (2020). Health risk assessments of polycyclic aromatic hydrocarbons and chlorinated/brominated polycyclic aromatic hydrocarbons in urban air particles in a haze frequent area in China. *Emerging Contaminants, 6*, 172-178. doi:10.1016/j.emcon.2020.04.002
Shirani, A. (2011). *Behaviour of Polycyclic Aromatic Hydrocarbons in Stabilised and Solidified Contaminated Soil.* (Doctor of Philosophy). Cardiff University, Retrieved from https://orca.cardiff.ac.uk/id/eprint/55081/1/U585470.pdf
Shrubsole, C., Ridley, I., Biddulph, P., Milner, J., Vardoulakis, S., Ucci, M., . . . Davies, M. (2012). Indoor PM2.5 exposure in London's domestic stock: Modelling current and future exposures following energy efficient refurbishment. *Atmospheric Environment, 62*, 336-343. doi:10.1016/j.atmosenv.2012.08.047
Sicard, P., & Dalstein-Richier, L. (2015). Health and vitality assessment of two common pine species in the context of climate change in southern Europe. *Environmental Research, 137*, 235-245. doi:10.1016/j.envres.2014.12.025
Simoneit, B. R. T. (1984). Organic matter of the troposphere-III. Characterization and sources of petroleum and pyrogenic residues in aerosols over the western united states. *Atmospheric Environment, 18*, 51-67. doi:10.1016/0004-6981(84)90228-2
Simoneit, B. R. T. (1989). Organic matter of the troposphere—V. Application of molecular marker analysis to biogenic emissions into the troposphere for source reconciliations. *Journal of Atmospheric Chemistry, 8*, 251-275. doi:10.1007/BF00051497
Simoneit, B. R. T., Kobayashi, M., Mochida, M., Kawamura, K., Lee, M., Lim, H. J., . . . Komazaki, Y. (2004). Composition and major sources of organic compounds of aerosolparticulate matter sampled during the ACE-Asia campaign. *Journal of Geophysical Research: Atmospheres, 109*. doi:10.1029/2004JD00459
Simoneit, B. R. T., Sheng, G., Chen, X., Fu, J., Zhang, J., & Xu, Y. (1991). Molecular marker study of extractable organic matter in aerosols from urban areas of China. *Atmospheric Environment. Part A. General Topics, 25*(10), 2111-2129. doi:10.1016/0960-1686(91)90088-O
Singh, V., Ravindra, K., Sahu, L., & Sokhi, R. (2018). Trends of atmospheric black carbon concentration over the United Kingdom. *Atmospheric Environment, 178*, 148-157. doi:10.1016/j.atmosenv.2018.01.030
Sirignano, C., Riccio, A., Chianese, E., Ni, H., Zenker, K., D'Onofrio, A., . . . Dusek, U. (2019). High Contribution of Biomass Combustion to PM2.5 in the City Centre of Naples (Italy). *Atmosphere, 10*(8). doi:10.3390/atmos10080451
Slota, P. J., Jull, A. J. T., Linick, T. W., & Toolin, L. J. (1987). Preparation of small samples for 14C accelerator targets by catalytic reduction of CO. *Radiocarbon, 29*(2), 303-306. doi:10.1017/S0033822200056988
Smallwood, B. J., Philp, R. P., T.W., B., & Allen, J. D. (2001). The Use of Stable Isotopes to Differentiate Specific Source Markers for MTBE. *Environmental Forensics, 2*(3), 215-221. doi:10.1006/enfo.2000.0023
Smith, D. J. T., & Harrison, R. M. (1998). *Polycyclic aromatic hydrocarbons in atmospheric particles*: Wiley.

Snape, C. E., Lafferty, C. J., Eglinton, G., Robinson, N., & Collier, R. (1994). The potential of hydropyrolysis as a route for coal liquefaction. *International Journal of Energy Research, 18*, 63-344. doi:10.1002/er.4440180221

Sparkman, O. D., Penton, Z. E., & Kitson, F. G. (2011). *Chapter 1 - Introduction and History* (2 ed.): Academic Press.

SPC. (2020). Cement industry's contribution to the Polish economy. Retrieved from https://www.polskicement.pl/wp-content/uploads/2020/10/EY-Raport-wp%C5%82ywu-podsumowanie-EN.pdf

Spengler, J. D., McCarthy, J. F., & Samet, J. M. (2001). *Indoor Air Quality Handbook.* New York: McGraw-Hill.

Stefanova, M., Markova, K., Marinov, S. P., & Simoneit, B. R. T. (2005). Biomarkers in the fossils from the Miocene-aged Chukurovo lignite, Bulgaria: Sesqui- and diterpenoids. *Bulletin of Geosciences, 80*(1), 93-97.

Stein, A. F., Draxler, R. R., Rolph, G. D., Stunder, B. J. B., Cohen, M. D., & Ngan, F. (2015). NOAA's HYSPLIT atmospheric transport and dispersion modeling system. *Bull. Amer. Meteor. Soc., 96*, 2059-2077. doi:10.1175/BAMS-D-14-00110.1

Stout, S. A., & Emsbo-Mattingly, S. D. (2008). Concentration and character of PAHs and other hydrocarbons in coals of varying rank – Implications for environmental studies of soils and sediments containing particulate coal. *Organic Geochemistry, 39*, 801-819. doi:10.1016/j.orggeochem.2008.04.017

Su, B., Zhang, G., Zhuo, Z., Xie, Q., Du, X., Fu, Y., . . . Zhou, Z. (2021). Different characteristics of individual particles from light-duty diesel vehicle at the launching and idling state by AAC-SPAMS. *Journal of Hazardous Materials, 418*. doi:10.1016/j.jhazmat.2021.126304

Su, D. S., Müller, J.-O., Jentoft, R. E., Rothe, D., Jacob, E., & Schlögl, R. (2004). Fullerene-like soot from EuroIV diesel engine: consequences for catalytic automotive pollution control. . *Topics in Catalysis, 30*, 241–245. doi:10.1023/B:TOCA.0000029756.50941.02

Szidat, S., Bench, G., Bernardoni, V., Calzolai, G., Czimczik, C. I., Derendorp, L., . . . Prévôt, A. S. H. (2013). Intercomparison of 14C Analysis of Carbonaceous Aerosols: Exercise 2009. *Radiocarbon, 55*(3), 1496-1509. doi:10.1017/S0033822200048426

Szidat, S., Jenk, T. M., Gäggeler, H. W., & Synal, H.-A. (2004a). Source apportionment of aerosols by 14C measurements in different carbonaceous particle fractions. *Radiocarbon, 46*, 475-484. doi:10.1017/S0033822200039783

Szidat, S., Jenk, T. M., Gäggeler, H. W., Synal, H.-A., Hajdas, I., Bonani, G., & Saurer, M. (2004b). THEODORE, a two-step heating system for the EC/OC determination of radiocarbon (14C) in the environment. *Nucl. Instrum. Meth. B., 223-224*, 829-836. doi:10.1016/j.nimb.2004.04.153

Tadsanaprasittipol, A., Tonrub, P., Beverland, I. J., & Kalin, R. M. (2021). Characterization of PM10-Bound Polycyclic Aromatic Hydrocarbons and Associated Carcinogenic Risk in Bangkok, Thailand. *Applied Science, 11*. doi:10.3390/app11104501

Tan, J. H., Bi, X. H., Duan, J. C., Rahn, K. A., Sheng, G. Y., & Fu, J. M. (2006). Seasonal variation of particulate polycyclic aromatic hydrocarbons associated with PM10 in Guangzhou, China. *Atmospheric Research, 80*(4), 250-262. doi:10.1016/j.atmosres.2005.09.004

Tang, X. L., Bi, X. H., Sheng, G. Y., Tan, J. H., & Fu, J. M. (2006). Seasonal variation of the particle size distribution of n-alkanes and polycyclic aromatic hydrocarbons (PAHs) in urban aerosol of Guangzhou, China. *Environmental Monitoring and Assessment, 117*, 193-213. doi:10.1007/s10661-006-0440-y

Tankersley, C. G., Bierman, A., & Rabold, R. (2007). Variation in Heart Rate Regulation and the Effects of Particle Exposure in Inbred Mice. *International Forum for Respiratory Research, 19*(8), 621-629. doi:10.1080/08958370701353049
Tankersley, C. G., Campen, M., Bierman, A., Flanders, S. E., Broman, K. W., & Rabold, R. (2004). Particle Effects on Heart-Rate Regulation in Senescent Mice. *Inhalation Toxicology, 16*, 381-390. doi:10.1080/08958370490439551
TfL. (2021). *Travel in London*. Retrieved from https://content.tfl.gov.uk/travel-in-london-report-14.pdf
The Air Quality England Regulations. (2000). Retrieved from https://www.legislation.gov.uk/uksi/2000/928/contents/made
The Air Quality Standards Regulations. (2010). Retrieved from https://www.legislation.gov.uk/uksi/2010/1001/contents/made
The Air Quality Standards Regulations Amendment. (2016). Retrieved from https://www.legislation.gov.uk/uksi/2016/1184/contents/made
The National Centre for Emissions Management - KOBiZE. (2018). *Poland's Informative Inventory Report*. Retrieved from Warszawa: https://www.kobize.pl/uploads/materialy/materialy_do_pobrania/krajowa_inwentaryzacja_emisji/IIR_2018_POL.pdf
Thornes, J. E., Hickman, A., Baker, C., Cai, X., & Saborit, J. M. D. (2017). Air quality in enclosed railway stations. *Proceedings of the Institution of Civil Engineers - Transport, 170*(2), 99-107. doi:10.1680/jtran.15.00094
Tobiszewski, M., & Namieśnik, J. (2012). PAH diagnostic ratios for the identification of pollution emission sources. *Environmental Pollution, 162*, 110-119. doi:10.1016/j.envpol.2011.10.025
Tomlin, A. S. (2021). Air Quality and Climate Impacts of Biomass Use as an Energy Source: A Review. *Energy and Fuels, 35*(18), 14213-14240. doi:10.1021/acs.energyfuels.1c01523
Toney, J. L., Huang, Y., Fritz, S. C., Baker, P. A., Grimm, E., & Nyren, P. (2010). Climatic and environmental controls on the occurrence and distributions of long chain alkenones in lakes of the interior United States. *Geochimica et Cosmochimica Acta, 74*(5), 1563-1578. doi:10.1016/j.gca.2009.11.021
Transport for Greater Manchester. (2016). *Greater Manchester Air Quality Action Plan 2016-2021*. Retrieved from
Transport for Greater Manchester. (2021). *Air Quality Annual Status Report (ASR)*. Retrieved from https://www.manchester.gov.uk/downloads/download/4166/air_quality_reports
Transport for Greater Manchester. (2023). Get Cycling in Greater Manchester. Retrieved from https://tfgm.pindarcreative.co.uk/
Transport for London: Travel in London (14). (2021). Retrieved from https://content.tfl.gov.uk/travel-in-london-report-14.pdf
Transport for Scotland. (n.d.). Chapter 13 - Environment. Retrieved from https://www.transport.gov.scot/publication/scottish-transport-statistics-2021/chapter-13-environment/
Transport Scotland. (2022). *Scottish Transport Statistics*. Retrieved from https://www.transport.gov.scot/publication/scottish-transport-statistics-2022/
Traversi, D., Schiliro, T., Degan, R., Pignata, C., Alessandria, L., & Gilli, G. (2011). Involvement of nitro-compounds in th emutagenicity of urban PM2.5 and PM10 in Turin. *Mutat. Res.*, 54-59. doi:10.1016/j.mrgentox.2011.09.002
Turrio-Baldassarri, L., Battistelli, C. L., & Iamiceli, A. L. (2003). Evaluation of the efficiency of extraction of PAHs from diesel particulate matter with pressurized

solvents. *Analytical and Bioanalytical Chemistry, 375*, 589–595. doi:10.1007/s00216-002-1733-9
Tzillah, A. (2009). *The emissions of selected air pollutants from biodiesel fuel usage.* (Master of Science). University of Cincinnati, Retrieved from https://www.proquest.com/openview/0461a7994a73c254f326bbd567566d8f/1?pq-origsite=gscholar&cbl=18750 (1473511)
UK Air. (n.d.-a). AQMA Summary. Retrieved from https://uk-air.defra.gov.uk/aqma/summary
UK Air. (n.d.-b). Daily Air Quality Index. Retrieved from https://uk-air.defra.gov.uk/air-pollution/daqi?view=more-info
UK Air. (n.d.-c). Local Authority Details: City of Glasgow. Retrieved from https://uk-air.defra.gov.uk/aqma/local-authorities?la_id=373
UK Air. (n.d.-d). Smoke Control Areas Map. Retrieved from https://uk-air.defra.gov.uk/data/sca/
UK Government. (2022a). *Chief Medical Officer's annual report 2022: air pollution.* Retrieved from https://www.gov.uk/government/publications/chief-medical-officers-annual-report-2022-air-pollution
UK Government. (2022b). *Statement on the differential toxicity of particulate matter according to source or constituents: 2022*. Retrieved from https://www.gov.uk/government/publications/particulate-air-pollution-health-effects-of-exposure/statement-on-the-differential-toxicity-of-particulate-matter-according-to-source-or-constituents-2022
UK Government. (2022c). *Transport and environment statistics 2022*. Retrieved from https://www.gov.uk/government/statistics/transport-and-environment-statistics-2022/transport-and-environment-statistics-2022
UK Parliament. (2022). Air quality: policies, proposals and concerns. Retrieved from https://commonslibrary.parliament.uk/research-briefings/cbp-9600/
Umbuzeiro, G. A., Franco, A., Martins, M. H., Kummrow, F., Carvalho, L., Schmeiser, H. H., . . . Claxton, L. D. (2008). Mutagenicity and DNA adduct formation of PAH, nitro-PAH, and oxy-PAH fractions of atmospheric particulate matter from São Paulo, Brazil. *Mutat. Res. Genet. Toxicol. Environ. Mutagen., 652*(1), 72-80. doi:10.1016/j.mrgentox.2007.12.007
United States Census Bureau. (2000, 08/10/2021). Historical Census of Housing Tables: House Heating Fuel. Retrieved from https://www.census.gov/data/tables/time-series/dec/coh-fuels.html
USEPA. (1993). *Provisional Guidance for Quantitative Risk Assessment of Polycyclic Aromatic Hydrocarbons*. Retrieved from
USEPA. (2011). *Integrated Risk Information System (IRIS) Glossary*. Retrieved from https://www.epa.gov/iris
USEPA. (2017). *Toxicological review of benzo[a]pyrene - integrated risk information system*. Retrieved from https://cfpub.epa.gov/ncea/iris_drafts/recordisplay.cfm?deid=329750
Van Leeuwen, F. W., De Kleijn, D. P. V., Van Den Hurk, H. H., Neubauer, A., Sonnemans, M. A. F., Sluijs, J. A., . . . Hol, E. M. (1998a). Frameshift Mutants of β Amyloid Precursor Protein and Ubiquitin-B in Alzheimer's and Down Patients. *Science, 279*(5348), 242-247. doi:10.1126/science.279.5348.242
Van Leeuwen, F. W., Hol, E. M., & Burbach, J. P. H. (1998b). Mutations in RNA: a first example of molecular misreading in Alzheimer's disease. *Trends in Neurosciences, 21*(8), 331-335. doi:10.1016/S0166-2236(98)01280-6
Van Pee, T., Hogervorst, J., Dockx, Y., Witters, K., Thijs, S., Wang, C., . . . Nawrot, T. S. (2023). Accumulation of Black Carbon Particles in Placenta, Cord Blood, and

Childhood Urine in Association with the Intestinal Microbiome Diversity and Composition in Four- to Six-Year-Old Children in the ENVIRONAGE Birth Cohort. *Environmental Health Perspectives, 131*(1). doi:10.1289/EHP11257

Vardoulakis, S., Giagloglou, E., Steinle, S., Davis, A., Sleeuwenhoek, A., Galea, K. S., . . . Crawford, J. O. (2020). Indoor Exposure to Selected Air Pollutants in the Home Environment: A Systematic Review. *Int. J. Environ. Res. Public Health, 17*(23). doi:10.3390/ijerph17238972

Vermulst, M., Denney, A. S., Lang, M. J., Hung, C.-W., Moore, S., Moseley, M. A., . . . Erie, D. A. (2015). Transcription errors induce proteotoxic stress and shorten cellular lifespan. *Nature Communications, 6*. doi:10.1038/ncomms9065

Visser, S., Slowik, J. G., Furger, M., Zotter, P., Bukowiecki, N., Canonaco, F., & Prévôt, A. S. H. (2015). Advanced source apportionment of size-resolved trace elements at multiple sites in London during winter. *Atmos. Chem. Phys., 15*, 11291-11309. doi:10.5194/acp-15-11291-2015

Wang, B., Lau, Y., Huang, Y., Organ, B., Chuang, H., Ho, S. S. H., . . . Ho, K. (2021). Chemical and toxicological characterization of particulate emissions from diesel vehicles. *Journal of Hazardous Materials, 405*. doi:10.1016/j.jhazmat.2020.124613

Wang, G., Huang, L., Zhao, X., Niu, H., & Dai, Z. (2006). Aliphatic and polycyclic aromatic hydrocarbons of atmospheric aerosols in five locations of Nanjing urban area, China. *Atmospheric Research, 81*(1), 54-66. doi:10.1016/j.atmosres.2005.11.004

Wang, G., Zhen, L., Lü, P., Jiang, R., & Song, W. (2013). Effects of ozone and fine particulate matter (PM2.5) on rat cardiac autonomic nervous system and systemic inflammation. *Journal of Hygiene Research, 42*(4), 554-560.

Wang, W., Huang, M., Kang, Y., Wang, H., Leung, A. O. W., Cheung, K. C., & Wong, M. H. (2011a). Polycyclic aromatic hydrocarbons (PAHs) in urban surface dust of Guangzhou, China: status, sources and human health risk assessment. . *Science of the Total Environment, 409*(21), 4519–4527. doi:10.1016/j.scitotenv.2011.07.030

Wang, W., Jariyasopit, N., Schrlau, J., Jia, Y., Tao, S., Yu, T.-W., . . . Simonich, S. L. M. (2011b). Concentration and Photochemistry of PAHs, NPAHs, and OPAHs and Toxicity of PM2.5 during the Beijing Olympic Games. *Environmental Science & Technology, 45*(16), 6887-6895. doi:10.1021/es201443z

Waters, C. N., Syvitski, J. P. M., Gałuszka, A., Hancock, G. J., Zalasiewicz, J., Cearreta, A., & Barnossky, A. (2015). Can nuclear weapons fallout mark the beginning of the Anthropocene Epoch? *Bulletin of the Atomic Scientists, 71*(3), 46-57. doi:10.1177/0096340215581357

Watson, A. Y., & Valberg, P. A. (2001). Carbon Black and Soot: Two Different Substances. *American Industrial Hygiene Association, 62*(2), 218-228. doi:10.1080/15298660108984625

Wei, X., Liu, M., Yang, J., Du, W., Sun, X., Huang, Y., . . . Zhou, Y. (2019). Characterization of PM2.5-bound PAHs and carbonaceous aerosols during three-month severe haze episode in Shanghai, China: Chemical composition, source apportionment and long-range transportation. *Atmospheric Environment, 203*, 1-9. doi:10.1016/j.atmosenv.2019.01.046

Weingartner, E., Burtscher, H., & Baltensperger, U. (1997). Hygroscopic properties of carbon and diesel soot particles. *Atmospheric Environment, 31*(15), 2311-2327. doi:doi.org/10.1016/S1352-2310(97)00023-X

Weissenbok, R., Biegalski, S. R., Currie, L. A., Klinedinst, D. B., Golser, R., Klouda, G. A., & Wild, E. (1998). 14C Measurements of Sub-Milligram Carbon Samples from Aerosols. *Radiocarbon, 40*(1), 265-272. doi:10.1017/S0033822200018130

WHO. (2000). *Air Quality Guidelines for Europe (Second Edition)*. . Retrieved from https://www.euro.who.int/en/health-topics/environment-and-health/air-quality/publications/pre2009/who-air-quality-guidelines-for-europe,-2nd-edition,-2000-cd-rom-version

WHO. (2012). *Health Effects of Black Carbon*. Retrieved from https://www.euro.who.int/__data/assets/pdf_file/0004/162535/e96541.pdf

WHO. (2017). *Guidelines for drinking-water quality*. Retrieved from https://www.who.int/publications/i/item/9789241549950

Wood, R. (2015). From revolution to convention: the past, present and future of radiocarbon dating. *Journal of Archaeological Science, 56*, 61-72. doi:10.1016/j.jas.2015.02.019

World Health Organisation. Air pollution. Retrieved from https://www.who.int/health-topics/air-pollution#tab=tab_2

Wu, H., Reis, S., Lin, C., Beverland, I. J., & Heal, M. R. (2015). Identifying drivers for the intra-urban spatial variability of airborne particulate matter components and their interrelationships. *Atmospheric Environment, 112*, 306-316. doi:10.1016/j.atmosenv.2015.04.059

Wurster, C. M., Lloyd, J., Godrick, I., Saiz, G., & Bird, M. I. (2012). Quantifying the abundance and stable isotope composition of pyrogenic carbon using hydrogen pyrolysis. *Rapid Communications in Mass Spectrometry, 26*(23), 2690-2696. doi:10.1002/rcm.6397

Wurster, C. M., Saiz, G., Schneider, M. P. W., Schmidt, M. W. I., & Bird, M. I. (2013). Quantifying pyrogenic carbon from thermosequences of wood and grass using hydrogen pyrolysis. *Organic Geochemistry, 62*, 28-32. doi:10.1016/j.orggeochem.2013.06.009

Xu, D., Huang, N., Wang, Q., & Liu, H. (2008). Study of ambient PM2.5 on the influence of the inflammation injury and the immune function of subchronic exposure rats. *Journal of Hygiene Research, 37*(4), 423-428.

Xu, R., Alam, M. S., Stark, C., & Harrison, R. M. (2020). Composition and emission factors of traffic- emitted intermediate volatility and semi-volatile hydrocarbons (C10–C36) at a street canyon and urban background sites in central London, UK. *Atmospheric Environment, 231*. doi:10.1016/j.atmosenv.2020.117448

Xu, S., Anderson, R., Bryant, C., Cook, G. T., Dougans, A., Freeman, S. P. H. T., . . . Scott, E. M. (2004). Capabilities of the new SUERC 5MV AMS facility for 14C dating. . *Radiocarbon, 46*(1), 59-64.

Yadav, S., Bamotra, S., & Tandon, A. (2020). Aerosol-associated non-polar organic compounds (NPOCs) at Jammu, India, in the North-Western Himalayan Region: seasonal variations in sources and processes. *Environmental Science and Pollution Research, 27*(15), 18875-18892. doi:10.1007/s11356-020-08374-3

Yadav, S., Tandon, A., & Attri, A. K. (2013a). Characterization of aerosol associated non-polar organic compounds using TD-GC-MS: A four year study from Delhi, India. *Journal of Hazardous Materials, 252–253*, 29-44. doi:10.1016/j.jhazmat.2013.02.024

Yadav, S., Tandon, A., & Attri, A. K. (2013b). Monthly and Seasonal Variations in Aerosol Associated n-alkane Profiles in Relation to Meteorological Parameters in New Delhi, India. *Aerosol and Air Quality Research, 13*(1), 287–300. doi:10.4209/aaqr.2012.01.0004

Yagoh, H., Murayama, H., Suzuki, T., Tominaga, Y., Shibuya, N., & Masuda, Y. (2006). Simultaneous Monitoring Method of Polycyclic Aromatic Hydrocarbons and Persistent Organic Pollutants in the Atmosphere Using Activated Carbon Fiber Filter Paper. *Analytical Sciences, 22*(4), 583-590. doi:10.2116/analsci.22.583

Yang, H., Yu, J. Z., Ho, S. S. H., Xu, J., Wu, W.-S., Wan, C. H., . . . Wang, L. (2005). The chemical composition of inorganic and carbonaceous materials in PM2.5 in Nanjing, China. *Atmospheric Environment, 39*(20), 3735-3749. doi:10.1016/j.atmosenv.2005.03.010

Yassaa, N., Meklati, B. Y., Cecinato, A., & Marino, F. (2001). Organic Aerosols in Urban and Waste Landfill of Algiers Metropolitan Area: Occurrence and Sources. *Environ. Sci. Technol., 35*(2), 306–311. doi:10.1021/es991316d

Yim, U. H., Hong, S. H., Shim, W. J., Oh, J. R., & Chang, M. (2005). Spatio-temporal distribution and characteristics of PAHs in sediments from Masan Bay, Korea. *Marine Pollution Bulletin, 50*(3), 319-326. doi:10.1016/j.marpolbul.2004.11.003

Yin, J., & Harrison, R. M. (2008). Pragmatic mass closure study for PM1.0, PM2.5 and PM10 at roadside, urban background and rural sites. *Atmospheric Environment, 42*, 980-988. doi:10.1016/j.atmosenv.2007.10.005

Youn, J. S., Kim, Y. M., Siddiqui, M. Z., Watanabe, A., Han, S., Jeong, S., . . . Jeon, K. J. (2020). Quantification of tire wear particles in road dust from industrial and residential areas in Seoul,Korea. *Science of the Total Environment, 842*. doi:10.1016/j.scitotenv.2021.147177

Zakaria, M. P., Takada, H., Tsutsumi, S., Ohno, K., Yamada, J., Kouno, E., & Kumata, H. (2002). Distribution of Polycyclic Aromatic Hydrocarbons (PAHs) in Rivers and Estuaries in Malaysia: A Widespread Input of Petrogenic PAHs. *Environ. Sci. Technol., 36*(9), 1907-1918. doi:10.1021/es011278+

Zencak, Z., Elmquist, M., & Gustafsson, O. (2007). Quantification and radiocarbon source apportionment of black carbon in atmospheric aerosols using the CTO-375 method. *Atmospheric Environment, 41*(36), 7895-7906. doi:10.1016/j.atmosenv.2007.06.006

Zenker, K., Sirignano, C., Riccio, A., Chianese, E., Calfapietra, C., Prati, M. V., . . . Dusek, U. (2020). δ13C signatures of organic aerosols: Measurement method evaluation and application in a source study. *Journal of Aerosol Science, 145*. doi:10.1016/j.jaerosci.2020.105534

Zenker, K., Vonwiller, M., Szidat, S., Calzolai, G., Giannoni, M., Bernardoni, V., . . . Dusek, U. (2017). Evaluation and Inter-Comparison of Oxygen-Based OC-EC Separation Methods for Radiocarbon Analysis of Ambient Aerosol Particle Samples. *Atmosphere, 8*(11). doi:10.3390/atmos8110226

Zhan, C., Han, Y., Cao, J., Wei, C., Zhang, J., & An, Z. (2013). Validation and application of a thermal–optical reflectance (TOR) method for measuring black carbon in loess sediments. *Chemosphere, 91*, 1462-1470. doi:10.1016/j.chemosphere.2012.12.011

Zhang, C., Ding, R., Xiao, C., Xu, Y., Cheng, H., Zhu, F., . . . Cao, J. (2017). Association between air pollution and cardiovascular mortality in Hefei, China: A time-series analysis. *Environmental Pollution, 229*, 790-797. doi:10.1016/j.envpol.2017.06.022

Zhang, R., Khalizov, A. F., Pagels, J., Zhang, D., Xue, H., & McMurry, P. H. (2008). Variability in morphology, hygroscopicity, and optical properties of soot aerosols during atmospheric processing. *Proc Natl Acad Sci U S A., 105*(30). doi:doi.org/10.1073/pnas.0804860105

Zhang, X., Li, J., Mo, Y., Shen, C., Ding, P., Wang, N., . . . Zhang, G. (2019a). Isolation and radiocarbon analysis of elemental carbon in atmospheric aerosols using hydropyrolysis. *Atmospheric Environment, 198*, 381-386. doi:10.1016/j.atmosenv.2018.11.005

Zhang, X., Li, J., Zhu, S., Liu, J., Ding, P., Gao, S., . . . Zhang, G. (2023). Technical note: Intercomparison Study of the EC Radiocarbon Analysis Methods Using Synthetic Known Samples (Pre-print). *Atmospheric Chemistry and Physics*. doi:10.5194/egusphere-2023-379

Zhang, Y., Albinet, A., Petit, J. E., Jacob, V., Chevrier, F., Gille, G., . . . Faveza, O. (2020). Substantial brown carbon emissions from wintertime residential wood burning over France. *Science of the Total Environment, 743*. doi:10.1016/j.scitotenv.2020.140752

Zhang, Y., Dong, S., Wang, H., Tao, S., & Kiyama, R. (2016). Biological impact of environmental polycyclic aromatic hydrocarbons (EPAHs) as endocrine disruptors. . *Environ. Pollut., 213*, 809-824. doi:10.1016/j.envpol.2016.03.050

Zhang, Y., Lou, D., Hu, Z., & Tan, P. (2019b). Particle number, size distribution, carbons, polycyclic aromatic hydrocarbons and inorganic ions of exhaust particles from a diesel bus fueled with biodiesel blends. *Journal of Cleaner Production, 225*, 627-636. doi:10.1016/j.jclepro.2019.03.344

Zheng, L., Huang, X., X., J., & Deng, C. (2020). Paleoenvironmental implications of molecular and carbon isotopic distributions of n-alkanes in the hominoid-bearing upper Miocene sediments from the Zhaotong Basin, southwestern China. *Palaeogeography, Palaeoclimatology, Palaeoecology, 544*. doi:10.1016/j.palaeo.2020.109627

Zheng, X., Wu, Y., Zhang, S., Hu, J., Zhang, K. M., Li, Z., . . . Hao, J. (2017). Characterizing particulate polycyclic aromatic hydrocarbon emissions from diesel vehicles using a portable emissions measurement system. *Nature, 7*. doi:10.1038/s41598-017-09822-w

Zischka, M., Schramel, P., Muntau, H., Rehnert, A., Gomez, M. G., Stojanik, B., . . . Maier, E. A. (2002). A new certified reference material for the quality control of palladium, platinum and rhodium in road dust, BCR-723. *TrAC Trends in Analytical Chemistry, 21*(12), 851-868. doi:10.1016/S0165-9936(02)01207-4